TRIUMF

ANNUAL REPORT
SCIENTIFIC ACTIVITIES
2002

TRIUMF

ANNUAL REPORT
SCIENTIFIC ACTIVITIES
2002

BEAM LINES AND EXPERIMENTAL FACILITIES

ISAC - I & ISAC - II EXPERIMENTAL HALLS

—— **PRESENT**
—— **FUTURE**
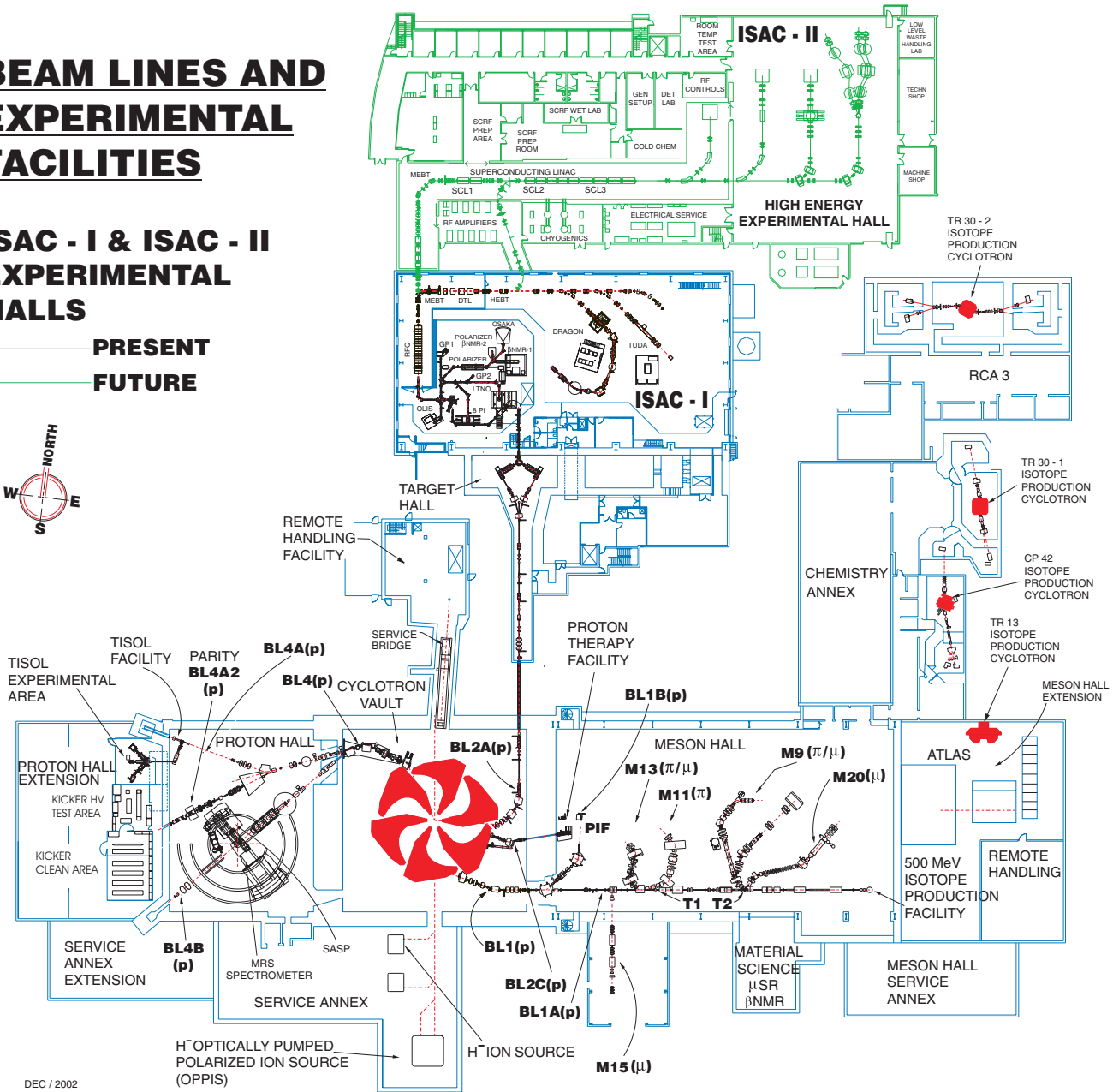
ISAC - II

ROOM TEMP TEST AREA

LOW LEVEL WASTE HANDLING LAB

TECHN SHOP

RF CONTROLS

GEN SETUP

DET LAB

SCRF WET LAB

SCRF PREP AREA

SCRF PREP ROOM

COLD CHEM

MACHINE SHOP

MEBT

SUPERCONDUCTING LINAC

SCL1   SCL2   SCL3

HIGH ENERGY EXPERIMENTAL HALL

ELECTRICAL SERVICE

RF AMPLIFIERS

CRYOGENICS

MEBT   DTL   HEBT

RFQ

OSAKA

GP1   POLARIZER   βNMR-2

POLARIZER   βNMR-1

GP2

DRAGON

TUDA

OLIS

LTNO

8 Pi

ISAC - I

TARGET HALL

REMOTE HANDLING FACILITY

SERVICE BRIDGE

PROTON THERAPY FACILITY

TR 30 - 2 ISOTOPE PRODUCTION CYCLOTRON

RCA 3

TR 30 - 1 ISOTOPE PRODUCTION CYCLOTRON

CP 42 ISOTOPE PRODUCTION CYCLOTRON

TR 13 ISOTOPE PRODUCTION CYCLOTRON

CHEMISTRY ANNEX

MESON HALL EXTENSION

TISOL FACILITY

TISOL EXPERIMENTAL AREA

PARITY
BL4A2 (p)

BL4A(p)

BL4(p)   CYCLOTRON VAULT

PROTON HALL

BL2A(p)

BL1B(p)

MESON HALL

M9 (π/μ)

ATLAS

PROTON HALL EXTENSION

KICKER HV TEST AREA

KICKER CLEAN AREA

M13 (π/μ)

M11 (π)

M20 (μ)

PIF

SERVICE ANNEX EXTENSION

BL4B (p)

MRS SPECTROMETER

SASP

BL1(p)

BL2C(p)

BL1A(p)

T1   T2

500 MeV ISOTOPE PRODUCTION FACILITY

REMOTE HANDLING

SERVICE ANNEX

MATERIAL SCIENCE μSR βNMR

MESON HALL SERVICE ANNEX

H⁻ OPTICALLY PUMPED POLARIZED ION SOURCE (OPPIS)

H⁻ ION SOURCE

M15 (μ)

NORTH

W   E

S

DEC / 2002

FOREWORD

On behalf of the TRIUMF Board of Management I am pleased to have the opportunity to comment on another very successful year for TRIUMF. Members of the Board are proud of the achievements of the many scientists from Canada and abroad who are making such good use of the facilities TRIUMF provides. These facilities support a truly exciting program of science in nuclear and astrophysics, precision tests of fundamental processes, medical physics, condensed matter physics, and nuclear chemistry. The scientific output of the lab is impressive for its breadth and scope, but especially for the high quality of the research that is accomplished. That quality has been recognized again by excellent support from the Natural Sciences and Engineering Research Council (NSERC). TRIUMF was also a key participant in the successful proposal to build WESTGRID, a computing facility that will, among other things, provide vital support for Canada's particle physics program.
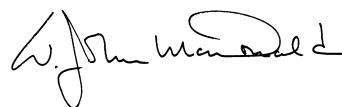
As part of their continuing support of the Canadian and international particle physics community, TRIUMF staff have continued to live up to their reputation for producing state of the art components as part of Canada's contribution to CERN. The ATLAS detector hadronic end-cap calorimeter components and the quadrupole magnets for the LHC continue to be assembled on time and on budget.

Equally important for TRIUMF's success is the professional and competent way the facilities are operated. Equipment has to be maintained and refurbished to meet ever-increasing demands for additional capability. This is particularly important in the case of the original H^- cyclotron that is the driver for multiple proton beams used for everything from medical treatment to the proton, meson, and radioactive beam programs. Staff members of the Cyclotron division are to be congratulated for their outstanding work in rebuilding and replacing key components of the cyclotron to ensure that it can continue to meet the demands placed on it. It is a tribute to their abilities that the cyclotron is operating at higher than ever efficiency despite the fact that it is now over 30 years old.

As in the past, the Board has been regularly considering matters brought to it from its standing committees: Finance, Human Resources and Safety. In addition, technology transfer was the focus of much discussion this year and the Board decided to establish a fourth committee specifically to consider how to best enhance and promote TRIUMF's existing strengths and future potential in this area. While it is the excitement of the unknown that drives all scientists and the support of good science will continue to be the first priority at TRIUMF, it is also the case that good science frequently leads to developments that can benefit society. The Board recognizes the need to encourage the transfer of ideas developed through the science activity to the wider community. Another matter that received Board attention this year is the search for resources for the replacement of TRIUMF House. The Board is seeking support from the universities to assist TRIUMF in maintaining this vital component to the success of the laboratory.

Finally, work has begun on preparing a new TRIUMF Five-Year Plan for 2005–2010. This exercise will involve considerable work by staff, the user community, administration and the Board to ensure the best possible plan for the future of TRIUMF results.

In closing, I would like to thank all members of the Board who give so generously of their time to assist TRIUMF in its important and exciting work. I would also like to acknowledge, on behalf of the Board, the core funding support of the Government of Canada through the National Research Council and the Government of British Columbia for its contribution to the ISAC-II building. Finally, I wish to personally thank President Arthur Carty of the National Research Council and his staff for their helpful advice and support.

W.J. McDonald
Chair, Board of Management

TRIUMF was established in 1968 as a laboratory operated by the University of Alberta, the University of British Columbia, Simon Fraser University and the University of Victoria under a contribution agreement from the National Research Council of Canada. The initial consortium has been expanded to include Carleton University as a full member, and the University of Manitoba, McMaster University, the Université de Montréal, Queen's University, the University of Regina and the University of Toronto as associate members. The facility is operated for all Canadian as well as foreign users.

The experimental program is based on a cyclotron which is capable of producing four simultaneous beams of protons, two of which are individually variable in energy from 180–520 MeV, the third from 472–510 MeV, and the fourth between 70 and 110 MeV. The potential for high beam currents – 100 μA at 500 MeV to 300 μA at 400 MeV – qualified this machine as a "meson factory". The third high intensity beam line feeds the new isotope production facility, ISAC, which started operation in 1998 and qualifies as a second generation radioactive beam facility.

Fields of research include basic science, such as particle physics, nuclear physics, nuclear astrophysics, and condensed matter research, as well as life sciences based primarily on isotope research. There is also a biomedical research facility which uses protons for treatment of ocular melanomae. TRIUMF is providing the Canadian contribution to the Large Hadron Collider at CERN and TRIUMF resources are also available to support the Canadian subatomic program at other laboratories.

The ground for the main facility, located on the UBC campus, was broken in 1970. Assembly of the cyclotron started in 1971. The machine produced its first full-energy beam in 1974 and its full current in 1977.

The laboratory employs approximately 325 staff at the main site in Vancouver and 19 based at the participating universities. The number of university scientists, graduate students and support staff associated with the present scientific program is about 625.

CONTENTS

viii

INTRODUCTION

For several years the central theme for TRIUMF development has been the ISAC facilities. Major milestones for these facilities were successfully met during the year.

The first significant nuclear physics results from the DRAGON experiment were published as a Physics Review Letter. These results tied down the production rates of ^{22}Na from stellar hydrogen burning of the radioactive nucleus ^{21}Na. They are of great interest as ^{22}Na is a gamma-ray marker for novae that the satellite INTEGRAL is searching for. This gamma-ray satellite was launched by the European Space Agency in 2002 with a mission to search for radioactive species in different stellar environments.

Various other experiments at ISAC are producing interesting and exciting results as new facilities come on line, such as the radioactive spin polarization system and the 8π gamma-ray spectrometer.

TRIUMF's next challenge is to build the ISAC-II accelerator and construct new experimental equipment required to exploit the scientific opportunities presented by ISAC-II. During the year the ISAC-II building was substantially completed and much detailed design of the superconducting accelerator cavities was undertaken. Scientifically and technically, ISAC is evolving into the premier world facility for science involving radioactive beams. TRIUMF and several Canadian universities are appointing an increasing number of young scientists specifically to work with the ISAC facilities.

TRIUMF's other scientific programs are proceeding vigorously. The μSR program is attracting an increasing number of users from within Canada and around the world. New Canadian university faculty appointments are being made to exploit the fast-developing and intriguing science of μSR. The unique sensitivity of TRIUMF's μSR program to the internal force fields of materials is attracting the attention of materials scientists worldwide.

The life sciences program continues to make an important impact towards the scientific reputation of the laboratory.

The TWIST experiment aims to measure with unprecedented accuracy the decay characteristics of the muon. The first extensive experimental data collection run for TWIST occurred during the year and the success of this run demonstrated very clearly that the TWIST experiment has the potential to fulfill all its ambitious aims.

Central to the internal activities of the laboratory, the 500 MeV cyclotron continues to function well. This success is due to the dedication of the machine staff who are always ready to give that extra effort when called upon.

TRIUMF is a national facility and has as its goal the support of the entire Canadian particle and nuclear physics community. Facilities are provided at TRIUMF but TRIUMF also provides scientific and engineering support to mount front-line experiments at other international laboratories. Over the last few years a large part of this work has revolved around the specialized equipment being built by TRIUMF and Canadian industry as Canada's contribution to the LHC at CERN as well as vital contributions of equipment and expertise to the ATLAS detector, which will form part of the LHC experimental facility. Many of the milestones for this work have been successfully passed; Canada, through TRIUMF, has established a reputation in the internationl community for excellence in design, construction, and delivery of advanced technology, on time and on budget.

TRIUMF's outreach program involves both technology transfer and education outreach. Technology transfer has many facets. One highlight is the collaboration between TRIUMF and MDS Nordion which continues to be the best known of TRIUMF's successful technology transfers to Canadian industry. During the year MDS Nordion installed a third cyclotron at TRIUMF to produce more radioisotopes for medical therapy and diagnostic purposes. Because the demand for such isotopes is rapidly growing (currently enough isotopes are produced at the TRIUMF/MDS Nordion site for over 2 million medical procedures per year), this third cyclotron will only just meet the demand.

It is important that Canadians be aware of and understand TRIUMF's mission. For many years TRIUMF has had a successful program in this area. This year a new outreach program was started specially aimed at schoolteachers. The idea is to provide teachers interaction opportunities with TRIUMF staff and involvement in experimental programs to both inspire and inform them about advanced technical and scientific technology, methods and procedures. Teachers are then able to take this information and their experiences back to their students.

A major activity during the year was the preparation of groundwork for TRIUMF's 2005–2010 Five-Year Plan. A series of workshops was held where different sections of the Canadian physics community were able to express their vision for the future. All these opinions were discussed in a town meeting at TRIUMF in September. From this meeting, a planning group was set up to take forward the ideas and construct a coherent and comprehensive plan for presentation in 2003.

In a laboratory the size of TRIUMF, staff undertake many different tasks; some jobs are highly visible, but many others, although essential, are less visible at first glance. Having now spent two years at TRIUMF, I have a greater insight into the many valuable contributions people make. I am impressed by the commitment and dedication of all staff members to TRIUMF's mission.

It has been a busy and exciting year at TRIUMF in terms of scientific output, interactions with society, and in establishing the foundation that will take TRIUMF, as a world-class laboratory, to 2010 and beyond.

A. Shotter,
Director

SCIENCE DIVISION

INTRODUCTION AND OVERVIEW

The year marked a new era in TRIUMF's scientific achievements. This report highlights the very new results coming out in publications from ISAC while the final papers related to experiments that took data in the proton hall before its decommissioning were released. Also, physics analyses of CHAOS data are being finalized.

In ISAC, a major accomplishment is reported by the DRAGON collaboration with the publication of the first direct proton capture measurement of the ^{21}Na(p, γ) reaction. It has demonstrated that the combination of ISAC accelerators and the DRAGON spectrometer has outstanding potential, as we had hoped. DRAGON has met its specifications very quickly. In parallel, the TUDA collaboration studied the level structure of ^{21}Mg and ^{22}Mg.

The refurbishing of the 8π spectrometer has been completed and a large collaboration is now exploiting the unique features of the twenty Compton suppressed germanium detector array. In this report the 8π group reports on a study of ^{11}Li high energy levels, a high precision lifetime measurement with ^{26}Na, a new value for the lifetime of ^{176}Lu, a geochronometer decay of $T_{1/2}$ = 40.8 ± 0.3 billion years, and a study of the long-lived isomer ^{178m2}Hf ($T_{1/2}$ = 31 years). The 8π spectrometer is already generating many interesting proposals and will be even more attractive when it is fitted with charged particle detectors next year.

Beautiful new results were obtained by two groups from Osaka University. Using ^{11}Li beams, several spin and parity assignments were made for states in ^{11}Be using a novel technique of β-delayed asymmetry measurements. Studies of aligned ^{20}Na nuclei will test the possible existence of non-standard interactions in the weak decay of ^{20}Na.

The TRINAT group has continued their studies of correlations in the beta decay of ^{37}K and ^{38m}K. These beautiful experiments rely on atomic trapping and polarizing techniques to test properties of the weak interaction.

This report demonstrates that science is coming out of our ISAC investments. This development is helping us attract new users and talented young physicists who want to exploit the unique opportunities created at ISAC.

Also, in this report, very important new results are presented linked to data taken some years ago with the CHAOS spectrometer. CHAOS has proven to be a very versatile and unique instrument to study pion physics and, in particular, to test predictions of chiral perturbation theories. New results on the analyzing power measurement of $\pi^{\pm}p$ elastic scattering at low energies are presented. Constraints on the πN coupling constant, the πN scattering length at low energies, and ultimately the πN sigma term were obtained.

The charge symmetry breaking experiment was the last experiment which took data in the proton hall. It used the SASP spectrometer to measure a forward-backward asymmetry in the charge exchange reaction $np \to d\pi^0$ to look for evidence of a charge symmetry breaking term in the strong interaction. This is related to the mass difference between an up and down quark. The TRIUMF result is new and has sent theorists back to their model to try and reproduce the experimental result.

The TWIST experiment was able to take its first complete data set. It is designed to make high precision measurements of the energy and angular distribution of the decay positrons in the decay of polarized muons at rest. This difficult experiment is limited by systematic effects and many data sets were taken in varying conditions to assess the systematic errors and learn ways to control them.

In the support TRIUMF gives to Canadian researchers in high energy physics experiments at facilities abroad, the main event was the delivery of all modules for the hadronic endcap calorimeter to the future ATLAS experiment at the LHC. The TRIUMF team, led by Dr. C. Oram, has delivered on time and on budget an $8 million contribution to the ATLAS experiment. Funds for the hardware were provided by NSERC (Natural Sciences and Engineering Research Council) while TRIUMF invested in infrastructure support and assembly personnel.

Another ATLAS project was brought to conclusion at the University of Victoria with the help of TRIUMF engineers and technicians: 55 feedthrough assemblies were produced and 50 delivered to CERN by year end. Both of these ATLAS project teams will now focus on the assembly and commissioning efforts at CERN in preparation for the completion of the detector by 2007. In a related activity, a demonstration test was carried out to transfer huge data sets (1 Tbyte) from TRIUMF to CERN over commercial networks and using commercial software tools. It established a world record for high speed transmission over long distances (12,000 km).

Other activities at DESY (HERMES experiment), at TJNAF ($G\emptyset$ and Qweak experiments), at BNL (rare kaon decay studies), and at SNO are also reported in this section.

Our condensed matter effort has continued to grow

with both polarized muons (μSR) and light ions (β-NMR). In particular, the considerable investments made at ISAC to generate low energy polarized light ion beams are now leading to new physics opportunities in the studies of thin films or multi-layered materials like recording media, superconducting films, etc. The commissioning phase for the beam line, the spectrometer and its data acquisition system is now complete and the physics program can now start in earnest.

The μSR facility is attracting many users (130) and materials developers who want to study the magnetic properties of new materials. This year a new superconductor material MgB_2 was tested at TRIUMF; new organic superconductors, C_{60}, molecular magnets, and new electron-doped superconductors found their way into our muon beams. The studies of muonium as analogue of hydrogen in semiconductors (GaAs, GaP, ZnS, etc.) continued in these industrially very important materials. The SFU chemistry group studied muonium in critical water and critical CO_2, while the UBC chemistry group focused on zeolites.

In the life sciences, TRIUMF plays an important role in delivering novel tracers to a variety of institutions ranging from the UBC Neurodegenerative Disorders Centre to the local hospitals, the Botany and Chemical Engineering departments, etc. The most important event was the funding of two new PET cameras (one for human brain studies, the other for small animal studies) by the Canadian Foundation for Innovation.

These experimental programs are complemented by a strong theoretical effort. The 4 permanent staff members and their 7 research assistants cover a wide range of topics from extra-dimension theories, to chiral perturbation theories, to quantum chromodynamics on the lattice, to standard model tests, to novel nuclear physics models to explore the region of neutron-rich nuclei.

A review of the Theory group activities took place early in the year and recommended a refocusing of the group's activities toward ISAC-related science. A search for a Theory group leader who would accomplish this task was initiated in collaboration with the UBC Physics department.

We continued to treat western Canadian patients with large ocular melanomae, as well as providing irradiation services for the space industries and high energy groups who need to test their detectors for radiation resistance.

Overall, this was a very successful year scientifically and I would be extremely satisfied if it were not for the loss of a very talented experimenter and friend in the person of Nate Rodning, the leader of the TWIST experimental team. He will be missed.

PARTICLE PHYSICS

Experiment 614
TWIST – the TRIUMF weak interaction symmetry test
(G.M. Marshall, TRIUMF)

TWIST is an experiment to measure precisely the parameters describing the energy and angular dependence of positrons (e^+) emitted from the decay of polarized positive muons (μ^+). It uses the M13 beam line to provide a high luminosity beam of highly polarized surface muons, produced by pions decaying at rest near the surface of the 1AT1 pion production target. The muons are guided axially into a large, uniform, 2 T solenoidal magnetic field where they stop in a thin planar target at the centre of a precisely constructed, low-mass array of drift chambers (Fig. 1). The polarization of the muon beam, $\vec{\mathcal{P}}_\mu$, is preserved to a high and predictable degree in the process. When the muons decay with a mean lifetime of 2.2 μs, the array of chambers records the tracks of the e^+ in the magnetic field, allowing the measurement of e^+ momentum for several thousand decays every second.

Such a large number of events means that the characteristics of the decay (e^+ energy and angular distributions) can be measured with unprecedented accuracy, and that the many possible sources of systematic uncertainties can be investigated efficiently. The distributions are described by four parameters (ρ, η, δ, and ξ), widely referred to as the Michel parameters. The distributions, and thus the values of the four parameters, are exactly predicted by the standard model. The goal of TWIST is to search for deviations from the predictions and thus to subject the model to very stringent tests, by measuring ρ, δ and $\mathcal{P}_\mu \xi$ to a few parts in 10^4.
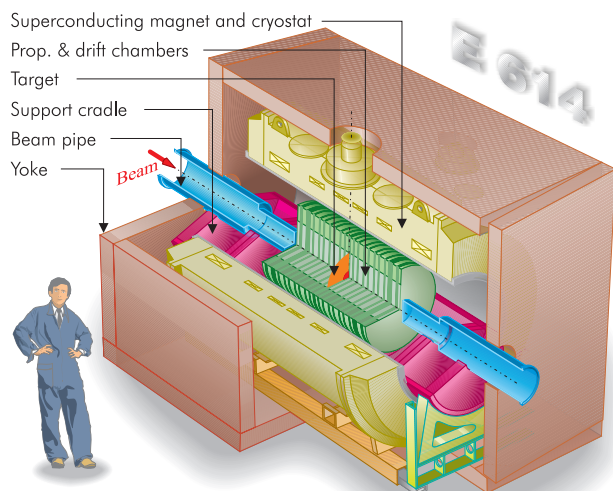
Fig. 1. The TWIST spectrometer.

This represents an improvement of more than one order of magnitude over the existing precision. An additional advantage is that the values are derived simultaneously and consistently from the same data set, thereby strengthening the outcome with respect to correlated uncertainties in the different parameters.

While the standard model has been very successful so far at predicting diverse phenomena in the interactions of subatomic particles, it is widely regarded as an approximation to a more fundamental theory, one which may be more symmetric in left-right handedness and in particle-antiparticle character. TWIST may be able to elucidate some of the qualities of the more fundamental theory.

Progress towards the goals of TWIST

Following the first operation of most of the spectrometer's components in beam during an engineering run in the fall of 2001, the TWIST experiment made significant progress in 2002, thanks to the support and assistance of many individuals at TRIUMF.

Solenoid

The solenoid magnetic field was mapped, using an array of Hall probes and a data acquisition system which automatically measured and recorded the longitudinal field components while the array was rotated and translated throughout the positron tracking volume. The probes were calibrated *in situ* with an NMR device, and a partial survey was also made using NMR to check for consistency and precision. The results were compared with predictions of the OPERA simulation program. Parameters were adjusted in OPERA by comparing with the measurements, enabling OPERA to provide a field map of the tracking volume which is in good agreement with the survey. This map is now used by the GEANT simulation of particles in the detector, and is being incorporated into the tracking and analysis software.

While ramping the field of the superconducting solenoid near its operating point in preparation for the first physics runs, the solenoid quenched. The resulting loss of cryogens (liquid helium and nitrogen), coupled with a previously identified small leak in the solenoid vacuum vessel, precipitated a nearly complete warmup of the cryogenic system of the superconductor. Subsequent cooling took much longer than anticipated, but the solenoid was again ready for operation in August. Fortunately, no damage to the solenoid or the detector system occurred from the quench.

Detector

There were only a few very minor problems encountered in the engineering run in 2001. One broken

wire (of 4608) and three oscillating planes (of 56) were quickly and completely repaired. The high quality and precision of construction of the chambers and their gas systems have led to a very reliable, robust detector assembly. The chambers demonstrated full efficiency (>99.9%) and experienced no high voltage trips during normal operation throughout six months of beam time in 2002.

Data acquisition

The on-line data acquisition was expanded and improved. The system is now capable of recording data at the high rates required (event rate 5000 s^{-1}, event size 1.5 kB, data rate 8 MB s^{-1}), and upgrades to this can be included if necessary. This is made possible in part by a new high-capacity tape system (SDLT 320 standard) which additionally reduces the cost of the recording medium by a significant amount. Precise periodic monitoring takes place for many parameters which can affect data quality, such as temperatures, pressures, voltages, currents, magnetic fields, primary and secondary beam parameters, etc. The values recorded are used not only during data analysis, but also to create alarms for conditions out of specification which signal problems that must be corrected by the experimenter. On-line documentation describing responses to most problems has been provided. Some of the periodically measured values, the NMR magnetic field measurements in the dipoles of M13, are now used to automatically control the fields within very tight tolerances by communication with the recently developed EPICS control system for M13.

Software and analysis

Throughout the year, taking advantage of data obtained in the engineering run as well as the physics runs, the software used in simulation and analysis was dramatically improved. The GEANT3 simulation was further customized by extending and including processes which are expected to be important for TWIST physics measurements. A procedure was established for testing and adjusting the alignment of the planar drift chambers in the analysis software. Another procedure for calibration of the times of drift chamber hits on a wire-by-wire basis was developed and applied. The helix fitting procedures used in the analysis code were tested on both simulated and real data, improving the precision of track reconstruction.

A procedure has been defined by which the data can be analyzed in a way which is blind to the final results, in order to avoid possible human biases. The principle has been used by many other collaborations, but the nature of the TWIST analysis requires some special techniques by which the data are fit to a sum of simulated spectra generated with hidden Michel parameters which are different from the accepted values.

When the fits are completed and satisfactory, the hidden values are revealed and the results of the fit are used to calculate the true experimental values for the Michel parameters.

In order to be able to process the large amount of data and to match it with a comparable number of simulated events, a small analysis cluster consisting of fifteen dual-CPU nodes (AMD 1.8 GHz processors) and a tape library device were purchased with an NSERC equipment grant. Although still inadequate for our full requirements, the analysis and simulation rates were greatly improved.

First measurements

Data were taken in the fall of 2002, with the goal of determining two of the Michel parameters, ρ and δ, with a precision of better that one part in 10^3. While this level of statistical precision can be reached using only a few days of beam (a data set of some 10^8 events is adequate), the investigation of possible systematic uncertainties takes much longer. Altogether, approximately 6×10^9 events were recorded, comprising many separate measurements of the Michel parameters under different experimental conditions, in order to measure quantitatively the effects of the changes. Data sets were obtained corresponding to such variables as different detector efficiencies, solenoidal fields, muon beam characteristics (polarization, stopping position, focus position), trigger rates, and backscattered event rates. Figures 2 and 3 show the momentum and angular distributions, respectively, from one data set.

A critical task for TWIST is to test and validate both the analysis software and simulation programs. With the availability of the first data, this has begun. Agreement between the simulated and measured muon stopping distributions is impressive. Although there is no truly monochromatic positron calibration source
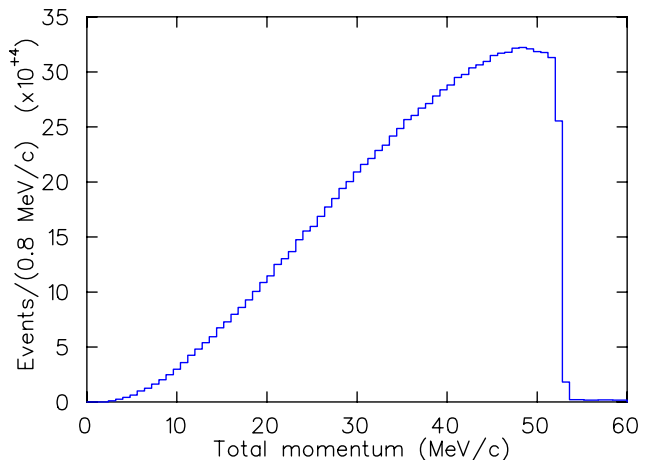
Fig. 2. Momentum distribution from one data set; events in the range of about 15 to 50 MeV/c are considered to be within the fiducial volume.

6
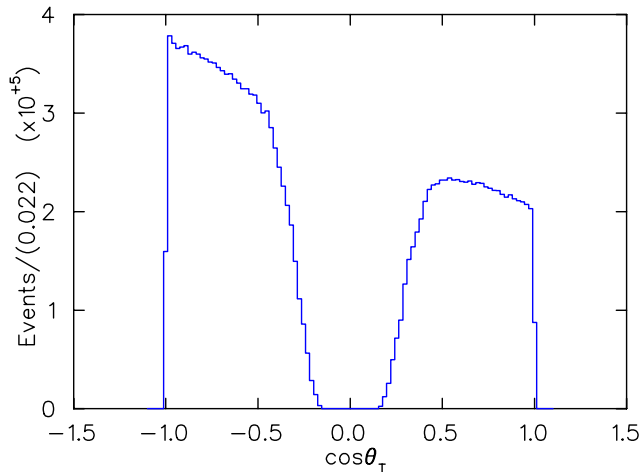
Fig. 3. Angular distribution from one data set; events in the range of about $0.5 < |\cos\theta_T| < 0.95$ are considered to be within the fiducial volume, while the region near $\cos\theta_T = 0$ is not within the spectrometer acceptance.

which can populate the spectrometer angular acceptance, the symmetry of the detector allows one half to be used to independently define a positron track to the limits of the detector precision, while the other half can be used to analyze another part of the same track. This is accomplished by using muons which have been selected to stop not in the target at the centre of the detector, but near either end of the detector. Comparison of the two halves permits checking characteristics such as pattern recognition, reconstruction efficiency, and resolution in angle and momentum. Moreover, comparisons can also be made using the simulation under the same conditions, to help to validate the physics of simulated positron motion through the detector.

Next steps

The analysis of the data taken in 2002 is proceeding at the limits of the human and computing resources of the group. It is expected that this analysis will be completed in 2003. Meanwhile, improvements to the muon beam and to its characterization, using a newly constructed low-density time expansion chamber, will enable TWIST to proceed with the measurement of $\mathcal{P}_\mu\xi$ to a precision of one part in 10^3. With the experience gained in the process, the challenges of the measurements to the ultimate statistical and systematic capabilities of the spectrometer can be met.

ATLAS Experiment at the LHC
(C. Oram, TRIUMF)

As described in detail in the 1996 Annual Report, ATLAS is building a general purpose pp detector which is designed to exploit the full discovery potential of the Large Hadron Collider (LHC) at CERN. The TRIUMF group is responsible for the management and engineering of the hadronic endcap (HEC) calorimeter, and the feedthroughs for the endcap cryostat. For the HEC, this year has seen the completion of module production and the assembly of the two wheels of the first endcap. The wheel assembly at CERN is led by a TRIUMF staff member.

Physics goals

The present theoretical understanding of elementary particles is in the context of the standard model. It is a remarkably successful model, providing predictions which have been consistently confirmed by experiments for over two decades. Its agreement with experimental results, to enormous accuracy in some cases, makes it the most accurately verified model in science. Of the many elementary particles contained in the standard model, only the Higgs remains to be discovered. The central goal of ATLAS is the search for the Higgs particle.

There are good theoretical reasons to believe that the discovery of the Higgs will at least contain hints at, and more likely direct evidence of, what lies beyond the standard model. If the Higgs is composite, its existence requires as yet unknown ultra-strong forces. If it is elementary, it would be the only spinless particle to be discovered so far. There is a theoretical "naturalness" problem for the masses of spinless particles. In the standard model, which is a highly nonlinear dynamical system, the elementary particles tend to take on the heaviest of all possible mass scales which in such a model are at inaccessible energies and inconsistent with other requirements of the model. All other particles discovered thus far have natural mechanisms, such as gauge and chiral symmetries, for protecting their masses so that they can lie in the observable range. For the Higgs particle, there is no such symmetry in the present model. The only theoretical scenarios which leave the Higgs particle light enough to observe are hypothetical ones, either technicolour or supersymmetry, both radical departures from the present structure of the standard model. If the Higgs is seen at the LHC, one of these scenarios should be seen at the same time.

Particle theory has progressed enormously over the last few decades with many appealing scenarios for physics beyond the standard model. The most likely of these is supersymmetry and the boldest of these is superstring theory. These theories are intimately related and are both radical ideas which promise a new conceptual framework for understanding elementary particles. Though far from being complete theories so far, there are superstring models which resemble the standard model in their low energy limit. These models have a great appeal as they contain a unification of fundamental forces which includes gravity. They have already had substantial impact on gravitational physics

where, for example, in addition to the long sought reconciliation of gravity with quantum mechanics, they have been used to derive a fundamental understanding of black hole thermodynamics. Superstring theory is still in its infancy, but progress has been dramatic and the promise of great things to come has captured the imagination of a substantial fraction of the world's theoretical particle physicists.

The present theoretical view is that the conventional grand unification of the strong, weak and electromagnetic forces can only work in the supersymmetric extension of the standard model. In that model, the grand unified energy scale is only two decades below the Planck scale, the ultimate energy where spacetime itself has quantum fluctuations. It is not out of the realm of imagination that, at energy scales where supersymmetry would be observed, evidence for an ultimate theory of everything, at least everything that can exist once spacetime is formed, is within human grasp.

Experiments at the LHC, where the ATLAS detector will take data, will probe the energy region where the Higgs particle, possibly supersymmetry, or other structures will be visible. This will be the first experimental probe of an energy region where fundamentally new physics is expected to occur in many years. There is every reason to believe that the results will be among the most dramatic ever.

Basic ATLAS design considerations

The most prominent issue for the LHC is the quest for the origin of the spontaneous symmetry-breaking mechanism in the electroweak sector of the standard model (SM). This is related to one of the most fundamental questions of physics: What is the origin of the different particle masses? New direct experimental insight is required to answer this question.

One of the possible manifestations of the spontaneous symmetry-breaking mechanism could be the existence of a SM Higgs boson (H), or of a family of Higgs particles ($H^{\pm}$, h, H and A) when considering the minimal supersymmetric extension of the standard model (MSSM). The Higgs search is therefore used as a first benchmark for the detector optimization. For the SM Higgs, the detector has to be sensitive to the following processes ($\ell = e$ or μ) in order to cover the full mass range above the discovery limit set by the final LEP operation in the fall of 2000:

$H \to b\bar{b}$ from WH, ZH and $t\bar{t}H$ using a $\ell^{\pm}$ and b-tagging,
mass range $80 < m_H < 100$ GeV;

$H \to \gamma\gamma$
mass range $90 < m_H < 150$ GeV;

$H \to WW^* \to \ell^{\pm}\nu\ell^{\pm}\nu$
mass range $150 < m_H < 200$ GeV;

$H \to ZZ^* \to 4\ell^{\pm}$
mass range 130 GeV $< m_H < 2m_Z$;

$H \to ZZ \to 4\ell^{\pm}, 2l^{\pm} + 2\nu$
mass range $m_H > 2m_Z$;

$H \to WW, ZZ \to l^{\pm}\nu + 2$ jets, $2\ell^{\pm} + 2$ jets
from WW, ZZ fusion using tagging of forward jets for m_H up to about 1 TeV.

In addition to signatures similar to these, the MSSM Higgs searches also require sensitivity to processes such as:

$$A \to \tau^+\tau^- \quad \to e\mu + \nu\text{'s}$$
$$\to \ell^{\pm} + \text{hadrons} + \nu\text{'s};$$
$$H^{\pm} \quad \to \tau^{\pm}\nu \quad \text{from } t\bar{t} \to H^{\pm}W^{\mp}b\bar{b} \text{ and using}$$
$$\ell^{\pm} \text{ tag and } b\text{-tagging}$$
$$\to 2 \text{ jets}.$$

The observable cross sections for most of these processes are small over a large part of the mass range to be explored at the LHC. Hence it is important to operate at high luminosity, and to maximize the detectable rates above backgrounds by high-resolution measurements of electrons, photons, and muons.

Canada's participation in ATLAS

The Canadian group consists of about 35 grant eligible physicists from TRIUMF, University of Alberta, Carleton University, Simon Fraser University, University of British Columbia, Université de Montréal, University of Toronto, University of Victoria, and York University. We are strongly involved in three construction projects centred around detecting hadrons in the endcap region: the hadronic endcap project, the hadronic portion of the forward calorimeter project, and the pipeline electronics for calorimetry. In addition, we are committed as part of our common project contribution to providing the feedthroughs for the two endcap cryostats. TRIUMF is directly involved in all of these projects, and in the trigger and physics simulations.

The hadronic endcap project

The hadronic endcap (HEC) calorimeter is a liquid argon sampling calorimeter with copper absorbers [ATLAS Collab., ATLAS Liquid Argon Technical Design Report, December 15 (1996)]. A concise overview of this design was provided in the 1996 TRIUMF Annual Report. An artist's impression of a module can be seen in Fig. 4. In each endcap cryostat sit four detector systems: nearest the interaction region is the presampler, followed by the electromagnetic endcap (EMEC) and the HEC. At the inner diameter around the beam pipe is the forward calorimeter (FCAL).
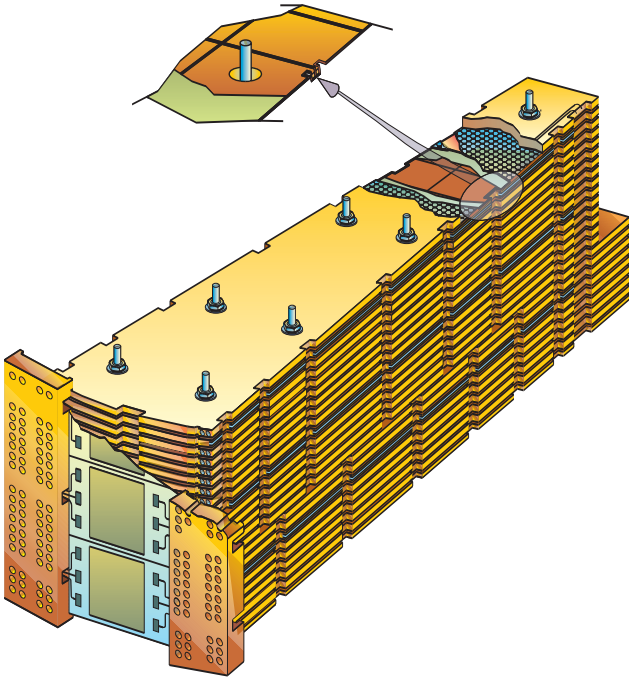
Fig. 4. Artist's impression of a hadronic endcap module.

Hadronic endcap module production

By the middle of the year the TRIUMF group was 100% complete on module production, and by September had shipped all major components. The copper machining facility at the University of Alberta completed all machining for the European groups early in 2002. Hence by year end, production at TRIUMF was limited to making dust covers for the completed wheels at CERN.

Test beam measurements of the hadronic endcap modules

This year saw the publication [Dowler *et al.*, Nucl. Instrum. Methods **A482**, 94 (2002)] of the extensive set of standalone beam tests of the hadronic endcap. This finished our quality control criteria in which we measured 1/8th of our series module production in the test beam at CERN. All the series modules are cold tested. By the end of 2002 we had tested 120 of the 132 modules that constitute the two HEC endcaps in ATLAS.

A test beam period in the summer on the CERN H6 beam line has successfully tested the combined performance of the HEC and EMEC series production modules of the endcap calorimeter system. The H6 beam line provides beams from 20 to 180 GeV. Initial analysis of the data shows the data is of good quality, and the response is within the design goals. This is an important milestone for the group as these measurements form the basis of the calibration of the system as it will be used at LHC beam startup.

To be ready for ATLAS, a further test beam measurement with the calorimeters near the beam line is required. This test will use standard EMEC and FCAL modules, along with purpose built small "inner radius" HEC modules. During 2003 these small inner radius HEC modules will be constructed.

Wheel assembly at CERN

32 modules of the HEC form a wheel. There are two wheels at each end of ATLAS, so we must construct 128 modules into four wheels. The equipment to undertake this is a Canadian responsibility. These four wheels and the two wheels of the EM calorimeter, which go in the same cryostat, are assembled in the horizontal orientation. Hence each wheel, which weighs about 90 tonnes, must be taken from its assembly table, rotated to the vertical and moved to the cryostat. This rotation and translation of equipment is a Canadian responsibility. The engineering was undertaken by a collaboration between Alberta and TRIUMF personnel. The production of the equipment was by Canadian industry. This equipment was delivered to CERN in January, 2002. It was successfully assembled and tested, both for mechanical loading and operation with other systems. Two wheels were constructed this summer, both on schedule. Both wheels have been rotated from the horizontal into the vertical. The rotated wheels have successfully passed all their extensive electrical tests, and are well within their allotted envelopes. The sag of the rotated wheel was measured to be 0.3 mm, which is in agreement with prior calculations. Figures 5 and 6 show respectively the first and second wheel being rotated. Wheel assembly will be completed in early 2004.
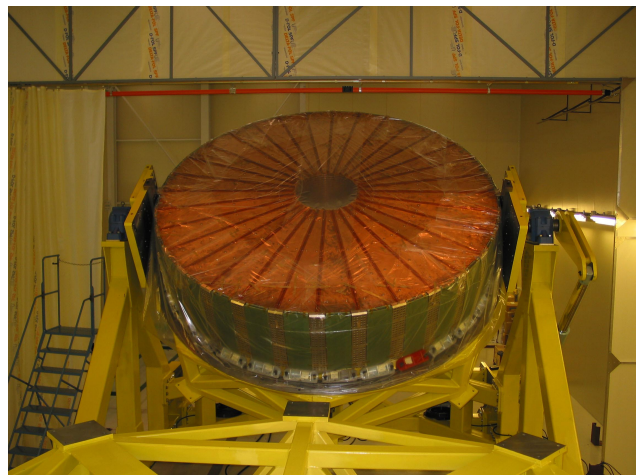
Fig. 5. First front HEC wheel being rotated.

Fig. 6. First rear HEC wheel being rotated.

The ATLAS endcap signal feedthroughs
(M. Lefebvre, Victoria)

The TRIUMF group is responsible for the engineering of the HEC and contributes to the production of high density cryogenic signal feedthroughs for both endcap cryostats. The feedthroughs are critical to the success of ATLAS. They have been built and tested at the University of Victoria by TRIUMF and Victoria staff. The endcap signal feedthroughs are currently (December, 2002) being installed on one of the two endcap cryostats. The operation is expected to last until the end of February, 2003. The second installation period is scheduled for early summer, 2003. The ATLAS endcap signal feedthrough project was covered in detail in the 2001 Annual Report. This report focuses on recent progress.

Reviews

A Canadian involvement in the endcap signal feedthroughs was already proposed in 1995. From the $12.2 M Major Installation Grant awarded to ATLAS in the 1997–98 competition, a total of $4.28 M is earmarked for the endcap signal feedthrough project. The most recent status report was presented at the last NSERC ATLAS Review, held at TRIUMF December 5–7, 2002.

Overview of the project

The ATLAS liquid argon calorimetry is composed of a barrel section and two endcap sections. Each endcap cryostat contains an electromagnetic calorimeter, two wheels of one HEC, and a forward calorimeter. The calorimeter signal and calibration lines are routed to the outside of each endcap cryostat via 25 feedthrough assemblies arranged approximately equally spaced in azimuth. The low voltage needed to operate the endcap hadronic calorimeter preamplifiers, which are located in the cold, are also supplied via the signal feedthroughs as well as various monitoring lines.

The design is based on gold plated conductive pins insulated and sealed by glass inserts in a stainless steel carrier. The carriers are then welded into the cold and ambient (temperature) flanges. A total of 1920 signal and calibration lines per feedthrough assembly is required in the chosen design. The ambient and cold flanges are connected by a bellows to isolate the feedthrough vacuum from the cryostat inter-vessel vacuum. The cold flange is attached to a transition piece, known as a funnel, which is welded to the cryostat via a bi-metallic joint. The electrical signals are brought from the calorimeter to the cold flange by coaxial kapton cables; these are called pigtail cables. Cables located in the vacuum between the cold and the ambient flange, i.e. inside the bellows, carry the signals through the cryostat wall; these are called vacuum cables. For each endcap, four feedthrough assemblies also carry the low voltage for the HEC preamplifiers. Figure 7 shows an overview drawing of one endcap signal feedthrough.

Procurement of components

Pigtail cables

The development of the pigtail cables was part of a larger effort to develop signal and calibration cables for the whole of the liquid argon (LAr) readout chain. They were purchased through Orsay, along with the other ATLAS LAr cables, from Axon. A Memorandum of Understanding for the procurement of the endcap pigtail cables was signed by Orsay and ATLAS-Canada. A detailed procurement schedule was developed, and reception of pigtails in Victoria was completed in the fall of 2002.

Pin carriers

Extensive and detailed tests comparing the ceramic and glass pin carrier technologies were made in 1997 and 1998. Both technologies were found suitable for our project. The green light was given at the feedthrough Production Readiness Review (held in CERN on January 29, 1999) to purchase glass technology pin carriers made of low inclusion 304 L stainless steel. The order was placed in June, 1999. Reception was completed early in 2002.

10
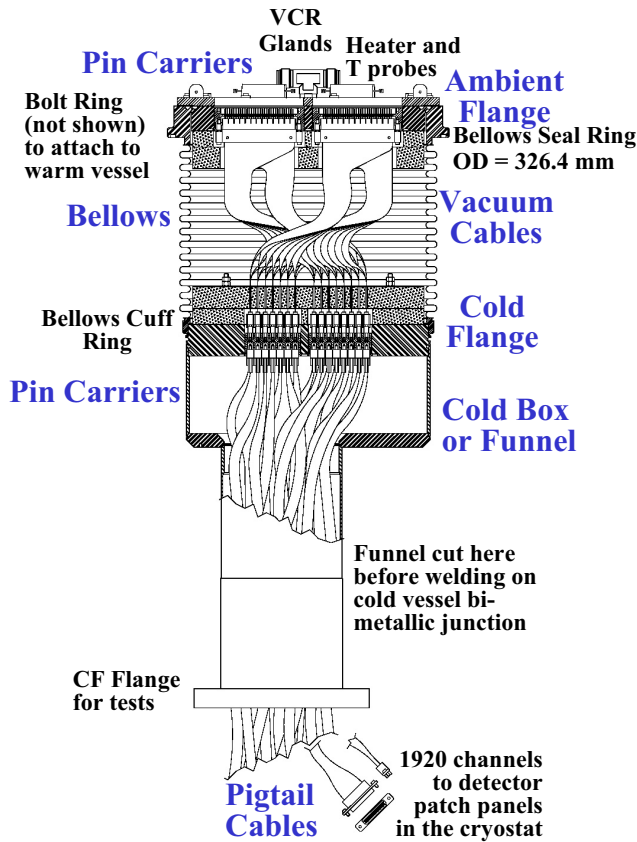
Fig. 7. Overview drawing of one endcap signal feedthrough, identifying its most important components.

Assembly and installation

A total of 50 feedthrough assemblies plus 5 spares have been produced (see Fig. 8) following a detailed assembly procedure, quality plan and quality assurance plan. These include the description of the testing of components from their arrival in Victoria through the completion of feedthrough units. Complete material traceability is ensured through the use of detailed traveller sheets. The funnel and cold flange of each feedthrough assembly are part of the cryostat pressure vessel. An officially licensed company has done the welding and extensive testing to conform to accepted welding code.

The shipment of feedthrough assemblies to CERN is done by air freight. All but five assemblies are now in CERN. Upon arrival at CERN, each feedthrough assembly is subjected to an ambient temperature leak test and a basic electrical test. We are responsible for these tests. The required testing equipment was commissioned at CERN in October, 2001, when the first feedthrough assemblies arrived at CERN.

The installation of the feedthrough assemblies on the cryostat is a delicate and complex operation. Although the feedthrough installation is not a Canadian responsibility, our group is actively assisting during the

Fig. 8. Vacuum cables being installed on a feedthrough by Paul Birney (TRIUMF) at the University of Victoria.

operation. In particular, given the softness of the pins, members of our team will manually connect the so-called warm cables that join the outside of the ambient flange to the electronics crate baseplane. Each feedthrough assembly, once welded on the cryostat, must also be electrically tested.

The installation of the feedthrough assemblies on the first endcap cryostat (see Fig. 9) started on December 2, 2002 and is expected to last until the end of February, 2003. As of December 20, 2002, six feedthrough assemblies have been successfully installed (see Fig. 10). Installation on the second cryostat is scheduled for early summer, 2003. It is expected that Canada's involvement in the feedthrough project will end during 2003 with the connection of the warm cables to the ambient flange.

Fig. 9. The first endcap cryostat of the ATLAS liquid argon calorimeter after arrival at CERN, still in its transport cradle (April, 2002).
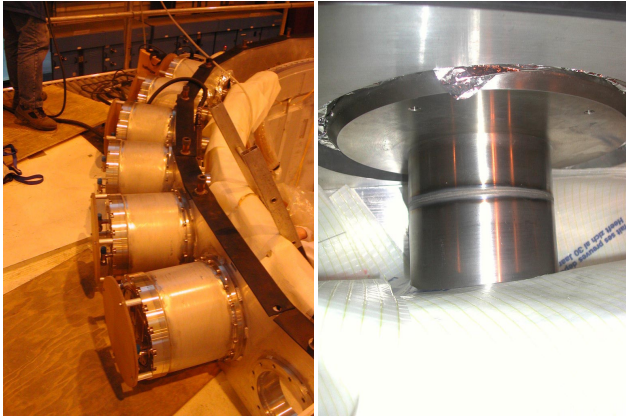
Fig. 10. First six feedthrough units installed on the first endcap cryostat (December, 2002) and a close-up of one of the welds. Photos by Aboud Falou, Orsay.

Canadian participants in ATLAS

Investigators: J. McDonald, J. Pinfold, M. Vincter (Alberta); D. Gingrich, P.W. Green (Alberta/TRIUMF); J. Armitage, M. Dixit, G. Oakham (Carleton); P. Depommier, C. Leroy, J.-P. Martin (Montréal); G. Azuelos (Montréal/TRIUMF); G. Couture (Montréal/UQAM); M.C. Vetterli (SFU/TRIUMF); D.C. Bailey, R.S. Orr, P. Sinervo, W. Trischuk (Toronto); P. Krieger, J.F. Martin (Toronto/IPP); M. Losty, C. Oram (TRIUMF); D. Axen (UBC); A. Astbury, R. Keeler, M. Lefebvre (Victoria); R. McPherson, R. Sobie (Victoria/IPP); S. Bhadra (York).

Collaborators: S. Liu, R. Soluk, S. Wheeler (Alberta); B. Caron (Alberta/TRIUMF); M. Khahkzad (Carleton); R. Mehdiyev (Montréal); Kyung Kwang Joo (Toronto); S. Chekulaev, H. Stenzel, M. Wielers (TRIUMF); M. Fincke-Keeler, N. Kanaya (Victoria).

Graduate students: N. Buchanan, L. Chen, C. Cojoocaru, B. Dowler, J. de Jong, R. McDonald, Wei-Yuan Ting (Alberta); G. Belanger, B. Williams (Carleton); P.H. Beauchemin, G. Fubiani, M.H. Genest, C. Lebel, R. Mazini, F. Marullo, P. Roy (Montréal); K. Martens (Toronto); M. Dobbs, T. Ince, V. Singh (Victoria).

BaBar Experiment at the Stanford Linear Accelerator Center

(C. Hearty, UBC)

Introduction

BaBar is an experiment to study the electroweak sector of particle physics using B mesons produced at the high-luminosity e^+e^- collider PEP-II. The primary physics goal is to observe and quantify CP violation in B mesons, but more generally, it is to test the standard model description of electroweak physics and to look for new physics beyond the standard model. The charged weak force is described by the CKM matrix in the standard model, and the central physics goals of BaBar are often described in terms of overconstraining the "unitarity triangle", a geometrical representation of the CKM matrix. BaBar's measurement in 2001 of the angle β of this triangle established that CP is violated in B decay.

The BaBar detector was designed, constructed and assembled prior to the start of the first data run in October, 1999. The drift chamber, one of six major detector systems, was constructed at TRIUMF.

Activities of the collaboration

BaBar collected data for seven months in 2002. The remaining five months constituted a major shut down, during which all components interior to the drift chamber (the support tube, silicon vertex tracker, beam pipe, and the final focus dipole and quadruple magnets) were removed. The primary purpose was to install additional cooling to allow beam currents above the design value. This seems to have been successful: as of early 2003, luminosity was approximately 30% above design. A small number of failed vertex tracker components were fixed as well.

An unfortunate accident during the removal of the support tube damaged the beryllium inner cylinder of the drift chamber, producing a crack approximately 10 cm in length. Although there was no loss of structural integrity, the chamber was unable to hold pressure. The crack was patched during the shutdown and subsequent measurements indicate that repairs are fully gas tight.

BaBar has made good progress in studying a second angle α of the unitarity triangle using the decay $B^0 \rightarrow \pi^+\pi^-$. Although higher-order diagrams make the extraction of α difficult, an initial step would be the observation of CP violation in this final state. BaBar, as of yet, does not see a significant asymmetry (Fig. 11). This is in contrast to Belle, which sees maximal asymmetry in this channel.

Activities of the local group

The local group continues to study charmonium ($c\bar{c}$) mesons. A paper describing the inclusive production of charmonium mesons in B decays was accepted for publication by Physical Review D. Branching fractions were measured for the inclusive production of the $J/\psi, \psi(2S), \chi_{c1}$, and χ_{c2}. The branching fractions were also presented as a function of the centre-of-mass momentum p^* of the mesons and of the helicity of the J/ψ.

The p^* distribution of the J/ψ (Fig. 12) is especially interesting. Compared to a recent non-relativistic QCD calculation, there is a significant excess at low momentum. Possible sources of the excess include an
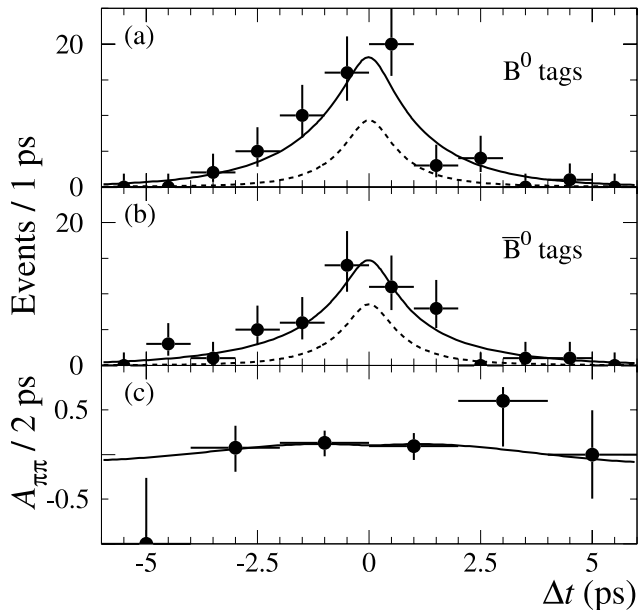
Fig. 11. Number of CP $(\pi^+\pi^-)$ final state candidates (a) with a B^0 tag N_{B^0} and (b) with a $\bar{B}^0$ tag $N_{\bar{B}^0}$, and (c) the raw asymmetry $(N_{B^0} - N_{\bar{B}^0})/(N_{B^0} + N_{\bar{B}^0})$, as functions of the time difference between the signal and tag decay.
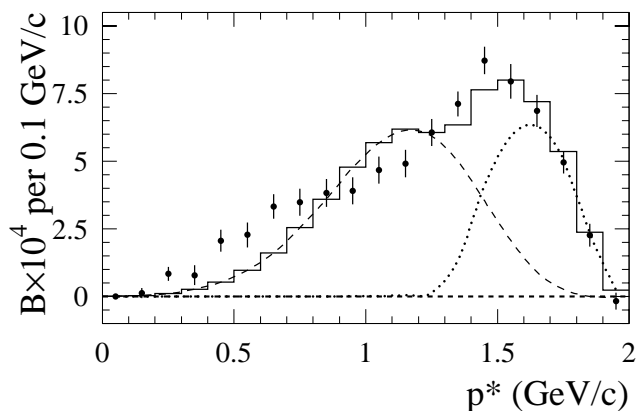
Fig. 12. Centre-of-mass momentum of J/ψ mesons produced directly in B decays (points). The histogram is the sum of the colour-octet component from a recent NRQCD calculation (dashed line) and the colour-singlet $J/\psi K^{(*)}$ component from simulation (dotted line).

intrinsic charm component of the B or the production of an $s\bar{d}g$ hybrid in conjunction with a J/ψ. Another possibility is that the excess is from decays of the form $B \to J/\psi$ baryon anti-baryon. The rate of this type of decay could be enhanced by the intermediate production of exotic states allowed by QCD but not yet observed, including nuclear-bound quarkonium (a $c\bar{c}$ pair bound to a nucleus) or baryonium, a baryon-antibaryon bound state.

These possibilities are being pursued in current analyses.

BNL E787/949/KOPIO
Measurement of $K \to \pi\nu\bar{\nu}$ and other rare decays
(D. Bryman, UBC)

Among possible measurements relating to CP violation, four "golden" processes which stand out as theoretically unambiguous will allow complete elucidation of CP violation in the standard model (SM). Two are the asymmetries in $B \to \Psi K_s$ decays, and the ratio of B_s to B_d mixing. The others are the branching ratios of the charged and neutral $K \to \pi\nu\bar{\nu}$ decays. These rare kaon decays offer unique opportunities to scrutinize higher order phenomena associated with quark mixing and charge-parity (CP) non-invariance.

In the SM, using current data on m_t, m_c, V_{cb}, $|V_{ub}/V_{cb}|$, ϵ_K, $\bar{B}-B$ mixing, etc., the branching ratio of $K^+ \to \pi^+\nu\bar{\nu}$ is expected to be $B_+ = 7.5 \pm 2.9 \times 10^{-10}$. SM expectations for the branching ratio of $K_L^0 \to \pi^0\nu\bar{\nu}$ are at the level $B_0 = 3 \times 10^{-11}$.

E787/949

The decay $K^+ \to \pi^+\nu\bar{\nu}$ has been the object of E787 and its sequel E949 at the Alternating Gradient Synchrotron (AGS) at Brookhaven National Laboratory (BNL). Initial data from E787 yielded the first evidence for the $K^+ \to \pi^+\nu\bar{\nu}$ decay. This year the final result from E787 was published [Adler *et al.*, Phys. Rev. Lett. **88**, 041803 (2002)] based on the full data set which doubled the previously reported sensitivity. Two events of the ultra-rare $K^+ \to \pi^+\nu\bar{\nu}$ decay have now been observed and the branching ratio remains consistent with the SM expectation.

Substantial upgrades to the E787 detector system have been made during the past two years in preparation for E949 aimed at reaching a sensitivity of $(8 - 14) \times 10^{-12}$, roughly an order of magnitude below the SM prediction. Since E949 will be the primary (or only) AGS user, the proton beam on target is intended to have an effective luminosity improvement of 56% over previous running conditions while keeping instantaneous rates at the same level. E949 running with higher instantaneous rates will also be attempted to increase the sensitivity.

In E949, a 700 MeV/c positive kaon beam with a K/π ratio of 4:1 passes through a series of active elements and passive degrader materials to be stopped in a scintillating fibre target at the centre of the detector. The TRIUMF group constructed a new set of more highly segmented beam counters designed to achieve improved spatial resolution at the hodoscope where the incoming particles enter the target. In order to improve photon detection efficiency in the beam corridor, the lead glass beam detector was replaced by a copper/scintillator sandwich active degrader of larger

diameter, also built at TRIUMF.

The TRIUMF-built central drift chamber (UTC) front end cathode pre-amplifiers and post-amplifier/discriminator electronics (768 channels) were replaced to overcome a problem associated with the cathode charge measurement system. As an additional benefit, improvements in the z position resolution along the wires were realized.

The energy, range, and decay sequence of charged particles are measured in the range stack scintillators. The two layers of limited-streamer mode straw tube tracking detectors within the RS were repaired and a new electronics front-end system was built and installed by the TRIUMF group. This resulted in greatly improved performance of the z-coordinate measurement used to suppress backgrounds from scattered muons.

After several months of parasite/shakedown operation, the initial data-taking for E949 took place during the period from mid-March to mid-June and delivered an exposure representing more than a third of E787's taken in one sixth of the time with higher relative sensitivity. Due to the problems with the AGS, the data were acquired at roughly twice the expected instantaneous rate and with the primary proton beam energy lowered from 24 to 20 GeV. Although most systems performed quite well, some problems arose with the upgrade of the central drift chamber cathode strip electronics system and the new beam hodoscope. These problems can be handled in the data analysis, but will be corrected in the hardware for the future.

Improvements were made to the reconstruction and calibration codes to combat high rates in the central drift chamber, and a double-pulse fit procedure for the CCD-digitized target fibre and beam counter pulses has been developed as well as an improved second-pulse-finding algorithm for the range stack.

In spite of strong endorsement of the science of E949 and myriad letters of support for the measurement by the world's leading scientists (including 15 Nobel Laureates), DOE funding for AGS running for E949 was curtailed in mid-2002. Various avenues of other funding for future running are being actively pursued.

KOPIO

The goal of KOPIO is to observe and measure the rate of the decay $K_L^0 \rightarrow \pi^0 \nu \bar{\nu}$. We aim to unambiguously detect a large sample of events so that η, the SM CP violation parameter, can be determined to 15% accuracy with minimal contributions from background or systematic effects. Like E787/E949, KOPIO has built-in redundancies and a reasonable level of contingency to meet the goal of a successful measurement.

In the KOPIO experiment, a 500 μsr solid angle

neutral beam is extracted at 45° to produce a "soft" K_L spectrum peaked at 0.65 GeV/c; kaons in the range from about 0.5 GeV/c to 1.3 GeV/c will be used. Downstream of the final beam collimator is a 3.5 m long decay region which is surrounded by the main detector. Approximately 16% of the kaons decay yielding a decay rate of about 25 MHz. The beam region is evacuated to a level of 10^{-7} torr to suppress neutron induced π^0 production. The decay region is surrounded by an efficient Pb/scintillator photon detector which serves to veto photons and charged particles. In the forward detection region the primary photon detector system consists of two sections: a fine grained preradiator in which the photons are converted and the first e^+/e^- pair is tracked, followed by an 18 radiation length (X_0) calorimeter in which the remaining energy of the photon shower is measured. The preradiator measures the photon positions and directions accurately in order to allow reconstruction of the K_L decay vertex while also contributing to the achievement of sufficient energy resolution.

The preradiator is the main hardware responsibility of the Canadian group, and consists of 64 0.03 X_0 layers, each with plastic scintillator, metal converter and dual-coordinate drift chambers. Each preradiator layer consists of four flat square cell drift chambers (2 m × 2 m) with extruded Al comb backplanes and independent extruded scintillator elements read out by wavelength shifter (WLS) fibres.

R&D projects are proceeding well. A stack of 5 small (8 cm × 15 cm) KOPIO chambers has been constructed and is under test, and initial measurements gave the expected level of performance for efficiency and position resolution. Two medium size KOPIO chambers (30 cm × 30 cm) are operational for electronics development and specification. Two other chambers with full scale (2 m) in one dimension (anode or cathode) are under construction. The final prototype level will be a full size pre-production module of eight chamber layers.

The anode and cathode signals from each preradiator layer will be read out near the chambers. The electronics is designed to enable a fully pipelined dead-timeless system. Front end chamber electronics systems for both the anodes (including HV distribution) and cathodes have been tested on the development chambers. Multi-channel boards are being constructed and designs have been developed for the receiver and processor boards.

The extruded scintillator for the preradiator has proven to require additional R&D effort and expense and we are working with several potential suppliers (including a local plastics company) to achieve the light output and mechanical tolerances that are required.

The HERMES Experiment

(C.A. Miller, S. Yen, TRIUMF; M.C. Vetterli, SFU/TRIUMF; M.G. Vincter, Alberta)

The HERMES experiment was designed to comprehensively study the spin structure of the nucleon. It has been running at the HERA electron accelerator at the DESY Laboratory in Hamburg, Germany since 1995, measuring spin asymmetries for deeply inelastic electron scattering (DIS). The combination of a polarized high energy electron beam in a storage ring with undiluted polarized atomic gas targets is unique in this field, and has important experimental advantages. Furthermore, the spectrometer detecting the scattered electrons also has substantial acceptance and the capability to identify all types of hadrons produced in coincidence.

Inclusive spin structure functions

The original goal of the collaboration was to precisely determine the polarizations of the quarks of all flavours relative to the spin direction of the nucleon. This requires the combination of longitudinal spin asymmetries on both hydrogen and deuterium polarized targets. HERMES ran with a hydrogen target in 1996/7, and deuterium in 1998–2000. Based on the latter extensive data set, a preliminary extraction of the spin structure function g_1^d of the deuteron has now been released. Its unprecedented precision is illustrated in Fig. 13, where the structure function ratio g_1^d/F_1^d is shown as a function of Bjørken-x, which can be interpreted as the momentum fraction carried in the proton by the struck quark.

The comprehensive set of hyperfine transitions available in the atomic beam source providing the polarized deuterium for the target made it possible to also make the first measurement of the tensor spin structure function b_1^d. (Such a measurement is impractical with conventional solid polarized targets.) This structure function vanishes if the spin-one target is made up of spin-half nucleons at rest or in a relative s-wave. Our preliminary result from less than one month of running in tensor-polarized mode offers support for a model prediction based on a combination of a shadowing mechanism and the d-state component of the deuteron [Bora and Jaffe, Phys. Rev. **D57**, 6906 (1998)]. Figure 14 shows this result in the form of the structure function b_2, which is simply related to b_1 by the indicated relationship.

Quark spin densities from semi-inclusive DIS

A combination of inclusive polarized DIS data sets from both proton and deuteron targets is inherently limited to defining only the particular non-singlet combination of polarized quark distributions that is associated with the fundamental Bjørken sum rule. Further inferences from such data must be model-dependent. Quarks and antiquarks of the same flavour can not be distinguished since these cross sections scale as the square of the quark charge. To distinguish the contributions of the quark flavours and in particular of the sea quarks, it is necessary to use other types of

Fig. 13. Structure function ratio g_1^d/F_1^d for the deuterium target, which is closely related to the measured polarization asymmetry in inclusive DIS.
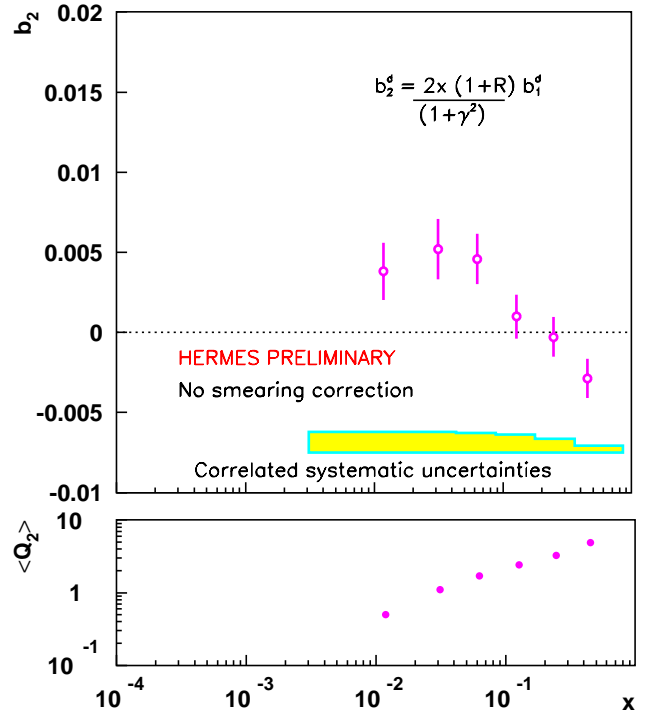
Fig. 14. The tensor spin structure function b_2^d on the deuteron target as measured for the first time by HERMES.

experimental information. In semi-inclusive scattering, a leading hadron is detected in coincidence with the deep-inelastic scattering of a lepton. This method exploits the correlation between the quark flavour and the type of leading hadron produced from the struck quark. Scattering asymmetries with various leading hadrons in the final state can be analyzed to determine the fractional contributions of the various quark flavours to the nucleon spin. Such an analysis uses data-constrained models for the fragmentation functions, which give the probability of a given flavour of quark to produce a given type of leading hadron.

The HERMES collaboration has released preliminary results for such a leading-order flavour decomposition from our complete data set recorded in the period 1996–2000. The data on the deuterium target recorded in 1998–2000 benefits from the dual-radiator Ring-Imaging Čerenkov detector (RICH) that identifies pions, kaons, and protons over the full momentum range. Hence kaon asymmetries are available for the first time, to provide sensitivity specific to the strange sea. The new preliminary results, now being prepared for publication, are shown in Fig. 15. They constitute the most precise information on quark helicity distributions, and for the first time provide separate determinations of the polarizations of the up, down and

Fig. 15. Polarized quark distributions extracted from HERMES semi-inclusive 1996–2000 data sets. The curves are NLO QCD parametrizations of previous world inclusive data assuming SU(3) flavour symmetry.

strange sea quarks. They reveal that the sea quark polarizations are all small – there is little evidence of the "cancellation" between the contributions of valence and sea quarks that had been hypothesized to explain the small net contribution inferred from inclusive data under the assumption of SU(3) flavour symmetry. In particular, there is no indication that Δs is negative as indicated by that model-dependent analysis. Two theoretical groups are ready to perform next-to-leading-order analyses of these HERMES asymmetries.

The Canadian group played a major role in this analysis. For example, treatment of kinematic smearing by radiative and instrumental effects was done for the first time in this field by full unfolding, resulting in well-defined and quantitative (and small) correlations between data points.

Deeply virtual Compton scattering

The field of hadron structure has rapidly evolved in recent years. It is blessed with an extraordinarily dynamic community of QCD phenomenologists, who have essentially re-invented our view of hadron structure. All types of experimental observables are now integrated into the unified framework of generalized parton distributions (GPDs). Hard exclusive reactions have been identified as the key to further progress. Two features of this development promise to be revolutionary. If the GPDs can be sufficiently constrained by measurements of various observables for several hard exclusive reactions, it should be possible for the first time to determine the net contribution of parton orbital angular momenta to the nucleon spin. Deeply virtual Compton scattering (DVCS) is considered to be the most interpretable of these hard exclusive processes, as NLO QCD corrections and those for higher twist are already under theoretical control. Furthermore, the DVCS process has the unique virtue that it interferes with the well understood process of radiative elastic scattering from the nucleon target, fortuitously giving rise to a rich variety of large asymmetries in either beam or target polarization or beam charge, appearing in the azimuthal distribution of detected photons. This interference provides access to the DVCS scattering amplitudes. In analogy to the formation of holograms using such interference with visible light, images of the proton in the plane transverse to the beam can effectively be formed. In particular, the correlations between transverse coordinate (impact parameter) and momentum fraction of the partons can be measured. This technique of "femto-photography" has now been placed on a firm theoretical basis [Burkardt, submitted to Int. J. Mod. Phys. A, hep-ph/0207047; Diehl, Eur. Phys. J. **C25**, 223 (2002)].

To fully exploit these new possibilities will require the next generation of accelerator now being designed
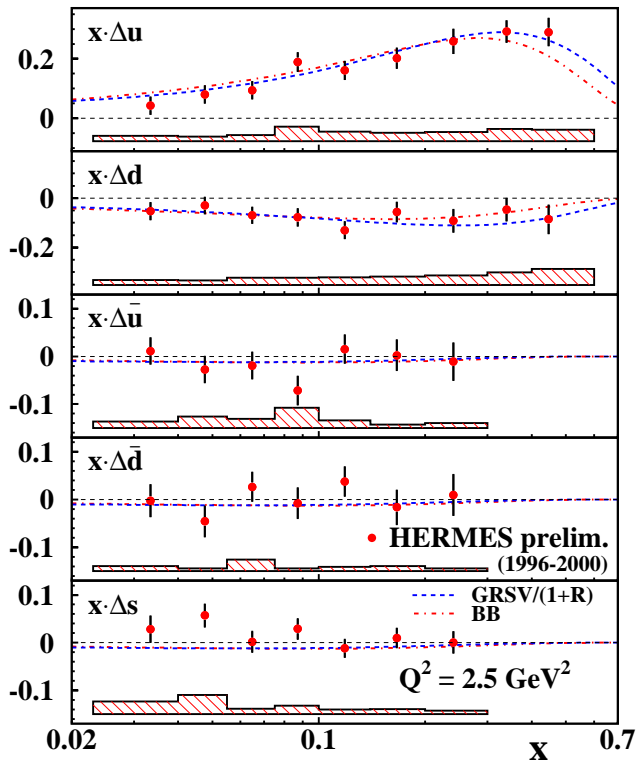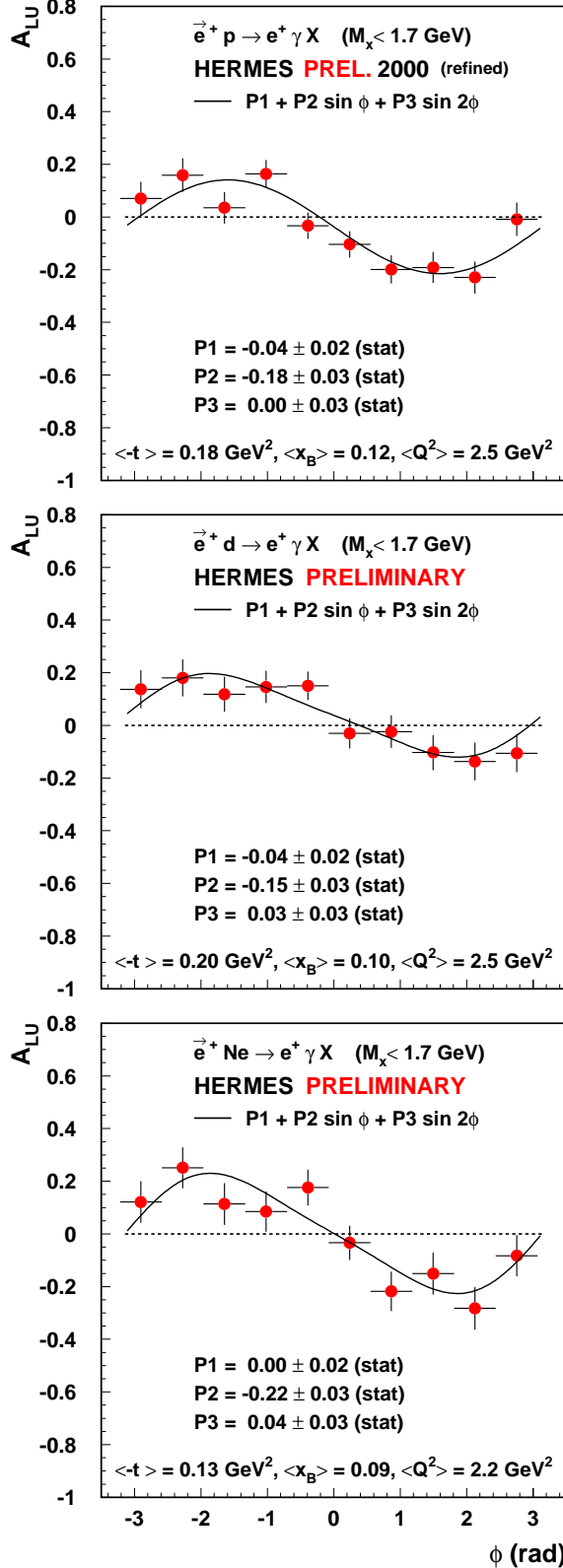
Fig. 16. Beam-spin asymmetries from DVCS/Bethe-Heitler interference on the three targets indicated, as a function of the angle of the detected photon azimuthally around the virtual-photon direction, relative to the lepton scattering plane.

for this purpose (e.g. e-RHIC at BNL, TESLA-N at DESY). However, HERMES now finds itself with the ability to make exploratory measurements that will guide this design. The first observation of a DVCS beam spin asymmetry was reported by HERMES in 2000. Now the collaboration has also recently released new and more precise DVCS beam-spin asymmetries for targets of hydrogen, deuterium and neon, based on the 2000 data set. Their azimuthal dependence for events selected in the kinematic region of the exclusive final state are shown in Fig. 16. Since the contribution of the coherent reaction on the deuteron is expected to be small, and the Bethe-Heitler cross section on the neutron is also small, the asymmetries for the proton and deuteron targets are expected to be similar, as is observed. On the other hand, the Z^2 amplification for the coherent reactions on neon makes this contribution important, as indicated by a more prominent peak in its t-distribution. An important reason for interest in the coherent reaction on nuclear targets is that the interpretation can be actually simplified in that the spin-flip amplitudes are suppressed by the preservation of the target ground state needed to allow the interference.

The above beam spin asymmetries constrain the imaginary part of certain DVCS amplitudes. The real part of these amplitudes is related to the asymmetry in the lepton beam charge. HERMES has recently released the first such measurement, shown in Fig. 17, revealing the expected cosine behaviour. The data are already able to discriminate among theoretical predictions corresponding to different choices for the
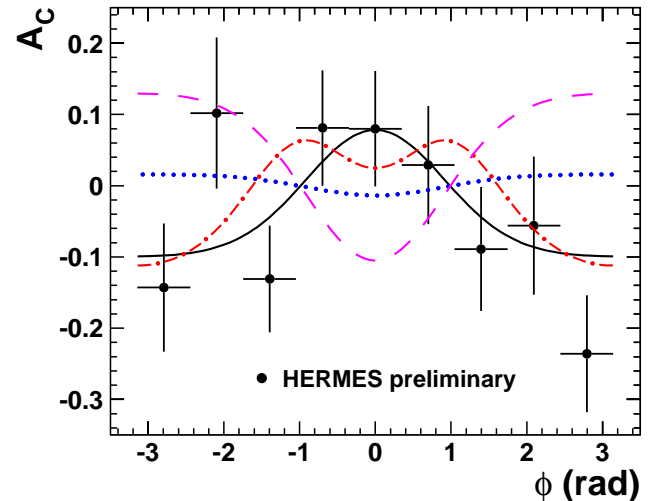
Fig. 17. Beam-charge asymmetries from DVCS/Bethe-Heitler interference on the hydrogen target. Three theoretical curves are shown; solid line: twist-2 + D term from a calculation in the chiral quark soliton model; dash-dotted: same calculation, but adding twist-3 effects; dotted: twist-2 without D term; dashed : same calculation as for solid line, but opposite sign for D term.

17

so-called "D term" in the generalized parton distribution, which is related to breaking of chiral symmetry. Refinements in the analysis that are presently under way will almost double the data available for this observable.

Asymmetries in the target spin are sensitive to other combinations of DVCS amplitudes. They have been extracted by a member of the TRIUMF group and have now been released. They indicate that the leading-twist $\sin\phi$ moment is small, but that the twist-3 moment $\sin 2\phi$ may be larger.

Single-spin azimuthal asymmetries

In 1999, HERMES and SMC released the first observations of semi-inclusive single-spin asymmetries that depend on the orientation of the hadron's momentum component $P_\perp$ azimuthally about the direction of the virtual photon. Relative to the lepton beam axis, the target polarization was transverse for SMC, and longitudinal for HERMES. In either case, the linear polarization of the virtual photon in the lepton plane selects transverse polarization of the struck quark. In leading twist and in this kinematic regime, $P_\perp$ can arise primarily from two sources: primordial p_T of the quark in the target, or k_T produced in the fragmentation process. A single-spin asymmetry requires the participation of some time-odd object correlating that p_T or k_T with some spin. Theoretical explanations of these asymmetries have focused on a T-odd fragmentation process sensitive to the transverse polarization of the fragmenting quark. The associated "Collins fragmentation function", designated $H_1^{\perp(1)}(z)$, is T-odd not in the fundamental sense, but only through the soft interactions in the final state. The wonderful implication of such an interpretation is that this "quark polarimeter" could provide access to the chiral-odd, and hence otherwise-inscrutable, transversity distribution. Transversity is the last remaining unmeasured one of the three leading-twist quark distributions that survive integration over intrinsic p_T. It is related to the probability of finding a transversely polarized quark in a nucleon polarized transversely with respect to its "infinite" momentum.

Unfortunately, almost all of the existing data revealing target-related single-spin asymmetries have been measured with a longitudinally polarized target. However, even these data can be interpreted in terms of the same Collins fragmentation function, operating together with transversity-related distribution functions – one twist-2 ($h_{1L}^\perp$, representing the probability of finding a transversely polarized quark in a longitudinally polarized nucleon) and one twist-3 (h_L). Hence such data from the HERMES collaboration, and now emerging from the CLAS collaboration at JLAB as well, offer important evidence that the Collins function has

a substantial magnitude. However, there are presently too many unknowns for an unambiguous interpretation. Some assumptions must be made – e.g. neglecting either the interaction-dependent part of h_L, or neglecting $h_{1L}^\perp$ altogether. It has then been found possible to explain most of the existing data.

HERMES has now also released results on the same observable for both pions and kaons from a deuterium target. Selected examples of these data are shown in Fig. 18, and compared to theoretical predictions where
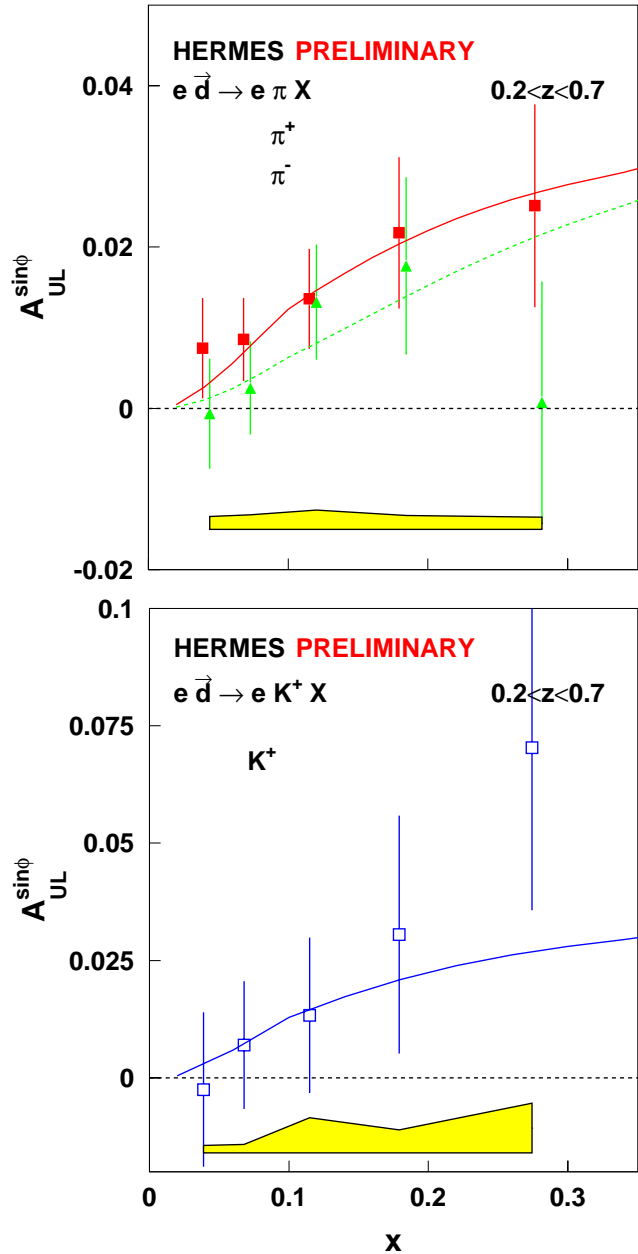
Fig. 18. Preliminary HERMES analyzing powers in the $\sin\phi$ moment of single-spin asymmetries with a longitudinally polarized deuterium target, as a function of Bjørken x. The curves are theoretical calculations [Efremov *et al.*, Eur. Phys. J. **C24**, 407 (2002)].

the transversity distributions are calculated in the chiral quark soliton model. In these calculations, the interaction-dependent part of h_L was neglected. The Collins function was parametrized to fit the HERMES proton data, now resulting in a magnitude which corresponds to the "optimistic" (large) extreme from a Delphi preliminary analysis of $e^+e^- \rightarrow 2$ jets: $\frac{\langle H_1^{\perp(1)} \rangle}{\langle D_1 \rangle} = (12.5 \pm 1.4)\%$. Previous estimates of the Collins function were only half this size, due to a theory-error in the sign of the contribution of that component of the target polarization that is orthogonal to the virtual photon direction. (This component appears even in the HERMES experiment with target polarization parallel to the lepton beam.) Another result of the corrected sign is that the sign of the SMC preliminary asymmetry with a transversely polarized target no longer appears to be theoretically consistent with that of the HERMES results with a longitudinally polarized target, although those SMC data are not statistically definitive.

Work by others is now under way to extract the Collins function from Belle e^+e^- data. This information can be used to interpret new data now being recorded by HERMES with a transversely polarized hydrogen target, in order to extract the quark transversity distribution.

Other results in spin physics

Space here does not permit an adequate summary of other new HERMES results related to spin physics. For example, using the polarized proton data, quark-hadron duality has been demonstrated for the first time in a spin asymmetry [Airapetian *et al.*, hep-ex/0209018]. Also an unprecedented and complete determination of the generalized Gerasimov-Drell-Hearn (GDH) integrals for the proton, deuteron and neutron was made over the range in exchanged photon virtuality $1.2 < Q^2 < 12.0\,\mathrm{GeV}^2$ and for photon-nucleon invariant mass squared W^2 ranging over $1 < W^2 < 45\,\mathrm{GeV}^2$, thus covering both the nucleon-resonance and DIS regions [Airapetian *et al.*, hep-ex/0210047]. No departure from leading-twist behaviour appeared over this entire kinematic range.

Quark fragmentation in the nuclear environment

The standard HERA operating procedure allows the routine use of thick unpolarized targets for higher luminosity (up to $3 \times 10^{33}\,\mathrm{cm}^{-2}\,\mathrm{s}^{-1}$) for one hour at the end of each beam fill. (This has been the main source of most of the data for the DVCS beam-related asymmetries.) In addition, various gaseous nuclear targets have been employed to study the hadronization process in the nuclear environment, through the measurement of nuclear attenuation of the multiplicity of identified hadrons. Such unique data from HERMES have been analyzed to extract the rate of energy loss

of partons in the nuclear medium. In one approach [Wang, Nucl. Phys. **A702**, 238 (2002)], the effect of gluon Bremsstrahlung induced by multiple scattering of a highly off-shell quark and the resulting parton energy loss is expressed in terms of in-medium modification to the quark fragmentation functions. This analysis is based on the original recognition that this soft gluon radiation is coherent in the sense of the LPM effect in QED [Baier *et al.*, Phys. Lett. **B345**, 277 (1995)], and that therefore the energy loss is remarkably proportional to the square of the distance in the medium [Baier *et al.*, Nucl. Phys. **B484**, 265 (1997)]. The A-dependence of the HERMES attenuation data supports this prediction, and not alternate models in which e.g. the attenuation is largely caused by ordinary nuclear absorption of either the QCD string stretched by the struck quark or subsequent absorption of the formed hadron. The Wang model employs the HERMES data to interpret observations of jet quenching in collisions of relativistic nuclei at, for example, RHIC.

Colour transparency

Among other new results from nuclear targets is the first clear evidence in lepton scattering of the effects of the phenomenon of colour transparency, in diffractive ρ^0 production on nuclei. Mesons produced by photons with large virtuality exist initially as "small-size configurations", and experience less attenuation in traversing the nuclear medium. The resulting paper has been accepted in Phys. Rev. Lett. [Airapetian *et al.*, hep-ex/0209072].

The ongoing HERMES program

DESY has promised beam for HERMES until at least the end of 2006. The plan that is approved by the DESY Physics Review Committee is to spend until the end of 2004 on a transversely-polarized hydrogen target to make the first measurement of quark transversity. (This intent was mentioned in the original proposal; since then a single-spin asymmetry that HERMES discovered revealed a suitable experimental signal.) This may also result in the first observation of a particular time-odd distribution function, which until very recently was thought to be excluded by basic time reversal invariance. It is expected there will be enough statistics for a preliminary result by the start of the 4-month HERA shutdown in March, 2003.

Meanwhile, HERMES is designing and constructing a new recoil detector to surround the target cell and detect the recoiling intact target nucleon from hard exclusive processes, in order to guarantee their exclusivity. This fully funded €1.4 M project is scheduled to be ready for two years of running on high density unpolarized targets in 2005/6. This will yield the first really high quality data on asymmetries in both beam

spin and charge for DVCS, the process that holds the most promise to shed light on the orbital angular momentum of partons.

HERMES collaborators in 2002: G. Gavrilov, J. Lu, C.A. Miller, S. Yen (TRIUMF); M.V. Vetterli (SFU/TRIUMF); M.G. Vincter (Alberta); K. Garrow (Alberta/SFU); J. Wendland (SFU).

KEK Expt. 246 and 470 (Japan-Russia-Canada-Korea-U.S.A. Collaboration)
Kaon decay studies
(M.D. Hasinoff, UBC; J.A. Macdonald, B. Shin, TRIUMF)

The KEK apparatus [Abe *et al.*, submitted to Nucl. Instrum. Methods A] at the 12 GeV Proton Synchrotron (PS) for the search for T-violation in the transverse polarization (P_T) of muons in $K_{\mu 3}^+$ decay has been demonstrated to be well suited to precision studies of other kaon decay modes, e.g., $K_{\pi 3}^+$ [Shin *et al.*, Eur. Phys. J. **C12**, 627 (2000)], K_{e3}^+ [Shimizu *et al.*, Phys. Lett. **B495**, 33 (2000)] and $K_{\mu 3}^+$ [Horie *et al.*, Phys. Lett. **B513**, 311 (2001)]. The detector consists of an active scintillating-fibre target which serves as a kaon stopper and vertex detector, a CsI(Tl) calorimeter system which detects photons including π^0 decay, and a superconducting toroidal magnet spectrometer system to analyze and select μ^+s e^+s, and π^+s. A muon polarimeter system is located at the quasi-focal planes of the toroidal magnet gaps. The complete kinematics from stopped K-decay can be reconstructed from the charged track obtained in the target, ring scintillators and spectrometer tracking chambers, and from photons and π^0s in the photon detector array.

Data-taking for the T-violation search was completed in 2000. In 1999, after the analysis of data taken in 1996 and 1997, we reported a value for P_T in $K_{\mu 3}$ of -0.0042 ± 0.0049(stat) ± 0.0009(syst) and Im(ξ) = -0.013 ± 0.016(stat) ± 0.003(syst) [Abe *et al.*, Phys. Rev. Lett. **83**, 4253 (1999)]. The analysis effort since then has been directed at the total data set taken 1996–2000. The strategy has been to undertake two independent analyses in order to check for errors and biases. In 2002, the first of the two analyses was completed and a new result was reported at the PANIC 2002 conference in Osaka [Abe *et al.*, hep-ex/0211049 (2002)]. This new result, $P_T = -0.00112 \pm 0.00217$(stat) ± 0.0009(syst) and Im(ξ) = -0.0028 ± 0.0069(stat) ± 0.003(syst), remains consistent with the standard model expectation of no T-violation, and should be considered preliminary until the second analysis is completed. The latter is in the final stages and is expected to be complete in early 2003. Additional analytical techniques are being used in order to better deal with systematic effects related to the stopping distribution of the kaons in the

target and the muons in the polarimeter.

In October, 2001, the last beam time with the apparatus was used to study the radiative $K_{\pi 2}$ decay, $K^+ \to \pi^+ \pi^0 \gamma$. This decay channel is unique, in which the direct photon emission from the vertex is easy to observe because the internal bremsstrahlung contribution is suppressed by the $\Delta I = 1/2$ rule. This direct emission is dominated by the chiral anomaly of magnetic transitions and the decay amplitude can be analyzed in terms of chiral perturbation theory (ChPT).

For this run, additional photon veto counters were added to detect photons escaping through the muon holes in the CsI(Tl) calorimeter, and the trigger demanded the presence of 3 photons in the calorimeter.

In 2002 the analysis was completed. The π^+ was distinguished from μ^+s and e^+s by time of flight. Most of the non-radiative $K_{\pi 2}$ two-body decays were excluded by momentum analysis. The difficult task of pairing the correct two photons to the π^0 was done by detailed kinematic analysis of the three possibilities. To extract the direct emission branching ratio, the detector response was simulated in GEANT3 and tested against the $K_{\pi 2}$ two-body decays. This measurement extends the recent result from BNL E787 [Adler *et al.*, Phys. Rev. Lett. **85**, 4856 (2000)] by virtue of its high kinematic resolution, and its capability to reach the lower π^+ energy region, $T_\pi > 35$ MeV where the direct photon emission is more important. Our result [Aliev *et al.*, Phys. Lett. B, in press] confirms the BNL result when the partial branching ratio for the π^+ kinematic region is taken into account. No evidence was found for an interference component between the direct photon emission and the dominant inner bremsstrahlung, which indicates the pure magnetic nature of direct emission in $K_{\pi 2\gamma}$ decay.

In early 2002, the apparatus was removed from the K5 channel at the KEK PS to make way for other experiments. Letters of Intent for a new T-violation experiment and for kaon decay spectroscopy of interest to members of the collaboration have been prepared for future extensions of this work at the J-PARC facility now under construction.

Sudbury Neutrino Observatory
(R. Helmer, TRIUMF)

Data-taking with salt in the heavy water continued throughout the year. As reported in last year's Annual Report, there is little need for TRIUMF infrastructure support at the present time. A small part for one of the calibration sources was designed in the Design Office and fabricated in the Machine Shop.

In the meantime, SNO reported an extremely important result; namely, solid evidence showing that electron neutrinos produced in the sun transform to

another active flavour during their transit to earth. Specifically, the flux of electron neutrinos was found to be

$$\phi(\nu_e) = 1.76 \pm 0.05(\text{stat}) \pm 0.09(\text{syst}) \times 10^6 \text{ cm}^{-2}\text{s}^{-1}$$

while the flux of active, non-electron neutrinos was found to be

$$\phi(\nu_{\mu\tau}) = 3.41 \pm 0.45(\text{stat})^{+0.48}_{-0.45}(\text{syst}) \times 10^6 \text{ cm}^{-2}\text{s}^{-1},$$

5.3 σ greater than zero. The total flux, measured with the neutral current reaction, was found to be

$$\phi(\text{NC}) = 5.09^{+0.44}_{-0.43}(\text{stat})^{+0.46}_{-0.43}(\text{syst}) \times 10^6 \text{ cm}^{-2}\text{s}^{-1},$$

consistent with solar models.

The day and night energy spectra measured with SNO were reported in a second publication. The night minus the day rate was found to be $14.0\% \pm 6.3\%(\text{stat})^{+1.5\%}_{-1.4\%}$ of the average rate, and the asymmetry in the flux of electron neutrinos was found to be $7.0\% \pm 4.9\%^{+1.3\%}_{-1.2\%}$, assuming the flavour transformation was to active neutrinos only. A global analysis using all other solar neutrino data, including SNO's day and night energy spectra, strongly favoured the large mixing angle solution of the solar neutrino problem.

TJNAF Experiment 00-006
Measurement of the flavour singlet form factors of the proton (G∅)
(W.T.H. van Oers, Manitoba)

The detailed structure of the nucleon at low energies is not well understood within the framework of quark and gluon degrees of freedom. For example, relatively little is known about the importance of the sea quarks at these energies. The G∅ experiment will measure two proton ground state matrix elements which are sensitive to point-like strange quarks and hence to the quark-antiquark sea in the proton. The matrix elements of interest are the elastic scattering vector weak neutral current charge and magnetic form factors, G_E^Z and G_M^Z, respectively. These can be extracted from a set of parity-violating electron-proton scattering measurements. If one assumes a relationship between the proton and neutron structure in that the proton and neutron differ only by the interchange of up and down quarks, i.e., isospin symmetry, the strange quark (as well as the up and down quark) contribution to the charge and magnetic form factors of the nucleon can be determined. This would result from taking appropriate linear combinations of the weak neutral form factors and their electromagnetic counterparts.

Determinations of both the charge and magnetic strange quark form factors are of fundamental interest, as these would constitute the first direct evidence of the quark sea in low energy observables. It is the objective of the G∅ experiment to determine these contributions to the proton form factors at the few percent level. Observations at high energy suggest that the strange quarks carry about half as much momentum as the up and down quarks in the sea. It is important to determine both the role of the quark sea and the relevance of strange quarks at low energy where there are voids in understanding the theory of the strong interaction (quantum chromodynamics, QCD). Even if the strange quark contributions are found to be below the sensitivity level of the experiment, upper limit determinations are as valuable as non-zero results. The matrix elements, G_E^Z and G_M^Z, are also relevant to discussions of the Ellis-Jaffe sum rule and the pion-nucleon sigma term; there is uncertainty in both of these about the strange quark contributions. The G∅ experiment will allow the determination of the strange contributions to the proton charge and magnetic form factors in a more straightforward manner.

In the G∅ experiment, which is being carried out at the Thomas Jefferson National Accelerator Facility (TJNAF), parity-violating longitudinal analyzing powers will be measured in electron-proton scattering in the range $0.1 \leq Q^2 \leq 1.0$ GeV^2 at both forward and backward angles. The longitudinal analyzing power is defined as

$$A_z = (1/P)\frac{[\sigma^+(\theta) - \sigma^-(\theta)]}{[\sigma^+(\theta) + \sigma^-(\theta)]}$$

where P is the polarization of the incident electron beam and the + and – signs indicate the helicity state. Making pairs of measurements at forward and backward angles will allow the separation of G_E^Z and G_M^Z. Predicted longitudinal analyzing powers range from about $(-3 \text{ to } 35) \times 10^{-6}$; it is planned to measure the longitudinal analyzing powers with statistical uncertainties of $\Delta A/A = 5\%$ and systematic uncertainties related to helicity correlated effects of $\Delta A/A \leq 2.5 \times 10^{-7}$. In the first phase of the experiment, longitudinal analyzing powers will be measured concurrently at several values of the momentum transfer in the range $0.1 \leq Q^2 \leq 1.0$ GeV^2. It now also appears that higher beam polarizations ($\sim 70\%$) will be available at the reduced beam pulse frequency of 31 MHz, decreasing the original estimate of 700 hours for the first phase of the experiment. However, it must be realized that the length of the experiment is in part governed by making rather elaborate control measurements to determine the corrections that have to be made to the measured asymmetries and to assess systematic errors. In the second phase of the experiment, each subsequent backward angle analyzing power measurement would require from one half to

one month of running time. The results of the SAMPLE experiment at the MIT-Bates Laboratory have shown the importance of measuring the axial form factor corrections, since these appear to be quite different from the theoretical predictions. Therefore, companion measurements of quasi-elastic scattering from deuterium will also be made at the backward angles. With these measurements, the effective axial current of the nucleon will also be determined. This current includes effects from the effective axial coupling of the photon to the nucleon or anapole moment, which are relevant also in other processes, e.g., parity violating Moller scattering and atomic parity violation.

The $G\emptyset$ collaboration

The $G\emptyset$ experiment is being carried out in Hall C at TJNAF by a collaboration of scientists from Canada, France, Georgia, and the United States, with funding provided through NSERC (Canada), IN2P3 (France), and DOE/NSF (US).

This past year has seen the completion of many critical milestones for the experiment. The apparatus for the forward angle measurements is now installed in Hall C and a first set of commissioning runs with beam was carried out from August, 2002 to January, 2003. As well, considerable progress has been made in the design, prototyping, and fabrication of critical components for the second phase backward angle mode of the experiment. The Canadian contributions to these efforts have been significant.

Canadian contributions

The Canadian members of the $G\emptyset$ collaboration, based at the Universities of Manitoba, Northern British Columbia, and TRIUMF, have been asked to:

(1) Develop and produce specialized photomultiplier tube bases for the main detector arrays;
(2) Design, build, and commission an automated magnetic field measuring apparatus complete with its own data acquisition system;
(3) Prototype and fabricate the cryostat exit detector arrays for the backward angle measurements;
(4) Prototype and fabricate (together with the Grenoble group) the aerogel Čerenkov arrays for background rejection in the backward angle measurements;
(5) Design the support structure for the aerogel Čerenkov and cryostat exit detector arrays;
(6) Coordinate the implementation of TJNAF built beam monitors and control apparatus with TRIUMF-built parity electronics;
(7) Provide design and implementation support for the liquid hydrogen target slow controls system;
(8) Provide support for the coordinating and

scheduling of resources for $G\emptyset$ commissioning and engineering runs at TJNAF.

Much progress has been made in the design and construction of the various subsystems listed above, many of which are now in operation.

Photomultiplier tube bases

The heart of the $G\emptyset$ detection system is a spectrometer which consists of an eight-sector toroidal magnet, with an array of scintillation detectors located at the focal surface of each sector (see Fig. 19). Since data will not be acquired in event-by-event mode in this experiment, and since the scintillator arrays are the only detectors to measure the scattered particles in the forward angle mode, the performance of these focal-plane detectors (FPD) is of critical importance. The timing and pulse shape characteristics of this system must be fine-tuned at the hardware level as it will not be possible to reconstruct individual events. Furthermore, the rates associated with many of the FPD elements will be quite high (1 MHz) and the photon yield(s) will have a large dynamic range. As such, special demands will be made on the photomultiplier tubes (PMT) and especially on their associated divider/base circuit. The design, development, and building of the $G\emptyset$ bases (for the North American FPD arrays) was carried out at TRIUMF. Several iterations of prototype high-rates bases were constructed at TRIUMF and tested at TJNAF, and in mid-1998, a set of final prototype bases was constructed and delivered to TJNAF for tests with the first set of prototype FPDs. Fabrication of the production bases began shortly thereafter. With the help of summer students (funded partly through the TRIUMF Summer Students program and partly through the $G\emptyset$ NSERC grant), the fabrication of the electrical components for all of the production bases was completed in late 1998. The design of the mechanical housing for the PMT-base subsystem depended on
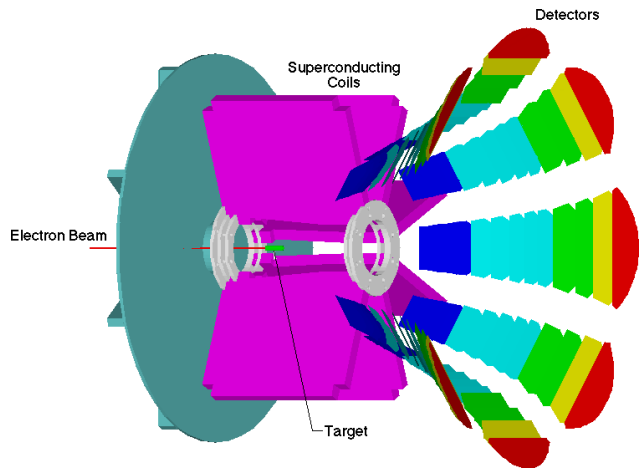
Fig. 19. Schematic layout of the $G\emptyset$ spectrometer.

the final design of the FPD support structure and, after much effort resolving subsystem integration issues, the final design for the PMT-base housing assembly was completed in late 1998. The fabrication and assembly of the mechanical housings and integration of the electrical components was completed over the summer of 1999 (again with the help of summer students at TRIUMF). Final testing of the completed bases was carried out in the fall of 1999, and shipment of all the bases (300 units) to TJNAF occurred at the end of calendar year 1999. Integration of this subsystem with the FPD arrays and the DAQ electronics, was completed at TJNAF in 2000 and 2001 during the final assembly of the FPD system. Presently, all of the FPDs are fully instrumented and have undergone tests of the detector "chain" (scintillator/PMT-base/electronics/DAQ/analysis) in Hall C using cosmics, beam background and, as of this summer, $G\emptyset$ test beam during the first sets of commissioning/beam-development runs.

Magnetic verification

An automated field measuring apparatus was constructed to provide a magnetic verification of the $G\emptyset$ superconducting toroidal magnet by determining the locations of a pre-specified set of magnetic reference points. These reference points correspond to the zero-crossing locations of specific field components at selected points of symmetry around the toroidal magnet, and they are a sensitive function of the coil positions. Determination of these zero-crossing points then allows the actual coil positions and, in principle, the magnetic fields to be completely determined. The measurements are carried out by scanning over a predefined set of zero-crossing lines, and determining where specific field components reverse signs. The system must be capable of providing a position determination of $\pm$ 0.2 mm and a field determination of $\pm$ 0.2 G, in order to reach the design goal of $\pm$ 0.2 $-$ 0.3 mm for the zero-crossing determination. Considerable effort went into the design, construction and commissioning of this magnetic field measuring apparatus or magnetic verification device at TRIUMF, the University of Manitoba and UNBC. The device consists of a programmable gantry with full 3D motion anywhere within a 4 m $\times$ 4 m $\times$ 2 m volume, and a set of high precision Hall probes, thermocouples, and clinometers (which measure tilt-angles) is mounted at the end of a probe boom on the gantry (see Fig. 20). Procurement of parts commenced in early 2000, and final assembly and testing began in late spring, 2000. With the support of TRIUMF Engineering and the TRIUMF summer/co-op student program, the magnetic verification device was completed in mid-summer, 2000 and transported to the University of Illinois (UIUC) where the magnetic measurements would
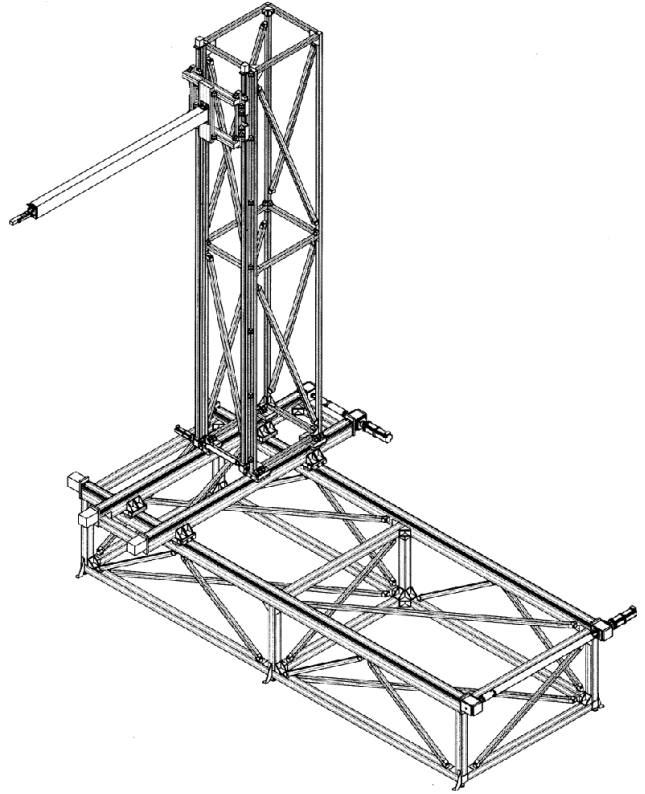
Fig. 20. Layout of the magnetic verification apparatus.

be carried out. In late 2000 and early 2001, much effort went into commissioning this device at UIUC and upgrading and modifying the motion control and data-acquisition software. In the spring of 2001, a series of test measurements were carried out with the magnet energized at room temperature and very low currents. The magnetic verification device yielded remarkably consistent results. Shown in Fig. 21 is the magnetic verification device and the $G\emptyset$ superconducting spectrometer.

In late 2001, after significant effort by the UIUC group to cool the $G\emptyset$ magnet to superconducting temperatures, the transition to superconducting mode was achieved and a set of magnetic field measurements was carried out. Due to limited cooling capacity and other magnet-related difficulties, the magnetic verification measurements were carried out with the coils energized at 1000 A (20% of the full-field value) and only a subset of the scans could be performed. Three sets of background magnetic field measurements were made, interleaved with two sets of foreground magnetic field measurements at 1000 A. In all, 30 zero-crossing points were scanned for each magnet sector, for a total of 240 zero-crossing values per data set. Preliminary processing of these data involved applying corrections for: Hall probe offsets and the background magnetic field; clinometer readings; and Hall probe
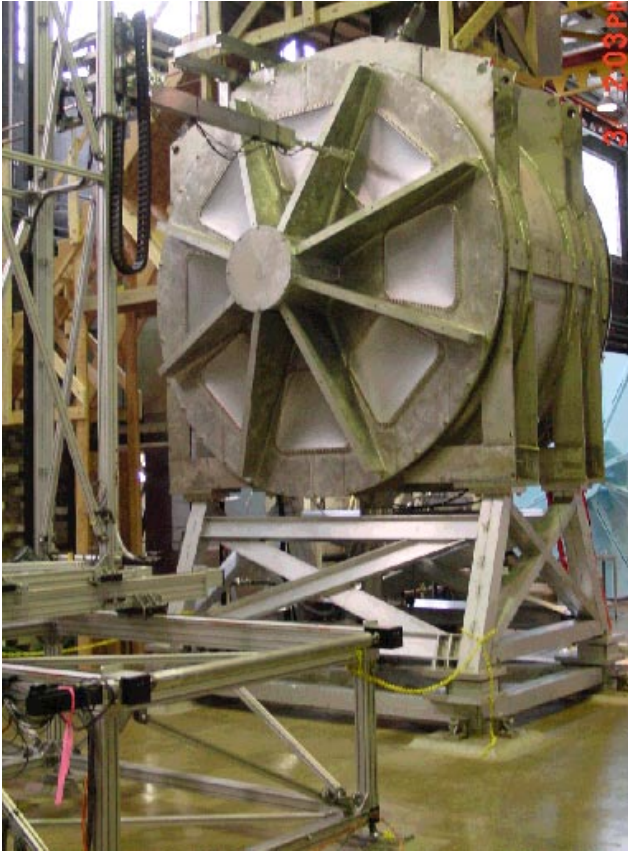
Fig. 21. The magnetic verification apparatus and $G\emptyset$ superconducting magnet at UIUC.

Fig. 22. Coil displacements for the $G\emptyset$ toroid extracted from the zero-crossing data.

misalignments. Various combinations of these corrections were applied and a total of 18 different raw data sets were generated. The zero-crossing points of the various field components were subsequently determined for each of these 18 different data sets. Measured uncertainties associated with these zero-crossing points varied widely, depending on the particular location of the scan. Typical errors were ± 0.15 mm, but in regions where the field gradients were small (down an additional factor of 5 due to the lower magnet currents) the errors were significantly larger.

The analysis procedure used to extract the coil positions from the zero-crossing points was tested against computer simulations, where known coil displacements were used to generate simulated data. Not only were the displaced coil positions correctly extracted, but the relative orientations and positions of the Hall probes themselves could also be extracted. This was due in part to the symmetry of the set-up and the large number of zero-crossing points involved. Analysis of the actual experimental data quickly revealed that the gantry frame was offset with respect to the toroid frame by about $\delta X = 0.62$ cm and $\delta Y = -0.33$ cm. Allowing the analysis procedure to correct for this resulted in the residual coil displacements shown in Fig. 22. Most

of the angular displacements were about $0.1°$, and the linear displacements less than 0.2 cm. This was well within the specifications for the tolerances on the coil positions laid out in the original design. The behaviour of dZ required further study. The shape of the curve suggested that the $X - Y$ plane mapped out by the gantry (with constant Z) was not parallel to the toroid $X - Y$ plane. A value of $0.11°$ was extracted for this angle between the planes. In addition, the fact that all (except for coil 4) dZ values were positive, suggested that there was also an offset in the Z-coordinate between the gantry and toroid frame. Indeed, further analysis revealed that the experimental data recorded with a Z-coordinate of 187 cm were actually recorded at 185.95 cm. When the magnet endcaps were later removed during repairs at the University of Illinois it was observed that the coils were closer to the downstream endcap by about $1/2$ in., in good agreement with the 1.05 cm found above.
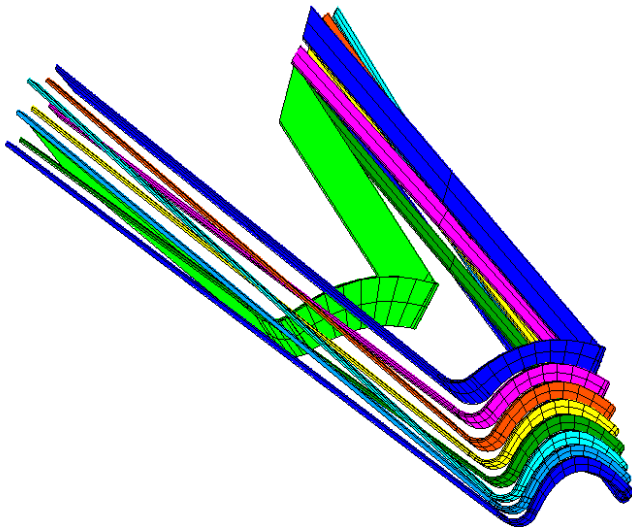
Fig. 23. Layout of a cryostat exit detector (CED) array for a single octant.

Cryostat exit detectors

For the backward angle measurements during the second phase of the $G\emptyset$ experiment, the addition of a second array of scintillation detectors, located near the spectrometer-cryostat exit windows, will be required in order to separate the elastic and inelastically scattered electrons. The geometry of these cryostat exit detector (CED) arrays (see Fig. 23) has been studied in detail and a reference design was completed in 1999. With the resident expertise at TRIUMF in producing high quality scintillation detectors and lightguides, the Canadian subgroup was asked to play the main role in the prototyping and production of the CEDs. A set of prototypes was built at TRIUMF and delivered to Louisiana Tech. University for further studies in 1999. Results from these studies indicated that the reference design and the prototype detectors met the specification requirements for the CED arrays. Production of a full set of dummy CED prototypes was then completed at TRIUMF in 2000, to aid in the design of the CED support structure. After finalizing the CED design, construction of the production versions of the CED arrays began in late 2000. Fabrication of the CED scintillators for all 8 octants was completed and delivered to TJNAF in late 2001, and fabrication of the special helical-bent lightguides began in 2002. In order to achieve the unique helical bend required in the $G\emptyset$ back angle geometry, customized bending jigs were designed and constructed at TRIUMF and tested on a first set of CED lightguides. Production of the lightguides is presently nearing completion and delivery to TJNAF is scheduled for summer, 2003. The CEDs will also make use of the same types of photomultiplier tubes and specialized TRIUMF/$G\emptyset$ bases as the FPDs.

Aerogel Čerenkov detectors

Monte Carlo simulation results have shown that backgrounds from negative pions will be problematic for the second phase backward angle measurements involving the deuterium target. The $G\emptyset$ simulation subgroup has focused on characterizing this π^- background and providing options regarding the design of an additional set of detectors to reject the background pions. The $G\emptyset$ Canadian and French (Grenoble) subgroups have been asked to jointly undertake the prototyping and construction of this crucial set of detectors, which will be made up of an array of aerogel Čerenkov counters. Much effort has gone into the design of this detector array and a conceptual design (see Fig. 24) was evolved into a first prototype at TRIUMF.

Prototype tests using the TRIUMF pion beam (M11) were carried out in December, 2001, but were hampered by the fact that there was insufficient aerogel to fully load the detector, which led to inconclusive results. This situation was rectified in early 2002, and further tests using cosmic rays were carried out at TRIUMF over the spring and summer of 2002. Issues that have been studied include: the optimal choice and configuration of reflective material within the light diffusion box; the choice of photomultiplier tube (PMT) and base; the best procedure to establish a hit (summed signal vs. multiplicity); characterization of the diffusion box response by Monte Carlo
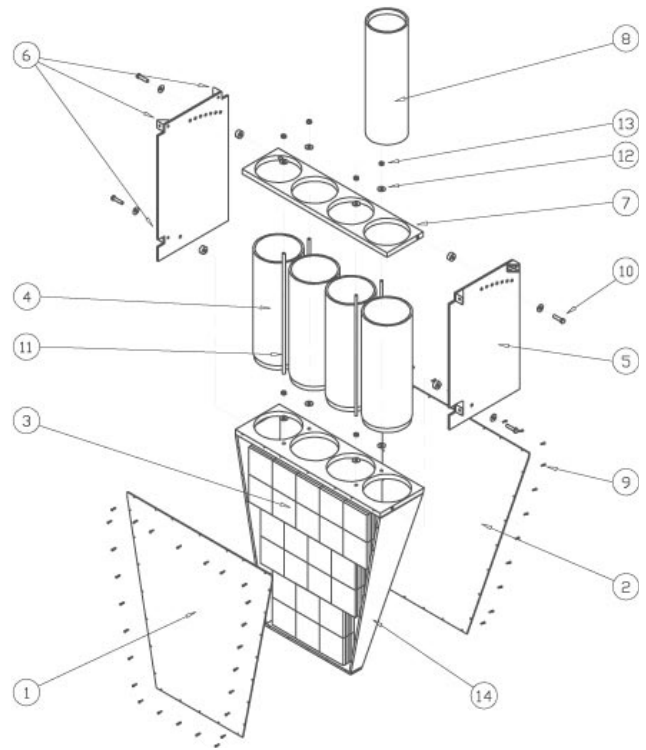
Fig. 24. Conceptual layout of aerogel Čerenkov detector.

simulations; magnetic shield requirements; radiation shielding requirements; and optimization of the solid angle of the detector.

In the recent tests with cosmic rays, different PMTs were tested in the detector box and the choice, thus far, is to retain the Photonis XP4572B. Millipore paper was chosen as the diffuse reflector in the box. Most of the inner surfaces of the box were lined initially with an underlayer of Tyvek and one layer of millipore. Later, a second layer of millipore was added. The collars around the PMTs were also lined with millipore. Measurements were made at different positions: (i) near the PMTs, (ii) at the centre of the box, and (iii) far from the PMTs, where, it should be noted, there were only four stacked aerogel tiles (as opposed to five in the rest of the box active area). Shown in Fig. 25 are ADC spectra for the summed pulse height of the four tubes for the three positions listed above.

Another issue, related to the inactive region of the photocathode around the PMT front face, was studied in detail. A reflective cone was designed to cover this region and to redirect the light toward the active portion of the PMT photocathode. Different reflective materials on this cone were tested, including an experimental reflective (dichroic) film from 3M (claimed to be a very efficient reflector at 320 to 430 nm). Although results with the dichroic reflector were initially encouraging, it was later demonstrated that good quality (thicker) aluminized mylar resulted in comparable or even slightly better detector efficiencies. The measured relative efficiency for cosmics passing near the centre of the detector is approximately 90% and 85%, for single- and two-photoelectron thresholds, respectively. Studies of light propagation in the diffusion box are also being carried out using the programs LITRANI, GEANT4, and a simple Monte Carlo.
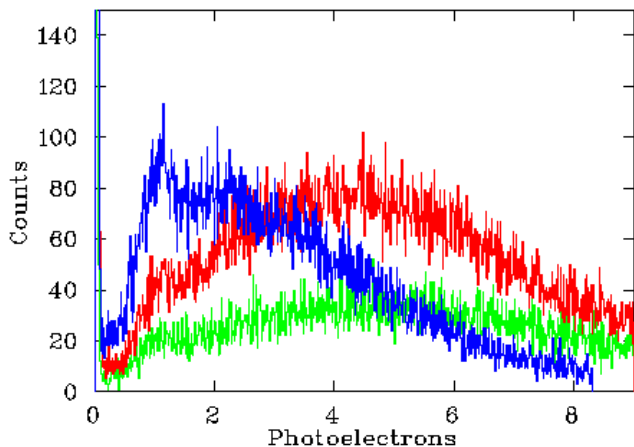
Further in-beam tests with the prototype Čerenkov detector were carried out in December, 2002 using the M9 beam line at TRIUMF and the data are currently being analyzed. A second iteration prototype is also presently being designed.

Backangle support structure

Considerable effort has gone into the engineering design of a support structure for the Čerenkov and CED arrays. Although the Canadian subgroup was initially responsible only for the design of the Čerenkov support structure, it was soon realized that the CED support structure would be closely coupled to the former due to the physical proximity of the two detector subsystems. As such, an integrated design for the two detector subsystems is presently being pursued. The support structure will centre around the use of pre-fabricated aluminum extrusions from Bosch because of their strength, versatility, and relatively low costs. A series of detailed finite-element analysis studies have been carried out at TRIUMF, using the program AN-SYS, to identify potential problems and to optimize the strength/cost of the support structure. The present design consists of a second Ferris wheel type support structure, which is to couple to the existing FPD support structure (also a Ferris wheel type design) and to the linear rails on the existing $G\emptyset$ detector platform. A conceptual illustration of the $G\emptyset$ backward angle configuration is shown in Fig. 26, with the superconducting magnet, the 3 detector arrays (FPD, CED, Čerenkov) in each of the 8 sectors, and their respective support structures.

Fig. 25. Pulse height spectra for the four-PMT summed signal for 3 trigger positions: (i) near the PMTs [green], (ii) near the detector centre [red], and (iii) far from the PMT [blue].
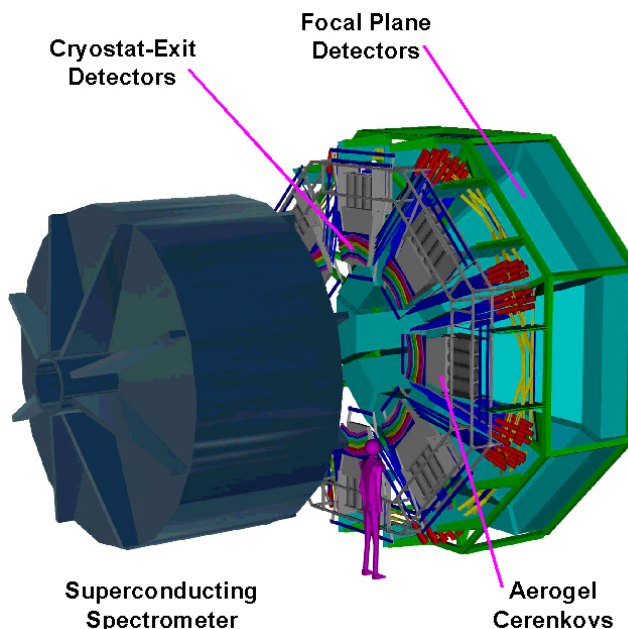
Fig. 26. Conceptual layout of the $G\emptyset$ backward angle configuration.

Beam line monitors

The success of the $G\emptyset$ experiment will be closely linked to the precise measurement and control of the electron beam properties. To make the subtle, refined asymmetry measurement of 1 ppm or better, the beam properties must be held within tight constraints. In pursuit of this, the beam position must be measured to better than 25 μm per 33 ms time window and the beam current to 40 ppm during the same 33 ms time window. To accomplish this, $G\emptyset$ uses two sets of XYQ microwave cavity monitors. These monitors require precision electronics designed and built by TJ-NAF and TRIUMF. Specifically, the position monitors produce a voltage signal based on position for the X and Y cavities, and a current proportional voltage signal for the current cavity. The voltage is amplified by dedicated amplifiers designed specifically for the dynamic range of the cavities expected during the course of the $G\emptyset$ experiment. The output from these amplifiers is fed into TRIUMF-built precision voltage to frequency converters and thence into the $G\emptyset$ DAQ scalars.

One set of these XYQ cavities is installed approximately 30 m upstream of the $G\emptyset$ target. The second set of XYQ cavities is installed on the $G\emptyset$ diagnostic girder immediately before the target. Also on this girder are a pair of standard stripline beam position monitors, a pair of super-harp wire scanners, and an optical transmission view. The combination of these monitors will allow a beam position measurement of better than 10 μm per helicity window and an angle measurement of better than 0.5 μrad.

In addition to measuring and tightly controlling the beam properties, there will also be a need to determine the false asymmetries contributed by the beam parameters of position, angle, and current on target. Knowledge of the false-asymmetries is required in order to extract the physics asymmetries and its associated uncertainties. The false asymmetries are given by

$$A_f = \sum \frac{\partial Y}{\partial X_i} \Delta X_i$$

where ∂Y is the change in the detector yield, ∂X_i is the change in the ith beam parameter, and ΔX_i is the helicity correlated asymmetry per quartet. To calculate these false asymmetries, the sensitivities $\frac{\partial Y}{\partial X_i}$ must be measured. To accomplish this, deliberate and controlled beam modulation is introduced. This is accomplished by sending a dc current to beam steering magnets far upstream from the $G\emptyset$ target. The steering magnet positions are chosen to minimize $x - y$ motion coupling at the target. By modulating a specific beam parameter, $\{X,\ Y,\ \Theta_x,\ \Theta_y,\ E\ \}$, and noting the detector yield response, $\partial Y / \partial X_i$ can then be extracted. These slopes will be measured at the beginning of each
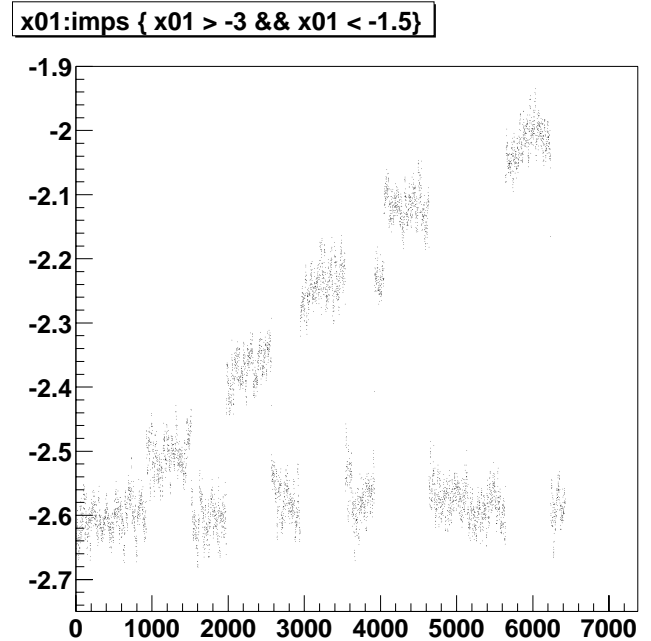
Fig. 27. Beam displacement resulting from modulation of upstream steering coils. The vertical axis gives a measure of the beam position (in mm) and the horizontal axis is in units of time (macro pulse signal).
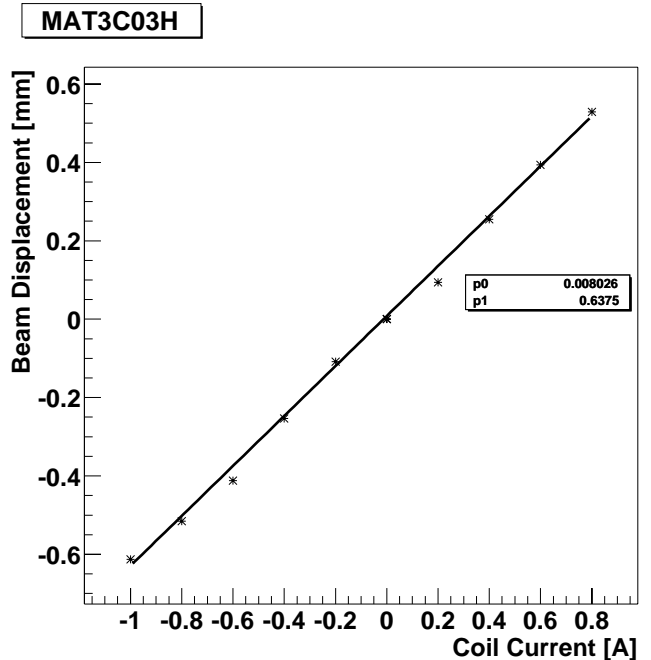
Fig. 28. Beam displacement as a function of steering coil excitation.

data run while the helicity asymmetry will be measured continuously throughout the run. This modulation system has recently been tested with beam and works as expected. Shown in Figs. 27 and 28 are plots of the beam displacements resulting from modulation of the upstream steering coil.

27

This modulation control system is being developed by members of the Canadian subgroup. Further developments of this system will include general beam/detector diagnostic software which will allow searches for the detector-magnet system asymmetry null coordinates, otherwise known as the sweet spot.

Target slow controls

The $G\emptyset$ experiment will use a 20 cm long liquid hydrogen (LH_2) target connected to a cryogenic loop to recirculate and cool the liquid. This target will operate at 20 K and 25 psia, and the heat deposited by the $40\,\mu A$ electron beam will be carried away from the hydrogen by a compressed He gas heat exhanger. The main components of the target system are a pump for circulating the target fluid in a closed cryogenic loop, a heat exchanger, the target cell and a manifold to direct the fluid flow down the centre of the target cell. A gas handling system is employed to provide gas to the target, the He coolant to the heat exchanger, and to evacuate the region surrounding the target. The state of the target (temperatures, pressures, position, etc.) and the gas handling system (valve settings) is monitored/controlled by what is called the slow controls system. This system sounds alarms when operating conditions become improper, monitors beam current and maintains a constant heat load on the target. The controls system also includes recording the target state at regular intervals to log files. The Canadian subgroup has been providing design and implementation support for the liquid hydrogen target slow controls system. Specifically, the responsibilities include: (a) participation in MEDM monitoring and control screens design; (b) installation and integration into the system of the Joule-Thompson valve controller to control the flow of the He coolant; (c) testing of target and He coolant temperature sensors; (d) participation in the pressure transducer calibration and target motion testing/calibration; and (e) configuration and management of the channel archiver software which logs and plots the target data. Members of the Canadian subgroup have taken part in the test cooldowns of the target and are also involved in the design of the $G\emptyset$ main screen software which displays the experiment and system status.

Under typical experiment running conditions, the heavy data load will need to be managed and stored in an efficient way. These data will be decomposed into one of two types: physics data and slow control data. The physics data involves yields and asymmetries, whereas the slow control data consists of temperatures, pressures, vacuums of various subsystems (target, magnet) and beam parameters such as polarization or helicity. The University of Manitoba/TRIUMF group along with New Mexico State University (NMSU) is success-fully carrying out the task of designing and implementing a MySQL database for the slow control part of the data. These data will be stored on a run by run basis and will be made available on the Web to the collaboration at large.

Engineering and commissioning runs

Several engineering runs have been carried out by the $G\emptyset$ collaboration, including studies of: (a) the helicity correlated properties of the TJNAF polarized electron beam and the noise characteristics of the Hall-C beam line monitors (July, 1997); and (b) the neutron background and energy spectrum in the vicinity of the $G\emptyset$ detector system (December, 1999). Both these efforts were coordinated by members of the Canadian subgroup and personnel from TJNAF (Hall-C) with much of the equipment provided by the Canadian subgroup.

This past year and a half, as the forward-angle mode of the $G\emptyset$ experiment entered the commissioning phase, the individually complex systems comprising the experiment had to be integrated into one overall system and tested. The commissioning was broken into three stages. The first stage, called the chain tests, was carried out from July through September, 2001. During this period, one fourth of the detector system was installed and cabled in the hall. In addition, about one half of the data acquisition system (DAQ), including the Trigger supervisor, was tested with beam in the hall. This test was used to identify shortcomings in the detector-DAQ-analysis chain. The second stage, carried out over the late summer and fall of 2002, involved the commissioning of the $G\emptyset$ cryogenic target, toroidal spectrometer and detector system with beam. The various subsystems were successfully commissioned, and the experiment is presently in the third stage, called the engineering run. The engineering run includes the fully operational spectrometer, the complete eight sector detection system, the full DAQ and electronics train, the cryogenic target system, $G\emptyset$ beam, beam modulation and beam diagnostics.

Canadian subgroup of the $G\emptyset$ collaboration: J. Birchall, J. Chang, B. Clemente, W.R. Falk, G. Faust, L. Lee, S.A. Page, W.D. Ramsay, A. Rauf, G. Rutledge, M. Steeds, W.T.H. van Oers (Manitoba); E. Korkmaz, T. Porcelli (Northern British Columbia); C.A. Davis (TRIUMF).

TJNAF Experiment 02-020

The Qweak experiment: a search for physics at the TeV scale via a measurement of the proton's weak charge

(S.A. Page, W.T.H. van Oers, Manitoba)

The standard model of electroweak interactions has been confirmed with impressive precision in a variety of experiments, ranging in energies from the eV scale in atomic parity violation to a few hundred GeV in collisions at HERA, LEP, SLC, and the Tevatron. Consequently, the particle physics community has turned from testing the standard model and measuring its parameters to searching for "new" physics beyond the standard model. In addition to searches for the Higgs boson, the searches for signatures of such new physics is one of the primary objectives of present and future high energy collider experiments.

However, an essential, but not well tested, prediction of the standard model is the variation of $\sin^2(\theta_W)$ with momentum transfer Q^2, referred to as the "running of $\sin^2(\theta_W)$" (see Fig. 29). Testing this prediction requires a set of precision measurements over a large range of Q^2 values, with sufficiently small and well understood theoretical uncertainties associated with the extraction of $\sin^2(\theta_W)$. It clearly requires a careful evaluation of the standard model radiative corrections to $\sin^2(\theta_W)$ in the context of the renormalization group
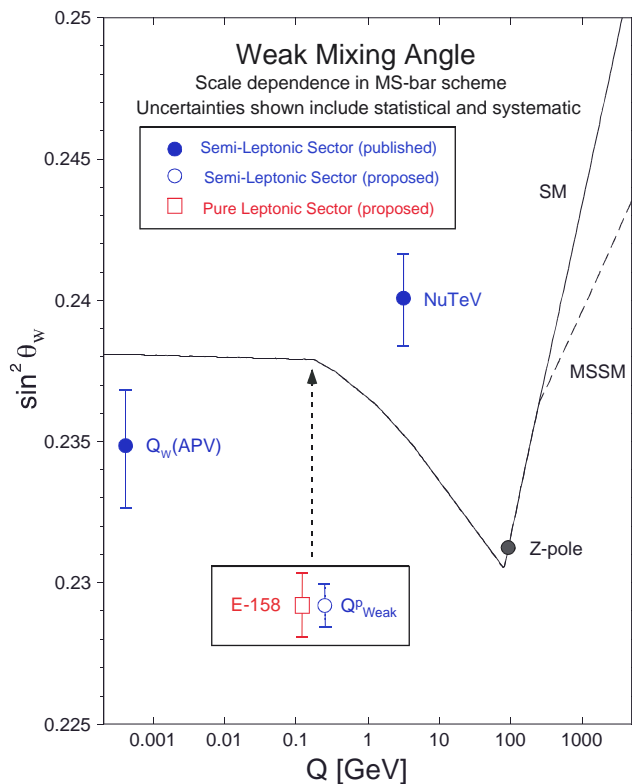
Fig. 29. Running of $\sin^2(\theta_W)$.

evolution of the gauge couplings. This has been crucial in establishing QCD as the correct theory of the strong interaction. But the gauge coupling of the weak interaction, at low energies represented by the weak mixing angle $\sin^2(\theta_W)$, has not yet been studied successfully in this respect.

The standard model has a well defined prediction for the Q^2 dependence of $\sin^2(\theta_W)$. The very precise measurements at the Z^0 pole (at LEP and SLC) set the overall scale of the "running" of $\sin^2(\theta_W)$. Currently there are only two other measurements of $\sin^2(\theta_W)$ which test the running at a significant level: one from an atomic parity violation (APV) experiment (a 2.6 σ deviation below the predicted value) [Bennett and Wieman, Phys. Rev. Lett. **82**, 2484 (1999); Wood *et al.*, Science **275**, 1759 (1997)] and one from high energy neutrino-nucleus scattering [Zeller *et al.* (NuTeV collaboration), Phys. Rev. Lett. **88**, 091802 (2002)]. The proposed measurement of the weak charge of the proton will be performed with significantly smaller statistical and systematic errors and has a much cleaner theoretical interpretation than existing low Q^2 data. It is complementary to, and will be carried out to higher precision than an approved experiment at SLAC (E158) [SLAC Proposal E158, spokespersons E.W. Hughes, K. Kumar, and P.A. Souder], which will attempt to determine $\sin^2(\theta_W)$ from parity violating electron-electron (Moeller) scattering. The importance of a new measurement of the weak charge of the proton is underlined by the current situation in atomic parity violation. To date, the most precise measurement of low energy neutral current interactions has been carried out by exploiting parity violating effects in cesium, which allow a determination of the weak charge of the cesium nucleus. Unfortunately, there continue to be considerable theoretical atomic structure uncertainties. Very recently, the NuTeV collaboration determined $\sin^2(\theta_W)$ at a Q^2 value of about 10 (GeV/c)^2 in deep inelastic scattering of neutrinos in an iron/scintillator target. The result is about 3 σ above the predicted value. The uncertainty is claimed to be dominated by statistics. However, it is conceivable that isospin symmetry violating parton distribution functions are responsible for part of the effect. Both the measurement of the weak charge of the proton and the polarized Moeller scattering experiment E158 at SLAC should be able to measure the weak mixing angle at low energies to unprecedented precision. These experiments will have different systematic errors and complementary dependences on physics beyond the standard model [Kurylov *et al.*, hep-ph/0205183]. A 4% measurement of the weak charge of the proton corresponds to an uncertainty of ±0.0007 in $\sin^2(\theta_W)$, and would establish the difference in radiative correc-

tions between $\sin^2(\theta_W)$ at low Q^2 and $\sin^2(\theta_W)$ at the Z^0 pole as a 10 standard deviation effect. For comparison, the E158 experiment anticipates a combined statistical and systematic error of about 9% on the measured asymmetry.

The Qweak experiment will measure the parity violating asymmetry in polarized electron-proton scattering at very low momentum transfer (Q^2 value of 0.03 (GeV/c)^2) and an energy of 1.12 GeV. These experimental conditions will suppress the hadronic form factor contributions to the measured asymmetry. The results of earlier electron-proton parity violating experiments will be used to constrain these hadronic corrections to the data. A 2200 hour measurement of the parity violating asymmetry in electron-proton scattering at the momentum transfer of 0.03 (GeV/c)^2 employing 180 μA of 80% polarized beam on a 0.35 m liquid hydrogen target will determine the proton's weak charge with a 4% combined statistical and systematic error. A longitudinally polarized electron beam, a liquid hydrogen target, a resistive toroidal magnetic spectrometer, detectors for the scattered electrons at forward angles complete with electronics, and a dedicated Compton polarimeter are the key elements of the experimental apparatus. The toroidal magnetic field will focus elastically scattered electrons onto a set of eight, rectangular quartz Čerenkov detectors coupled to photomultiplier tubes, which will be read out in current mode to achieve the high statistical precision required for the measurements. The acceptance averaged asymmetry in the designed experiment is –0.3 ppm. The asymmetry will be measured to $\pm 1.9\%$ statistical and $\pm 1.7\%$ systematic error, leading to the determination of $\sin^2(\theta_W)$ at the 0.2% level.

Major stakeholders in the experiment are JLab, who will provide the polarized beam, the beam line instrumentation and required shielding, and the liquid hydrogen target; LANL, who lead the design and construction of the detector package and associated electronics; Louisiana Tech, who lead the effort in computer simulations of the detector and detector response; MIT-Bates, who will play a significant role in the design and implementation of a dedicated Compton polarimeter for the experiment; and the Manitoba/UNBC/TRIUMF group who are leading the magnetic spectrometer construction project.

The resistive toroidal magnet with eightfold symmetry has been defined in a working group meeting held at TRIUMF on July 22 in which physicists and engineers from JLab, Louisiana Tech, Manitoba, MIT-Bates, and TRIUMF participated. The engineering concept has been worked out in a series of follow-up meetings with MIT-Bates engineers at Jefferson Laboratory and TRIUMF. This has led to requests for quotes for the copper conductor wire, the eight coils, their support structure, and the power supply. These quotes are currently being evaluated. Simulations of the particle-tracking through magnetic field configurations deviating from the specified ideal field, as well as systematic error analyses, are under way.

Canadian subgroup of the Qweak collaboration: J. Birchall, W.R. Falk, L. Lee, S.A. Page, W.D. Ramsay, G. Rutledge, W.T.H. van Oers, (Manitoba); E. Korkmaz, T. Porcelli, (Northern British Columbia); C.A. Davis, J. Doornbos, (TRIUMF).

NUCLEAR AND ATOMIC PHYSICS

Experiment 560
πp analyzing powers with the CHAOS spectrometer
(G.R. Smith, TRIUMF, G. Hofman, Colorado)

This experiment made use of the CHAOS spectrometer and a specially designed CHAOS polarized proton target (CPPT). The goal was to measure the analyzing powers (A_y) for $\pi^{\pm}p$ scattering to better than 0.05 between angles of 60° and 180° at several bombarding energies between 30 and 140 MeV. In 1995/1996 we made measurements at resonance energies only, due to persistent problems with the polarized target. In the fall of 1997, however, the target (and spectrometer) operated flawlessly, which permitted us to successfully explore the low energy region with incident π^- down to 51 MeV. Unfortunately, the beam time available to us in the fall of 1997 was insufficient to measure below 51 MeV, or to pursue the π^+ part of the low energy program.

Using the technique of partial wave analysis (PWA), the data obtained in this experiment are being used to improve the knowledge of the smaller scattering amplitudes. Analyzing power results in the forward angle (Coulomb nuclear interference) region for π^+p scattering, and in the $S-P$ interference region at backward angles near 50 MeV for π^- scattering are especially useful in this regard. With accurate πN partial waves, in particular at low energies, the physics goals of Expt. 560 are then to provide improved values for the πN coupling constant, to extrapolate to threshold where the πN scattering lengths can be obtained, and to extrapolate below threshold as well as to obtain a more accurate measure of the πN sigma term. The πN sigma term is an explicit measure of chiral symmetry breaking from which the strange sea quark content of the proton can be deduced. In addition there has been substantial interest in using πp observables to investigate isospin violations. These modern analyses use only data below about 100 MeV.

In 1997 the analysis of the resonance energy experiment was completed, and a Ph.D. thesis [Hofman, Physics, Univ. of British Columbia] was obtained based on those data. In 1998 the resonance energy results were published [Hofman *et al.*, Phys. Rev. **C58**, 3484 (1998)].

During the years 1998–2001 much effort was expended in designing and implementing an analysis procedure for the data which emphasized increased efficiency. The linear data streams were converted into a tree structure built around the CERN ROOT system. This led to an extremely fast, robust, and automated analysis that lets us adjust parameters such as
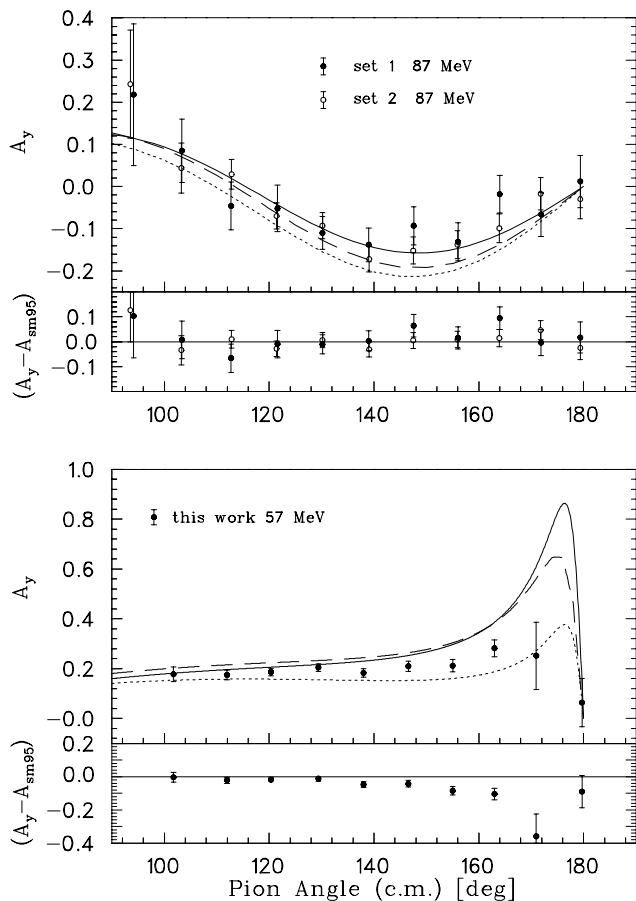
Fig. 30. The analyzing powers compared to phase shift solutions 87 and 57 MeV π^-. In each case the solid line is the SM95 phase-shift solution, the dotted line the SM02 solution and the dashed line the KH80 solution. The lower graphs show the new experimental analyzing powers subtracted from the SM95 solution.

kinematic cuts and angular binning, checking the new results in seconds rather than days.

The data analysis was performed by J. Patterson. Much effort went into reconstructing so called short tracks in CHAOS. Since the energy available to the recoil proton is very low, it does not penetrate all the detector planes. A special hardware trigger was developed to record events of this type and new off-line algorithms were required to reduce the large number of false tracks. Analysis was completed in late 2001 and a Ph.D. thesis (University of Colorado) submitted.

A typical result at the lowest energy of 57 MeV is shown in Fig. 30 and compared to 3 existing phase shift analyses. All the data have been submitted to the Virginia-GWU partial wave analysis group and were published [Patterson *et al.*, Phys. Rev. **C66**, 025207 (2002)].

Although the Expt. 560 program was (successfully) completed, the same spin polarized target was employed in Expt. 862 (see elsewhere in this Annual Report). As a by-product of that effort in summer, 2002, elastic πp analyzing power data were collected at 280 MeV. These have been analyzed and will be submitted for publication.

Experiment 704
Charge symmetry breaking in $np \to d\pi^0$ close to threshold
(A.K. Opper, Ohio; E. Korkmaz, UNBC)

Experiment 704 has final results from its precision measurement of charge symmetry breaking in the strong interaction. The observable of interest is the forward-backward asymmetry (A_{fb}) in $np \to d\pi^0$, which must be zero in the centre of mass if charge symmetry is conserved and has a predicted value that ranges between $(-35 \to +70) \times 10^{-4}$ [Niskanen, Few-Body Systems **26**, 241 (1999); van Kolck *et al.*, Phys. Lett. **B493**, 65 (2000)] depending on the strengths of the various contributions. The forward-backward asymmetry is defined as

$$A_{fb}(\theta) \equiv \frac{\sigma(\theta) - \sigma(\pi - \theta)}{\sigma(\theta) + \sigma(\pi - \theta)}$$

with the relevant contributions being the neutron-proton mass difference, exchange of an isospin mixed $\eta - \pi$ meson, and the effect of the d u quark mass difference on pion nucleon scattering.

The experiment was carried out with a 279.5 MeV neutron beam, a liquid hydrogen target, and the SASP spectrometer positioned at $0°$. With these kinematics and the large acceptance of SASP the full deuteron distribution was detected in one setting of the spectrometer thereby eliminating many systematic uncertainties. Deuterons from this reaction form a kinematic locus in momentum vs. lab scattering angle, shown in Fig. 31.
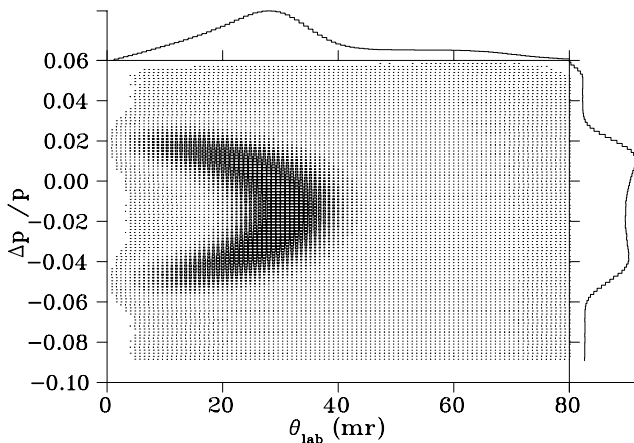
Fig. 31. Kinematic locus of all $np \to d\pi^0$ data.

Measurements of np elastic scattering with incident neutron beams that fill the same target space and produce protons that span the momentum distribution of the $np \to d\pi^0$ reaction provide a stringent test of the acceptance description of the spectrometer. With over seven million $np \to d\pi^0$ events and six million np elastic events the statistical uncertainty of this measurement is 8×10^{-4}. The systematic uncertainties add in quadrature to 5.5×10^{-4}.

Extraction of A_{fb}

The data have the accumulated effects of multiple scattering, energy loss, and other physical processes which make extracting A_{fb} directly from the locus impossible. As such, Monte Carlo techniques are used to extract the angle integrated A_{fb}. Close to threshold the $np \to d\pi^0$ cross section in the centre of mass frame is given by:

$$\frac{d\sigma}{d\Omega} = A_0 + A_1 P_1(\cos(\theta)) + A_2 P_2(\cos(\theta)),$$

where P_i are Legendre polynomials, and θ is the centre of mass scattering angle [Hutcheon *et al.*, Nucl. Phys. **A535**, 618 (1991)]. The presence of charge symmetry breaking is reflected in the A_1 term as it is odd in terms of $\cos \theta$. The angle integrated form of A_{fb} is given by

$$A_{fb} = \frac{1}{2} A_1 / A_0.$$

Due to the strong sensitivity of A_{fb} to the central momentum of the spectrometer (p_0), the LH$_2$ target thickness, and the average energy of the primary beam (T_{beam}) the simulation spanned a four dimensional space defined by these three experimental parameters and A_1/A_0. This procedure required generating simulations at the nominal values, plus a canonical step, and minus a canonical step for each parameter. With a four dimensional parameter space needing to be covered, 81 (i.e. 3^4) independent simulations had to be generated. The comparison of data to these simulations produced a four dimensional χ^2 space and the values of the four parameters that gave a global minimum of that χ^2 space determined the value of A_1/A_0 and consequently A_{fb}.

Simulation

The simulation is based on GEANT and begins with a proton beam incident on a ^{7}Li target to reproduce the energy loss effects in that target. The model of the equipment is in agreement with the best known blueprints, "as-built" drawings, and recent measurements. The SASP dipole field used in the simulation is a map of that magnet at 875 A, scaled up to the running current of 905 A. Data were acquired in 19 different periods spanning two years and the simulation

"scheduled in" measured detector efficiencies, scintillator thresholds, and missing wires in a manner consistent with the actual running periods. Deuteron reaction losses, which account for 1–2% of all deuteron events, have a significant momentum dependence over the 8% momentum range of the experiment. These losses were parameterized from the world's data on deuteron elastic and reaction cross sections from hydrogen and carbon, and included in the simulation.

To reduce the possibility of psychological bias in matching simulation to data, a blind analysis technique was used which incorporated a "black box" subroutine into the simulation. This routine added a (hidden) offset to the A_1/A_0 asymmetry parameter used to set up the $np \to d\pi^0$ generator. After selecting the value for the offset, a member of the collaboration not involved in simulation development compiled the subroutine on all simulation computer clusters, mailed the source code to two people outside the collaboration, and deleted the source code.

Model of SASP acceptance

The acceptance of SASP is a complicated function of the position and angle at which the deuteron is produced and its momentum (X_i, θ_i, Y_i, ϕ_i, and δ). Describing this acceptance properly required an accurate model of the magnetic fields and interior surfaces of SASP because (1) deuterons can collide with interior surfaces of SASP and be lost from the locus and (2) the reconstructed momentum variable, which is a function of the focal plane variables X_f and θ_f, may be distorted in a momentum dependent way by an inaccurate model.

The np elastic scattering data provide the best means to determine the acceptance in that the incident beam of this reaction fills the target parameter space in a way that is similar to that of the $np \to d\pi^0$ reaction. The $np \to d\pi^0$ momentum space was spanned with np elastic scattering data taken with the SASP fields set to those used for the $np \to d\pi^0$ reaction and changing the energy of the primary proton beam so that the elastically scattered protons had momenta equal to -4, 0, and $+4\%$ of the central momentum of the deuterons of interest. To investigate momentum dependent effects, projections of θ_i and ϕ_i were made for slices in X_i and Y_i, respectively, and ratios of these distributions made for the -4% and $+4\%$ momentum sets. The basic features of these ratios are understood in terms of the focusing action of the SASP entrance quads, Q1 and Q2. These features appear in both data and GEANT but GEANT does not accurately represent the shoulder region where the acceptance in θ_i and ϕ_i begin to change. Consequently, we have determined cuts which exclude those portions of the acceptance that cannot be adequately modelled. These cuts are on target position
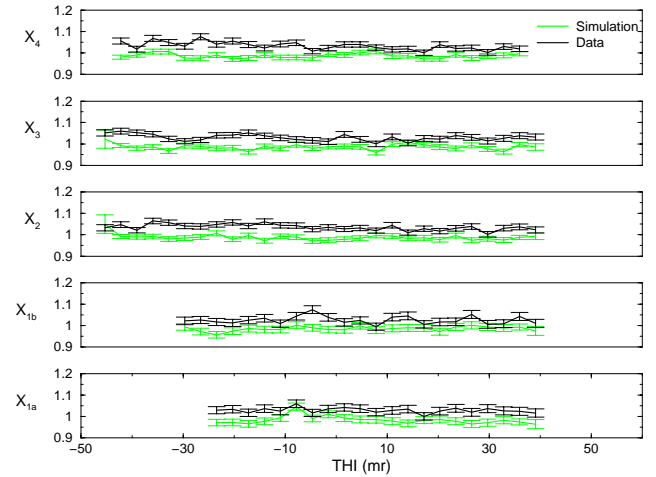
Fig. 32. Elastic np scattering ratio ($-4\%/+4\%$) vs. THI for five slices in X_i with final acceptance cuts applied.

and angle and define regions of uniform acceptance.

Prior to August, position and angle acceptance cuts were only applied in the horizontal direction to avoid non-uniformities due to the dipole gap of SASP. Subsequent inspection of the ($-4\%/+4\%$) ratio in the vertical direction showed clear discontinuities and analogous cuts were determined for the vertical direction. Applying these acceptance cuts yields distributions of the ($-4\%/+4\%$) ratio that are essentially flat in θ_i and ϕ_i for all X_i and Y_i slices used; the magnitudes of the slopes of these distributions are all less than $5 \times (10)^{-4}$.

Verification of acceptance model

In a robust test of the uniformity of the acceptance, A_1/A_0 was extracted for various subsets of the target space and compared to the result for the full acceptance. Carrying out such a comparison for each data cycle was hampered by limited statistics so a group of cycles were analyzed together. Six of the ten data cycles have calibration data that allowed the relative target thickness for each cycle to be determined; these relative thicknesses were "scheduled" into the appropriate cycles of the simulation. This allowed the six "good LH$_2$ cycles" to be added together and treated as a single high statistics set in both data and simulation.

Figure 33 shows the value of [(A_1/A_0)+ black box offset] independently determined for the full acceptance and each of four acceptance subspaces for the six good LH$_2$ cycles. Note that while data in the bottom and top (left and right) subspaces are independent, they make up the data in the full acceptance. The values of [(A_1/A_0)+ black box offset] were determined both by analyzing the summed cycles (red squares) and by calculating the error weighted average of the individually analyzed cycles (black circles). These two methods give good agreement and the small differences
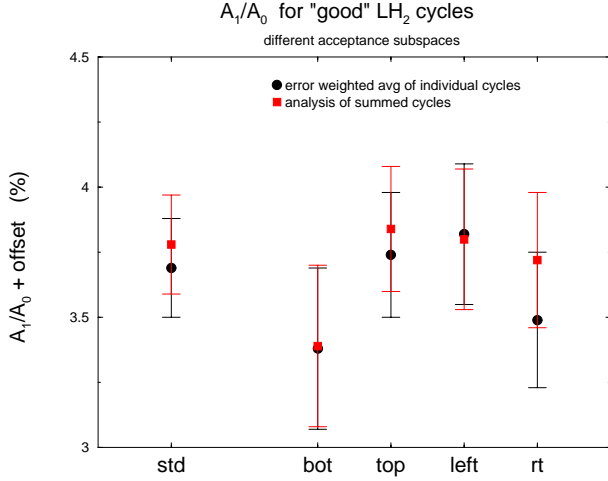
Fig. 33. A_1/A_0 for different acceptance subspaces.

in their results are thought to arise from effects that are not fully accounted for when data cycles are added together. The consistency of $[(A_1/A_0)+$ black box offset$]$ for all acceptance subspaces suggested that the acceptance was well described in the simulation and the value of the black box offset was revealed.

Result and error budget

Simulation vs. simulation comparisons were carried out to determine how strongly experimental parameters are correlated with A_1/A_0. For each parameter this involved simulating kinematic locus scatter plots for a 3×3 grid of the experimental parameter vs. A_1/A_0, calculating the χ^2 of those 9 plots when compared to a plot simulated with nominal values, and fitting the χ^2 space. The correlation of A_1/A_0 with the experimental parameter was then obtained from the error matrix based on the curvature of the χ^2 space. Combining this correlation with the independently determined uncertainty of the parameter gives the systematic uncertainty of A_1/A_0 due to that experimental parameter.

Table I. Error budget.

	Uncertainty A_{fb} (10^{-4})
FEV threshold	2.5
FEC separation	2.5
Li target position	2.5
A_2/A_0	2
Deuteron losses	1.5
Efficiencies	1.5
$\sigma(T)$	1
Neutron angle	1
Background	1
FET threshold	0.5
Total systematics	5.5
Fit & statistics	8
Total uncertainty	10
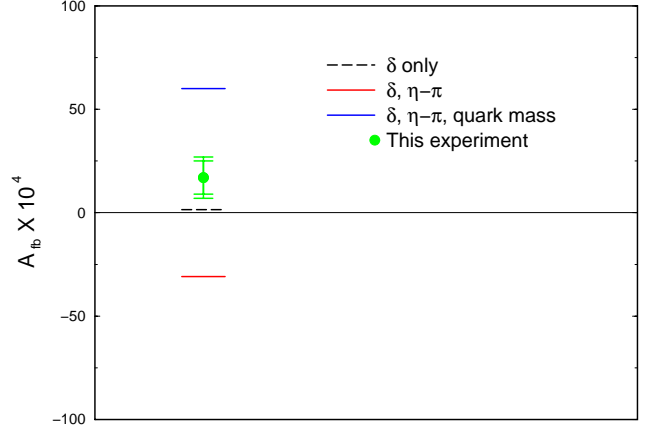
Fig. 34 A_{fb}, error weighted average of all ten cycles, standard acceptance. Incident $T_{\text{neutron}} = 279.5$ MeV.

The error weighted average of A_{fb} for all ten cycles with standard acceptance cuts applied is 17×10^{-4} and is shown in Fig. 34. This figure also shows the results of calculations done by van Kolck, Niskanen, and Miller which include contributions from the np mass difference effect on the OBEP (δ), the exchange of an isospin mixed $\eta - \pi$ meson, and the effect of the $d\,u$ quark mass difference on π^0 nucleon scattering. A_{fb} can be expressed as

$$A_{fb} = -0.28\% \times \left[\frac{\langle \pi^0 | \mathcal{H} | \eta \rangle}{-0.0059 \text{GeV}^2} - \frac{0.87}{\text{MeV}} (\delta m_N - \frac{\bar{\delta} m_N}{2}) \right]$$

where the first term arises from the exchange of an isospin mixed $\eta - \pi$ meson and the second from π^0 scattering from the nucleon. The neutron proton mass difference can be expressed in terms of δm_N and $\bar{\delta} m_N$

$$m_n - m_p = \delta m_N + \bar{\delta} m_N = 1.3 \text{ MeV}$$

where δm_N is the ud quark mass difference and $\bar{\delta} m_N$ is the contribution due to electromagnetic effects.

Experiment 715
Weak interaction symmetries in β^+ decay of optically trapped ^{37,38m}K
(J.A. Behr, M. Pearson, TRIUMF; K.P. Jackson, TRIUMF/SFU)

TRIUMF neutral atom trap (TRINAT)

TRIUMF's neutral atom trap (TRINAT) captures radioactive atoms in a 1 mm-sized cloud using the pressure of laser light, with goals of precision standard model weak interaction tests in both the charged and neutral current sectors. To date, the trap techniques have shown great promise to provide greater precision in two broad types of experiments in nuclear β decay. The low-energy recoiling nuclei produced in the decays freely escape the trap, and by measuring their

momenta in coincidence with the β, the ν momentum can be deduced more directly than in previous experiments. In addition, the nuclei can be highly polarized by atomic techniques, and their polarization measured atomically independent of their decays. We have pioneered the β-recoil coincidence techniques at TRIUMF/ISAC, and are learning to polarize the nuclei to realize unique spin-correlation experiments.

Progess in ^{36}K trapping is updated in the Expt. 925 report.

Technical progress

Production

The CaZrO$_3$ production target has recently been replaced with a TiC target which can withstand 40 μA of 500 MeV proton beam, producing ^{37}K yields of 6×10^7/sec, a 6-fold increase.

Laser development

Laser development has been ongoing on two fronts within the TRINAT collaboration.

Firstly, in order to enhance the current trapping efficiencies, a second, basic titanium sapphire ring laser has been purchased. This ring is currently being pumped by an existing argon ion laser returned from long term loan to Expt. 497. Currently this new ring is capable of producing in excess of 2 W of single frequency, narrow linewidth laser power. Work is currently ongoing in order to frequency stabilize and control this laser. It will increase collection efficiency in the capture MOT by a factor of three.

With a view to producing a purely optical dipole force trap (see below), an existing standing wave titanium sapphire laser has been converted into a single mode ring laser. This has reduced its linewidth from a factory specification of 40 GHz to an unstabilised linewidth of less than 40 MHz. This transformation has ensured a narrow, low divergence, gaussian output that is required in order to produce a tight, diffraction limited focus to create the trap. In order to successfully load this trap using circularly polarized light (required for 100% polarization) the laser frequency has to be shifted by approximately 2 nm on a rapid ($\sim$1 μs) time-scale. A scheme for a reliable, controllable, method of operation has been devised using an electro-optic modulator to make controllable changes in the birefringence within the laser cavity. Arrangements have been made to borrow equipment for initial tests in order to ascertain the feasibility as well as the final design requirements.

Beta-neutrino correlations

The weak interaction is mediated by vector bosons with spin one. By measuring the β-ν angular distribution in the decay of ^{38m}K, which is one of the pure Fermi $I^\pi = 0^+ \rightarrow 0^+$ decays, we can test whether bosons with spin zero produce a scalar interaction contributing to β decay. The best present β-ν experiment is the Seattle/Notre Dame/ISOLDE collaboration's β-delayed proton decay of ^{32}Ar, with published result $a = 0.9989 \pm 0.0052 \pm 0.0039$.

We have taken data with statistical error in the β^+-ν correlation coefficient a of $\sigma_a \approx 0.33\%$. We are presently evaluating systematic errors, which will limit us to total σ_a between 0.5% and 0.7%. This accuracy will let us constrain the mass/coupling ratio of non-standard model spin-0 bosons as great as 4 times the mass of the spin-1 W boson. We analyze data taken in October, 2000 in two ways: 1) fitting the experimental time-of-flight spectra of the recoils as a function of β energy; 2) reconstructing the β-ν angle from the position and energy information in both detectors. With help from our new collaborator F. Glück, we have included radiative corrections in our full Monte Carlo simulations. These are dominated by the momentum perturbations caused by real bremsstrahlung photons. The perturbation of the recoil TOF spectra turns out to be small in our experiment, but the perturbation on the β^+ singles spectrum from which our energy calibration comes is larger and still being evaluated. We have published the main method in a conference proceedings [Gorelov et al., Hyp. Int. **127**, 373 (2000)] and expect to publish a result soon.

By reconstructing the ν momentum, we have completed and published a missing mass search for heavy ν's with masses 0.7 to 3.7 MeV mixing with the electron ν, [Trinczek et al., Phys. Rev. Lett., in press]. Although recent results exclude a sterile ν_x as an explanation for the atmospheric and solar neutrino anomalies, the small admixture limits for heavy masses explored by TRINAT are still allowed. The length of the ν pulse from SN1987A also allows ν_e to have relatively large admixtures with a ν_x with mass a few MeV, so experiment must constrain these.

Our kinematic coincidences reduce the 3-body kinematics to 2-body, allowing a search for peaks in a TOF spectrum instead of the more conventional search for kinks in continuous β spectra. Figure 35 shows the reconstructed zero-mass peak and a simulation of an admixture with a massive ν for a particular data cut, and the results. The admixture upper limits are as small as 4×10^{-3}, and are the most stringent for ν's (as opposed to $\bar{\nu}$'s) in this mass range, although there are stronger indirect limits from other experiments. This constitutes the first real physics measurement in β decay from neutral atom traps.

Polarized measurements

The weak exchange bosons also couple only to left-handed (negative helicity) ν's, and in that sense parity – mirror symmetry – is said to be fully violated.
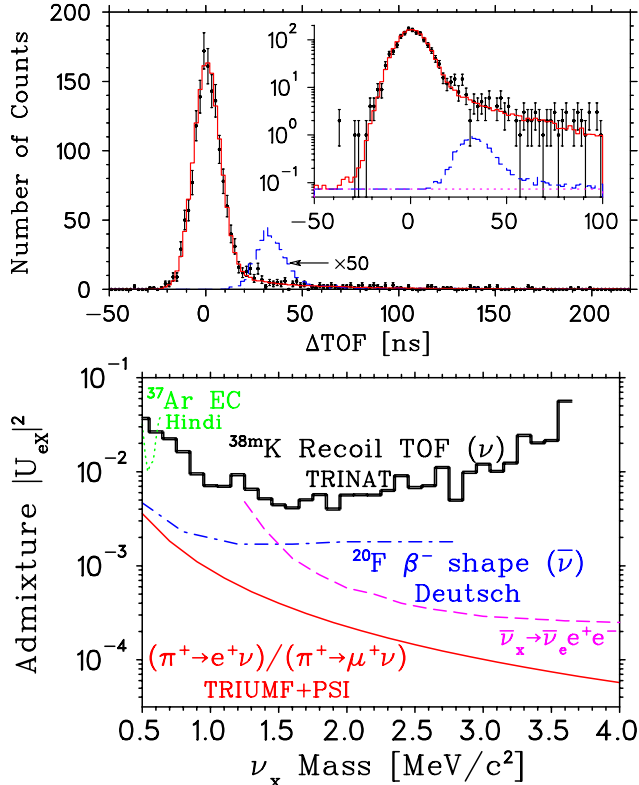
Fig. 35. Top: Kinematic reconstruction of events for $T_\beta = 1.7 - 1.9$ MeV bin, and simulation including a 1 MeV ν_x. Bottom: Present 90% CL upper limits, and those of other experiments.

By measuring β-ν angular distributions from the decay of polarized ^{37}K, we can search for production of right-handed ν's. Since β-decay is semileptonic, these experiments are complementary to the purely leptonic TWIST experiment. Measurements of the β asymmetry A_β and neutrino asymmetry B_ν in ^{37}K to accuracy 10^{-2} compete with the world average of neutron β decay, and experiments to $\leq 10^{-3}$ accuracy are necessary to be complementary to TWIST or collider searches for higher-mass extra W's. We also plan a search for nonstandard model time-reversal violation in ^{37}K, flipping the nuclear spin to simulate the reversal of time in a correlation involving the nuclear spin and the β and ν momenta.

We have begun spin-correlation measurements in the mixed Fermi/Gamow-Teller decay of ^{37}K. We have achieved polarization precision 0.001 in trapped stable ^{41}K atoms, which has almost identical hyperfine splitting to ^{37}K. We are in the process of calibrating the absolute accuracy and applying the techniques to β-decaying ^{37}K.

We have implemented optical pumping in a geometry with back-to-back β^+ detectors along the optical pumping axis (Fig. 36). We use high-reflectivity dielectric mirrors on 0.1 mm thick fused silica substrates, to minimize energy loss and angle straggling. The circular polarization distortion from the 11° mirror is cancelled by a mirror with the same coating outside the vacuum rotated by the same angle in the other plane. The β^+ detectors are plastic/CaF$_2$(Eu) phoswiches designed to contain the 10 MeV β^+'s from ^{36}K. The electrostatic field electrodes are made from glassy carbon to minimize eddy currents when the trap B field is switched on and off.

Figure 36 also shows data from our recent ^{37}K run using this geometry. MCP position asymmetries are shown for the nuclear recoils in coincidence with β^+'s at 90° to the polarization axis (not shown in the figure). Assuming the standard model, the X asymmetry implies that $(107 \pm 5)\%$ nuclear vector polarization was achieved. The atomic probe also indicated over 95% polarization. When the polarization is known better, the ν asymmetry B_ν can be determined from this observable – the β^+ is detected at $\approx 90°$, so that the recoil momentum is directly opposite the ν momentum. Preliminary results are in press in a refereed conference proceedings [Melconian et al., EMIS14, Nucl. Instrum. Methods B, in press]. We have extracted polarization information from nuclear recoil singles in the past tests and will attempt to do this here as well. B_ν could be determined with $\sigma_{\text{stat}} \approx 0.001$ in 1 month at demonstrated rates in this geometry.

We learned that β singles measurements in this geometry are difficult. See Expt. 925 report for details.

We will simultaneously search for time-reversal violation in the triple product of vectors involving the nuclear spin, the term D $\vec{J}_N \cdot (\vec{p}_\beta \times \vec{p}_\nu)$. We will look for distortions of the position spectrum along the axis perpendicular to the polarization when the spin is flipped, rather than looking at rate changes as in previous experiments. Unwanted polarization along this axis will be tested by recoil singles asymmetries. The location of the cloud is determined in 3D by photoionization using a small 355 nm frequency tripled diode-pumped Nd::YAG laser, and we have shown this method works for the radioactive ^{37}K (see below). Constraints on the β^+ detector position and orientation will come from measurements of the β^+ asymmetry in the silicon strip detector ΔE.

Polarization probe and calibration

Our most important recent advance is the demonstration that we can make measurements of the polarization of the same nuclei that are decaying by using atomic techniques *in situ* on ^{37}K. The atoms stop absorbing optical pumping light after they are fully polarized, and we monitor the vanishing atomic excitation with two-step photoionization. The knowledge of polarization is a limiting systematic in many experiments in this field, including those in neutron β-decay and μ decay.

Fig. 36. Top: 2D side view of additional detectors and optical pumping light for polarized geometry, showing the 0.1 mm-thick mirrors, plastic/CaF$_2$(Eu) phoswiches, copper tungsten collimators, and 405 nm probe beam. Bottom: Asymmetry in MCP position for β^+-Ar coincidences for 1 day of data, with optical pumping polarization axis in X-direction. The X-asymmetry is dominated by B$_\nu$; the standard model was assumed in this test to "measure" the polarization. The Y-asymmetry would be from a time-reversal violating D term (residual polarization will be tested by recoil singles asymmetries, not shown).

Oct11 ^{37}K Data

! runs9944−74 bias B constant

χ^2/N 9.56

a= 2.992E+02± 1.634E+01

Pow= 0.312± 0.152 mW/cm^2

δ=−3.52± 0.66 MHz

$B_\perp$= 0.000E+00fixed G

S_3=0.9859 ± 0.0003

photoions — time [μs]

Oct11 ^{37}K Data

! runs9944−74 bias B constant

χ^2/N 6.15

a= 1.682E+02± 9.822E+00

Pow= 0.329± 0.143 mW/cm^2

δ=−2.78± 0.64 MHz

$B_\perp$= 0.000E+00fixed G

S_3=0.9859 ± 0.0004

PMT — time [μs]

Fig. 37. Vanishing of fluorescence for ^{37}K atoms whose nuclear decays are shown in Fig. 36, showing P> 95%, for both signs of polarization.

We show in Fig. 37 the fluorescence spectrum determined by photoionization with the 355 nm laser for ^{37}K, showing the vector polarization P is greater than 95%. About half the size of the tail is from β^+ decay "backgrounds" that must still be subtracted.

The most direct way to probe the sub-level population is to Zeeman-split the sub-levels with a B field and use resonant fluorescence. Resolution is limited by the natural linewidth Γ of the excited states, which is 6 MHz for the $4P_{1/2,3/2}$ first excited states used for trapping and optical pumping. The $4P$ hyperfine splitting is very small in ^{41}K and ^{37}K, so B fields large enough to resolve the sub-levels will hurt the optical pumping process by decoupling the nuclear and atomic spin.

Instead, we use the second excited $5P_{1/2}$ state, where Γ=1.1 MHz. Diode lasers at 404 nm have recently become commercially available. We have not achieved routine operation, but a first scan over the ^{41}K Zeeman substructure measured polarization of 90%, in good agreement with the vanishing of fluorescence measured at the same time. When this method becomes more reliable, we will be able to absolutely calibrate the fluorescence vanishing in a model-independent way.

CFORT: A trap with perfect polarization

The future of these experiments lies in a remarkable dipole force trap using circularly polarized light developed at JILA. This will trap atoms in one magnetic substate only, with no known systematics to spoil the polarization; the resulting nuclear polarization should be better than 99.99%. 1 W of circularly polarized σ^+ light is focused to a diffraction-limited spot, with frequency between the D1 and D2 resonances. With light detuned just blue of the D1 resonance, repulsive dipole forces ("optical tweezers") expel all the spin sub-levels except M_F=F, whose coupling to the D1 vanishes for σ^+ light. The light is to the red of the D2 resonance, which produces a weaker attractive force that traps the M_F=F state only. This state (and this state only) is then trapped by the attractive force produced because the same light is red-detuned from the D2 resonance. This trap is unique to neutral atoms, and it would let us compete with the new generation of neutron β-decay experiments coming on line.

If the circular polarization of the light is imperfect, the trap becomes shallower but still only traps the one sub-level. The quantization axis will be determined by the laser light direction. (For gaussian beams the wavefronts are parallel at the focus, so even the small angle of the light focus does not spoil the polarization!) We have diverted 10 W of power from an existing Ar$^+$ laser to pump a ring laser constructed by us from a used standing-wave cavity. This trap will be the M.Sc. thesis for Erika Prime at UBC.

The potential of this technology is enormous, but this trap is extremely difficult to load. It took JILA approximately two years to load it for Rb atoms. Some of the atomic physics complications will be different for K atoms, and it is difficult to foresee when it will be ready. We will develop this in parallel with on-line experiments using the present optical pumping methods.

Expt. 956: search for tensor interactions in recoil nucleus singles in decay of polarized ^{80}Rb

The EEC has approved this experiment with medium priority. The recoiling nuclei in singles have spin asymmetry A_{recoil}= A_β+B_ν, which vanishes for pure Gamow-Teller decays. Right-handed current effects also cancel. A_{recoil} is sensitive to fundamental tensor interactions, on which the best limits are from ^{6}He β-ν correlations. A_{recoil} measurements with error 1% accuracy would be competitive and, given the vanishing observable, it is foreseeable to do much better. We have made optical pumping tests in ^{80}Rb, and we can adapt methods developed in ^{37}K (for example using MCP pulse heights to distinguish ions from backgrounds) to ^{80}Rb. A heavy Gamow-Teller decay like ^{80}Rb will be ultimately limited by nuclear-structure dependent recoil order corrections. ^{8}Li is a case where nuclear structure-dependent corrections are better understood.

Fr atomic spectroscopy

Including Stony Brook collaborators, we (M. Pearson *et al.*) have submitted a LOI for hyperfine anomaly measurements in Fr isotopes. Comparison of precision hyperfine splitting measurements in $7S_{1/2}$ and $7P_{1/2}$ states is more sensitive to higher-order moments of the nuclear magnetism distribution than the magnetic

dipole. This is because the two atomic states have different overlap with the nucleus. The result is a probe of the spatial distribution of nuclear magnetism. Since the proton distribution is given by the charge radius to this order, it can be calculated, allowing the spatial distribution of the valence neutron to be deduced in odd-odd Fr isotopes. Among the physics interests are proton-rich isotopes with spin isomers, where differences in the spatial neutron distribution would come from higher-order interactions between the valence neutron and the core. The LOI was favourably received and it is hoped these measurements will begin when an actinide target is available.

Experiment 778
Pion proton cross sections in the Coulomb-nuclear interference region
(H. Denz, R. Meier, Tübingen)

Several quantities of fundamental importance to the strong interaction can be extracted from πp observables. Examples include the πNN coupling constant, the sigma-term of the proton and a measure of isospin breaking.

Presently, there is no agreement on the values of these quantities. For example, recent extractions of the pion nucleon sigma-term from elastic pion-proton scattering vary by up to a factor of 2, including results which imply a strangeness content of the nucleon of up to 25% in contrast with extractions of the sigma-term from baryon masses.

These discrepancies are at least partly due to the status of the πp data base, in particular at low energies. There are regions where information is still missing, and there are regions where the available experimental data are contradictory. New measurements of πp observables at low energies are aimed at providing additional information and resolving the discrepancies. The goal of Expt. 778 is to determine differential cross sections of pion proton elastic scattering at low energies, in particular at small scattering angles in the so-called Coulomb-nuclear interference (CNI) region.

This experiment received beam time in 1998, 1999, and 2000. The data were taken using the CHAOS detector. A planar liquid hydrogen target was used. For each event, the incoming particle and the outgoing reaction products were detected. At large scattering angles, both the elastically scattered pion as well as the backscattered proton were tracked. At forward scattering angles the protons had too low energy to leave the target, therefore only the outgoing pion track was seen. For normalization purposes, elastic scattering of muons was measured simultaneously using muons originating from a point close to the production target which could be separated from pions by the time of

flight through the secondary beam line. A major difficulty for measurements in the Coulomb-nuclear interference region at low scattering angles was overwhelming muon background from pion decay close to the hydrogen target. These decay muons could only partly be separated from scattered pions by kinematical constraints. Therefore a muon-pion identification detector was built for this experiment and included in the CHAOS data acquisition.

Data were taken for $\pi^{\pm}p$ differential cross sections at 8 energies between 15 and 67 MeV, in an angular range from 8° to 180°.

The analysis efforts are ongoing. The raw data (4.7 TB) have been reduced by a factor of 10 by removing obvious decay events in a first analysis stage. Now enough disk space is available to keep all remaining information on disk and simultaneous analysis of the full data set at several energies is possible. This greatly facilitates the study of systematic effects. In the GEANT simulation for the experiment, further details have been incorporated, e.g. structural elements of the 4th wire chamber which are thick enough to affect pions at very low energies, thus modifying the acceptance of the detector.

In the forward angle region, the decay background poses a challenging problem. Most of it can be removed by applying the neural net for pion-muon identification, but the problem of background subtraction is not yet fully solved for a few angular bins. Preliminary results from the analysis of the larger angle data show good agreement of the shape of angular distributions with current phase shift analyses at the higher measured energies, but deviate at very backward angles and low energies. The currently applied absolute normalization, based on acceptances determined in Monte Carlo simulations, leads to reasonable agreement with phase shift analyses and previous experiments (where data exist), but the normalization uncertainty is still large. This uncertainty will be reduced by matching the angular distribution at larger angles with the forward angle data and the μp scattering which was measured simultaneously.

We expect to have final results for a subset of the data in 2003.

Experiment 781
Investigations of the $\pi\pi$ invariant mass distributions of nuclear $(\pi, \pi\pi)$ reactions with CHAOS
(N. Grion, INFN Trieste; M. Sevior Melbourne)

In earlier CHAOS experiments investigating nuclear pion induced pion production, data were collected at a single energy (280 MeV) for a variety of nuclei. Of particular interest we note that typical differential dis-

tributions such as the cross section as a function of the dipion invariant mass, $M_{\pi\pi}^2$, were reasonably well described by phase space for the isospin 2 reactions $(\pi^+, \pi^+\pi^+)$ on several nuclei. However, the same distribution for the isospin 0 reactions $(\pi^+, \pi^+\pi^-)$ on the same nuclei were not well described by phase space. In particular the process leads to strength in the low end of the $M_{\pi\pi}^2$ distribution for the reaction on nuclei relative to that on the nucleon. These results have generated considerable excitement because they are consistent with a modification of the $(\pi\pi)$ interaction due to nuclear matter when the interaction occurs in the $I = J = 0$-channel, which is conventionally called the σ-channel. This behaviour might be explained by the partial restoration of the chiral symmetry in nuclear matter, which was observed to occur at nuclear densities below the saturation density. Similar results were subsequently found in the crystal ball studies of the reaction $(\pi^-, \pi^0\pi^0)$ on several nuclei at the AGS [experiment: Starostin et al., Phys. Rev. Lett. **85**, 5539 (2000); discussion: Camerini et al., Phys. Rev. **C64**, 067601 (2001)], and in studies of photo pion production at MAMI by the TAPS collaboration [Metag et al., nucl-ex/0205009 (2001)]. Although the coupling of the pions to particle hole and delta hole configurations may also play a role, its effect is much smaller.

In this experiment additional data were collected for the pion induced pion production reactions on ^{45}Sc at a variety of incident energies between 240 MeV and 320 MeV. Data were analyzed in Trieste using the same algorithm as in the earlier work.

The data were obtained in M11 using a solid slab of ^{45}Sc. Incident beam was detected with in-beam counters and observed in the two inner wire chambers. Particle identification is achieved with the CHAOS fast trigger array, which is composed of 20 segments, each with two layers of thin plastic scintillation counters (the second of which is segmented) and 3 lead glass Čerenkov detectors. CFT segments were removed for the incident and exit beam. Particle identification is generally achieved through the CFT detector pulse heights and the track momentum. Of particular importance is the separation of pions from electrons and positrons which is achieved to better than 95% per track using the lead glass Čerenkov detectors. The rate of misidentified electron-positron pairs is further reduced to about 0.1% by an opening angle cut at 3°.

Events of interest are binned in the angle and energy of both of the pions detected. All quantities, such as the $M_{\pi\pi}^2$ discussed above, the missing energy, and the opening angle between the pions, are then determined. The CHAOS geometry has a large acceptance near the horizontal plane, but no coverage beyond seven degrees out of the plane. In this work the in-

plane acceptance has been determined with a Monte Carlo simulation, however, any out of plane correction necessarily has a model dependence. Fortunately, comparisons with theoretical predictions can be made within the CHAOS acceptance to avoid the impact of a model dependence. It is also possible to consider ratios of the various quantities between the reaction on nuclei and the reaction on ^{2}H, as a second approach to avoid the impact of any model dependence in forming the conclusions.

In order to determine a total cross section a correction reflecting the in-plane acceptance must, however, be applied. One choice would be to impose a phase space expectation as a model for out of plane extrapolation. In this work a different out of plane correction was determined. This correction factor is based simply on an interpolation between the dipion opening angles near 0° and near 180°. Clearly this choice preserves the shape of the in-plane distribution, which is dominated by the CHAOS acceptance.

As shown in Fig. 38, the shape and magnitude of the dipion invariant mass distributions for the pion production on ^{45}Sc in this work confirm earlier results on, for example, calcium [Bonutti et al., Nucl. Phys. **A677**, 213 (2000)]. The phase space for the ^{45}Sc reactions is represented by the shaded regions in each part of the figure, and the curves are theoretical results of Vincente-Vacas et al. [Phys. Rev. **C60**, 064621 (1999)], determined within the CHAOS acceptance. One can readily see that the shape of the $M_{\pi\pi}^2$ near threshold for the reaction $(\pi^+, \pi^+\pi^+)$ on nuclei is essentially the same as that for the ^{2}H$(\pi^+, \pi^+\pi^+)$ reaction, whereas the shape changes dramatically for the reaction $(\pi^+, \pi^+\pi^-)$ on nuclei compared to that for the ^{2}H$(\pi^+, \pi^+\pi^-)$ reaction. This trend was reproduced throughout the energy range studied. An
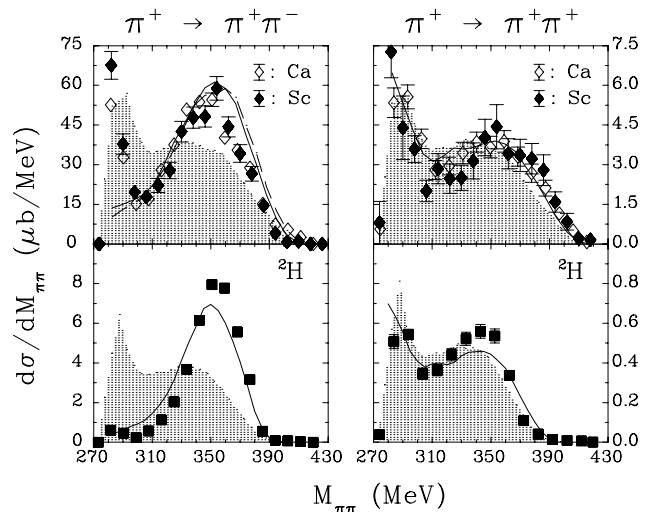
Fig. 38. Invariant mass distributions (see text for details).

interpretation of this trend is that the dynamical traits of the I=2, J=0 interaction are understood on nuclei as on the nucleon, whereas the I=0, J=0 interaction is specifically different in nuclei than on the nucleon.

Experiment 823
Pure Fermi decay in medium mass nuclei
(G.C. Ball, TRIUMF)

Precise measurements of the intensities for super-allowed Fermi $0^+ \rightarrow 0^+$ β-decays have provided a demanding test of the CVC hypothesis at the level of 3 $\times$ 10^{-4} and also led to a result in disagreement with unitarity (at the 98% confidence level) for the CKM matrix. Since this would have profound implications for the minimal standard model, it is essential to address possible "trivial" explanations for this apparent non-unitarity, such as uncertainties in the theoretical isospin symmetry-breaking correction. Uncertainties in the calculated Coulomb corrections can be studied by extending the precision β-decay measurements to heavier ($A \geq 62$, $T_z = 0$) odd-odd nuclei where these corrections are predicted to be much larger [Towner and Hardy, Phys. Rev. **C66**, 035501 (2002)]. The primary goal of the Expt. 823 experimental program is to measure the half-lives and branching ratios for the superallowed β-decay of these radioactive nuclei produced at ISAC. The early measurements have focused on ^{74}Rb (see 1999–2001 Annual Reports).

High-precision β-decay branching-ratio measurements for ^{74}Rb

The goal of this experiment was to determine the branching ratio of the superallowed $0^+ \rightarrow 0^+$ transition from ^{74}Rb to the ground state of ^{74}Kr. However, the ground-state branch cannot be measured directly, but is determined by subtracting the (non-superallowed) feeding to excited levels from the total intensity of the decay. However, since the Q_{EC}-values are large ($\sim$10 MeV) for the heavier $T_Z = 0$ nuclei, there are a large number of excited 1^+ states in the daughter nucleus predicted to be populated through GT transitions [Hardy and Towner, Phys. Rev. Lett. **88**, 211801-1 (2002)]. These transitions, together with non-analogue Fermi (F) branches must be taken into account to determine the partial half-life of the superallowed transition. Yet their individual intensities are very small and many of them cannot be detected with high resolution gamma spectroscopy. In the present experiment we have shown that this problem can be overcome with the help of theory. It is not necessary to reconstruct the GT strength function of the ^{74}Rb decay, only the total amount of non-superallowed feeding must be determined. The low-lying levels in ^{74}Kr act as collector states for a large fraction of the non-superallowed feeding and by observing their de-excitation, the larger

part of their feeding can be determined. The remaining component, which directly feeds the ^{74}Kr ground state can be estimated from shell-model calculations [Towner and Hardy, *op. cit.*] provided they reproduce well the relative feeding to excited levels in ^{74}Kr.

The experiment was carried out at ISAC in May, 2001. In this measurement the ^{74}Rb atoms were implanted into a $\frac{1}{2}$ in. wide conducting collector tape which was viewed by two LN-cooled Si(Li) diodes for the detection of conversion electrons, two large plastic scintillation counters (one thin ΔE and one thick E counter) to detect positrons and an ($\sim$80%) HPGe detector for γ-rays. A more complete description of the experiment together with preliminary results was reported previously in the TRIUMF 2001 Annual Report. Analysis of the data has now been completed. Table II summarizes the experimental feeding of the lowest six 0^+ and 2^+ levels in ^{74}Kr resulting either from the γ-decay of states above the third 2^+ level at 1742 keV (following GT or F decay) or from direct F decay to the lowest two excited 0^+ levels. The sum of the six feedings is equal to the sought branching ratio, namely the sum of all branches other than the superallowed branch in the β-decay of ^{74}Rb. This experimental sum shown at the bottom of the second column amounts to 0.336(20)%; however, this sum is incomplete since much of the γ-ray feeding of the ground state from states above 1742 keV likely remains unobserved in this experiment. Also shown in Table II are the predictions of recent shell model calculations [Towner and Hardy, *op. cit.*]. In these calculations, two quantities affect the total GT strength, namely the effective axial-vector coupling constant g_A and the excitation energies of the predicted 1^+ states in ^{74}Kr. In the published calculations g_A was set to 1.0 (a typical quenched value for shell model calculations in complete 0 hbar ω oscillator model spaces) and the lowest 1^+ state was at 3.2 MeV excitation energy. The results of this calculation appear in the fourth column of Table II, where it can be seen that they give relative feeding intensities in reasonable agreement with experiment but absolute values that are too large by a factor of two.

The purpose of the shell model calculations is to provide an estimate of the missing strength not seen in the experiment. To this end we have adjusted the calculation to reproduce the intensity of the strongest γ-ray transition seen, the $2_1^+ \rightarrow 0_1^+$ 456 keV transition. Since the model space is not that of a complete 0 hbar ω oscillator space, it is not clear what an appropriate quenched value of g_A should be: we now choose to use $g_A = 0.8$. Further, we raise the spectrum of 1^+ states relative to the 0^+ and 2^+ states such that the lowest 1^+ state occurs at 3.6 MeV. Again there is very little experimental data to guide us here. The

Table II. γ-ray and direct non-superallowed beta feeding to the 6 lowest states in ^{74}Kr, expressed per ^{74}Rb beta decay.

Level	Exp.	Theory			
	GT +F $[\times 10^5]$	GT^a + F $[\times 10^5]$	GT^b + F $[\times 10^5]$	GT^a [%]	GT^b [%]
gs, 0_1^+	12(2)	103	259	26.4	28.2
456, 2_1^+	142(18)	145	324	37.3	35.2
509, 0_2^+	39(11)	60+36	158+36	15.3	17.2
1204, 2_2^+	53(14)	41	87	10.6	9.4
1654, (0_3^+)	52(5)	20+23	46+23	5.0	5.0
1742, (2_3^+)	38(6)	21	46	5.4	5.0
Sum	336(20)	449	979	100	100

^{a} lowest 1^+ level at 3.6 MeV, $g_A = 0.8$
^{b} lowest 1^+ level at 3.2 MeV, $g_A = 1.0$

feeding intensities predicted by the adjusted shell model calculation, which are also shown in Table II, are in reasonable agreement with experiment. Notice that between the two calculations there is little difference in the relative feedings; the adjustments principally altered the absolute intensity. From the first row of Table II we estimate that the missing strength feeding the ground state is 0.10%. To place an error on this estimate we take the spread of the two calculations to give an upper error, while arguing that the missing strength is unlikely to be less than half our estimate to get the lower error. This results in a missing strength of 0.15(10)% with symmetrized errors. This missing strength is now added to the observed strength to get the summed branching ratio for all non-superallowed beta decays of 0.336(20) + 0.15(10) = 0.5(1) %.

The Q_{EC} value for the β-decay of ^{74}Rb can be predicted using the previously measured half-life [Ball et al., Phys. Rev. Lett. **86**, 1454 (2001)], the present branching ratio, the average Ft value measured for the nine well-known superallowed emitters together with the theoretical corrections from Towner and Hardy [op. cit.]. The result, 10405(9) keV, is in agreement with the measured value of 10425(18) keV [Herfurth et al., Eur. Phys. J. **A15**, 17 (2001)]. It is important to note that the error in the predicted Q_{EC} value is dominated by the theoretical uncertainty in the nuclear-structure dependent correction δ_C - δ_{NS} = 1.50(40)%.

The present experiment also provides a test for part of the analogue-symmetry breaking correction, δ_C, by observing limits on the strength of the Fermi transition to excited non-analogue 0^+ states (see below). For the ^{74}Rb decay, 80% of the non-analogue Fermi strength is predicted to be shared by the two lowest excited 0^+ levels. The predicted branches to the 0_2^+ and 0_3^+ levels are 36×10^{-5} and 23×10^{-5}, respectively, in agreement with the experimental upper limits of 50×10^{-5} and 57×10^{-5} (see Table II).

These results show that the precise determination of the superallowed branching ratio in the presence of non-negligible, strongly-fragmented GT branches is achievable and suggests improved results can be obtained by using refined experimental techniques. Such measurements using the reconfigured 8π spectrometer are planned [Svensson et al., TRIUMF Expt. 909]. Finally, a paper describing these results has been submitted to Phys. Rev. C.

Measurement of the non-analogue $0^+ \to 0^+$ transition in ^{38m}K

The determination of the transition strengths for non-analogue $0^+ \to 0^+$ decays provides a critical test of the model predictions for superallowed β-decays. In particular, they provide a direct measurement of the isospin-mixing component of the Coulomb correction. Branching ratios for Fermi transitions to non-analogue states have been measured previously [Hagberg et al., Phys. Rev. Lett. **73**, 396 (1994)] for ^{46}V and ^{54}Co. In this experiment it was only possible to set a limit for the non-analogue transition in ^{38m}K of <19 ppm corresponding to an isospin mixing correction of <0.28%. Recently, Towner and Hardy [op. cit.] have recalculated the nucleus-dependent corrections for the nine well-known superallowed β emitters for several shell model effective interactions. The values for ^{38m}K range from 0.062 to 0.186%.

An experiment designed to measure this weak decay branch was carried out in October. The measurement used the same basic method developed previously [Hagberg et al., Nucl. Phys. **A571**, 555 (1994)] and modified as described in the 2000 Annual Report for the ^{74}Rb branching ratio measurements. The fast tape transport system was used to collect and move the ^{38m}K samples out of the vacuum chamber and position them between two thin plastic scintillator paddles each backed by a HPGe detector. However, the

large HPGe detectors used previously were replaced by two Compton suppressed ($\sim25\%$) HPGe detectors from the 8π spectrometer. As a result, the sensitivity for detecting the 1209 keV γ-ray following the β-decay of ^{38m}K($t_{1/2} = 0.925$s) to the first excited 0_2^+ state in ^{38}Ar at 3377 keV was greatly enhanced by the reduction in the background coming from the decay of the long-lived isobaric contaminant ^{38}K$_{gs}$($t_{1/2} = 7.64$ min) which emits a 2168 keV γ-ray with a branching ratio of 99.8%. The ^{38}K$_{gs}$ contaminant was minimized by collecting the ^{38m}K samples for only 0.3 s. Unfortunately with the ISAC TiC target used to produce the ^{38m}K beam, the yield of the short-lived ^{38m}K isomer relative to the long-lived ^{38}K$_{gs}$ was found to be substantially reduced (by a factor of ~5) compared with that obtained using a CaZrO$_3$ target. As a consequence, the ratio of the ^{38m}K/^{38}K$_{gs}$ initial activities was only ~4:1. Under these conditions the background (during the initial 0.5 s counting period) coming from the decay of the long-lived ^{38}K$_{gs}$ contaminant in the vicinity of 1209 keV is estimated to be approximately a factor of ten higher than the present upper limit for the non-analogue 0^+ decay branch for ^{38m}K. Approximately 2 $\times$ 10^{10} ^{38m}K β-decays were observed. Analysis of the data is in progress. These data should be sufficient to confirm the present upper limit of <19 ppm. However, we plan to repeat the measurement with a CaZr0$_3$ production target and the full 8π spectrometer.

Experiment 824
Measurement of the astrophysical rate of the ^{21}Na$(p,\gamma)^{22}$Mg reaction
(J.M. D'Auria, SFU)

Experiment 824 has essentially completed the data-taking phase using the new DRAGON facility in 2002 and several papers have been submitted for publication on the facility and some results of the experiment. The objective of this experiment is to measure for the first time the rate of the ^{21}Na$(p,\gamma)^{22}$Mg reaction at explosive stellar temperatures. This reaction is thought to play a key role in the production and destruction of the long-lived isotope, ^{22}Na, during nova and X-ray bursts. Unsuccessful searches in the universe for the observation of its unique (1274 keV) decay γ-ray in such cataclysmic events using γ-ray observatories, e.g. COMPTEL, have indicated that present models on the mechanism of such events require improvement [Iyudin *et al.*, Astron. & Astrophys. **300**, 422 (1995); Starrfield *et al.*, MNRAS **296**, 502 (1998); José and Hernanz, Astrophys. J. **494**, 680 (1998)]. In the energy region of interest, such radiative proton capture reactions are governed primarily by narrow resonances, requiring direct and indirect studies to elucidate. In order to perform this study directly, we require an intense beam of the

radioactive isotope, ^{21}Na, a gaseous helium target and a detection system able to separate the relatively rare reaction products from the much more intense beam particles (~1 in 10^{12}).

The DRAGON (Detector of Recoils And Gammas Of Nuclear reactions) facility consists of a windowless, recirculating gas target (with a cold cleaning trap), surrounded by a BGO gamma array (30 units) to detect the prompt reaction gamma, followed by a multi-component recoil mass separator (RMS) system to separate the recoiling reaction products. For Expt. 824 a DSSSD (double sided silicon strip detector) was used at a position just past the focal plane of the RMS to detect separated reaction recoiling ions. A more complete description can be found elsewhere [Hutcheon *et al.*, Nucl. Instrum. Methods A (in press); Liu *et al.*, *ibid.*].

Within the past 12 months considerable time was devoted to studying the performance of the DRAGON, particularly measuring the incident beam energy using the first magnetic dipole of DRAGON, studying the optics of the system, measuring the efficiency of the gamma array, and measuring the omega gamma of well-known resonances in order to "calibrate" DRAGON. These studies were performed using stable heavy ion beams, and a description of some of these studies can be found elsewhere in this Annual Report.

The stellar reaction rate, $N_A\langle\sigma v\rangle$, for a narrow resonance, expected for nova conditions, is directly proportional to the resonance strength, $\omega\gamma$, and depends exponentially on the resonance energy, E_R. In units of cm^3 s^{-1} mol^{-1}, it is given by [Fowler *et al.*, Ann. Rev. Astron. Astrophys. **5**, 525 (1967)]:

$$N_A\langle\sigma v\rangle = 1.54\times10^{11}(\mu T_9)^{-3/2}\omega\gamma \exp\left[-11.605\frac{E_R}{T_9}\right],$$
(1)

with N_A Avogadro's number, μ the reduced mass in amu, T_9 the temperature in units of GK, $\langle\sigma v\rangle$ the thermally averaged nuclear cross section and $\omega\gamma$ and E_R in MeV. The narrow resonance thick target yield, Y, at maximum is,

$$Y = \frac{\lambda^2}{2}\frac{M+m}{m}\omega\gamma\left(\frac{dE}{dx}\right)^{-1},$$
(2)

with λ the centre-of-mass de Broglie wave length, M the (heavy) projectile nucleus mass, m the (light) target nucleus mass, and $\frac{dE}{dx}$ the energy loss per atom/cm^2(lab). Thus, measurement of the maximum thick target yield can determine the resonance strength, $\omega\gamma$.

Figure 39 shows the ^{22}Mg level scheme. Calculations of the Gamow window for the ^{21}Na$(p,\gamma)^{22}$Mg reaction at estimated ONe nova temperatures from
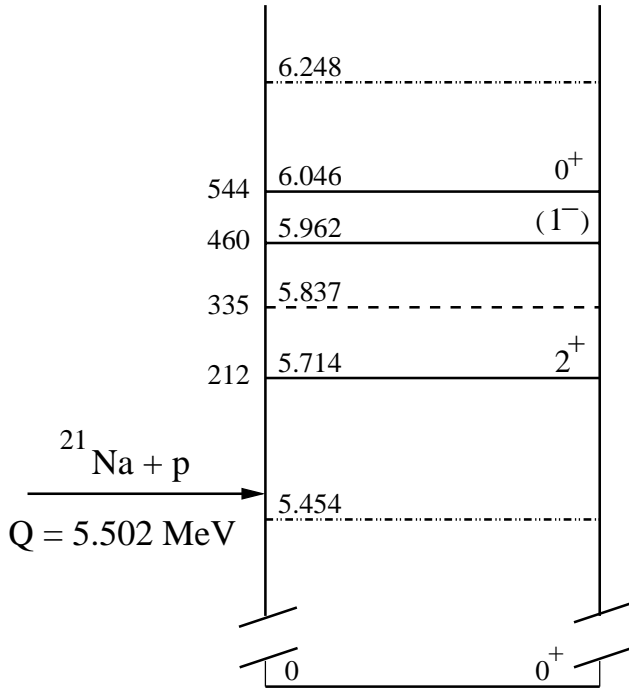
Fig. 39. The ^{22}Mg level scheme of those states of astrophysical interest for ONe nova, shown with solid lines. The numbers on the far left denote centre-of-mass energies ($E_x - Q$), in units of keV. The state at 5.837 MeV was observed once and not confirmed in other studies [Bateman *et al., op. cit.*; Michimasa *et al.*, Eur. Phys. J. **A14**, 275 (2002); Chen *et al.*, Phys. Rev. **C63**, 065807 (2001)].

Fig. 40. Resonant-capture spectra for a ^{21}Na beam energy of 220 keV/u. (a) Valid events enclosed by a two-dimensional-cut box above a background of random-coincidence events, (b) the recoil-energy distribution of the events in the DSSSD, selected by the box in (a), (c) the recoil TOF distribution for events above the γ-ray threshold energy, (d) distribution of box-selected γ-ray events observed in the BGO array along the target length, with a Gaussian fit.

0.2 to 0.35 GK at peak temperature suggest that throughout the duration of the outburst the 212 keV, $l = 0$ resonance will be dominant in the nucleosynthesis of ^{22}Na.

The experiment was carried out at the TRIUMF-ISAC radioactive beam facility. A radioactive beam of pure ^{21}Na ($q = 5^+$) at typical intensities up to 5×10^8 s^{-1} was delivered to the DRAGON hydrogen gas target (4.6 torr). The gas target received a total of $\sim 10^{14}$ ^{21}Na atoms for this study. Data-taking was done in both singles and coincidence modes; the coincidence mode required a "start" timing signal from the γ-array in coincidence with a "stop" timing signal from the DSSSD. Figure 40 shows resonant-capture spectra for a beam energy of 220 keV/u. Counts within the box in Fig. 40a were considered to be valid capture events. Their recoil energy distribution is presented in Fig. 40b. Figure 40c is the recoil time-of-flight spectrum for events satisfying the cut on γ-ray energy. The distribution of the hit BGO detector position along the beam axis (Fig. 40d) shows that the resonance was near the centre of the gas target at beam energy 220 keV/u ($E_{cm} = 211$ keV).

The beam energies were measured by adjusting the field of the first magnetic dipole in the separator so as to position the beam on the ion-optical axis at an energy-dispersed focus. Using the design bending radius of the dipole (1 m), it was possible to calculate beam energy in terms of the dipole field. The expected relationship was confirmed by measuring a number of known resonances with stable beams. The lower panel of Fig. 41 shows the yield curve for one of these studies, the ^{24}Mg$(p, \gamma)^{25}$Al reaction, demonstrating our agreement (inflection point of 214.4 ± 0.5 keV) with the literature resonance energy of 214.0 ± 0.1 keV [Uhrmacher *et al.*, Nucl. Instrum. Methods **B9**, 234 (1985)]. As shown in the upper panel, we find the energy (inflection point) for the ^{21}Na$(p, \gamma)^{22}$Mg resonance to be 205.7 ± 0.5, and not 212 keV (see Fig. 39), the difference between the Q value and the level excitation energy, 5713.9 ± 1.2 keV [Endt, Nucl. Phys. **A521**, 1 (1990)]. Given that the latter value is based upon a direct gamma de-excitation measurement of the 5713.9 keV level, this disagreement could be explained by a modified mass excess for ^{22}Mg; our data imply a value of -403.2 ± 1.3 keV rather than -396.8 keV.

Figure 41 (upper panel) shows the thick target yield curve corrected/scaled for various factors listed in Table III. The efficiency of the BGO array as a function of γ-ray energy and resonance position in the target was calculated using the GEANT program. The variation of resonance position with beam energy resulted in the
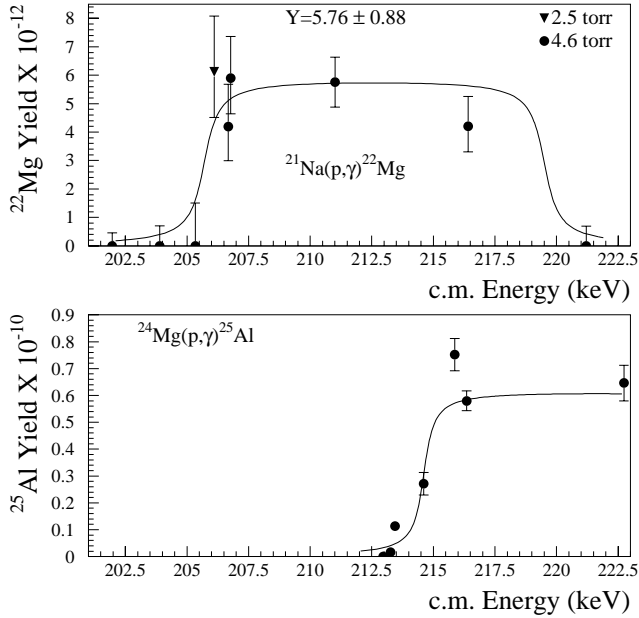
Fig. 41. The upper panel displays the thick target yield data for the ^{21}Na$(p, \gamma)^{22}$Mg reaction, with the solid line showing the nominal target thickness for 4.6 torr. Yield of the ^{24}Mg$(p, \gamma)^{25}$Al reaction for the resonance at $E_{cm} = 214$ keV, used for beam energy calibration, is displayed in the lower panel. Statistical errors only are displayed in both.

Table III. Summary of systematic errors.

Factors	Value	Syst. error
BGO array efficiency (211 keV)	0.48	12%
Separator transmission	0.98	2%
DSSSD efficiency	0.99	1%
Charge state fraction	0.44	3%
Integrated beam (211 keV)	3.62×10^{13}	4%
dE/dx (eV/(atom/cm^2))$_{\text{lab}}$	8.18×10^{-14}	5%

following calculated efficiencies: 45% for 202 keV $\leq$ E $\leq$ 207 keV, 48% at 211 keV, and 46% above 216 keV. The systematic error was deduced from values of the array efficiency measured with stable beam reactions. The separator transmission (98%) and DSSSD detection efficiency (99%) were determined separately, and the fraction of the charge state selected (44%) was measured with a ^{24}Mg beam of 220 keV/u. At 4.6 torr, charge state equilibrium in H$_2$ gas was measured to be attained within 4.4 mm [Liu *et al., op. cit.*]. The energy loss in the target (4.6 torr) was measured to be 14.4 keV/u (lab) or 8.18×10^{-14} eV/(atom/cm^2), in agreement with SRIM [Biersack and Haggmark, Nucl. Instrum. Methods **174**, 257 (1980)].

The data of Fig. 41 (upper panel) were obtained by maximum likelihood combination of several runs at each energy. The error bars on the zero counts seen at off-resonance energies are 68% confidence limits. Table III presents a summary of systematic
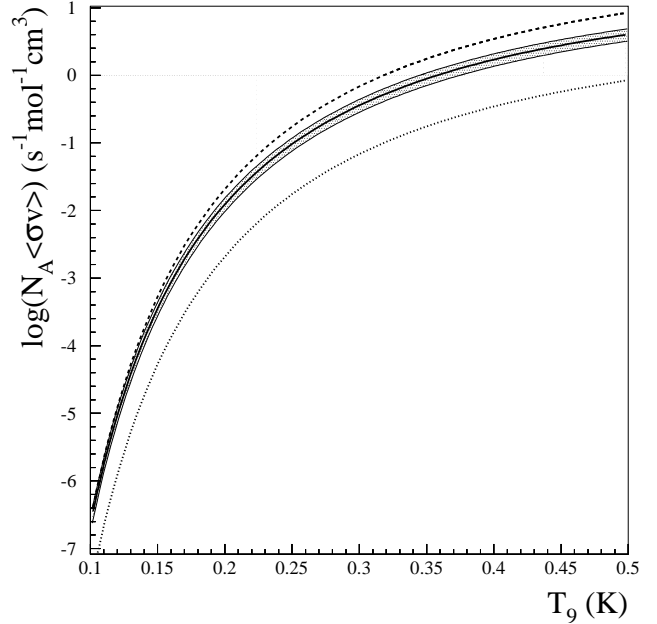
Fig. 42. ^{21}Na$(p, \gamma)^{22}$Mg reaction using Eq. 2 with typical novae temperatures and our measured values for $\omega\gamma$ and $E_{\text{R}} = 0.206$ MeV (solid line with hatched area reflecting errors), in comparison with other works; upper curve [Bateman *et al., op. cit.*] and lower curve [José *et al., op. cit.*].

errors. Using Eq. 2 and only the mid-target data point (211 keV), a yield of $(5.76 \pm 0.88) \times 10^{-12}$ per incident ^{21}Na results in a resonance strength of $\omega\gamma = 1.03 \pm 0.16_{\text{stat}} \pm 0.14_{\text{syst}}$ meV.

The effect of these results on the calculated stellar reaction rate is shown in Fig. 42. The rate is reduced over that determined by shell model calculations of $\omega\gamma$ as reported in Bateman *et al.* [Phys. Rev. **C63**, 035803 (2001)], and enhanced over that found in José *et al.* [Astrophys. J. **520**, 347 (1999)]. An analysis of the impact of the new measurements on the synthesis of ^{22}Na in novae was performed. A new model of a nova outburst, using an ONe white dwarf of 1.25 solar mass, has been computed from the onset of accretion up to the explosion and ejection stages, by means of a spherically symmetric, implicit, hydrodynamic code, in Lagrangian formulation (see José and Hernanz [*op. cit.*] for details). Results have been compared with a model evolved with the previous prescription of the ^{21}Na$(p, \gamma)^{22}$Mg rate [José *et al., op. cit.*]. As a result of the higher contribution of the 5.714 MeV level (Fig. 42), a slightly lower amount of ^{22}Na (a mean mass fraction of 2.8×10^{-4}, compared with the previous estimate of 3.5×10^{-4}) is found. The small decrease in the ^{22}Na yield results from the fact that increasing the proton capture rate on ^{21}Na favours the synthesis path through ^{21}Na$(p, \gamma)^{22}$Mg$(\beta^+)^{22}$Na, hence reducing the role of the alternative ^{21}Na$(\beta^+)^{21}$Ne$(p, \gamma)^{22}$Na path. In these newly derived conditions of increased proton

capture on ^{21}Na, ^{22}Na production takes place earlier in the outburst, at a time when the envelope has not yet significantly expanded and cooled down (contrary to the case when a lower ^{21}Na(p,γ) rate is adopted), and hence the temperature in the envelope is still high enough to allow proton captures on ^{22}Na, that reduce its final content in the ejecta.

Up to now, γ-ray flux determinations were limited by a large uncertainty in the ^{21}Na(p,γ) and ^{22}Na(p,γ) rates, which translated into an overall uncertainty in the ^{22}Na yields of a factor of $\sim$3. The maximum detectability distance was, accordingly, uncertain by a factor of $\sim$2. Such uncertainty, mainly due to the previously unknown reaction rate, has been largely reduced with the present experimental determination of $\omega\gamma = 1.03 \pm 0.16_{\text{stat}} \pm 0.14_{\text{syst}}$ meV. These results provide a firmer basis for predictions of the expected γ-ray signature at 1.275 MeV associated with ^{22}Na decay in ONe novae, and confirm the previous determination of 1 kiloparsec for a typical ONe nova [Gómez-Gomar et al., MNRAS **296**, 913 (1998); Hernanz et al., Proc. 4$^{\text{th}}$ Integral Workshop Exploring the Gamma-Ray Universe (ESA SP-459, ESA Publ. Div.:ESTEC, Noordwijk, 2001) p.65] observed with ESA's (European Space Agency) INTEGRAL spectrometer, SPI. Furthermore, the smaller uncertainty in the rate also indicates that the predicted ^{22}Na yields are not in conflict with the upper limits derived from several observational searches.

Additional details of this study can be found elsewhere [Bishop et al., Phys. Rev. Lett. (in press); Bishop, "The ^{21}Na(p,γ)^{22}Mg reaction and O-Ne Novae" (Ph.D. thesis, SFU, in preparation)].

Experiment 862
Analyzing powers in the $\vec{p}(\pi,\pi\pi)$ reactions with CHAOS
(E.L. Mathie, Regina)

In this experiment, the Canadian High Acceptance Orbit Spectrometer, CHAOS, was used to observe at least two charged reaction products from 280 MeV negative pion interactions with polarized protons in the CHAOS polarized proton target. Of particular interest are reactions with two pions in the final state, which have proven to be excellent tests of the predictions of chiral perturbation theory (ChPT). Tests of ChPT at energies near threshold constitute some of the rare tests of QCD possible at low energies. Comparisons of the theory with experiment afford the opportunity to determine low energy constants (LEC) of the theory. Previously only total and differential cross sections could be used for this purpose. Experiment 862 is the first attempt to measure a polarization observable. The pion energy was chosen as a compromise between $\vec{p}(\pi,\pi\pi)$ cross sections, which rise steeply above threshold, and the near threshold kinematic regime, where the theory is best understood.

The polarization observable is sensitive to the spin orientation of the target proton and is defined in terms of the differential cross sections σ^+ (σ^-) for positive (negative) target polarization according to

$$A = \frac{1}{P_{\text{tgt}}} \frac{\sigma^+ - \sigma^-}{\sigma^+ + \sigma^-}$$

where P_{tgt} refers to the magnitude of target polarization and σ refers to any one of several differential cross sections which may be determined. In earlier CHAOS experiments, such as Expt. 624, it has been demonstrated that the differential distributions for ($\pi,\pi\pi$) reactions can be expressed in terms of: the square of the dipion invariant mass, $M_{\pi\pi}^2$; the square of the momentum transfer to the nucleon, t; and the angle between the two final state pions in the dipion system. The essentially full horizontal angle coverage of CHAOS permits the determination of two distributions for any one differential cross section, where for example the dipion system is moving to the left of the beam and to the right.

The polarized target was first developed for CHAOS experiment Expt. 560. The control system was extensively changed to operate in a more modern control environment. The orientation of the proton spins is accomplished in an external, high homogeneity magnetic solenoid. The target material is first cooled to low temperatures using a helium 3-4 dilution refrigerator. Bombardment with suitably tuned microwaves induces polarization of the electron system, which is subsequently transferred to the proton system. Upon completion of this dynamic phase, the microwaves are turned off, leading to a rapid drop in temperature and the proton spin relaxation time to increase suddenly, effectively freezing the proton spin polarization. Once frozen, the target was physically moved from the polarizing solenoid above CHAOS into the spectrometer, where the normal magnetic field serves to preserve the polarization for days. During the actual movement of the target, a third small superconducting magnet, local to the target cryostat, was used to preserve the polarization.

The target polarization may be determined either by calibration of the NMR with the signal due to the small natural polarization arising from thermal equilibrium, or through measurement of a nuclear reaction with a known analyzing power. Numerous target studies including optimizing the NMR system, thermal equilibrium calibrations, and thermal equilibrium buildup studies at different temperatures were completed.

In previous pion production experiments, limitations to the maximum data acquisition rate meant the trigger had to discriminate against the prolific pion proton elastic scattering reaction. Recent improvements in data acquisition meant that this was no longer required, and new data for pion proton elastic scattering were simultaneously obtained. These new pion proton elastic scattering data may be used to improve the current appreciation of the analyzing power or alternatively, knowledge of the analyzing power can be used to provide an independent determination of the target polarization.

Experiment 862 received beam in the summer of 2002. However, from early in the running period it became clear that the septum magnet at the entrance to the channel had an ever worsening coolant leak. The magnet is located in a very difficult location, immediately downstream of the meson production target with vacuum connections to beam line 1A as well as the meson channel, M11. A valiant effort was made to repair the magnet remotely, however, the leak grew worse steadily until its operation was untenable and it became impossible to run M11. During this time data were collected for three cycles of the target polarization (both spin orientations form a cycle) and for one series of measurements with the background target configuration.

In principle the improved trigger arrangement allowed the simultaneous collection of data for $\vec{p}(\pi^-, \pi^-\pi^0)p$, however, the reaction rate is low and, due to the meson channel failure, the amount of data even for the reaction $\vec{p}(\pi^-, \pi^-\pi^+)n$ is minimal. Furthermore, the truncated run limits the scope of systematic checks which are normally a strong point in polarization experiments.

Analysis effort since the end of the run has primarily been focused upon the thousands of NMR spectra and temperature calibrations to determine the target polarization for all runs. Analysis of these data continues in 2003.

Experiment 863
Ground state magnetic moments of ^{75,77,79}Ga (LTNO)
(P. Mantica, Michigan State)

The focus of Expt. 863 is to study the evolution of the single-particle structure of medium-mass nuclides above $_{28}$Ni toward the $N = 50$ shell closure. A well-known shape transition from spherical to moderate deformation ($\beta_2 \approx 0.2$) occurs in the neutron-rich $_{31}$Ga and $_{32}$Ge isotopes between $N = 40 - 42$. Since the ground state magnetic dipole moment can serve as a sensitive probe of the nuclear ground state wavefunction, the experimental determination of the magnetic

moments of heavy, odd-A Ga isotopes can address the extent to which quadrupole deformation persists toward $N = 50$.

A low energy beam of ^{75}Ga was produced at the TRIUMF-ISAC facility using a surface ion source equipped with a Ta production target. The ^{75}Ga nuclei were implanted into an iron foil mounted on the cold finger inside the ^{3}He/^{4}He dilution refrigerator of the LTNO. The nuclear orientation of ^{75}Ga was monitored by measuring the angular distribution of β particles emitted from the radioactive parent ($T_{1/2}(^{75}$Ga$) = 126$ s). Two plastic scintillator ΔE-E telescopes were placed at 0° and 180° relative to the external magnetic field provided by a superconducting split-coil magnet surrounding the ^{75}Ga implantation position. Three Ge detectors were also placed around the sample position at 0°, 90°, and 180° relative to the external magnetic field. These detectors were used to monitor the γ-rays emitted from the ^{60}Co<u>Fe</u> thermometer as well as the ^{75}Ga γ-ray activity.

The angular distribution of β particles can be written in the form $W_\beta(\theta) = 1 + AP\cos(\theta)$, where P is the fractional polarization of the sample and A is the β-decay asymmetry parameter which depends on the spins and parities of all populated levels in the daughter nucleus, as well as their absolute branching ratios. Since only relative intensities were known for β-delayed γ-rays from ^{75}Ga, absolute γ-ray intensities were first measured in order to determine A, and hence the fractional polarization P from the measured angular distribution of β particles from ^{75}Ga.

In order to extract absolute branching ratios, care was taken to evaluate spectra from runs where the ^{75}Ge daughter activity was saturated, thus ensuring that the activities of the parent and daughter were in
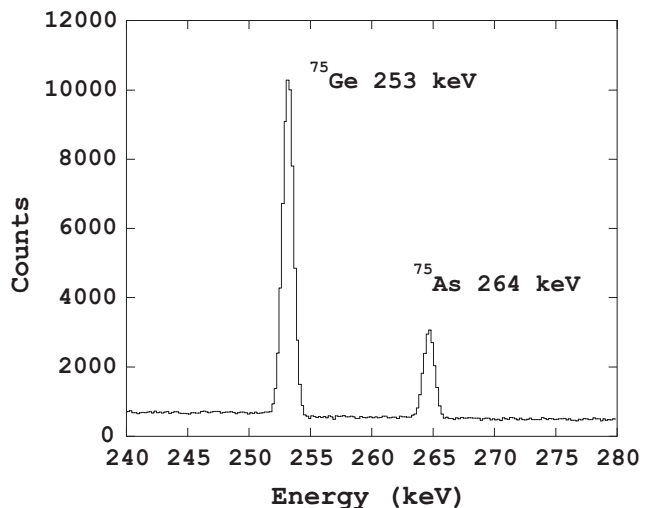
Fig. 43. Summed γ-ray spectrum in the range 240–280 keV taken with the 0° Ge detector during runs with an equilibrium of ^{75}Ga and ^{75}Ge activity.

equilibrium. Absolute γ-ray intensities in the stable [75]As granddaughter populated by the decay of [75]Ge ($T_{1/2} = 82.78$ m) are known, hence all that is required for determining absolute branching ratios from parent [75]Ga is knowledge of relative intensities of daughter [75]Ge γ-rays combined with the total activity of the sample. Since the most intense γ-ray transitions in the [75]Ge daughter and [75]As granddaughter are close in energy (253 keV and 264 keV, respectively, see Fig. 43), the peak efficiency for each γ-ray can be assumed to be identical. Thus the ratio of counts at 253 keV to 264 keV can be used to determine absolute branching ratios from the parent [75]Ga.

Taking into account the deduced branching ratios and assuming the β-decay in this neutron-rich system to be pure Gamow-Teller, $A = -0.40(3)$ was obtained. This value permits the determination of the polarization of [75]Ga.

Experiment 870
The $^{17}O(p, \alpha)^{14}N$ reaction – a probe of the O isotope ratios in giant stars
(D. Groombridge, York)

Phase I of the He gas target tests was carried out in May/June. This preliminary test was unsuccessful due to a fault with the initial design of the gas target that caused unacceptable rates of scattered beam into our detection system. Following a small modification to the initial design of the gas target, the TUDA collaboration is pleased to announce that phase II of the tests, carried out in December, were successful.

The aims of these tests were (a) to commission the new gas target using a stable beam, in preparation for use with a ^{18}Ne beam (Expt. 870) and (b) to demonstrate the success of the experimental set-up in reconstructing the trajectories of the reaction protons and in the identification of the elastic proton background originating from the window at the entrance of the gas target.

Past experience of (α, p) measurements have shown that it is crucial to have a more complete understanding of the proton background. With this in mind, a ^{20}Ne beam was requested at a similar energy to that which will be used in the future ^{18}Ne measurement. In the attempt to fulfil the second aim, it was our intention to use a stable beam that also had the potential of yielding some astrophysically interesting physics. The $^{17}O(p, \alpha)^{14}N$ reaction affects the $^{16}O/^{17}O$ isotope ratio in intermediate mass stars undergoing hot bottom burning on the asymptotic giant branch. A measurement of the $^{14}N(\alpha, p)^{17}O$ reaction at high energies was performed. The (p, α) rate can be inferred using the principle of detailed balance and the resulting rate extrapolated down to stellar energies.

The gas target consists of a cylindrical chamber, 226 cm^3 in volume with a 0.75 μm Ni entrance window (8 mm dia.) and a 6 μm Ni segmented exit window. A thick Ta foil centered on the exit window served to stop the beam in the target. These windows were designed to hold He gas at a pressure of 250 mbar.

The beams were generated by ISAC using the off-line ion source (OLIS). Typical beam currents on target were 180 pA, and during the experiment a ^{14}N beam at 1.45 MeV/u and a ^{20}Ne beam at 1.0 MeV/u were requested.

Detection of the elastic and reaction protons was acheived using 4 MSL type QQQ (single sided) 45 μm strip detectors in the "CD" configuration and 8 MSL type YY1 strip detectors in the "LEDA" configuration. These were placed at distances of 11 cm and 35 cm downstream of the entrance window, respectively. One feature of this set-up is that protons can be tracked to a position of origin within the gas target. This information, used together with energy loss information, has the advantage of reducing any ambiguity in the assignment of the final state.

Data were obtained with both ^{14}N and ^{20}Ne beams which indeed looked promising on-line, and detailed analysis of these data is currently being undertaken.

Experiment 871
Meson and quark effects in nuclear β-decay of ^{20}Na
(K. Minamisono, JSPS Postdoctoral Fellowship/TRIUMF; K. Matsuta, T. Minamisono, Osaka)

In preparation for the measurement of the alignment correlation terms in the β-ray angular distribution of ^{20}Na, several test experiments using Na isotopes (on the mass $A = 20, 21, 26,$ and 28) have been performed. These were to demonstrate both nuclear polarization by optical pumping of neutral Na atoms in the ISAC polarized beam line and the preservation of that polarization following implantation of the activity in a lattice of single crystals. In addition, hyperfine studies were needed to find a suitable crystal in which spin manipulation could be used to convert the laser-induced nuclear polarization into nuclear alignment. As a result, a large nuclear polarization of $\sim 50\%$ was produced by the laser-pumping method for four Na isotopes and successfully maintained in the crystal lattice (NaF and TiO_2 single crystals). The electric quadrupole coupling constant eqQ/h of $^{20,21}Na$ in TiO_2 and the asymmetry parameter η of the field gradient in the crystal were also determined for the first time.

Introduction

Alignment correlation term

The β-ray angular distribution from oriented nuclei is given by $W(E,\theta) \sim 1 + APp/E(1+\alpha E) + \hat{A}\alpha E$, where A is the asymmetry parameter, P the polarization, p and E the momentum and energy of the electron, respectively, $\hat{A}$ the alignment, and α the alignment correlation coefficient given by [Holstein, Rev. Mod. Phys. **46**, 789 (1972)]

$$\alpha_{\mp} \sim \frac{1}{3M}\left(\mp\frac{b}{c} + \frac{d_{\mathrm{I}}}{c} \pm \frac{d_{\mathrm{II}}}{c} - 1\right).$$

Here $\mp$ is for the electron and positron decays, respectively, M the nucleon mass, b the weak magnetism, c the Gamow-Teller matrix element, d_{II} the G-parity irregular induced tensor term, and d_{I} the nuclear structure dependent time component in the main axial vector current, which is known to have a huge enhancement relative to a value calculated by impulse approximation because of the meson exchange effect inside the nucleus. Taking advantage of the symmetry between the mirror pair, ^{20}Na and ^{20}F in the mass $A = 20$ system, we can extract the induced tensor term from the difference of the alignment correlation coefficients if the weak magnetism is known.

$$\alpha_{-} - \alpha_{+} = -\frac{2}{3M}\left(\frac{b}{c} - \frac{d_{\mathrm{II}}}{c}\right).$$

On the other hand, the time component can be purely obtained from the sum as $\alpha_{-} + \alpha_{+} = 2\left(d_{\mathrm{I}}/c - 1\right)/3M$. Here, the higher order matrices are neglected for simplicity. The polarization term also has α but since the parity violating large term 1 prevents us from extracting very small α (~ 0.01), the alignment term is the best observable to extract d_{II} and d_{I}.

Hyperfine interaction

One important key for measurement of the alignment terms is to create a purely nuclear spin aligned Na nucleus. For this purpose, the spin manipulation technique is used, which is an artificial interchange and/or equalization of the population of the magnetic sublevels. For the spin manipulation, the Na atoms are implanted into the single crystal, which has a proper electric field gradient q, under a strong magnetic field H_0. The quadrupole interaction between q inside the crystal and the quadrupole moment Q of the nucleus, superposed on the magnetic interaction between the magnetic moment μ of the nucleus and H_0, changes the energy between each magnetic sublevel so that the single nuclear magnetic resonance (NMR) frequency splits into $2I + 1$ lines depending on the nuclear spin I. Thus, a transition between specific two magnetic substates can be induced applying an rf field and it becomes

possible to convert a polarization into an alignment. Accurate knowledge of the quadrupole interaction is required for a reliable spin manipulation and artificial creation of alignment.

Experiment

Production of Na atoms and laser-pumping method

The experiment was performed at the radioactive beam facility ISAC. The 500 MeV proton beam from the TRIUMF cyclotron was used to bombard a thick production target, which is coupled to the ionization source. For the production of ^{20}Na, a SiC target and a surface ionization source were used. ^{20}Na ions were extracted at an energy of 40.8 keV, mass separated, and transferred to the polarized beam line at the ISAC experimental hall, where Na atoms were polarized by the laser-pumping method. The atomic polarization was created by pumping Na atoms on the D_1 transition with circularly polarized light. Both ground state hyperfine levels were pumped to achieve high polarization. Essentially the same technique was used as the previous work [Levy *et al.*, Proc. 9$^{\text{th}}$ Int. Workshop on Polarized Sources and Targets (World Scientific, 2002) p.334] but the optical pump laser was a coherent 899-21 frequency stabilized dye ring laser pumped by a 7 W argon-ion laser. The NMR vacuum chamber was placed 40 cm downstream of the polarimeter and a NMR magnet made of permanent magnet (5250 Oe at the centre) was used.

β NMR

The polarized Na ions were stopped on the surface of the crystal (catcher) placed at the centre of the NMR magnet and the β-rays from the stopped Na were counted by a set of plastic-scintillation counter telescopes placed above and below the catcher relative to the polarization axis. The solid angle was 2.6% in total. Each telescope consisted of three thin plastic-scintillation counters and a veto counter to reject the scattered β-rays from the NMR magnet. The amount of polarization was deduced from the asymmetry measured by the β-ray counting ratio between up and down counters. The NMR signals were measured as a function of applied rf frequencies.

Results

Measured asymmetry and polarization

First of all, Na ions were implanted into a NaF single crystal, which is known to keep 100% of Na polarization created by the laser-pumping method. The ground state properties of the Na isotopes measured in the experiment and the results are summarized in Table IV. The measured asymmetry AP depends on the asymmetry parameter A, the spin-lattice relaxation time T_1, the timing program used to measure AP, and other corrections. In Table IV, a typical value of

Table IV. Measured Na isotopes. Here A is the asymmetry parameter, which is the integrated value of all measured decay branch, AP the measured asymmetry, T_1 the spin lattice relaxation time, P_0 the initial polarization created by laser-pumping method (corrected value for A and T_1), eqQ/h the electric quadrupole coupling constant, and η the asymmetry parameter of the electric field gradient.

Catcher	Structure		^{20}Na	^{21}Na	^{26}Na	^{28}Na
		$T_{1/2}$	447.9 (ms)	22.49 (s)	1.072 (s)	30.5 (ms)
		I^{π}	2^+	$3/2^+$	3^+	1^+
		A	0.33	0.81	−0.94	−0.76
NaF	cubic	AP (%)	16.0 ± 0.4	21.8 ± 0.5	-46.6 ± 1.1	-35.9 ± 2.5
		T_1 (s)	9.9 ± 3.1	9.0 ± 0.2	24.6 ± 4.2	–
		P_0 or P (%)	51.0 ± 1.3	61.9 ± 1.4	52.8 ± 1.3	47.3 ± 3.3
TiO$_2$	rutile	AP (%)	5.3 ± 0.3	13.7 ± 0.3	-44.8 ± 0.5	-34.1 ± 2.5
		T_1 (s)	3.4 ± 1.3	13.0 ± 0.5	32 ± 11	–
		P_0 or P (%)	18.3 ± 1.5	24.0 ± 0.5	46.8 ± 0.9	44.9 ± 3.3
		eqQ/h (MHz)	2.2 ± 0.2	5.20 ± 0.03	–	–
		η	0.33 ± 0.03		–	–
LiNbO$_3$	ilmenite	AP (%)	4.3 ± 0.3	5.3 ± 1.6	-40.4 ± 0.6	-26.3 ± 3.0
		T_1 (s)	1.8 ± 0.5	1.3 ± 0.3	5.3 ± 0.5	–
		P_0 or P (%)	17.0 ± 1.7	56 ± 28	51.8 ± 1.5	34.7 ± 4
MgF$_2$	rutile	AP (%)	–	–	-18.6 ± 0.6	–
		T_1 (s)	–	–	7.4 ± 2.0	–
		P_0 or P (%)	–	–	22.3 ± 1.3	–
Pt	ccp	AP (%)	–	–	-14.5 ± 0.4	–
		T_1 (s)	–	–	0.78 ± 0.08	–
		P_0 or P (%)	–	–	55.0 ± 5.9	–
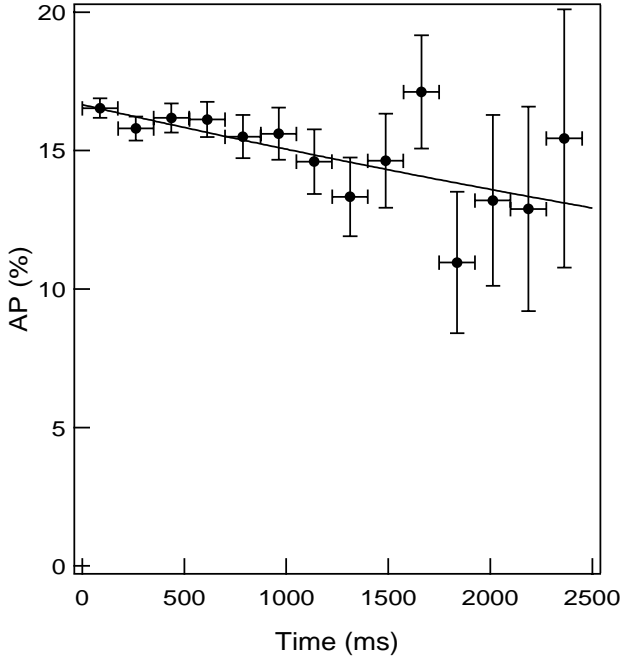
Fig. 44. A typical result of spectrum of spin–lattice relaxation time of ^{20}Na in NaF. Solid line is best fit.

measured AP during the run and the corrected value P_0 for T_1 and A are listed. For the run, in which T_1 was not measured, a value P corrected for A is presented. The typical result of T_1 measurement of ^{20}Na in NaF is shown in Fig. 44, where a pulsed-beam method was employed and the beam was chopped at time 0. Because of the limited beam time, the electro-optic modulators (EOMs) for the laser pumping were not fully optimized to cover the line width of the hyperfine splitting of the ground state in D_1 transition. Thus a higher asymmetry can be expected for the future run.

Quadrupole interaction of ^{20,21}Na in TiO$_2$: preliminary results

For the spin manipulation to create an alignment, TiO$_2$ single crystal will be used as a catcher. For this purpose, the quadrupole coupling constant eqQ/h and the asymmetry parameter η of the field gradient of ^{20,21}Na in TiO$_2$ were determined for the first time. η is defined as $\eta = (V_{XX} - V_{YY})/V_{ZZ}$, where the electric field gradient is defined by the principal components of $V_{ii} = d^2V/dX_i dX_i$ as $|V_{XX}| \leq |V_{YY}| \leq |V_{ZZ}|$ and $V_{ZZ} = q$. NMR spectra of ^{21}Na in TiO$_2$ were measured with crystal orientations $c \parallel H_0$ and $c \perp H_0$ and eqQ/h and η were extracted as listed in Table IV. Then, using the obtained information, we measured the NMR spectrum of ^{20}Na in TiO$_2$, $c \parallel H_0$, which is shown in Fig. 45, where the solid circles were the data measured with rf modulation of $\pm$ 150 kHz and open circles with FM = $\pm$ 50 kHz. From the measured coupling constant listed in Table IV, we have

$$\frac{Q(^{20}\text{Na})}{Q(^{21}\text{Na})} = 0.43 \pm 0.03 \; : \; preliminary.$$
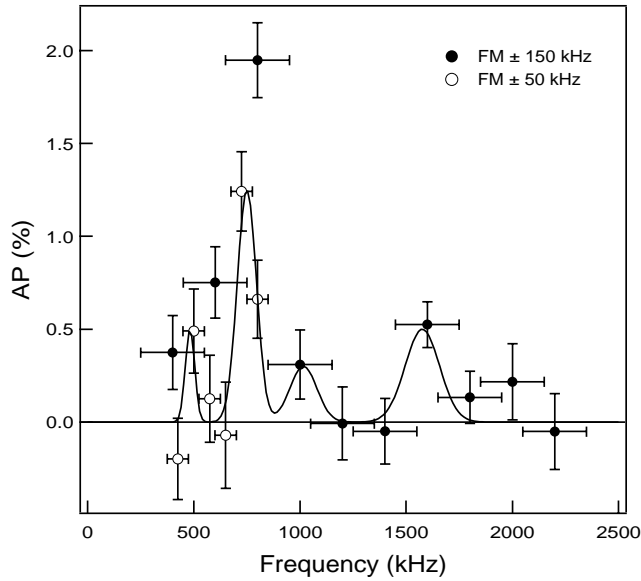
Fig. 45. NMR spectrum of ^{20}Na in TiO$_2$, c // H_0. The solid circles are the data measured with FM = $\pm$ 150 kHz and open circles with FM = $\pm$ 50 kHz. Solid line is best fit.

The Q moment of ^{21}Na has been measured as $Q(^{21}$Na$) = 50 \pm 37$ (mb) [Touchard *et al.*, Phys. Rev. **C25**, 2756 (1982)] and thus the Q moment of ^{20}Na can be extracted as $Q(^{20}$Na$) = 22 \pm 16$ (mb). To have a more precise value, we have to measure eqQ/h of a Na isotope in TiO$_2$ whose Q moment has been precisely measured.

In the next run, we will confirm the spectrum of ^{20}Na in TiO$_2$ and measure the alignment correlation term. The precise measurement of the Q moment of ^{20,21}Na is also planned.

Experiment 875
MuScat: muon scattering in low Z materials for muon cooling studies
(R. Edgecock, RAL)

As explained in the Annual Reports for 2000 and 2001, MuScat is making a precise measurement of the multiple scattering of muons in the momentum range 150–200 MeV/c as input to cooling studies for both a neutrino factory and a muon collider [MUCOOL Collab., Fermilab Proposal P904 (1998)]. Due to the complexity of the cooling process and the fact that ionization cooling has never been demonstrated to work, MuScat is one of three cooling projects. The second of these, MuCool, is studying the components of a cooling channel, while the third, the international Muon Ionisation Cooling Experiment (MICE), will show that a cooling channel can be built and will work.

The layout of MuScat during the first run in 2000 is shown in Fig. 46 and its performance was described in the 2000 Annual Report. As a result of this, it was
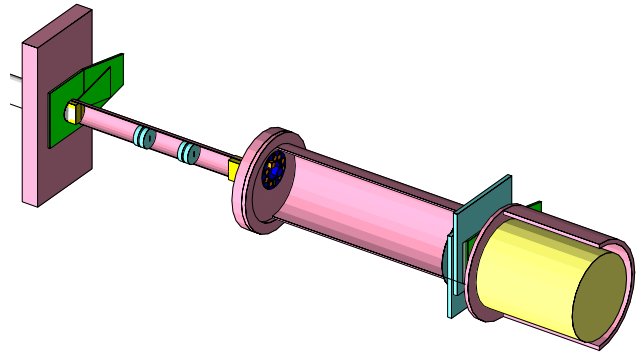
Fig. 46. The layout of the MuScat experiment in 2000, shown from below.

decided to make a number of modifications to the experiment for a second run. These are described in the 2001 Annual Report, and summarized in the following.

New tracking detectors

Three new chambers, using scintillating fibres, have been built. These consist of two offset planes of 1 mm thick fibres in each dimension, to give a uniform efficiency and two dimensional readout. There is a total of 1024 fibres per chamber. The light from the scintillating fibres is transmitted to photomultipliers using clear fibres. The PMTs used are Hamamatsu R5900 L16s (see http://cat1.hpk.co.jp/Eng/catalog/ETC/R5900U-L16_TPMH1146E06.pdf) and contain 16 anodes, each 16 mm long and 0.8 mm wide. Bundles of 16 by 16 clear fibres are formed to match these anodes, thus giving a 16-fold multiplexing. To ensure that signals can be de-convoluted, the scintillating fibres are read out at both ends and the PMTs at each end are rotated by 90° with respect to each other. One of the chambers, with the bundles of clear fibres clearly visible, is shown in Fig. 47. The PMTs sit outside the vacuum vessel and the fibre arrays form the vacuum seal. Tests show that the leak rate from these is sufficiently small to allow a vacuum of less than 10^{-6} torr.
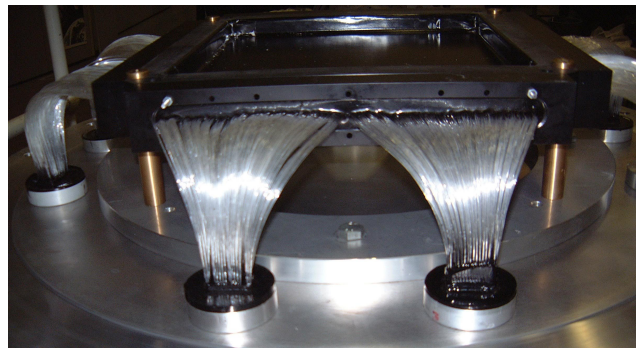
Fig. 47. One of new scintillating fibre detectors.

Collimation system

The performance of the collimation system has been improved by making a number of changes. In particular, the existing collimator disks in the collimator tube have been moved to the ends, two to each, to increase the thickness of the 40 mm and 160 mm thick end collimators. The disks have been replaced by another four, each 10 mm thick, but with 2 cm radius holes through the centre. As well as reducing the penetration through the collimators, this dramatically reduces large angle scatters off the internal faces of all the collimators. The large angle scatters will be further reduced as the collimator tube has been wrapped with 6 mm thick lead sheet and the thickness of the front flange of the main vacuum vessel doubled. Finally, an active collimator has been added to the front face of the 160 mm collimator block. This was done by placing small blocks of scintillator above and below the slit of the collimator. This will eliminate particles that just clip this edge of the collimator. These improvements are demonstrated in Fig. 48.

Targets

In the 2000 run, nine different solid targets were used, mounted on the ten hole target wheel. The tenth hole was used for measuring the intrinsic distribution of the beam. For the run in 2003, a twelve hole wheel has been created. This will allow nine targets of the
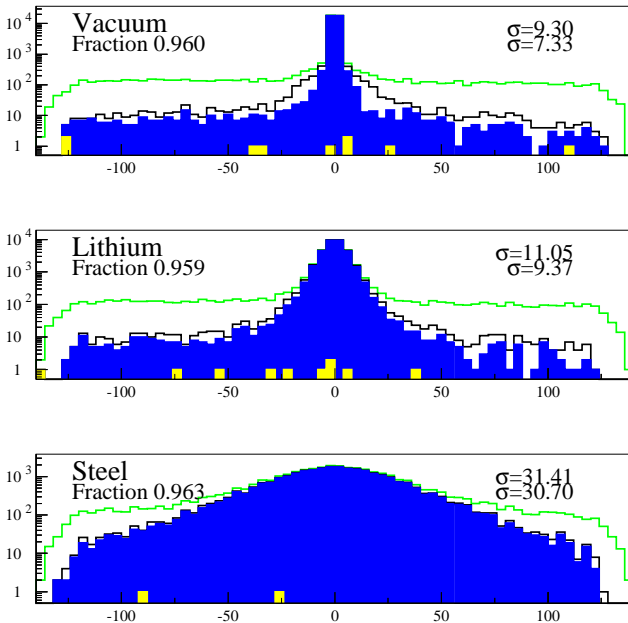
Fig. 48. A comparison of simulated scattering distributions with no target, 10 mm of lithium and 2 mm of iron using the old and new collimation systems. In each case, the upper line is the old collimation system, with no software cuts, the middle line is the new system and the dark shaded area is the new system using the active collimator. The light shaded blocks are from decays in flight.

same type as in 2000 to be used, but thicker to allow for the use of a higher beam energy than originally expected. In addition, one target from 2000 will be re-used, to have a comparison with the previous data. Finally, it is hoped to use a lithium hydride target, if a solid piece of the required size can be obtained. However, the main change compared to 2000 will be two liquid hydrogen targets, one 100 mm thick and the other 150 mm. These have been built by the Cryogenics Group at TRIUMF. Two thicknesses are to be measured to make it easier to de-convolute the effects of the target windows.

Vacuum vessel

Due to the new scintillating fibre detectors and the liquid hydrogen targets, a new main vacuum vessel has been built.

The construction of the new version of the experiment was completed in the middle of 2002 and the rest of year was used to test it, especially the new tracking detectors, in a proton beam from the ISIS accelerator at RAL. The first results of these tests are described in the next section.

Beam tests

The new tracking chambers were tested with beams of protons and muons at a variety of energies. The entire experiment is shown in the HEP test beam line at RAL in Fig. 49. When the collimation system was used, a reasonable trigger rate could only be achieved using protons at 700 MeV/c. The bulk of these data were taken just before Christmas and are still being analyzed. Nevertheless, two plots are shown in Figs. 50 and 51. The first shows the number of photo-electrons measured on individual fibres from a proton hit. From these individual fibre hits, clusters are formed in each projection and then combined into a space point in the
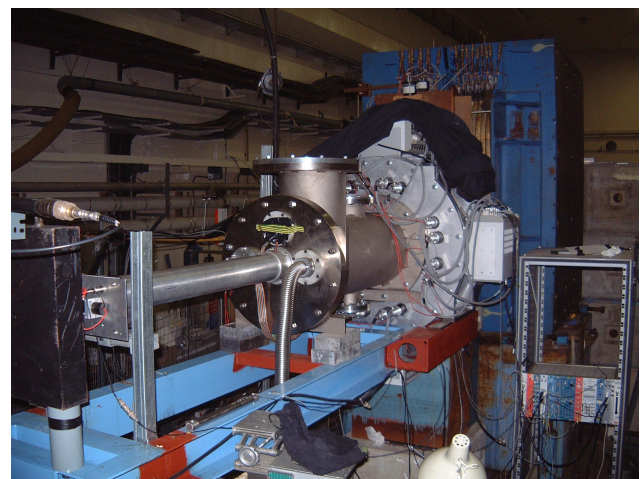
Fig. 49. The MuScat experiment in the test beam line at RAL.

chamber. Figure 51 shows the total number of photo-electrons in these space points.

Although the analysis of the data taken is not yet complete, it is sufficiently well advanced for us to be confident that the new detectors will work as required during our run in TRIUMF in 2003.
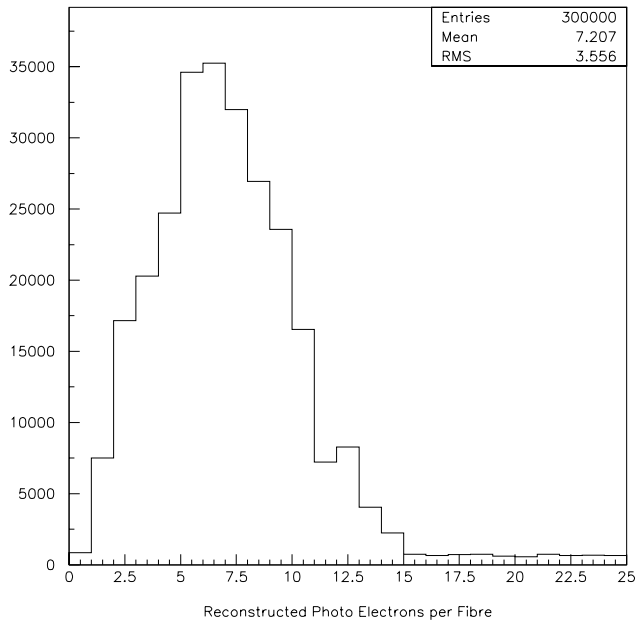
Fig. 50. The number of photo-electrons seen on individual fibres from 700 MeV/c protons.
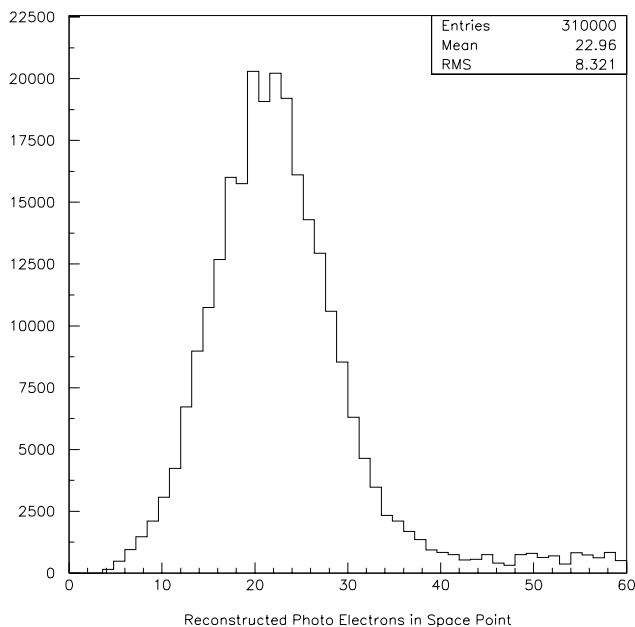
Fig. 51. The number of photo-electrons in a reconstructed space point in a single chamber.

Experiment 893
The hyperfine field of Rb in Fe, Ni and Co (LTNO at ISAC)
(P. Delheij, TRIUMF)

Principle

In the low temperature nuclear orientation set-up, a polarized nuclear ensemble is created by implanting the radioactive beam from the ISAC facility into a ferromagnetic target foil which is kept at a temperature near 10 mK. For these systems the polarization is determined by the factor $\mu H/kT$ through the Maxwell Boltzmann distribution. Here, μ is the magnetic moment, H the hyperfine field, T the temperature and k the Boltzmann constant. This polarization produces an anisotropy in the emission of the decay products which depends on nuclear structure properties like spins, multipole mixing and parity mixing. By raising the temperature, the normalization (isotropic distribution) is measured. The normalized anisotropies determine the parameter values.

If two of the three parameters in $\mu H/kT$ are known for the parent ground state, the third one can be determined. In this way (because μ and H are known) the temperature is determined by attaching a long lived source like ^{60}CoFe (for which μ and H are known) to the cold finger that cools the target foil.

The product μH can be determined directly with rf irradiation (NMRON technique). As the frequency of the rf field is stepped, the anisotropy of any subsequent transition is measured to detect the change of this anisotropy when the Larmor frequency is passed. This technique avoids the complication of the temperature determination. Then the accuracy is typically improved by an order of magnitude. Either the magnetic moment or the hyperfine field can be determined if the other quantity is known.

Development

A major disassembly included removing the refrigerator from the set-up to replace the O-rings on the actuator shafts for the baffles and the needle valves of the supply line to the 1 K pot. Also, a vacuum leak had developed in the cold beam line. This occasion was used to redesign the bellows section of the cold beam line which contains the iris to introduce more mechanical flexibility at that point.

To improve the diagnostics for the beam tuning, several changes were implemented. Microswitches were mounted on the 4 K shield below the target to verify the position of the movable Faraday cup. Furthermore, a Faraday cup was built that can be inserted to replace the cold finger with the target. In this way 90–100% transmission was obtained during tuning with stable

beam from the on-line source. These modifications performed very well.

On-line measurements

At ISAC the on-line ion source that was available was of the surface ionization type which is particularly suitable to produce alkali beams like Rb. The calculated and experimental values of the hyperfine field for Rb implanted in Fe differ by a factor 5. The best isotope to solve this problem is ^{79}Rb. The hyperfine field for alkalis is typically rather small compared to, e.g., noble gases or halogens. This feature of the experimental data is counter to what one would expect intuitively. Nevertheless, we observed sizable polarization for implanted ^{79}Rb. It has a number of other favourable properties. The decay scheme provides several internal consistency checks. Furthermore, the lifetime of 22 min is long enough to close off the beam after a few minutes of implantation. This provides a fixed source and allows the target to cool a few mK.

From several production targets enough ^{79}Rb intensity (20 pA) can be produced to take wirescans and measure the beam position every few hours. However, due to problems with the production target in the past year this goal could not be met. The intensity was also too low for NMRON measurements. An integral measurement at a temperature of 16 mK showed an anisotropy from which a preliminary lower limit of 14.5 ± 1.5 T is determined for the hyperfine field. It is assumed for this result that all the implanted ions experience the full hyperfine field. An NMRON measurement will verify this condition.

Off-line measurements

After the on-line measurements it was decided to verify quantitatively with a long lived source the status of the set-up. ^{60}Co was diffused into a thick Fe foil (0.25 mm thick). In Figs. 52 and 53 the intensity of the ^{60}Co γ-rays is shown as a function of the rf frequency for the detectors that were mounted parallel to the polarization direction. A magnetic field of 0.2 and 0.5 T respectively was applied to the sample. For this geometry an anisotropy in the gamma emission produces a reduction in the intensity. At the Larmor frequency the gamma anisotropy is reduced by the rf irradiation and therefore the measured intensity increases towards the normalization value wcts. From a gaussian fit to the data it follows that the destroyed fraction of the anisotropy exceeds 30%. The resonance frequency ν_2 of 165.1 MHz and the width W of 1.07 MHz agree very well with previous observations. In each graph an error bar is plotted for the measurements with the highest and lowest value.
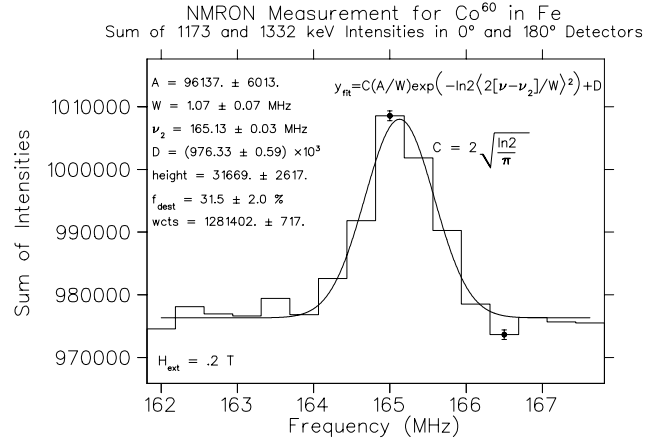
Fig. 52. NMRON resonance for ^{60}Co$\underline{\text{Fe}}$ at 0.2 T.
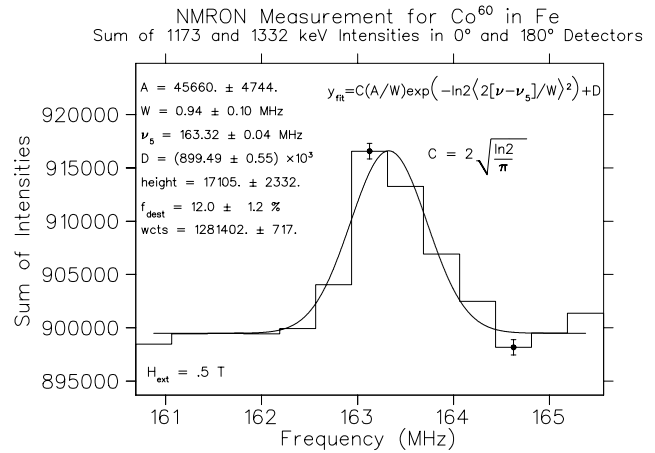
Fig. 53. NMRON resonance for ^{60}Co$\underline{\text{Fe}}$ at 0.5 T.

The shift of 1.8 MHz in the resonance frequency reflects exactly the magnetic field shift of 0.3 T (Fig. 53). The reduction of the destroyed anisotropy fraction follows the decrease of the tipping angle at higher external magnetic field.

The isolated spin assumption is verified by measuring the intensities with the frequency modulation on (N_{on}) and off (N_{off}) for equal time intervals at each rf frequency (Fig. 54). Their difference is the destroyed anisotropy which is normalized with the undisturbed anisotropy($N_{warm} - N_{off}$). These time intervals were split in four equal parts of 150 s each.

From the dropoff in intensity, when the modulation is turned off (Fig. 55), a longitudinal relaxation time of approximately 50 s is determined, as expected.

Through these off-line measurements it has been demonstrated quantitatively that the sample fabrication and the cryogenic set-up for NMRON measurements as well as the sample fabrication are operating very well.

54
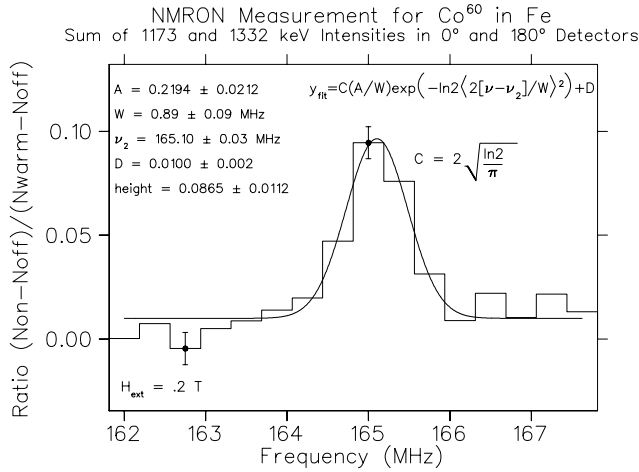
Fig. 54. NMRON resonance as determined by toggling the frequency modulation on and off at each frequency.
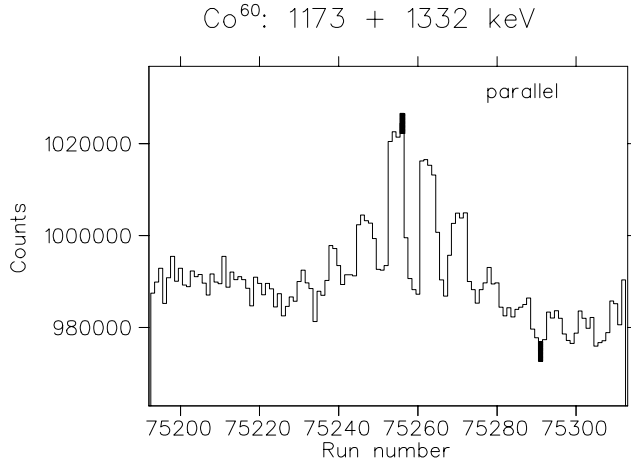
Fig. 55. Raw data with frequency modulation that is toggled every fourth run.

Experiment 903
Spectroscopic study of ^{11}Be with polarized ^{11}Li beam
(T. Shimoda, Osaka)

Although the establishment of a level scheme is of primary importance to understanding the nuclear structure, essentially no "firm" spin-parity assignments have been made for a neutron-rich nucleus ^{11}Be, except for the famous abnormal parity ground state ($1/2^+$) and the first excited state (0.320 MeV, $1/2^-$). This experiment aims at establishing firm spin-parity assignments and level scheme of ^{11}Be by observing β-delayed neutrons and γ-rays from a spin-polarized ^{11}Li$_{g.s.}$. The present method takes advantage of the fact that the allowed β-decay from a polarized nucleus shows significantly different asymmetry depending on the spin values of both the initial and final states. The difference comes from the asymmetry parameter A as shown

in the following expression of the β-ray angular distribution $W(\theta)$ as a function of the emission angle θ with respect to the polarization axis,

$$W(\theta) \propto 1 + AP\cos\theta,$$

where P is the polarization of the parent nucleus. In the allowed transition from ^{11}Li$_{g.s.}$ ($I^\pi = 3/2^-$, $T_{1/2}$ = 8.5 ms, $Q_\beta = 20.61$ MeV) the asymmetry parameter A is restricted to very discrete values of -1.0 or -0.4 or $+0.6$, corresponding to the final state spin-parity of $1/2^-$ or $3/2^-$ or $5/2^-$, respectively, of ^{11}Be. The spin polarization P can be evaluated from the β-ray asymmetry coincident with the γ-ray from the first excited state at 0.32 MeV ($1/2^-$) to the ground state in ^{11}Be. Thus, from the β-ray asymmetry measurements of β-n and β-n-γ coincidence for other states in ^{11}Be, the associated A's can be determined, and consequently their spin-parities can be assigned, in addition to the level scheme of ^{11}Be and the decay schemes of ^{11}Li$_{g.s.}$ and ^{11}Be*. Highly polarized radioactive nuclear beams at ISAC are best suited for this kind of experiment.

Since the proposal of Expt. 903 has been approved in the beginning of 2001, preparation for the experiment has been made extensively in the following three major parts: (i) development of spin-polarized ^{11}Li beam, (ii) construction of the Osaka beam line which delivers the polarized ^{11}Li beam to the area where the present experiment is performed, (iii) development of the detector system for the β-n and β-n-γ coincidence measurements.

Polarized ^{11}Li beam

Polarization of ^{8}Li beam as high as $\sim$70% has been achieved in August, 2001 after introducing a set of EOMs into the pumping laser system so as to match the laser line width to the broadened absorption line of the neutral ^{8}Li beam [Levy *et al.*, PST2001 (World Scientific, 2002) p.334; Hatakeyama *et al., ibid.* p.339]. The same scheme is applicable for ^{11}Li beam. After installing a ring dye laser system, $\sim$50% polarization of ^{11}Li was achieved in July, 2002.

Detector system

A schematic of the detector set-up is shown in Fig. 56. The spin-polarized ^{11}Li beam is stopped in a thin Pt stopper foil in vacuum. The polarization is preserved with the help of a static magnetic field applied by a pair of permanent magnets. The β-ray asymmetry is measured with two sets of plastic scintillator telescopes placed along the polarization direction, free from spurious asymmetry due to the detector geometry or efficiency by inverting spin orientation. The inversion is achieved by flipping the laser helicity for optical pumping. High energy β-delayed neutrons ($E_n = 0.5$–9 MeV) are detected with six TOF plastic scintillators
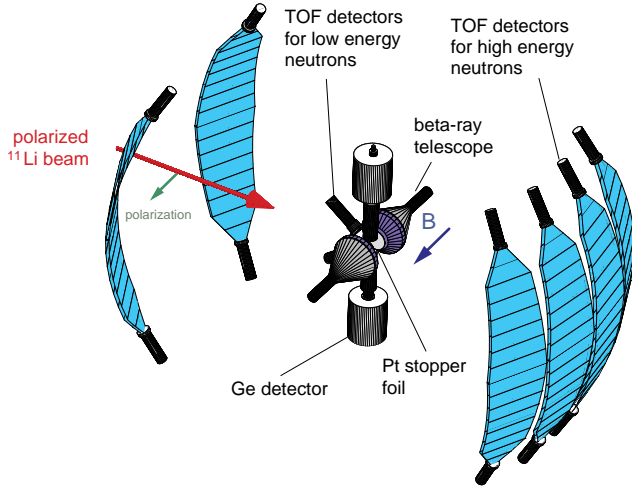
Fig. 56. Detector system for β-n and β-n-γ coincidence measurements from spin-polarized ^{11}Li.

with an arc shape. Low energy β-delayed neutrons (E_n = 10–500 keV) are detected with two TOF Li-glass scintillators. γ-rays from ^{11}Li and ^{11}Be are detected with two HPGe detectors placed above and below the Pt stopper.

Results of July, 2002 run

Following the first test experiment in December, 2001 to examine the performance of the low energy neutron detectors, the second test experiment with polarized ^{11}Li beam and full detector set-up was performed in July, 2002. Even with many troubles such as the limited beam intensity to $\sim$200 pps (10 times less than expected) and not optimum laser conditions, significantly high polarization brought fruitful results as follows.

In the upper and lower panels of Fig. 57, the neutron TOF spectrum with the high energy neutron detectors and the observed asymmetry parameters A for β-rays coincident with the neutrons are shown, respectively, as a function of the flight time. The expected A values for β-decay to a specific spin state in ^{11}Be* are shown by horizontal lines in the lower panel. Better time resolution and less background than the previous
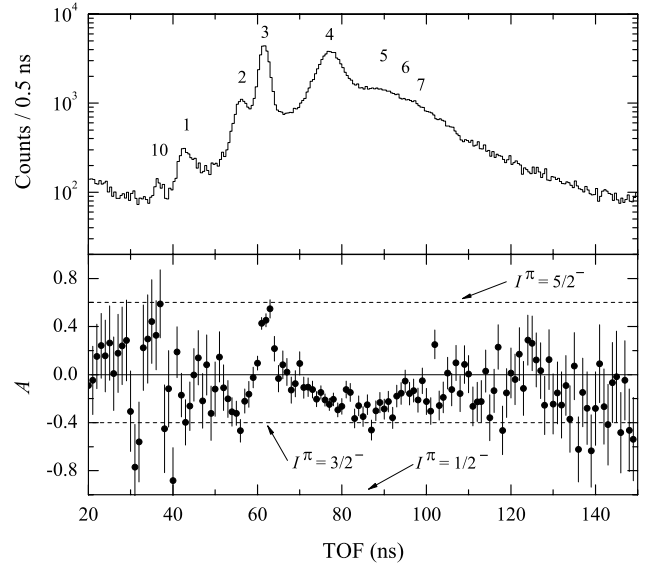
Fig. 57. Neutron TOF spectrum and associated β-ray asymmetry.

works at fragment separator facilities [Aoi *et al.*, Nucl. Phys. **A616**, 181c (1997); Morrissey *et al.*, Nucl. Phys. **A627**, 222 (1997)] enabled observation of a new peak 10 which corresponds to the neutron decay from a state at E_x = 10.6 MeV in ^{11}Be to the ground state of ^{10}Be. For the peak 1 Aoi *et al.* proposed a neutron decay from a "new state" at E_x = 8.03 MeV, but Morrissey *et al.* assigned the peak 1 as due to the neutron decay from the known 10.6 MeV state to the first excited state in ^{10}Be(3.368 MeV, 2^+). Our observation of the peak 10 shows that these are decays from the 10.6 MeV state, and our β-n-γ coincidence measurements also indicate decay from the 8.03 MeV state. Table V lists the observed neutron energy, the states in ^{11}Be from which the neutrons are emitted, the measured asymmetry parameter A, and the spin-parity assignments, for the prominent neutron peaks.

The spin-parities of the state decaying to the ground state of ^{10}Be are decisively assigned. Namely, the states at E_x = 2.69, 8.03, and 10.6 MeV are assigned to be of $3/2^-$, $3/2^-$, and $5/2^-$, respectively. The

Table V. Results of β-n coincidence measurements for prominent neutron peaks observed with the high energy neutron detectors.

Peak number	TOF (ns)	E_n (MeV)	E_x in ^{11}Be (MeV) [Ajzenberg-Selov]	A (measured)	I^π (assigned)
10	36.2 ± 0.5	8.86 ± 0.25	10.6	$+0.89 \pm 0.52$	$5/2^-$
1	41.9 ± 0.5	6.61 ± 0.15	8.03, 10.6	-0.33 ± 0.14	$3/2^-$
2	55.7 ± 0.5	3.74 ± 0.07	8.03, 10.6	-0.42 ± 0.09	$3/2^-$
3	60.8 ± 0.5	3.14 ± 0.05	3.89, 3.96	$+0.44 \pm 0.05$	$5/2^-$
4	76.8 ± 0.5	1.97 ± 0.03	2.69	-0.36 ± 0.02	$3/2^-$

observed asymmetry of +0.44 for the peak 3, which is due to neutron decays from both the states at $E_x = 3.89$ MeV and 3.96 MeV to the ground state of ^{10}Be, indicates that one of these states, of which neutron yield dominates the other one, is of $5/2^-$ and the other state is of either $1/2^-$ or $3/2^-$.

Figure 58 shows the TOF spectrum with the low energy neutron detectors. A large peak at ~20 ns is due to efficiency enhancement by the resonance of n + ^{6}Li ($E_x(^7\text{Li}) = 7.460$ MeV, $5/2^-$, $E_n = 0.245$ MeV). Peaks 8 and 9 are most possibly due to decays from the 3.89 MeV and 3.96 MeV states, respectively, to ^{10}Be(3.368 MeV, 2^+). After correcting for detection efficiency, the neutron energy and the branching ratio (the ratio normalized to a parent nucleus ^{11}Li$_{g.s.}$) were determined as listed in Table VI.

Aoi *et al.* observed 80 keV neutrons with plastic scintillators, but their detectors were not sensitive to the 17 keV neutrons. They ignored such neutron decay in their decay scheme, according to Liu *et al.*'s assignment for the 3.89 MeV state to be $3/2^+$ from DWBA analyses of the ^{9}Be(t,p)^{11}Be reaction [Liu and Fortune, Phys. Rev. **C42**, 167 (1992)]. On the other hand, Morrissey *et al.* included the β-decay to the 3.89 MeV state and the successive 17 keV neutron decay, although they did not observe low energy neutrons. Their decay scheme was presumably claimed after Azuma *et al.* [Phys. Rev. Lett. **43**, 1652 (1979)] who have
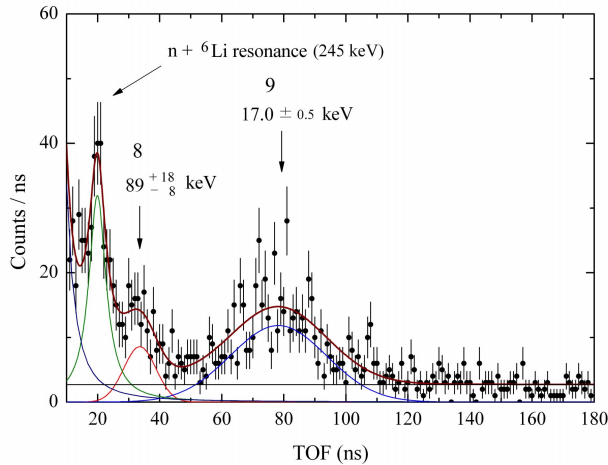
Fig. 58. Neutron TOF spectrum with low energy neutron detectors.

observed 18 keV neutrons as well as the 80 keV neutrons with ^{3}He proportional detectors. Our results apparently support the work by Azuma *et al.* Therefore, the 3.89 MeV state must be of minus parity.

Although the small statistics of the low energy neutron spectrum make it impossible for us either to deduce β-ray asymmetries for the neutron peaks 8 and 9 or to examine the β-n-γ coincidence, we could assign the spin values of the 3.89 and 3.96 MeV states. The key quantities are the branching ratios and asymmetries concerning the first excited state of ^{10}Be ($E_x = 3.368$ MeV, 2^+): We determined (i) the branching ratios of the neutron decays from the 3.96 MeV and 3.89 MeV states to the 2^+ state of ^{10}Be as 5.3% and 14.0%, respectively, (ii) the branching ratio and asymmetry of the γ-decay from the 2^+ state of ^{10}Be to the ground state as 37.0% and +0.16, respectively, (iii) the branching ratio and asymmetry of the γ-decays leading to the ^{10}Be(2^+) state as 12.7% and $A = -0.27$, respectively. Therefore the following relation must be fulfilled,

$$A_{3.96} \times \frac{0.053}{0.370} + A_{3.89} \times \frac{0.14}{0.370} + (-0.27) \times \frac{0.127}{0.370}$$
$$+ \overline{A} \times \frac{0.060}{0.370} = +0.160,$$

where A_i is the asymmetry parameter of the labelled state and $\overline{A}$ is the average asymmetry for all states which decay to the 2^+ state of ^{10}Be by emitting neutrons. For all possible combinations of A_i, $\overline{A}$'s were evaluated. From the condition that $-1.0 \leq \overline{A} \leq 0.6$, there are three possible cases where the spin-parity of the 3.89 MeV state is always $5/2^-$. Thus, the spin-parity of the 3.89 MeV must be $5/2^-$. As for the 3.96 MeV state, any of three possible spin values can not be excluded because of large errors in $A_{3.96}$. For this state two groups have proposed $3/2^-$ assignment from the DWBA analyses of the ^{9}Be(t,p)^{11}Be reaction at $E_t = 23$ MeV [Ajzenberg *et al.*, Phys. Rev. **C17**, 1283 (1978)] and at 15 MeV [Liu and Fortune, *op. cit.*], and the energy-level compilation [Ajzenberg-Selov, Nucl. Phys. **A506**, 1 (1990)] has adopted this assignment. In the next beam time with higher beam intensity and higher polarization, the spin-parity assignments of the 3.89 and 3.96 MeV states will be confirmed.

Table VI. Low energy neutron peaks detected with the low energy neutron detectors.

TOF (ns)	E_n (keV)	FWHM (keV)	Branching ratio (%)	E_x in ^{11}Be (MeV) [Ajzenberg-Selov]
$75^{+1.1}_{-2.1}$	17.0 ± 0.5	16.4	$14.0 \pm 2.4(\text{stat})^{+2.1}_{-4.0}(\text{syst})$	3.89
$32.7^{+1.5}_{-2.9}$	89^{+18}_{-8}	65.8	$5.3 \pm 1.9(\text{stat})^{+4.0}_{-0.8}(\text{syst})$	3.96

Many neutron decays leading to the excited states of ^{10}Be exhibit neutron peaks overlapping with each other as typically shown in the energy region below that of peak 4 in Fig. 57. The neutron peaks were decomposed by the β-n-γ coincidence analyses with the help of β-ray asymmetry, and the neutron decay paths were determined. In the case that the small statistics prevented such analyses, the following γ-ray shape analyses were very successful: Some of the γ-rays from ^{10}Be* showed significantly broader line shapes than the detector resolution. This is due to the neutron recoil effect. The line shapes were analyzed by assuming the neutron decay paths and by taking into account the stopping process of ^{10}Be* in the Pt stopper foil and the lifetimes of the γ-ray emitting states of ^{10}Be*, similarly to the Doppler shift attenuation method. It was found, for the first time, that the 8.82 MeV state in ^{11}Be decays to the 6.263 MeV state of ^{10}Be(2^-). In addition, the β-ray asymmetry coincident with the subsequent γ-decay in ^{10}Be (6.263 MeV state (2^-) $\rightarrow$ 3.368 MeV state (2^+)) was measured to be $-0.44(33)$. The neutron decay intensity from the 8.82 MeV state exhausted the γ-decay intensity. Therefore, it is strongly suggested that the 8.82 MeV state is of $3/2^-$. Other neutron decay paths determined from the γ-ray line shape analyses were very consistent with those determined by the β-n-γ coincidence analyses.

Neutrons with $\sim$96 ns flight time in Fig. 57 ("6") are due to the decay from the 5.24 MeV state in ^{11}Be to the 2^+ state of ^{10}Be [Aoi *et al., op. cit.*; Morrissey *et al., op. cit.*]. This was also confirmed by the β-n-γ coincidence measurement in the present work. The β-ray asymmetry in this region in Fig. 57 tends to increase toward positive value. This strongly suggests $5/2^-$ assignment, because the $5/2^-$ state uniquely gives positive asymmetry. Somewhat smaller asymmetry than the expected value of $+0.6$ is due to the many overlapping peaks in this region and the asymmetry cancellation occurs to a large extent. We therefore assign the 5.24 MeV state to be of $5/2^-$ with high probability.

From the β-n-γ coincidence we could determine the widths of the neutron peaks 5 and 7 which are due to the decay from the 8.03 MeV state. The widths were much smaller than assumed by Aoi *et al.* The widths for other states are known from the ^{9}Be(t,p)^{11}Be reaction [Liu and Fortune, *op. cit.*]. By assuming all the assigned states and decay paths, we reproduced the TOF spectrum and asymmetry as shown in Fig. 59a, but we failed to reproduce the experimental results to a large extent. Therefore, we assumed, in addition, three unknown states in ^{11}Be at 5.61 MeV ($1/2^-$ or $3/2^-$), 9.1 MeV ($3/2^-$), and 10.0 MeV ($5/2^-$) so as to better reproduce both the TOF spectrum and asymmetry. The experimental data are reproduced rather well, as
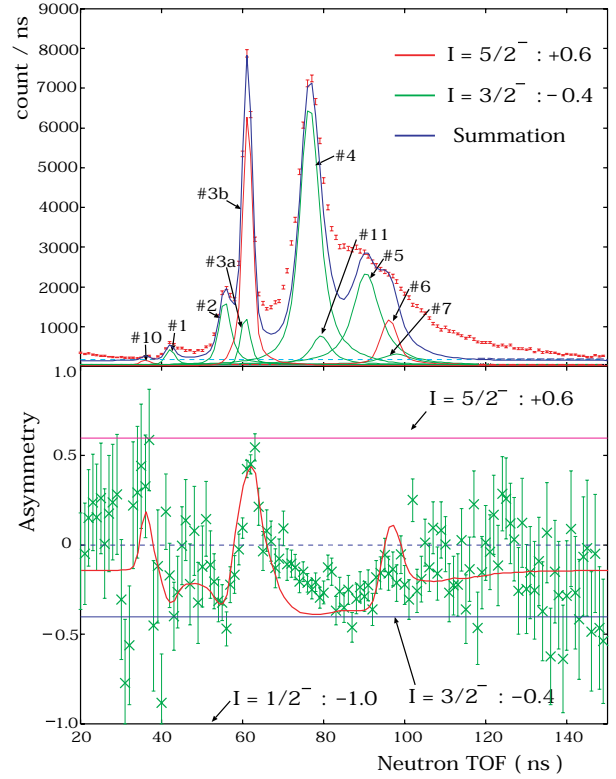
Fig. 59a. Reproduction of TOF spectrum and asymmetry with known states and presently assigned I^π and branching ratio.
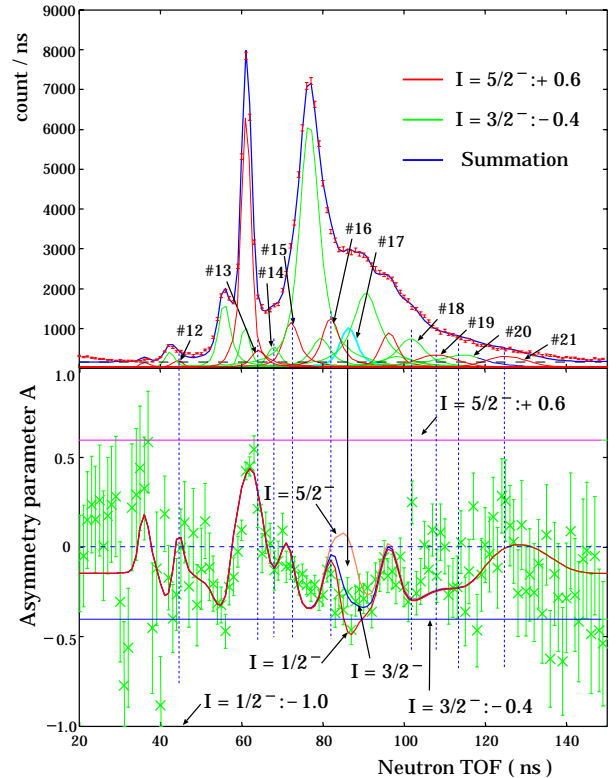
Fig. 59b. Reproduction of TOF spectrum and asymmetry with three more assumed states at 5.61 MeV ($1/2^-$ or $3/2^-$), 9.1 MeV ($3/2^-$), and 10.0 MeV ($5/2^-$).

Table VII. Assigned energy levels in ^{11}Be and $\log ft$ values of the β-decay of ^{11}Li$_{\mathrm{g.s.}}$ to these states. The AMD calculations were made for two cases with different spin-orbit interactions. Very strong interaction of $u_{\ell s} = 3700$ MeV was used so as to reproduce the level inversion of the ground state $1/2^+$ and the first excited state $1/2^-$, but Kanada-En'yo *et al.* recommend $u_{\ell s} = 2500$ MeV to describe the excited states of ^{11}Be.

I^π	E_{x}	$\log ft$			
		Present work	AMD by Kanada-En'yo *et al.*		
	(MeV)		$u_{\ell s} = 3700$ MeV	$u_{\ell s} = 2500$ MeV	K^π
$1/2^-$	0.32	5.67(8)	5.0	5.5	$1/2^-$
$3/2^-$	2.69	5.0(1)	4.4	5.0	$1/2^-$
$5/2^-$	3.89	4.80(7)	4.5	5.0	$1/2^-$
$3/2^-$	3.96	5.3(1)	4.9	6.2	$3/2^-$
$5/2^-$	5.24	5.55(8)			$3/2^-$
$3/2^-$	8.03	4.30(8)	3.9	4.3	
$3/2^-$	8.82	4.46(7)			
$5/2^-$	10.6	4.13(12)			

shown in Fig. 59b. We therefore claim these three new states in ^{11}Be. These speculations will be confirmed by the asymmetry associated with the β-n-γ coincidence measurements with much higher statistics in the next beam time.

Comparison with theoretical prediction

So far we have assigned spin-parities of some of the levels in ^{11}Be and decay schemes of ^{11}Li and ^{11}Be. The results were compared with theoretical predictions level by level. A recent shell model calculation by Millener [Nucl. Phys. **A693**, 394 (2001)] predicted an excited state with $I^\pi = 3/2^+$ located at 3.89 MeV with the 1-$\hbar\omega$ configuration and another state of $5/2^-$ at 3.96 MeV with the 0-$\hbar\omega$ configuration. Both predictions do not agree with the present assignments. On the other hand, the level sequence and the $\log ft$-values are in good agreement with predictions by a fully microscopic calculation of anti-symmetrized molecular dynamics (AMD) [Kanada-En'yo *et al.*, Nucl. Phys. **A687**, 146c (2001); Phys. Rev. **C66**, 024305 (2002)] as listed in Table VII. The $\log ft$-values are displayed in four groups, following Kanada-En'yo *et al.*: (i) The states at $E_{\mathrm{x}} = 0.320$ ($1/2^-$), 2.69 ($3/2^-$), and 3.89 ($5/2^-$) MeV have $\log ft$-values of 4.8–5.7. It is understood that these are the members of the rotational band with $K^\pi = 1/2^-$. (ii) The states at 3.96 ($3/2^-$) and 5.24 ($5/2^-$) MeV have larger $\log ft$-values than the first group. These are the members of the rotational band with $K^\pi = 3/2^-$, where development of α-cluster is more dominant than in the $K^\pi = 1/2^-$ band. (iii) The 8.03 and 8.82 MeV states have very small $\log ft$-values. One of these may correspond to a state for

which it is predicted that the α-clustering is completely broken. (iv) The 10.8 MeV state, for which a large $\log ft$ value was observed, may have dominant single particle configuration, but there is no corresponding state in AMD.

Experiment 909
Isospin symmetry breaking in superallowed Fermi β-decays
(C.E. Svensson, Guelph)

Precision measurements of the ft values for superallowed $0^+ \to 0^+$ Fermi β-decays between isobaric analogue states provide demanding tests of the standard model description of electroweak interactions. To date, superallowed ft values have been determined at the $\pm 0.1\%$ level for nine nuclei between ^{10}C and ^{54}Co and, once corrected for small radiative and isospin symmetry-breaking effects, their consistency has confirmed the conserved vector current (CVC) hypothesis at the level of 3×10^{-4}. However, the value of V_{ud} derived by comparing these β-decay data with the purely leptonic muon decay, combined with present knowledge of V_{us} and V_{ub}, indicates a violation of the unitarity of the Cabibbo-Kobayashi-Maskawa (CKM) quark-mixing matrix at the 98% confidence level [Towner and Hardy, Phys. Rev. **C66**, 035501 (2002)]. Should this discrepancy be firmly established, it would indicate the need for new physics, either in terms of explicit quark effects in nuclear structure or an extension of the minimal electroweak standard model. Before a definitive conclusion can be reached, all uncertainties contributing to the unitarity test must be carefully scrutinized and, if possible, reduced. For V_{ud}, the dominant uncer-

tainties are those associated with theoretical corrections to the ft values, and the search for systematic effects has focused on the nuclear-structure dependent δ_C corrections that account for the breaking of isospin symmetry by charge-dependent forces in the nucleus.

Experiment 909 involves a series of measurements with the 8π spectrometer and SCEPTAR β array aimed at constraining the above-mentioned isospin symmetry-breaking corrections in superallowed Fermi β-decays. This program will take advantage of the unique beams of radioactive ions available at ISAC to study particular decays in which the predicted δ_C corrections show the greatest model sensitivity. An initial focus of Expt. 909 will be on precise lifetime and branching ratio measurements for ^{34}Ar, with the aim of establishing the superallowed ft value at the $\pm 0.1\%$ level. The uncertainty in the ^{34}Ar superallowed ft value is currently dominated by the uncertainty in the half-life, 844.5 ± 3.4 ms. With high-intensity beams of ^{34}Ar expected from the new ISAC ECR ion source in the spring of 2003, the first objective will be to improve this half-life precision by approximately an order of magnitude. These measurements will be carried out by collecting samples of ^{34}Ar at the centre of the 8π and following their decay for ~ 30 half-lives by time-stamping γ-rays emitted from excited states in the daughter ^{34}Cl populated in Gamow-Teller decay branches of ^{34}Ar.

In anticipation of ^{34}Ar beams from the ISAC ECR ion source in early 2003, two commissioning runs with radioactive ^{26}Na beams were carried out as part of Expt. 909 during 2002. This isotope was chosen because i) high yields were available from ISAC surface ion sources, ii) the half-life (~ 1.07 s) is similar to ^{34}Ar, iii) the daughter ^{26}Mg is stable, and iv) $\sim 99\%$ of ^{26}Na β-decays are followed by the 1809 keV γ-ray transition in ^{26}Mg, facilitating tests of the γ-ray lifetime technique to be employed for ^{34}Ar. The first requirement was to determine a precise value for the ^{26}Na lifetime. To this end, a ^{26}Na beam was delivered in May to the fast tape system at the ISAC GPS station and its lifetime determined to high precision by the well-established and well-understood 4π gas proportional β counter technique. A sample of the data from a single run from this experiment is shown in Fig. 60. A total of 32 runs were conducted under various experimental conditions to check for systematic effects. The analysis of these data is nearing completion, and will establish the ^{26}Na lifetime at the desired $\pm 0.05\%$ level (20 times better than previously known). During the May run, the ^{26}Na beam was also delivered to the 8π spectrometer at ISAC as the first radioactive beam commissioning of the newly completed low energy beam transport to the 8π.
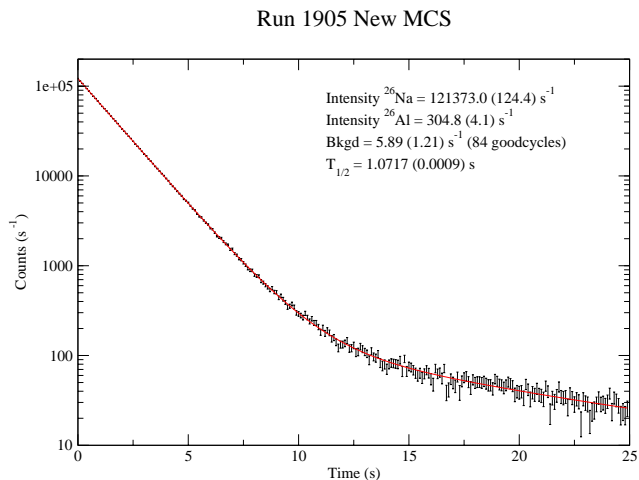
Fig. 60. Decay curve from a single run of β counting ^{26}Na samples with the 4π gas proportional counter at the ISAC GPS station.

With upgrades to the 8π electronics completed in the summer of 2002, a second ^{26}Na experiment was carried out in August, 2002. The spectrum of γ-rays from approximately the first 2.5 hours of collecting continuous ^{26}Na beam at the centre of the 8π is shown in Fig. 61. γ-rays with yields down to $\sim 10^{-5}/\beta$-decay, including many transitions above 5 MeV not previously known in ^{26}Na β-decay, were observed. These data, together with simultaneously recorded high-efficiency γ-γ coincidence data that will establish coincidence relationships between transition in the daughter nucleus, illustrate the power of a large multi-detector such as the 8π spectrometer for performing high-precision branching ratio measurements. The primary objective of the August experiment, however, was to test the γ-ray lifetime technique. For the majority of the experiment, samples of ^{26}Na ions were thus collected during a brief (~ 1 s) beam-on period and their
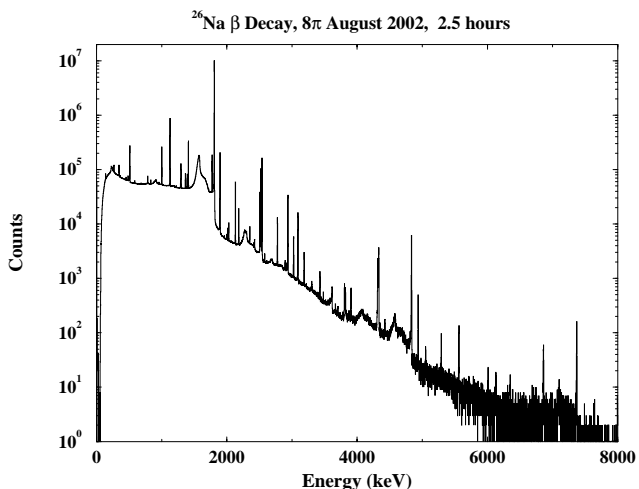
Fig. 61. γ-ray spectrum from ~ 2.5 hours of continuous ^{26}Na beam to the 8π spectrometer at ISAC.

^{26}Na β Decay, 8π August 2002

Average DeadTime Corrected

Total Gamma Activity
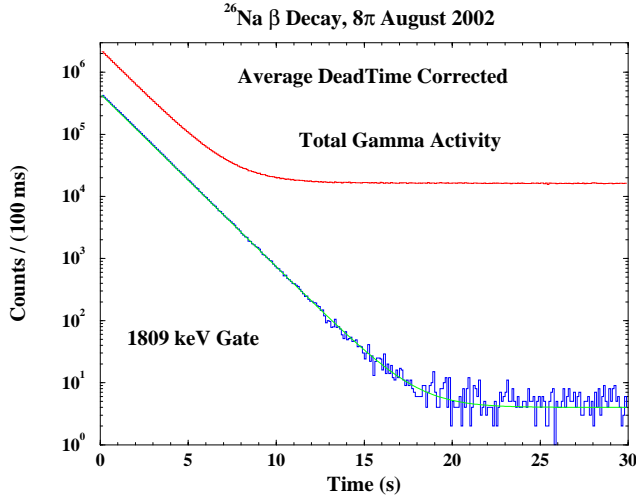
1809 keV Gate

Fig. 62. Summed γ-ray decay curves from a single run of the August ^{26}Na experiment with the 8π spectrometer at ISAC. The upper curve is the total γ activity, while the lower curve has been gated on the photopeak of the 1809 keV transition in the daughter ^{26}Mg.

decay then followed over a 30 s (28 half-lives) beam-off period. Figure 62 shows the data from a single run of this experiment. While the total γ activity in the HPGe detectors of the 8π becomes dominated by room background after about 8 half-lives, the decay curve measured in coincidence with the 1809 keV photopeak from ^{26}Mg provides more than 16 half-lives before the background is reached. This single run provides a statistical precision of ±0.05% for the ^{26}Na half-life. A total of 36 runs under intentionally varied experimental conditions were performed during the August experiment. These data are currently being analyzed to constrain systematic effects associated with the γ-ray lifetime technique that will be used to perform the high-precision lifetime measurement for the superallowed emitter ^{34}Ar when beams from the ISAC ECR ion source become available in early 2003.

Following measurement of the ^{34}Ar lifetime, subsequent measurements with the 8π and SCEPTAR will focus on an improved determination of the ^{34}Ar superallowed branching ratio. Large, and model-dependent, isospin symmetry-breaking corrections are also predicted for the $A \geq 62$ odd-odd $N = Z$ nuclei. A program of precision lifetime measurements (Expt. 823) for these nuclei with the 4π gas proportional counter at the ISAC general purpose station is being led by G.C. Ball of TRIUMF. Future experiments with the 8π spectrometer and SCEPTAR will provide branching ratio measurements for these short-lived isotopes. Weak non-analogue Fermi decay branches that provide direct, and absolute, information on one component of the isospin symmetry breaking will also be measured. Initial measurements of ^{74}Rb decay by our collaboration with a single HPGe detector have identified a num-

ber of high-energy γ-rays from excited states in the daughter ^{74}Kr [Piechaczek *et al.*, submitted to Phys. Rev. C]. The high γ-γ efficiency of the 8π spectrometer will be used to clarify the coincidence relationships between these γ-rays and identify further γ-ray transitions following weak Gamow-Teller decay branches, with the aim of establishing the superallowed branching ratio at the ±0.05% level. With the continued development of ion source technology at ISAC, these superallowed and non-analogue Fermi β-decay branching ratio studies will be extended to include ^{62}Ga and ^{70}Br.

Experiment 925
Isospin mixing in ^{36}Ar via spin-polarized observables in ^{36}K $β^+$ decay
(J.A. Behr, M.R. Pearson, TRIUMF; K.P. Jackson, TRIUMF/SFU)

This experiment would measure the isospin mixing between the first two $I^{\pi} = 2^+$ excited states of ^{36}Ar and the lowest 2^+ T=1 isobaric analogue state, using spin-polarized ^{36}K beta decay observables with TRIUMF's neutral atom trap. The main purpose is to help test isospin mixing models in the *sd* shell needed for determination of the superallowed Fermi strength in $0^+ \rightarrow 0^+$ decays (and hence CKM matrix unitarity), as the calculation's methodology is the same. The β asymmetry A_β and neutrino asymmetry B_ν would show deviations linear in the ratio M_F/M_{GT} produced by isospin mixing from the values of 1/3 and –1/3 predicted if they were pure Gamow-Teller transitions.

^{36}K was successfully trapped, the shortest-lived isotope ($t_{1/2}$=0.34 s) for which neutral atoms have been trapped. ^{36}K was produced from the TiC target at ~1×10^6/s, which allowed trapping and initial tests but was insufficient for the isospin mixing experiment. The additional Ti:sapph when frequency-locked is expected to produce 3× more capture efficiency, and we had better ^{36}K/^{37}K production ratio for Ca. There are conceptual designs for CaZrO$_3$/Zr foil hybrid targets to handle more beam than the 2.5 μA limit of our CaZrO$_3$ ceramic target.

To do a viable experiment for A_β in ^{36}K, $β^+$ tracking is needed to ensure the atoms decay from the trap volume. We intend to build Be-windowed wire chambers for this purpose. We did not polarize ^{36}K, but tests done with polarized ^{37}K demonstrated the difficulties of measuring A_β with a trap. The trap has a lifetime for stable species of 45 s, limited by the 3×10^{-10} torr vacuum, so some atoms decay from the walls and not from the trap, producing β singles backgrounds. Shown in Fig. 63 is the effective asymmetry measured as a function of vacuum, with vacuum deliberately spoiled to enhance this effect. A correction of ≈1% can be deduced by extrapolating to the known ^{37}K decay rate
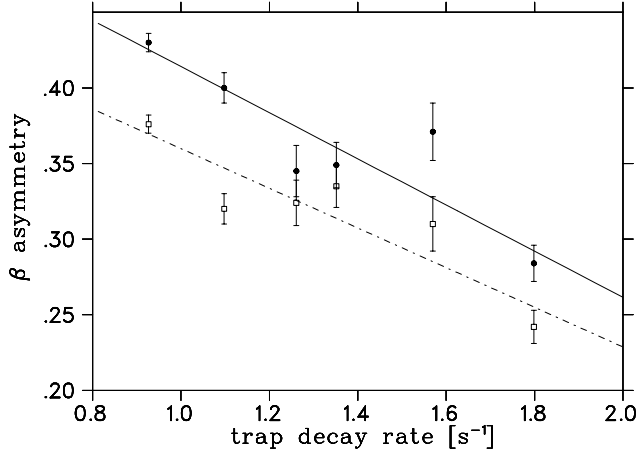
Fig. 63. The measured ^{37}K β singles asymmetry as a function of trap lifetime for the two CaF$_2$(Eu) detectors. This demonstrates the difficulty of measuring β singles to the accuracy required for ^{36}K isospin mixing experiments without β^+ tracking.

Fig. 64. Hyperfine structure of $S_{1/2}$ F=5/2 to $P_{3/2}$ F=7/2, 5/2, 3/2 states in ^{36}K, as measured by resonant excitation with the trap off followed by non-resonant photoionization.

Fig. 65. Deduced ^{36}K charge radius plotted with potassium isotopes previously measured at TRIUMF and at ISOLDE [Mårtensson-Pendrill *et al.*, J. Phys. **B23**, 1749 (1990)]. The K isotopes for N < 20 follow the finite-range droplet model (FRDM). The dashed lines show systematic effect of the specific mass shift.

of 0.81 s^{-1} (i.e., no trap losses). The lack of agreement between the two back-to-back detectors is not understood, and implies additional backgrounds.

The same isospin mixing information is contained in B_ν, which can be measured using β-recoil coincidences free of such backgrounds, but this would be severely statistics limited at present rates.

Polarization of ^{36}K was not attempted. The M.Sc. thesis of O. Aviv from Tel Aviv is to extract the $\beta - \nu$ correlation parameter a from the Gamow-Teller and the analogue transitions to the accuracy allowed from the present 600 coincidences measured. Momentum reconstruction techniques developed for the ^{38m}K experiment are being used to separate the different final states.

The optical hyperfine structure needed for future optical pumping was measured, from which the charge radius and the quadrupole moment can be derived. USD calculations [Brown, private communication] predict the quadrupole moment to be an order of magnitude smaller than for other potassium isotopes, and our preliminary result is not in agreement. We show the preliminary result for the ^{36}K measurement in Fig. 64 and the deduced ^{36}K charge radius in Fig. 65. The charge radii for N < 20 are in agreement with the finite range droplet model, in contrast with those for N > 20. These data were taken in 8 hours, with ~20 atoms trapped, and demonstrate the sensitivity of our two-step photoionization methods to perform accurate atomic spectroscopy on small numbers of atoms.

Experiment 928
Level structure of ^{21}Mg: nuclear and astrophysical implications
(A. Murphy, Edinburgh)

The TUDA collaboration is pleased to announce that Expt. 928 successfully took data in November. Good statistics were accrued with all necessary stable and radioactive beams, and analysis of the data taken is currently progressing.

The objective of the experiment was to measure the parameters of states in the resonant ^{21}Mg nucleus, which determine the ^{20}Na$(p,\gamma)^{21}$Mg reaction rate. This reaction is thought to be an integral link in

62

the path of breakout from the hot-CNO cycle to the rp-process that may occur in novae and X-ray bursts. Furthermore, accurate knowledge of these excited states may be compared to those of isobaric analogue states and thus a study of the Thomas-Ehrman shifts made.

In order to determine the parameters of resonant states in ^{21}Mg, resonant elastic scattering of protons was employed. Experimentally, this consisted of impinging a radioactive ^{20}Na beam on to a hydrocarbon foil, and then detecting the recoil protons. The beam was generated by ISAC, using a primary silicon-carbide target with a driver beam of typically $20\,\mu$A of 500 MeV protons. Typical beam currents on target in the TUDA chamber were a few pA, and during the experiment beam energies of 1.25 MeV/u and 1.60 MeV/u were requested. Accurate confirmation of the beam energies was assured by making measurements in both the Prague magnet, and then cross checking with the DRAGON spectrometer. This consisted of sending the beam in to each device and focusing the beam on to a set of exit slits (after the first magnetic dipole in the case of DRAGON), and then measuring each independently calibrated field. For the higher beam energy, where the maximum rigidity of the DRAGON MD1 magnet was unable to sufficiently bend the beam, this required first introducing gas in to the DRAGON target volume to slow the beam. Measurements of the required magnetic field were performed with various pressures of gas, and an extrapolation to zero gas pressure made. In all cases, an agreement between the beam energy measured with the Prague magnet and with DRAGON of $\sim$1 keV/u was observed.

The target consisted of $\sim$795 μg/cm^2 of CH$_2$. Such a thickness results in a significant spread of energies at which elastic scattering reactions can take place, corresponding to the depth in the target at which the reactions occur. For the lower beam energy, reactions can occur at $\sim$0.51–1.20 MeV in the centre-of-mass, and for the higher beam energy between $\sim$0.91–1.54 MeV.

Detection of the recoiling protons was achieved in two LEDA-design silicon detector arrays. These were placed downstream of the target at 19 and 62 cm. Preliminary spectra of protons observed in detecting elements placed at a laboratory scattering angle of 15.6° are shown in Fig. 66. This shows protons being detected with a range of energies in agreement with that predicted due to the width of the target. Rutherford scattering determines that the yield in general falls off with higher energy, but superimposed on this are three distinct resonances, with approximate energies of 4.01, 4.26 and 4.44 MeV (excitation energy in ^{21}Mg). Observation of the lowest energy state was the primary goal of this experiment. The states at 4.01 and 4.26 had
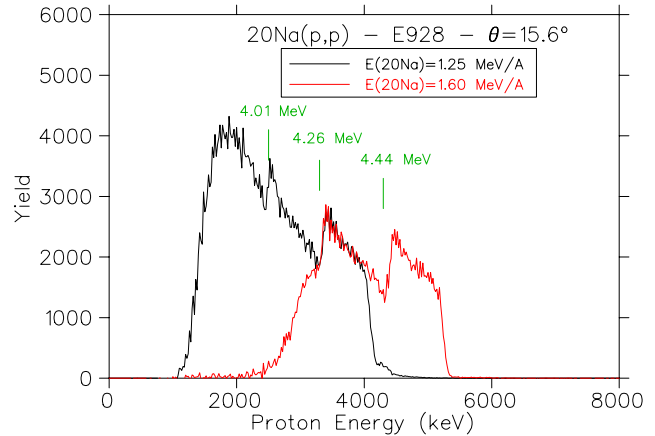
Fig. 66. Preliminary spectrum of proton energy observed in the ^{1}H(^{20}Na,^{1}H)^{20}Na reaction.

already been observed, but the highest energy state is entirely new. Accurate determination of the energies, widths and spins of these states will require R-matrix analysis (multi-channel and allowing the possibility of non-zero angular momentum transfer), and this is currently getting under way.

Experiment 930
π^- capture in water and light materials
(Y. Efremenko, Tennessee; T. Numao, TRIUMF)

Asymmetric production of neutrino species is an essential factor in appearance experiments of neutrino oscillation. The production of $\overline{\nu}_e$ at low energy is thought to be significantly suppressed over that of ν_e; the conventional belief is that π^+'s freely decay but π^-'s, after stopping in the beam moderator, are immediately absorbed by a nucleus without a chance of decay. This results in a large asymmetry in the $\overline{\nu}_e$ and ν_e productions, which is further enhanced by the larger π^+ production cross section by a factor of $\sim$5. However, if a π^- stays long enough either freely or bound in an atomic orbit, it has a chance to decay to a μ^- that would subsequently produce a $\overline{\nu}_e$.

The goal of Expt. 930 is to measure the free-decay fraction of the π^- stopped in water and light materials at a sensitivity of <0.1 %. Direct modes of search are to detect delayed electrons from the decay $\pi^- \rightarrow e\overline{\nu}$ and from the main pion decay mode, the decay $\pi^- \rightarrow \mu^-\overline{\nu}$ followed by $\mu^- \rightarrow e^-\nu\overline{\nu}$, ($\pi \rightarrow \mu \rightarrow e$ chain). The backgrounds come from Compton scattering of radiative pion capture γ-rays for the decay $\pi^- \rightarrow e\overline{\nu}$ and from decay-in-flight of π^-'s in the beam (or muon contamination in the beam) for $\pi \rightarrow \mu \rightarrow e$ chain. Other modes to be sought are $\pi^- + (Z) \rightarrow (Z-1)^* + \gamma$, $\pi^- + p \rightarrow n + \pi^0$, and $\pi^- + O \rightarrow X + p$. These capture modes are almost background-free in the delayed part, but a good time resolution (about 200 ps or better) is required to reach a sensitivity of 10^{-3} in the free-decay fraction.

A 75 MeV/c π^- beam at M9A was stopped at rates of 10–30 KHz in an 8 mm thick water target after passing through two sets of wire chambers and beam counters. The decay (and reaction) products were observed by two arm telescope systems located at $\pm 90°$. Each telescope consisted of three plastic counters spanning about 2–5% in solid angle followed by a large NaI crystal (46 cm$\phi \times$ 51 cm and 36 cm$\phi \times$ 36 cm) placed about 30 cm from the beam axis. Data were taken with a π^- beam as well as a π^+ beam to calibrate the system and provide normalizations. Other possible moderator materials, such as beryllium and aluminum, were tested as well.

In the data analysis, events originating from a pion were selected based on the energy losses in the two beam counters and the time of flight (TOF) with respect to the cyclotron rf phase. Each type of decay product was selected based on the energy loss measurements in the telescope counters and the remaining energy in the NaI detectors.

Figure 67 shows energy spectra of positrons (closed triangles) and electrons (open triangles). The electron spectrum is based on a higher statistic π^- sample by more than an order of magnitude. The peak around 70 MeV in the positron spectrum is from the decays $\pi^+ \to e^+ \nu$, and the bumps around 50 MeV in both spectra are from the $\pi \to \mu \to e$ chain (including the contribution from muons in the beam). For the measurements of proton time spectra, the time zero position was corrected for the time walk, momentum dependences (beam and proton) and TOF. Figure 68 shows a time spectrum of protons after π^-

Fig. 68. Time spectrum of protons after corrections.

capture, which is consistent with a gaussian distribution with $\sigma \sim$ 200 ps. No events in the region $t > 5$ ns were present in the spectrum. This preliminary result indicates that the free-decay fraction of the π^- in water is <1%. A preliminary study of the decay $\pi^- \to \mu^- \to e^-$ also provided a similar limit. The analysis that aims for a sensitivity of <0.1% is in progress.

Other studies with the 8π spectrometer

Several nuclear physics experiments have been performed with the 8π γ-ray spectrometer in either off-line or parasitic mode. These are reported below.

The half-life of ^{176}Lu
(G.F. Grinyer, Guelph)

Measurements of the half-lives of certain long-lived isotopes are typically dominated by experimental uncertainties in detector efficiencies, solid-angle coverage, internal conversion, self-absorption, angular correlations and true-coincidence summing. In particular, published half-life values for ^{176}Lu, of interest for geochronological studies, range from 21 to 73 billion years and show scatter far greater than the experimental uncertainties. As a result, the precision of Lu-Hf deduced ages is currently limited by uncertainties in the ^{176}Lu decay constant. We have employed a unique γ-γ coincidence method that takes advantage of the inherent symmetry within the 8π γ-ray spectrometer at ISAC, and eliminates many of the above uncertainties. The experiment was performed in February, 2002, and was the first on the 8π since its relocation to TRIUMF in 2001. A small sample of enriched Lu_2O_3 powder was placed at the centre of the 8π array and data were

Fig. 67. Energy spectra of positrons (closed triangles, connected) and electrons (open triangles).

taken for 48 hours live time. Our method reduces the calculated corrections to only 3% and led to the result $T_{1/2} = 40.8 \pm 0.3$ billion years [Grinyer *et al.*, Phys. Rev. C (in press)] which is now sufficiently precise for geochronological work.

The spontaneous decay of ^{178m2}Hf ($T_{1/2} = 31$ y)
(P.M. Walker, TRIUMF/Surrey, UK)

Nuclear isomers provide probes into a variety of nuclear-structure facets [Walker and Dracoulis, Nature **399**, 35 (1999)], especially the interplay between individual-particle and collective modes of excitation. An outstanding isomer is the 31 year, 2.4 MeV state in ^{178}Hf. This, the second metastable state of ^{178}Hf, is designated ^{178m2}Hf. It carries 16 units of angular momentum. On account of its long half-life and high excitation energy, ^{178m2}Hf has attracted much interest. In particular, it has been reported [Collins *et al.*, Phys. Rev. Lett. **82**, 695 (1999)] that the decay of ^{178m2}Hf can be induced by X-rays, opening up the possibility of novel energy-storage devices. However, the issue remains controversial [Ahmad *et al.*, Phys. Rev. Lett. **87**, 072503 (2001)].

The X-ray-induced decay may proceed through new pathways, from the 31 year isomer at 2.4 MeV to the ground state. Also, the known [van Klinken *et al.*, Nucl. Phys. **A339**, 189 (1980)] spontaneous decay path may involve additional weak γ-ray branches, which are important for understanding the breakdown of the K quantum number. (K is the projection onto the nuclear symmetry axis of the total angular momentum.)

In order to clarify the nature of the decay of this exceptional isomer, we have used the 20-Ge detector, 8π Compton suppressed spectrometer at TRIUMF, to obtain a high statistics γ-γ coincidence data set. The 0.4 μCi source of ^{178m2}Hf (provided by SRS Technologies, Alabama) was extracted from a Los Alamos beam dump, and placed at the centre of the 8π spectrometer. No TRIUMF or ISAC beams were involved. The ^{178m2}Hf source also contained ^{172}Hf ($T_{1/2} = 1.9$ years) with an approximately equal decay rate. More than 10^9 two-fold γ-γ coincidence events have been recorded during four weeks of data-taking, including, for each event, the relative γ-ray times over a $2\,\mu$s range.

Preliminary analysis of the data has revealed two new γ-ray transitions emitted directly from the 31 year isomer, each accounting for about one part in 10^4 of the total decay rate. One is a 310 keV transition with M4 multipolarity, and the other is a 587 keV, E5 transition. The observation of these two high-multipolarity, K-forbidden transitions establishes the quality and sensitivity of the new data set. Other possible transitions are under investigation.

The β decay of ^{150g}Eu ($T_{1/2} = 36$ y)
(P. Schmelzenbach, Oregon State)

Numerous studies have been made of nuclei that are sufficiently far enough away from a closed shell that they exhibit collective behaviour. In the past, and now recently, there has been particular interest in such a region of nuclei with 90 neutrons. In these nuclei, the addition or removal of a pair of neutrons results in a sudden change in nuclear properties. The onset of this transition is observed in nuclei with 88 neutrons. By studying N = 88 nuclei, a more stringent test can be applied to transition models. In particular, it is important that nuclear levels and γ-ray intensities be well known, especially those below the pairing energy of about 2 MeV. In an effort to establish a more correct level scheme for ^{150}Sm, nuclear levels of ^{150}Sm were studied through the β decay of ^{150}Pm ($T_{1/2} = 2.9$ h, Q = 3454 keV, $J^\pi = 1^-$), ^{150m}Eu ($T_{1/2} = 12.8$ h, Q = 2303 keV, $J^\pi = 0^-$), and ^{150g}Eu ($T_{1/2} = 35.8$ y, Q = 2261 keV, $J^\pi = 5^-$). In combination with other experiments, these β decay experiments are particularly useful in determining levels because of the parent's various spins, and Q values. The three parent nuclei were all produced at the 88″ cyclotron located at Lawrence Berkeley National Laboratory. The short-lived parent nuclei were counted in 1999 at the 8π, then located at LBNL. This particular study investigated the levels of ^{150}Sm, populated through the beta decay of ^{150g}Eu ($T_{1/2} = 35.8$ y). This source was allowed to cool for 3 years. A portion of this source, with an activity of 6.8 μCi, was counted for a total of 175 h in December, 2002 at TRIUMF using the 8π spectrometer. Preliminary results have revealed approximately 165 γ-rays placed in a consistent level scheme (including about 35 new γ-rays previously unreported from this decay.) No new levels have been proposed below 2 MeV based on this decay, although some known levels have been seen for the first time from the long-lived europium. Further analysis, including angular correlations, may help determine uncertain spin assignments for some of these levels.

β-decay of ^{11}Li
(F. Sarazin, TRIUMF)

The structure of ^{11}Li, a ^{9}Li core surrounded by two distant neutrons (the so-called halo), has been investigated in many different ways in the past two decades to improve our understanding of the halo wave function. Among them, the study of the ^{11}Li β-decay has provided very useful information on how the halo wave function influences the weak interaction process. It has also been found that the daughter nucleus, ^{11}Be, has an abnormal level sequence, suggesting an inversion of the $1p_{1/2}$ and $2s_{1/2}$ single particle neutron orbits. However, discrepancies in γ-ray intensities exist among

these previous experiments, mostly due to low statistics and large background. A more precise study of the ^{11}Li β-decay is likely to resolve these discrepancies and bring new insights on these two important topics.

In August, a beam of ^{11}Li was implanted into a thin Al foil at the centre of the array of 20 HPGe detectors comprising the 8π γ-ray spectrometer. In this experiment, the ^{11}Li β-decay was investigated for the first time with a high-efficiency γ-array of Compton-suppressed germanium detectors. A total of 8.1M γ-singles and γ-γ coincidence events were collected over a 2.5 day period.

Because of the very neutron-rich nature of ^{11}Li and ^{11}Be, their mass difference is quite large (Q_β = 20.61 MeV) and their neutron separation energies are low (S_n = 0.503 MeV for ^{11}Be). Therefore, the ^{11}Li β-decay leads almost exclusively to unbound states in ^{11}Be, which subsequently decay mainly by neutron emission. To study these states, one is required to detect the neutron(s) emitted and/or the γ-ray cascades in the corresponding daughter nucleus. In the present case, the dominant β-decay path of ^{11}Li, besides the direct decay to the first and only bound excited state of ^{11}Be, is via β-delayed one-neutron emission into ^{10}Be. The level structure of ^{10}Be is well known up to the one-neutron separation energy at 6.812 MeV (see Fig. 69). It is therefore not necessary to detect the neutron to identify the states that are populated by one-neutron emission in ^{10}Be.
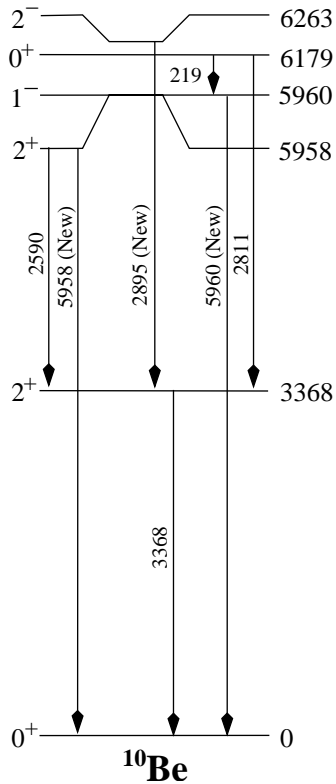
The γ-decay cascades of the ^{10}Be excited states observed in this experiment are shown in Fig. 69. Three new transitions have been observed for the first time in a ^{11}Li β-decay experiment, as a result of the unique capability of the 8π for decay studies.

The relatively high efficiency of the array makes it possible to observe weak branches of the decay, even at high energy. Although observed in other types of experiment, a transition at 5.96 MeV has been observed for the first time following the β-decay of ^{11}Li. It could have been assumed that only very weak branches would remain to be seen at lower γ-energy. However, thanks to the Compton suppressed configuration of the array, a new transition, shadowed in previous experiments by the strong contribution of the single escape peak of 3368 keV, has been observed at 2895 keV (see Fig. 70). This 2895 keV transition is a signature that the 6263 keV 2^- state is fed by a neutron branch never observed before.

The relative intensities of the γ-rays observed in this experiment for the β-decay of ^{11}Li are about a factor of 10 more precise than previous data [Morrissey *et al.*, Nucl. Phys. **A627**, 222 (1997)], sufficient to resolve previous discrepancies.

To push the analysis further, the neutron energies are required to determine which states in ^{11}Be are linked with which states in ^{10}Be. In this experiment, we are investigating the possibility of deducing the neutron energy information from the lineshape analysis of the γ-peaks recorded with the 8π spectrometer. Indeed, as can be seen in Figs. 70 and 71, these peaks display Doppler-broadened lineshapes, due to the ^{10}Be momentum kick induced by the β-delayed neutron emission. The lineshapes observed for the γ-decay of a given excited state in ^{10}Be depends on the relative intensities

Fig. 69. Level scheme of ^{10}Be below S_n = 6.812 MeV and γ-transitions observed in this experiment.
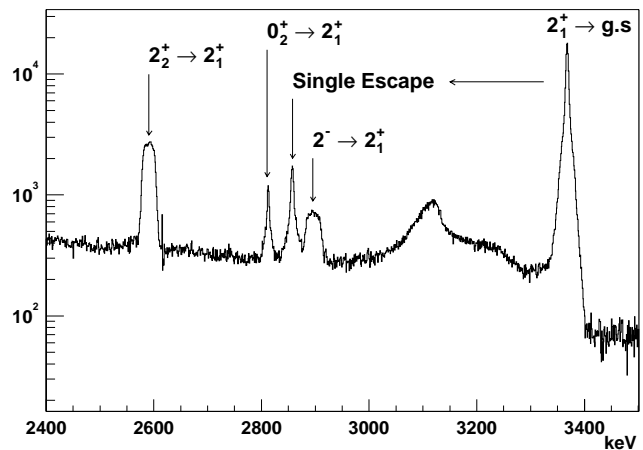
Fig. 70. γ-transitions in ^{10}Be observed in the 2.4–3.5 MeV range.

66
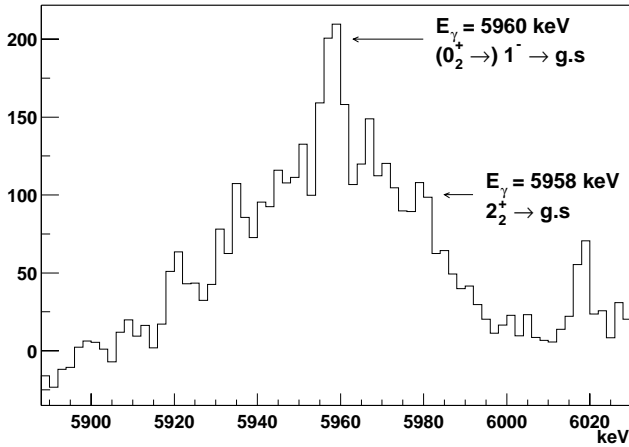
Fig. 71. Structure of the 5.96 MeV peak after room background subtraction.

of all the neutron branches feeding the state either directly or indirectly, and on the lifetimes of the excited states in ^{10}Be involved in a particular decay path. It is possible, in principle, to deduce the neutron energies of these branches from a careful lineshape analysis. A Monte Carlo simulation is under development to reproduce the lineshapes of the peaks of interest and possibly extract new information such as lifetime measurements of excited states in ^{10}Be and/or previously unobserved neutron branches.

In the meantime, one can already immediately extract information from the lineshape of the 5.96 MeV peak. As shown in Fig. 71, the lineshape of the 5.96 MeV peak clearly displays 2 separate components: a broad one corresponding to the decay of the short-lived ($\tau < 55$ fs) 5958 keV state and a sharper one corresponding to the longer-lived ($\tau \sim 800$ fs) 6179 keV state, which is observed to decay to the 5960 keV level (see Fig. 69).

The present study is complementary to Expt. 903 (Shimoda *et al.*), also being performed at ISAC, which makes use of a polarized ^{11}Li beam to measure β-n and β-n-γ coincidences and deduce the spin and parity of the excited states populated in ^{11}Be. The comparison between our lineshape analysis and the Osaka data should provide a more detailed understanding of the ^{11}Li β-decay through β-delayed one-neutron emission.

LANSCE Experiment NPDGamma
Measurement of the parity-violating gamma asymmetry A_γ in the capture of polarized cold neutrons by para-hydrogen, $\vec{n} + p \rightarrow d + \gamma$.
(S.A. Page, W.D. Ramsay, Manitoba)

Introduction

Despite several decades of intense experimental and theoretical effort, the strength of the pion exchange contribution to the weak nuclear force [Desplanques *et al.*, Ann. Phys. **124**, 449 (1980)] remains a mystery. The most precise measurements to date from parity mixing in ^{18}F [Page *et al.*, Phys. Rev. **C35**, 1119 (1987); Bini *et al.*, Phys. Rev. Lett. **55**, 795 (1985)] indicate a coupling constant consistent with zero, in contrast to a relatively large value implied by measurements of the anapole moment of ^{133}Cs via atomic parity violation. The np system is the only two nucleon system that is sensitive to the weak meson-nucleon coupling f_π^1 and can provide a clean measurement free of nuclear structure uncertainties. The up-down γ-ray asymmetry relative to the neutron spin direction in the reaction $\vec{n} + p \rightarrow d + \gamma$ at very low energy is sensitive almost exclusively to f_π^1. Previous measurements [Cavaignac *et al.*, Phys. Lett. **B67**, 148 (1977); Alberi *et al.*, Can. J. Phys. **66**, 542 (1988)] of A_γ failed to reach sufficient precision to test model predictions, and set only upper bounds that were less definitive than the ^{18}F experiments noted earlier. Advances in techniques for producing high intensity beams of polarized, cold neutrons now make possible for the first time a measurement of A_γ and hence f_π^1 to within 10% of model predictions [Desplanques *et al.*, Ann. Phys. **124**, 449 (1980); Bowman *et al.*, experiment proposal: "Measurement of the Parity-Violating Gamma Ray Asymmetry A_γ in the Capture of Polarized Cold Neutrons by Para-Hydrogen, $\vec{n}+p \rightarrow d+\gamma$", submitted to the US DOE (1998); Wilburn and Bowman, Phys. Rev. **C57**, 3425 (1998), and references therein].

The $np \rightarrow d\gamma$ experiment [Bowman *et al.*, *op. cit.*; Wilburn and Bowman, *op. cit.*] will be the first of a new program of fundamental electroweak symmetry experiments to be run at the Lujan Center spallation neutron source at LANSCE, Los Alamos National Laboratory. An international team from 12 scientific institutions has been assembled to prepare the experiment.

Two University of Manitoba researchers (S.A. Page and W.D. Ramsay) joined the collaboration in the fall of 1999. We have taken responsibility for precision monitoring of the neutron beam flux, and have designed a new current mode beam monitor that was tested successfully in the fall of 2001 at LANSCE. Three additional beam monitors based on this new design are currently under construction for the experiment. During the past year we expanded our role, with vital infrastructure support from TRIUMF, to include design and construction of an integrated stand for the gamma detector array and liquid hydrogen targets. TRIUMF also engineered a computer controlled motion system to move the CsI array horizontally and vertically by precisely determined distances up to ± 5 mm. The Manitoba/TRIUMF group will work on commissioning of the apparatus and on diagnosis and minimization of systematic errors. The experiment is sched-

uled for installation and testing during 2003, followed by a full calendar year of data-taking.

Apparatus

The basic requirements of the experiment are an intense source of polarized cold neutrons, a liquid para-hydrogen target, a high-efficiency, large solid angle γ-ray detector, and a means of reversing the spin of the neutron beam with minimal effect on other beam properties. At LANSCE, the neutron beam will be produced by a 200 μA 800 MeV proton beam pulsed at 20 Hz impinging on a tungsten spallation target; MeV neutrons emerging from the target will be cooled in a liquid hydrogen moderator and transported via a supermirror guide to the experimental apparatus (Fig. 72), where they will emerge with a time-of-flight distribution indicated in Fig. 73. The supermirror guide will enhance the total neutron flux in the desired energy range (0–15 meV) by about a factor of 3 with respect to the Maxwellian distribution of neutrons emerging from the moderator. The pulsed beam enables the neutron energies to be determined from their times of flight.

Neutrons will be polarized in the vertical direction by selective transmission through a nuclear-polarized ^{3}He gas cell which acts as a spin filter, producing the energy dependent polarization spectrum indicated in Fig. 73. The neutron beam intensity will be measured with a ^{3}He/N$_2$ ionization chamber before the ^{3}He cell, and again at the end of the beam line with a similar device. A third beam monitor will be inserted downstream of the ^{3}He cell for diagnostic purposes; the transmission of the ^{3}He cell serves as an on-line measurement of its polarization and hence that of the neutron beam.
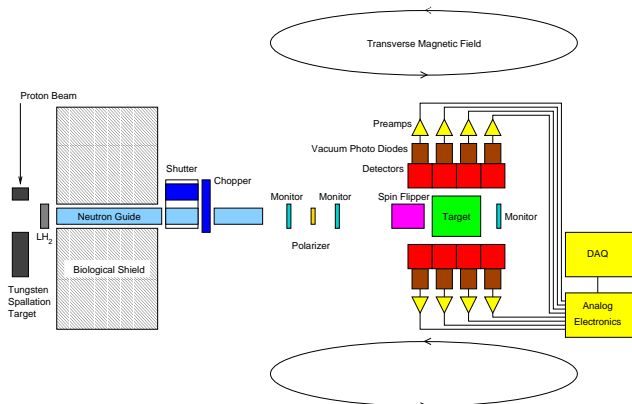
Fig. 72. $np \rightarrow d\gamma$ experimental apparatus at LANSCE. Cold neutrons from the LH$_2$ moderator travel through a supermirror neutron guide, are polarized by a polarized ^{3}He spin filter and are captured in the liquid para-hydrogen target. The 2.2 MeV capture γ-rays are detected by an array of CsI(Tl) crystals.
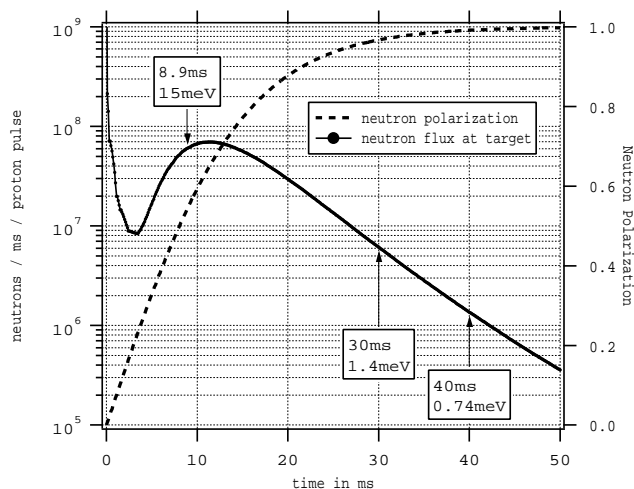
Fig. 73. Cold neutron beam flux and polarization for $\vec{n}+p \rightarrow d+\gamma$, assuming a 15 m flight path. Neutrons arriving early in the frame with energy >15 meV are energetic enough to excite para-to-ortho transitions in the target, so there is no physics asymmetry during this time. After 40 ms, a frame overlap chopper will block slow neutrons. (For the 22 m flight path of FP12, 40 ms will correspond to 1.5 meV.)

A uniform vertical guide field, $B_{\rm o} = 10$ G, preserves the neutron beam polarization as it is transported to the liquid hydrogen target. Low energy neutrons depolarize rapidly in ortho-hydrogen, while those below 15 meV retain their polarization in a parahydrogen target; hence, it is important to ensure that the target is prepared and maintained with the very low equilibrium ortho-hydrogen concentration of <0.05%. On-line monitoring of the target transmission provides a measure of the ortho:para hydrogen ratio, since the cross sections for the two species are markedly different. Only 60% of the beam neutrons will be captured in the target; those that scatter through the target walls will be absorbed in a ^{6}Li liner surrounding the target vessel, and the remaining 15% will be transmitted to the ionization chamber at the end of the beam line for monitoring purposes.

The 2.2 MeV γ-rays from neutron capture in the target will be detected with an array of 48 (15 cm)^3 CsI(Tl) crystals read out in current mode by vacuum photodiodes coupled via low noise I-V preamplifiers to transient digitizers. The time-of-flight information from the CsI detectors will allow the γ-ray asymmetry A_γ with respect to the neutron spin direction to be deduced as a function of incident neutron energy; A_γ should be constant, but the experimental asymmetry $\varepsilon = P_n A_\gamma$ will reflect the energy dependence of the beam polarization from Fig. 73. A beam chopper will eliminate frame overlap by blocking the low energy tail of the flux distribution, which would otherwise be superposed on the spectrum of fast neutrons from the next beam pulse. A resonant rf spin flipper upstream of

the target will reverse the direction of the neutron spin every beam pulse according to a $+--+-++-$ reversal pattern, cancelling systematic drifts to second order. The expected asymmetry is $A_\gamma = -5 \times 10^{-8}$ based on the best available theoretical predictions [Bowman *et al., op. cit.*; Wilburn and Bowman, *et al., op. cit.*], and we plan to measure A_γ to $\pm 5 \times 10^{-9}$ with systematic errors less than 5×10^{-10}.

Prototype beam monitor

During 2001, a prototype beam flux monitor was constructed according to our specifications by LND, Inc., of Oceanside, NY. The beam monitor is a parallel plate ionization chamber with 12×12 cm^2 active area. It was filled by LND with a gas mix consisting of 50% N$_2$ and 50% ^{3}He at 1 standard atmosphere. The chamber consists of an outer aluminum box with entrance and exit windows each 1 mm thick, and it contains 3 internal aluminum electrodes, each 0.5 mm thick for a total of 3.5 mm Al. The outer box and central internal electrode are grounded; the other electrodes are intended to be biased at –5 kV. A current signal is derived from the sum of the ionization collected when neutrons are captured on the ^{3}He in either of the two central 1 cm gaps, as indicated in Fig. 74.

Neutron capture on ^{3}He produces a triton, a proton, and 0.77 MeV of kinetic energy. Not all of the kinetic energy released contributes to the ionization signal, because of the finite detector geometry. To design the beam monitor, a simple Monte Carlo program was written to simulate the capture of neutrons and collection of charge in the ionization medium. The program calculates the distribution of energies deposited in the detector for a uniform flux of incident neutrons distributed over a given area. For fixed detector dimensions, the mean of this distribution decreases, and the variance increases slightly, with increasing beam size. The additional noise due to the variance of the energy deposited per neutron is given by $\sqrt{1 + (\sigma/E)^2}$. This noise factor depends only weakly on the choice of filling gas and the transverse detector size, for reasonable options that were considered in the design.
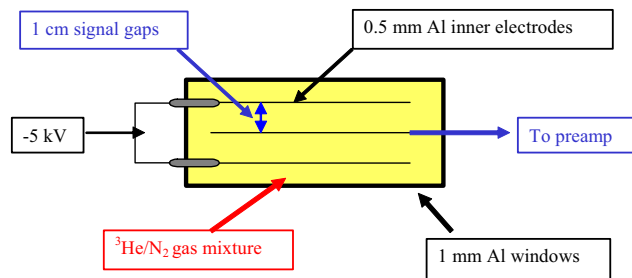
Fig. 74. Sketch of the LND 27527 prototype monitor. The beam enters vertically in this orientation. For the upstream monitors, enough ^{3}He is added to capture about 1% of the neutrons.

For the upstream monitors in the NPDGamma experiment, we plan to absorb about 1% of the beam to produce the signal. This corresponds to about 22 torr of ^{3}He in N$_2$ at 1 Atm. The reason for choosing a relatively heavy filler gas is to maximize the energy that is deposited in the sensitive region, and hence also to minimize a slow contribution to the current signal that would result from ionization occurring in the low field regions between the edges of the inner electrodes and the outer can. The lower ion mobility is compensated for by operating the chamber at a higher voltage than would be necessary with a lighter gas. At –5 kV, the response time for the 1% detectors is estimated to be 80 μs.

Test run data

A first look at M1 at the beginning of the test run produced the scope plot shown in Fig. 75. Note the significant frame overlap indicated by the tail at the start of the beam pulse. The plot is averaged over 8 beam pulses at 54 μA proton current. The Al Bragg edges at 14.1 and 16.3 ms locate the detector at 14.05 m from the source. The maximum signal is 2.7 volts at 16.9 ms, corresponding to an energy of 3.6 meV. The capture probability at 3.6 meV is 0.223. The preamp feedback resistor was 5.0 MΩ. From these data, we deduce the test run neutron flux at 3.6 meV to have been 1.4×10^6 neutrons/ms/pulse.

A detailed comparison of the fluctuations in the beam monitor signals for the prototype monitor M1 and the reference monitor M2 was carried out. The integrated charge between 2 and 40 ms within a beam pulse was recorded, and the variance in the ratio of integrated charges, R=(M1/M2), was used to assess the intrinsic noise in the two monitors, in
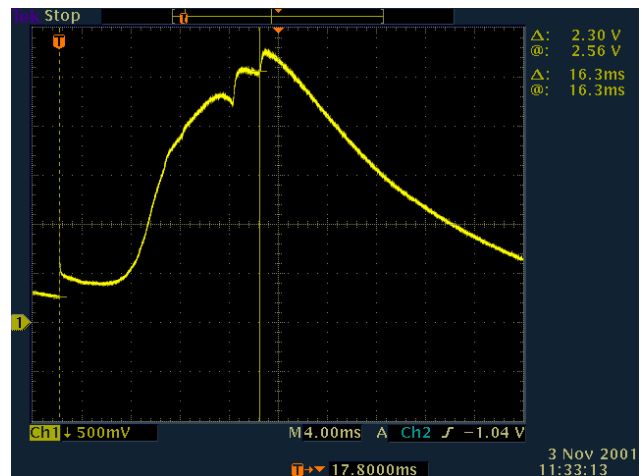
Fig. 75. Digital scope plot from prototype monitor during the test run. No frame overlap chopper was in operation, so some overlap is seen at the start of the frame. The two notches near the top are Bragg edges from aluminum.

69

comparison with model predictions. It was found that $\sigma_R/R = 1.0 \times 10^{-3}$, which compared well with a prediction of 0.9×10^{-3} based on the expected number of neutrons detected by the two monitors in this time window (N1, N2) and the predicted noise factors $1.1/\sqrt{N1}$ and $1.2/\sqrt{N2}$ respectively.

Finally, an absolute comparison of the neutron flux at 3.12 meV was carried out, using the prototype monitor M1, the reference monitor M2, and a ^{6}Li-doped scintillation counter for normalization purposes. The beam was tightly collimated for these measurements. The resulting flux values at 3.12 meV were deduced to be 36, 33, and 32 kn/ms/pulse for M1, M2 and the ^{6}Li counter respectively, in agreement to within the uncertainties associated with the experimental conditions.

We conclude that the performance of the prototype monitor M1 was entirely satisfactory, with gain and noise characteristics in agreement with expectations. We also found that the design was very insensitive to mechanical vibrations – one could barely detect a change in the output signal when the monitor was struck firmly on the side with a wrench. Very little 60 Hz pickup was experienced with this configuration. Based on the test run results, 3 similar beam monitors, filled to appropriate gas mixtures for the final NPDGamma experiment, have been obtained and are now at LANSCE.

TRIUMF detector stand project

A crucial issue for the experiment is the ability to determine the effective detector alignment, *in situ*, to within ± 20 mr with respect to the magnetic holding field direction, in order to suppress the contribution of a small parity-allowed left-right asymmetry to the parity-violating up-down asymmetry that we are seeking to measure. One possible approach for this determination is to calibrate the detector alignment via a capture reaction with a known and relatively large left-right gamma asymmetry. Part of our test run time was spent searching for such asymmetries in several nuclei which had exhibited significant parity-violating up-down asymmetries, but no suitable candidates were found. An alternative scheme based on scanning a small target within the beam envelope in x and y was explored, but this was found to be unsuitable due to nonuniformities in the beam intensity distribution. As a result, we have concluded that the preferred method to calibrate the detector alignment is to scan the entire detector array in x and y with the liquid hydrogen target in place. This method places stringent requirements on the detector stand design and construction that were not envisioned when the experiment was originally proposed.

As part of our contribution to the project, the Manitoba/TRIUMF team has taken on the responsibility for design and construction of an integrated stand for both the CsI detector array and the liquid hydrogen target. This task relies heavily on crucial engineering and infrastructure support provided by TRIUMF. The design and construction of the stand and motion controller is now complete and the apparatus has been shipped to Los Alamos for final assembly and testing by TRIUMF and Manitoba personnel. A drawing of the integrated stand concept is shown in Fig. 76. Early in the project, one of the 4-detector support panels was shipped to LANL, where it was loaded with detectors and preamps. Deflections under load were within tolerances, as predicted by the FEA analysis of the design undertaken by TRIUMF engineer Tom Ries. Figure 77 shows Tom with the completed CsI array
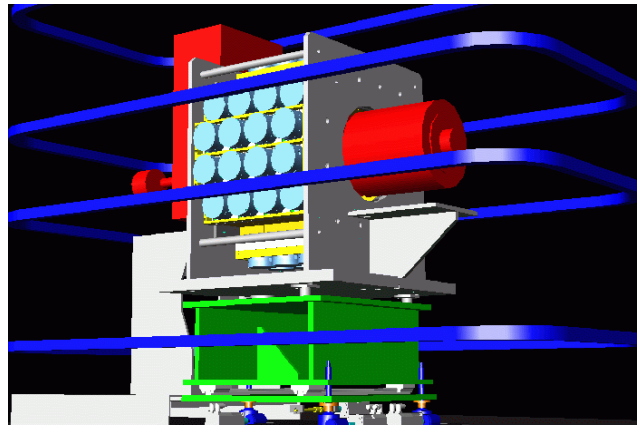
Fig. 76. Drawing of NPDGamma equipment. The CsI array is seen in the centre, supported by the TRIUMF $x - y$ motion stand. The cylinder at the right is the rf spin flipper, which moves with the CsI array. Part of the LH$_2$ target services box is visible at the left. The large horizontal coils provide the 10 G guide field.

Fig. 77. CsI mounting frame during installation in the ER-2 area of Lujan Center.

70

mouning frame. Tom and engineering coop student, Justin Ho, will go to Los Alamos early in 2003 to set up the TRIUMF apparatus.

Future plans

The construction of the beam line is currently under way, and the cave to house the experimental equipment is planned to be ready in late May, 2003. The liquid hydrogen target should be delivered to LANL in early May, 2003, for assembly and mounting on the stand structure (Fig. 76). We will provide manpower for installation and commissioning of the apparatus. The stand assembly was completed at TRIUMF in December, 2002. The experiment is scheduled to be commissioned starting in June, 2003, followed by one year of data acquisition, starting November–December, 2003 and likely spread over 2 calendar years. A new Manitoba graduate student has been recruited and will be starting work in summer, 2003.

Collaborators: C.S. Blessinger, M. Gericke, G.L. Greene, G. Hansen, G.L. Morgan, H. Nann, W.M. Snow (Indiana University); J.D. Bowman G.E. Hogan, J.N. Knudson, S.K. Lamoreaux, G.S. Mitchell, C.L. Morris, S.I. Penttila, D.A Smith, W.S. Wilburn, V.W. Yuan (Los Alamos National Laboratory); R.D. Carlini (Thomas Jefferson National Accelerator Facility); T.E. Chupp, K.P. Coulter, R.C. Welsh, J. Zerger (University of Michigan); M.S. Dewey, T.R. Gentile, D.R. Rich, F.E. Wietfeldt (National Institute of Standards and Technology); T. Case, S.J. Freedman, B.K. Fujikawa (University of California, Berkeley); S. Ishimoto, Y. Masuda, K. Morimoto (KEK National Laboratory, Japan); G.L. Jones (Hamilton College); W.M. Hersman, M.B. Leuschner, V.R. Pomeroy (University of New Hampshire); S.A. Page, W.D. Ramsay (University of Manitoba); E.I. Sharapov (Joint Institute for Nuclear Research, Dubna); T.B. Smith (University of Dayton).

CHEMISTRY AND SOLID-STATE PHYSICS

Experiment 768
Generalized FFLO state and anomaly of flux line lattice state in novel superconductors
(R. Kadono, J. Akimitsu, KEK-IMSS, Aoyama-Gakuin)

The revelation of superconductivity in a binary intermetallic compound, MgB_2, has attracted much interest because it exhibits a transition temperature T_c almost two times higher than those of all other intermetallic superconductors known to date [Nagamatsu, *et al.*, Nature **410**, 63 (2001)]. The most interesting issue associated with this compound is whether or not it belongs to the class of conventional BCS type superconductors. In order to obtain information on the order parameter in MgB_2, we have observed the temperature and field dependence of magnetic penetration depth λ by muon spin rotation.

This μSR experiment was performed on the M15 beam line at TRIUMF using the high time resolution spectrometer Belle which allows μSR measurements up to 5 T. A muon-veto counter system was adopted to eliminate positron events from muons which missed the sample so that the relative yield of such events was less than 5% of the total positron events. The sample was field-cooled at the measured magnetic fields in order to eliminate the effect of flux pinning.

We show the temperature dependence of the muon depolarization rate σ_1 in Fig. 78. These data were obtained under a field $H \simeq 0.5$ T which is well above $H_{c1} \sim 10^{-2}$ T. The data were fitted by the two-gap model [Bouquet *et al.*, Europhys. Lett. **56**, 856 (2001); Ohishi *et al.*, J. Phys. Soc. Jpn., in press]. The solid line in Fig. 78 is the best fit result with Δ_1 = 4.9(1) meV, Δ_2 = 1.2(3) meV, w = 0.84(3) and T_c = 36.48(3) K. The dotted line shows the result of
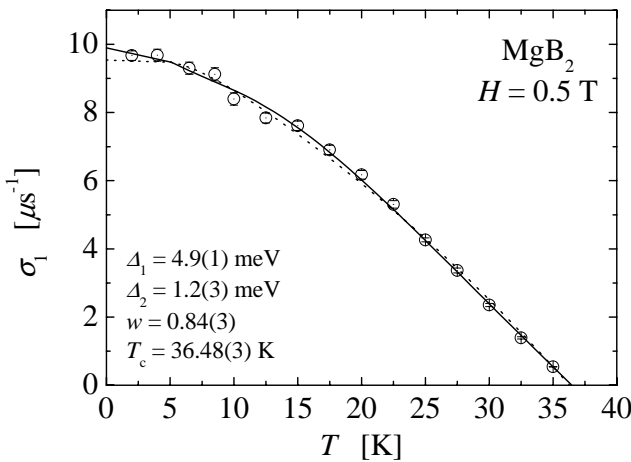
fitting using the values of Δ_1, Δ_2 and w in Niedermayer *et al.* [Phys. Rev. **B65**, 094512 (2002)]. Although our result shows reasonable agreement with Niedermayer *et al.*, the value of Δ_2 is considerably smaller than the reported value of 2.6(2) meV.

The field dependence of λ is shown in Fig. 79. It clearly exhibits a strong field dependence where $\lambda(h)$ increases almost linearly with $h \equiv H/H_{c2}$. This is similar to the cases of YNi_2B_2C [Ohishi *et al.*, Phy. Rev. **B65**, 140505R (2002)], $NbSe_2$ [Sonier *et al.*, Phys. Rev. Lett. **79**, 1742 (1997)] and high-T_c cuprate superconductors [Sonier *et al.*, Rev. Mod. Phys. **72**, 769 (2000)], where the increase of λ is attributed to the anisotropic order parameters and the associated nonlinear effect due to the Doppler shift of the quasiparticles in the nodal region ($\Delta(k) \simeq 0$) [Volovik, JETP Lett. **58**, 469 (1993)]. The field dependence of λ is expected to be stronger when the phase space satisfying $\Delta(k) \simeq 0$ has larger volume. A fitting by the relation $\lambda(h) = \lambda(0)[1 + \eta \cdot h]$ provides a dimensionless parameter η which represents the strength of the pair breaking effect. We obtain $\eta = 1.27(29)$ with $\lambda(0)$ = 116.1(6.2) nm which is shown as the solid line in Fig. 79. The obtained value of η is intermediate between that in YNi_2B_2C and $NbSe_2$ (e.g., $\eta = 0.97$ at $0.2\ T_c$, $\eta = 1.61$ at $0.33\ T_c$, respectively) and is smaller than those in d-wave superconductors (e.g., $\eta = 5.5 \sim 6.6$ for cuprates).

Our result on the temperature dependence of σ_1 is qualitatively consistent with earlier results [Niedermayer *et al., op. cit.*], suggesting that the order parameter in MgB_2 may be effectively described by adopting the two-gap model. However, the observed field dependence of λ is not expected for the isotropic order parameter irrespective of the multiplicity of the

Fig. 78. T dependence of σ_1 at $H \simeq 0.5$ T.
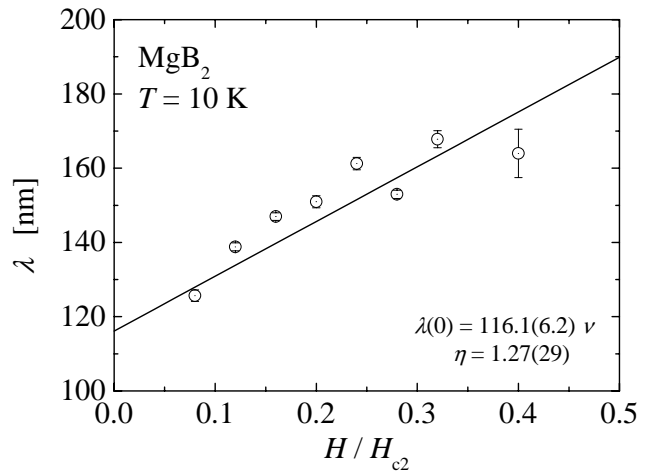
Fig. 79. H dependence of λ at $T \simeq 10$ K.

band structure and the associated gap energy. Considering that the current result on the field dependence of λ was obtained at $T \simeq 10$ K, this energy scale of $\varepsilon \equiv k_B T \sim 1$ meV places an upper boundary on the smaller gap energy Δ_2 in order to explain the observed effect of the Doppler shift. Since our estimation for $\Delta_2 = 1.2(3)$ meV is very close to ε, the observed H-linear behaviour of λ may be attributed to the quasiparticle excitations in the vicinity of the smaller gap. While this cannot be distinguished from the case of a nodal structure in the order parameter (i.e., considering a region where $\Delta(k) \ll \varepsilon$), our result is clearly inconsistent with the two-gap model with $\Delta_2 \gg \varepsilon$. On the other hand, it is also quite unlikely that the d-wave pairing is realized in MgB_2, because the coefficient η is much smaller than those in high-T_c cuprates. The recent observation that the order parameter in YNi_2B_2C (where the pairing symmetry has been identified as s-wave [Shu et al., Phys. Rev. **B54**, 15341 (1996)]) has point nodes [Izawa et al., Phys. Rev. Lett. **89**, 137006 (2002)] exhibits a good correspondence with the intermediate value of $\eta (\sim 1)$ obtained by μSR [Ohishi et al., Phys. Rev. **B65**, 140505R (2002)], suggesting that there is a similar situation in MgB_2. Thus, the present μSR result leads us to conclude that the order parameter in MgB_2 has a structure with an energy gap smaller than $\varepsilon \simeq 1$ meV. The field dependence of λ measured at a much lower temperature would provide more useful information to distinguish the anisotropic order parameter from the isotropic one described by the two-gap model.

In summary, we have performed TF-μSR measurements in MgB_2 to obtain the temperature and magnetic field dependence of the penetration depth λ and the associated spin relaxation rate σ_1. Our result is perfectly in line with the presence of an anisotropic order parameter with a nodal structure, and it sets an upper boundary $\varepsilon \simeq 1$ meV for the smaller gap energy in the two-gap model. The magnetic field dependence of λ exhibits a linear dependence on the external field up to 5 T with the gradient η being considerably smaller than that in d-wave superconductors, which may disfavour the occurrence of d-wave pairing in MgB_2.

Experiment 782
Non-Fermi-liquid behaviour and other novel phenomena in heavy-fermion alloys
(D.E. MacLaughlin, California, Riverside)

Isotropic pairing in superconducting $PrOs_4Sb_{12}$

In most heavy-fermion (HF) metals and superconductors the f ion (Ce, Yb, U) has a magnetic ground state. HF behaviour has, however, been reported in a small number of praseodymium-based alloys and compounds [Yatskar et al., Phys. Rev. Lett. **77**, 3637

(1996)], in which the crystalline electric field (CEF) ground state of the non-Kramers Pr^{3+} ion could be nonmagnetic and degenerate. In this case a charge-scattering analogue of Kondo spin scattering can give rise to the so-called "quadrupolar Kondo effect", an example of the two-channel Kondo effect that has been invoked to explain non-Fermi-liquid behaviour in HF systems [Cox and Jarrell, J. Phys.: Cond. Matter **8**, 9825 (1996)].

Superconductivity has recently been discovered in the cubic HF compound $PrOs_4Sb_{12}$ [Bauer et al., Phys. Rev. **B65**, 100506 (2002)]. From thermodynamic measurements it is found that a large carrier effective mass $m^* \approx 50\, m_e$ characterizes both the normal and superconducting states, and the transition temperature $T_c = 1.85$ K is relatively high for a HF superconductor. Although a conventional spin-based HF mechanism has not been completely ruled out, thermodynamic properties of $PrOs_4Sb_{12}$ suggest a Pr^{3+} nonmagnetic doublet Γ_3 CEF ground state, so that the quadrupolar Kondo effect is a candidate mechanism for the HF behaviour. The symmetry of the superconducting pairing in such a system is a fundamental question.

In general the muon spin relaxation rate is related to the rms width $[\overline{(\Delta B)^2}]^{1/2}$ of the internal magnetic field distribution $n(B)$ in the vortex state of type-II superconductors [Sonier et al., Rev. Mod. Phys. **72**, 769 (2000)]. In turn $[\overline{(\Delta B)^2}]^{1/2}$ is inversely proportional to the square of the magnetic penetration depth λ, which is related to the density n_s of superconducting carriers and m^* by the London equation

$$1/\lambda^2 = 4\pi n_s e^2/m^* c^2 . \tag{1}$$

The temperature dependence of λ at low temperatures is therefore sensitive to the lowest-lying superconducting excitations, the thermal population of which reduces n_s with increasing temperature. In the presence of an isotropic or nearly isotropic energy gap, $\lambda(T) - \lambda(0)$ varies exponentially with temperature, whereas nodes in the gap function characteristic of non-s-wave pairing lead to power-law dependences.

We have carried out zero- and transverse-field μSR experiments in the superconducting state of $PrOs_4Sb_{12}$ using the dilution refrigerator at the TRIUMF M15 beam line. The penetration depth derived from the vortex-lattice field distribution width exhibits the temperature dependence characteristic of isotropic s-wave pairing. Isotropic p-wave pairing, which is indistinguishable from s-wave pairing by thermodynamic or electrodynamic measurements, is also possible. To our knowledge this is the only example to date of an isotropic gap in a HF superconductor. It suggests the possibility of (a) marked differences in superconducting properties between HF materials with magnetic and

nonmagnetic f-ion ground states, and (b) a relation between the pairing symmetry and the mechanism (spin or quadrupole Kondo effect) for the HF normal state from which the superconductivity evolves.

Zero-field μSR experiments were performed to determine whether static magnetism exists in the superconducting state of PrOs$_4$Sb$_{12}$. The zero-field data are well fit by the product of a damping exponential and the Kubo-Toyabe (K-T) function expected from nuclear dipolar fields. The exponential damping rate $W(T)$ is already appreciable in the normal state, increases only slightly more than experimental uncertainty below T_c, and is (negatively) correlated with the K-T rate $\Delta_{\mathrm{KT}}(T)$ in the fitting process. Thus there is no statistically significant evidence for static magnetism below T_c; the present data place an upper limit of ~ 50 μT on any static field below T_c.

The internal field distribution in the vortex state is the convolution of the field distributions due to the vortex lattice and to the electronic and nuclear moments of the host material; by the convolution theorem the muon-spin precession signal is the product of the Fourier transforms of these distributions. The superconducting-state data have been fit to a product of exponential and Gaussian functions, where the latter is taken as an approximation to the relaxation function due to the vortex-lattice field distribution.

The temperature dependence of the Gaussian relaxation rate σ_s is shown in Fig. 80 for an applied field of 200 Oe. Salient features of these data are that $\sigma_s(T)$ varies only slowly at low temperatures, and that the $T = 0$ value $\sigma_s(0) = 0.91(1)$ μs^{-1}. This is large for a HF superconductor and is much larger than changes
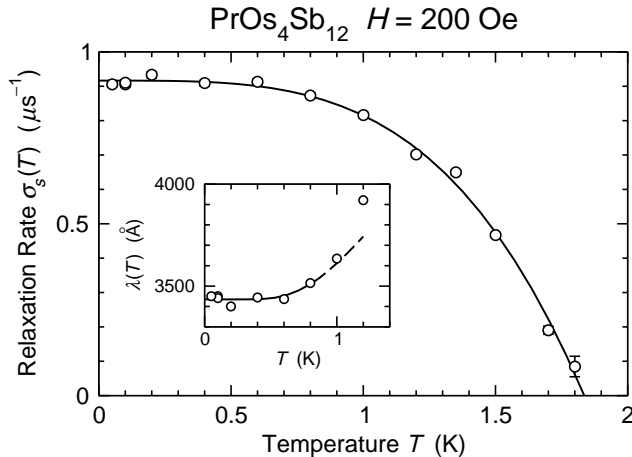
Fig. 80. Temperature dependence of vortex-state μ^+ relaxation rate $\sigma_s(T)$ in the superconducting state of PrOs$_4$Sb$_{12}$. Curve: $\sigma_s(T) = \sigma_s(0)[1 - (T/T_c)^y]$, $\sigma_s(0) = 0.91(1)$ μs^{-1}, $T_c = 1.83(2)$ K, $y = 3.6(2)$. Inset: low-temperature penetration depth $\lambda(T)$ derived from $\sigma_s(T)$. Curve: $\lambda(T) = \lambda(0)[1 + (\pi\Delta/2T)^{1/2}\exp(-\Delta/T)]$, $\lambda(0) = 3440(20)$ Å, $\Delta/T_c = 2.1(2)$, from fit to data for $T \leq 0.8$ K.

in the ZF-μSR rates, so that σ_s is dominated by the vortex-state field distribution.

We obtain λ from σ_s and the expression

$$\overline{(\Delta B)^2} = 0.00371\,\Phi_0^2\lambda^{-4}\,, \qquad (2)$$

appropriate to an isotropic extreme type-II superconductor, where Φ_0 is the flux quantum. The data are shown in the inset to Fig. 80. The BCS low-temperature expression $\lambda(T) = \lambda(0)[1 + (\pi\Delta/2T)^{1/2}\exp(-\Delta/T)]$ was fit to data for $T \leq 0.8$ K $< 0.4\,T_c$; the curve in the inset to Fig. 80 shows this fit and its extension (dashed) up to 1.2 K. The fit value $\lambda(0) = 3440(20)$ Å is short for a HF superconductor. The fit value of the ratio $\Delta/T_c = 2.1(2)$ is somewhat larger than the BCS value 1.76, suggesting strong coupling. Over the entire temperature range $\sigma_s(T)$ is consistent with the phenomenological "two-fluid" temperature dependence $1/\lambda^2(T) \propto 1 - (T/T_c)^4$, although the data are slightly better fit with an exponent of 3.6(2) (curve). All these properties indicate that the gap is isotropic or nearly so. Proportionality between $\overline{(\Delta B)^2}$ and λ^{-4} should survive vortex lattice disorder as long as the distance between vortices is much smaller than λ ($H \gg H_{c1}$); disorder increases the numerical coefficient in Eq. (2) but should not affect the temperature dependence of $\overline{(\Delta B)^2}$.

Early studies of the penetration depth in cuprate superconductors using unaligned powders also observed little temperature dependence of λ at low temperatures, and concluded that the pairing was s-wave [Sonier $et\ al.,\ op.\ cit.$]. Later measurements in high-quality aligned crystals revealed the linear temperature dependence characteristic of d-wave pairing. The early results appear to have been due to a combination of circumstances: strong anisotropy in λ, oxygen inhomogeneity, and sensitivity to hole doping due to the low density n_s of superconducting carriers. None of these factors would seem to affect the current measurements. The crystal structure of PrOs$_4$Sb$_{12}$ is cubic, so that the penetration depth is isotropic. With $m^* \approx 50\,m_e$ we find $n_s \approx 10^{22}$ carriers/cm^3 from Eq. (1), so that PrOs$_4$Sb$_{12}$ is a good metal and the carrier concentration is insensitive to chemical inhomogeneity. Thus it seems unlikely that the observed temperature dependence of $\lambda(T)$ is due to extrinsic effects.

The resistive mean free path ℓ can be calculated from the residual resistivity $\rho(0) \approx 5$ $\mu\Omega$-cm using n_s as an estimate of the normal-state carrier concentration, and can be compared with the superconducting coherence length ξ_0 [Bauer $et\ al.,\ op.\ cit.$]. We find $\ell/\xi_0 \approx 3$, so that PrOs$_4$Sb$_{12}$ is a rather clean superconductor (and Eq. (1), derived in the clean limit, is

valid); this is of importance in the analysis of thermodynamic properties.

The isotropy of the superconducting energy gap indicated by the temperature dependence of σ_s (Fig. 80) strongly suggests that superconductivity in $PrOs_4Sb_{12}$ is in some sense "conventional." In this regard $PrOs_4Sb_{12}$ differs markedly from other HF superconductors studied to date, a difference that may possibly be related to a nonmagnetic or quadrupolar Kondo state in this compound. Better understanding of the quadrupolar Kondo lattice will be needed to elucidate the questions of whether $PrOs_4Sb_{12}$ is indeed such a system and, if so, whether this property is related to the conventional superconducting behaviour.

Experiments 815, 816 and 817: β-NMR
(W.A. MacFarlane, R.F. Kiefl, TRIUMF/UBC)

The positive muon beams at TRIUMF and associated instruments are an excellent way to probe the magnetic properties of bulk materials. Over the past few years we have developed a closely related technique called β-detected NMR which uses the low energy radioactive ion beams from ISAC. These instruments complement muon spin rotation in that they can be used to probe magnetic and electronic properties of nanostructures and ultrathin films. Recently we have commissioned a second β-NMR spectrometer for carrying out nuclear quadrupole resonance in zero static external field. In particular we have observed nuclear quadrupole resonances of ^{8}Li in several crystals such as $SrTiO_3$, Al_2O_3 and Sr_2RuO_4. We anticipate that, as in the case of μSR, the ability to carry out measurements in zero external magnetic field will have significant applications in the area of magnetism and superconductivity. More details are given in the next section.

We also made progress in quantifying the beam spot imaging that we perform with a CCD camera by correlating these images with the β count rates. An example of the light output in a section through the beam spot is shown in Fig. 81, indicating the high quality of the beamspot for this energy and magnetic field.

β-detected pure quadrupole resonance

The most significant advance over the last year is the demonstration of β-detected nuclear quadrupole resonance. Nuclei with spins greater than $\frac{1}{2}$ possess electric quadrupole moments which couple the nuclear spin to the local gradient of the electric field (EFG). In a single crystal for a single site with an axially symmetric EFG, this leads to an effective spin Hamiltonian of the form [see Das and Hahn, *Nuclear quadrupole resonance spectroscopy* (Academic, NY, 1958) for example]: $H_Q = \frac{1}{6}h\nu_Q[3m^2 - I(I+1)]\delta_{mm'}$, where $h\nu_Q$ is the scale of the quadrupolar coupling, I and m are the
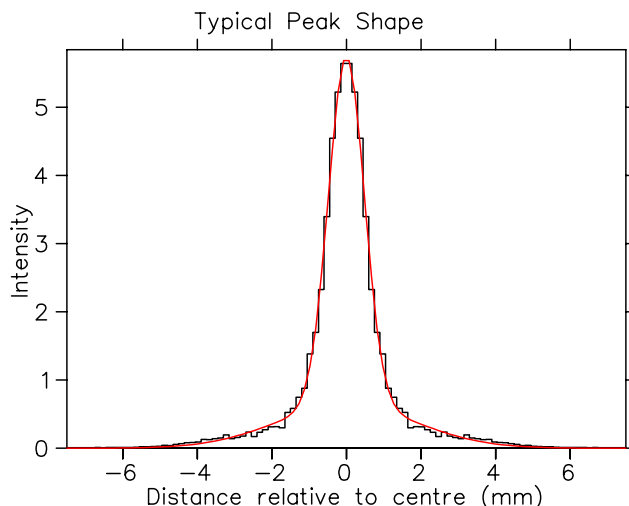
Fig. 81. A quantitative measure of the beam spot as measured by a CCD camera imaging a scintillator mounted at the sample position.

nuclear spin quantum number and the magnetic quantum number with a quantization axis (z) defined by the direction of maximal EFG. The quadrupolar spectrum is thus very simple with just two transition frequencies at $\frac{\nu_Q}{2}$ and $\frac{3\nu_Q}{2}$. Provided the initial polarization has a component in the z direction, then we should observe a resonant loss of the β decay asymmetry when the frequency of H_1 (the oscillating transverse magnetic field) matches the quadrupolar level splitting.

By analogy with conventional nuclear magnetic resonance, we call this zero field technique β-NQR. For light nuclei like ^{8}Li, the nuclear electric quadrupole moment is small ($+32$ mB), so the quadrupole coupling ν_Q is small. For ^{8}Li we expect it to be less than 200 kHz in most cases. These low frequencies were beyond the range of the rf system designed for the high field spectrometer. Consequently we developed a radio/audio frequency irradiation system which can irradiate either with a single frequency ν or an equal combination of ν and 3ν. In the case of high initial polarization, only the $m = \pm 2$ state is initially occupied and irradiation at $\frac{3\nu_Q}{2}$ will yield a small change in the asymmetry as the transition is saturated. To achieve full saturation, i.e. equalization of the populations of the magnetic states, yielding zero asymmetry, we thus require the two frequency irradiation. Figure 82 shows such a signal in an epitaxially prepared $\langle 100 \rangle$ crystal of $SrTiO_3$ at room temperature. We expected this value for ν_Q from our prior observations of quadrupolar splitting of the high field resonance in this material.

Conventional metals

Previously we observed a split resonance of ^{8}Li near the Larmor frequency in high magnetic field (3 T) in Ag and Au. We have proposed that this was due to two distinct Li sites differing in their Knight shifts. In
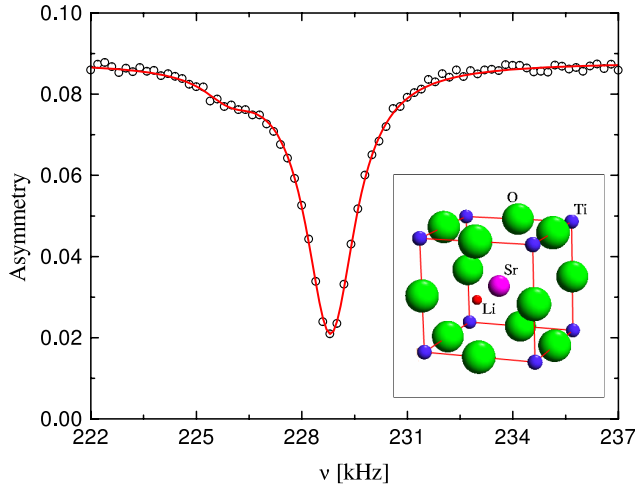
Fig. 82. The β-NQR signal of interstitial ^{8}Li SrTiO$_3$. The spectrum is taken at room temperature in zero applied field.

Fig. 83. The β-NMR signal of interstitial ^{8}Li in a high purity annealed Au foil. These data were taken with 1.7 W of rf power and full beam energy (30 keV). Notice the broad line superimposed on the narrow line at the Larmor frequency which is likely due to Li that is trapped adjacent to an Au vacancy.

order to test this hypothesis it was necessary to carry out measurements in much lower magnetic field (0.3 T) where the back detector has a very small effective solid angle due to the reduced magnetic field. This is now possible since we have also commissioned a new neutral beam monitor (NBM), which detects βs from polarized neutral Li that is not reionized in the He cell of the polarizer. This in turn allows measurements with a single forward detector which can be normalized to the incoming beam rate as measured at the NBM. The NBM is now commissioned and fully integrated into the data acquisition system. The data on Ag were taken at 0.3 T and show a very narrow line at all temperatures. This confirms that the lines at high field are split because of a site dependent Knight shift.

In Ag and Au we have observed the split resonance now in several samples, but in addition only in Au in a temperature range around 225 K, at 0.3 T, we find a broad line in addition to the narrow one corresponding to the 2 cubic sites (unresolved here). Figure 83 shows an example of this line. We speculate that it is due to a transition state, i.e. the Li spends significant time just adjacent to a local-cubic-symmetry-breaking vacancy. It occurs in the same temperature regime where the amplitudes of the two lines we resolve at high field are changing.

Having developed the low frequency capability in order to measure the β-NQR, we also demonstrated that we can observe conventional β-NMR resonances in very small applied magnetic fields. Note the β-NQR spectrometer at the polarimeter station is equipped with a Helmholtz coil, allowing a static field of up to 0.015 T to be applied. Figure 84 shows such a resonance. Conventional NMR relies on thermal polarization of the nuclear spins (unlike the highly athermal polarization produced optically in the ^{8}Li beam), thus resonance in such low fields is nearly impossible.
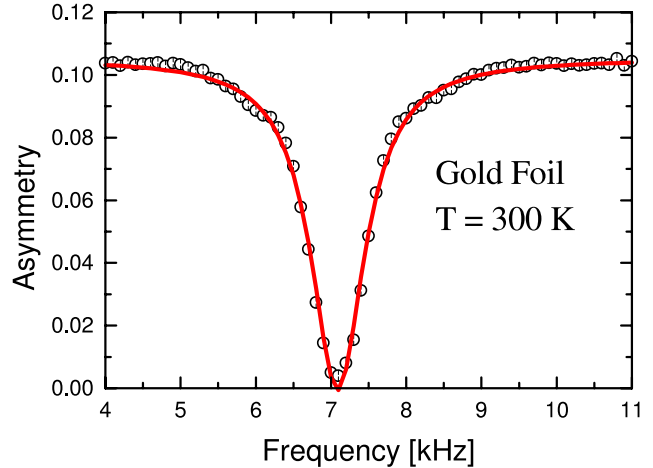
Fig. 84. The β-NMR signal of interstitial ^{8}Li in annealed high purity gold at room temperature in a field of about 11 G.

Superconductors

Recently, we have implanted ^{8}Li near the surface of a conventional superconductor NbSe$_2$. We find a remarkably small quadrupolar frequency ν_Q for interstitial ^{8}Li, even though the crystal is noncubic. From the asymmetry of the resonances for the two nuclear helicities, we estimate that $\nu_Q < 1$ kHz, considerably smaller than what is seen in analogous stable Li intercalation compounds [Prigge *et al.*, Z. Phys. Chem. **189**, 153 (1995)]. Above the critical temperature we observe a single resonance at the Larmor frequency with unresolved quadrupolar effects.

When a type II superconductor is cooled in a magnetic field H, for H in a certain range, the field will become inhomogeneous due to the formation of a lattice
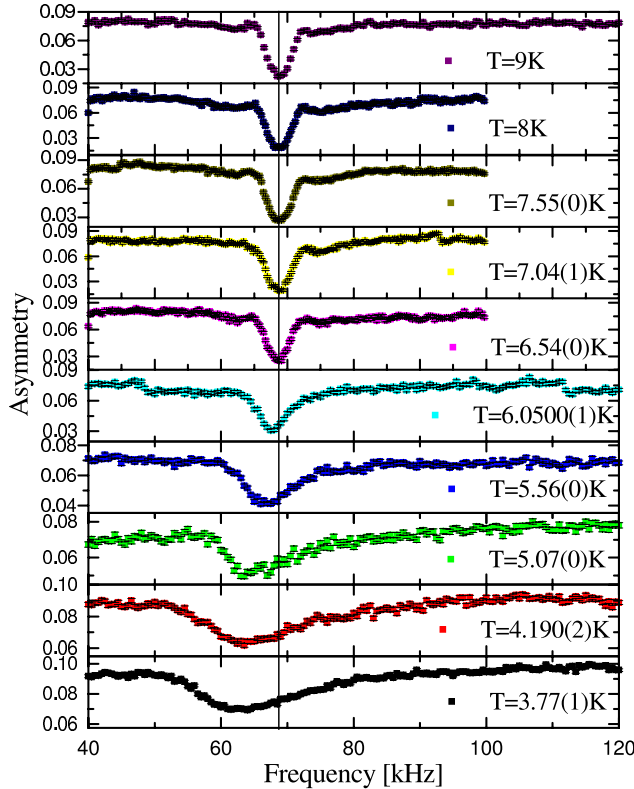
Fig. 85. The β-NMR signal of interstitial ^{8}Li in a crystal of NbSe$_2$ with $H//c$ (the hexagonal axis). The field H was about 110 G.

of magnetic vortices, a consequence of the superconductor's tendency to screen the field. Such a field inhomogeneity gives rise to the well-known broadening of the magnetic resonance in the superconducting state. In Fig. 85, we detect this effect by observing a broadened line possessing the expected long high frequency tail. Establishing the technique in a well studied superconductor such as NbSe$_2$ is an important step towards the application of β-NMR to the study of properties of the vortex state in exotic and thin film superconductors.

Semiconductors

We have also begun experiments on semiconductors in which the implanted radioactive atom is used to simulate the behaviour of an isolated Li impurity. The inset of Fig. 86 shows the β-NMR resonances at room temperature and at low temperature. In both cases there is a large amplitude line which is attributed to Li at sites which are close to being cubic and thus have no resolved quadrupole splitting. There is, however, a strong temperature dependence to the linewidth shown in the main part of Fig. 86. At low temperatures the width is attributed to nuclear dipolar broadening from the abundant ^{69}Ga, ^{71}Ga and ^{75}As nuclear moments. A slight decrease as the temperature increases from 5 K to 150 K is attributed to motional narrowing
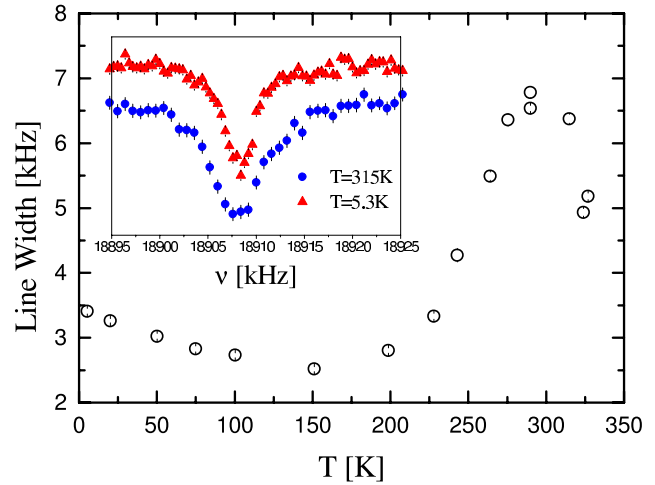
Fig. 86. The linewidth of the β-NMR resonance of ^{8}Li in semi-insulating high purity GaAs with $H \parallel < 100 >$.

as the Li begins to hop. However, above 150 K the line broadens significantly. This may be due to small unresolved quadrupolar splittings as the Li approaches the vacancies which are presumably created when the Li is implanted. Note the linewidth peaks at about 290 K. The drop at higher temperatures is likely due to the Li occupying the vacancy where the quadrupolar splitting is identically zero. This behaviour is very similar to that seen in the annealed Au foil. Further measurements are required to confirm this scenario.

Experiment 822
Effect of disorder on quantum spin liquid state
(A. Koda, R. Kadono, KEK)

The primary goal of the Expt. 822 collaboration is to elucidate the implicit correlation of quantum spin systems through the effect of controlled disorder on the magnetic property of parent compounds which is best probed by muon-spin-rotation/relaxation (μSR). Recently, an anomalous behaviour reminiscent of heavy f-electron systems, observed in a metallic spinel LiV$_2$O$_4$, has been drawing much interest as strong evidence for heavy quasiparticles which are carried by d-electrons. In order to identify the origin of such an enhanced density of states, we have carried out μSR experiments on polycrystalline samples of LiV$_2$O$_4$ and Li$_{1-x}$Zn$_x$V$_2$O$_4$ ($0.025 \leq x \leq 0.3$) under zero and longitudinal fields (ZF/LF-μSR) up to 300 mT.

In Fig. 87, typical ZF/LF-μSR time spectra in Li$_{1-x}$Zn$_x$V$_2$O$_4$ with $x = 0$ and 0.05 are shown. No remarkable increase of the relaxation rate corresponding to the development of staggered magnetic moments, as reported for one of the samples (#3) in previous reports [Kondo *et al.*, Phys. Rev. Lett. **78**, 3729 (1997)], was observed in a specimen with $x = 0$ over the investigated range of temperature. The result suggests
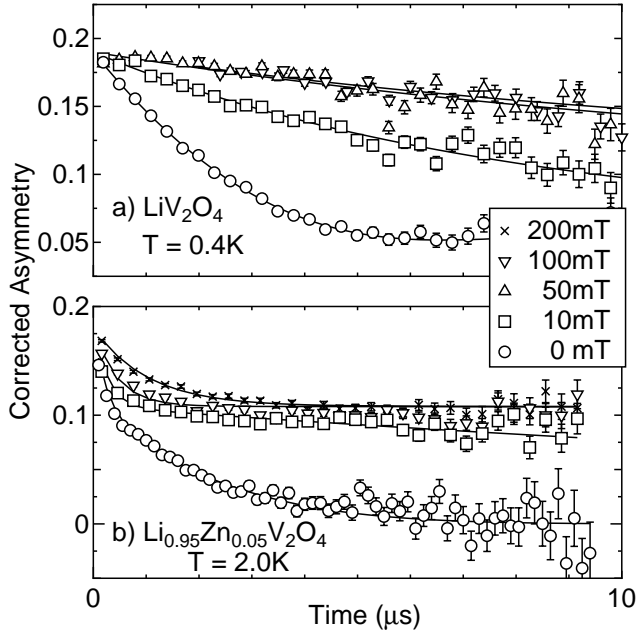
Fig. 87. Time evolution of muon spin polarization in LiV$_2$O$_4$ ($T = 0.4$ K) (a) and Li$_{0.95}$Zn$_{0.05}$V$_2$O$_4$ ($T = 2.0$ K) (b) under zero or longitudinal fields up to 200 mT.

the presence of two magnetic components, one which leads to a quasi-static internal field, which is readily quenched under $H \leq 100$ mT, and the other portion, which exerts dynamically fluctuating fields with a considerably high fluctuation rate. This situation is described by the following model of the relaxation function:

$$A_0 G_z(t) = A_0 [(1 - f) \exp(-\lambda_S t) + f \exp(-\lambda_D t)] G_{\text{KT}}^{\text{nuc}}(t) + A_{\text{BG}},$$

where A_0 is the initial asymmetry, λ_S is the relaxation rate for the quasi-static component, f is the fraction of the dynamically fluctuating component with the relaxation rate (λ_D), $G_{\text{KT}}^{\text{nuc}}$ is a relaxation function arising from the nuclear magnetic moments, and A_{BG} is the background contribution of the silver sample holder. The relaxation rate ($\lambda_i; i = S, D$) is given by Redfield's spectrum density function,

$$\lambda_i(\omega_\mu) = \frac{2\delta_i^2 \nu_i}{\omega_\mu^2 + \nu_i^2}, (i = S, D),$$

where $\omega_\mu \equiv \gamma_\mu H$ with γ_μ being the muon gyromagnetic ratio and H the external field; δ_i and ν_i are the dipolar width and fluctuation rate of each component, respectively. The temperature dependences of δ_i and ν_i in undoped LiV$_2$O$_4$ are shown in Figs. 88(a) and (b). The dynamically fluctuating component (λ_D) exhibits a relatively large dipolar width ($\delta_D \sim 10$ μs^{-1}), which is independent of temperature, while the quasi-static one has a much smaller coupling ($\delta_S \sim 1$ μs^{-1}). We
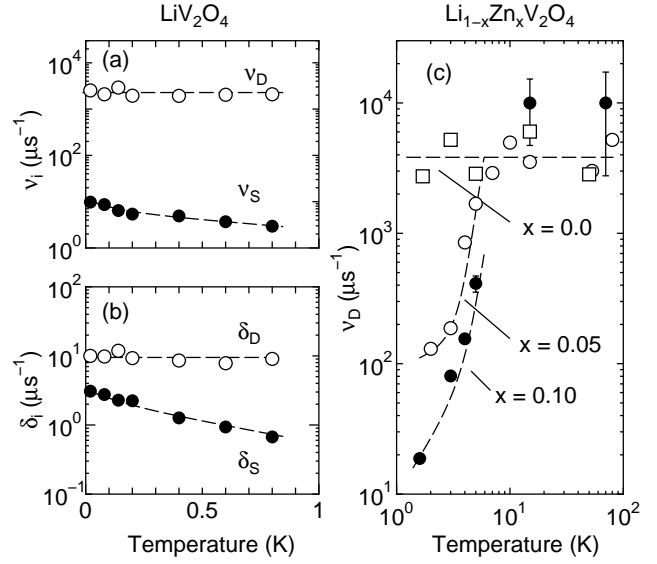
Fig. 88. Temperature dependences of (a) the fluctuation rate (ν_i) and (b) dipolar width (δ_i) in LiV$_2$O$_4$. The solid and open symbols represent the quasi-static (S) and the dynamical (D) component, respectively. (c) The fluctuation rate (ν_D) for different Zn concentrations (x), where those with $x > 0$ exhibit a clear tendency of slowing down below ~ 10 K.

note that the fraction of each component is independent of the temperature below 1 K with almost equal partition. The best-fit result was obtained for $f \sim 0.4$, which rules out the possibility that one of these components may be attributed to an impurity phase.

More direct evidence of phase segregation was obtained by the muon Knight shift in LiV$_2$O$_4$ deduced from TF-μSR measurements. In Fig. 89, the fast Fourier-transform (FFT) spectra of the μSR signal at a field of 1 T are shown, together with the Knight shift K vs. susceptibility plot. Two precession signals with different frequencies were observed over the investigated range of temperature (0.02 K < T < 300 K). One having a smaller hyperfine coupling (HFC) constant of -0.27 kOe/μ_B exhibits a nearly temperature-independent behaviour down to 20 mK, implying a narrowed coupling due to a high fluctuation rate corresponding to the dynamical component identified by ZF/LF-μSR. On the other hand, it is notable in Fig. 89 that another part showing a greater HFC constant of $+5.57$ kOe/μ_B exhibits a broadening of the linewidth, which is in line with the temperature dependence of the quasi-static component. This result strongly supports the interpretation that the two components observed in the ZF/LF-μSR spectra originate from different magnetic couplings.

We believe that this phase segregation is intrinsic to LiV$_2$O$_4$, because a similar behaviour has been commonly observed in Li$_{1-x}$Zn$_x$V$_2$O$_4$ with varying Zn concentrations, whereas the dynamical property is

strongly dependent on x. In Fig. 88(c), the fluctuation rate (ν_D) exhibits a clear tendency of slowing down with increasing x below $\sim$10 K. These features indicate that phase segregation into two components having different dynamical character occurs in $Li_{1-x}Zn_xV_2O_4$ irrespective of x, in which the singularity of the undoped LiV_2O_4 is primarily related to the spin fluctuation of the dynamical component (ν_D) persistent even at 20 mK. Thus, we conclude that the observed duality in the magnetism of LiV_2O_4 is intrinsic and cannot be attributed to the second phase or imperfectness of the crystal lattice.
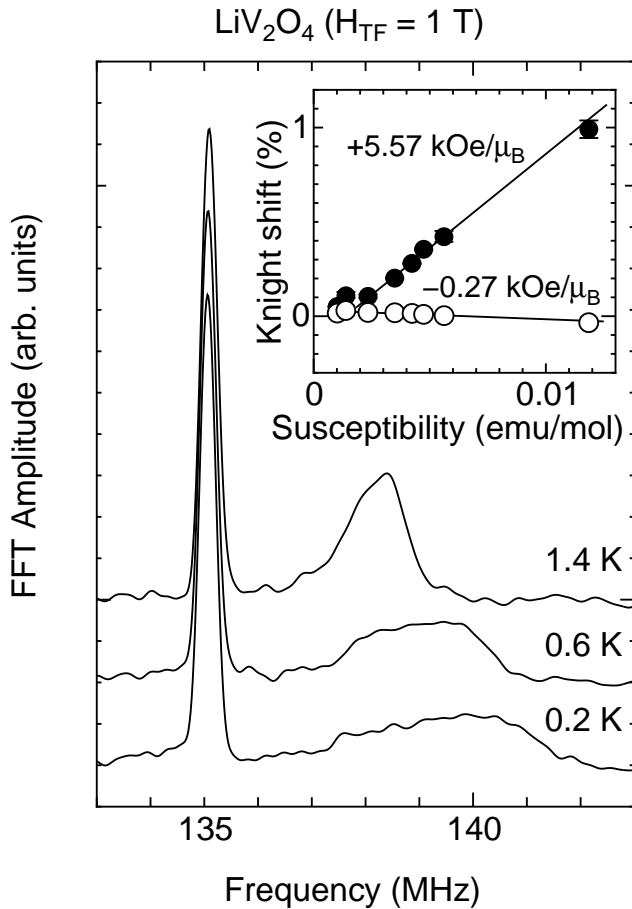
Fig. 89. FFT spectra of the TF-μSR signal under a field of 1 T. The inset shows a Knight shift (K) vs. susceptibility plot at $T > 2$ K.

Experiment 833
Muon spin relaxation studies on MnSi under applied pressure
(I.M. Gat, Columbia)

MnSi is one of the most investigated magnetic systems with itinerant electrons. The compound orders at $T_c = 29.5$ K in a helical magnetic structure with a long period (180 Å). We present μSR studies of a single crystal of MnSi at ambient pressure and under an applied pressure of 8.3 kbar. The critical temperature under 8.3 kbar is reduced to $T_c = 17$ K. At $p_c = 14.6$ kbar, the system becomes a correlated paramagnet.

The unexpected field dependence of the relaxation time T_1 in the paramagnetic phase, for magnetic fields less than 3000 G, is explained based on the helical nature of the magnetic structure. The relaxation time in the paramagnetic state, under the applied pressure of 8.3 kbar and the applied magnetic field of 61.3 G, shows a pronounced curvature when plotted vs. $1/T$. This might be due to the system approaching the ferromagnetic to paramagnetic crossover, where the spin fluctuations with small wave-vector and small energy are predominant, producing a deviation of the uniform susceptibility from the Curie-Weiss law close to the transition. Accordingly, a $T_1 \propto (T/T_c - 1)^2/T$ dependence is expected right above T_c. There is also an intermediate region between the critical region and the high temperature region, where $T_1 \propto ((T/T_c)^{4/3} - 1)/T$.
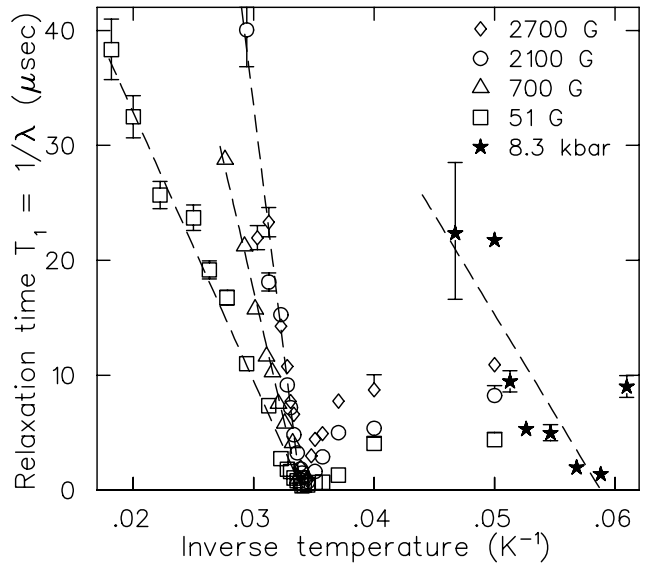
Fig. 90. The muon spin relaxation time T_1 vs. $1/T$ plot under applied magnetic fields of 51.5 G, 2115 G and 2700 G at ambient pressure and under 61.3 G under an applied pressure of 8.3 kbar. Data under 700 G and ambient pressure taken by Dr. Hayano's group [J. Phys. Soc. Japan **49**, 1773 (1980)] confirm our findings.
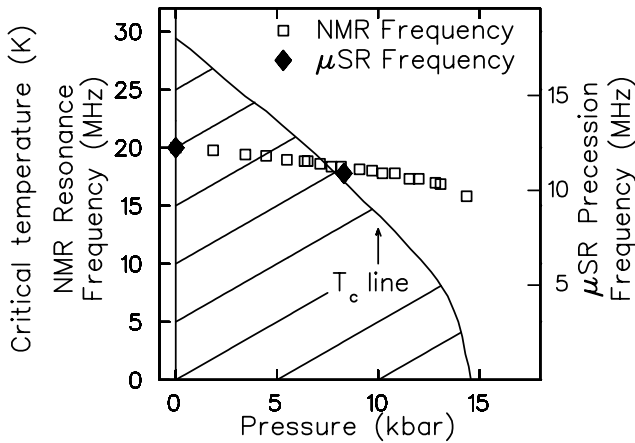
Fig. 91. The muon spin precession frequency in MnSi at 5 K at ambient pressure and under an applied pressure of 8.3 kbar is plotted together with the NMR resonance frequency at 1.4 K measured by Dr. Thessieu's group [J. Magn. Magn. Mater. **177-181**, 609 (1998)]. The μSR data confirm the small decrease of the magnetic moment with increasing pressure. This result might be related to the first order nature of the transition at p_c.

Experiment 834
μSR study of transverse spin freezing in a site-frustrated magnetic glass
(D.H. Ryan, McGill)

Random addition of antiferromagnetic (AF) exchange interactions to an otherwise ferromagnetic (FM) Heisenberg spin system leads to a loss of FM order through the effects of exchange frustration. In extreme cases, a spin glass (SG) is formed with random isotropic spin freezing and neither net magnetization nor long range order. At lower levels of frustration the system exhibits characteristics of both extremes as long-ranged FM order co-exists with SG order in the plane perpendicular to the FM order. On warming such a system from $T = 0$ K, the SG order first melts at T_{xy} followed by the loss of FM order at T_c. This picture has emerged from experimental measurements [Ren and Ryan, Phys. Rev. **B51**, 15885 (1995)], numerical simulations [Thomson *et al.*, Phys. Rev. **B45**, 3129 (1992)] and mean field calculations [Gabay and Toulouse, Phys. Rev. Lett. **47**, 201 (1981)]. The infinite-ranged interactions implicit in mean-field spin glass models make all forms of exchange frustration equivalent. However, real systems are generally dominated by shorter-ranged interactions, and for the case of first-neighbour-only exchange coupling, two distinct situations can be identified: (i) bond frustration [Thomson *et al.*, *op. cit.*] and (ii) site frustration [Nielsen *et al.*, Phys. Rev. **B53**, 343 (1996)].

Bond frustration arises when each exchange bond to a moment's nearest neighbours may be either positive (i.e. ferromagnetic) or negative (i.e. antiferromagnetic). Our earlier work under Expt. 834 has allowed us

to use zero-field muon spin relaxation (ZF-μSR) to establish the magnetic phase diagrams of two bond frustrated systems in great detail [Ryan *et al.*, J. Appl. Phys. **89**, 7039 (2001)]. We have shown that the static and dynamic signatures of both T_c and T_{xy} coincide within experimental error: the fluctuation rate diverges at the same temperature at which static order develops. These results are in perfect agreement with the predictions of numerical simulations [Thomson *et al.*, *op. cit.*], and a cross-check using selective excitation double Mössbauer spectroscopy has confirmed that the fluctuations sampled by interstitial muons and those seen at the nuclei of the moment-carrying iron atoms are identical [van Lierop and Ryan, Phys. Rev. Lett. **86**, 4390 (2001)].

Site frustration is achieved by introducing a dopant with AF coupling to all of its nearest neighbours so that the frustration is introduced site-wise rather than bond-wise. While the gross magnetic behaviour is expected to be the same as the bond frustrated case (the system exhibits non-collinear order at low temperatures, there are two magnetic transitions at intermediate dopings and a spin glass at higher dopings), numerical simulations show that there are two striking differences [Nielsen *et al.*, *op. cit.*]. Firstly, low levels of doping do not cause frustration as isolated AF-coupled sites simply order anti-parallel to the majority FM order. Frustration only appears when the dopant density is high enough for AF-AF pairs to occur. Secondly, the transverse correlations below T_{xy} exhibit short-range AF character rather than forming the xy-spin glass observed in the bond frustrated case. The first of these distinctions is clearly seen in the magnetic phase diagrams of manganese-doped metallic glasses, while Mössbauer spectroscopy in a–$(Fe_{1-x}Mn_x)_{78}Sn_2Si_6B_{14}$ [Kuprin *et al.*, Phys. Rev. **B61**, 1267 (2000)] and polarized neutron diffraction from a single crystal of Fe_2MnSi [Ersez *et al.*, J. Phys. : Cond. Matter **7**, 8423 (1995)] have confirmed that the transverse spin components exhibit AF correlations.

While the consistency between experiment and simulation for the two types of frustration appears excellent, one sharply conflicting result exists. A recent ZF-μSR study of a–$(Fe_{0.74}Mn_{0.26})_{75}P_{16}B_6Al_3$ [Mirebeau *et al.*, Hyp. Int. **104**, 343 (1997)] suggested that the static and dynamic signatures of transverse spin freezing at T_{xy} did not coincide. They argued that their data provided evidence for two distinct transitions below T_c: a canting transition at T_K that leads to the development of non-collinearity but involves no dynamical anomaly, followed by a freezing transition at T_F which is associated with strong energy losses and a peak in the fluctuation rate, but no specific change in the magnetic correlations. This three-transition inter-

pretation of the magnetic ordering in this single sample is inconsistent with numerical simulations of site frustrated Heisenberg spin systems [Nielsen *et al., op. cit.*], and the reported disagreement between the static and dynamic signatures of transverse spin freezing in the ZF-μSR data stands in stark contrast to the almost perfect agreement observed at T_{xy} in bond frustrated systems [Ryan *et al., op. cit.*].

The aim of the Expt. 834 runs in the summer was to re-visit this issue in a systematic way in order to clarify the situation. We carried out an extensive study of the entire magnetic phase diagram of a–$(Fe_{1-x}Mn_x)_{78}Si_8B_{14}$ for $0 \leq x \leq 0.5$, covering the full range of magnetic behaviour from ferromagnetic to spin glass, with five compositions in the two-transition region. These materials were studied using both bulk techniques (magnetization and susceptibility) and microscopic probes (Mössbauer spectroscopy and ZF-μSR). We found perfect agreement between the static and dynamic signatures of T_{xy} obtained from all techniques. There is no evidence for separate static and dynamic transitions below T_c. The phase diagram derived from our measurements is fully consistent with numerical simulations and the observed signatures of T_{xy} in this site frustrated material are identical to those observed previously in bond frustrated alloys.

Fitting procedure

Above T_c, fluctuations lead to an exponential dephasing of the muon polarization: $A_d = A_o \exp(-\lambda t)$ where λ is an effective relaxation rate. Below T_c, a static magnetic field will be present at the muon sites. However, the materials studied here are both structurally disordered (i.e. glassy) and magnetically disordered as a result of both random Mn substitution and also exchange frustration, therefore we expect a distribution of local fields to be present. In this case, the asymmetry will decay according to the Kubo-Toyabe (K-T) form:

$$G_z(\Delta, t) = \frac{1}{3} + \frac{2}{3}\left(1 - (\Delta t)^\alpha\right)\exp\left(-\frac{(\Delta t)^\alpha}{\alpha}\right)$$

with $\alpha = 2$, so that Δ/γ_μ is the rms field. In cases where both static order and fluctuations are present the asymmetry decays according to the product:

$$A = A_d \times G_z,$$

and both a K-T contribution at early times, and a slower exponential decay are seen. Note, we were able to fully fit all of our data using these functions, without resorting to the use of stretched exponentials.

Results

Fitting the μSR data using the functions described earlier yields the temperature dependences of the static
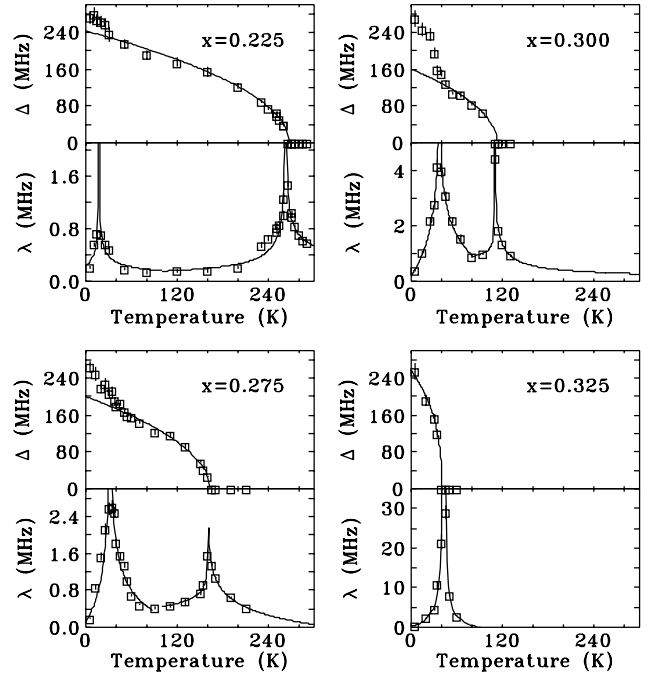
Fig. 92. Temperature dependence of the static (Δ) and dynamic (λ) signals from ZF-μSR for several a–$(Fe_{1-x}Mn_x)_{78}Si_8B_{14}$ alloys. In every case, the increase in static order (at T_c, T_{xy} or T_{sg}) is associated with a peak in the fluctuation rate.

relaxation rate (Δ), a measure of the static field seen by the muons, and the dynamic fluctuation rate (λ) which tracks the fluctuations in the field at the muon sites. These fits are summarized in Fig. 92 for four samples. The changeover from two transitions to one clearly occurs between $x = 0.30$ and $x = 0.325$, placing x_c in this range. Only a single transition is seen for the $x = 0.350$ sample as it is beyond x_c and is therefore a spin glass. The four samples $0.225 \leq x \leq 0.30$ each exhibit two distinct peaks in $\lambda(T)$. The higher temperature peak is associated with the onset of a non-zero static contribution and thus clearly corresponds to T_c, while the lower peak is aligned with the break in the slope of $\Delta(T)$ and therefore marks the freezing of the transverse spin components at T_{xy}. As the Mn content is reduced, the contribution of the transverse spin components to the total ordered moment declines, so that the increase in Δ below T_{xy} becomes difficult to localize reliably. Even with the high density of points apparent in Fig. 92, the error on T_{xy} at $x = 0.225$ is about 16 K, however, the derived value is fully consistent with the two dynamic determinations. At $x = 0.20$, only the fluctuation peak at T_{xy} was detected.

The transition temperatures deduced from the ac-susceptibility data (χ' for T_c, χ'' for T_{xy}), $<B_{hf}>(T)$ from Mössbauer spectroscopy, and both Δ and λ from the ZF-μSR data are summarized in the phase diagram shown in Fig. 93. Manganese doping has a severe
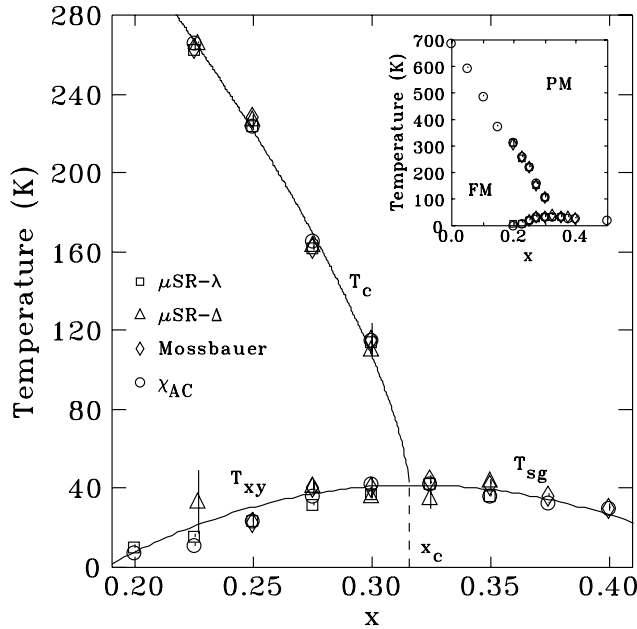
Fig. 93. Magnetic phase diagram for a–$(Fe_{1-x}Mn_x)_{78}Si_8B_{14}$ derived from ac-susceptibility data (χ' for T_c, χ'' for T_{xy}), $< B_{hf} > (T)$ from Mössbauer spectroscopy, and both Δ and λ from the ZF-μSR. Three transitions can be identified: ferromagnetic ordering at T_c, transverse spin freezing at T_{xy}, and spin glass ordering only for $x > x_c$ at T_{sg}. Note the perfect agreement between independent determinations of T_{xy}. Inset shows data for whole composition range studied.

effect on the magnetic ordering of this system, driving T_c down from 695 K at $x = 0$ (inset to Fig. 93), to ~40 K at $x_c = 0.31$. A power-law does not fit the composition dependence of T_c particularly well, and extrapolating T_c to zero yields a rather poor estimate for the critical composition of $x_c = 0.33 \pm 0.02$. This failure is not unexpected, as the FM–SG boundary is not marked by $T_c \rightarrow 0$, but rather by $T_c \rightarrow T_{xy}$. Indeed, a power-law fit to $1 - T_{xy}/T_c$ is far superior, and yields $x_c = 0.309 \pm 0.004$, in perfect agreement with $x_c = 0.306 \pm 0.006$ derived from field-cooled magnetization data.

The excellent agreement between T_c values derived from χ', Mössbauer spectroscopy and ZF-μSR, coupled with consistent T_{sg} values obtained above x_c, provides strong evidence that the analysis and transition assignments are correct and self-consistent. However, it is the behaviour at T_{xy} that is the primary focus of this work. Only for $x \geq 0.2$ do we see a second transition below T_c, a result that is in full accord with numerical simulations [Nielsen et al., op. cit.]. There is excellent agreement between T_{xy} values derived from the various techniques. For $x = 0.275$ and 0.300, we have four independent determinations of T_{xy} that agree to better than 5 K. The static, dynamic and loss signatures of T_{xy} are in perfect agreement, with no systematic

bias apparent in any of the measurements. While at $x = 0.250$, static data from Mössbauer, and dynamics from both $\lambda(T)$ and χ'' are in complete agreement. By $x = 0.225$, the change in the static order at T_{xy} is too small for its onset to be reliably determined from $< B_{hf} > (T)$ and the estimate from $\Delta(T)$ exhibits a substantial (~50%) uncertainty. However, the ZF-μSR fluctuation peak, and the maximum in the χ'' loss signal are still clear and coincident. As was found in our earlier work on bond-frustrated alloys [Ryan et al., op. cit.], all observed signatures of T_{xy} line up perfectly.

It is important to emphasize that the techniques that have been used to determine T_{xy} with such good agreement probe a very wide range of frequencies: ZF-μSR–Δ (~10^8 Hz), $< B_{hf} >$–Mössbauer (~10^7 Hz), ZF-μSR–λ (~10^6 Hz) and χ'' (~10^2 Hz), yet they yield T_{xy} values that agree within a few K for five samples that exhibit transverse spin freezing transitions at temperatures that change by more than a factor of three. Furthermore, there is no systematic frequency related trend in the T_{xy} values for a given sample. The scatter is random. A separation of T_{xy} into distinct static (T_K) and dynamic (T_F) events can therefore be ruled out. There is no evidence in our data to support the existence of a third transition below T_{xy}.

Experiment 842
Mu-substituted free radicals in sub- and super-critical water
(P.W. Percival, SFU)

Experiment 842 and its predecessor, Expt. 713, were designed to study muonium chemistry under hydrothermal conditions, i.e. aqueous solutions at high temperatures and pressures. The motivation is to investigate the chemistry of reactive intermediates under the extreme conditions found in supercritical water reactors, used for the destruction of hazardous waste, and in the cooling water cycles of pressurized water nuclear reactors. Direct measurements of "pressure-cooker" chemistry are technically very demanding, and engineering studies have had to rely on extrapolation of lower temperature data. On the other hand we have demonstrated that muon spin rotation circumvents many of the limitations of conventional spectroscopic probes, and that it is therefore feasible to investigate muonium chemistry in such difficult environments. Since muonium behaves chemically as a light isotope of hydrogen it can be used to study H atom chemistry and the properties of free radicals which incorporate H (almost all organic free radicals).

Only one week of beam time was taken in 2002; it was used for measurements of muonium reaction rates. Two H abstraction reactions were investigated:
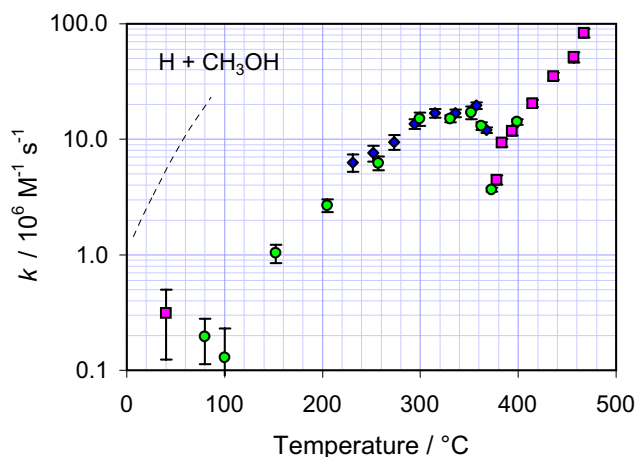
Fig. 94. Rate constants for Mu + methanol in water at 230 bar. The new data are denoted with square symbols. The dotted line indicates the best literature data for the equivalent reaction of H atoms.

1) $Mu + CH_3OH \longrightarrow MuH + \cdot CH_2OH$ and

2) $Mu + NH_2NH_2 \longrightarrow MuH + \cdot NHNH_2$.

We have already made extensive measurements of Mu kinetics for the reaction with methanol (TRIUMF Annual Report 2000) and some of the data have been published [Ghandi *et al.* (Physica B, in press)]. The new measurements extend the study to higher temperatures. Our earlier work for this and other reactions has shown that the rate constants go through a maximum as the temperature is raised, but we had very little data on either the "dip" or the "recovery" at higher temperatures. Since the dip occurs in the region of the critical point of water (374°C) the density is very sensitive to temperature and pressure. Precise control of the pressure is therefore essential to avoid huge systematic errors.

Figure 94 displays a selection of data at constant pressure (230 bar, except for a few points at lower temperature where the pressure effect is negligible). Also shown is the (very limited) range of published data for the H atom [Mezyk and Bartels, J. Phys. Chem. **101**, 1329 (1997)].

In addition to completing the study of Mu + methanol we began an investigation of the reaction with hydrazine (NH_2NH_2). Hydrazine is commonly used as a corrosion inhibitor in steam generators, including those in the nuclear power industry. Despite the obvious importance of understanding the radiation chemistry of water and additives, there are relatively little data on the reactions of radiolysis transients in aqueous solutions of hydrazine. Moreover, a recent study [Buxton and Sims, Phys. Chem. Chem. Phys. **2**, 4941 (2000)] calls into question published data on the reactions of H atoms with hydrazine. The situation is complicated by the existence of the hydrazinium
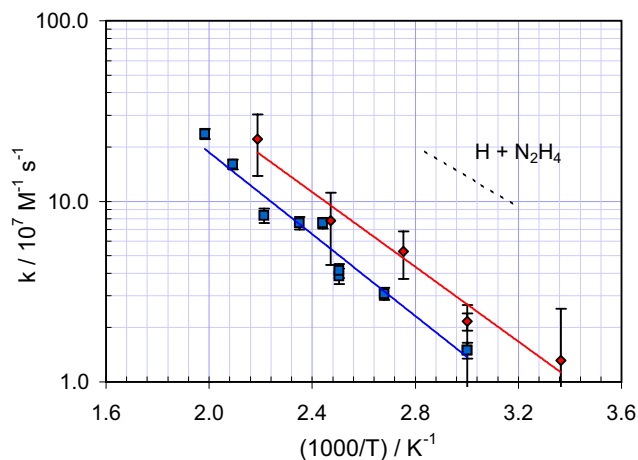
Fig. 95. Arrhenius plot of rate constants for Mu + hydrazine in water at pressures at or below 250 bar. The squares correspond to solutions at natural pH (mixture of N_2H_4 and $N_2H_5^+$) while the circles represent measurements on solutions at pH 1.5 (overwhelming $N_2H_5^+$).

ion ($N_2H_5^+$) in acidic solution, and the possibility of alternative reaction channels.

Our preliminary results for the muonium rate constant are displayed in Fig. 95. The activation energies derived from the slopes of the data sets at different pH are similar to the published result for H + N_2H_4 but not that for H + $N_2H_5^+$ [Mezyk *et al.*, J. Chem. Soc. Far. Trans. **92**, 2541 (1996)].

Experiment 843
Quadrupole ordering in dense Kondo systems studied by μLCR
(R. Kadono, J. Akimitsu, KEK-IMSS/Aoyama-Gakuin U.)

It has been reported by Young *et al.* that lightly doped divalent hexaboride $Ca_{1-x}La_xB_6$ shows a ferromagnetism [Young *et al.*, Nature **397**, 412 (1999)]. The ferromagnetic state has a number of unprecedented features, e.g., it appears only over a narrow carrier concentration range ($0 < x < 0.01$) with a small magnetic moment (< 0.07 μ_B/La) and a remarkably high Curie-temperature ($T_c \approx 600$ K). Various studies have been performed after this report to understand the mechanism of the ferromagnetism in this material. However, it turned out that this compound exhibits extremely strong sample dependence in bulk properties, and it is not clear whether or not impurities affect this ferromagnetic behaviour. Thus, there is no general consensus on the intrinsic character of ferromagnetism among researchers.

We have been studying this compound by μSR technique to elucidate the microscopic character of the reported ferromagnetism. We have found that the relaxation rate of CaB_6 is apparently larger than that

of CeB_6 in the paramagnetic phase over the low temperature region ($T < 150$ K). Since the contribution of nuclear dipolar field from boron nuclei is presumed to be the same between isostructural CaB_6 and CeB_6, the difference of relaxation rate for both systems suggests an additional contribution of magnetic moments in CaB_6.

In the 2002 beam time, we performed muon level-crossing resonance (μLCR) measurements to determine the electric field gradient q at the boron site in CaB_6. In the case of ^{11}B ($I = 3/2$), only one resonance signal is expected at a field,

$$B_{\text{res}} \simeq \frac{3e^2qQ}{4\hbar\gamma_\mu}.$$

The time-integrated and field-differentiated asymmetry δA is shown in Fig. 96. The resonance signal is
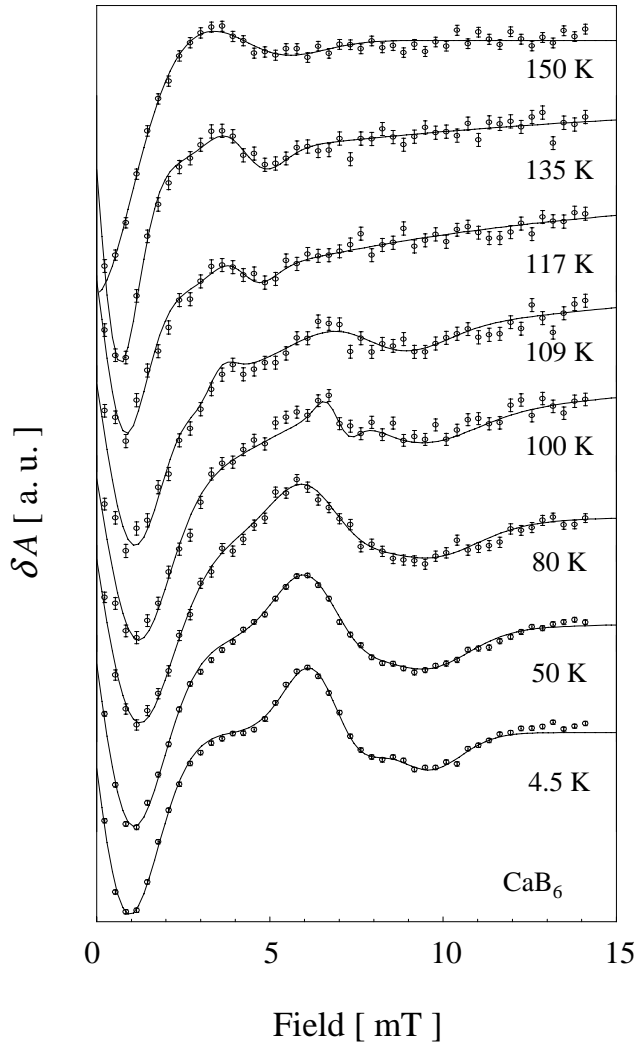
Fig. 96. Time-integrated μLCR spectra in CaB_6 at various temperatures. The solid curves are results of fitting by the function described in the text.
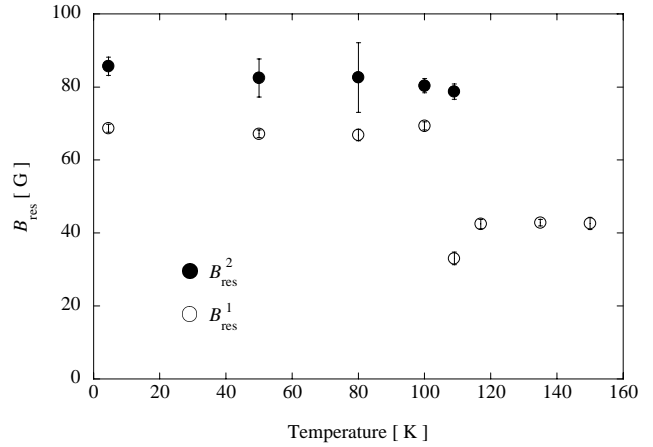
Fig. 97. Temperature dependence of muon level-crossing resonance field in CaB_6.

observed near 4 mT above 110 K, whereas it is shifted to near 7 mT below 110 K. It should be emphasized here that two resonance signals are clearly observed at the lowest temperature (4.5 K). These spectra can be described as

$$\delta A = \sum_{n=0}^{m} -c_n(B - B_{\text{res}}^n)\exp(-\gamma_\mu^2(B - B_{\text{res}}^n)^2/\Lambda^2)$$

$$\left(\begin{array}{l} T < 110\,\text{K} : m = 2 \\ T > 110\,\text{K} : m = 1 \end{array} \right),$$

where c_n are the amplitudes determined by the relaxation rate, and Λ is the linewidth obtained from the second moment. The term of $n = 0$ corresponds to the zero-field crossing. The solid curves in Fig. 96 are the fitting results by the above equation, where we obtained the resonance fields ($B_{\text{res}}^n : n = 1, 2$) as shown in Fig. 97. The resonance field above 110 K is in good agreement with those obtained from ^{11}B-NQR in the paramagnetic phase of CeB_6, thereby indicating that there is no muon-induced effect. On the other hand, however, there are two resonance fields below 110 K, being larger than that above 110 K. Since the change of a crystal structure in CaB_6 can not be observed around 110 K, two resonance peaks might be attributed to the change of electronic arrangement around boron atoms. Preparation of a more detailed report is now in progress.

Experiment 846
Complex order parameter symmetry in YBa$_2$Cu$_3$O$_{7-\delta}$ at low T and high magnetic field
(J.H. Brewer, UBC; J.E. Sonier, SFU)

Superconductivity in YBa$_2$Cu$_3$O$_{7-\delta}$ depends both on the oxygen content, δ, as well as the oxygen ordering properties of the CuO chain layers. While early ZF-μSR measurements on underdoped polycrystalline samples displayed clear signatures of ordered and/or fluctuating Cu electronic magnetic moments, studies of

optimal and fully oxygenated samples showed sensitivity only to the static nuclear dipoles. More recent ZF-μSR measurements on high-quality superconducting single crystals showed that the muon-spin relaxation signal does in fact evolve considerably as a function of temperature at optimal doping, indicating the presence of an additional source of local magnetism [Sonier *et al.*, Science **292**, 1692 (2001)]. In order to gain more insight into the physical origin of the additional magnetism sensed by the μ^+, we carried out ZF-μSR experiments on a series of $YBa_2Cu_3O_{7-\delta}$ single crystals with different oxygen content. In 2002 we completed this study, and began work on the $Y_{1-x}Ca_xBa_2Cu_3O_{7-\delta}$ system. The substitution of Y^{2+} by Ca^{2+} introduces extra hole carriers into the superconducting CuO_2 layers. This allows for hole concentrations greater than that in fully-oxygenated $YBa_2Cu_3O_7$, thus enabling investigations of the overdoped regime over a wider range of hole doping.

Figure 98 shows measurements of the muon-spin relaxation rate in single crystals of Ca-doped $YBa_2Cu_3O_{6.99}$ at zero external field. Qualitatively the temperature dependence of the relaxation rate resembles that in the pure (nearly) fully-oxygenated compound $YBa_2Cu_3O_{6.99}$. In particular, a minimum near $T = 60$ K and a significant increase below $T = 35$ K are observed. We have previously attributed these features in the pure system $YBa_2Cu_3O_{7-\delta}$ to a redistribution of the hole carriers in response to local structural distortions. The observation of the same features in the Ca-doped sample supports our assertion that these structural changes occur at temperatures that are independent of hole concentration.
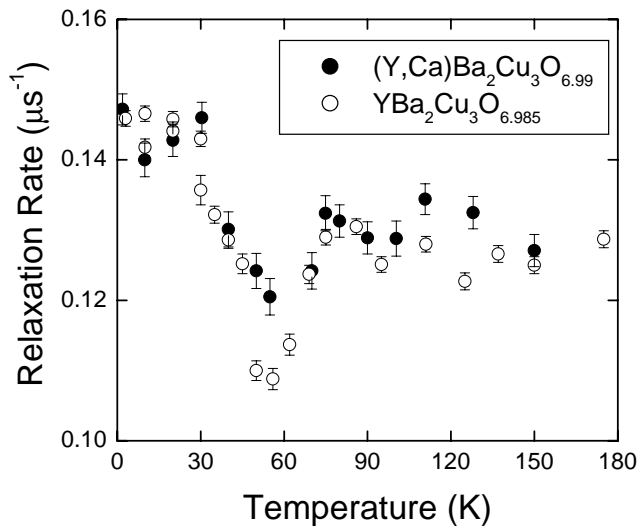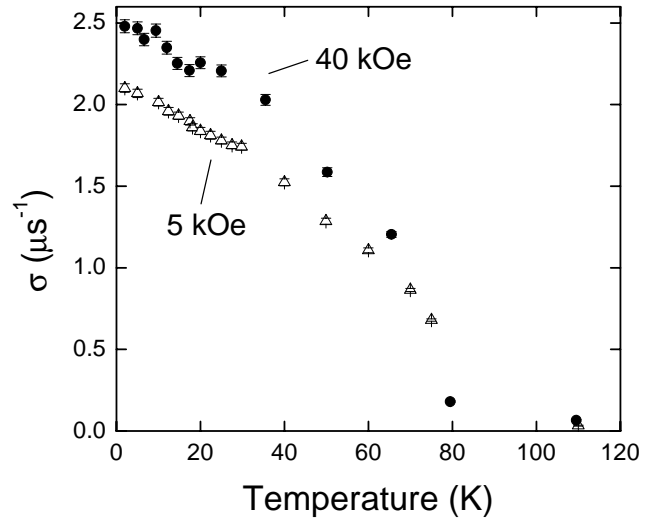
Fig. 99. Temperature dependence of the muon-spin depolarization rate in Ca-doped $YBa_2Cu_3O_{6.99}$ single crystals at $H = 5$ kOe and $H = 40$ kOe applied parallel to the *c*-axis of the crystals.

Figure 99 shows the temperature dependence of the muon-spin depolarization rate in Ca-doped $YBa_2Cu_3O_{6.99}$ single crystals in the vortex state. These results were obtained from a preliminary on-line analysis of the data. Both sets of data show the linear temperature dependence at low T that is characteristic of a "clean" *d*-wave superconductor. A detailed analysis of this data, assuming an appropriate theoretical field distribution for the vortex lattice, will ultimately lead to a precise determination of the temperature dependence of the in-plane magnetic penetration depth λ_{ab}.

Experiment 847
Electron-doped high-T_c superconductors
(J.E. Sonier, SFU)

While there now exists a large body of convincing experimental work on high-T_c superconductors with hole-type carriers, the intrinsic properties of the electron-doped cuprates $R_{2-x}Ce_xCuO_4$ ($R \equiv$ La, Pr, Nd, Sm or Eu) have remained very elusive. Part of the problem stems from the difficulty of preparing single phase superconducting samples. An additional complication is the presence of both Cu and rare-earth (R) moments. The interplay between these two magnetic sublattices has been studied extensively in the undoped parent compounds R_2CuO_4. In Ce-doped samples, there is the possibility that the magnetic exchange interactions involving the CuO_2 planes play an important role in superconductivity. There is also some uncertainty about the symmetry of the superconducting order parameter (i.e. *s*-wave, *d*-wave, *p*-wave etc.). In 2002 we continued our study of superconducting $Pr_{2-x}Ce_xCuO_4$ (PCCO) single crystals.

Fig. 98. Temperature dependence of the muon-spin relaxation rate measured at zero external field in Ca-doped and pure $YBa_2Cu_3O_{6.99}$ single crystals.

TF-μSR and magnetization measurements were carried out under both field-cooled (FC) and zero-field cooled (ZFC) conditions. Typical asymmetry spectra are shown in the inset of Fig. 100. In the ZFC case, pinning at the sample edges prevents flux from entering the bulk at $T = 2.3$ K and $H < 300$ Oe. Thus, the ZFC time spectrum in Fig. 100 resembles that observed in ZF. We note that this is also the case in high-quality YBa$_2$Cu$_3$O$_{7-\delta}$ single crystals. Above 300 Oe, flux fully penetrates the sample at $T = 2.3$ K, but pinning centres prevent the formation of an equilibrium vortex lattice configuration. On the other hand, a well-ordered vortex lattice is achieved in the FC procedure. Fast Fourier transforms (FFT) of the corresponding muon-spin precession signals at $H = 91$ Oe are shown in Fig. 100. The FFT provides an approximate picture of the internal magnetic field distribution $n(B)$. Above T_c, the linewidth is due to the electronic and nuclear magnetic moments. Below T_c, the lineshape is further broadened and becomes asymmetric as a result of the inhomogeneous field distribution created by a lattice of vortices.

Below T_c, there is a substantial increase of the average internal field B_0 at the μ^+ stopping site that nearly coincides with the increase of the diamagnetic signal observed in bulk susceptibility $\chi^\parallel$ measurements under FC conditions (see Fig. 101 inset). From μ^+ Knight shift measurements carried out in the normal state we have verified that this increase of B_0 cannot be explained by the formation of Cooper pairs. We surmise that the increased field at the μ^+ site is due to

Fig. 101. $B_0(T) - B_0^{\mathrm{N}}$ vs. B_0^{N} at $T = 5$ K (solid circles) and 10 K (open circles). The solid curves are described in the text. Inset: Temperature dependence of B_0 and $\chi^\parallel$ taken under FC conditions.

supercurrents induced in the CuO$_2$ layers by the Pr $4f$-moments. The screening of R magnetic moments has previously been considered in the RBa$_2$Cu$_3$O$_{7-\delta}$ system, where TF-μSR measurements show large shifts of B_0 in the superconducting state. The main panel of Fig. 101 shows a plot of the difference between the value of B_0 below and above T_c. The solid curve is a fit assuming $B_0(T) = [(B_0^{\mathrm{N}})^2 + (B_\perp)^2]^{1/2}$, where B_0^{N} is the average internal field in the normal state and $B_\perp \approx 43$ G and 28 G, at 5 K and 10 K, respectively. This indicates that the additional field $B_\perp$ that appears at the μ^+-site is primarily directed in the ab-plane.

The in-plane magnetic penetration depth λ_{ab}, which is related to the density of superconducting carriers, was determined from an extensive analysis of the TF-μSR time spectra. The fits accounted for both the inhomogeneous field distribution associated with a vortex lattice and the local field distribution due to the nuclear and electronic magnetic moments. Figure 102 shows the temperature dependence of λ_{ab}^{-2}. The absence of data below $T = 2.3$ K forbids an accurate determination of the limiting temperature dependence of $\lambda_{ab}^{-2}(T)$. However, above this $\lambda_{ab}^{-2}(0)/\lambda_{ab}^{-2}(T)$ shows reasonable agreement with that determined by μSR in the hole-doped high-T_c systems La$_{2-x}$Sr$_x$CuO$_4$ and YBa$_2$Cu$_3$O$_{7-\delta}$. The zero-temperature value $\lambda_{ab}(0) \approx$ 3370 Å suggests our sample is primarily underdoped. Recently it has been suggested that there is a crossover from s-wave to d-wave behaviour in the underdoped regime of electron-doped cuprates. Our results could

Fig. 100. Fourier transforms of the muon-spin precession signal in PCCO. Below T_c, the measurements were taken in an arbitrary sequence as a function of T under FC conditions. The dashed vertical line indicates the value of the external field $H = 91$ Oe. Inset: Asymmetry spectra taken at $T = 2.3$ K under both FC and ZFC conditions.
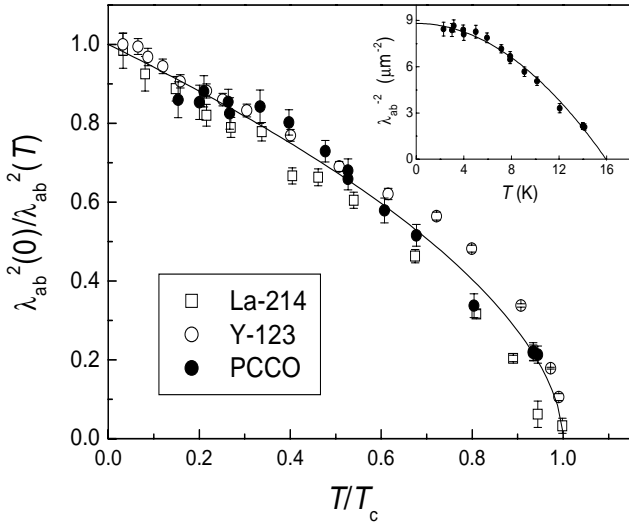
Fig. 102. Normalized magnetic penetration depth $\lambda_{ab}^2(0)\lambda_{ab}^2(T)$ as a function of T/T_c for single crystals of PCCO at $H = 90$ Oe (solid circles), $La_{2-x}Sr_xCuO_4$ at $H = 2$ kOe (open squares) and $YBa_2Cu_3O_{6.95}$ at $H = 5$ kOe. Inset: Temperature dependence of λ_{ab} in a PCCO single crystal.

be interpreted as consistent with d-wave pairing in the presence of sample impurities. However, a unique determination of $\lambda_{ab}^{-2}(T)$ at low temperatures by μSR awaits the availability of larger high-quality single crystals.

Experiment 851
μSR in ruthenate and cuprate high-T_c compounds
(D.R. Harshman, Physikon Research Corp.)

Over the last year, our research program has focused on answering two basic questions regarding high-T_c superconductivity: (1) "What is the pairing state symmetry?", and (2) "Where does the hole condensate actually reside?" To this end, we have concentrated on measurements of $YBa_2Cu_3O_7$ and $Sr_2Y(Ru_{1-u}Cu_u)O_6$, respectively.

Proof of nodeless pairing state in single-crystal $YBa_2Cu_3O_7$

Muon spin rotation (μ^+SR) measurements were conducted on a single-crystal of $YBa_2Cu_3O_7$ with a superconducting transition temperature of $T_c \approx 91.3$ K and a transition width of $\Delta T_c < 0.5$ K in zero applied field. Data were taken at applied magnetic fields along the c-axis of 0.05, 1.0, 3.0, and 6.0 T. We found, by taking into account the expected field-dependent and temperature-activated flux-line disorder, that our results were in fact consistent with a nodeless (s-wave) superconducting order parameter and that they appeared to be inconsistent with order parameters possessing nodes, such as those having $d_{x^2-y^2}$ symmetry.
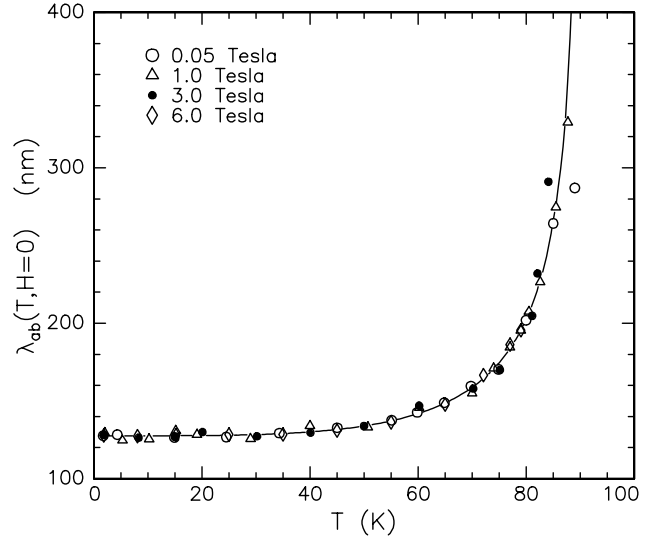
Fig. 103. The temperature dependence of the zero-field penetration depth, $\lambda_{ab}(T, H=0)$, with the fitted effects of pinning removed. The curves are fitted with a London penetration depth value of $\lambda_{ab}(T, H=0) = 127.6 \pm 1.5$ nm.

This result (shown in Fig. 103) is consistent with early μ^+SR measurements on sintered samples in which (we believe) strong pinning eliminated the temperature and field dependence of the vortex lattice disorder. These data (including their observed dependences on magnetic field) are, however, completely consistent with s-wave (or extended s-wave) pairing, provided that field-dependent and temperature-activated vortex de-pinning is also accounted for. Our results (i) confirm the s-wave superconductivity character originally observed in 1989, and (ii) show that the features of μ^+SR (and microwave) data claimed by other authors to be evidence for d-wave superconductivity are instead symptomatic of temperature-dependent de-pinning of vortices, which results in long-ranged distortion of the flux lattice. Indeed, the probability that any d-wave model gives a better fit than the two-fluid s-wave model is less than 4×10^{-6}.

Spin-glass behaviour, spin-fluctuations and superconductivity in $Sr_2Y(Ru_{1-u}Cu_u)O_6$

Muon spin rotation studies of $Sr_2Y(Ru_{1-u}Cu_u)O_6$ (for u = 0.1) reveal two distinct muon sites; one located in a SrO layer (which is superconducting at low temperatures) and the other in a $Y(Ru_{1-u}Cu_u)O_4$ layer (which is magnetically ordered at low temperatures). A precursor spin-glass state due to Ru moments is detected in high-fields ($\approx$3.3 kOe) in the $Y(Ru_{1-u}Cu_u)O_4$ layers, with a spin-glass temperature, $T_G \approx 29.25$ K. The $Y(Ru_{1-u}Cu_u)O_4$ layers layers order ferromagnetically in the a-b planes at a Néel temperature, $T_N \approx 23$ K. This in-plane ferromagnetism alternates direction between adjacent $Y(Ru_{1-u}Cu_u)O_4$

planes, resulting in a net antiferromagnetic structure. Although the onset of superconductivity is observed both by electron spin resonance and by dc-susceptibility to occur for temperatures up to about $T_{c,onset} \approx 49$ K, this superconductivity is adversely affected by the Ru moments that fluctuate for $T > T_N$ producing magnetic fields that break pairs in the SrO layers. The muons, as well as other probes, sense the more-robust static superconductivity for $T < T_G$. In fact, resistance measurements only show zero resistance below T_N, at which temperatures the Ru moments that fluctuated for $T > T_N$ are frozen in-plane (resulting in a net zero field along the SrO layers). Hence, strictly speaking, the superconducting transition temperature is the same as T_N, which is far below $T_{c,onset}$. Below T_N there are no pair breaking fluctuating magnetic fields in the SrO layers where the hole condensate resides.

Experiment 877
μSR studies on strongly correlated electron systems under high pressure
(W. Higemoto, KEK-IMSS)

Pressure appears as an experimental parameter of primary interest in the field of strongly correlated electron physics. For the heavy fermion system (HF), volume reduction changes the strength of hybridization between conduction and f electrons and this in turn controls the behaviour of heavy-mass quasiparticles.

CeRh$_2$Si$_2$ shows two antiferromagnetic long-range ordering at ambient pressure ($T_{N1} = 36$ K and $T_{N2} = 27$ K). Magnetic Bragg peaks for $T_{N2} < T < T_{N1}$ were indexed to a $(\frac{1}{2}\frac{1}{2}0)$ magnetic structure; whereas below T_{N1} additional peaks corresponding to $(\frac{1}{2}\frac{1}{2}\frac{1}{2})$ appeared. Application of pressure suppresses T_N to 0 K at $P_c \sim 1$ GPa. Neutron diffraction study under high pressure shows decreasing of the saturated sublattice moment μ and transition temperature with increasing pressure [Kawarazaki *et al.*, Phys. Rev. **B61**, 4167 (2000)]. They found that μ becomes $\mu \sim 0$ at quantum critical point P_c. We study the magnetism of CeRh$_2$Si$_2$ by means of μSR method under high pressures. A high pressure μSR experiment was carried out at the M9B beam channel at TRIUMF. A piston cylinder type high pressure cell, which is made from CuBe alloy, was used. A positive muon of 102 MeV/c was implanted into a single crystalline sample of CeRh$_2$Si$_2$ through a thick wall of high pressure cell.

Figure 104 shows the typical μSR spectra in CeRh$_2$Si$_2$ under zero magnetic field (ZF) in the high pressure cell. Here about 40% of the implanted muons stopped at CeRh$_2$Si$_2$ and the rest of the muons stopped at the CuBe wall or the pressure medium (Fluorinert FC77/70). In $T_{N2} < T < T_{N1}$, no spontaneous muon
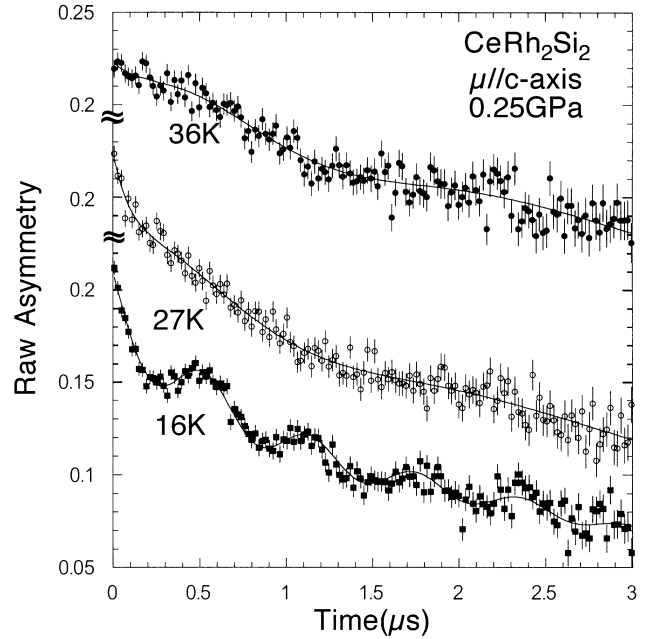
Fig. 104. ZF-μSR spectra in CeRh$_2$Si$_2$ at 0.25 GPa.

spin precession, but the fast spin relaxation is observed. In the lower magnetic ordering phase, $T < T_{N2}$, we observed both the fast relaxation and the spontaneous muon spin precession under ZF, which means that two kinds of the local fields exist at the muon site. The transition temperatures T_{N1} and T_{N2} decrease with increasing pressure. These behaviours are in good agreement with other experiments.

The precession frequency is almost temperature independent below T_{N2}, which shows the feature of the first order phase transition at T_{N2}. The pressure dependence of precession frequency below 10 K is plotted in Fig. 105. The precession frequency is nearly independent to the applied pressure up to 0.45 GPa. This result implies that the internal field and the saturated
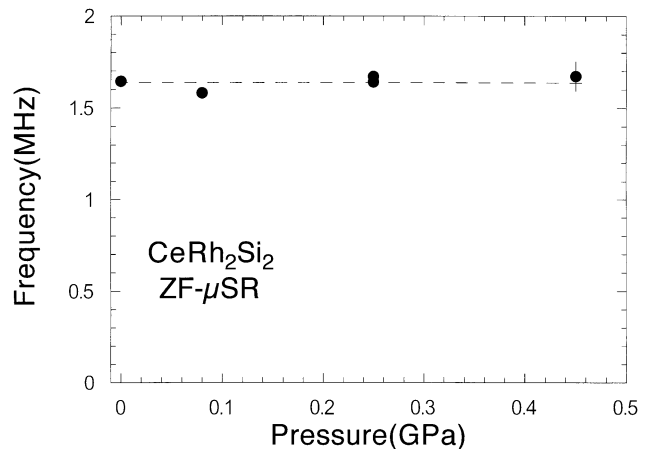
Fig. 105. Pressure dependence of ZF muon spin precession frequency below 9 K.

sublattice magnetic moment around the muon site are nearly independent to the applied pressure. It was proposed, based on the assumption of 4-**q** spin structure, that the saturated sublattice magnetic moment decreases with increasing pressure and disappears around 1 GPa [Kawarazaki *et al., op. cit.*]. These interpretations are inconsistent with each other. This fact implies that it is necessary to re-examine the magnetic structure below T_{N2}.

Experiment 881
Magnetism of Ce-based heavy fermion superconductor
(A. Koda, R. Kadono, KEK)

It is of principal interest whether or not magnetism coexists with superconductivity. Heavy fermion superconductors provide important opportunities to investigate the interplay between magnetism and superconductivity. $CeCu_2Si_2$ is an archetypal heavy fermion superconductor, which exhibits a magnetic phase (*A*-phase) adjacent to the superconducting phase as well. We have performed the muon spin rotation measurements of $Ce_{0.99}Cu_{2.02}Si_2$ under high transverse fields ($B_{TF} \leq 3$ T), proving coexistence of the *A*-phase and the superconductivity in a microscopic level.

The chemical composition of the employed specimen is situated in the region where the dominance of the magnetic *A*-phase is observed. The hyperfine coupling (HFC) constant of muon spin has turned out to be $-3.36 \, kOe/\mu_B$ from a Knight shift vs. susceptibility plot at high temperatures ($T > 15$ K), which is comparable to the values reported on Cu and Si nuclei.

Below 15 K, on the other hand, the obtained TF-μSR signal exhibits a splitting with different HFC. We consider that this behaviour is attributed to the anisotropy of HFC, since a qualitatively similar anisotropy has been observed in Cu-/Si-NMR experiments [Ohama *et al.*, J. Phys. Soc. Jpn. **64**, 2628 (1995)]. In addition, extrapolation from higher temperatures approximately divides the result at lower temperatures into a ratio of 1:2 as expected, because the isotropic Knight shift K_{iso} is given by $K_{iso} = \frac{2}{3}K_\perp + \frac{1}{3}K_\parallel$, where $K_\perp$ ($K_\parallel$) is the Knight shift for the field perpendicular (parallel) to the *c*-axis. It is noteworthy that these μSR signals come from a unique domain in the sample.

In Fig. 106, the temperature dependences of $K_\parallel$ and the transverse depolarization rate T_2^{-1} under several fields are shown. With decreasing temperature, T_2^{-1} shows a pronounced increase below ~ 0.8 K. Since this temperature dependence well reproduces previous ZF-/LF-μSR results, we consider that the increasing of the depolarization rate is due to the onset of the *A*-phase. A remarkable finding is that the central
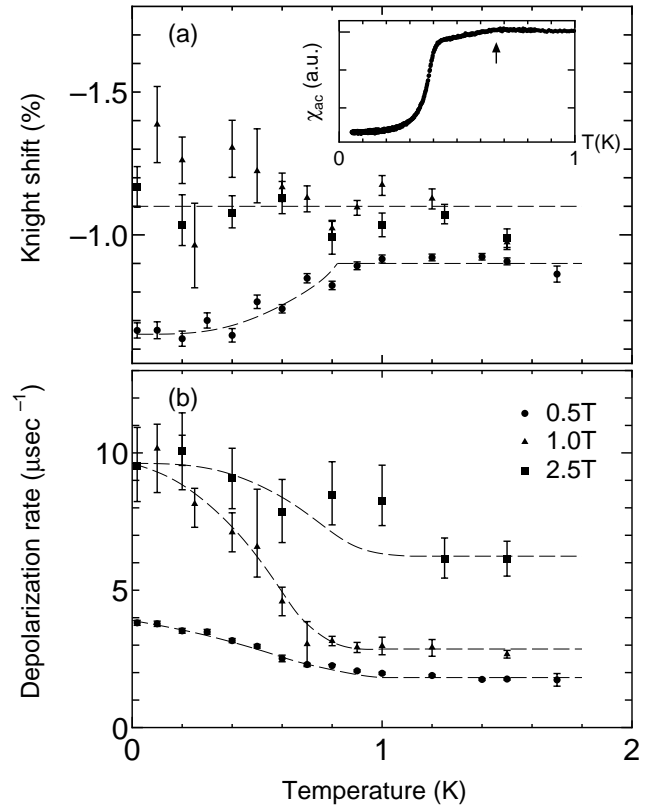
Fig. 106. Temperature dependences of the Knight shift parallel to the *c*-axis, $K_\parallel$, (a), and the transverse depolarization rate, T_2^{-1}, (b), at several magnetic fields. The broken lines are guides to the eye. In the inset of the upper panel, the ac-susceptibility of the present specimen is shown.

frequency of the broadening spectra is slightly shifted under the field of 0.5 T at lower temperatures, as shown in Fig. 106. The reduction of the Knight shift coincides with the appearance of the *A*-phase and is quenched by applying further high fields ($B_{TF} \geq 1.0$ T). It is reasonable to interpret this field dependence as the suppression of superconductivity when $B_{TF} \geq B_{c2}$. In summary, we have found evidence that superconductivity may exist within the magnetic *A*-phase in $CeCu_2Si_2$.

Experiment 883
Muoniated methyl and associated free radicals
(P.W. Percival, SFU)

In view of our successful detection in 2001 of the muoniated methyl radical, $\cdot CH_2Mu$, we had expected to study isotopomers such as $\cdot CD_2Mu$ in 2002. As it happens we used both weeks of beam time on some of the "associated free radicals" of the project title. These radicals are characterized as α-muoniated, because the Mu atom is directly bound to the radical centre, i.e. the atom which is the principal site of unpaired spin density in the molecule. Common methods for producing muoniated radicals involve addition of

Mu to a double bond (C=C, C=O) or aromatic ring, resulting in attachment of Mu to the radical centre or conjugated system. The methyl radical is the simplest α-muoniated organic radical, and we detected it as a product of the reaction between muonium and ketene ($CH_2C=O$). As part of the preliminary investigations for Expt. 883 we explored various other methods of generating α-muoniated radicals [McKenzie *et al.*, Physica B, in press]. One of these is the direct addition of Mu to a carbene:

$$\overset{R}{\underset{R}{\diagdown}}C: \quad \xrightarrow{\text{Mu}} \quad \overset{R}{\underset{R}{\diagdown}}\overset{\cdot}{C}-Mu$$
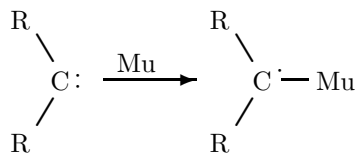
The relationship of such radicals to methyl is obvious when one replaces the alkyl groups (R) with H atoms.

Carbenes are relatively exotic species in chemistry. They possess a neutral dicoordinate carbon atom with a lone pair of electrons, so they are generally extremely reactive and are usually only postulated as reaction intermediates. However, over the past decade the synthesis and isolation of several singlet carbenes have been accomplished. A preliminary exploration with a commercially available carbene (**1** = 1,3,4-triphenyl-4,5-dihydro-1*H*-1,2,4-triazol-5-ylidene studied as a 0.25 M solution in tetrahydrofuran) gave encouraging results: A single pair of radical precession frequencies was detected by transverse field μSR, indicating that only one type of radical is formed, and this was tentatively assigned as radical **1a** (Fig. 107).

This result was very significant, since it represents the first example of radical formation by direct H (Mu) addition to a carbene. In fact, the addition of a hydrogen atom to a dicoordinate carbon constitutes one of the most fundamental addition reactions in chemistry – involving the creation of only one new chemical bond. The study of radicals formed from carbenes may permit the exploration of fundamental questions concerned with bond formation, such as: 1) How does the electronic structure of the reaction site change when the singlet carbene (sp^2 hybridized?) is converted into a doublet state? 2) Does the previously empty π-orbital accommodate the extra electron, or does the singly-occupied molecular orbital have more sp^3 character? The unpaired spin distribution in the radical and the geometry at the radical centre may provide valuable clues.

To investigate further we embarked on a collaboration with Dr. Jason Clyburne of the SFU Chemistry Department, who has considerable expertise and interest in carbene chemistry. The first step in the investigation was to confirm that Mu addition occurs at the carbene centre rather than elsewhere in the molecule. To
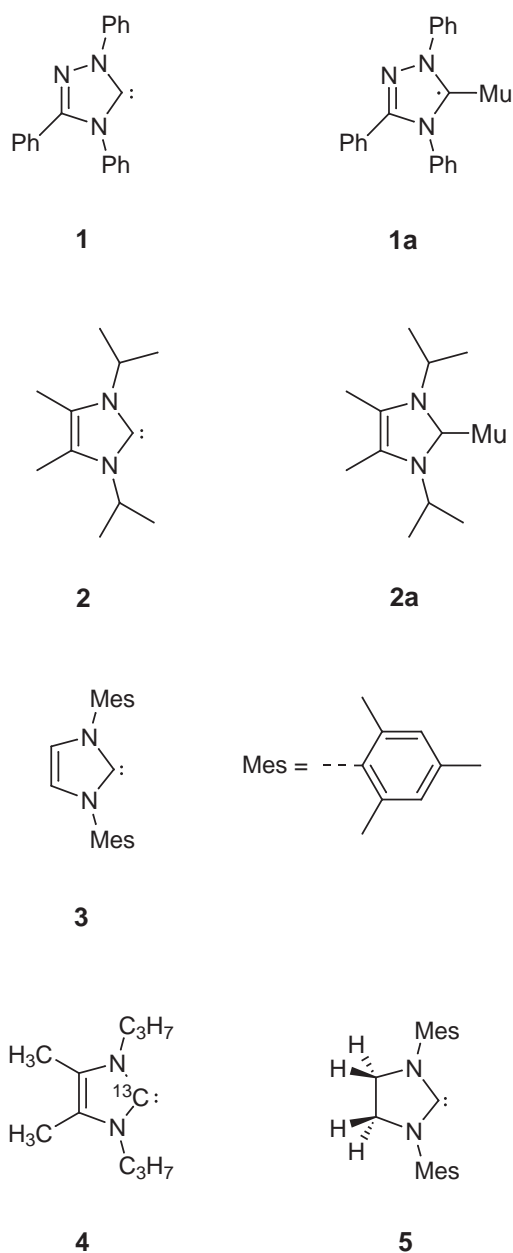
Fig. 107. The structures of carbenes (**1**–**5**) and some typical radical products (**1a**, **2a**) formed by Mu addition.

minimize the possible products, symmetrical carbenes are needed, so carbenes **2** and **3** were synthesized.

There are two obvious sites of Mu addition – at the carbene and alkene carbons (see Fig. 108).

Computational studies indicate that addition of hydrogen atoms to either site is exothermic, but addition to the carbene carbon is favoured (i.e. it gives the less energetic radical product).

Muon irradiation of **2** was found to produce only one type of radical. The muon hyperfine constant (hfc) was determined by TF-μSR (Fig. 109) and found to be 246.43 ± 0.02 MHz. One resonance was observed in
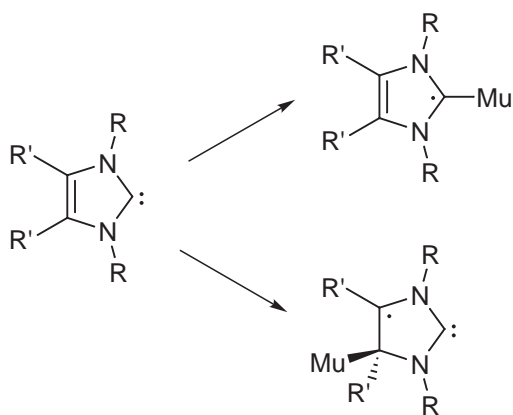
Fig. 108. Possible reactions of stable imidazole-type carbenes with muonium.
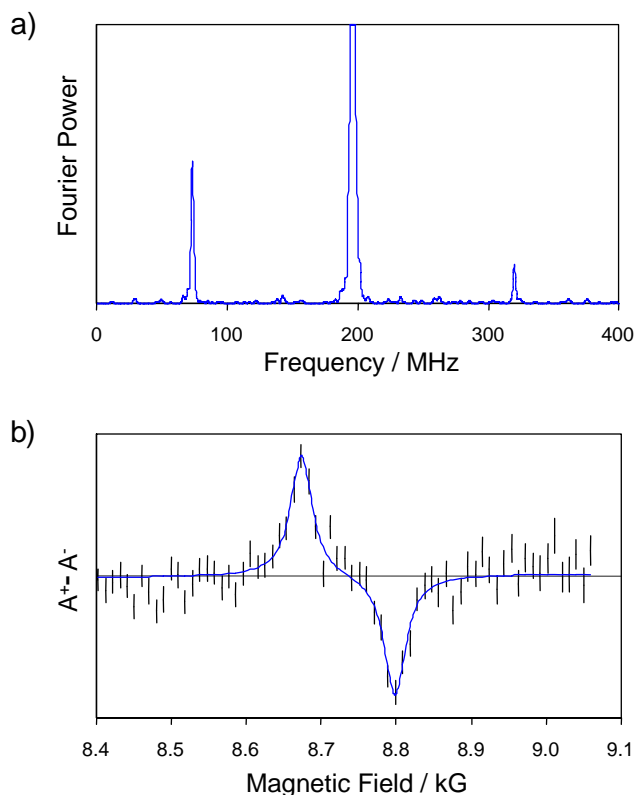
Fig. 109. (a) TF-μSR, and (b) μLCR spectrum of **2** in tetrahydrofuran at 298 K.

the μLCR spectrum at 8736.44 ± 1.24 G corresponding to either ^{14}N nuclei with hfc $A_N = 13.73 \pm 0.04$ MHz or protons with $A_p = 82.88 \pm 0.03$ MHz. Similar experiments were carried out with carbene **3**. The results for both carbenes are in good agreement with the predictions of density functional calculations, and we conclude that Mu adds exclusively to the carbene centre.

Two new avenues were explored in a second week of beam time. First, a ^{13}C-enriched version of carbene **2** was synthesized and investigated. The molecule was labelled at the carbene carbon (structure **4** in Fig. 107) to provide a clear signature of spin localization at this centre. Synthesis difficulties resulted in an enrichment of only 40%. In addition, the μLCR signal is predicted to be relatively weak, so it was a time-consuming exercise to locate the resonance and record it with adequate signal-to-noise. Nevertheless, this was achieved and the ^{13}C hfc was determined.

Second, a sample of a saturated imidazolylidene (**5**, the dihydro derivative of **3**) was obtained and investigated, the idea being to remove the possibility of Mu addition at the alkene site. The TF-μSR spectrum revealed a single radical but with a much smaller muon hfc than for **2** and **3**. This was unexpected and clearly merits further investigation. One possible explanation is that the Mu adduct of the saturated carbene has a more planar geometry at the radical centre. We plan to investigate this through measurements of the temperature dependence of muon and ^{13}C hfcs. However, such studies extend beyond the original scope of Expt. 883, and accordingly we have launched a new proposal, Expt. 945, which was approved by the Experiments Evaluation Committee in December, 2002.

The research carried out in Expt. 883 will form the major part of the Ph.D. thesis of Iain McKenzie (Chemistry Department, SFU).

Experiment 888
Test of delayed-muonium model for hydrocarbon liquids
(D.C. Walker, UBC)

These experiments were designed to test directly whether the "delayed" muonium-formation mechanism of low temperature inert materials [eg. Storchak *et al.*, Phys. Rev. Lett. **76**, 2969 (1996); Morris, Ph.D. thesis, University of B.C. (1997)] also applies to common chemicals like water, alcohols and hydrocarbons at room temperature. This possibility acquired extra importance for the Muonium Chemistry community when a theoretical model [Siebbeles *et al.*, J. Chem. Phys. **111**, 7493 (1999); Siebbeles *et al.*, Physica **B289-290**, 404 (2000)] was able to simulate the yields of muonium atoms (and their "complementary" diamagnetic species, D) in liquid hexane [Ito *et al.*, Can. J. Chem. **58**, 2395 (1980); Ito *et al.*, Hyp. Int. **8**, 355 (1981)] based on this delayed formation mechanism. In this model, the muonium atoms are predicted to be formed $\sim$60 nm beyond the end of the muon's radiation-track and to take microseconds to form [Siebbeles *et al., op. cit.*]. This picture is a time-dilation of the old "spur" model [Percival *et al.*, Advances in Chemistry Series **175**, 335 (1979)] and both are in direct conflict with the even older hot model of muonium formation [Fleming *et al.*, Advances in Chemistry Series **175**, 279 (1979);

Walker, Muon and Muonium Chemistry (Cambridge University Press, 1983)], where the latter is based on reactions occurring at the pre-thermalization stage.

In both the delayed and spur models it is presumed that the positive muons survive as unattached μ^+ particles from the charge-exchange cycles of thermalization. Some of them form muonium atoms (Mu, μ^+e^-) later by combining with an electron produced in the muon's radiolysis track in the simple thermal neutralization reaction (1):

$$\mu^+ + e^- \rightarrow \text{Mu}. \tag{1}$$
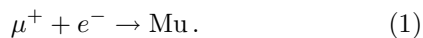
Muons which do not undergo reaction (1) constitute the "diamagnetic" species, D. Mu formation is predicted to occur close to where the muon comes to rest, with the distance being within a nanometer or two of the muon's last track-ionization (i.e. very close to the last spur) in the spur model [Percival et $al.$, $op.$ $cit.$], and about 60 nm beyond that for the delayed model [Siebbeles et $al.$, $op.$ $cit.$]. As the electrons will not be distributed randomly around the muons in either case, nonhomogeneous kinetics will apply to reaction (1) giving a range of formation times. In these experiments solutes were added to scavenge e^- and μ^+ under pseudo-first order conditions. If reaction (1) occurred then the solutes would reduce the yield of Mu and increase that of D.

These were muon spin rotation studies using the SFUMU cart with backward muons on the M9B beamline and supported through the μSR Facility. About one hundred samples of pure liquids and solutions of selected solutes in these liquids were studied during the one week of beam time available. The samples were all deoxygenated and contained in 50 mL glass vessels. They were subjected to the usual on-line μSR fitting analysis [Percival et $al.$, $op.$ $cit.$; Fleming et $al.$, $op.$ $cit.$] to evaluate the initial asymmetry A (proportional to yield), the initial phase ϕ and the relaxation constants, for both Mu (M) and D. Muonium atoms were found to have lifetimes >1 μs in our hexane (and methanol and water) so Mu is directly observable, as shown in Fig. 110(a) for n-hexane (C_6H_{14}). To this hexane, a variety of solutes were then added which are known to scavenge electrons with rate constants in the 10^{12} $M^{-1}s^{-1}$ range (CCl_4, nitrobenzene, benzophenone, styrene, tempo and oxygen) or proton (μ^+) scavengers (methanol and triethylamine).

Our initial experiments used solutes at concentrations that targeted the delayed model – they used millimolar concentrations to reduce the electron lifetimes to <10^{-7}s. These results are indicated in Fig. 110 (same initial yield with or without CCl_4) and in Tables VIII and IX, where the fitted initial phases of Mu and D are seen to be unaffected by added
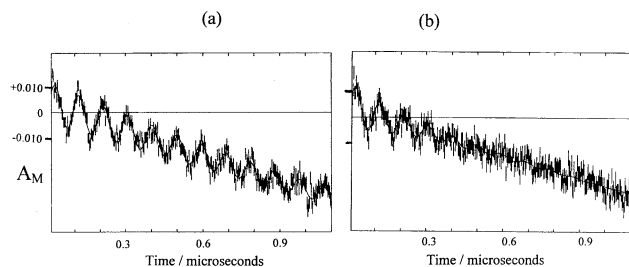
Fig. 110. (a) Plot of the TF-μSR muonium asymmetry (A_M) over the first μs in neat n-hexane at room temperature (293 $\pm$ 5 K) with an applied transverse magnetic field of 7.5 G. (b) Analogous plot to that in (a) except the hexane contains CCl_4 at a concentration of 0.0044 M (which reduces the electron lifetime to $\sim$$10^{-10}$ s). The initial yield of Mu is seen to be the same, only the relaxation has changed.

Table VIII. Values of the initial phase of Mu (ϕ_M) recorded for experiments in neat hexane and various solutions of electron scavengers, in fields of 7.5 G at room temperature with diagonally opposite counters called UP and DOWN.

System	ϕ_M (DOWN)	ϕ_M (UP)
neat hexane (Fig. 110a)	265.32 $\pm$ 3.88	67.13 $\pm$ 4.74
neat hexane	266.30 $\pm$ 3.65	81.66 $\pm$ 4.52
neat hexane	272.48 $\pm$ 3.54	75.38 $\pm$ 4.48
CCl_4 in hexane (Fig. 110b)	270.94 $\pm$ 5.80	—
0.15 mM NitroB in hexane	262.11 $\pm$ 5.25	81.81 $\pm$ 6.83
0.30 mM NitroB in hexane	269.18 $\pm$ 6.11	71.77 $\pm$ 8.56
0.09 mM NitroB in hexane	254.70 $\pm$ 5.33	80.15 $\pm$ 8.03
21 μM Tempo in hexane	264.13 $\pm$ 5.00	79.38 $\pm$ 5.00
30 μM Tempo in hexane	265.79 $\pm$ 4.12	72.44 $\pm$ 5.60
46 μM Tempo in hexane	272.89 $\pm$ 5.45	81.89 $\pm$ 6.01

Table IX. Values of the initial phase of D (ϕ_D) recorded for experiments in neat hexane and solutions of electron and muon scavengers, in fields of 91 G at room temperature.

System	ϕ_D (DOWN)	ϕ_D (UP)
neat hexane (Fig. 111a)	87.75 $\pm$ 0.40	278.15 $\pm$ 0.44
neat hexane	88.35 $\pm$ 0.58	279.96 $\pm$ 0.68
Fig. 111b solution	89.18 $\pm$ 0.39	279.66 $\pm$ 0.45
0.5 M Methanol in hexane	87.17 $\pm$ 0.41	278.24 $\pm$ 0.47
Oxygen in hexane	86.15 $\pm$ 0.38	277.40 $\pm$ 0.44
0.2 M (NitroB + TEA) in hexane	89.15 $\pm$ 0.41	280.33 $\pm$ 0.48
0.2 M NitroB in hexane	88.23 $\pm$ 0.54	280.73 $\pm$ 0.64
0.1 M Benzophenone in hexane	87.60 $\pm$ 0.36	279.56 $\pm$ 0.42
0.2 M Triethylamine in hexane	87.55 $\pm$ 0.44	278.98 $\pm$ 0.50

scavengers of both e^- and μ^+. This shows clearly that Mu is not formed to any significant extent on the microsecond timescale by reaction (1).

The experiments were thus extended to much higher concentrations of scavengers to cover the nanosecond timescale corresponding to the spur model. Those results are represented by Fig. 111 (same initial

92

Fig. 111. (a) Plot of the TF-μSR diamagnetic asymmetry (A_D) against time over 5 μs for neat n-hexane at room temperature (293 ± 5 K) with a transverse magnetic field of 91 G. (b) Analogous plot to (a) except the hexane contains 0.49 M methanol + 0.087 M styrene (which essentially eliminates both e^- and μ^+). The initial yield of D is seen to be the same and no relaxation is observable.

yield and no decay, with or without e^- and μ^+ scavengers) and in Table X as the yields are unaffected by added scavengers in methanol and hexane. D was not measurably affected by the inhibition of reaction (1), so we deduce that Mu is not formed by that mechanism. (Mu itself could not be directly observed in those systems as all powerful electron scavengers react with Mu to some extent, as seen in Fig. 110(b) for 4.4 mM CCl_4.)

Having eliminated the delayed and spur models one is left with the hot model, the only model proposed so far whose precursor ($Mu_{(hot)}$) is not scavengable on the 10^{-11}s timescale. The hot model thus wins by default – at least in these chemical-active media at room temperature.

Unfortunately, similar scavenging experiments would be very difficult to do in the low temperature inert liquids or solids where electric field effects have shown reaction (1) to occur [Storchak et al., op. cit.]. But these are such inert systems that μ^+ and Mu have no other chemical reaction channels available, which is not the case in hexane, methanol or water.

Table X. Yields of D(P_D = 0.62 $A_D/A_{(water)}$) obtained in various solutions of hexane with electron or muon scavengers.

Solution	P_D
n-hexane	0.61
+ nitrobenzene (0.2 M)	0.59
+ benzophenone (0.1 M)	0.60
+ CCl_4 (4 mM)	0.60
+ oxygen (8 mM)	0.60
+ $N(C_2H_5)_3$ (0.2 M)	0.60
+ methanol (0.5 M)	0.61
+ $N(C_2H_5)_3$ (0.2 M) + nitrobenzene (0.2 M)	0.60
+ methanol (0.5 M) + styrene (0.1 M)	0.61

Experiment 891
Superconductivity and magnetism in $Ce_nM_mIn_{3n+2m}$
(G.D. Morris, LANL)

Experiment 891 is investigating superconductivity and magnetism in Ce-based heavy-fermion materials $Ce_nM_mIn_{3n+2m}$, M=Rh, Ir, Co. These materials exhibit a wide range of complex magnetic order and superconductivity which may be tuned with composition. The family of materials enables a systematic study of the relation between magnetism and unconventional superconductivity. Recently, our μSR experiments showed that antiferromagnetic order in $CeRh_{0.5}Ir_{0.5}In_5$ coexists microscopically with superconductivity [Morris et al., Physica B, in press].

In 2002 we studied magnetic properties in several $n = 2$, $m = 1$ samples. Antiferromagnetic order is known from neutron scattering experiments to be present in Ce_2RhIn_8. Specific heat data show that T_N decreases on substitution of Rh with Ir and hint at the possibility of a quantum critical point (QCP) where T_N seems to approach zero temperature for the M=Ir material. Using μSR as a sensitive local probe of magnetism, we carried out experiments on several samples to follow the development of electronic magnetic moments with varying composition in the vicinity of this proposed QCP.

Representative muon relaxation spectra recorded in Ce_2IrIn_8 are shown in Fig. 112. Samples with Ir substituted with 5% Co or 5 and 10% Rh displayed qualitatively the same behaviour. At temperatures of about 1 K and above, the muon spin relaxation function follows a Gaussian Kubo-Toyabe form characteristic of isotropic nuclear dipolar fields. On cooling, an additional relaxation mechanism is apparent as an increase in spin depolarization rate. No coherent

Fig. 112. Muon spin polarization functions in Ce_2IrIn_8 at $T = 1.0$ (circles) and 0.022 K (squares).

precession signal indicative of ordered magnetism was found; the muons see only randomly oriented magnetic fields. Assuming the nuclear dipolar broadening to be T-independent, the zero-field muon relaxation spectra were fitted with a polarization defined in terms of a product of Kubo-Toyabe functions

$$
\begin{aligned}
G(t) \quad = \quad & \left[\frac{1}{3} + \frac{2}{3}(1 - \Delta_n^2 t^2) \exp(-\Delta_n^2 t^2/2) \right] \\
& \times \left[\frac{1}{3} + \frac{2}{3}(1 - \Delta_{el}^p t^p) \exp(-\Delta_{el}^p t^p/p) \right]
\end{aligned}
$$

where the widths due to nuclear dipolar and electronic magnetic moments are characterized by Δ_n and Δ_{el} respectively. (A non-relaxing background signal was also present in this dilution refrigerator data.) Δ_n for each sample was obtained from high temperature data and these values were held constant in fitting the low temperature spectra. The exponent p was found to be 0.6–0.7 in all samples. Figure 113 shows the temperature dependences of Δ_{el}. In all samples Δ_{el} is not large; the additional local magnetic field is comparable to nuclear dipolar fields, implying the electronic moments are small. High transverse field data in Ce_2IrIn_8 also revealed two lines and hence two muon sites with different Knight shifts. The anomolous value of p may

Fig. 113. Linewidths $\Delta_{el}(T)$ characterizing the electronic contribution to muon spin relaxation in several $Ce_2Ir_{1-\delta}M_\delta In_8$ samples.

therefore result from characterizing the sum of two signals (resulting from Lorentzian field distributions with differing values of Δ_{el}) with one signal. Nevertheless, this phenomenological fitting model accomplishes the goal of extracting a measure of the additional line broadening from electronic magnetic moments and identifies their onset temperatures. Electronic magnetic moments appear at about 700 mK in all four samples, however, the widths $\Delta_{el}(T = 0)$ do vary with composition. These widths are highest for the $Ce_2Ir_{0.95}Co_{0.05}In_8$ sample and decrease by a factor of 2 across the series to the smallest value in $Ce_2Ir_{0.90}Rh_{0.10}In_8$.

Runs with a longitudinal field of 20 mT applied parallel to the muon spin resulted in complete decoupling of the muon spin from the internal field, indicating the electronic moments are static on timescales of μs. We conclude that all the samples near the M=Ir composition develop weak, static and disordered electronic moments. These μSR results rule out the possibility of a quantum critical point at M=Ir in the Ce-218 family.

Experiment 894
Muonium kinetics and free radical formation in solutions of fullerenes
(P.W. Percival, SFU)

Aqueous solutions of fullerenes have long been sought for their application in biological systems. However, fullerenes are notoriously difficult to dissolve, and being hydrophobic their solubility in water is even more of a problem. One approach has been to generate fullerene sols, i.e. colloidal suspensions. Various methods of producing sols have been developed in the past few years, including (a) sonication of millimolar concentrations of fullerenes in organic solution in the presence of water; (b) preparation of organic solutions of the mono-anion, which are then added drop-wise to water; and (c) direct injection of a small amount of a concentrated solution of fullerene in an organic solvent into water. In all cases the organic solvent is removed, leaving fullerene clusters suspended in water.

Experiment 894 was conceived to explore muonium chemistry in aqueous fullerene sols. We set out to answer questions such as: How does fullerene aggregation affect chemical kinetics? Is the reaction between Mu and the sol clusters diffusion-controlled? What is the nature of the reaction? Can we identify the product? The chemistry is well understood for organic (true) solutions of fullerenes: In previous work (TRIUMF Expts. 654 and 749) we have clearly shown that Mu adds to fullerene molecules to form the radical adduct, e.g.

$$
Mu + C_{60} \rightarrow C_{60}Mu \, .
$$

Radio frequency muon spin resonance, low-field

muon spin rotation (μSR), and muon level-crossing resonance (using ^{13}C-labelled material) have all been used to characterize the radicals formed from C_{60} and C_{70} in organic solvents. Only the second, low-field μSR is appropriate for aqueous sols, but unfortunately our experiments have been indeterminate. We had hoped to detect a clear signature of the Mu adduct, $(C_{60})_N$Mu, but the lack of a radical signal could be due to several reasons: a different product, broad lines due to a spread of hyperfine constants, or (most likely) simply inadequate concentration to achieve sufficient signal to noise at the radical precession frequencies.

Most of our beam time in 2002 was spent on a different type of measurement, albeit again with frustrating results. Regardless of product, it is possible to measure the damping of the Mu precession signal in low transverse field to determine the rate of reaction. If it is assumed that Mu reacts with a fullerene cluster (sol particle) containing N C_{60} molecules, then the Mu decay rate is given by

$$\lambda - \lambda_0 = k_{\mathrm{sol}}[\mathrm{sol}] = (k_{\mathrm{sol}}/N)[C_{60}]$$
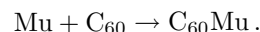
where λ_0 is the Mu decay rate in pure water. To interpret the chemical kinetics we need the second-order rate constant k_{sol}, but the usual plot of decay rate versus reactant (C_{60}) concentration would give us (k_{sol}/N). However, the aggregation number N is related to the size of the sol particle, which can be determined by dynamic light scattering (DLS). This we have done. In principle, then, we can determine the rate constant k_{sol} and compare it with the prediction for a diffusion-controlled reaction.

Muonium decay measurements have now been made in three different beam periods, but with inconsistent results. Some of the early data can be explained by technical problems, but the use of improved apparatus in 2002 has eliminated this source of error. The explanation for the scattered results seems to lie in the dependence of the reaction rate on the aggregation number N. Not only does N vary with method of sol preparation, it can also have a spread of values in fresh solutions prepared by the sonication method. To get around this problem we tried "aged" samples, which DLS measurements showed to be monodisperse (sol particles with a narrow size distribution). We were able to accumulate a set of consistent and reliable data, only to discover that the Mu decay rate (λ) in such sols is not a simply linear function of C_{60} concentration, as implied by the equation given earlier. Some of these data are shown in Fig. 114. Perhaps N varies with fullerene concentration? Detailed interpretation of the Mu decay results awaits further DLS studies.

Experiment 894 research will form the major part of the M.Sc. thesis of Sonja Kecman (Chemistry, SFU).
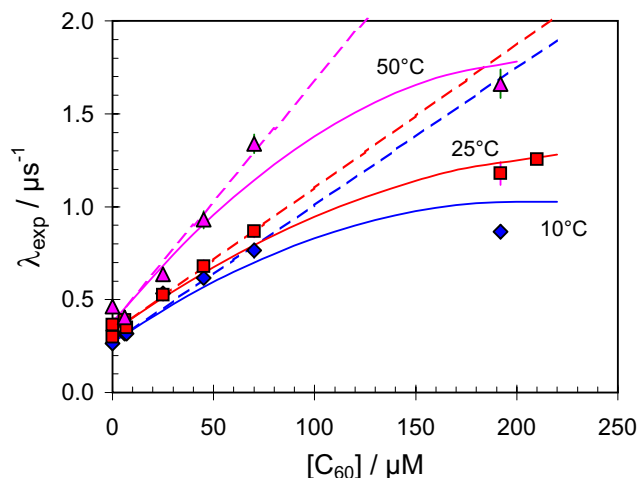
Fig. 114. Muonium decay rates as a function of C_{60} concentration for aqueous sol samples generated by the sonication method. The deviation from the expected linear behaviour is evident at all three temperatures.

Experiment 895
The vortex structure and magnetism of electron-doped cuprate superconductors
(R. Kadono, KEK-IMSS; K.M. Kojima, Tokyo)

Electron-hole asymmetry in the phase diagram of cuprate superconductors is one of the key issues for selecting the models of pairing mechanisms being proposed. Despite its importance, however, so far the study of electron-doped cuprates is far behind that of hole-doped systems. This is partly because of the limited variety of compounds and associated difficulty of obtaining them as large single crystal specimens; earlier works have been done mostly on $L_{2-x}Ce_xCuO_{4-\delta}$ (where L=Nd, Pr, and Sm) which are available only as a small amount of tiny crystals. This situation has been changed recently by Fujita and co-workers from ICR, Kyoto, who succeeded in growing a large single crystal of $Pr_{1-x}LaCe_xCuO_{4-\delta}$ (PLCCO).

Another important issue related to the electron-doped cuprates is the microscopic nature of the oxygen depletion process which is needed to turn the as-grown material into superconducting. It is believed that the excess oxygen atoms occupy apical sites between the CuO_2 planes, and that the removal of those leads to the electron doping. In this regard, the newly synthesized PLCCO has an interesting character in that it is stable over a wide range of the oxygen depletion, $0 \leq \delta \leq 0.12$. In the 2002 beam time, we concentrated on the μSR experiment to map out the magnetic phase diagram of this PLCCO system with δ as the primary parameter. (The phase diagram as a function of carrier concentration x has been reported by other groups, yielding a result similar to $Nd_{2-x}Ce_xCuO_{4-\delta}$ with a little wider region of superconductivity.)

The results of ZF-μSR measurements on
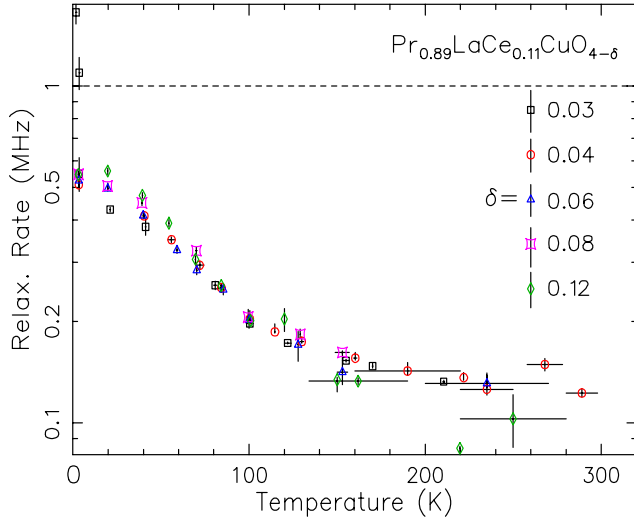
Fig. 115. Muon spin relaxation rate under zero field in $Pr_{0.89}LaCe_{0.11}CuO_{4-\delta}$. It is almost common among all the specimens except for $\delta = 0.03$, where the relaxation rate shows a steep increase below $\sim$2 K.

$Pr_{0.89}LaCe_{0.11}CuO_{4-\delta}$ with δ=0.03, 0.04, 0.06, 0.08, and 0.12 are summarized in Fig. 115. The relaxation rate exhibits a universal behaviour of increase with decreasing temperature below about 150 K regardless of the oxygen depletion. The observed time spectra in those specimens are common to show an exponential depolarization overlapped with Gaussian-like damping due to nuclear dipolar fields, indicating that the origin of the exponential relaxation is due to random magnetic moments. The absence of δ dependence further suggests that the random moments are carried by Pr^{3+} ions, although the ground state of which is presumed to be nonmagnetic. This means that there is a significant contribution of magnetic excited levels split by the crystal electric field over this temperature range. A similar situation has been reported to occur in $Pr_{1.85}Ce_{0.15}CuO_{4-\delta}$ (see 2000 TRIUMF Annual Report). A more detailed report is now in preparation.

Experiment 912
Formation, structure and dynamics of muonium in GaAs studied by EF-RF μ^+SR
(V.G. Storchak, Kurchatov)

Studies of traps and recombination centres in semiconductors is of fundamental and technological interest. Muon spin relaxation experiments with electric fields (EF) have shown that in condensed samples the stopped muon is very close to (at distances less than 10^{-5}cm) or even surrounded by its own track products. Some excess electrons generated in the track are close enough to reach and to be captured by the stopped muon and form a muonium atom. This process of delayed muonium formation is relevant to the process of trapping excess electrons by an attractive centre.

Radio frequency (rf) μSR is particularly well suited for investigating such processes because this technique can detect final states that are formed within a μs timescale, rather than only prompt or formed within nanoseconds scale fractions which are detected by conventional time-differential (TD) μSR. Here we report an EF + RF-μSR experiment in semi-insulating GaAs providing a demonstration of the role of track electrons in muonium dynamics.

Time-differential μSR experiments show that at low temperatures, $T < 100$ K, virtually no diamagnetic muonium (i.e. Mu$^+$ or Mu$^-$) is formed after muon implantation into semi-insulating GaAs RF-μSR studies detect a significant diamagnetic fraction at low temperatures: the diamagnetic fraction appears at $T \sim 20$ K and rises to about 0.4 at $T \sim 60$ K. Electric field dependences of the diamagnetic rf fraction measured at two different temperatures are presented in Fig. 116.

At $T = 61.5$ K the diamagnetic fraction in small electric fields $|E| < 2$ kV/cm is big; at high electric fields data tend to low temperature points.

There are two alternative explanations of this behaviour. According to the first approach the diamagnetic signal seen at low electric fields at $T = 61.5$ K is due to slow thermal ionization of Mu$^0_{BC}$. To explain the decrease of the diamagnetic signal in moderate electric fields one has to include rapid track electron recapture by the Mu$^0_{BC} \rightleftharpoons$ Mu$^+_{BC}$ process.

An alternative model involves Mu$^-_{BC}$ formation. Just after the slowing down process, the bare muon is surrounded with a cloud of its own track electrons. Due to strong Coulomb interaction, the muon captures one of the track electrons and forms Mu$^0_{BC}$. At this stage Mu$^0_{BC}$ is still surrounded by electrons. Neutral muonium can attract a second electron and form Mu$^-$.
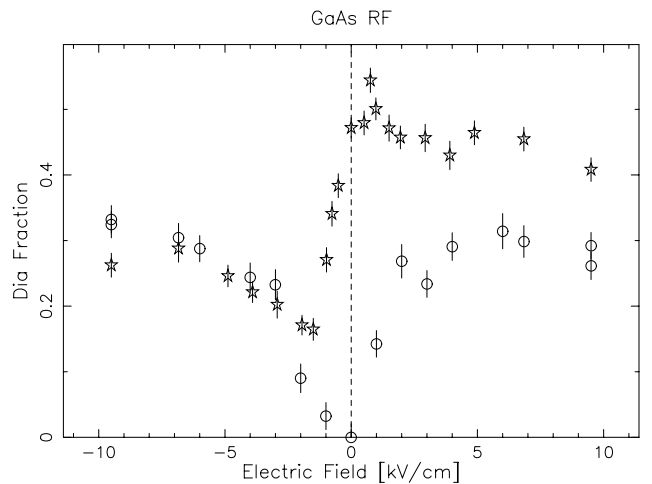
Fig. 116. Diamagnetic RF fraction in semi-insulating GaAs as a function of electric field. Circles: $T = 15$ K; stars: $T = 61.5$ K. Positive electric field is in the direction of the initial muon beam momentum.

96

The muonium-electron interaction is a weak charge-induced dipole attraction and muonium-electron mutual motion is a diffusion controlled random walk. At low temperatures the diffusion coefficient is small ($D = \frac{kTb}{e}$, where b is the electron mobility) and the probability of Mu^- formation is negligible. As the temperature is raised, D becomes larger and the probability of Mu^- formation increases. At some temperature Mu^- starts to ionize and the fraction we observe in zero electric field is a result of the $Mu^0 \rightleftharpoons Mu^-$ exchange process. This is valid until Mu^0_{BC} starts to ionize. According to the model of Mu^0_{BC} formation through the intermediate shallow state, this critical temperature is about 100 K. Electric fields higher than $E_c \approx 5$ kV/cm prevent Mu^0_{BC} formation and the diamagnetic fraction corresponds to the bare muon. Low electric fields move the cloud of track electrons away from the already formed Mu^0_{BC} and thus diminish the probability of Mu^- formation.

In conclusion, EF + RF-μSR experiments have been successfully carried out in semi-insulating GaAs. The results suggest Mu^- formation at $T < 100$ K and open new opportunities to study electron capture by positive and/or neutral centre in a semiconductor.

Experiment 915
Muonium in semiconductor alloys
(R.L. Lichti, Texas Tech)

TRIUMF Expt. 915 consisted of two separate parts, one to study the silicon-germanium alloys and the second to examine II-VI alloys with Cd and Zn mixed on one sublattice. The first week of beam time, taken in 2001, concentrated on the $Si_{1-x}Ge_x$ system, while the second week taken this year was on the (Cd,Zn)X chalcogenide alloys.

Figure 117 gives an update on results for the (Si,Ge) alloys, showing the mean hyperfine parameter for the bond-centred (BC) Mu^0 state as a function of alloy concentration. Although this graph shows that the average hyperfine interaction is remarkably linear across the full alloy range, a more detailed examination of the lineshapes and temperature dependences suggests that there may be a slight site preference for Si-Si bonds for Mu^0_{BC} at low temperatures. This is one of several areas to be pursued in future Expt. 915 allocations.

The metastable Mu^0_T state was only observed cleanly in one sample with low Ge content, $x = 0.2$; while any possible spin precession signal from Mu^0_T for $x = 0.45$ and 0.77 was very broad if observed at all. From the one data point, it appears that the hyperfine constant decreases from $A_{hf}(T)$ for Si for small x instead of increasing toward the value for Ge. The implied non-monotonic behaviour for the T-site Mu^0 will
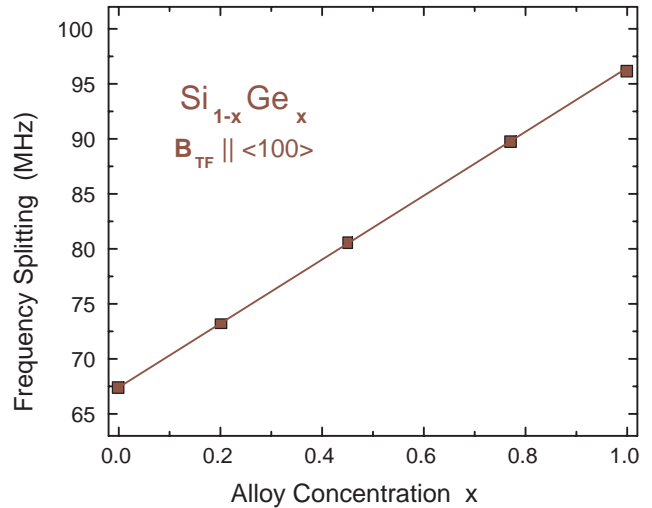
Fig. 117. The average hyperfine splitting obtained for Mu^0_{BC} as a function of concentration in the $Si_{1-x}Ge_x$ alloys. This variation, representing the isotropic part of $A_{hf}(BC)$, is surprisingly linear across the full range.
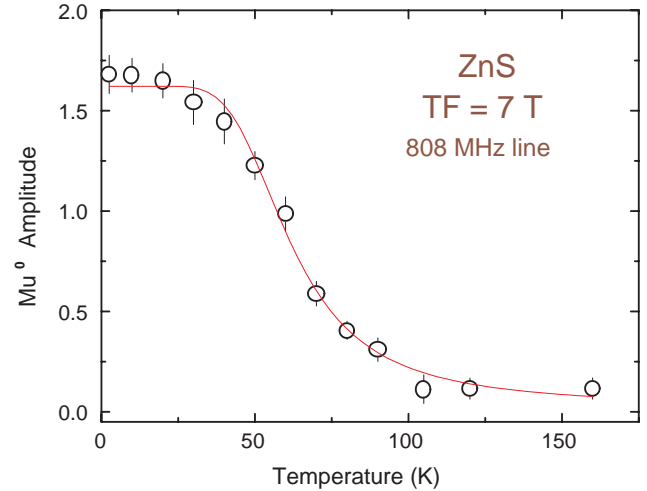
Fig. 118. The temperature dependent amplitudes for the Mu^0 signal in ZnS suggest a very low ionization energy, although the hyperfine constant implies a highly localized impurity-like electronic wavefunction for Mu^0 rather than that for an effective-mass shallow donor.

be investigated further with additional samples having low Ge concentration to follow the hyperfine splitting in more detail.

During the week of time dedicated to the II-VI alloys, we looked at several samples with low Zn content for both the (Cd,Zn)S and (Cd,Zn)Te systems. Unfortunately, we did not observe either a shallow donor or an atomic-like Mu^0 spin precession signal in any of these II-VI alloy samples. However, for Zn content below about 15% in both systems, at temperatures below 30 K there were changes in the relaxation functions associated with the diamagnetic signals that suggested the possibility of a shallow Mu^0 state undergoing very

fast dynamics of some sort. We suspect charge transfer with other defects since the impurity and native defect concentrations are quite high in the samples available during that beam time. Only an atomic-like Mu^0 signal was seen in the ZnS binary compound; however, this signal disappears by about 100 K as seen below.

The temperature dependence for the atomic-like (deep) Mu^0 centre in ZnS is shown in Fig. 118. Although the temperature at which the Mu^0 signal disappears is quite low, the large hyperfine constant, nearly the full free-atom value, identifies this state as a deep Mu^0 defect. Investigation of muonium states in the II-VI alloys as well as in the parent binary compounds will continue as part of a newly proposed experiment to determine the muonium (or hydrogen) defect energy level for comparison to recent theoretical predictions.

Experiment 916
QLCR of diamagnetic muonium states in GaP
(R.L. Lichti, Texas Tech)

Zero-field depolarization functions demonstrated that several different diamagnetic muonium states exist in doped GaP. The aim of TRIUMF Expt. 916 is identification of these states using quadrupolar level-crossing resonances (QLCR). The two Ga isotopes produce a clear signature of a Ga near neighbour to the muon, while P has no quadrupolar nuclei, and thus is invisible to this technique. We initially examined a mid-$10^{16}cm^{-3}$ n-type sample near room temperature where the expected state is an isolated Mu^-; however, the resonances were weak and identification was not conclusive. Two higher concentration n-type samples and a heavily Zn-doped p-type sample have now been examined at temperatures where isolated Mu^- and Mu^+ were expected. We used earlier spectra for these states in GaAs as a guide in searching for their signature in GaP. The results confirm our preliminary identification of those states based on zero-field assignments.

Figure 119 (top) shows the Mu^- QLCR signature at 140 K with $B\|\langle 100 \rangle$ for a $10^{18}cm^{-3}$ n-type GaP:S sample. This resonance is essentially identical to that for Mu^- in GaAs except that it is shifted to higher fields, implying an electric-field gradient (EFG) about 15% larger at the Ga neighbours in GaP compared to GaAs. The Mu^- location is assigned to the T-site with Ga nearest neighbours in both materials.

The diamagnetic fraction does not appear to change with n-type concentration as expected. There is essentially no major difference in three samples covering more than 2 orders of magnitude in electron concentration: Fig. 119 (bottom) shows the temperature dependence [Expt. 916 data below 300 K] for the high concentration sample. The state identity above 200 K
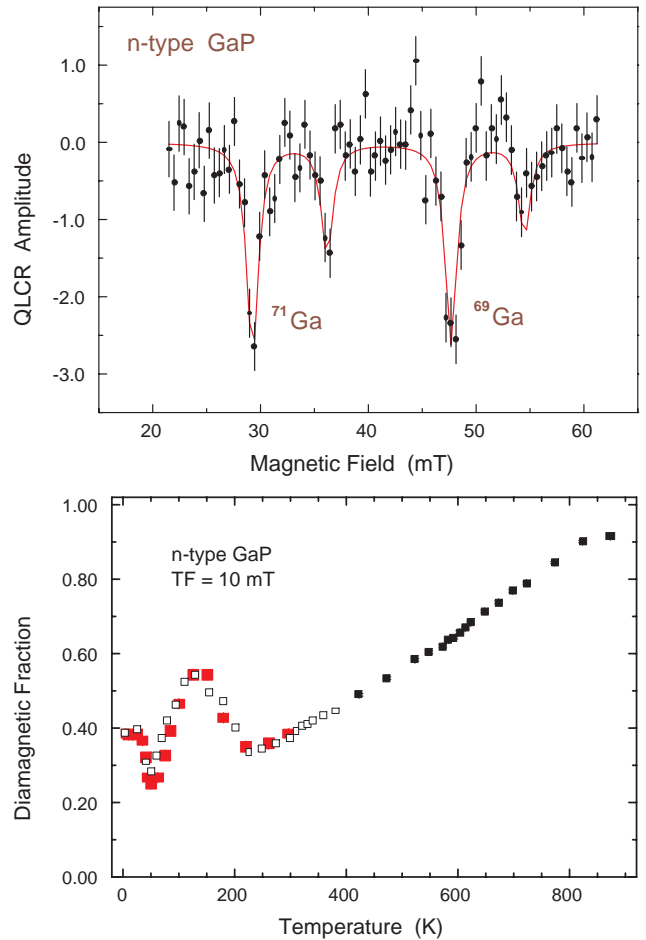
Fig. 119. QLCR spectra (top) confirm Mu^- in the T_{Ga} site at 140 K for heavily doped n-type GaP. However, the temperature-dependent diamagnetic fraction (bottom) is not as expected and further tests are required above 200 K.

remains in doubt pending QLCR tests in that range.

Most recently we examined the QLCR for Mu^+ in p-type GaP, finding the largest amplitude lines from both Ga isotopes. These lines are again at slightly higher fields compared to the GaAs spectra. These data confirm Mu^+ at the BC location at 150 K in GaP:Zn and indicate a somewhat larger EFG at Ga than for the Mu^+ state in GaAs. This trend in EFG is present for all states observed by QLCR thus far.

In addition to data at 150 K, the ^{71}Ga resonance was recorded at 50 K. A reduced amplitude at 50 K is consistent with zero-field data which suggest that up to 1/3 of the Mu^+ related centres may be paired with the Zn acceptor below about 100 K. A search for a different QLCR spectra to confirm a second state at low temperatures is planned for future Expt. 916 beam time.

To date, we have confirmed preliminary identification of three of the five proposed diamagnetic states in doped GaP; Mu^- at T_{Ga}, Mu^+ at BC, and a high-
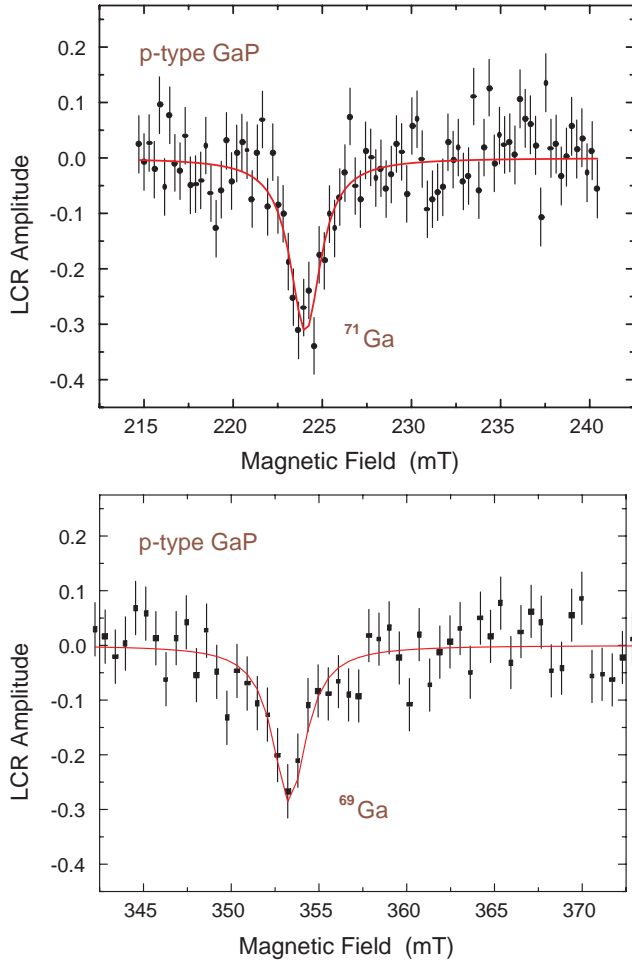
Fig. 120. QLCR spectra for the main line from ^{71}Ga (top) and ^{69}Ga (bottom) for Mu$^+$ in heavily doped p-type GaP at 150 K confirming the BC site based on similarity to the results for p-type GaAs.

temperature Mu-Zn paired state formed by Coulomb capture of mobile Mu$^+$ by Zn$^-$. We still seek confirmation of low-temperature pair formation proposed to occur by charge transfer interactions between mobile Mu$_T^0$ centres and neutral donors or acceptors below their respective ionization temperatures.

Experiment 917
Correlation between magnetism and transport properties of thermoelectric oxides
(J. Sugiyama, Toyota CRDL Inc.; J.H. Brewer, UBC-TRIUMF)

The "good" thermoelectric layered cobaltites Ca$_3$Co$_4$O$_9$ and Na$_x$CoO$_2$ share a common structural component: the CoO$_2$ sheets, in which a two-dimensional-triangular lattice of Co ions is formed by a network of edge-sharing CoO$_6$ octahedra. Charge carrier transport in these materials is thought to be restricted mainly to these CoO$_2$ sheets, as in the case of the CuO$_2$ planes for the high-T_c cuprates.

A recent μ^+SR experiment [Sugiyama *et al.*, Phys. Rev. **B66**, 134413 (2002)] indicated the existence of an incommensurate (IC) spin density wave (SDW) state below 100 K in Ca$_3$Co$_4$O$_9$, which was not detected previously by other magnetic measurements [Masset *et al.*, Phys. Rev. **B62,** 166 (2000)]. Meanwhile, the resistivity $\rho(T)$ exhibits a broad minimum around 80 K. Since the behaviour of conduction electrons is strongly affected by their magnetic order, this suggests a strong electron-electron correlation in Ca$_3$Co$_4$O$_9$. In order to further clarify the role of magnetism in thermoelectric layered cobaltites, we have measured both weak ($\sim$100 Oe) transverse-field positive muon spin rotation and relaxation (wTF-μ^+SR) and zero field (ZF-) μ^+SR time spectra in Ca$_3$Co$_4$O$_9$ at temperatures below 700 K.

Figures 121(a) and (b) show the temperature dependences of the paramagnetic asymmetry A_{para} and the corresponding relaxation rate λ_{para} in three Ca$_3$Co$_4$O$_9$ samples: a randomly oriented polycrystalline sample, a c-aligned polycrystalline sample and single crystal platelets. The large decrease in A_{para} below 100 K (and the accompanying increase in λ_{para}) indicates the existence of a magnetic transition with an onset temperature $T_c^{\mathrm{on}} \approx 100$ K and a transition width $\Delta T \approx 70$ K. The single crystal data suggest that the
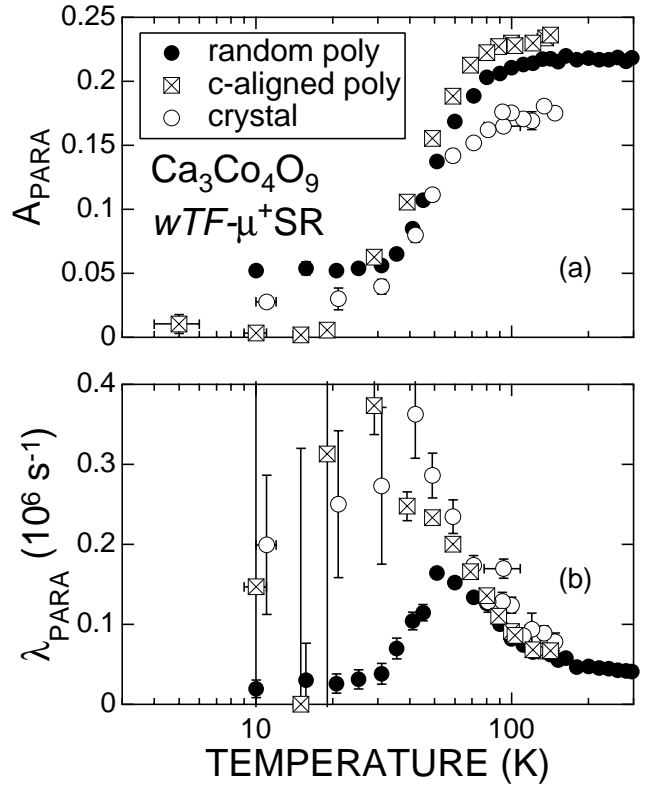
Fig. 121. (a) Paramagnetic asymmetry A_{para} and (b) relaxation rate λ_{para} as functions of temperature for the three Ca$_3$Co$_4$O$_9$ samples.
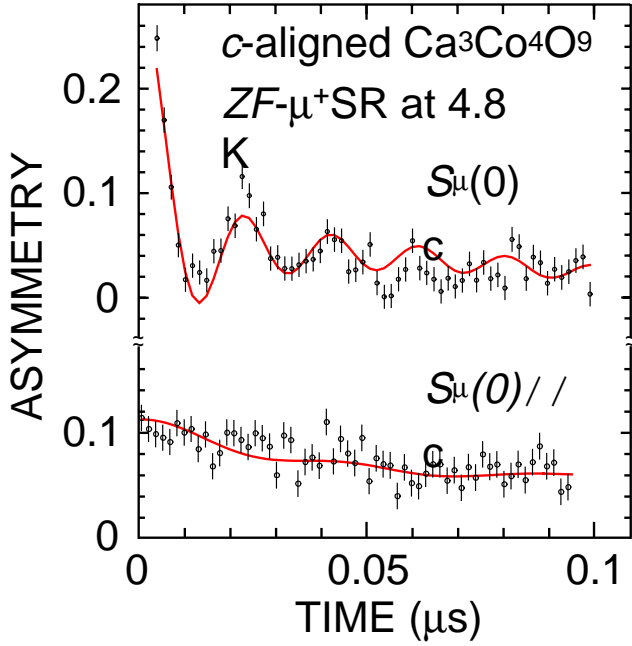
Fig. 122. ZF-μ^+SR time spectra of the c-aligned $Ca_3Co_4O_9$ plate at 4.8 K.

large ΔT is not caused by inhomogeneity of the sample but is an intrinsic property of this compound.

Figure 122 shows ZF-μ^+SR time spectra at 4.8 K in the c-aligned sample; the top spectrum was obtained with the initial μ^+ spin direction $\mathbf{S}_\mu(0)$ perpendicular to the c-axis and the bottom one with $\mathbf{S}_\mu(0) \parallel \hat{\mathbf{c}}$. A clear oscillation due to quasi-static internal fields is observed only when $\mathbf{S}_\mu(0) \perp \hat{\mathbf{c}}$. This oscillating spectrum is reasonably well fitted by the phenomenological function for an incommensurate spin density wave (IC-SDW) state [Kalvius et $al.$, in $Handbook$ on the $physics$ and $chemistry$ of $rare$ $earths$ **32** (North-Holland, Amsterdam, 2001) p. 55], namely a zeroth-order Bessel function of the first kind. We therefore conclude that $Ca_3Co_4O_9$ undergoes a magnetic transition from a paramagnetic state to an IC-SDW state (i.e. $T_c^{on} = T_{SDW}^{on}$). The absence of a clear oscillation in the bottom spectrum of Fig. 122 indicates that the internal magnetic field $\mathbf{H}_{int}$ is roughly parallel to the c-axis, since the muon spins do not precess in a parallel magnetic field. The IC-SDW is therefore considered to propagate in the a-b plane, with oscillating moments directed along the c-axis.

The high-temperature wTF-μ^+SR spectra in the c-aligned $Ca_3Co_4O_9$ sample indicate the existence of a broad shoulder in the $\lambda_{para}(T)$ curve at 400–600 K, although such a shoulder seems to be ambiguous in the Y-doped sample (Fig. 123(a)). This behaviour is in good agreement with the results of $\chi(T)$ measurements (see Fig. 123(b)). At these temperatures muons are diffusing rapidly, so that the relaxation rate usually decreases monotonically with increasing temperature.
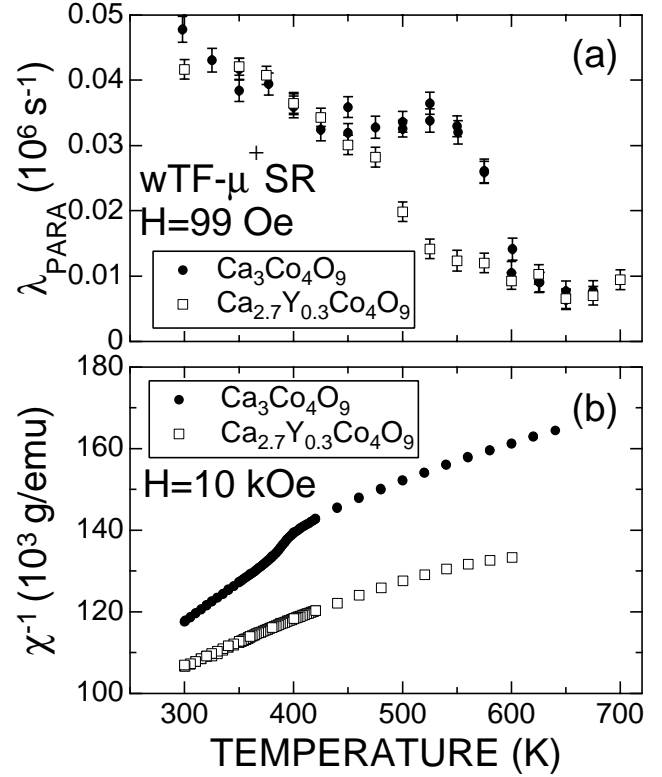
Fig. 123. Temperature dependences of (a) λ_{para} and (b) the inverse susceptibility χ^{-1} in polycrystalline $Ca_3Co_4O_9$ and $Ca_{2.7}Y_{0.3}Co_4O_9$ samples.

Furthermore, above 150 K A_{para} levels off to its maximum value ($\sim$0.23) – i.e., the sample volume is almost 100% paramagnetic. Hence we can conclude that this shoulder is induced by the spin state transition. Since H_{int} increases due to the spin state transition above T_{SS}, λ_{para} is expected to increase with increasing T. On the other hand, both the rapid muon diffusion and the fast exchange rate of electrons between Co^{3+} and Co^{4+} ions decrease λ_{para} with increasing T. The competition between these three factors is likely responsible for the broad shoulder in $\lambda_{para}(T)$ around 400–600 K.

The broad shoulder also indicates that the spin state changes gradually in the temperature range between 400 and 600 K. If the transition occurs abruptly at T_{SS}^χ as seen in the $\chi^{-1}(T)$ curve, then a calculation [Koshibae et $al.$, Phys. Rev. **B62**, 6869 (2000)] using the degeneracy of spin and orbital degrees of freedom of Co ions predicts that the thermoelectric power should show a dramatic change at T_{SS}^χ. Therefore, this gradual change in the spin state is apparently essential to the large thermoelectric power at elevated temperatures.

Figure 124 summarizes the magnetic transitions in $Ca_3Co_4O_9$. The two magnetic transitions detected by μ^+SR, i.e. the IC-SDW and the spin state transitions, are found to correlate closely with the transport properties of $Ca_3Co_4O_9$. The existence of the IC-SDW transition indicates an enhancement of the effective mass
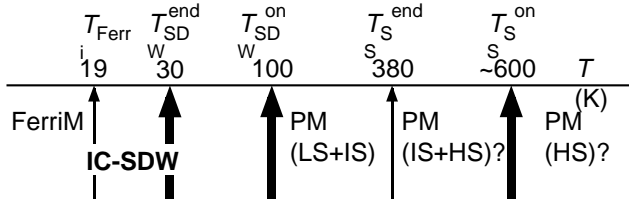
Fig. 124. Successive magnetic transitions in $Ca_3Co_4O_9$. The bold arrows indicate the transitions found by Expt. 917, while the narrow arrows show those detected by the previous susceptibility measurements.

of charge carriers (and thus the thermoelectric properties) by strong electron correlations. The existence of the spin state transition suggests that the crystal-field splitting between t_{2g} and e_g levels is comparable to $\sim$400 K. Furthermore, the gradual change in the spin state prevents a decrease in thermoelectric power above T_{ss}^{end}. In other words, these transitions are likely to be key factors in achieving a good thermoelectric performance.

Experiment 918
High field study of La_2CuO_4 based superconductors
(G.M. Luke, McMaster; Y.J. Uemura, A.T. Savici, Columbia)

Experiment 849 revealed the coexistence of static magnetic order and superconductivity in several La_2CuO_4 based samples, relatively close to hole concentration of 1/8 per Cu atom in spatially separated regions. Computer simulations suggest a radius of the magnetic regions on the order of 30 Å.

Mostly neutron inelastic scattering, but also some older μSR data, show that a high magnetic field tends to induce magnetic correlations in these samples. We therefore decided that it might be interesting to determine if we have an increase in the size of the magnetic moments or if we have an increase in the size of the magnetic regions.

We performed high magnetic TF-μSR measurements on several samples of $La_{2-x}Sr_xCuO_4$ (LSCO) and $Bi_2Sr_2CaCu_2O_{7-\delta}$ (Bi2212). While in Bi2212 we see no field induced magnetism in either underdoped or optimally doped samples, the picture for LSCO is completely different. We fitted the data by a gaussian damped cosine function. As we can see in Fig. 125, the TF relaxation rate increases with the applied field in the case of underdoped and optimally doped samples, but there is no field induced effect in the case of the overdoped one. The value of the relaxation rate at low temperatures is dependent on the time domain of fitting, which implies that this simple model is not enough.

We therefore need a better way to look at the data, even before we propose a model. Beside the standard
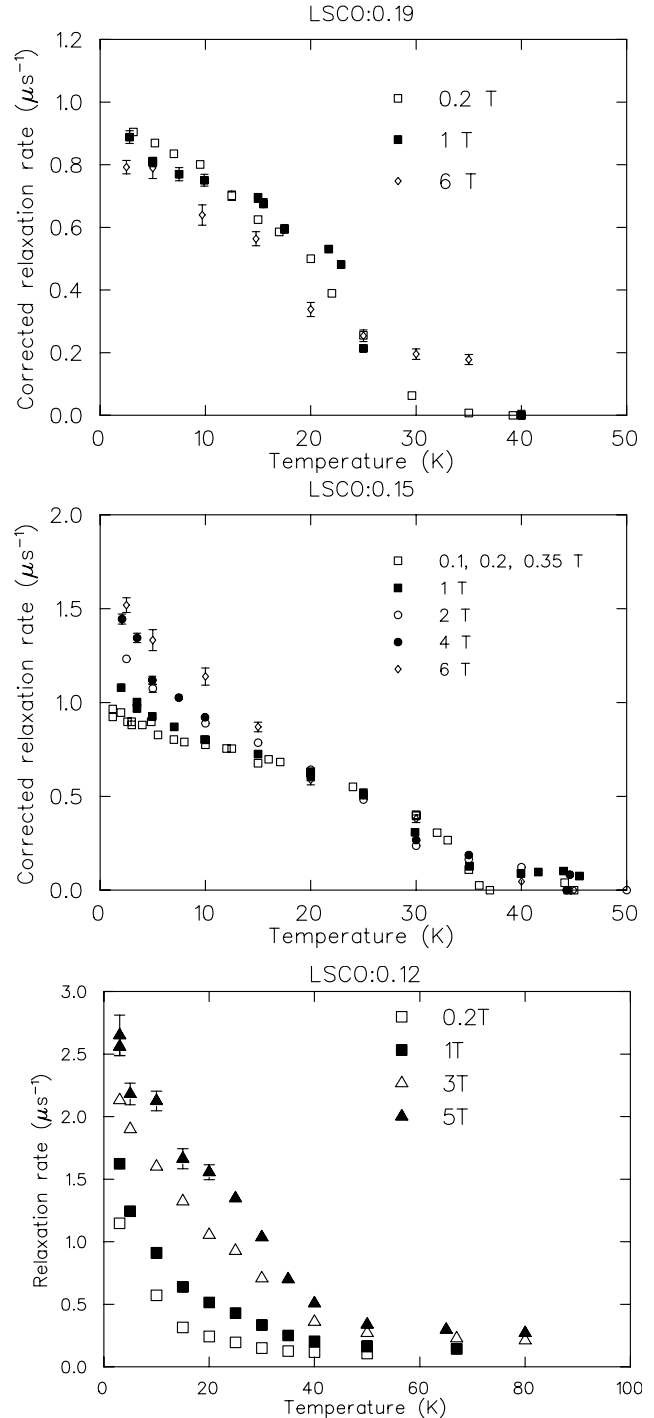
Fig. 125. Relaxation rates for TF-μSR signal in several LSCO samples.

way of looking at the asymmetry in rotated reference frame, we found that the Fourier transform does not produce enough new information to be useful in understanding the data. Another way to get useful results is looking at the envelope function. The results for $La_{2-x}Sr_xCuO_4$ are shown in Fig. 126. In the case of overdoped LSCO ($x = 0.19$) we see no change. For
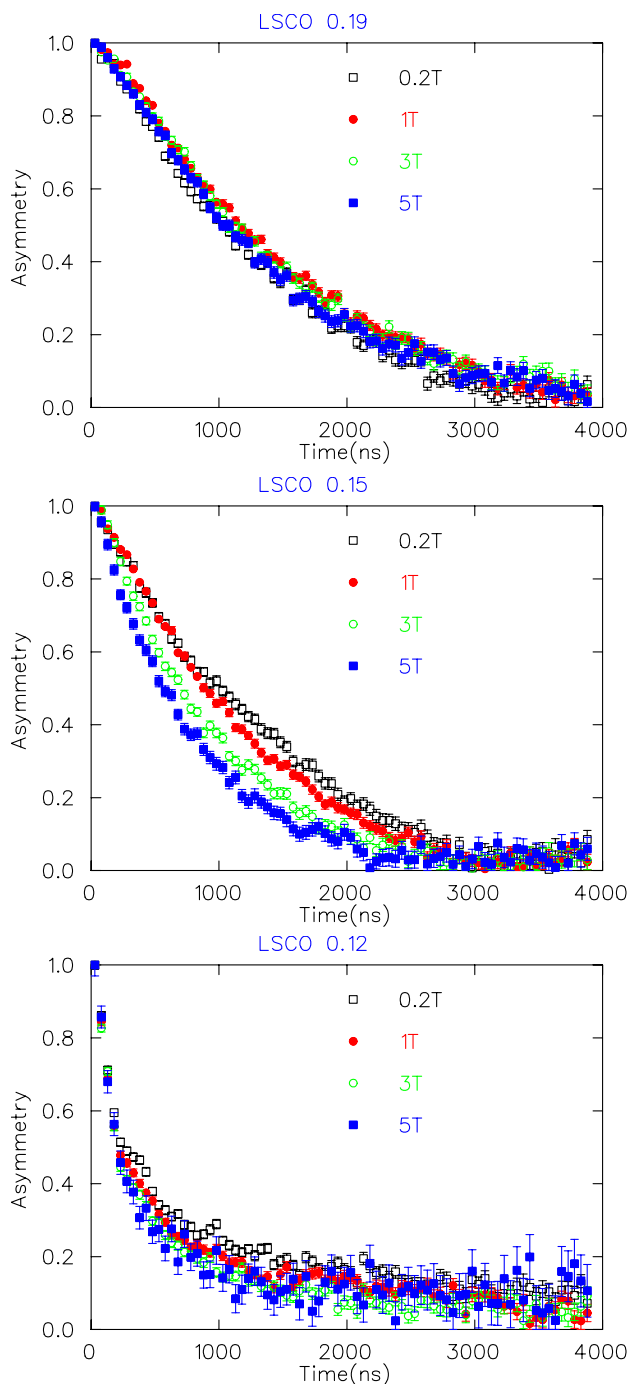
Fig. 126. Envelope functions for TF-μSR signal in several LSCO samples.

$x = 0.15$ we see a gradual change, all across the time spectrum. The $x = 0.12$ sample exhibits a two component signal, with a fast relaxation due to the magnetically ordered regions.

For the optimally doped LSCO sample, we see no volume fraction of sites with high magnetic fields. The field-induced relaxation in LSCO:0.15 seems to be due to slowing down of spin fluctuations occurring in the whole volume of the sample.

Experiment 931
Magnetic properties of multinuclear, open-shell coordination complexes and polymers probed by μSR
(J.E. Sonier, D.B. Leznoff, SFU)

Compounds that contain unpaired electrons, also called "open-shell" systems, can be found throughout chemistry, from the active sites in many proteins to magnetic materials. Every open-shell compound contains a particular "spin carrier" that actually carries the unpaired electron(s), such as transition metal ions, lanthanides and organic radicals. Molecular magnetism deals with the magnetic properties of isolated molecules and groups of molecules, which contain one or more spin carriers. It is the combination of these spin carriers, the bridges connecting them, and their multidimensional assembly that generates materials with unique properties. At the heart of these investigations are two general goals: first, we seek to understand the magnetic interactions between spin carriers, both via direct bonding and mediated by ligand bridges. The key issue of interest is the strength and type of magnetic coupling (ferromagnetic or antiferromagnetic) for a given system. Second, methods to generate high-dimensional systems in a controlled fashion must be explored and applied to open-shell systems. Generally, high-dimensionality systems can show bulk properties (magnetic, thermal, optical) attributable to their polymeric nature.

$Cu[Au(CN)_2]_2 \cdot H_2O$

The coordination polymer $Cu[Au(CN)_2]_2 \cdot H_2O$ shows ferromagnetic coupling down to 2 K. μSR measurements of this compound in zero external magnetic field show a first-order transition to magnetic order near 0.19 mK. Upon warming, hysteresis is observed (see Fig. 127). An outstanding question is whether the magnetic exchange coupling is mediated by the Au(I) centre or the copper(II)-bound H_2O via an H-bonding array.

$C_{24}H_{60}N_4Si_4O_2Fe_2$

The metal-diamidoether complex $C_{24}H_{60}N_4Si_4O_2Fe_2$ is unstable in air. Consequently, a special sample cell was prepared for use in a conventional He gas-flow cryostat. This limited the lowest temperature to $\sim$2.3 K. Measurements in zero external magnetic field indicated a slowing down of the spin dynamics with decreasing temperature (see Fig. 128). However, no magnetic transition was observed.

Cu(II)/Au(I) and Cu(II)/Hg(II) 2-D arrays

The reaction of $Cu(ClO_4)_2 \cdot 6H_2O$ with tmeda (tmeda = $Me_2NCH_2CH_2NMe_2$) and two equivalents of

102
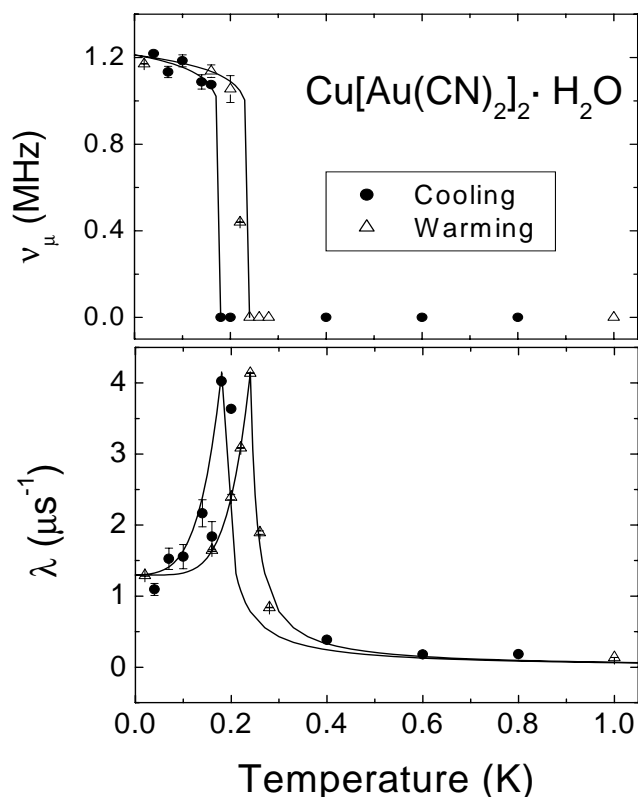
Fig. 127. Zero-field μSR measurements on polycrystalline Cu[Au(CN)$_2$]$_2$·H$_2$O taken as a function of increasing (open circles) and decreasing (solid circles) temperature. The top and bottom panels show the temperature dependence of the muon-spin precession frequency ν_μ and muon-spin relaxation rate λ, respectively.
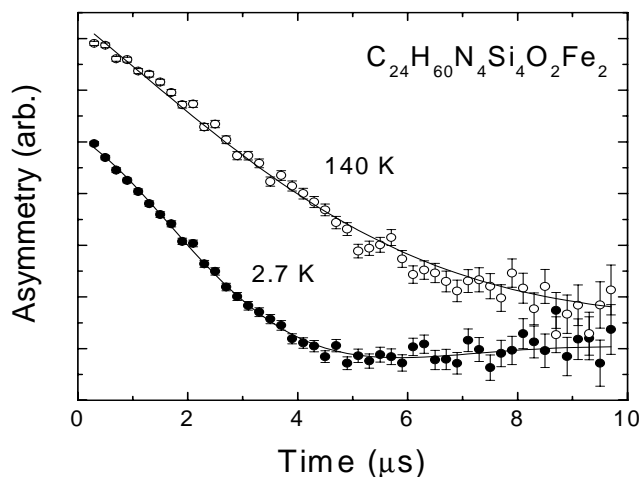
Fig. 128. Asymmetry spectra in C$_{24}$H$_{60}$N$_4$Si$_4$O$_2$Fe$_2$ at zero external field. The increased relaxation rate at lower temperatures is consistent with the slowing down of fluctuating magnetic moments, but no onset of magnetic order is observed.

K[Au(CN)$_2$] yields Cu(tmeda)[Au(CN)$_2$]$_2$, a 3-D polymer which shows ferromagnetic interactions mediated by the Au(I) centre. We carried out ZF-μSR measurements of this compound to probe the nature of the
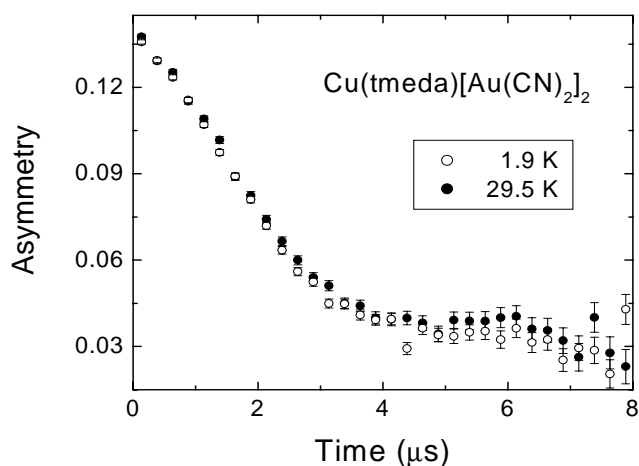
Fig. 129. Asymmetry spectra in Cu(tmeda)[Au(CN)$_2$]$_2$ at zero external field. The change upon cooling the sample below $T = 25$ K is very subtle.

transition observed at $T = 25$ K in bulk susceptibility measurements. While we did observe a subtle but abrupt change in the muon spin relaxation signal below 25 K (see Fig. 129), no clear evidence for magnetic order was found.

Experiment 932
Improving μ^-SR performance
(J.H. Brewer, CIAR/UBC/TRIUMF)

The applications of μ^+SR to condensed matter physics and chemistry are legion and familiar; by comparison, the uses of μ^-SR are rare and obscure. This is because of the well known disadvantages of μ^-SR (relative to μ^+SR), all of which are related to the formation of muonic atoms in which the μ^- orbits a positive nucleus roughly 200 times closer than a $1s$ electron:

- Lifetime: For heavy nuclei, the μ^- actually spends most of its time inside the nucleus. This has an adverse effect on μ^-SR because, in all but the lowest-Z materials, the muon lifetime τ_μ is dramatically shortened by nuclear capture involving the elementary reaction $\mu^- + p \rightarrow n + \nu_\mu$. In ^{16}O$\mu^-$, $\tau_\mu \approx 1.8$ μs, not much shorter than the free muon decay lifetime of 2.197 μs, but in ^{58}Niμ^- it is only 152 ns and in ^{208}Pbμ^- it is only 75 ns. The fraction of muons producing a decay electron to be detected in a normal μ^-SR experiment is reduced by the lifetime ratio (e.g. 3.4% for ^{208}Pb). On the other hand, higher μ^- stop rates (by the same factor) can be accommodated as long as the extra beam intensity is available and the sample contains no light elements.

- Depolarization: Meanwhile, strong L-S coupling in the radiative transitions of the muon on its way to the muonic $1s$ state cause a dramatic loss of polarization, with the result that no more than

20–25% remains in the ground state. This reduces the sensitivity of μ^-SR (relative to μ^+SR) by the same factor.

- Giant hyperfine interactions: The majority of nuclei have spins of their own. The extreme proximity of the muon to the nucleus causes an enormous hyperfine interaction (in muonic niobium the effective field of the nucleus on the muon is comparable to magnetic fields at the surfaces of neutron stars!) which effectively "locks" together the muon and nuclear spins into an F^+ state (parallel) or an F^- state (antiparallel). The energy difference between these states is often sufficient to eject core electrons in Auger processes accompanying hyperfine transitions. Because of these transitions, and the fact that the $F^\pm$ states precess in magnetic fields at their own characteristic Larmor frequencies different from that of the free muon, conventional wisdom holds that muonic atoms with nonzero-spin nuclei are not useful for μ^-SR studies of condensed matter.

On the other hand, μ^-SR reveals something that μ^+SR cannot: the local magnetic fields at lattice sites occupied by what is essentially a $Z_{\text{eff}} = Z - 1$ impurity nucleus – usually $B_\mu = {}^{12}C\mu^-$ or $N_\mu = {}^{16}O\mu^-$, because most applications of μ^-SR as a condensed matter probe have relied upon muonic atoms of spinless nuclei, primarily ${}^{16}O\mu^-$ in oxides. However, a number of muonic atoms of nuclei with spin (notably ^{7}Li, ^{9}Be, ^{11}B, ^{14}N, ^{19}F and ^{27}Al) produce useful μ^-SR signals of sufficient strength to be used as magnetic probes of materials that contain these isotopes but no convenient spinless nuclei. Their possible applications have never been seriously explored. Experiment 932 was therefore undertaken to explore some possible ways to make μ^-SR more efficient and versatile.

In the first year of Expt. 932 I have made a few calibration measurements on spinless nuclei and obtained new TF-μ^-SR spectra from ${}^{19}F\mu^-$, ${}^{14}N\mu^-$ and ${}^{23}Na\mu^-$ in chemical compounds, where the F^+ frequency is easily separated from the free μ^- signal of muons captured on ^{12}C and ^{16}O.

${}^{12}C\mu^-$ lifetime

As usual, graphite was used for calibration. In the process I obtained a ${}^{12}C\mu^-$ lifetime (Fig. 130) of 2016.5 ± 1.0 ns (500 ppm), which is about half as precise as the best value to date. However, people preparing to measure the μ^+ lifetime to high precision should note that I made no effort to minimize the effects of the muon's polarization and asymmetric decay; instead, I made sure to understand (and fit) it.
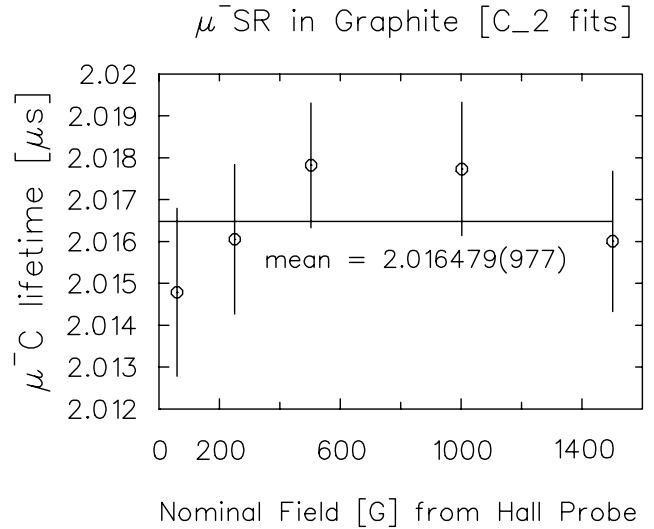
Fig. 130. μ^- lifetime in graphite vs. transverse magnetic field.

Relativistic shifts

I also obtained a nominal value for the ${}^{12}C\mu^-$ relativistic shift ($-0.035\pm5\%$) [which should not be taken too seriously because there were no controls for systematic errors], as well as those of ${}^{208}Pb\mu^-$ and natural $Cd\mu^-$ (where systematics are less of a problem) for comparison with the measurements of Yamazaki *et al.* [Phys. Lett. **B53**, 117 (1974)]. Also, shown in Fig. 131 are the relativistic shifts of ${}^{14}N\mu^-$ (in melamine, see below), ${}^{19}F\mu^-$ (in Teflon, see below) and ${}^{27}Al\mu^-$, where in each case the reference frequency is that calculated for the F^+ hyperfine state (see below).
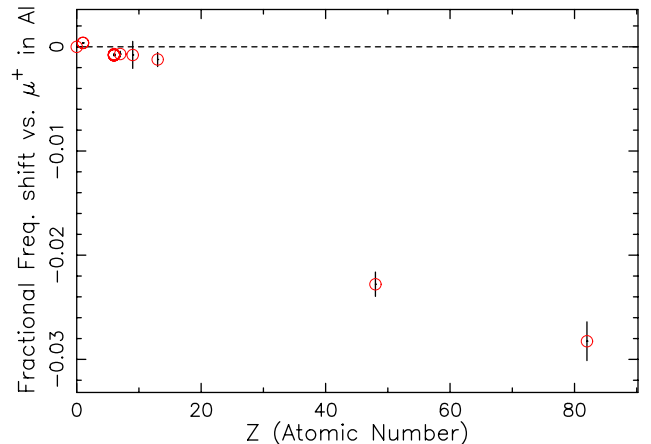
Fig. 131. Relativistic shift of negative muon precession frequency expressed as a fraction of the μ^+ frequency in aluminum at the same transverse magnetic field (0.7 T). Points at $Z = 0$ and $Z = 1$ are for μ^+ in aluminum and graphite, respectively. (In graphite the μ^+ has a large positive Knight shift.)

Giant hyperfine interactions

Since the muon penetrates deep into the nucleus in its $1s$ state, the hyperfine splitting for muonic atoms with nonzero-spin nuclei can be huge. In ^{93}Nbμ^- and ^{209}Biμ^- the energy difference between the F^+ state (muon and nuclear spins parallel) and the F^- state (muon and nuclear spins antiparallel) is ~ 5 keV – equivalent to a magnetic field of $\sim 10^{14}$ G on the muon. (This is comparable to the magnetic fields at the surfaces of neutron stars!) Even in light nuclei, this interaction rigidly "locks" the muon spin to that of the nucleus in either the F^+ or the F^- state; these states then precess in an external field at well defined Larmor frequencies ν_+ and ν_- quite different from that of the "bare" muon (ν_μ). One can therefore measure the time evolution of the μ^- polarization in any such states independently of each other in a sufficiently strong transverse magnetic field (high enough that the muon survives in the state of interest for at least several periods of the corresponding frequency).

Hyperfine transitions

The hyperfine splitting is often sufficient to eject core electrons in Auger processes, the dominant mechanism for hyperfine transitions. The rates of these transitions are known for a few cases where it has been important to semileptonic nuclear physics experiments, but most have never been measured since the calculations of Winston in 1963 [Phys. Rev. **129**, 2766 (1963)]. As a general rule, the initial $F^\pm$ populations are stable in the lightest elements and transitions begin to be detectable by about ^{11}B.

^{19}Fμ^- in Teflon

The HF transfer rate R_{HF} in muonic ^{19}F is the best known of all such cases, so it made a nice "proof of principle" calibration. As can be seen from Fig. 132, the F^+ signal was easily observed in a Teflon $((\mathrm{CF}_2)_n)$ sample and impossible to confuse with the carbon background signal by virtue of their radically different frequencies. Its "relaxation" rate was also easy to measure; with just under 18 hours of data accumulation I was able to determine $R_{\mathrm{HF}} = 5.2(5)\ \mu\mathrm{s}^{-1}$, consistent with previous measurements using neutrons from nuclear muon capture (which is strongly dependent upon the HF state).

I was also able to determine the product of $P_+(0)$ (the initial polarization of the muonic fluorine F^+ state) and the fraction $f_F \cdot f_+$ of muons initially in that state (which includes the fraction f_F initially captured on fluorine as opposed to carbon). The result was $f_F \cdot f_+ \cdot P_+(0) = 0.31(3)\%$.

Hyperfine transition rate in ^{23}Naμ^-

Measurements on sodium metal at a transverse field of about 0.7 T produced a tantalizing result, shown
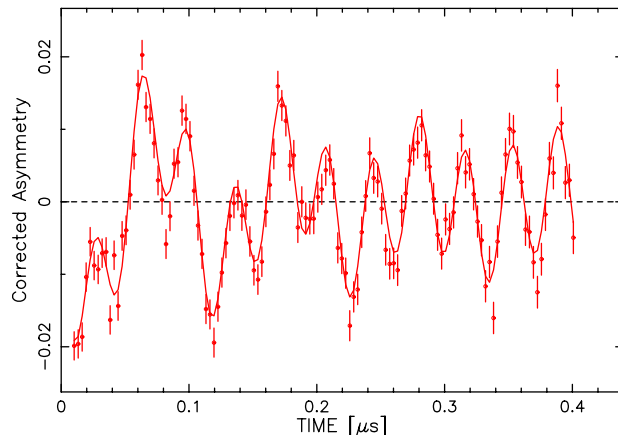
Fig. 132.   Negative muon precession signal in Teflon $((\mathrm{CF}_2)_n)$ at room temperature in a transverse magnetic field of 2040 G. The long-lived signal at higher frequency is from ^{12}Cμ^- and the rapidly decaying signal is from the F^+ state of ^{19}Fμ^- before its transition to the (singlet) F^- state.
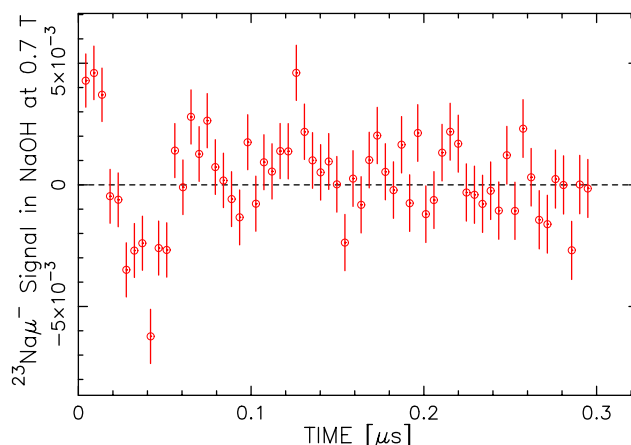
Fig. 133.   Precession signal of the F^+ state of ^{23}Naμ^- in sodium metal, showing the apparent relaxation caused by the hyperfine transition to the F^- ground state.

in Fig. 133: a weak signal at a frequency about 0.18 times that of the free muon, consistent with the theoretical frequency of the F^+ state in muonic ^{23}Na ($\nu_+/\nu_0 = 0.18765$), with a "relaxation" rate of about $13 \pm 3\ \mu\mathrm{s}^{-1}$, consistent with the HF transition rate calculated by Winston in 1963 ($R_{\mathrm{HF}} \approx 14\ \mu\mathrm{s}^{-1}$).

^{14}N in melamine ($\mathbf{C_3H_6N_6}$)

The F^+ signal in ^{14}Nμ^- is large and long-lived; its frequency is easily distinguished from that in ^{12}Cμ^-, and so it was easy to measure in a compound containing both nitrogen and carbon, as shown in Fig. 134. The ratio of the fitted ^{14}Nμ^- F^+ frequency to that of ^{12}Cμ^- was $\nu_+/\nu_C = 0.3180(3)$, in agreement with the theoretical value of $\nu_+/\nu_0 = 0.3182$ relative to the free muon frequency ν_0. (Since ^{12}Cμ^- and ^{14}Nμ^- will have
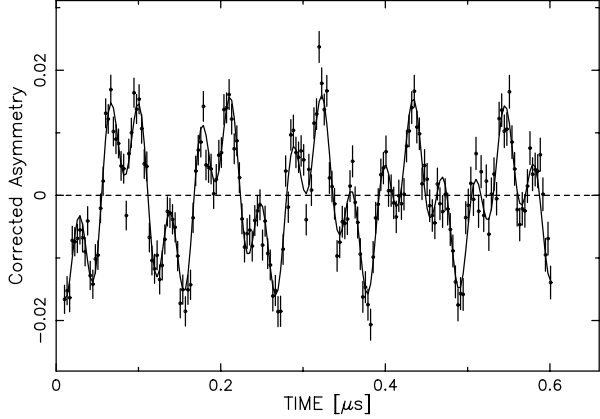
Fig. 134. Negative muon precession signal in melamine ($C_3H_6N_6$) at room temperature in a transverse magnetic field of 2000 G. The higher frequency signal is again from $^{12}C\mu^-$ and the slower decaying signal is from the F^+ state of $^{14}N\mu^-$; in this case the decay is not due to a transition to the F^- state but is caused by some sort of conventional magnetic or chemical spin relaxation mechanism.
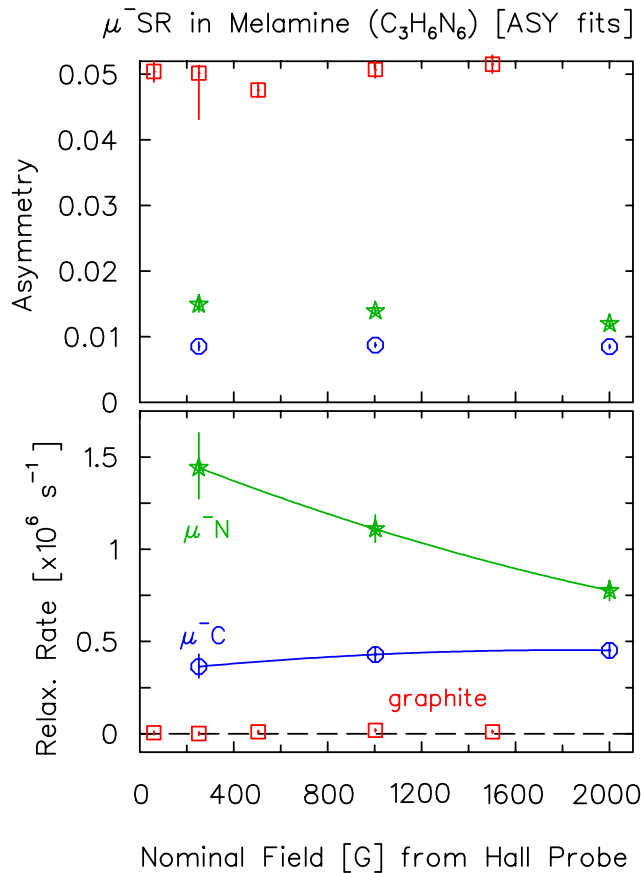
Fig. 135. Fitted asymmetry (top) and relaxation rate (bottom) of negative muon precession signals from $^{12}C\mu^-$ (circles) and $^{14}N\mu^-$ (stars) in melamine ($C_3H_6N_6$) at room temperature for several transverse magnetic fields. Results for pure graphite (squares) are shown for comparison. The relaxation rates are much too high to be caused by random local fields from neighbouring nuclear dipole moments.
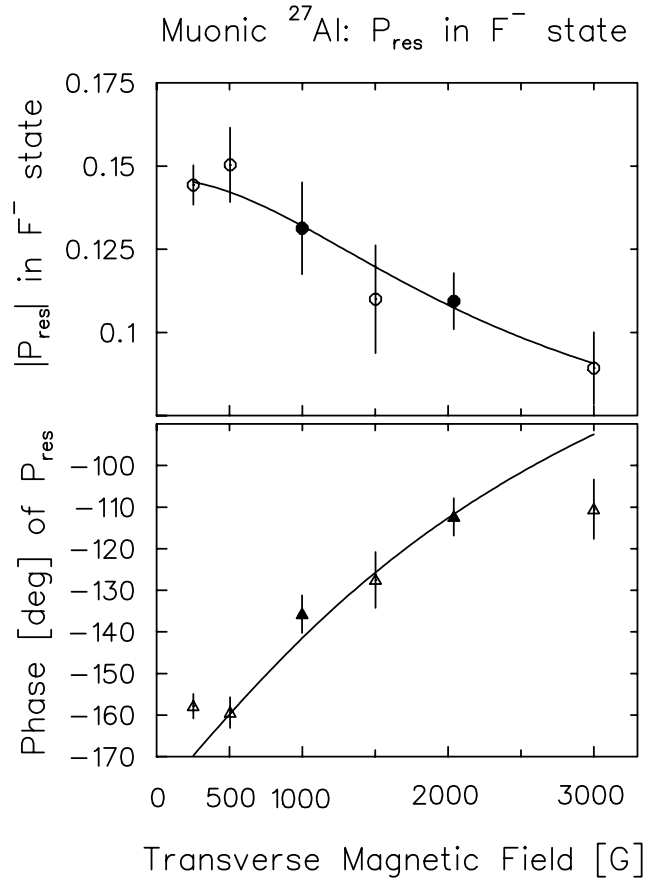
Fig. 136. Magnitude (top) and initial phase (bottom) of the residual polarization of the F^- state in $^{27}Al\mu^-$ as a function of transverse magnetic field. Lines are fits to a simple model.

roughly the same relativistic shift, this complication has been ignored.)

As shown in Fig. 135, the product $f_N \cdot f_+ \cdot P_+(0)$ and the relaxation rate of the F^+ signal were both sharply decreasing functions of increasing magnetic field, starting from 0.01495 ± 0.00129 and 1.44 ± 0.19 μs^{-1}, respectively, at 251 G and dropping to $0.0120(4)$ and $0.776(5)$ μs^{-1} at 2000 G. This behaviour is mysterious. The $F^+ \to F^-$ transition is thought to be energetically forbidden, leading to skepticism about the association of R_{HF} with the (much slower) relaxation rate observed in a liquid nitrogen target in 1983 by Nagamine et $al.$ [Phys. Lett. **B167**, 31 (1986)]. The present result is clearly not a HF transition rate, but a "real" spin relaxation by random local magnetic fields; the question is, what could produce such large fields? The rate is too high to be due to nuclear moments, even those of protons. It seems likely that paramagnetic moments are involved, but it is anybody's guess which. This system may be very interesting for reasons as yet unguessed, but it will not make a good one for determining R_{HF} for muonic nitrogen.

Hyperfine transition rate in ^{27}Alμ^-

For elements heavier than sodium, R_{HF} becomes larger than ν_+ in experimentally accessible magnetic fields, so that direct observation of "relaxation" of the F^+ signal is no longer a feasible method for measuring R_{HF}. However, at lower magnetic fields the muon polarization can be transferred efficiently to the lower F^- state with a field-dependent amplitude and phase shift. Using this "residual polarization" method I made the first measurement of R_{HF} in ^{27}Alμ^- at SIN in 1982 [Brewer, Hyp. Int. **17-19**, 873 (1984); Brewer, *ibid.*, p.879]. Under Expt. 932 the number of measurements at different fields was increased to confirm this "residual polarization" effect and improve the precision of the measurement (see Fig. 136). As soon as the data analysis is complete, I will publish a new value for the HF ($F^+ \rightarrow F^-$) transition rate R_{HF} as well as the products of initial polarization and population for each of the HF states, which is difficult to determine any other way. It will then be interesting to investigate other muonic atoms of intermediate mass where this method might be used to determine these HF parameters.

Experiment 934
μSR study of polymerized C$_{60}$
(Y.J. Uemura, Columbia; T. Makarova, Umeå Univ.)

Recently, Makarova *et al.* [Nature **413**, 716 (2001)] reported that polymerized C$_{60}$ exhibited ferromagnetic behaviour at room temperatures. The C$_{60}$ polymerizes into an oriented rhombohedral C$_{60}$ phase (Rh-C$_{60}$). We performed μSR measurements in ZF and LF on this sample.

We ran two samples of polymerized C$_{60}$ with slightly different annealing temperatures of 750°C and 775°C. Results were extremely similiar for both samples. SQUID magnetometry was performed in the range of –2 kOe$< H <$2 kOe, for temperatures of 10 K and 300 K. The room temperature magnetization hysteris loops are shown in Fig. 137. One can clearly see a saturation of the magnetization at higher fields 2×10^4. These SQUID results are consistent with the Makarova *et al.* measurements and seem to indicate the presence of ferromagnetic order within the sample.

Our group performed μSR on the Rh-C$_{60}$ samples mentioned above. The results are summarized in Fig. 138. The ZF and WTF measurements show no substantial internal magnetic field within the bulk of the sample. The asymmetry in the ZF measurement does not oscillate, and the WTF measurement does not show any effect of dephasing except due to perhaps lifetime effects of the muon. Hence, there does not seem to be any static internal magnetic field in the sample. We find no evidence of static magnetic order in
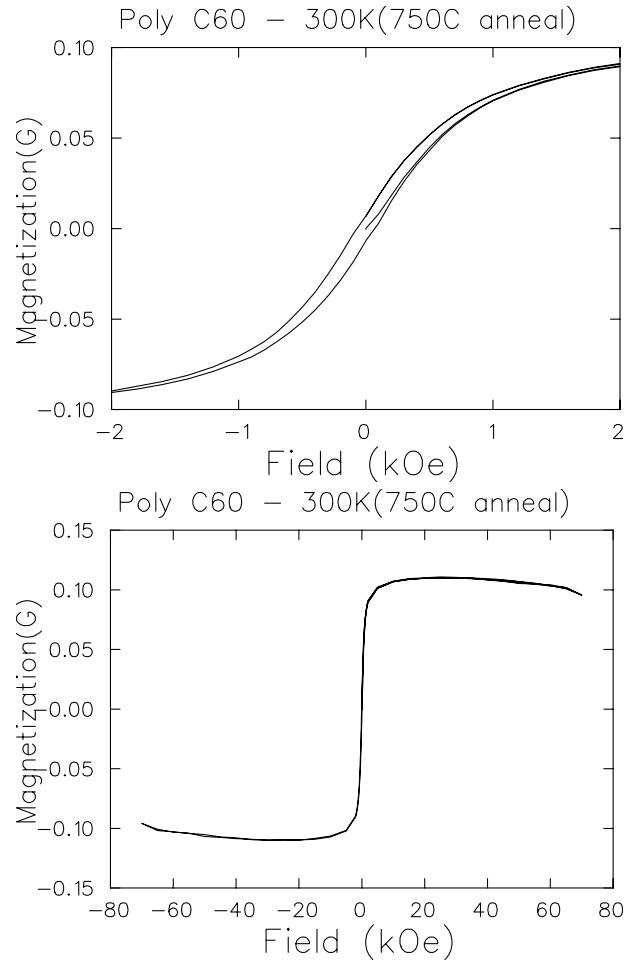
Fig. 137. Magnetic susceptibility for Rh-C$_{60}$ (annealed at 750°C).
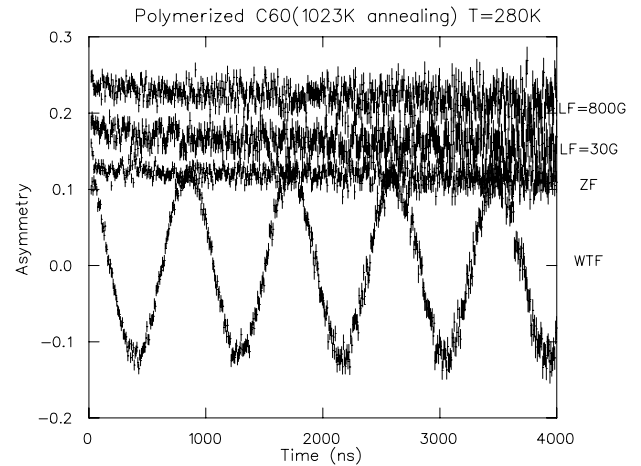
Fig. 138. Results of μSR experiments on Rh-C$_{60}$.

polymerized C$_{60}$. The ferromagnetism in the sample may be due to localized impurity. The ZF and LF results indicate that about half of the implanted muons form muonium. Characterization of this muonium state is currently under way.

107

Experiment 937
Muonium in hexagonal semiconductors
(R.L. Lichti, Texas Tech)

TRIUMF Expt. 937 was given time specifically to investigate the differences in muonium behaviour in single crystal AlN compared to that in sublimation grown thick films or those deposited by CVD. We have obtained the temperature dependence of the qlcr resonances for a single crystal of AlN. The sample, obtained on loan from Crystal IS, Inc., had a cross section slightly under 80 mm^2 and was sufficiently thick to stop all muons hitting the sample; those hitting the Ag holder do not contribute to any resonance feature.

The main spectral features are associated with N neighbours of diamagnetic Mu$^+$ centres, specifically yielding information related to the sites and dynamics of these defects. The likely stable site for an isolated Mu$^+$ is a nitrogen anti-bonding location oriented into the channels formed by the 2H wurtzite stacking order, commonly noted as AB$_\perp$[N]. The other likely site based on our previous results in GaN is a second N anti-bonding location with Mu$^+$ inside the most tightly confined cage region of the structure. The strong qlcr line observed near 4.5 mT was initially assigned to this metastable AB$_\parallel$[N] cage site.

For thick AlN films grown by CVD or sublimation techniques, the 4.5 mT resonance is strongest in samples with the smallest grain sizes or otherwise visually defective. Preliminary single crystal data at room temperature showed only a very weak resonance in this range, consistent with formation of the responsible Mu state primarily in defective regions. If this state requires migration of Mu$^+$ to a grain boundary or some other highly stressed region, one might expect the resonance to grow at higher temperatures where the main Mu$^+$ centre can rapidly diffuse through the crystal. Zero-field depolarization functions imply a second Mu$^+$ centre in AlN films. This state was assigned to the stable Mu$^+$ site and is mobile within the wurtzite channels. Hints in the depolarization data suggest a change from local tunneling to diffusive motion above 300 K in AlN films, but the details are highly sample dependent. Our main goal for Expt. 937 was to examine the temperature dependence of the 4.5 mT line in single crystal AlN.

Figure 139 shows the qlcr spectra for single crystal AlN at a few temperatures between 500 and 1050 K. The 4.5 mT line increases in intensity up to 800 K and then decreases at higher temperatures. The decrease is consistent with earlier data on AlN films which gave a state dissociation energy of 1.0 eV. This energy had been tentatively assigned to the cage to channel site change for Mu$^+$ based on initial signal identifications.

Figure 140 shows the T-dependent amplitudes for
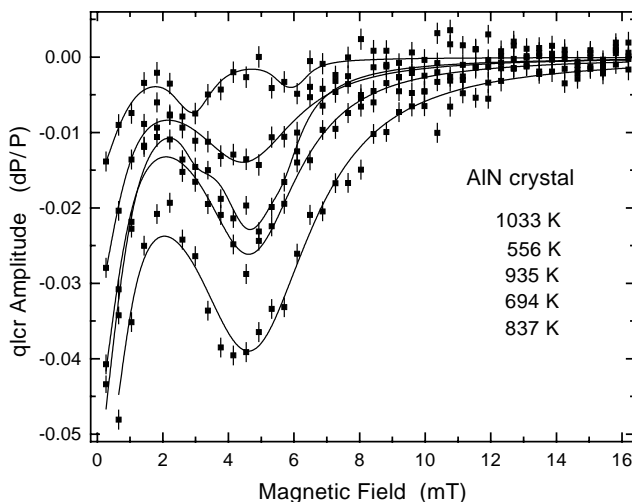
Fig. 139. The qlcr spectra obtained for single crystal AlN at several temperatures between 500 and 1050 K. The large resonance near 4.5 mT represents a trapped Mu$^+$ state.
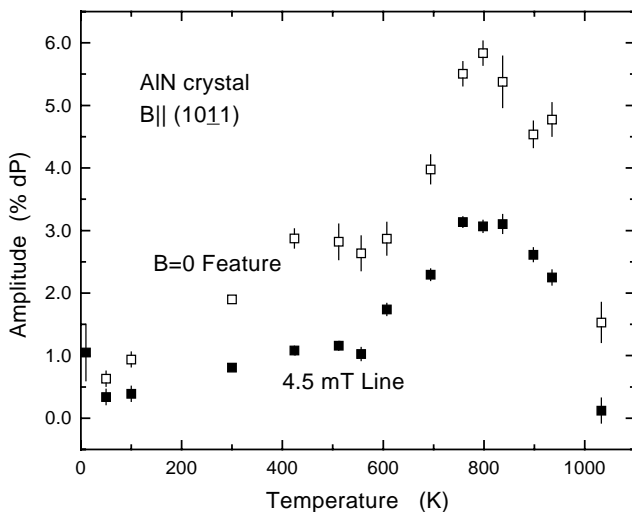
Fig. 140. Temperature dependence for the amplitudes of the main 4.5 mT qlcr line (filled squares) and the zero-field feature (open squares) due to non-resonant interactions.

the main qlcr line and the zero-field feature for this AlN crystal. The spectra for 935 and 1033 K have two additional lines present. These lines are from a different Mu$^+$ state (or states) and verify earlier conclusions that, at temperatures above the stability limit for the state responsible for the 4.5 mT resonance, Mu$^+$ can trap at another site, presumably paired with a specific, as yet undetermined, defect.

Because the T-dependence (and intensity) for the 4.5 mT line in various AlN samples is very different below 800 K, but very similar above 800 K, we conclude that the same trapped state is seen in films and single crystal samples, but that its formation is controlled by encounter rates between a mobile Mu centre and the relevant parent defect, grain boundary, or stressed region. These results suggest that this state is probably
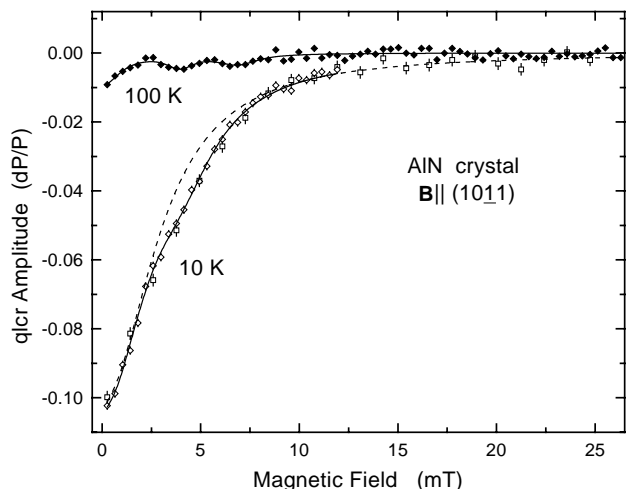
Fig. 141. Comparison of spectra taken at 10 K and 100 K displaying the large zero-field relaxation feature at the lowest temperatures. The 100 K data show a two-line qlcr spectrum shifted from that at 1000 K.

associated with an Al vacancy or a more extended defect rather than residing at the $AB_\parallel[N]$ cage site in the regular wurtzite lattice. Details of Mu^+ motion and an estimate of the density of trapping sites yielding the 4.5 mT qlcr resonance await zero-field depolarization measurements to quantify Mu^+ diffusion rates.

We took a few spectra at cryogenic temperatures. The resonance amplitudes are included in Fig. 140. The spectra at 50 and 100 K are basically consistent with the overall trends seen above room temperature. However, at 10 K there is a large-amplitude, broad zero-field feature reminiscent of II-VI materials that show a shallow-donor Mu^0 state. Figure 141 shows the 10 K and 100 K spectra for comparison. Hyperfine decoupling curves had earlier implied an atomic-like Mu^0 up to at least 300 K. No hyperfine precession signals have yet been observed for either a shallow or deep (atomic-like) Mu^0 in AlN. Either a neutral muonium state is present or a much different relaxation mechanism is active at 10 K compared to 50 K and above. Spectra at 300 K and below show two extra lines, similar to those near 1000 K but at higher fields, as well as a weak 4.5 mT line. It is not obvious whether or not these high-T and low-T extra resonances represent the same state.

Experiment 938
Muonium formation and ionization in semiconductors and insulators
(V.G. Storchak, Kurchatov)

Properties of impurities in semiconductors have been the subject of substantial experimental and theoretical interest due to their physical properties as well as important applications, most notably in studies of metal-insulator transition. Atomic hydrogen represents the simplest and the lightest impurity in semiconduc-

tors, therefore its electronic structure and dynamics are of special interest. Even so, very little is known about isolated hydrogen impurity in bulk semiconductors due to its high mobility and reactivity: most of our knowledge is accumulated on hydrogenic-impurity complexes in which hydrogen removes electrically active levels from the band gap and thus passivates electrical and optical activities of other impurities. As a result of binding with other impurities, hydrogen removes its own electrically active levels from the semiconductor band gap as well.

In this regard the technique of muon spin rotation/relaxation/resonance (μSR) has made a significant contribution in clarifying the electronic structure of the isolated state of muonium ($Mu = \mu^+e^-$) atom. The structure and dynamics of muonium in semiconductors have been suggested to be directly relevant to understanding the analogous hydrogen defect: Muonium has a reduced mass almost the same as that of H, so its electronic states and chemical interactions are literally those of a light hydrogen isotope ($m_\mu \simeq m_p/9$); as such, and with due regard to isotope effects, muonium is expected to provide an accessible model for isolated hydrogen defect centres in semiconductors.

In μ^+SR experiments one accumulates the necessary statistics into a time spectrum that reveals the spin polarization of positive muons stopped in the sample. Each incoming 4 MeV muon leaves behind an ionization track of excess electrons and ions liberated during the μ^+ thermalization process. Experiments in insulating and more recently in semiconducting media (Si and GaAs) have shown that the ionization track products are very close to the thermalized muon. (The characteristic distance is about $10^{-5} - 10^{-6}$ cm.) Some of the excess electrons generated in the end of the μ^+ track are mobile enough to reach the thermalized muon and form the muonium atom.

The phenomenon of delayed muonium formation described above implies that as the electron approaches the stopped muon it may be captured initially into an excited electronic state. In semiconductors with low electron effective mass and high dielectric constant, an electron and a positively charged centre can form a hydrogen-like weakly bound state with macroscopic-sized orbits. In particular in GaAs, the binding energy of such a shallow donor is $U \approx 7$ meV while its characteristic radius $a \approx 8 \times 10^{-7}$ cm.

The phenomenon of formation of this weakly bound muonium centre may serve to model the process of a free electron capture (or electron localization) by an attractive centre. What is relevant to current studies is the magnetic-field effects on shallow-impurity (hydrogen-like) states. It is suggested that in semiconductors the presence of an external magnetic field en-

hances the binding energy of the impurity atom. The point here is the effect of competition of the magnetic energy and the Coulomb energy: when the magnetic field is strong enough so that cyclotron energy $\frac{1}{2}\hbar\omega_c$ is comparable or larger than Coulomb interaction, a considerable compression of the electronic wave function of the atomic state occurs because its orbital radius tends to decrease as the field is increased. This shrinkage of the wave function in turn causes the electron to be affected by stronger binding of the attractive Coulomb potential, and thus results in an increase of the ionization energy. This effect of magnetic freezing out could be observed as a decrease in number of conduction carriers due to thermal deionization against an increase of the field H.

In bulk semiconductors, the phenomenon of metal-insulator transition is typically studied using "electrical" techniques (such as measurements of magnetoresistance or Hall coefficient). In these experiments, however, the conclusion on electron localization is made indirectly based on measuring properties of the electrons "left" as delocalized and thus available for conduction. The phenomenon of delayed muonium formation via capture of the free electron by positive muon gives an opportunity to study the elementary act of metal-insulator transition. These studies are carried out in extremely dilute limit of a single impurity in the sample thus avoiding complications related to impurity-impurity interactions. Here we present the results of our study of magnetic freezing out of electrons into muonium atoms in GaAs in magnetic fields up to 7 T.

Muonium centres in semiconductors typically ionize above several hundred K, with the Mu^0_{BC} signals not observed above roughly 150–200 K in GaAs. Ionization of Mu^0_{BC} in GaAs is accompanied with an increase of the diamagnetic fraction (diamagnetic polarization). In the middle of the ionization curve it is very hard to detect the Mu^0_{BC} signal as it relaxes too fast. An influence of the magnetic field on muonium formation may, however, be studied by measuring the magnetic field dependence of the diamagnetic fraction: a decrease in diamagnetic signal amplitude signifies an increase of muonium fraction (although unobservable).

Figure 142 presents the magnetic field dependence of the diamagnetic polarization in GaAs at T=190 K. The diamagnetic signal amplitude in GaAs is normalized to that in Ag in order to take into account effects of the final time resolution of the spectrometer (it is known that in Ag 100% of polarization is diamagnetic). The data are normalized at every temperature point.

A significant decrease of the diamagnetic fraction is seen at high magnetic field (above about 1 T). We consider this decrease as a result of freezing out of free electrons into muonium atom energy level.
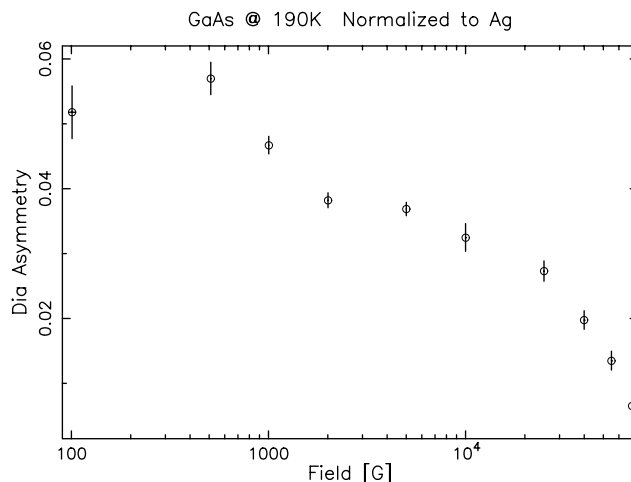
Fig. 142. Magnetic field dependence of the diamagnetic polarization in semi-insulating GaAs at T=190 K.

Experiment 939
Guest-host interactions and Hfcs of Mu-radicals in zeolites
(D.G. Fleming, UBC)

In Expt. 677, the guest-host interactions and hyperfine coupling constants (Hfcs) of the Mu-cyclohexadienyl radical were studied in various zeolites [Fleming *et al.*, J. Phys. Chem. **B106**, 6395 (2002)]. Particular focus was on the NaY, HY and USY zeolites for their distinct differences in SiO_2/Al_2O_3 ratio and charge-balancing-cation type. In the 2002 beam time of its successor, Expt. 939, the Mu-ethyl and Mu-*t*-butyl radicals in NaY and HY, formed by Mu addition to ethylene and isobutene, respectively, were investigated by both TF-μSR and ALC-μSR. Preparation of the alkene-loaded zeolites is identical to the technique used in Expt. 677. Two zeolite loadings were used in this experiment, 1 and 3 per supercage (SC). Here we report on the data obtained from ethylene- and isobutene-loaded NaY. Results from HY are incomplete and will be reported at a later time.

Figure 143 shows the Hfc data obtained for the Mu-*t*-butyl radical in NaY (3 per SC loading), compared to data for the same radical in bulk solid and liquid isobutene [Yu, Ph.D. thesis (SFU, 1989)]. For the temperature range of 150–300 K, the reduced muon Hfc ($A'_\mu = A_\mu/3.184$) curve follows a similar trend as seen in the liquid, albeit with somewhat higher values. At lower temperatures, 5–120 K, this trend also looks similar to that of solid isobutene, though with reduced values that also flatten out, likely due to "freezing" at the favourable low-T orientation of hindered rotation from the McConnell equation of β-Hfcs ($A(\theta) = L + M\langle\cos^2(\theta)\rangle$), where θ is the dihedral angle between the p_z-orbital of the free-radical electron and

Hyperfine Couplings - Mu-t-butyl
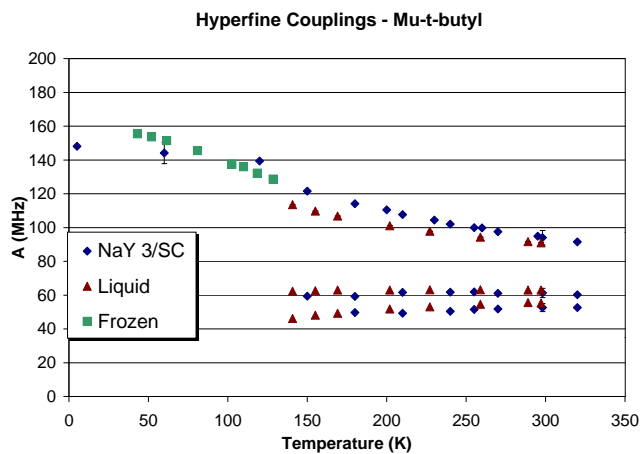
Fig. 143. T-dependence of the muon and proton Hfcs for the Mu-t-butyl radical compared in NaY zeolite (Expt. 939) and in the solid and liquid bulk. Note that the reduced muon Hfc ($A'_\mu = A_\mu/3.184$) is plotted.

Hyperfine Couplings - Mu-ethyl
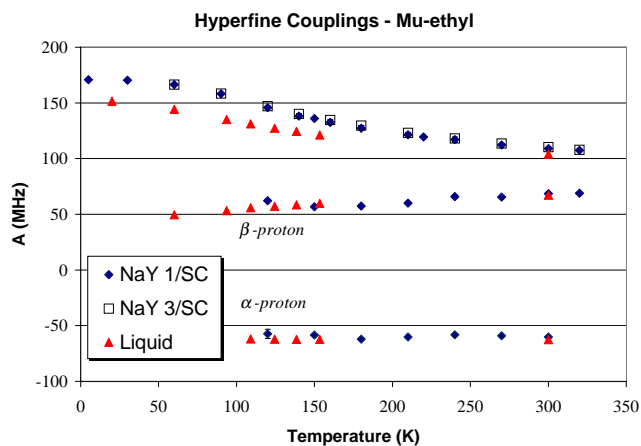
Fig. 144. Muon ($A'_\mu(T)$) and proton Hfcs for the Mu-ethyl radical in NaY zeolite at 1 and 3 per SC loadings (Expt. 939), compared with similar data in the bulk. Note that there is little or no loading dependence in the zeolite.

the β C-H bond). Both proton Hfc-temperature dependences are linear with slightly positive slopes, and are close to the values seen in liquid isobutene, though in the zeolite the proton couplings are 3 to 4 MHz lower than in the bulk.

Hfc data obtained for the Mu-ethyl radical in the NaY zeolite are shown in Fig. 144. Reduced muon Hfcs were obtained for loadings of both 1 and 3 per SC and show little loading dependence. When compared to data for the same radical in bulk ethylene and on a silica surface (not shown in figure) [Schwager et $al.$, Hyp. Int. **87**, 859 (1994)], deviations due to interactions with the zeolite framework begin to show. The temperature dependence of the muon Hfc ($A'_\mu(T)$) for the zeolite-loaded Mu-ethyl radical is $\approx 10\%$ higher than found in the bulk, at lower temperatures, indicating enhanced binding to the Na$^+$ cation of NaY. In contrast, the proton Hfcs for both the α- and β-protons are very

similar to those found in the bulk (and on the silica surface), all seemingly giving (within errors) a linear trend with a very shallow slope. The α-protons (bound to the carbon radical centre) display essentially no temperature dependence, though the hyperfine couplings of the β-protons do show some intra-molecular rotational T-dependence, closely following the trend seen in the bulk. Future beam shifts will obtain more data for ethylene-loaded HY, as well as additional temperature points for ethylene and isobutene in NaY zeolite.

Experiment 940
Thermoelectrics II: μSR in layered manganese oxides
(J. Sugiyama, Toyota CRDL Inc.; J.H. Brewer, UBC-TRIUMF)

Perovskite manganites, AMnO$_3$ ($A = AE_{1-ny}RE_{ny}$, $AE =$ Ca or Sr, RE = rare earth element), are known to exhibit n-type conductivities, if the average valence of Mn ions ≥ 3.5 [Hejtmanek et $al.$, Phys. Rev. **B60**, 14057 (1999); Martin et $al.$, $ibid.$, **B62**, 6442 (2000)]. In addition, both transport and magnetic properties are reported to depend on the average ionic radius of the A-site ions. That is, for $(Sr_{1-x-y}Ca_xRE_y)MnO_3$ ($0 \leq x \leq 0.92$, $y \sim 0.1$), the dependence of the resistivity $\rho(573 \text{ K})$ on the tolerance factor Γ exhibits a broad minimum at around $\Gamma \sim 0.96$ [Hirano et $al.$, Meeting Abstract, Phys. Soc. Japan **57**, 556 (2001) (in Japanese)] (see Fig. 145),
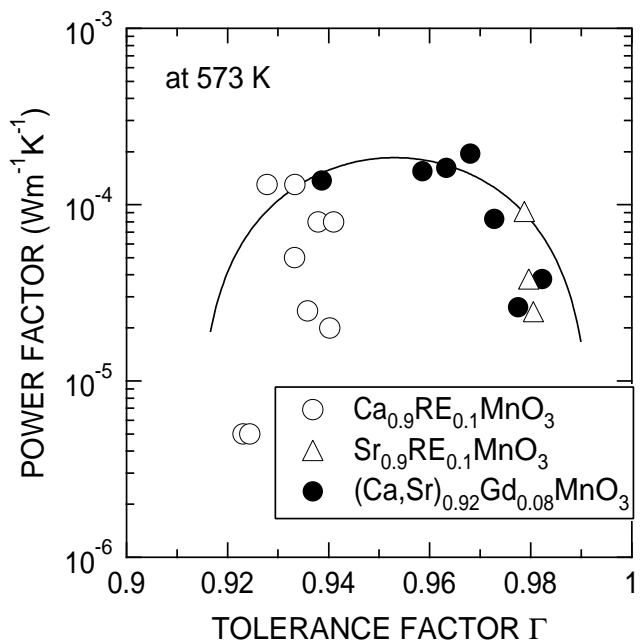
Fig. 145. Thermoelectric power factor ($=S^2/\rho$) at 573 K as a function of tolerance factor Γ of various $(Sr_{1-x-y}Ca_xRE_y)MnO_3$ samples, where $y \sim 0.1$ and RE = rare earth elements. Since S is approximately independent of Γ, ρ exhibits a broad minimum at $\Gamma \sim 0.955$.

where $\Gamma = (r_A + r_O)/\sqrt{2}(r_B + r_O)$; r_A, r_B and r_O are the ionic radii of the A-site, B-site and oxygen, respectively. This is considered to be a typical "chemical pressure effect" on ρ induced by the substitution of Sr by Ca. Since the Seebeck coefficient S is found to be insensitive to Γ, the magnitude of the thermoelectric figure of merit $ZT = S^2T/(\rho\kappa)$ (where T is the absolute temperature and κ is the thermal conductivity) approaches ~ 0.18 at 800 K; this is the highest ZT value for manganese oxides at present.

According to dc susceptibility (χ) measurements on $(\mathrm{Sr}_{0.92-x}\mathrm{Ca}_x\mathrm{Gd}_{0.08})\mathrm{MnO}_3$, antiferromagnetic (AFM) transitions were observed for the samples with $x \leq 0.5$, whereas ferromagnetic (FM) transitions for the samples with $x \geq 0.8$ (see Fig. 146). It should be noted that the highest thermoelectric power factor ($= S^2/\rho = Z/\kappa$) was obtained for the sample with $x \sim 0.5$ ($\Gamma \sim 0.96$); that is, in the phase boundary between AFM and FM phases. Therefore, the competition between AFM and FM interactions seems to be significant to increase ZT. Indeed, both direct and superexchange interactions between Mn ions should be altered by the substitution of Sr by Ca without a change in carrier concentration. In order to investigate the change in magnetism as a function of x, i.e., chemical pressure, we measured both weak (~ 100 Oe) transverse-field (wTF-) μ^+SR and zero field (ZF-) μ^+SR time spectra in $(\mathrm{Sr}_{0.92-x}\mathrm{Ca}_x\mathrm{Gd}_{0.08})\mathrm{MnO}_3$.

Figures 147(a) and (b) show the temperature dependences of the paramagnetic asymmetry A_{para} and the corresponding relaxation rate λ_{para} in the three $(\mathrm{Sr}_{0.92-x}\mathrm{Ca}_x\mathrm{Gd}_{0.08})\mathrm{MnO}_3$ samples. The large decrease

Fig. 147. (a) Paramagnetic asymmetry A_{para} and (b) relaxation rate λ_{para} as a function of temperature for the three $(\mathrm{Sr}_{0.92-x}\mathrm{Ca}_x\mathrm{Gd}_{0.08})\mathrm{MnO}_3$ samples.

in A_{para} is clearly observed at $T_\mathrm{C}/T_\mathrm{N}$. On the other hand, as temperature decreases from 300 K, λ_{para} decreases at T_N, while it increases at T_C. It is worth noting that $A_{\mathrm{para}} \sim 0.1$ even at 0 K for all the three samples indicating the phase separation, as reported for several perovskite manganites [Martin et al., op. cit.; Moritomo et al., Phys. Rev. **B64**, 214409 (2001)]. Furthermore, ZF-μ^+SR spectra of the three samples at 2.5 K showed no muon precessions but probably very fast relaxations. This suggests an inhomogeneous or a fast fluctuating distribution of an internal magnetic field.

Experiment 942
Magnetic fluctuations near metal-insulator transitions in ruthenate pyrochlores
(S. Dunsiger, LANL; R. Kiefl, UBC)

The nearly free electron model may often successfully describe the band structure of a crystal, the highest band being completely filled for insulators or only partially so for metals. However, many transition metal oxides with partially filled d-electron bands have nonetheless been found to be poor conductors or indeed insulators. The origin of this behaviour is thought to be the Coulomb repulsion between electrons: strong

Fig. 146. Magnetic phase diagram of $(\mathrm{Sr}_{0.92-x}\mathrm{Ca}_x\mathrm{Gd}_{0.08})\mathrm{MnO}_3$ determined by dc susceptibility measurements.

electron-electron correlations. Indeed, an otherwise insulating material may be driven into a metallic state in a controllable way with doping, chemical composition, pressure or magnetic field. Such metal-insulator transitions are widely observed in condensed matter physics.

The scientific interest in these materials is based on the fact that near the transition point the metal shows fluctuations of spin, charge and orbital degrees of freedom. There has been extensive theoretical and experimental work in the past 60 years to explain metal-insulator transitions driven by strong electron-electron correlations. Muon spin relaxation is one of the principal methods we use to characterize the dynamic behaviour since it is uniquely sensitive to the low frequency magnetic fluctuations which are often present in these systems.

The focus of Expt. 942 is the study of pyrochlores with chemical composition $A_2B_2O_7$ where only the B site is occupied by a magnetic ion, in particular $Y_{2-x}Bi_xRu_2O_7$. This system may be driven in a controlled manner from a geometrically frustrated insulator, $Y_2Ru_2O_7$, to a Pauli paramagnetic metal with increasing Bi doping.

Susceptibility measurements on $Y_2Ru_2O_7$ by Yoshii *et al.* [J. Phys. Soc. Jpn. **68**, 3034 (1999)] yield a Curie-Weiss temperature of $\Theta_{CW} = -1000$ K, indicating antiferromagnetic interactions between Ru moments. The system undergoes an ordering transition at $T_G \sim 76$ K. This suppression of T_G relative to Θ_{CW} is characteristic of a geometrically frustrated system. Macroscopically, the susceptibility of $Y_2Ru_2O_7$ is history dependent below the ordering temperature. Yoshii *et al.* argue that the observed behaviour is evidence of a spin glass transition. However, recent neutron diffraction studies [Ito *et al.*, J. Phys. Soc. Jpn. **69**, 888 (2000)] show an increase in intensity of resolution limited 111 and 220 reflections below the transition temperature. This is consistent with a non-collinear antiferromagnetically long range ordered state, even though the system appears spin glass-like macroscopically.

Muon spin relaxation measurements on four members of the family $Y_{2-x}Bi_xRu_2O_7$ ($x = 0, 0.9, 1, 2$) were undertaken during the autumn of 2002 on the M20 beam line at TRIUMF. The measurements were taken in a longitudinal field of 15 Oe. Above the transition temperature, the muon spin depolarization in $Y_2Ru_2O_7$ is too slow to be observed. This is likely because of the large value of the exchange coupling between Ru moments and associated rapid Ru spin fluctuation rate in the paramagnetic regime. In low longitudinal field experiments in the "motionally narrowed" limit of rapid spin fluctuations, the muon spin depolarization may be characterized by a single exponential

$\exp(-t/T_1)$, where

$$1/T_1 = \frac{2\Delta^2}{\nu}.$$

The second moment of the internal magnetic field B_i ($i = x, y, z$) is given by $\Delta^2/\gamma_\mu^2 = \langle B_i^2 \rangle$, of the order of 1–2 kOe in $Y_2Ru_2O_7$; ν is the mean fluctuation rate for fluctuations in B_i, and γ_μ is the muon gyromagnetic ratio. As may be seen in Fig. 148, spontaneous muon spin precession develops below 76 K. This indicates a well defined static local magnetic field at the muon site, consistent with long range order. The precession frequency increases as the temperature is reduced, as a measure of the growing sublattice magnetization (see Fig. 149).

Doping with Bi on the Y site increases the lattice constant and the system becomes progressively more metallic as the Bi $6p$ states mix with $4d$ states of Ru
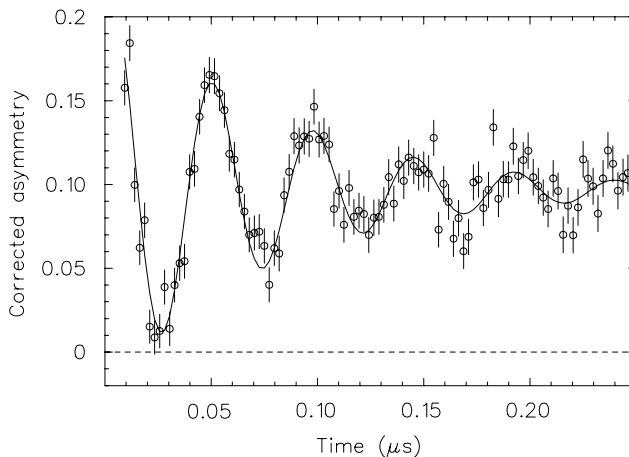
Fig. 148. Typical muon spin depolarization spectrum of $Y_2Ru_2O_7$ taken in a longitudinally applied field of 15 Oe at T = 2.4 K.
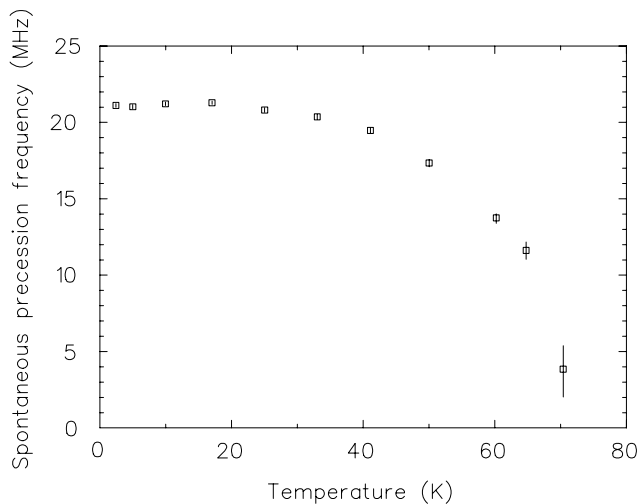
Fig. 149. Spontaneous muon spin precession frequency in $Y_2Ru_2O_7$ as a function of temperature.

113

via the framework oxygen [Cox *et al.*, J. Solid State Chem. **62**, 360 (1986)]. The ordering transition temperature is also suppressed and broadened. Muon spin relaxation measurements on $Y_{2-x}Bi_xRu_2O_7$ ($x = 0.9$, 1.0) in a longitudinally applied field of 15 Oe are summarized in Figs. 150 and 151. As the temperature is reduced, two components are observed in the signal: an increasingly rapid initial loss of polarization and a slowly relaxing "tail". The data have been analyzed using the fitting function

$$G_Z(t) = A_1 \exp[-(\lambda_1 t)^\beta] + A_2 \exp[-\lambda_2 t].$$

The peak in λ_2, the muon depolarization rate of the tail, corresponds to a peak observed in the zero field cooled dc susceptibility and the onset of history dependent behaviour. This is indicative of a freezing of the Ru spins. The depolarization rate λ_1 gives a measure of the static, highly disordered internal magnetic field which develops with decreasing temperature.

Bulk measurements by Yoshii *et al.*, *op. cit.* indicate that the metal-insulator transition point occurs in $Y_{1.1}Bi_{0.9}Ru_2O_7$. It is interesting to note that as the metal-insulator transition is approached, the specific heat coefficient γ and Pauli paramagnetic susceptibility are enhanced compared to values expected from band theory. This attribute reflects a thermal effective mass m^* of the conduction electrons which is orders of magnitude larger than the bare electron mass. The effect is usually believed to derive from strong correlations.

From published work [Yoshii *et al.*, *op. cit.*], T_G is expected to go to zero in $Y_1Bi_1Ru_2O_7$. The higher transition temperatures observed in the 2 non-stoichiometric samples used in our μSR study (see Fig. 151) indicate a lower Bi concentration than anticipated. The cause of this difference is currently under investigation.

Finally, as anticipated, the muon spin depolarization rate in $Bi_2Ru_2O_7$ is too slow to be observed using the μSR technique. This is fully consistent with the rates associated with Korringa relaxation in a normal metal [Abragam, Principles of Nuclear Magnetism (Clarendon Press, Oxford, 1961)].

Further μSR measurements on the family of compounds $Y_{2-x}Bi_xRu_2O_7$ are planned. In particular, new samples of $Y_{1.1}Bi_{0.9}Ru_2O_7$ and $Y_1Bi_1Ru_2O_7$ will be investigated, to shed light on the enhanced magnetic fluctuations associated with the metal-insulator transition.
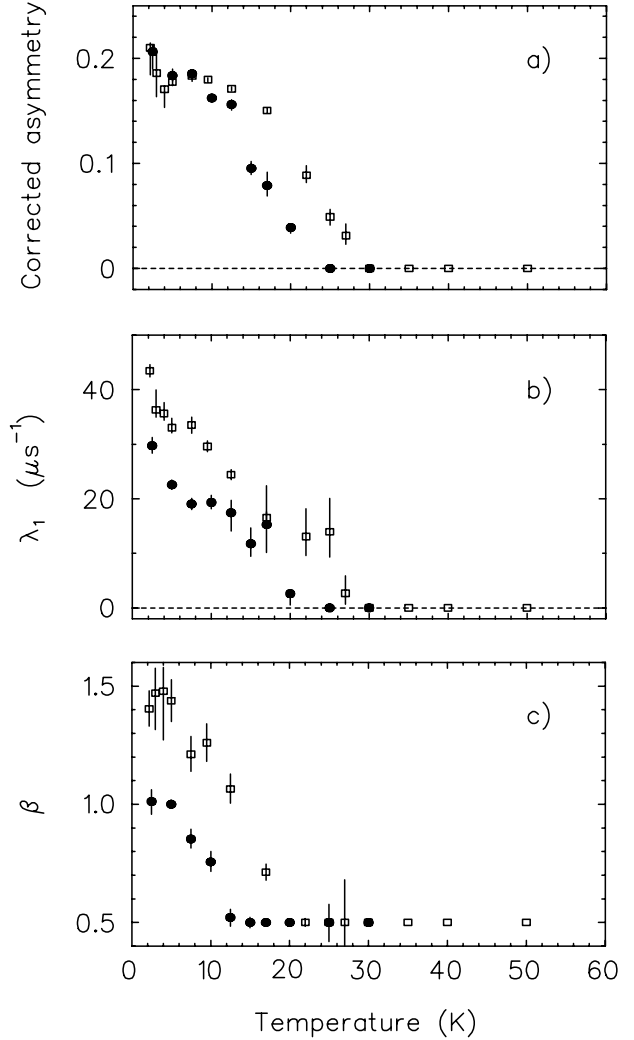
Fig. 150. (a) Corrected asymmetry A_1, (b) muon spin depolarization rate λ_1 and (c) parameter β as a function of temperature in $Y_{2-x}Bi_xRu_2O_7$ ($x = 0.9$, 1.0) in a longitudinally applied field of 15 Oe. The fitted function is described in the text. Filled circles and unfilled squares indicate data on $YBiRu_2O_7$ and $Y_{1.1}Bi_{0.9}Ru_2O_7$, respectively.
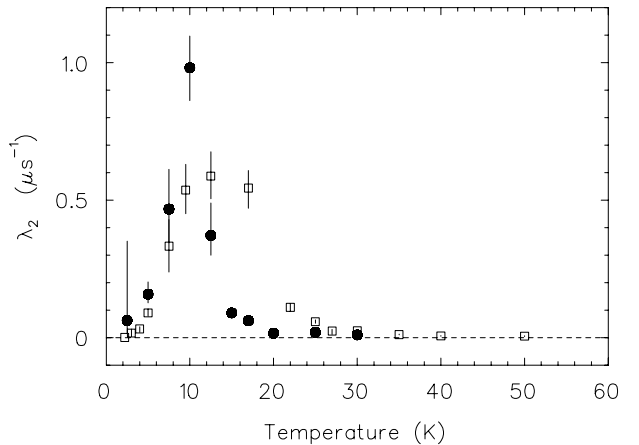
Fig. 151. Muon spin depolarization rate λ_2 as a function of temperature in $Y_{2-x}Bi_xRu_2O_7$ ($x = 0.9$, 1.0).

Experiment 943

Muonium and muoniated free radical formation and reactivity in sub- and supercritical carbon dioxide

(K. Ghandi, SFU)

The purpose of Expt. 943 is to study: 1) the radiation chemistry, 2) the free radical chemistry and 3) chemical kinetics of transient species in supercritical CO_2 ($ScCO_2$) and $ScCO_2$/cosolvents at the microscopic level using μSR as the experimental tool. These three areas are closely related by the common theme of green chemistry, a topic of significant recent interest (the entire ninth issue of 2002 Acc. of Chem. Res. was devoted to this topic).

Before giving the report on different stages of the project, we will list only a small number of the questions that were planned to be tackled during the course of this study:

1. Are these experiments feasible? Are muonium and diamagnetic species long lived under sub- and supercritical conditions?
2. Can radiation chemistry be tuned with the solvent thermodynamic state under sub- and supercritical conditions?
3. What kind of free radicals would react with CO_2 under sub- and supercritical conditions?
4. Are free radicals free or do some complex with CO_2?
5. Under what conditions are the fluctuations of the solvent cage significant?
6. Can we tune the electron wave functions of a radical by applying modest pressure in a supercritical fluid?
7. Under what conditions and for what kind of radicals do solvent cages exist? If there is a significant change in the solvent cage, how would that affect hyperfine interactions and chemical kinetics?
8. What are the optimum thermodynamic conditions for different types of reaction?

We have answered several of these questions during one-week (fragmented) data-taking at M9 and M15. Studies were first carried out in standard samples. This determined the scaling factors to convert muon signal amplitudes to fractions of initial polarization: PD, diamagnetic fraction, PMu, muonium fraction and PL = 1 – PD – PMu, the "missing fraction", which is of particular interest since it points to the mechanism of muon depolarization in the radiolysis environment. The muon spin precession frequencies were used to distinguish between muons in the muonium atom and those incorporated in diamagnetic molecules. The diamagnetic signals were measured in experiments at fields around 100 G and muonium signals were
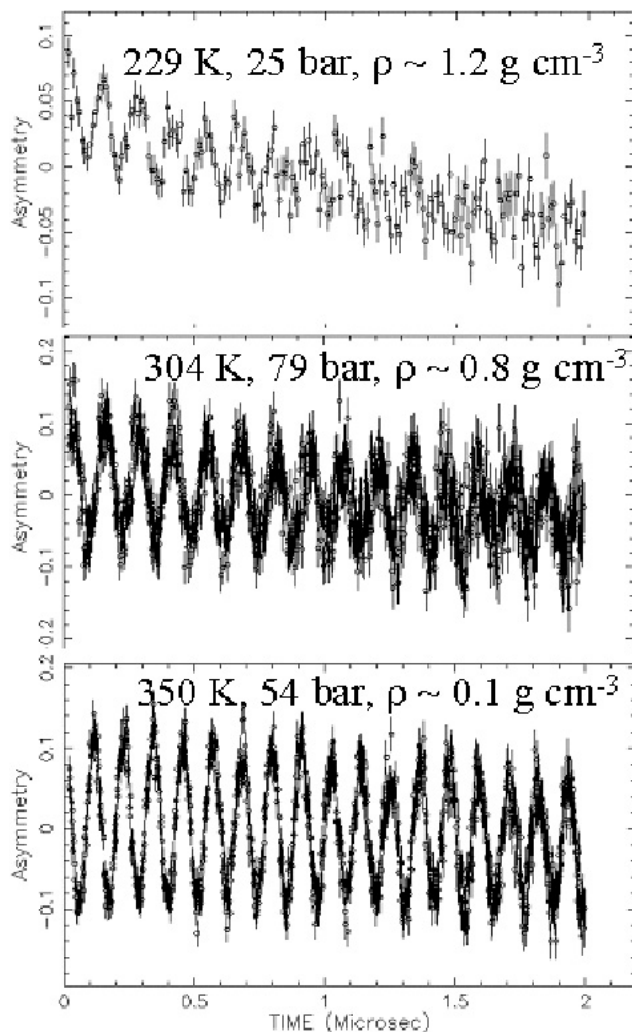
Fig. 152. Mu precession at 6G in CO_2.
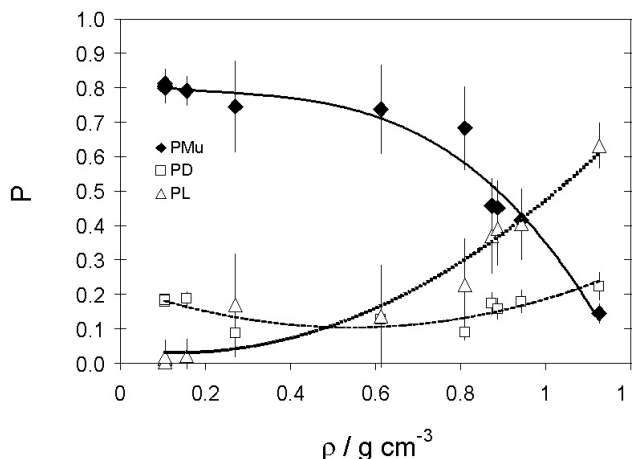
Fig. 153. Mu, diamagnetic and missing fraction in CO_2.

measured in fields smaller than 8 G, where a single frequency was detected (Figs. 152 and 153).

Based on our result, the answer to question 1 is that the experiment is feasible since Mu is formed and

115

long lived over a broad range of conditions from liquid to supercritical conditions (Fig. 152). However, the Mu fraction changes with density (Fig. 153). This may suggest that radiation chemistry can be tuned with the solvent thermodynamic state under sub- and supercritical conditions (question 2). More detailed studies are necessary to understand the factors affecting this significant change in Mu fraction.

At this stage our answer to question 3 is only limited to the reaction of Mu with CO_2 and our data suggest that Mu does not react with CO_2 under the conditions we have studied (thermal Mu does not add to CO_2). The only suspicious conditions are at very low temperature ($-40°C$) where the relaxation was significant ($0.8\,\mu s$), which needs more experiment to explore the cause of this high relaxation; under all other conditions the maximum background relaxation was less than $0.3\,\mu s$.

A magnetic field around 100 G, transverse to the muon polarization was used to determine the hyperfine coupling in muonium. At these intermediate fields the muonium precession signal splits into two (Fig. 154). The splitting was used to determine muon hyperfine coupling in muonium. The results are presented in Fig. 155 and suggest that Mu is free at lower pressure (question 4) since the hyperfine coupling is not much different from the value for vacuum Mu, but at higher densities there is a significant intermolecular interaction between Mu and CO_2 molecules.

The local minimum close to the critical density probably suggests that the fluctuations of the solvent cage are significant under these conditions and lead to local density enhancement (question 5). Theoretical calculations to describe these results are in progress, however, the result itself is very significant since it shows that we can tune the electron wave functions of as simple a radical as Mu by applying modest pressure in a supercritical CO_2 (question 6).

To answer question 7 we need to study the temperature dependence of hyperfine interactions at constant densities, which is in our future plans.

In our original proposed plan for these experiments, we listed studies for the reactions of Mu with O2 and Br2. The first one was to study diffusion process and cage effects in $ScCO_2$ while the latter was a chemical reaction with no electronic barrier. In the interim we changed our plans and studied instead the reaction between Mu and NO for two reasons: 1) Br2 is corrosive and the addition reaction with NO is similar to Br2 in that both have no electronic barrier; 2) by studying Mu decay rates at two fields, one less than 8 G and one around 80 G, we could determine both the spin exchange rate and addition rate. Our preliminary results are shown in Figs. 155 and 156. Much more

experimental data is needed but even from this little amount of data we can see that the addition of Mu to NO and likely to small molecules in general is much more efficient in $ScCO_2$ compared to the other usual moderators, particularly at higher densities.
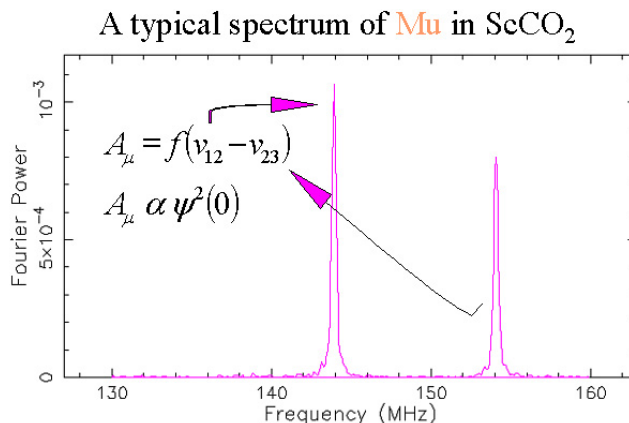
Fig. 154. $v12$ and $v23$ frequencies of Mu in 100 G magnetic field.
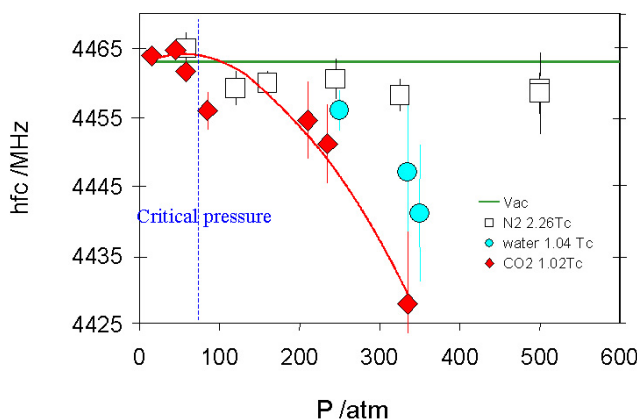
Fig. 155. Hyperfine coupling constants of Mu in $ScCO_2$.
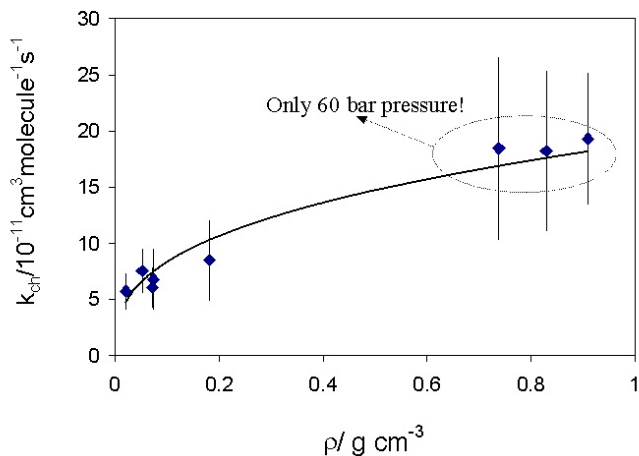
Fig. 156. Rate constants of Mu addition to NO in CO_2.

Experiment 944
Muonium in silicon carbide
(R.L. Lichti, Texas Tech.; K.H. Chow, Alberta)

TRIUMF Expt. 944 received its initial week of beam time late in 2002. Our main goal was to examine high frequency spin precession spectra for the three main structural phases of SiC; namely 3C, 4H, and 6H. High resistivity wafers of the two hexagonal structures were obtained commercially: the original source was Cree, Inc. The 3C sample is *n*-type at 2×10^{16}cm^{-3} and was provided by H. Nagasawa, Hoya Corp., from their substrate development program. The experiment was performed with the HiTime spectrometer in M15.

Our initial intent was to confirm the hyperfine values and then examine the temperature dependence for the three Mu^0 signals previously observed in 6H-SiC [Patterson *et al.*, Hyp. Int. **32**, 625 (1986)] and the two states seen in 4H-SiC. Cubic 3C-SiC is predicted to give a shallow donor state for H or Mu [Deak *et al.*, J. Phys. Cond. Mat. **13**, 9019 (2001)].

Figure 157 shows precession spectra obtained at low temperatures for the 6H and 4H structural phases. In both cases the magnetic field was nominally applied along the hexagonal *c*-axis, i.e. (0001). There do indeed appear to be three Mu^0 signals in 6H-SiC; however, these are not consistent with published hyperfine values. Spectra at higher temperatures imply that all three states are still there at 300 K in the present 6H sample, again contrary to earlier reports. The present data yield hyperfine values of 2826, 2984, and 2999 MHz for the three Mu^0 states at 4 K.

Figure 158 shows the detailed temperature dependence for the amplitudes and relaxation rates of each Mu^0 line and the diamagnetic signal in the 6H sample. The origin of the large amplitude variation for the Mu^0 states around 150 K is not understood at present. It is not completely reflected in the diamagnetic amplitude, and thus may represent Mu^0 motion in part. However, the hyperfine constants vary as expected for

Fig. 157. Low temperature hyperfine spectra for 6H-SiC and 4H-SiC in a field of 6.0 T applied along the *c*-axis. The diamagnetic line is at 813 MHz and the other lines represent negative frequencies for Mu^0 ν_{12} transitions.
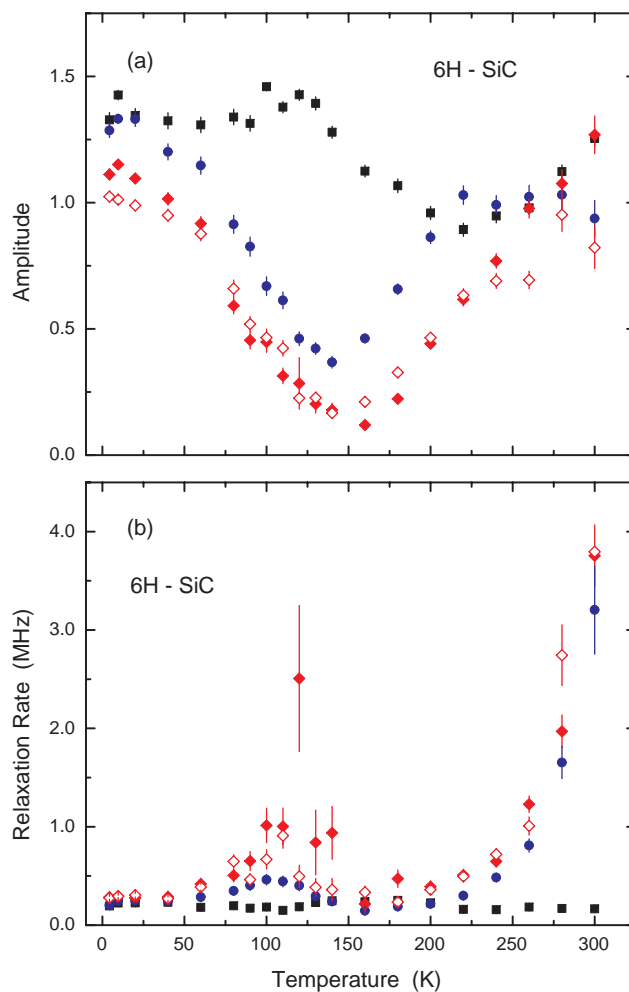
Fig. 158. Temperature dependence for amplitudes (a) and relaxation rates (b) for 6H-SiC (squares (black), μ^+, 813 MHz; circles (blue), Mu1, 559 MHz; filled diamonds (red), Mu2, 678 MHz; open diamonds (red), Mu3, 687 MHz).

individual Mu^0 states, so transitions among different types of Mu^0 sites are apparently not observed since that should lead to motional averaging of the relevant frequencies. The rate increase above 200 K is likely due to ionization. Higher temperatures are needed for confirmation.

In the case of 4H, five Mu^0 signals may be present at the lowest temperatures: the 678 MHz line appears to be split. Thus far we have only one other spectrum at 100 K where a single weak Mu^0 line is seen. It is not obvious whether the unexpected additional signals at low T are from a possible inclusion of a different structural phase (15R may be present and would have both 4H and 6H type sites) or from impurity-related sites. Most of the Mu^0 signals in 4H are very close to a 6H frequency.

We did not observe any Mu^0 signals in the n-type cubic (3C) SiC crystal. There is, however, a significant amount of relaxation in the diamagnetic signal which must arise from interactions between the muon and conduction electrons or with a magnetic impurity, given the very low fraction of host Si or C nuclei with magnetic moments. Both the absence of spectral evidence for a shallow donor and evidence of interactions between the muon and electrons in this sample are consistent with low-field results from measurements at ISIS a few months earlier.

We will need to examine additional samples of all three structures and obtain a more detailed temperature dependence for the 4H phase before drawing too many conclusions concerning differences with the older data and possible origins for the unexpected additional Mu^0 signals.

LIFE SCIENCES

Introduction

The use of clinical PET reached a critical point within Canada, and in Vancouver in particular, this past year. The TRIUMF Life Sciences program has played a large role in bringing this technically challenging imaging modality from the research bench to the bedside. During this past year TRIUMF supplied the Cross Cancer Centre (CCC) at the University of Alberta with ^{18}F over a 9 month period (125 shipments) that enabled the Centre to begin its research and clinical program in the use of PET in the diagnosis of cancer. Locally, the supply of the radiotracer FDG was drawing to an end as the Vancouver Hospital prepared to take over this task and MDS Nordion showed interest in becoming more involved in the supply of PET tracers.

The applications of radiotracers for various projects at UBC continued to play a significant part of the program with the addition of radiochloride isotopes for visitors from the University of Toronto. Possible new tracers utilizing metallic isotopes will expand the already significant array of radiotracers available for the research PET at UBC. Plans are under way for expanding the facilities available for the Life Sciences program in the next 5 year plan.

Experiment LS0
PET facilities
(K.R. Buckley, TRIUMF)

The PET facilities comprise the TR13 13 MeV H$^-$ cyclotron, the ECAT 953B/31 tomograph, and ancillary equipment such as counting and data acquisition systems.

Personnel

Carolyn English left for maternity leave this fall and a part time technologist (Hosien Kamrudin) has been hired to work Fridays. Caroline Williams will work extended hours Monday to Thursday to cover the scanning day and Hosien will work on Fridays. This allows us to continue operating the extended days required to accommodate our scanning protocols though it is dependent on the good graces of our technologists to keep up with the workload.

Dr. John Wilson from the Cross Cancer Institute in Edmonton stayed with us until the summer, learning cyclotron operation and carrying out the irradiations for the production of ^{18}F for shipment to Edmonton. Following John's departure, the Cross Cancer Institute sent Wayne Logus for the summer for training and to continue the irradiations. Wayne returned to Edmonton at the end of summer when their cyclotron began operations.

TR13 cyclotron

Usage of the TR13 cyclotron increased significantly this year in both runs conducted and delivered beam due to the irradiation of two high dose lithium targets for the production of ^{7}Be (LS8), the irradiation of a palladium target for ^{110m}Ag (LS8) and the routine supply of ^{18}F to the Cross Cancer Institute in Edmonton. The total number of runs increased to 1038 vs. 848 last year and delivered beam doubled to 1,258 mA min from 631 mA min.

Downtime this year was caused by two rf system problems and a cooling water leak under the cyclotron. These repairs required several days to complete. The cooling water leak resulted in the failure of the cryohead drive electronics in the compressor due to a poorly made splice to an electrical cable that ran in the vicinity of the water leak.

Nine extraction foil changes were required through the year and all targets where rebuilt at least once. Four ion source filament changes have been done along with other miscellaneous service items.

Presently there are six target locations occupied of the available eight. These consist of

- one ^{18}O-O$_2$ gas target
- one ^{18}O-water target
- one ^{16}O-water target
- one N$_2$/H$_2$ gas target
- two experimental gas targets.

A number of irradiations took place this year in support of LS8. The lithium target was operated twice this year, both times at 50 μA. One run was performed in early January for approximately 60 hours and a second run was performed in May for just over 100 hours. It is anticipated that that was the last run required.

We have been operating the niobium body gas target for the production of ^{14}O. This is the same target body we use for the production of fluoride from ^{18}O gas. We did another irradiation of an iron foil for production of ^{56}Co for calibration of the 8π detector in ISAC, and we irradiated another palladium foil for production of silver isotopes ^{110m}Ag for Brian Turrell in UBC Physics.

A fumehood was situated beside the TR13 cyclotron this summer to aid in development of ^{14}O production. The ^{14}O, with a half-life of 70 s, is recovered from the target in the form of H$_2$O. It was found to be too difficult to achieve this transport to the chemistry labs approximately 50 m away.

ECAT tomograph

Block detector failures and programmable array logic chips continue to be the dominant modes of failure for the camera. We are routinely repairing blocks in-house and have replaced 7 blocks again this year. We have still not assembled the necessary components to properly calibrate the blocks prior to returning them to the scanner. At present only a simple visual balance of PMT outputs is performed on the bench and the block set-up routine in the scanner performs the fine tuning. Programmable logic chips in the buckets continue to fail. Chips for nine channels have been replaced this year.

The array processor in the front end for 2D reconstructions had to be replaced again this year. A replacement was purchased from Byar's Consulting for a much better price than the last unit obtained from CTI.

A high voltage power supply was obtained to replace a drifting supply for the PMT high voltage. TRIUMF Electronics has not been able to isolate a fault in the original supply though the camera stability improved with the replacement of the supply. There is still a lingering drift in the ECAT calibration which is larger than the camera exhibited in previous years. We have been unsuccessful in determining the cause of this, however, it simply means that a calibration is performed more often to maintain the camera in allowable limits.

The ^{68}Ge transmission rods and uniform calibration cylinder were replaced this year with sources purchased from Sanders Medical.

Renovations in the UBC hospital have been completed for the installation of the HRRT from CTI. This new scanner will be installed in the space previously occupied by the original PETTVI scanner. This allows both the ECAT and the HRRT to be operated from the same control room. Delivery of the camera is expected early in 2003.

A small animal PET camera has also been purchased from Concorde Microsystems and is due for delivery in April, 2003.

Statistics

Table XI. ECAT scanning statistics.

		2002	2001
Total scans conducted		383	379
Total scans lost		37	52
Lost to	– patient	8	10
	– cyclotron	16	8
	– chemistry	3	6
	– scanner	7	13
	– staff sick/away	0	9
	– investigator	3	6

Table XII. TR13 run statistics.

		2002	2001
Total runs conducted		1038	848
Total runs lost		16	8
Total beam delivered (μA min)		1,258,376	631,357
Delivered to	– LS2	–	160
	– LS 3	301,611	262,573
	– LS 4	40,411	55,327
	– LS 8	605,500	14,4199
	– LS 13	51,410	33,611
	– LS 24	17,246	33,172
	– LS 32	240,995	91,240
	– LS 33	–	477
	– LS 39	1203	4580
	– LS 47	–	300
	– LS 49	–	3282
	– LS 52	–	2436

Experiment LS3
Synthesis of radiopharmaceuticals for positron emission tomography
(M.J. Adam, TRIUMF)

Daily routine production of up to 11 radiopharmaceuticals is currently performed with 3–4 radiophamaceuticals synthesized on any given day. FDG continued to be sent once per week to each of Vancouver, Lions Gate and St. Paul's Hospitals for research in cardiology and oncology. Out of these 11 radiopharmaceuticals, five (FDOPA, Raclopride, TBZ-OH, SCH23390 and MP) are used most heavily. There has been an increase in the number of Raclopride preparations from last year, making Raclopride the most heavily used radiopharmaceutical. Most of the Raclopride preparations this year are for the "Scatchard Analysis" experiment that Doris Doudet is performing on monkeys. These experiments require 3–4 Raclopride preparations each day where one is at high specific activity (5–10 Ci/μmol) and the others have carrier added to give a range of SAs of 2–35 Ci/μmol at time of injection. All preparations for these experiments are assayed by HPLC prior to injection to confirm the specific activity. There was a total of 642 production runs in 2001 for CIHR/PET and external users with 412 radiopharmaceutical syntheses carried out just for the TRIUMF/UBC PET Program.

The demand for FDG for our group remains low. However, most of our FDG production is being used by Lions Gate, St. Paul's and Vancouver General Hospitals for studies in oncology and cardiology (details in LS13, 24, 40, 48, 49 proposals). We currently send FDG to these hospitals one day per week in an amount

enough for imaging approximately 3–4 patients. Vancouver General Hospital is setting up an FDG synthesis system and the plan in the future is to send only ^{18}F-fluoride to Vancouver General Hospital and they will make the FDG for themselves and for all other local hospitals.

One of the main reasons for the large increase in the total production runs this year was the increase in shipments of ^{18}F-fluoride to Edmonton to three days each week for clinical cancer imaging (see LS32 proposal). The Cross Cancer Centre in Edmonton sent a chemist/trainee (Dr. John Wilson) to TRIUMF for a few months to carry out these runs and to learn cyclotron operations and PET chemistry. MDS Nordion handled the airline transport and Edmonton is paying all the transportation costs and the cost of the ^{18}O-water used in the target. The Cross Cancer Centre was able to carry out 5–6 patient scans with each shipment of radiofluorine from TRIUMF.

This year the preliminary experiments, carried out by Dr. Chong, using ^{11}C-PMP to study dementia in Parkinson's disease and diffuse Lewy body disease were completed. Previous studies in postmortem brains have shown that choline acetyltransferase activity, but not muscarinic cholinergic receptors, was markedly reduced in PD, diffuse Lewy body disease and Alzheimer's disease, and that neocortical cholinergic deficits correlate with severity of dementia in PD, diffuse Lewy body disease and Alzheimer's disease. As reduced cholinergic activity in the neocortex correlates with marked neuronal loss in the nucleus basalis of Meynert, these observations suggest that loss of cholinergic neurons in the basal forebrain may play a significant role in the pathogenesis of dementia in PD and diffuse Lewy body disease as well as in Alzheimer's disease.

This project has now been put on hold pending the analysis of data and the success of submitted grant applications.

The synthesis of ^{11}C-Carfentanil was successfully completed this year and will be ready for human use early in 2003. Dr. de la Fuente previously demonstrated, for the first time, that there was a measurable increase in the amount of dopamine released into the synapse when a placebo was administered, thus showing a chemical basis for the placebo affect. We now want to extend this research to look at other receptor systems that might be involved such as the opioid system. As with most new radiopharmaceutical projects, the synthesis of the precursor was the most labour intensive part.

The synthesis of ^{18}F-labelled oligonucleotides has also been started this year to compliment the Antisense research that has been ongoing in Dr. Stoessl's

lab. To start, we tried repeating the procedure of the INSERM French group and are attempting to attach a fluorinated aromatic group to the phosphorothioate end of the above oligo. We demonstrated that we can attach the non radioactive label to the oligo and purify it on HPLC. However, attempts to synthesize the ^{18}F-labelled version have proven to be somewhat problematic. Unfortunately, it requires a multistep synthesis where the ^{18}F is introduced in the first step, making the procedure very difficult to carry out. We are attempting to find alternative, simpler methods to the ^{18}F-labelling of these oligos.

We continue to use TBAF in most of the ^{11}C methyl iodide reactions to enhance and stabilize the yields. We are fortunate to still obtain the nitro precursor of Setoperone as a gift from Jannsen Pharmaceuticals. We also are grateful to ASTRAZENECA AB for the gift of Raclopride Tartrate, used as carrier for the Scatchard experiments, and dihydroxy Raclopride as the precursor for labelling.

The separation of $\pm$ DTBZ into its active enantiomer was also achieved this year. We began imaging with the $+$, active enantiomer in 2002 and the images are much clearer without the significant background image created by the inactive isomer. We are currently comparing both images from the active isomer and the racemic mixture before completely converting to the active isomer.

Experiment LS4
TR13 targets for PET radioisotope production
(T.J. Ruth, TRIUMF)

Progress for 2002

At this stage we have the targets required for our PET program, namely a target to produce ^{18}F-F$_2$ and ^{11}C-CH$_4$. These two tracers represent starting material for the bulk of our radiopharmaceuticals. We have built back-up targets to reduce the downtime associated with window failures and target cleaning. However, they have not been installed as of this time due to scheduling. Because of a failure of our Ti water target in 2000, we redesigned the target and built it from niobium. This new target material has performed exceedingly well. Results were reported at the 8th Workshop on Targetry and Target Chemistry (WTTC), Turku, Finland in May, 2002.

^{18}F-fluoride system

Following on our experience with the stainless steel target, we wanted to build a target system capable of producing multi-curie quantities of ^{18}F-fluoride while being able to recycle the target material.

Methods

We have reported our work on a gas target system to produce ultra-high quantities of ^{18}F-fluoride at the WTTC and in the literature using a stainless steel target body. While these results demonstrated proof-of-principle concepts, there were improvements to be made around the efficiency of ^{18}F extraction from the target walls and the chemical reactivity of the ^{18}F-fluoride. Since that time, we have designed another gas/liquid handling system and other target bodies.

Our experience with a niobium bodied water target led us to use niobium for the target we report on here. Three features, in addition to material, separate this target from the previous designs: i) cartridge heaters mounted in the target body, ii) vent port at the rear of the target, made possible by the change in the water jacket design, and iii) zero dead-volume fittings in the target body.

The design of the gas and liquid handling system for this target is also different than that used previously. The key feature is the use of a heat trace and insulation around the transfer lines to and from the target. This allows the lines to be dried quickly and efficiently and may also aid in the transfer of the fluoride.

The transfer lines were constructed by wrapping two 3 mm O stainless steel lines together and wrapping this assembly with the heat trace. The heat trace was assembled by feeding Chromel-A heater wire through a 1.6 mm O teflon tube 5 m long, the Chromel-A wire is 5.417 Ω/m, yielding a total resistance of 34.7 Ω. The entire assembly was wrapped in standard plumbing insulation sleeves. Operating the heat trace at 48VAC results in 66 W which warms the transfer lines to approximately 75°C.

To conduct an irradiation, the target is first evacuated to a pressure less than 200 m torr by a mechanical vacuum pump. The target is then loaded by opening the 95% ^{18}O-O_2 reservoir to the target. The fill pressure is approximately 2060 kPa (300 psi). After the irradiation the O_2 is cryotrapped back to the reservoir with only small losses. The reservoir is 25 ml volume and the target is 24 ml volume. While the gas is being recovered (5 minutes) the target cooling water is shut off and the target and transfer lines are heated to 80 ± 5°C.

The mechanical vacuum pump is then used to evacuate the target which is next opened to a reservoir of HPLC grade water. The temperature on the rear of the target can be seen to drop 5°C when the target is full. The water is left in the target for 5 minutes before being pushed by 140 kPa (20 psi) helium over the ion separation column (Waters QMA Sep-Pak for example). The wash volume is approximately 50 ml.

A second target rinse is performed by partially evacuating the target with the mechanical pump and drawing a second volume of water into the target. Again, this is left in the target for 5 minutes before being pushed over the ion separation column. At this point in our work the column is removed and counted in an ion chamber or attached to an FDG synthesis module.

To dry the target in preparation for the next irradiation the target and transfer line heaters are left on at 80°C while helium at 140 kPa (20 psi) flows through the system. To determine that the system has dried, the mechanical pump vacuum pump is used to evacuate the system. The system is assumed dry when a pressure of less than 200 m torr can be obtained. In our tests, the time until the target was deemed dry and ready for the next irradiation was approximately 2 hours but no effort was made to determine the minimum time required.

Results

This target performs at near theoretical levels to 25 μA and with decreasing production rate for higher beam currents. Up to 50 μA, the higher beam current outweighs the loss of target thickness from density reduction to result in a net increase in yield. A 2 hour irradiation at 13 MeV and 50 μA yields 130 GBq (3.5 Ci). The ^{18}F-fluoride recovered from the target is equivalent in reactivity to that obtained from conventional targets irradiating ^{18}O-H_2O.

Conclusions

A gas target for producing ^{18}F-fluoride has been demonstrated to operate at 50 μA with the possibility of even higher beam currents which would result in extremely high production rates.

There are 2 patents pending for this system.

^{11}C-CH$_4$ production

Our previous work on static irradiations of a H_2/N_2 target gas for the production of methane indicated that recoverable yields at 13 MeV plateaued at about 750 mCi at EOB. The relatively poor yields were attributed in part to hot atom interactions with the target chamber walls. In order to try and overcome this limitation, an aluminum bodied flow-through gas target was implemented and tested for the production of ^{11}C-CH$_4$ on the TR13 cyclotron at TRIUMF. Nitrogen gas with varying quantities of hydrogen has been used to investigate the optimum ratio for methane production. Comparison of the flow-through target with the static-target irradiations for production of methane are given.

Methods

Aluminum body gas targets were designed with cylindrical bores of 12.7 mm ID and 120 to 127 mm lengths. A water-cooled support grid with 34 × 1.59 mm holes arranged in a hexagonal pattern with

1.78 mm between centres supported aluminum target window foils $25.4\,\mu$m thick. Transmission through the grid was calculated to be approximately 70%. Beam transmission studies indicated 64% transparency. Mixtures of N_2 with up to 20 percent H_2, pressurized up to 3.1 MPa were used to make ^{11}C-CH_4. For comparison, ^{11}C-CO_2 was produced in the same target system with a mixture of N_2 and 0.5% O_2, pressurized at 0.69 to 2.28 MPa. Gas flow in each case was 200 to 600 ml/min. Irradiations of up to 32 μA lasted up to 60 minutes. The radiolytic production of ammonia could be a concern for post production processing, e.g. ^{11}CH3I synthesis. To measure the ammonia thus produced we passed the target gas through a series of HCl traps and back-titrated to a phenolphthalein end point.

Results

Testing of the flow-through target gave a saturation yield of up to 2.89 GBq/μA (79 mCi/μA) ^{11}C-CH_4 at 32 μA with a correction for the grid transmission (both beam current on target gas and saturation yields). For comparison, ^{11}C-CO_2 was produced with a saturation yield of 2.66 GBq/μA (73 mCi/μA) at 27 μA with correction for grid losses. Yields did not improve above approximately 10% H_2. The maximum ^{11}C-CH_4 produced after a 35 minute run at 30 μA was 57.3 GBq (1.55 Ci). Preliminary measurements of the specific activity (SA) via the synthesis of ^{11}C-raclopride indicate that the EOS SA is approximately 13.5 GBq/μmole (500 mCi/μmole). In the static target we found that ammonia production reached equilibrium quickly, resulting in a production of 0.13 mmoles. The flow-through target generated 8 mmoles of ammonia for a 50 μA $\times$ 20 minute irradiation.

Conclusion

The flow-through target system for the production of ^{11}C-CH_4 provides increased radioactivity over single shot low volume, high pressure gas targets. The ^{11}C-CH_4 saturation yield is within experimental errors to that for ^{11}C-CO_2 under similar conditions and is 72% of calculated theoretical maximum yield, allowing for the support grid transmission. The cause for the relatively low specific activity is under investigation. The high quantity of ammonia co-produced will adversely affect the production of CH3I and must be removed for a useful system.

Experiment LS8
Radiotracers
(T.J. Ruth, TRIUMF)

(A.D.M. Glass, Botany Department, UBC)

During 2001–2002, my group has diminished in size as Ph.D. students completed their programs and two PDFs accepted positions as research associates elsewhere. Also, my long-time research associate, Dr. Yaeesh Siddiqi, retired. We have therefore made much less use of ^{13}N during this period. Nevertheless, in September, 2002, a visiting scientist joined my group and will possibly begin her Ph.D. studies in September, 2003, two new PDFs will begin their tenures in my laboratory in January, 2003, and a scientist from New Zealand will join my group in May, 2003. I therefore anticipate a renewed requirement for ^{13}N in the coming year.

Ph.D. students: Anshuman Kumar (current), Yu Wang (likely) Mamoru Okamoto, Dev Britto (completed). PDF: Manuela Simon, Yaeesh Siddiqi. Visitors: Herbert Kronzucker, Dev Britto, Yu Wang.

Rice research

Anshuman Kumar has now cloned three ammonium transporter genes from rice and successfully demonstrated that the expression of two of these genes (AMT1.1 and AMT1.2) is strongly correlated with root N status. By measuring ammonium influx using ^{13}NH$_4^+$, he has shown that the control of influx, mediated via changes of root glutamine and asparagines, appears to be via changes of transcript abundance of AMT1.1 and AMT1.2. A third gene, AMT1.3, is relatively insensitive to root N status but is responsive to diurnal irradiance at leaf level. Thus a strong correlation was observed between the pattern of incoming light, AMT1.3 expression and ammonium influx.

Nitrogen uptake in trees
(Collaboration with CELLFOR: M.Y. Siddiqi, M. Simon, J.J. Vidmar)

Our goal of increasing nitrate uptake in plants overexpressing the high-affinity NO_3^- transporter gene, (AtNrt2.1) has been unsuccessful in tobacco and in poplar seedlings. Based on work on an algal model system, it appears that a second family of genes (the NAR2 family) must be co-expressed in order to achieve efficient NO_3^- uptake. Mamoru Okamoto (Ph.D. candidate) has cloned the algal counterpart from the higher plant Arabidopsis and we are investigating the importance of the Arabidopsis NAR2 homologue in mutants that are blocked in the expression of this gene. Preliminary findings suggest that the mutant is unable to grow normally when nitrate is the sole source of N. Assays of NO_3^- uptake will be conducted in standard fashion using $^{13}NO_3^-$.

^{13}NO$_3$ influx in the fungus aspergillus nidulans: a structure function study of gene sequence and NO_3^- uptake
(Collaboration with S. Unkles, J. Kinghorn, St. Andrews, Scotland; A.D.M. Glass, Y. Siddiqi)

Together with our Scottish collaborators, we have cloned and sequenced the two NO_3^- transporters of this

fungus. They have similar (but not identical) gene sequences but have very different affinities for NO_3^- and different maximum velocities.

Having the gene sequences and the physiological characterization, it will be possible to generate chimeric proteins and switch the gene's function from high to low affinity, etc. We will test the resultant strains using $^{13}NO_3^-$. This will make it possible to place NO_3^- transport kinetics on a sound structural basis and to manipulate transport within existing genes. This project has been on hold awaiting NSERC funding that is now in place. A PDF will begin this work in January, 2003.

Studies of fluxes and compartmentation of chloride ions in barley plants
(D.T. Britto, H.J. Kronzucker, Toronto)

With the increasing use of irrigation and fertilizers throughout the world, there have been associated increases in salt accumulation in agricultural soils, affecting ~50% of the irrigated agricultural land base globally. Soil solution concentrations of sodium, chloride, and other ions can sometimes reach excessively high levels, resulting in suppression of plant growth and, ultimately, loss of arable land. Because of the severity of this problem, much research has been focused on salt stress and its avoidance by tolerant species or cultivars. However, while the physiology of plant-sodium relations has been particularly well studied, the chloride ion, which often accompanies sodium, has been understudied in relation to salt stress in plants. The objective of our study was to establish a baseline of information regarding the transport and subcellular accumulation of chloride in barley (Hordeum vulgare) roots, particularly with regard to the influence of nitrogen strength and source.

Due to the provision of short-lived radioisotopes of chlorine ($^{38,39}Cl$) provided by TRIUMF, we have made major progress towards this objective. We grew barley seedlings under ten nutritional conditions, varying both external chloride concentrations and nitrogen sources and concentrations. Chloride was varied between 0.1 mM and 100 mM externally, covering a range that included both benign and toxic concentrations. Nitrogen was provided as either ammonium (NH_4^+) or nitrate (NO_3^-), at low (0.1 mM) or high (10 mM) concentrations. We examined the influx, efflux, shoot translocation, subcellular turnover, and pool size of Cl^- under these nutritional conditions. We found that, overall, these parameters follow the general pattern we have observed using isotopes for other nutrient ions, particularly nitrogenous ones. Steady-state Cl^- influx increased with increasing external Cl^- and was generally lower when NO_3^- was the nitrogen source (in keeping with findings by other workers). Cl^- efflux in-

creased to a greater extent along this gradient, resulting in a low efflux-to-influx ratio (10–20%) at moderate Cl_{ext}^-, and an exceptionally high one (~90%) at high external Cl_{ext}^-. This ratio tended to be higher when NO_3^- was the N source. Because the efflux increased with Cl_{ext}^-, the resulting net flux (accumulation) increased much more moderately than either influx or efflux. The high fluxes observed at high Cl_{ext}^- suggested that there would be an associated high respiratory cost, as has been shown previously for NH_4^+, but preliminary respiration experiments have not demonstrated this.

Our results disagree with a previous model for cellular Cl^- compartmentation, which had maintained that this ion is held at a homeostatically constant concentration in the cytosolic compartment. What we observed using compartmental analysis by tracer efflux (CATE) was substantial variability in the size of this pool, and in its turnover, both of which increased with increasing Cl_{ext}^-. One question we wanted to pose was whether we would see high accumulation of Cl^- ions in the cytosol of plant cells exposed to high external NH_4^+, since we have found that high accumulation of the latter ion occurs cytosolically under this condition, and we hypothesized that Cl^- could act as a counterion to NH_4^+, providing electroneutrality to this metabolically critical cellular compartment. While we did observe a generally higher cytosolic accumulation of Cl^- with NH_4^+ treatments relative to NO_3^- treatments, this accumulation was not high enough to satisfy the anion requirement demanded by high cytosolic NH_4^+, and further possibilities must be sought.

Radiotracers for chlorine and sodium

Dr. Herbert Kronzucker of the University of Toronto (former student of Dr. Glass) is developing a program to study kinetics of various elements in plant systems. This past summer he returned to Vancouver to conduct a series of studies using $^{38,39}Cl$. These isotopes can be easily produced by irradiating natural Ar with protons of about 40 MeV as described in the literature.

^{110m}Ag in nuclear orientation experiments
(B. Turrell, Physics, UBC)

In April, 2001, the PET group made us a sample of ^{110m}Ag produced by proton irradiation of a Pd foil. This procedure also produces other silver isotopes, in particular ^{105}Ag. Measurements in our laboratory at UBC in May indicated that the activity of ^{110m}Ag was 280 μCi while that of ^{105}Ag was 3.5 mCi. However, the relative half-lives of two isotopes are 255 d and 40 d respectively. Therefore, by waiting a few months, the ^{105}Ag activity would decay by an amount sufficient that a low temperature nuclear orientation (LTNO) experiment on ^{110m}Ag could be performed.

The motivation for the experiment is that there have been relatively few studies of impurities in insulating, ordered magnets, and we decided to study oriented Ag nuclei in a suitable antiferromagnet to determine the hyperfine field which reflects the atomic magnetization. A previous experiment at Louvain-La-Neuve by a UBC-Leuven collaboration had indicated a small anisotropy for γ-rays in the decay of ^{104}Ag that had been implanted into $MnCl_2.4H_2O$. However, the sample temperature in this experiment was relatively high ($\sim$90 mK) and, subsequently, thorough analysis showed that this effect could not be distinguished from zero within experimental error. Therefore, the original intent of the present experiment was to dope ^{110m}Ag into the same crystal and perform an LTNO experiment at a much lower temperature ($\sim$35 mK).

In May and June, 2001, attempts were made to grow a crystal of $MnCl_2.4H_2O$ from a saturated solution of $MnCl_2$ containing both ^{54}Mn and ^{110m}Ag (and ^{105}Ag). The former grew into the crystal as expected, but very little of the silver isotopes went in. It was concluded that this was due to Ag being monovalent whereas Mn is divalent. A literature search was then made for insulating magnets with a composition that included a monovalent, metallic ion. The candidate that emerged was $Rb_2MnCl_4.2H_2O$.

This is an antiferromagnet with a Néel temperature $TN = 2.2$ K. We have grown some crystals of this salt, but we have to refine the technique to produce some plate-like samples, incorporating ^{54}Mn and ^{110m}Ag, on which to perform the LTNO measurements. We plan to do this in the next two or three months.

In the LTNO technique, one measures the directional distribution of radiation from an oriented ensemble of nuclei. For the axially symmetric case, the normalized intensity of γ-radiation in direction θ to the orientation axis, normalized to the warm count at 1 K, is given by

$$W(\theta) = \sum B_k A_k Q_k P_k(\cos\theta). \qquad (1)$$

Here the B_k describe the orientation of the nuclei and contain the solid state information, the A_k depend on the observed and preceding transitions in the nuclear decay, the Q_k are detector solid angle corrections, and the P_k are the ordinary Legendre polynomials. Significant values of B_k are obtained when the nuclei experience a sizeable hyperfine interaction and are cooled to millikelvin temperatures in a dilution refrigerator.

In the decay of ^{110m}Ag, there are several γ-rays that can be studied, but an outstanding candidate for LTNO measurements is the 1384 keV transition. For this γ-ray the values of the A_k coefficients are A2 =

0.894 and A4 = 0.080. The hyperfine field, B_{hyp}, for the Ag nuclei is unknown. However, we note that Ag is a 4d element and, with one unpaired electron, we would expect $B_{hyp} \sim 35$ T. If we assume this value then, at temperature T = 40 mK, we would obtain for the B_k coefficients, B2 = 0.200 and B4 = 0.007. We can then estimate that the normalized intensities at $\theta = 0°$ and $\theta = 90°$, using $Q_k \approx 1$, would be $W(\theta) = 1.18$ and $W(\pi/2) = 0.91$. Measuring $W(\theta)$ in the experiment would allow B_{hyp} to be determined.

If a sizeable effect is indeed measured, we could then perform NMR on the oriented nuclei (NMRON). The NMRON technique not only measures the hyperfine field, B_{hf}, very precisely, but also the nuclear spin lattice relaxation (NSLR) and these give, respectively, details of the electronic magnetization and its dynamic behaviour. It is convenient for discussing NMRON to re-express Eq. (1) in the form

$$W(\theta) = \sum a_m(\theta) p_m. \qquad (2)$$

Here p_m is the population of a magnetic substate, labelled by m, and $a_m\theta$ includes the nuclear decay scheme and angular factors. NMR alters the substate population distribution and can be detected by observing the change in $W(\theta)$. The recovery to thermal equilibrium allows the determination of the NSLR time T1.

^{22}Na source for positron tomoraphy
(C. Thompson, McGill)

In positron emission tomography (PET), the most important correction required is the accurate measurement of γ-ray attenuation. Two approaches are currently used today: orbiting rod sources with 2D acquisition and single photon attenuation correction with ^{137}Cs. Rod-source windowing is the most widely implemented mechanism. ^{68}Ge/Ga rod sources rotate around the subject and, thanks to a coincidence circuit between two opposed detectors, the line of response (LOR) from the annihilation γ-rays is identified. The main advantage of this technique is the use of a concentrated source which reduces random events.

The collinearity criterion of both detectors and the orbiting rod sources eliminates most of the scatter events. Unfortunately the use of orbiting rod sources in transmission scans remains limited by low count rates due to close proximity of the near detectors.

The other alternative used is a rotating point source of 662 keV γ-rays of ^{137}Cs. This technique relies on the detection of photons in "single" mode rather than "coincidence" mode and no longer restricts the choice of transmission sources to those that decay by positron emission. The motivation for using ^{137}Cs as a transmission source comes from its higher count rate capability

due to a decreased detector dead time and increased object penetration. Since 662 keV γ-rays are being used for transmission, scanning measured attenuation coefficients will be 10% lower than 511 γ-rays of emission data and scaling of the measured attenuation factors to make them applicable to the emission data is thus necessitated. Several scaling methods are currently under study. Finally, a new approach using ^{137}Cs has been proposed by Jones *et al.* using collimated coincidence point sources with dedicated reference detector.

We propose a different approach of coincidence point sources using beta-gamma coincidence and 3D acquisition to improve the quality of transmission scans. This method would combine the advantages of single photon attenuation correction with ^{137}Cs without having the problem of scaling the attenuation coefficients due to a different energy from the annihilated photons. It is well known that a positron must lose an appreciable amount of its energy before annihilation with an electron can occur. In our case, the energy lost is spread inside a plastic scintillator material which produces light detectable by a photomultiplier tube (PMT). This PMT signal can then be used to trigger a coincidence circuit and identify a line of response between the plastic scintillator and the PET detectors. The concept of beta-gamma coincidence was proposed by our group in 1999 and used PIN diodes to detect the positron. This will be the first implementation of beta-gamma coincidence on an actual PET scanner.

^{38,39}Cl irradiations, targetry and chemistry

We converted the old neon target that was used to produce ^{18}F at 41 MeV (on the CP42) into a ^{38}Cl and ^{39}Cl-producing target ($t_{1/2}$ = 38–37.2 min; 39–55.7 min). At 41 MeV, the isotopic ratio for ^{38}Cl to ^{39}Cl is approximately 1.6. The experiment involved irradiating argon gas at a pressure equivalent to that of the Ne target ($\sim$300 psi) with a 41 MeV proton beam of 5–15 μA for times up to 30 minutes. The theoretical production rate is about 10 mCi/μA at saturation, thus we should be able to make <100 mCi. All the chlorine isotopes produced would stick to the walls of the aluminum target after they are produced. The gas can be vented directly since there are no gas phase radioisotopes produced with this method. The only other radioisotope (besides the chlorines) produced in any appreciable quantity is a small amount of ^{38}K (this would also stick to the walls of the target body) but since the half-life of this isotope is only $\sim$7 min it can decay away almost entirely before delivery. The Cl ions are removed by rinsing the target with a rinse of water ($\sim$70 ml) which is returned remotely to the lab via argon pressure (10 psi). This procedure is conducted remotely. The chlorine is then trapped on a small ion exchange column, which can then be shipped to the Botany Department via the pipeline, or alternatively the chemist can elute the ions in a few ml of potassium carbonate that can then be shipped in a small vial.

Seventeen shipments were made during the 30 day period of July/August, 2002.

Production of ^{110m}Ag

A stack of two natPd foils was bombarded in February, 2000. The chemical processing involved dissolving the palladium target, removing excess acid through evaporation followed by taking up the Pd in 0.01 M HCl. The Pd and Ag are separated on an alumina column with the Pd fraction eluting with the 0.01 M HCl. All indications are that the Ag fraction remains at the top of the column. Once all of the Pd has been removed as evident by colour change of the column, the Ag fraction can be eluted with 0.1 M HCl. The Ag is eluted in less than 10 ml.

Aliquots of both fractions were assayed for radioactive species. The Pd fraction does not have a strong γ-ray for identification. We will have to develop a technique to determine the relative radiochemical purity although from the colour change on the column we are certain that it is greater than 90% separation.

The silver fraction contained radioisotopes which could be identified as $^{105, 106m, 110m}$Ag. We performed a γ-ray spectroscopic analysis on the unseparated foil to estimate production rates. The estimated EOB yields are as follows:

^{105}Ag-combined foils – 26 mCi/μA at saturation;

^{106m}Ag-combined foils – 2.3 mCi/μA at saturation;

^{110m}Ag-combined foils – 0.75 mCi/μA at saturation.

At this rate it would require about 1250 μA h to achieve the required 100 μCi. However the co-production of ^{105,106m}Ag would be about 15 and 2.2 mCi, respectively. The exact mix would depend upon the beam current and length of bombardment.

In order to proceed we have had to modify a target so that we can irradiate with a beam of about 50 μA. At this intensity it will require about 25 hours of beam that could be spread over several days. Following irradiation, the foil would be left in place for at least 40 days to allow the decay of ^{105}Ag (50% remaining) and ^{106m}Ag (0.04 remaining).

In January, 2001 a Pd foil was irradiated at approximately 35 μA for a total proton dose of 90011 μA min (1500 μA h). We allowed the various radioisotopes to decay for 3 months before performing the chemical separation. In early May the dominant radioactive species were ^{105}Ag 3.5 mCi and ^{110m}Ag 280 μCi.

An additional Pd foil was irradiated in August, 2002. Processing will be performed in January, 2003.

Implantation of ^{22}Na

Two $10\,\mu$Ci sources will be prepared by implanting the separated ^{22}Na into plastic scintillator material. At a rate of 10^9 atoms/s it would take about 12 hours of beam time per source. A beam flux of 10^{10} atoms/s (which has been achieved at ISAC) would obviously enable the experiment to be performed in less than 2 hours for each source. To control spot size, a mask will have to be used which will lower the effective implantation rate.

Experiment LS29
Production and distribution of FDG for clinical studies
(T.J. Ruth, TRIUMF)

Final report

Following the workshop on the distribution of FDG held at the LSPEC Review of 1996/1997, discussions ensued as to how best to provide FDG to the local community for clinical utility. There is no mechanism established for the real-cost reimbursement. In addition, TRIUMF management does not wish to engage in a commercial venture dealing with radioactive substances. However, there continues to be interest in access to FDG and other tracers, both for research purposes and for clinical applications. While the research uses for these tracers can continue to be supplied under existing protocols, there is still a growing need for access to large quantities of either the radiopharmaceuticals such as FDG or ^{18}F-fluoride as precursor.

Since this project's first submission in 1998 a number of new and continuing developments warrant mentioning. First, a local company, IPET, has established a pay-for-fee Clinical PET Centre at the BC Research Facility adjacent to TRIUMF. IPET tried negotiating with MDS-Nordion for the supply of FDG. As indicated above, TRIUMF has chosen not to be involved as a supplier for non research purposes.

Over the last year IPET has received an Investigative New Drug application from Health Canada for the safety of ^{18}F-FDG prepared on the IPET site. That trial was completed in December, 2001. IPET has begun a Clinical Trial Application for the efficacy of FDG in monitoring metabolic status in cancer patients. In addition, MDS Nordion has expressed interest in supplying ^{18}F-fluoride once their new TR30 cyclotron has been installed and commissioned.

The Vancouver General Hospital is currently modifying its manufacturing laboratory to allow the production of ^{18}F-FDG. This site will receive the ^{18}F-fluoride from TRIUMF and, using the method of Hamacher *et al.* will synthesize the ^{18}F-FDG. After quality control, this material will be sent to all hospitals that have research proposals for clinical use of ^{18}F-FDG. The proposal is for TRIUMF to ship ^{18}F-fluoride to VGH twice a week (1 Ci per shipment). The object of this project is to gain experience in routine clinical supply of ^{18}F-FDG. From this experience we will prepare and submit a CTA and eventually a new drug application (NDA) which will allow the routine distribution of ^{18}F-FDG in British Columbia.

It should be noted that MDS Nordion has been approached to supply ^{18}F-FDG alone or ^{18}F-fluoride to VGH in a similar arrangement and they have refused.

With the transfer of the production of FDG from TRIUMF to VGH, this LSPEC project comes to an end and a separate mechanism needs to be considered.

BC Children's Hospital: No progress has been made on this project in 2002.

Vancouver General Hospital (Oak Street Site): A total of 24 FDG shipments were made in 1999, a further 30 shipments in 2000, 24 in 2001 and 18 in 2002, all part of LS28 and LS47.

St. Paul's Hospital: A total of 19 shipments of FDG were made in 2002 as part of LS48, 49 and 54.

Lions Gate Hospital: A total of 15 FDG shipments were made in 1999 and a further 27 shipments in 2000, 35 in 2001 and 42 in 2002 (see LS24 and LS41.

Over the last 4 years, TRIUMF has supplied 232 batches of ^{18}F-FDG to the local hospitals as well as 30 batches of ^{18}F-tracer for physics experiments. This program has been a success enabling the local clinicians to develop realistic protocols for using positron tracers for diagnosis in their patient populations. Now that the use of FDG has reached a clinical stage the support from LSPEC should be terminated and a new direction should be explored whereby TRIUMF/MDS Nordion can consider supplying the radiochemical ^{18}F-fluoride, with the production of FDG being handled by the lab in VGH.

No reports for the more clinically based projects will be presented (LS24, 28, 41, 42, 47, LS48, 49 and 54).

LS29 has evolved into LS58, production and distribution of FDG for clinical studies.

Experiment LS32
^{18}F-H$_2$^{18}O supply to the University of Alberta
(T.J. Ruth, TRIUMF)

Final report

Purpose: This project provided the researchers at the University of Alberta with ^{18}F-fluoride to support the development and commissioning of a new PET facility located in the Centre of Biological Imaging and Adaptive Radiotherapy (CBIAR) at the Cross Cancer Institute.

The research involved three primary aspects: i) a training component, ii) a radiopharmaceutical devel-

opment component, and iii) a technology assessment program for translational research.

i) Two staff from the University of Alberta spent a combined period of 9 months learning to operate and perform routine maintenance for the TR13 cyclotron in preparation for the delivery of their machine in Edmonton.

The staff at the University of Alberta PET Centre used the ^{18}F to gain experience in the labeling and handling of fluorinated compounds having applications in oncology. Proficiency in the operation and modification of the automated synthesis of commercial radiopharmaceutical modules supplied by Coincidence Technologies and Ebco Technologies was gained by both students and staff at CBIAR-PET. In particular, skills have been acquired for the preparation and use of ^{18}F-fluorodeoxyglucose (FDG). The vaule of FDG in cancer diagnosis and in the assessment of treatment outcomes has been well documented.

ii) A second project has established a synthesis of ^{18}F-estradiol using a semi-automated synthesis apparatus. The product will be used in a research project to identify and determine treatment outcomes of breast cancer patients who show positive estrogen receptor status in their disease. The PET Centre has received funding from the Canadian Breast Cancer Foundation, which has assisted in the development of a semi-automated synthesis unit for the ^{18}F-estradiol. The development and preliminary investigations with these agents required routine supply of ^{18}F-fluoride. This material has not yet been used in human studies.

iii) A descriptive and analytical epidemiology study of primary lung cancer in a 1998 Alberta cohort was completed and submitted for publication. The cohort's health care utilization experience, both in terms of costs and volumes of specific interventions, was analyzed using regression analysis to derive a cost formula. This phase is nearing completion. The final phase is to model our data (FDG PET in lung cancer), with respect to the costs benefit and survival. Modelling will initially use the methodology published by Gambhir and co-workers.

The cost effectiveness of FDG PET for other cancers was also explored in a manner similar to that described above. We are still in the introductory information gathering stage.

The activity received allowed for a total of 655 ^{18}F-FDG PET scans (ADAC C-PET) of which 598 were new patients and 67 were follow up PET scans for further assessment.

Summary

The delivery of ^{18}F from TRIUMF was established in the first quarter of 2001. The shipping schedule provided the delivery of one shipment per week, trans-

ported by ground carrier to Vancouver International Airport and then as Air Canada Dangerous Goods to Edmonton. Originally the irradiations were performed by the TRIUMF PET Chemistry group but at a later stage a chemist from Edmonton trained to perform the operations from the period December, 2001 to September, 2002.

- Produced a total of 178 Ci of ^{18}F from the TR13 cyclotron of the PET group at TRIUMF for shipments to Edmonton.
- Edmonton received a total of 16.8 Ci in 125 shipments (12 January to 19 September, 2002).
- The Edmonton cyclotron began producing ^{18}F on 19 September, 2002.
- MDS Nordion provided the packaging and shipping in Vancouver.

Experiment LS33
Evaluation and improvement of a dual head coincidence camera
(V. Sossi, UBC)

The performance measurements of the Siemens E.Cam Duet camera located at St. Paul's Hospital have been completed and submitted for publication.

Quantification studies for dual head coincidence imaging

The development of the analytical scatter correction is progressing. Since the last report, significant development of the scatter correction calculation for single scatters has been achieved. The sofware is written in Matlab because of its flexibility, portability and simple memory management. Some preliminary scatter distributions have been obtained for simple cylindrical phantoms. These results are being compared to results from Monte Carlo and initial results show the correct gross features of the scatter distribution.

The COincidence Data Examiner (CODEX) graphical user interface software for analyzing simulated data sets from SimSET is under continual updating, debugging and feature adding. CODEX is being updated to also analyze ADAC MCD dual head camera measured data and output from the scatter and randoms calculation code.

Presently the MCD camera does not have a correction for random events. A new method for random correction is therefore under development.

Matlab code to perform Fourier rebinning (FORE) [Defrise *et al.*, IEEE Trans. Med. Imaging **16**, 145 (1997)] is still in the process of development and needs to be completed. This is necessary to handle the scatter and randoms from oblique angles in the scatter and randoms correction code. This will be used to study

the effects of FORE on image quality and will be compared to measurements done on the MCD camera using FORE. The spatial resolution of the MCD camera will be measured and the data will be used to validate the FORE code.

Research plan

The scatter correction development

The optimization of the scatter correction code is continuously ongoing. The following issues are being investigated:

- Effects of detector materials and axial shielding, are still being studied to improve the accuracy of the calculation.
- The choice of scatter calculation parameters, such as object and angular sampling.
- The possibility of pre-calculations of a "scatter system matrix" which would only require the manipulation of the specific emission and transmission data for the scatter calculation. This is needed to speed up the calculation.
- A graphical user interface to simplify the set-up and use of the scatter correction and to interface with the CODEX environment.

When correct results are obtained for simple cylinders then scatter distributions in anthropomorphic phantoms (Zubal phantom) will be studied in comparison to results from Monte Carlo simulations. As well, when the correction code is fully validated with simulation studies a number of phantom studies will be done on the MCD camera.

Random correction method development

A new random correction method is under development.

Experiment LS35
Development of ^{18}F labelled nitroimidazole PET imaging agents for tissue hypoxia
(M.J. Adam, TRIUMF)

Hypoxia in cells and tissues is an important component of various pathological states (e.g. ischemia and stroke). Hypoxic tumour cells are extremely important within cancer treatment because they are more likely to survive radiation and chemotherapy, leading to an increase in tumor resistance to treatment. More recent evidence suggests that hypoxia is related to the aggressiveness of disease. Such studies employed a microelectrode, used in many centres, but were limited because of invasiveness and requirement for an accessible tumour.

Derivatives of 2-nitroimidazole are used extensively as hypoxia markers. The 2-nitroimidazoles are not metabolized in oxygenated tissues, but bind to macromolecular proteins after reduction in hypoxic cells.

This permits detection by a variety of techniques. For example, the products of such binding for the (pentafluoropropyl)acetamide (EF5) and (trifluoropropyl)acetamide (EF3) derivatives of 2-nitroimidazole can be detected by specific fluorescent antibodies.

The synthesis of ^{18}F-EF5 has now been developed and was achieved by preparing the allyl percursor and fluorinating it with ^{18}F elemental fluorine in trifluoroacetic acid. The radiochemical yield is 17% after HPLC purification.

Several syntheses have been performed for cell and animal studies. Initially we carried out cell studies to determine the effects of hypoxic and aerobic conditions on the uptake of EF5. This experiment indicates that about 10-fold more hot EF5 is concentrated in cells under hypoxic conditions as compared to aerobic conditions, and that the addition of cold EF5 has little effect. The gamma counting results were basically the same as those obtained by using cold EF5 and flow cytometry. These cell experiments were followed by rat experiments; rats with 9L tumours were injected with ^{18}F-EF5 and imaged on our PET tomograph, followed by dissection to determine biodistribution. An image of the brain tumour in the rat was obtained. The next stage of the research is to proceed to human studies.

Progress this year has been slow due to a lack of funds and the fact that a researcher at the Cancer Research Center (BCCRC) has not taken this project on as a priority. However, this has now changed and Dr. Donald Yapp has been hired by BCCRC to champion this project. A British Columbia Lung grant to Skov and Gelman will allow for an initial screening test of cold EF5 in 12 patients along with 6 hot EF5 experiments in humans. Ethics approval for these experiments is still required. Since Dr. Yapp's involvment, several other researchers have become more interested in using EF5 in their research. We expect to be able to carry out human imaging early in 2003.

Experiment LS39
Positron emission profiling (PEP) for pulp and paper fluid dynamic studies
(T.J. Ruth, TRIUMF)

Recently positron emission profiling has been shown to have utility in following certain physiochemical processes that have aided in the understanding of the mechanisms of these processes. The models used to describe the motion of fibres in the manufacturing of paper are limited by a lack of understanding about the micro-dynamics of the interaction of the various fibre sizes during motion. By labelling the fibres with a positron-emitting isotope, it may be possible to monitor the sedimentation process to provide better parameters for the models.

Previously we have visualized the motion of different fibre sizes during sedimentation and we are in the midst of developing this method to visualize fibre motion in a new geometry, namely a hydrocyclone. A hydrocyclone is an industrial apparatus used to separate fibres into different length or weight fractions.

Flow visualization of a hydrocylone using PET with applications for the pulp and paper industry

Papermaking fibres are hollow, flexible rod-like particles that have a wide distribution in both length and diameter depending upon species and growing conditions; when liberated from the tree they can curl or kink. North American fibres are typically 40–50% cellulose, 20–35% hemicellulose, 15–35% lignin, with the remaining fraction containing resins, tannins, ash and miscellaneous compounds. Solid-solid separation of papermaking fibre suspensions is of importance to the pulp and paper industry. Traditional unit operations such as screening, cleaning, and fractionation are traditionally described as solid-solid separation processes. For example, during fractionation, a dilute fibre suspension is separated into a number of different length-fractions. Despite the longstanding use of these unit operations, little is known about the mobility of the various fibre fractions that make up the suspension. One of the essential difficulties lies in the incomplete understanding of the long-range multi-body hydrodynamic interactions. Another difficulty is that these properties are strongly dependent upon the microstructure of the suspension which itself changes as these fibres tend to mechanically entangle or flocculate. Ascertaining these effects is not easy as these suspensions are opaque and difficult to visualize at reasonable penetration depths. These issues make the understanding of the behaviour of these suspensions particularly difficult. Clearly, there is a need to visualize the motion of the individual classes of components in a fibre suspension in order to better control the physical properties of paper.

Over the last number of years, we have conducted gravity-settling experiments at TRIUMF to test the feasibility of using PET as the visualization method. In this work, a selected class of fibres was radioactively labelled and allowed to settle in an untreated fibre suspension. The suspension was agitated and allowed to settle under the action of gravity in a cylindrical jar. Last year a similar study was carried out and we have now used these data to develop a mathematical description of the motion of fibres in a network. From these studies it is clear that this visualization technique has the potential to help clarify the behaviour of mixtures of fibres. We would like to extend this technique to measure the motion of fibres in a flowing device, in general, and to a hydrocyclone, in particular. We

propose a hydrocyclone as this device (i) has relevance to industry; (ii) has a size and is operated in a manner which allows for PET profiling; (iii) has a geometry that is amenable to numerical analysis; and (iv) is supported by local experts in Vancouver who would help develop an industrially-relevant experimental protocol.

Recently, we have tested the feasibility of this idea by building a "transportable hydrocyclone" which we could profile using PET. An initial test of this configuration was conducted on November 18.

Experiment LS42
Configuration modelling and image reconstruction studies on a depth encoding research tomograph
(V. Sossi, UBC)

This study can be logically divided into two parts: simulation of the effect of the γ depth of interaction correction on resolution uniformity, and development of an optimum reconstruction algorithm for a depth encoding, list mode acquisition, high resolution research tomograph (HRRT). The first part has been completed and submitted for publication while studies relative to the second part are still under way.

Simulation of the effect of the γ depth of interaction correction on resolution uniformity

One of the most important parameters in positron emission tomography (PET) imaging is detection sensitivity, since it has a direct bearing on the statistical quality of the images. Detection sensitivity is proportional to the tomograph solid angle and a cost-effective way of increasing the solid angle is achieved by reducing the detector-to-detector distance. However, such reduction increases the fraction of detected events where the γ-ray hits the detector surface at an oblique angle, thus reducing the probability of the interaction to occur in the same crystal, where the photon first entered the detector. This leads to the parallax error, which can significantly degrade the position resolution uniformity. The parallax error can be reduced by determining and accounting for the depth of the γ interaction (DOI) in the crystal. Several DOI determination schemes have been proposed [Jones *et al.*, "LSO PET/SPECT Spatial Resolution: Critical On-line DOI Rebinning Methods and Results", CTI PET Systems Inc., Free University Hospital (Amsterdam, Netherlands); Moses *et al.*, J. Nucl. Med. **32**, 995 (1991); Moisan *et al.*, IEEE Trans. Nucl. Sci. **42**, no. 4 (1995)] and one of them is currently implemented in a human size brain tomograph, the high resolution research tomograph (HRRT) [Wienhard *et al.*, IEEE Trans. Nucl. Sci. **49**, no. 1 (2002)]. This scheme employs a two-layer crystal configuration, where the two crystal layers are characterized by two different scintil-

lation decay times. Pulse shape discrimination is used to distinguish events originating from each layer [Wienhard *et al., op. cit.*]. We have evaluated the impact of such a correction scheme on the resolution uniformity for the HRRT geometry (octagonal design) using GEANT and a modified version of DETECT and compared it to that obtained for a circular tomograph design with the same detector-to-detector distance. In both cases four crystal configurations were simulated: two LSO layers 7.5 mm deep (LL_7.5), two LSO layers 10 mm deep (LL_10), a 7.5 mm deep LSO layer followed by a 7.5 mm GSO (LG_7.5) layer and finally a 10 mm deep LSO layer followed by a 10 mm deep GSO layer (LG_10). Resolution with and without DOI correction is presented in Table XIII. It can be observed that both the absolute resolution and resolution uniformity improve significantly with DOI correction for both tomograph configurations [Astakhov *et al.* (submitted to IEEE Trans. Med. Imag.)].

Table XIII. Overall spatial resolution for three source positions. Data are shown in the format a/b, where a is the resolution obtained with DOI correction and b is the resolution obtained without DOI correction. All values are expressed in mm.

	Crystal config.	0 cm	5 cm	10 cm
Octagonal geometry	LL_7.5	1.9/2.0	1.9/2.2	2.1/2.9
	LL_10	2.0/2.6	2.0/2.7	2.3/3.6
	LG_7.5	2.1/2.4	2.1/2.5	2.5/3.4
	LG_10	2.3/3.0	2.4/3.1	2.8/4.1
Circular geometry	LL_7.5	1.4/1.4	1.9/2.2	2.0/2.9
	LL_10	1.4/1.4	2.0/2.6	2.1/3.3
	LG_7.5	1.6/1.6	2.2/2.5	2.3/3.3
	LG_10	1.6/1.6	2.3/3.0	2.3/3.7

Image reconstruction strategies for the HRRT

The HRRT, when used in fully 3D mode, provides a total number of 4.486 billion LORs. In a dynamic scanning situation the duration of a time frame is often so short (30 s or less) that the number of acquired events might be much less than the number of bins in a full sinogram data set. A reconstruction algorithm that would not require event histogramming might thus reduce the size of the data sets. An additional advantage of list mode acquisition is the elimination of the need to *a priori* define frame duration.

We have thus developed and implemented an attenuation-normalization weighted listmode expectation maximization (EM) algorithm (ANW-LM-EM), based on the approach originally developed by A. Reader *et al.* [Phys. Med. Biol. **43**, 835 (1998); *ibid.*, IEEE Nucl. Sci. Symp. Conf. Record. **3**, 1853 (2001)]. In this algorithm the image update is based on the following expression:

$$\lambda_j^{m+1} = \frac{\lambda_j^m}{\sum\limits_{i=1}^{I} p_{ij}} \sum\limits_{k=1}^{N} p_{i_k j} \frac{1}{\sum\limits_{j=1}^{J} p_{i_k j} \lambda_j^m}$$

where λ_j^m is the mth iteration of the image estimate for pixel j, k is the event and i is the LOR index. Preliminary results obtained with this algorithm are shown in Fig. 159. Currently we are exploring various random event correction schemes and evaluating the quantification accuracy of various statistical reconstruction algorithms.
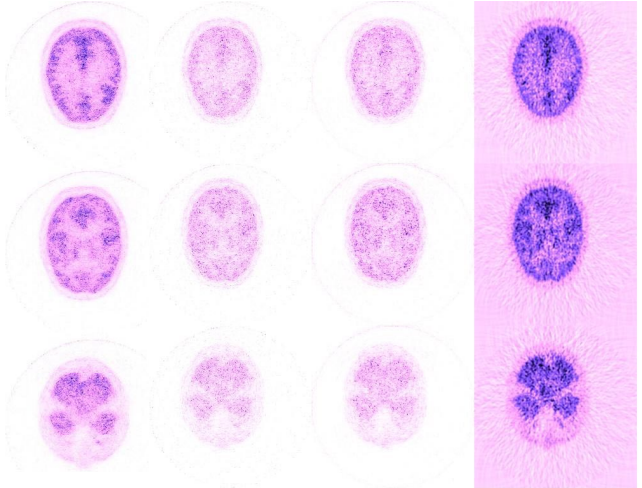
Fig. 159. Three different slices through images reconstructed using different reconstruction schemes. Columns, from left to right, correspond to LM-EM (1B counts), LM-EM (0.5B), 3D-OSEM (0.5 B) and FORE+2D-FBP (0.5 B).
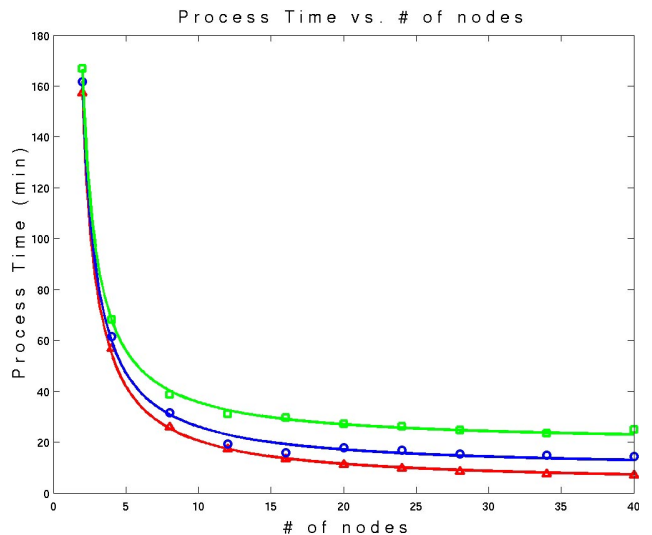
Fig. 160. Processing time for iterative list mode reconstruction for 40 M events as a function of number of 1 GHz Pentium nodes. Lower curve: 8 subsets ($x = 0.98$), middle curve: 32 subsets ($x = 0.94$) and upper curve: 64 subsets ($x = 0.88$) where x is the parallelized fraction of the reconstruction code.

We are also in the process of exploring various parallelization methods for the statistical reconstruction methods using a Linux cluster (Fig. 160).

Printed paper sources

Since the resolution of current scanners approaches 1–2 mm, it is important that the size of the sources used to measure the resolution is very small. We have successfully tested a set of printed sources using a regular ink-jet printer. We are currently refining the printing procedure and exploring possible source holder mechanisms.

Future work

The following topics are either on-going or to be started:

- Data reconstruction techniques with particular emphasis on random correction.
- Final design of a point source to map the tomograph point spread function.
- Implementation of the ^{22}Na source mechanism developed by Prof. Chris Thompson to investigate the impact of his time alignment procedure on this scanner.
- Detector normalization algorithms.
- Data transfer and storage schemes.
- Patient motion correction.

Experiment LS50
Antisense imaging nucleic acids for Parkinson's disease
(H. Dougan, TRIUMF)

For many years, Parkinson's disease has been a principal research interest of the TRIUMF PET group and the Neurodegenerative Disorders Centre at UBC. Many imaging agents labelled with positron emitters have been developed at TRIUMF for this program. Recently the UBC collaborators introduced Parkinson's related antisense DNA directed to the D2 receptor mRNA and to dopamine transporter mRNA into rat brains. The rats developed behavioural disorders and biochemical changes consistent with depletion of the "sense" mRNA by the "antisense" DNA probe. Last year's Annual Report related how the UBC investigators wished to extend their observations with unlabelled DNA to make new imaging agents based on DNA radiotracers. Progress was made at TRIUMF during 2002 developing radioactive ligand, (4-halogen-benzyl)-2-bromoacetamide (BBA) capable of labelling the needed antisense DNA. The chemical reactions leading to radiofluorine $[^{18}$F$]$F-BBA and the labelled DNA were carried out and examined in detail. It was determined that the reactions were too difficult and inefficient to be practical for the routine preparation of ^{18}F DNA in the immediate future. This prompted

the radiofluorine chemists to commence development of innovative practical methods for obtaining ^{18}F DNA. Meanwhile it was decided to work with the more attainable radioiodinated I-BBA and DNA modified with I-BBA ligand. Antisense DNA was first made modified with the non-radioactive I-BBA ligand and tested for biological activity in rat brains. Rats developed the characteristic behavioural disorders in the presence of antisense DNA modified with I-BBA. Finding reduced D2 receptor levels will be a further test of whether I-BBA interferes with antisense DNA activity. A mass spectroscopy technique was developed with the UBC Mass Spectroscopy Unit, which verified that the DNA bioconjugates had the expected mass. Radiolabelling antisense DNA proceeded successfully with $[^{125}$I$]$I-BBA, leading to $[^{125}$I$]$DNA at nearly 2,200 Ci/mmole. We hope to utilize the $[^{125}$I$]$DNA to visualize the site of antisense action in the rat brain by autoradiography.

Experiment LS51
Auger therapy for prostate cancer
(H. Dougan, TRIUMF)

Radioisotope induced therapy is of interest at TRIUMF because numerous radioisotopes possessing diverse decay characteristics are available here. Project LS51 examines the treatment of prostate cancer through DNA damage and cell killing induced by the Auger electrons released following the decay of ^{123}I and ^{125}I. Radioiodine incorporated into an iodoandrogen steroid is brought into proximity of DNA by the androgen receptor protein (AR); the cancer cell DNA is consequently targeted by the Auger electrons of the radioiodine decay, followed by death of the cancer cell. Prostate cancer is the most prevalent cancer in men and the second leading cause of cancer death in Canada. The Auger therapy research is carried out in collaboration with the Prostate Centre in Vancouver. Additional explanation of the prostate cancer biology was given in last year's Annual Report. In progress to date, stannyl precursors have been prepared for two suitable iodoandrogen steroids (EMIVNT and ZMIVNT) with potential for Auger therapy. The stannyl precursor permits $[^{125}$I$]$EMIVNT to be prepared with approximately 2,200 Ci/mmole, while $[^{123}$I$]$EMIVNT is labelled to much higher specific radioactivity. The binding of $[^{125}$I$]$EMIVNT has been assayed with androgen receptor (AR) from the rat and human. It was found that EMIVNT binds AR with roughly the affinity of the natural ligand, testosterone, so that EMIVNT will be useful for tests of Auger therapy. The potential of EMIVNT for AR-dependent Auger electron cell killing will presently be determined in cancer cell strains at the Prostate Cen-

tre. Two of the strains express AR while two strains do not express AR. The team at The Prostate Centre is prepared to characterize the biochemical changes induced by Auger decay, and to attempt Auger therapy in whole animals.

Experiment LS52
Comparison of commercial FDG synthesis systems
(T.J. Ruth, TRIUMF)

Final report

Scientific justification

The production of ^{18}F-FDG involves the production of ^{18}F-fluoride, typically in a target chamber containing ^{18}O-H$_2$O followed by reaction with mannose triflate and subsequent de-blocking of the protected sugar resulting in the production of the ^{18}F-fluorodeoxyglucose. These steps are generally controlled by one of several commercially available synthesis systems. The efficiency for the conversion of the label varies between 50 and 70%. The cause of this variability is not understood.

This retrospective study was aimed at determining the efficiency of ^{18}F-FDG production from several commercially available automated synthesis systems. In addition, a comparison of the efficiency for the incorporation of ^{18}F-fluoride was made as a function of the target chamber used to produce the ^{18}F. In addition, the yields from the various boxes were compared.

Description of the research

All synthesis systems made use of the Hamacher method where fluoride displaces the triflate-leaving group and the labelled acetylated fluorodeoxyglucose is then de-blocked using either HCl or NaOH. The yields were determined by comparing the quantity of ^{18}F-fluoride at the start of synthesis and the quantity of FDG produced at the end of synthesis. Values were decay corrected to a common time. In addition, the quality control metrics of the final product were compared for each unit. For the production of ^{18}F-fluoride, the ^{18}O$(p, n)^{18}$F reaction was used with a H$_2$^{18}O target on either a 13 MeV cyclotron (TR13) with a niobium target chamber or an 11 MeV cyclotron (RDS111) using a silver target chamber. For the production runs at the PETScan facility the ^{18}F-fluoride was loaded onto an ion-retardation resin before shipment from either P.E.T. Net in Seattle (about 3 hours for transit) or the TRIUMF facility (about 30 minutes). The shipments to Edmonton (about 8 hours) and Vancouver General Hospital (about 2 hours) involved shipping the irradiated water.

The three commercial synthesis units (Coincidence at the Cross Cancer Centre, CTI-CPCU at the PETScan Centre and the Ebco unit at VGH) provided similar yields (approximately 60% decay corrected) while the two targets had a significant difference in the yield of FDG, 60% for the niobium target body vs. 50% for the silver target body. All units provided FDG of the highest quality, meeting USP specifications.

The results of this study were presented at the Canadian Society of Nuclear Medicine Annual Meeting in Edmonton in April.

From these results it appears that the commercially available synthesis units provide similar yields of FDG with comparable quality of final product. While the results from VGH appear a little lower than the other two sites, the number of runs is small and the uncertainties associated with these results certainly overlap with those of the other units.

However, the efficiency of FDG production appears to be dependent upon the source of ^{18}F-fluoride. The yields using the same synthesis system (at PETScan) gave statistically significant different results for the two sources of ^{18}F-fluoride. The ^{18}F-fluoride produced in the niobium target body provides higher yields than a silver target body. The reason(s) for this difference is not understood and is currently under investigation to determine whether the material for the target chamber is the primary cause or whether radiolysis to the resin during shipment causes a poorer reactivity of the ^{18}F-fluoride ion. Another possibility is the purity of the target material (H$_2$^{18}O) for producing the ^{18}F. It should be noted that P.E.T.Net claims to have >65% FDG yield for in-house productions which could eliminate the target and water as problems.

Experiment LS53
Synthesis of ^{99m}Tc and ^{186,188}Re sugar derivatives
(M.J. Adam, TRIUMF)

An NSERC strategic grant was awarded (October, 2001, M.J. Adam, PI, $78,200/year for 3 years) to carry out research on the synthesis of technetium and rhenium labelled carbohydrates for use in nuclear medicine imaging and therapy. Dr. Adam is collaborating with Dr. Orvig in the UBC Chemistry Dept. and AnorMED (M. Abrams, CEO). A post doctoral fellow (Dr. Simon Bayly) and a graduate student (Cara Fisher) have also been working on this project for approximately one year.

Radiolabelled carbohydrates have been of significant interest to nuclear medicine due to the success of 2-^{18}F-fluoro-2-deoxy-glucose (FDG) as an imaging agent in positron emission tomography (PET). This success has naturally raised the question of whether a single-photon emitting glucose analogue with similar properties to FDG can be developed for use with single-

photon emission computed tomography (SPECT). Because of the relatively short half life of ^{18}F (110 min) its use is limited to facilities that have an accelerator in close proximity to chemistry laboratories and medical facilities. This fact makes it impractical for the FDG method to be widely used in medicine. ^{99m}Tc is the most widely used isotope in SPECT due to the fact that it is a generator produced, commercial isotope which makes it convenient to use and relatively inexpensive. It also has ideal physical properties for imaging. The drawback to this isotope is that it must be attached to the molecule via a chelate or organometal conjugate, which may perturb the system being studied. A SPECT analogue based on a widely available isotope such as ^{99m}Tc would make these agents available to the broader medical community. Among elements of the same series as Tc, the isotopes ^{186}Re and ^{188}Re show promise in the development of therapeutic strategies. For a β-emitting radioelement to be therapeutically useful, a half-life of between 12 h and 5 days is preferred: moreover, for a 1 MeV β-particle, the depth of penetration into tissue is approximately 5 mm. Furthermore, if some of the disintegrations are accompanied by 100–300 keV gamma photon, the behaviour of the radioelement can be conveniently followed by using a gamma camera. The nuclear properties of ^{186}Re and ^{188}Re are optimal for these purposes.

There has been significant progress in the first year with both the organometallic approach and the chelation approach. Cara Fisher has synthesized several ferrocenyl sugars including some that have not been reported before. Attempts to carry out the DLT reaction on these have proven difficult and new routes to the Cp-tricarbonyl metal compounds are being planned. Simon Bayly has established the aqueous based rhenium chemistry in the lab and has prepared at least one sugar-Re complex. The next step will be to prepare a chelate of the ^{99m}Tc radioisotope. A conference presentation and a paper are being prepared for submission in 2003.

Experiment LS57
Quantitative imaging with the Concorde microPET
(V. Sossi, UBC)

The UBC/TRIUMF PET group has recently been awarded funds to purchase a small animal scanner (CFI, BCKDF – P.I. Dr. T. Ruth). The Concorde microPET R4 (rat scanner) has been identified as the scanner of choice. Scanner delivery is expected in April, 2003.

Although the tomograph is a commercial scanner, the quantitative aspect of the data has not been fully characterized and implemented. We are proposing to

assess the quantification accuracy of the camera and to implement an iterative list mode reconstruction code. We are also planning to improve the quantification algorithms, if they are found not to be sufficiently accurate. In addition we want to implement the time alignment method developed by Prof. C. Thompson on this camera and compare its impact on the camera performance to that observed on the HRRT. The currently proposed studies are:

- Performance of phantom studies to assess the quantitative accuracy of the camera.
- Implementation of a list mode reconstruction algorithm for this camera based on the work performed for the HRRT (see LS42).
- Design of a point source to map the tomograph point spread function based on the paper point source design (see LS42).
- Implementation of the ^{22}Na source mechanism developed by Prof. Thompson to investigate the impact of his time alignment procedure on this scanner.

Since the data acquisition hardware and software of the microPET R4 and the HRRT have many similar aspects (LSO crystals, list mode acquisition capabilities), many of the studies proposed here are a natural extension of the work being developed for the HRRT (LS42). We are therefore in a unique situation where we can directly transport the expertise acquired in a human sized tomograph to a small animal imaging situation.

We are concentrating on the data quantification and image reconstruction aspect of small animal imaging, since they are a prerequisite condition to obtaining biologically meaningful information. Once this part is completed we anticipate the development of new imaging protocols associated with small animal scanning, in particular the development of bloodless scanning protocols. This will be an exciting area of investigation and we anticipate it to be a natural continuation of the studies proposed.

It is also important to provide a short overview of the breadth of the medical and biological research to be performed with the R4, since it will expand the current PET applications at UBC/TRIUMF and will require the development of new imaging agents and protocols. The proposed research to be conducted with the R4 spans the neurosciences, physiology, enzyme chemistry and tumour biology. In the neurosciences the microPET will complement and extend numerous studies already under way in the human UBC/TRIUMF PET program such as dopamine turnover, antisense studies and gene expression *in-vivo* (existing PET group plus Dr. Phillips, Psychiatry). The other areas of research are new to our imaging group. They will cover

hypoxia and blood flow in tumour studies (Dr. Durand, BCCA), investigation of type 2 diabetes (Dr. McIntosh, Physiology), brain control on its own sensory input as a function of behavioural and/or spinal cord state (Dr. Soja, Pharmaceutical Sciences), investigation of glycolipid storage disease and *in-vivo* monitoring of enzyme replacement therapy (Dr. Withers, Chemistry and Biochemistry). This research program will bring a larger research community together, thus strengthening and enriching PET imaging at UBC and TRIUMF.

THEORETICAL PHYSICS

Introduction

The TRIUMF Theory group consists of four staff members, six to seven research associates plus a number of students and visitors. The main research interests are physics beyond the standard model, hadron physics and nuclear physics. In addition to carrying out their own research programs, the members of the Theory group provide support for the TRIUMF experimental program and are available for consultation and collaboration with the experimentalists.

The four permanent staff members of the group are: Harold W. Fearing, Byron K. Jennings (group leader), John N. Ng and Richard M. Woloshyn. Erich W. Vogt (professor emeritus, UBC) is an associate member. During 2002 the Theory group had three sabbatical visitors, Chaoqiang Geng, Colston Chandler and Stephen Godfrey. The research associates are: R. Allahverdi (from September), S. Ando (from November), C. Barbieri (from September), W. Chang, A.K. Dutt-Mazumder, J. Escher (until October), S. Kondratyuk (until October), A.D. Lahiff (until August), C.P. Liu, and J.-M. Sparenberg (from September). The graduate students associated with the group are: C. Bird, F. Okiharu, C.C. Ho, I.L. Ho, and T.H. Wu.

The visitors to the Theory group this year included: J. Al-Khalili, N. Barmbilla, M. Butler, H.C. Chang, M. Chen, H.R. Fiebig, V. Flambaum, S. Godfrey, S. Groot Nibbelink, F. Herwig, S.W. Hong, G. Kribs, H. Lipkin, A. Lisetskiy, M. Locher, I. Low, A. Majumder, K. Maltman, E. Ormand, M. Pospelov, G. Prézeau, M. Ramsey-Musolf, M. Rozali, H. Sherif, A. Vairo, D. Wilkinson, Y.-P. Yan, J. Zanotti.

The Theory Research Program

Neutrino masses in a 5D SU(3)$_W$ TeV unification model
(W.-F. Chang, J.N. Ng; C.-H. Chang, Taiwan Normal Univ.)

We study an SU(3)$_w$ unified theory in the $M_4 \times S_1/(Z_2 \times Z_2')$ orbifold. The theory provides a tree-level mixing angle $\sin^2 \theta = 1/4$ at the compactification scale. The SU(3)$_w$ symmetry is broken down to SU(2)×U(1) at one of its two fixed points by choosing adequate boundary conditions. For leptons, e_L, ν_L and e_R^c form an SU(3)$_w$ triplet and are placed at the SU(3)$_w$ invariant fixed point. On the other hand, the quarks can not fit into any SU(3)$_w$ multiplet are to be put at the SU(2)×U(1) fixed point. To give correct fermions masses pattern, the minimum Higgs sector contains a bulk Higgs triplet and a bulk anti-sextet. The tree-level neutrino Majorana masses are forbidden by the orbifold boundary conditions. However, we show that the neutrino Majorana masses can be generated through 1-loop quantum corrections by adding a parity odd bulk Higgs triplet without introducing the right-handed neutrino. Furthermore, the resulting neutrino masses observe the inverted hierarchy and can easily accommodate the bilarge mixing angle solution favoured by the recent neutrino experiments without much fine tuning of parameters. Finally, the $\mu \to 3e$ transition and neutrinoless double β decays were shown to be safely below the current experimental bounds.

Lepton universality, rare decays and split fermions
(W.-F. Chang, I.-L. Ho, J.N. Ng)

Theories with split fermions (SFs) in extra dimension(s) are devised to give an alternative view of fermion masses hierarchy problems. We investigate the constraint on the SFs in extra dimensions by considering the universality of W leptonic decays $W \to l_i \nu_i$, the charged lepton decays $l_i \to l_j \nu_i \bar{\nu}_j$, and the lepton flavour violating process $l_i \to \bar{l}_j l_k l_h$ where $l_i = e, \mu$ or τ. For the standard model (SM) background of $W \to l_i \nu_i$, we extended the one loop quantum correction to include effects of order m_l^2/M_W^2 and the Higgs mass dependence. We find that in general the SF scenarios give rise to a 4D effective Yukawa matrix of the Kaluza-Klein (KK) Higgs bosons which is misaligned with respect to the fermion mass matrix. This holds true for gauge bosons as well. This leads to decays of $l_i \to \bar{l}_j l_k l_h$ at tree level and muonium antimuonium conversion. Interestingly the leptonic universality of W boson decays is not affected at this level.

CP violation in 5D split fermion models
(W.-F. Chang, J.N. Ng)

We give a new configuration of SF positions in one extra dimension with two different Yukawa coupling strengths for up-type, h_u, and down-type, h_d, quarks at $\frac{h_u}{h_d} = 36.0$. The new configurations can give enough CP violating (CPV) phase to accommodate all currently observed CPV processes. Therefore, a 5D SM with SFs is viable. In addition to the standard CKM phase, new CPV sources involving KK gauge bosons coupling which arise from the fact that unitary rotation which transforms weak eigenstates into their mass eigenstates only holds for the zero modes which are the SM fields and not for the KK excitations. We have examined the physics of kaon, neutron, and B/D mesons and found the most stringent bound on the size R of the extra dimensions comes from $|\epsilon_K|$. Moreover, it depends sensitively on the width, σ, of the Gaussian wavefunction in the extra dimension used to describe the fermions. When $\sigma/R \ll 1$, the constraint will be

lifted due to GIM suppression on the flavour changing neutral current and CPV couplings.

Constraint on the MSSM baryogenesis scenario from electric dipole moment
(W.-F. Chang; D. Chang, W.Y. Keung, CTS, Taiwan)

A commonly accepted mechanism of generating baryon asymmetry in the minimal supersymmetric standard model (MSSM) uses the CPV relative phase between the gaugino mass and the Higgsino μ term. The most severe constraint on this phase is from the limit on electric dipole moments of various light fermions. To avoid such constraint, a popular scheme with the first two generation sfermions naturally heavy is always used to suppress the one-loop level contributions. We point out that under such a scheme the most severe constraint may come from a new (two-loop level) contribution to the electric dipole moments of the electron, the neutron or atoms via the chargino sector in MSSM. As a result, the allowed parameter space of MSSM is severely constrained independent of the masses of the first two generation sfermions for baryogenesis.

Leptogenesis with superheavy Majorana neutrinos
(R. Allahverdi; A. Mazumdar, McGill)

Leptogenesis is an elegant mechanism which connects the observed baryon asymmetry of the universe to tiny masses of the light neutrinos. In the standard scenarios of leptogenesis the out-of-equilibrium decay of heavy Majorana neutrinos into the standard model Higgs and leptons generates a lepton asymmetry which is partially converted to baryon asymmetry through non-perturbative electroweak processes. We showed that successful leptogenesis is possible even if Majorana neutrinos are too heavy to be excited in the early universe, e.g. for Majorana masses as high as 10^{16} GeV. In our proposed model, the lepton asymmetry is directly produced from decay of the inflaton, the scalar field which drives cosmic inflation, into the standard model Higgs and leptons occuring via superheavy off-shell Majorana neutrinos. This model also naturally satisifies the bounds on the highest temperature in the early universe allowed in supersymmetric models.

Sleptogenesis
(R. Allahverdi; B. Dutta, Regina; A. Mazumdar, McGill)

As another alternative to standard leptogenesis, we propose that the lepton asymmetry can be created in inflaton decay to supersymmetric partners of Majorana neutrinos. The main feature of this scenario is decoupling of the generated asymmetry from the neutrino Yukawa sector. As a consequence, it can accommodate leptogenesis for Majorana masses as low as 10 TeV, without unnatural assumptions, fine-tuning or complications which arise otherwise. Our scenario can be naturally embedded within models which seek the origin of a tiny mass for the light neutrinos, e.g. models with a left-right symmetry.

Non-thermal dark matter
(R. Allahverdi; M. Drees, Munich)

The parameter space of various supersymmetric extensions of the standard model has been explored extensively, and regions which allow the lightest supersymmetric particle to be a viable thermal dark matter candidate are identified. New possibilties will arise by invoking non-thermal dark matter. On the one hand, some of the regions ruled out from thermal dark matter considerations can still be allowed. More generally, weakly interacting particles heavier than 100 TeV, ruled out as thermal dark matter by the unitarity bound, can be viable candidates. The important question is how to produce such particles abundantly. We considered various processes occuring in inflaton decay and thermalization of decay products. It was shown that stable (or long-lived) particles within a wide mass range, as heavy as 10^{12} GeV, can be copiously produced from reactions not considered before, without requiring non-perturbative processes. Therefore cosmological constraints on models containing such particles are (much) more severe than had previously been thought.

Cosmological bounds on large extra dimension models
(R. Allahverdi; C. Bird, S. Groot Nibbelink, M. Pospelov, Victoria)

Models with large extra spatial dimensions can solve the gauge hierarchy problem by bringing down the quantum gravity scale close to the electroweak scale. In these models, matter and gauge fields live on a 3-brane while gravity propagates in the bulk of the space, and hence a tower of Kaluza-Klein modes appears for the graviton. This leads to constraints on the fundamental scale from collider experiments and, more tightly, cosmology. So far, on the cosmology side, all studied processes only result in significant production of Kaluza-Klein gravitons which are lighter than 50 MeV, from the primordial bath. The current limits on the diffuse photon background from the late decay of such modes then translates into a bound on the fundamental scale. We show that much heavier Kaluza-Klein gravitons, with a mass of order TeV, can be efficiently produced directly from inflaton decay. These modes decay rather early which can lead to dissociation of the light elements from big bang nucleosynthesis. In

this case, the requirement for successful nucleosynthesis constrains the abundance of Kaluza-Klein gravitons and, consequently, sharpens the cosmological bounds on large extra dimension models.

Parity violation in deuteron electrodisintegration
(C.P. Liu; G. Prézeau, Caltech; M.J. Ramsey-Musolf, Caltech/Connecticut)

Parity violating (PV) electron-nucleus scattering provides more observables, normally not accessible by parity conserving (PC) scattering experiments, to study the structure of a nucleon. By measuring the asymmetry factors in elastic electron-proton and quasielastic (QE) electron-deuteron scattering at backward angles, one can determine the strange magnetic form factor G_M^s, and the isovector axial form factor (seen by the electron), $G_A^e(T = 1)$. The former provides a way to explore the strangeness content of a nucleon, which is a result anticipated by QCD, while the latter could be used to constrain the anapole form factor of a nucleon, which could be understood as a radiative correction in the unified electroweak theory. The surprising result published by the SAMPLE collaboration which gave a much larger $G_A^e(T = 1)$ than the theoretical prediction, has already caught a lot of attention. One possibility for this huge discrepancy is ignorance of the contribution from the PV NN interaction. However, our calculation – using AV_{18} as the PC interaction, and DDH potential (a $\pi^{\pm}$-, ρ-, and ω-meson exchange potential formulated by Desplanques, Donoghue, and Holstein) as the PV interaction – showed that while the effect of hadronic PV dominates in the threshold region, it is negligible at the QE kinematics relevant to SAMPLE experiments. In other words, quasi-elastic PV electron-deuteron scattering is indeed a clean probe of nucleon structure. The discrepancy still persists at the current stage.

Deuteron photodisintegration
(C.P. Liu; B. Desplanques, Grenoble; C.H. Hyun, Sungkyunkwan)

Threshold deuteron photodisintegration is another possible way to examine nuclear PV besides the radiative neutron capture and deuteron electrodisintegration. The existing analysis, using basically the zero-range approximation for the strong interaction, is being updated by modern high-quality NN potentials, given the fact that several groups are planning to do the experiments.

Deuteron anapole moment
(C.P. Liu; B. Desplanques, Grenoble; C.H. Hyun, Sungkyunkwan)

A previous work by B. Desplanques and C.H. Hyun was done in the model only with pion exchanges. Though the pion sector is the dominant subset in the DDH potential, as our work on deuteron electrodisintegration showed, the ρ and ω sectors give negligible contributions to the parity admixtures in the deuteron wave function, thus to the deuteron anapole. We are doing a complete calculation by including everything allowed by the DDH model.

Parity violating electromagnetic meson exchange currents
(C.P. Liu; B. Desplanques, Grenoble; C.H. Hyun, Sungkyunkwan)

The existence of meson exchange currents (MECs) has been acknowledged for quite a long time, and the inclusion of these currents is essential to guarantee the gauge invariance of any related calculation. Though the PV EM MECs in the framework of DDH scheme have been derived, it was pointed out by B. Desplanques that there might be some problems involved in the derivation of the heavy meson sectors, i.e., ρ and ω exchanges, so that they are not fully conserved. This new work aims to check the original derivation, fix the mistake if any, and get the correct result by explicitly showing the continuity equation is satisfied.

Reanalysis of nuclear parity violating observables in the framework of effective field theory
(C.P. Liu; M.J. Ramsey-Musolf, Caltech/Connecticut; B.R. Holstein, Massachusetts)

Traditional analyses of nuclear PV observables are done by using the DDH potential and then the experimental results are used to constrain the six PV meson-nucleon coupling constants, h_π^1, $h_\rho^{0,1,2}$, and $h_\omega^{0,1}$. However, one big puzzle in this field is that the current constraints on h_π^1, obtained from various nuclear PV observables, have not been very consistent, and they also do not agree well with the theoretical predictions, e.g., the DDH "best" value. One possible source of this inconsistency might be due to the fact that this widely-adopted potential is model-dependent. A new development by M.J. Ramsey-Musolf *et al.* of formulating a model-independent PV potential within the framework of effective field theory has been in progress. Our goal here is using this new potential – parametrized by various low energy constants (LECs) – to reanalyze nuclear PV observables and see if one can get a more consistent results in this framework.

Induced pseudoscalar coupling of the proton weak interaction

(T. Gorringe, Kentucky; H.W. Fearing)

The induced pseudoscalar coupling g_p is the least well known of the weak coupling constants of the proton's charged-current interaction. Its size is dictated by chiral symmetry arguments, and its measurement represents an important test of quantum chromodynamics at low energies. During the past decade a large body of new data relevant to the coupling g_p has been accumulated. This data includes measurements of radiative and non radiative muon capture on targets ranging from hydrogen and few-nucleon systems to complex nuclei. We have reviewed the theoretical underpinnings of g_p, the experimental studies of g_p, and the procedures and uncertainties in extracting the coupling from data. Current puzzles are highlighted and future opportunities are discussed. The review has been prepared for and submitted to Reviews of Modern Physics.

Solar-neutrino reactions on deuteron in effective field theory

(S. Ando; Y.H. Song, Seoul National Univ.; H.W. Fearing; T.-S. Park, K. Kubodera, South Carolina)

The cross sections for low-energy neutrino-deuteron reactions are calculated within heavy-baryon chiral perturbation theory employing the cut-off regularization scheme. The transition operators are derived up to next-to-next-to-next-to-leading order in the Weinberg counting rules, while the nuclear matrix elements are evaluated using the wave functions generated by a high-quality phenomenological NN potential. With the adoption of the axial-current-four-nucleon coupling constant fixed from the tritium beta decay data, our calculation is free from unknown low-energy constants. Our results exhibit a high degree of stability against different choices of the cutoff parameter, a feature which indicates that, apart from radiative corrections, the uncertainties in the calculated cross sections are less than 1%.

Radiative corrections for neutron β-decay revisited

(S. Ando; V. Gudkov, K. Kubodera, F. Myhrer, South Carolina; S. Nakamura, T. Sato, Osaka)

The recent very accurate measurements of the lifetime and the correlation coefficients of neutron β-decay play a key role in deducing precise values of physical constants, e.g., a K-M matrix element V_{ud} and axial vector coupling constant g_A. Furthermore, they probe for new physics beyond the standard model. The radiative corrections in $\mathcal{O}(\alpha)$ have been well established by Sirlin, where α is the fine structure constant. On the other hand, since the energy scale of the reaction is very small (about the electron mass), we can employ an effective Lagrangian in which the nucleon is treated as a heavy-baryon field and pions are integrated out. We re-examine the life time and correlation coefficients of neutron β-decay up to $\mathcal{O}(\alpha)$ and including the $1/m_N$ correction (where m_N is the nucleon mass) within this formalism.

Radiative corrections for solar-neutrino reactions on deuteron in effective field theory

(S. Ando; V. Gudkov, K. Kubodera, F. Myhrer, South Carolina; S. Nakamura, T. Sato, Osaka)

The recent experimental results at SNO show that the flavour of solar-neutrino changes while it flies to the Earth. This provides strong evidence that the neutrino has a mass. The neutrino reactions on deuteron are the detecting reactions of solar-neutrinos and, therefore, it is essential to provide the cross sections of the reactions as accurately as possible by theory, to deduce the mass and the mixing angle of neutrinos from the data. Moreover, it is known that radiative corrections of the reactions are significant, leading to a few percent corrections to the cross sections, which is comparable to an unknown constant in the hadronic sector in effective theory calculations. In this work, we incorporate the photon degree of freedom into an effective Lagrangian to study the radiative corrections of the reactions within the frame work of effective field theory.

The process $\pi p \to n e^+ e^-$ in heavy baryon chiral perturbation theory

(H.W. Fearing)

Heavy baryon chiral perturbation theory is an effective field theory approach which allows one to evaluate low energy processes using a Lagrangian which has the same symmetries as the underlying QCD, but which however contains some parameters, the so called low energy constants (LECs) which must be evaluated by fits to experiment. Earlier we looked at the process $\pi p \to n\gamma$ and used data from TRIUMF and Saskatoon to fit the S and P wave amplitudes and thus evaluate the appropriate LECs. [Fearing *et al.*, Phys. Rev. **C62**, 054006 (2000)]. We have now extended this calculation to the process $\pi p \to n e^+ e^-$. This latter process is of particular interest because it in principle provides information about the axial form factors in the timelike momentum transfer region. To extend the original calculation one has to allow for off shell photons, attach the $e^+ e^-$ pair, and evaluate a more complicated phase space. The required LECs are all known from the earlier calculation, and so the result here becomes a prediction for the rate, or alternatively a consistency check on the LECs previously evaluated. The $n e^+ e^-$ final state has been measured in a TRIUMF experiment and we expect to be able to compare our theoretical

results with the data, once the experimental analysis is complete.

Low-energy pion-nucleon scattering and the Adler-Weisberger sum rule in a unified dynamical description
(S. Kondratyuk)

An effective Lagrangian model for pion-nucleon scattering is utilized to address the following problem: "What can one learn from a comparison of the isospin-odd amplitude obtained in the low-energy limit with the value of the calculated Adler-Weisberger sum rule?". It is essential that the two methods of evaluation are done within the same dynamical approach. Since the model used – the dressed K-matrix approach – includes dressing of the nucleon two- and three-point Green's functions up to infinite order and successfully describes pion-nucleon scattering at low as well as intermediate energies, it is uniquely suited to study the above question. The basic assumptions on which the Adler-Weisberger sum rule rests are chiral symmetry and causality, both of which are, in principle, satisfied only approximately. The difference between the low-energy and sum-rule evaluations of the isospin-odd amplitude can be related to the degree to which these physical properties are violated. In the dressed K-matrix approach, a satisfactory agreement is found between the low-energy and sum-rule calculations. The remaining small discrepancy is in part due to omitted ingredients in the procedure for dressing the four-point $\pi\pi NN$ Green's functions, which causes only partial fulfilment of analyticity constraints.

Cutoff as an energy scale in pion-nucleon scattering
(S. Kondratyuk, B.K. Jennings)

Realistic dynamical models describing hadronic interactions from low to resonance energies typically rely on the usage of an energy-momentum cutoff. For theories applicable in a very wide energy span, such as quantum electrodynamics, the Wilson renormalization techniques offer a useful interpretation of a cutoff as a "floating" energy scale. By imposing the condition that the cutoff should not affect quantities observable at much lower energies, one calculates a beta-function whose properties can be used to describe dynamics of the system at various energy regimes. The main purpose of the present study is to apply Wilsonian methods to the pion-nucleon interaction at low and intermediate energies. The dynamics of this system are quite distinct in that they are essentially nonperturbative and typical cutoffs are not much larger than the nucleon mass. Therefore we use a nonperturbative dynamical model to compute beta-functions by sliding the cutoff in the pion-nucleon vertex while keeping low-energy observables, such as scattering lengths, fixed. A possible application for the obtained beta-functions could be to gain insight into the problem of connecting the low- and intermediate-energy regimes of pion-nucleon dynamics.

The Bethe-Salpeter equation and the low energy theorems for pion-nucleon scattering
(A.D. Lahiff; I.R. Afnan, Flinders)

The Bethe-Salpeter amplitude for πN scattering is evaluated at the off-mass-shell points corresponding to the low energy theorems based on PCAC and current algebra. We find that chiral symmetry is broken via the higher-order multiple scattering of t-channel ρ exchange. The results suggest a way of maintaining consistency between the Bethe-Salpeter amplitude and the low energy theorems.

Baryon resonance extraction from pion-nucleon scattering data in a covariant approach
(A.D. Lahiff; C. Bennhold, George Washington Univ.)

There are a large number of baryon resonances observed experimentally in meson-baryon scattering processes. It is important to be able to extract the properties of these resonances in a reliable way. We are developing a relativistic model of pion-nucleon scattering based on the 4-dimensional Bethe-Salpeter equation including the πN, ηN, $K\Lambda$, and $K\Sigma$ channels, as well as an effective $\pi\pi N$ channel. This covariant model is intended to be used for extracting resonance masses and partial decay widths from experimental data.

Heavy baryons in lattice NRQCD
(N. Mathur, R.M. Woloshyn; R. Lewis, Regina)

The mass spectrum of charmed and bottom baryons was calculated using quenched lattice nonrelativistic QCD. The mass splittings between spin $3/2$ and spin $1/2$ baryons were calculated and no evidence was found to suggest that there is a suppression of the colour hyperfine effects in baryons as is seen in quenched lattice simulations of the meson sector. In the charm sector the results using NRQCD are compatible with those obtained earlier using a Dirac-Wilson action of the D234 type for the charm quarks.

Strangeness matrix elements in the nucleon
(R. Lewis, Regina; W. Wilcox, Baylor; R.M. Woloshyn)

Quenched lattice QCD simulations and quenched chiral perturbation theory were used together to study matrix elements of strange quark currents in the nucleon. Dependences of the matrix elements on strange quark mass, valence quark mass and momentum transfer calculated in the chiral framework were used to extrapolate lattice QCD results to the physical region.

The main conclusions of this work are that the lattice QCD results for the strange-quark vector current matrix elements in the nucleon are very small in the quark mass range of the simulations and remain small when extrapolated to the physical region. The results of this analysis are consistent with existing experimental results.

Quark interactions in baryons
(F. Okiharu, Nihon Univ.; R.M. Woloshyn)

The interactions of static quarks within baryons is being studied using the methods of lattice QCD. The three quark potential has been calulated and it has been confirmed that the spatial dependence is not that given by either the simplest Y-shaped or triangluar-shaped flux tube models. For large quark separations the Y-shaped flux tube potential seems to be slightly favoured. The distribution of chromo-electric and chromo-magnetic field within the static baryon are being calulated directly to see if this can distingush between the different flux tube configurations. The results of this simulation have large statistical errors and techniques to improve the signals are being studied.

Omega meson propagation in dense nuclear matter and collective excitations
(A.K. Dutt-Mazumder)

The bosonic excitations induced by omega meson propagation in dense nuclear matter are studied within the framework of random phase approximation. The collective modes are then analyzed by finding the zeros of the relevant dielectric functions. Subsequently we present closed form analytical expressions for the dispersion relations in different kinematical regime. Next, the analytical behaviour of the in-medium effective propagator for the omega meson is examined. This is exploited to calculate the full spectral function for the transverse (T) and longitudinal (L) mode of the omega meson. In addition, various sum rules are constructed for the omega meson spectral density in nuclear medium. Results are then discussed by calculating residues at the poles and discontinuities across the cuts.

Aspects of meson properties in dense nuclear matter
(O. Teodorescu, C. Gale, McGill; A.K. Dutt-Mazumder)

We investigate the modification of meson spectral densities in dense nuclear matter at zero temperature. These effects are studied in a fully relativistic mean field model which goes beyond the linear density approximation and also includes baryon resonances. In particular, the role of $N^*(1520)$ and $N^*(1720)$ on the

rho meson spectral density is highlighted. Even though the nucleon-nucleon loop and the nucleon-resonance loop contribute with the opposite sign, an overall reduction of rho meson mass is still observed at high density. Importantly, it is shown that the resonances cause substantial broadening of the rho meson spectral density in matter and also induce non-trivial momentum dependence. The spectral density of the a_0 meson is also shown. We study the dispersion relations and collective oscillations induced by the rho meson propagation in nuclear matter together with the influence of the mixing of rho with the a_0 meson. The relevant expression for the plasma frequency is also recovered analytically in the appropriate limit.

The low-energy nuclear density of states and the saddle point approximation
(A.K. Dutt-Mazumder, B.K. Jennings; S.K. Ghosh, Calcutta)

The nuclear density of states plays an important role in nuclear reactions. At high energies, above a few MeV, the nuclear density of states is well described by a formula that depends on the smooth single particle density of states at the Fermi surface, the nuclear shell correction and the pairing energy. We have presented an analysis of the low energy behaviour of the nuclear density of states using the saddle point approximation and extensions to it. Furthermore, we prescribe a simple parabolic form for excitation energy, in the low energy limit, which may facilitate an easy computation of level densities.

Signatures of broken symmetry at GSI
(O. Teodorescu, C. Gale, McGill; A.K. Dutt-Mazumder)

The possibility of observing exclusive matter induced processes in high energy heavy ion collision is discussed. This involves mixing of different quantum states in nuclear matter as a result of broken symmetry in a thermal bath. It is argued that such processes could be observed in the dilepton spectra at GSI energy. Results are compared with CERN dilepton data. We highlight the qualitative difference that one might expect to observe at GSI energies stemming from the matter induced processes with that of CERN/SPS. The most dramatic effect is the clear appearance of an additional peak caused by the matter driven process like π-η annihilation which essentially is related with the broken symmetry in nuclear matter. The whole analysis is performed with the equation state determined from a interacting nuclear matter within the scope of a mean field model.

Low-energy nuclear structure and one-hole spectral function of ^{16}O

(C. Barbieri; W.H. Dickhoff, Washington Univ. (St. Louis))

The best theoretical calculations presently available for the nucleus of ^{16}O are still in disagreement with the experimental data obtained from $(e, e'p)$ reactions. In particular, the theory predicts too high values of the spectroscopic factors at small missing energies. In order to approach this problem we developed a formalism based on Green's function theory and the Faddeev equations technique. Results from such calculations have eventually been obtained during the last year. While discrepancies with the experiment still persist, the new results tend to reduce the disagreement with data and suggest that further improvement should come from better treatment of long-range correlations. In particular, it appears that a better description of the lowest positive parity excited state of the ^{16}O core is required to solve the problem. As a first step in this direction, we have studied the low-energy spectrum of ^{16}O by including the effects of the mixing of two-phonon states. This was done by means of an extension of the random phase approximation equations.

Study of short-range correlation by means of the $(e, e'pN)$ reactions

(C. Barbieri; W.H. Dickhoff, Washington Univ. (St. Louis); C. Giusti, F.D. Pacati, Pavia)

Two-nucleon emission reactions have recently proved to be a powerful tool to study two-body short-range and tensor correlations in nuclei. In these studies, the effects of long-range motion are also important and need to be properly accounted for. The recent Faddeev studies of low-energy structure of ^{16}O (described above) have also produced improved results for the two-hole spectral function. These include the effects of self-consistency and of ground state correlation in the target nucleus. We are now employing these two-hole spectral functions to study the two-proton and the proton-neutron emission from the nucleus of ^{16}O.

Rescattering contribution to $(e, e'p)$ cross section at high missing energy and momenta

(C. Barbieri; W.H. Dickhoff, Washington Univ. (St. Louis); L. Lapikás, NIKHEF; D. Rohe, Basel)

The one-hole spectroscopic function has been measured at Jefferson Laboratory for different nuclei, by the E97-006 collaboration. This experiment focused on the region at high missing energy and missing momenta, where the effects of short-range and tensor correlations are predominant. The data obtained show that a sizable contribution to the experimental cross section comes from processes involving the rescatter-

ing of the detected proton against other nucleons in the target. These effects are to be subtracted from the data in order to obtain meaningful results. The contribution of rescattering processes is presently being computed by applying a semiclassical model. This takes into account both the effects of nuclear transparency and the in-medium dependence of the proton-nucleon rescattering rate.

Nucleon-nucleus optical potential at low energy and proton capture

(C. Barbieri, B.K. Jennings)

The proton capture reactions $^7\text{Be}(p, \gamma)^8\text{B}$ and $^{16}\text{O}(p, \gamma)^{17}\text{F}$ at low energy play an important role in the understanding of stellar evolution. In this regime, the nuclear optical potential that describes the nucleon-nucleus interaction can present substantial energy dependence and is expected to be sensitive to the surface of the target nucleus. Such low-energy correlations have been considered for ^{16}O in earlier works, based on the self-consistent Green's function theory. The nuclear self-energy obtained in the latter works is expected to account for the most relevant features of the collective motion on the target nucleus. In general, the nuclear self-energy at positive energies is a realization of the optical potential for the nucleon-nucleus scattering, while at negative energies it gives information on the binding of the final A+1 body system. We are beginning to employ the above self-energy as an optical potential to analyze the scattering of protons by a finite nucleus. The final goal is to eventually reach a reliable theory of proton capture processes and to apply it to the reactions mentioned above.

Numerical calculation of the phase shift with an integral formula

(J.-M. Sparenberg)

A new integral formula for the scattering phase shift has been recently established by Chadan *et al.* [J. Math. Phys. **42**, 4031 (2001)]. Contrary to previous ones, this formula provides the absolute phase shift (no π ambiguity) and does not require a particular normalization of the scattering wave function. It seems thus particularly well suited for numerical calculations. Indeed, both finite-difference and Lagrange-mesh implementations of this formula have revealed several advantages: (i) easy calculation of narrow resonances, (ii) wave function needed on a limited interval only (potential range), (iii) good robustness with respect to imprecise wave functions, (iv) validity in presence of a Coulomb potential. The only drawback appearing up to now is the behaviour of this formula at very low energies in the presence of bound states or narrow resonances. The integrand then presents quasi-singularities that are difficult to handle numerically. A

theoretical study of the position of these singularities has been performed and has been able to relate them to the zero-energy wave function. Numerically, the use of an adaptive-step integration method makes things better without totally solving them (increase of computing time).

Study of the nucleon-hyperon interaction by the supersymmetric inversion method
(J.-M. Sparenberg; D. Baye, Free University of Brussels; Y. Fujiwara, Kyoto)

The construction of nucleon-hyperon interaction potentials is interesting for structure studies of hypernuclei, i.e. of nuclei containing one or several hyperons. Since experimental data are rather scarce for these systems, an interesting alternative is to estimate these potentials from theoretical models. For instance, by applying the resonating group method to a constituent quark model, one can get nucleon-hyperon elastic-scattering phase shifts, which can then be turned into potentials through the use of inversion techniques. We have applied an inversion method based on the algebraic formalism of supersymmetric quantum mechanics to analyze the $^1S_0$ and $^3S_1$ $\Lambda - N$ phase shifts. The corresponding potentials are smooth as long as the inverted data lie below the first inelastic threshold. The $^1S_0$ potential is not deeper than the $^3S_1$ one but has a longer range.

Analysis of the ^{12}C + α elastic scattering data by the supersymmetric inversion method
(J.-M. Sparenberg, L. Buchmann)

The ^{12}C (α, γ) ^{16}O radiative capture reaction plays an important role in nuclear astrophysics during the helium combustion phase in stars. Unfortunately, for the very weak energies of astrophysical interest (typically 300 keV in the centre-of-mass frame), this reaction cannot be measured directly in the laboratory (minimal energy: 1 MeV). A theoretical model is thus generally adjusted to available experimental data (radiative capture, α emission of ^{16}O excited states and ^{12}C + α elastic scattering data) to extrapolate them to low energies. The most commonly used model is the R matrix. In principle, an interesting alternative to the R matrix is the potential model; however, no satisfactory potential has been found up to now to describe the ^{12}C + α system. Since the ^{12}C + α elastic scattering has been recently remeasured with a very high precision, inversion techniques can now be used to construct such a potential. We have applied an inversion method based on supersymmetric transformations of the radial Schrödinger equation to construct a potential which reproduces the $l = 0$ phase shifts and which has no bound state. It presents a rather long range, which suggests a polarization phenomenon. Phase-equivalent addition

of bound states to this potential as well as inversion of other partial waves are currently under study.

Comparison of calculation methods for resonance widths
(B.K. Jennings, J.-M. Sparenberg)

The calculation of resonance widths is an important issue in nuclear physics, e.g. for the calculation of proton or α decays (see below). The most common method to do so is probably the R matrix, in which the width is expressed in terms of the wave function calculated at some sufficiently large radius (outside the range of nuclear forces). An alternative and elegant method has been proposed by Gurwitz and Kalbermann for the two-body case in which the width is expressed in terms of the Wronskian of the wave function and of a modified Coulomb regular solution, calculated at a particular radius (the top of the potential barrier). This method has been extended to the many-body case and the limitation to a particular radius has been shown to be unnecessary. We have compared these two formalisms in the two-body case, both from the theoretical and numerical point of view. From the theoretical point of view, the equivalence between both methods can be established for narrow resonances without background, provided the radius is chosen inside the barrier and sufficiently far from the classical turning points. The comparison has also revealed the interest of an integral formula for the resonance width. The two methods have been compared numerically for a narrow resonance of a Coulomb + square well potential. Well inside the barrier, both methods provide similar results, as expected from the theoretical analysis. In the vicinity of the turning points, Gurwitz' method provides much better results than the R-matrix without surface correction. Applying the surface correction to the R matrix makes it very precise (much more precise than Gurwitz' formula) in the vicinity of the internal turning point. The comparison in the case of wider resonances and of continuous potentials is in progress.

One-body overlap functions, equations of motion and phenomenological potentials
(J. Escher, B.K. Jennings)

One-body overlap functions play an important role for the description of nuclear structure and nuclear reactions. Equations of motion for the one-body overlaps, based on particle-only, hole-only, and particle-hole approaches, are studied. A given overlap function is shown to satisfy four different Schrödinger-like equations, all of which can be derived in the framework of the Feshbach projection operator formalism. Approximating the relevant potential by a local potential is only valid in the particle-hole approach. Previously proposed one-body functions, which can be derived

from the overlap functions, are also considered. It is argued that the latter do not satisfy a Schrödinger-like equation with an approximately local potential.

Contemplating a new measure for nuclear shell closures
(J. Escher, B.K. Jennings)

A special class of low-energy states has been identified for $(A \pm 1)$-body nuclei adjacent to even-even systems for which the independent-particle model (IPM) predicts closed (sub)shells. The states are characterized by spin-parity quantum numbers which match the quantum labels of the associated $(A \mp 1)$-body ground states and by small spectroscopic factors for one-nucleon transfers to/from the ground states of the even-even nuclei. A study of the associated Fliessbach functions shows that these states are structurally correlated with A-body g.s. components other than closed (sub)shell configurations. Under these circumstances, the spectroscopic factors provide a measure of the softness of the Fermi surface in the A-body nucleus. This measure, which is complementary to the systematic features usually employed to study shell closures, was tested for various well-studied nuclei and found to be very reasonable. An application to the ^{22}O region indicates that measuring the spectroscopic factors for the one-body transitions between the ^{22}O ground state and the low-lying $(1/2)^+$ and $(3/2)^+$ states of ^{21}O as well as the low-energy $(5/2)^+$ states of ^{23}O will provide valuable information about the shell structure of ^{22}O.

Proton emission and spectroscopic factors
(J. Al-Khalili, Surrey; J. Escher, B.K. Jennings, J.-M. Sparenberg)

We have shown how to embed the elegant results for proton emission [Gurvitz, Phys. Rev. **A38**, 1747 (1987)] into the full many-body problem. At first sight the results are very encouraging. We have seen that it is possible to express the decay width as the single particle result times the spectroscopic factor. This reinforces the procedure of S. Åberg *et al.* [Phys. Rev. **C56**, 1762 (1997)] where the spectroscopic factor was obtained by dividing a single particle calculation by the experimental lifetime. The decay width is proportional to the square of the matrix element $\langle \psi_0 | HQ | \zeta_{E'} \rangle$

(the Q is optional). We now understand how this expression arises and why it is not zero. Neither $|\psi_0\rangle$ nor $|\zeta_{E'}\rangle$ is an eigenfunction of H but both are well defined. If either were eigenfunctions then the matrix element would be zero because $|\psi_0\rangle$ and $|\zeta_{E'}\rangle$ are orthogonal. This should resolve an old dispute.

Unfortunately there is a serious problem: the spectroscopic factor is not actually an observable in proton emission but rather $\int^{r_t} dr \phi_R^*(r) \left(1 - \frac{\partial H_R(E)}{\partial E}\right) \phi_R(r)$ is the observable. The optical potential dependence noted in calculations is not just a practical detail but an important matter of principle. If the phenomenological potential does not correspond to the potential in the Hamiltonian for the spectroscopic factor but rather a different Hamiltonian then S_0 does not occur, but rather a different normalization constant. Indeed, K. Varga and R.G. Lovas [Phys. Rev. **C43**, 1201 (1991)] argue strongly that it is $\bar{\phi}(r)$ that corresponds to the phenomenological potential. There the argument is applied to alpha emission but a similar analysis will carry over for proton emission.

Partial dynamical symmetry in an interacting fermion system
(J. Escher; A. Leviatan, Hebrew Univ.)

We present an example of a partial dynamical symmetry (PDS) in an interacting fermion system and demonstrate the close relationship of the associated Hamiltonians with a realistic quadrupole-quadrupole interaction, thus shedding new light on this important interaction. Specifically, in the framework of the symplectic shell model of nuclei, we prove the existence of a family of fermionic Hamiltonians with partial SU(3) symmetry. We outline the construction process for the PDS eigenstates with good symmetry and give analytic expressions for the energies of these states and E2 transition strengths between them. Characteristics of both pure and mixed-symmetry PDS eigenstates are discussed and the resulting spectra and transition strengths are compared to those of real nuclei. The PDS concept is shown to be relevant to the description of prolate, oblate, as well as triaxially deformed nuclei. Similarities and differences between the fermion case and the previously established partial SU(3) symmetry in the interacting boson model are considered.

EXPERIMENTAL FACILITIES

Proton Irradiation Facility
(E.W. Blackmore, TRIUMF)

Once again there was considerable demand for beam time for proton irradiation work with six scheduled beam periods during the year. A group from Sandia National Laboratories and CEA in France carried out Expt. 919, "Proton irradiation effects in SOI devices", in two beam periods, one on BL2C at lower energies and then on BL1B at energies up to 500 MeV. This experiment aimed at determining which laboratory radiation source, Co-60 gammas or low energy X-rays, best simulated proton-rich space environments. The ATLAS group from the University of Alberta also used two sessions for further testing of the readout electronics for the liquid argon calorimeters for the high radiation environment at the LHC.

In order to satisfy the demand for higher fluences from several groups who wished to carry out displacement damage tests of harder devices, such as GaN devices and GaAs light emitting diodes, several improvements were made to enable more efficient use of protons. The maximum proton beam current is limited by neutron shielding to about 10 nA at 70 MeV and 2 nA at 500 MeV. As the devices to be tested are typically a few mm or less in size, smaller beam spots can be used. However, using a smaller beam spot makes it more important to have the beam well centered on the device during irradiation. This has been made easier by fabricating a new multiwire profile monitor which is located and aligned to the device under test. The beam profile and shape can be continuously monitored, both by the experimentalist and the cyclotron operators, during the irradiation. In addition, improved MATLAB software was developed by a summer student for analyzing the scanned images of the beam from Gafchromic (radiosensitive) film. Figure 161 shows a small beam profile from BL2C. The high intensity capability is available on both beam lines as the new profile monitor is portable and can be moved from one beam line to the other. Proton rates of 10^{10} protons/cm^2/s have been achieved. Groups from Defence Research and Development Canada (DRDC), previously called DREO, the Naval Research Laboratory, Oregon State, and the Canadian Space Agency made use of this capability during the year.

The neutron flux and energy spectrum was measured 1.4 m downstream of a 20 mm thick lead absorber for 110 MeV protons from BL2C. The measured and calculated neutron energy spectrum is shown in Fig. 162, together with the sea level neutron spectrum due to cosmic rays. For neutrons above 10 MeV the BL2C neutron flux is a factor of 2.5×10^6 per nA of
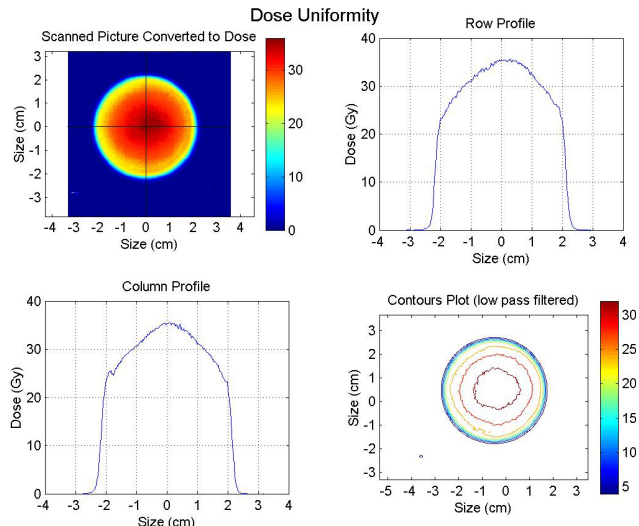
Fig. 161. Beam profile for 105 MeV protons at the BL2C high intensity test location.
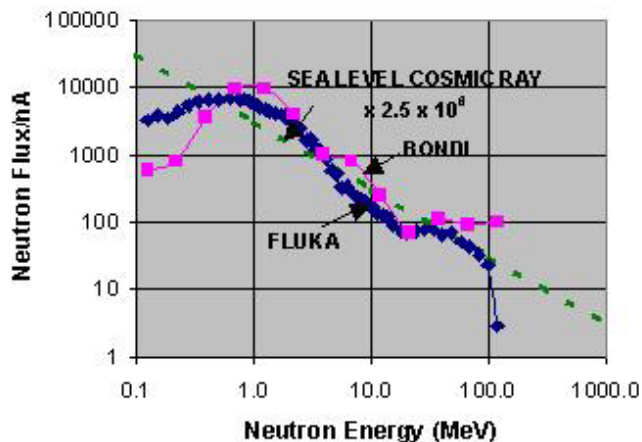
Fig. 162. The measured and calculated neutron energy spectrum.

protons above the sea level neutron flux. This beam was used by a Vancouver power supply company to test if an observed failure of power MOSFETS in certain types of their power supplies was due to cosmic ray neutrons. This was established quite convincingly and helped to solve a reliability problem that had been perplexing the company.

Other groups that used proton beam time during the year included MD Robotics (three occasions), Dynacon and UTIAS (three occasions) and QinetiQ, Farnborough, UK. In addition there were two series of irradiations for other applications. In one case samples of palladium were irradiated at three proton energies to determine certain radioisotope production rates from activation analysis. In another a group from Los
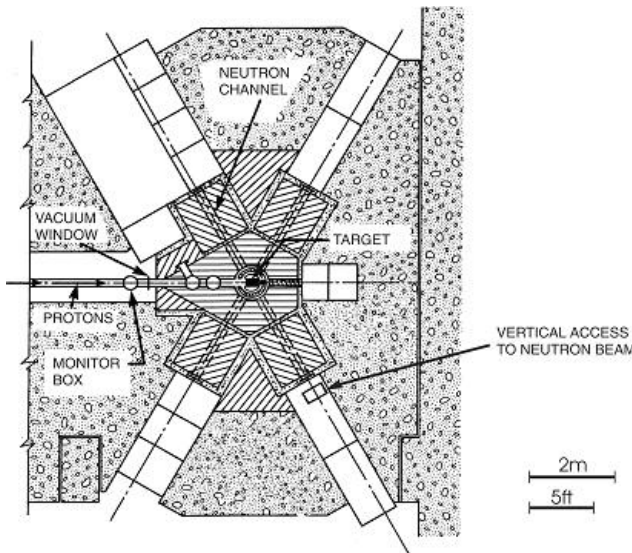
Fig. 163. Plan view of the TNF showing the vertical access to the neutron beam.

Alamos and UCLA carried out a proton RBE measurement in collaboration with the BC Cancer Research Agency. For this measurement a simple 2-step modulator was designed to give a spread out Bragg peak of 3 mm at 70 MeV. This measurement was requested by the CERN program committee to demonstrate the technique to be used in a future experiment to measure the RBE of antiprotons.

The BL1A beam dump (previously called the thermal neutron facility (TNF)) was designed with several neutron channels for thermal neutrons. These thermal neutrons were used for neutron scattering experiments in the 1980s when there was a lead beam stop and a heavy water moderator in the TNF. The beam dump is now aluminum and the moderator is ordinary water. A series of activation and other measurements were carried out in the summer to determine the flux of high energy neutrons (greater than 1 MeV) in this channel. There is vertical access to the southeast neutron channel as shown in Fig. 163, and a track with a pulley system was installed to allow measuring instrumentation to be lowered to beam level. This study has been docu-

mented in "Use of the TNF neutron beam for radiation damage studies" [TRI-DN-02-16] and shows that there is a significant high energy neutron flux corresponding to a 1 MeV equivalent flux of 1.2×10^7 neutrons/cm^2/s with 140 μA extracted down BL1A. As this neutron beam is available parasitically for about 3000 hours per year, there is a good possibility that it could be useful for SEU tests with neutrons. The only other neutron irradiation facility for electronic device testing available in North America is at LANSCE in Los Alamos and it is heavily booked. The TRIUMF neutron rate is similar to LANSCE although the testing area that is presently available at the TNF is smaller.

Proton Therapy Facility
(E.W. Blackmore, TRIUMF)

During the year, 9 patients were treated with protons, bringing the total number of patients treated at TRIUMF to 77. This total is made up of 75 treated for choroidal melanoma, 3 with tumours of the iris, and 2 with hemangiomas.

Dr. K. Paton and E. Blackmore attended the PTCOG meeting in Catania, Italy, May 29–31, and presented a paper on the results of proton and plaque therapy on ocular tumours treated in Vancouver. For that report a summary of the patient and tumour statistics was prepared for the first 70 proton patients (Table XIV).

Since 1995 the treatment planning program EYE-PLAN has run on the VAX computers ERICH/REG which were part of the TRIUMF cluster running VMS. These computers were retired and the planning software transferred to one of the Central Controls System computers which use the VMS operating system. This is an interim measure only as a PC version of EYE-PLAN has been obtained from Clatterbridge, UK, and it is presently being tested at the BC Cancer Agency.

The iris tumours typically require thinner modulators than used for choroidal melanomas. A new series of modulators from 5 mm to 10 mm were machined for this application.

Table XIV. Proton patient and tumour statistics. Total patients: 70 (67 choroidal melanoma, 2 iris, 1 hemangioma). Ages 17–80, 40 M, 30 F.

	Max. width	Min. width	Height mm	Volume cc	Range mm	Modulator mm
Maximum	23.0	19.1	12.6	1.68	31.4	23.8
Minimum	8.2	6.7	1.5	0.12	10.1	10.1
Mean	15.1	12.6	6.0	0.62	21.5	17.6

Location: 45% <2 mm macula, 55% < 2 mm optic desk

μSR User Facility
(S. Kreitzman, TRIUMF)

Overview

Operational snapshot

μSR user facility operations in 2002 reflected the availability of the 500 MeV proton beam and the operational status of the secondary beam lines. To that end, 66 beam weeks of μSR experiments were carried out. This number was somewhat reduced from the previous year's (70 beam weeks) insofar as the proton beam was off for a week during schedule 102a and the high momentum M9B channel was lost during schedule 103a due to a failure of a He turbo compressor. The major spectrometer utilization was found to be (given in weeks) LAMPF 22, Helios 13, HiTime 11, DR 8, OMNI 7, and SFUMU/OMNI$'$ 10.

Proposals and personnel

The μSR science program continues to flourish, with 19 new proposals submitted during the two semi-annual Experiments Evaluation Committee reviews. A change of staff in the facility has also occurred with a new design technologist joining the group. This individual has extensive 3-D design experience and comes with a strong background in mechanical design previously applied to the field of fuel injector design/manufacture for the liquid natural gas industry.

Funding and planning

As mentioned in the 2001 Annual Report, the Natural Sciences and Engineering Research Council (NSERC) unilaterally extended the μSR facility's funding that year (for an additional two) so that it could be put onto a 5 year funding cycle, replacing the 3 year cycle previously used. At that time, we petitioned NSERC to also grant us an inflationary supplement for that 2 year period so salaries, which are supported by the relevant Major Facility Access (MFA) grant, could manage to keep pace with inflation and the normal career progress of the facility staff. We are pleased to report here that NSERC granted our request for the required supplement thereby allowing us to maintain the necessary staffing levels. A further result of the shift to 5 year MFA funding is that now the μSR Facility will be making its funding case to NSERC in synchronization with the 5-year planning cycle that TRIUMF itself maintains. An imminent example of this correlated planning will be found in the upcoming MFA 2004–9 proposal, due to be submitted in the fall, 2003. The proposal in question will envision a significantly increased scope for the Facility operations so that the aggressive μSR expansion plans which TRIUMF will be putting forth in its 5 Year Plan can be adequately supported.

Facility developments

The major facility developments which highlighted the year were:

- Design of the OMNI$'$ spectrometer.
- Reconfiguration of the Helios spectrometer front end.
- Design and construction of an in-house VME timing/gating/counting module.
- Commissioning of new Linux data acquisition computers.
- Introduction of β-NQR capabilities in ISAC.

The following material outlines these and related developments more fully.

Spectrometers
OMNI$'$

OMNI$'$ is the last of the traditional facility spectrometers to undergo its rebuild into an instrument suited for the requirements of modern μSR research. It has been designed to be the instrument of choice for zero and longitudinal field studies on the high momentum M9B channel. Insofar as the Japanese μSR research community makes heavy use of this beam line, the spectrometer makes the facilitation of their traditional experimental set-ups very easy. In addition, the standard experimental configurations which the facility provides are also built into the design for straight forward installation. A new feature in this spectrometer
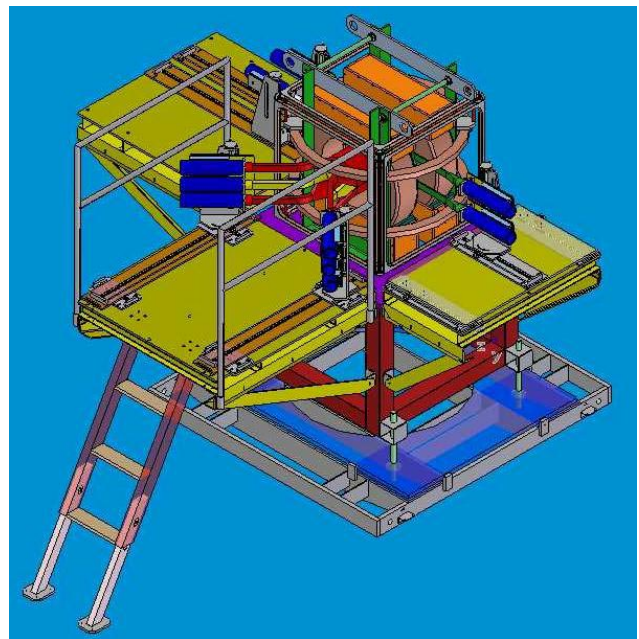
Fig. 164. A 3D rendering of the new OMNI$'$ spectrometer with a standard set of counters. The spectrometer is also fitted with specialized counters and mounting systems to accommodate experimental set-ups for the Japanese μSR research community which often utilize M9B.

is the use of carefully designed saddle coils to provide to a weak (up to 20 G) horizontal field perpendicular to the main field direction. The use of saddle coils best utilizes the available real estate inside the magnet and does not restrict either counter, cryostat or other cell access into the central field region. Finally, in addition to the large Z axis coils (3.5 kG) and weak (20 G) X/Y axis transverse field coils, the spectrometer has an independent set of zero field coils to remove small magnetic contributions from the earth and the cyclotron.

Helios front end

In 2001 the 7T solenoid workhorse spectrometer Helios was rebuilt to accommodate the current needs of the μSR research community. Envisaged at the time was a short large diameter front end geometry that had a significantly higher solid angle acceptance to the muon beams that could be injected into the apparatus. This front end has been implemented in 2002, resulting

in an increase of 25–40% (a field dependent value) in the available muon luminosity at the sample position.

Data acquisition

Hardware – GGL VME module

The correct set-up of a μSR time-differential experiment requires defining a time domain of interest (the Data Gate), and then ensuring (to within a reasonable probability) that only one muon is in the sample during that time. This requirement, and the way in which the TRIUMF μSR TDC (time-to-digital converter) operates, necessitates that a series of gates are set up which all depend on the data gate in a well defined manner. In the past, when the time of interest needed to be altered, manual intervention was required to appropriately change the data gate and its derivative TDC and reference gates. With the advent of the TRIUMF designed μSR gate generator logic module (i.e. GGL, pronounced "giggle"), these operations are
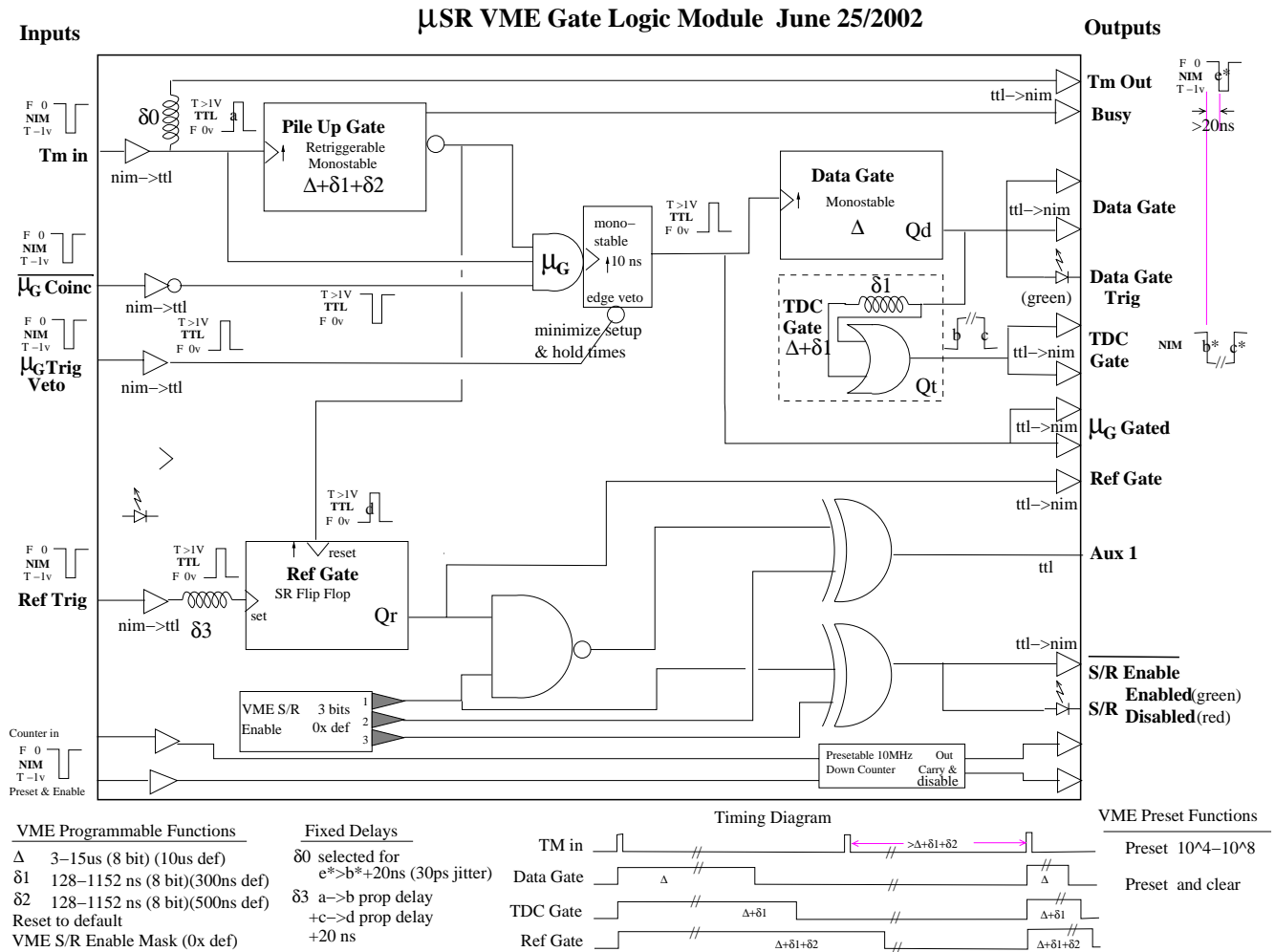
Fig. 165. The logic diagram of an integrated VME module that provides all the gating and timing delays required for the TRIUMF μSR time differential data acquisition mode. The module is meant to work efficiently with the μSR TDCs and the data acquisition software to remove the previous requirements for direct user intervention in the setting of the required gate intervals.

now automated by the DAQ system thereby obviating the requirement for any manual intervention after the initial electronics set-up. A further functionality of this board for TD μSR is that it supports the logic to switch to the so-called μSR $\times 2$ mode, in which sample and reference spectra are simultaneously acquired.

In addition to providing TD μSR mode support, the GGL module also contains preset scalers and DAC capabilities that allow I μSR (integral μSR) experiments to proceed solely with VME system support. Therefore the venerable CAMAC nuclear instrumentation interface is now being removed from the μSR DAQ configurations at TRIUMF.

Software – Linux DAQ

The new μSR Linux based DAQ and user interface continues to be refined. Automatic logging of the statistics of monitored CAMP variables (like temperatures, fields) is fully functional as is the automation of the gate generation mentioned in the previous section. A user friendly interface for I μSR (similar in look and feel to its TD counterpart) has been under development, to be deployed in the spring/summer schedule of 2003.

β-NQR at ISAC

Because ^{8}Li is a spin 2 nucleus, in principle it can (and often will) be found in a non-cubic microscopic environment after implantation. The existence of an electric field gradient makes it therefore natural to extend the β-NMR capabilities into the regime of NQR experiments in zero or low magnetic fields. To this end, the facility has expanded its support for the β-NMR program to assist in the magnetic excitation and control of samples in the 1–500 kHz frequency domain, which is the domain of typical β-NQR studies.

The near future: planning for an broad community spectrometer

Background

The field of μSR research in Canada has of late entered a significant growth phase earmarked by the appointment of a number of young professors (with extensive post graduate μSR experience) to universities across the country. Not only have these new faculty members invigorated (and indeed overburdened) the demand for current facilities, but they have catalyzed a broader interest in the field by providing their local university research colleagues with a knowledge and insight that is prompting some to utilize μSR as a research tool in their own studies. To meet this growing demand, we envisage developing a turnkey μSR spectrometer/system to be used as a tool which is easily accessible to the general research community.

The rig and the beam line

In accordance with TRIUMF's plans, the beam line to be utilized will be a refurbished version of M9B. It will contain dual achromatic spin rotators to achieve both 90° spin rotation, muon/positron separation and high flux transmission. Also featured will be an intermediate focus prior to the last triplet allowing for remote collimation of the beam spot. The spectrometer itself will consist of a 2T split coil magnet, with access into the field from both the axial and side directions. The former geometry is ideal for TD μSR while the latter will be optimized for LF and ZF studies. Counters and cryostats associated with both entry directions can be selected and controlled remotely into their experimental positions so that the optimal experiments can be switched in with ease.

Philosophy

Save for the sample mounting, the entire operation will be remotely controlled. It is envisioned that a full time liaison scientist will assist in the data-taking and analysis so that the visiting scientists involved can go back to their home institution with a complete set of analyzed data relevant to the system they are investigating. This planned ease of use will emulate the experimental environment that is found in modern neutron user facilities.

Facility information and documentation

Please refer to our Web site http://musr.triumf.ca for full access to a broad range of facility resources and information.

Computing Services
(C. Kost, TRIUMF)

Overview

A major accomplishment was the successful transfer of over a Tbyte of ATLAS Monte Carlo simulated data from TRIUMF to CERN, disk to disk, using a record spanning (12,000 km) end-to-end (single-hop) lightpath at record transfer rates (corresponding to transferring some 1500 CDs full of data at a rate of one every 8 seconds). This test was successfully demonstrated at the iGrid 2002 conference held in Amsterdam. It was the culmination of 3 months of intensive effort involving a partnership with CANARIE Inc., ATLAS Canada and other organizations, in addition to the tireless efforts of the 4 member research team – Corrie Kost, Steven McDonald, Bryan Caron, and Wade Hong. Besides the obvious spin-off benefits to TRIUMF, our network speed to BCNET was improved by a factor of 40. With WestGrid coming on stream by mid-2003, the rapid acquisition of small Linux based clusters at TRIUMF, the preparations under way to move into ISAC-II in early 2003, the retirement of our

VAX/VMS data analysis cluster, as well as the continued expansion of the local network, it has meant that our small group was under severe strain. Nevertheless we are optimistic that 2003 will herald in a new and substantially improved era in computing as we reap the rewards of extraordinary efforts made in 2002.

Modular approach

TRIUMF continues to take a modular approach in providing an integrated computing environment. Enhancements to several modules took place this year:

- Replacement of some colour X Window (NCD) terminals with PCs running Linux.
- Our central mail facility was upgraded with new hardware and new software packages including the Webmail service, antivirus program, LDAP server etc., and a Web-based version of the user configuration tool.
- The TRIUMF Router has been replaced with a Nortel Passport 8003, enabling gigabit routing. A second unit will be installed in early 2003, to increase capacity and provide some redundancy.
- Hardware for a new central Web server was installed. The new site, developed to enhance public exposure of TRIUMF, with suggestions for sitewide standards, should be released early in 2003.

Hardware/network

The TRIUMF network backbone configuration remains much like it was illustrated in the 2001 Annual Report, albeit with more BayStack switches. There are currently some 1850 nodes defined in the domain name server, with only about 50% (896) in active use. Most of those active ports are managed by the over 900 ports connected via Nortel BayStack switches. Some additional switches will be required to address capacity overloads in certain areas – the goal being to have all devices (with the exclusion of compute farm nodes, which should be on private networks) connected to managed ports.

Computer security

The number of network worms continues to grow. Code Red and Nimda are still active and show a marked monthly periodicity. In September a new worm, "Opaserv-A", started propagating across Windows networked disks and generated enough scan activity to overwhelm our reporting mechanism. We have not yet restarted the full reporter. We see more wide scan activity for proxy servers and other services. Some of this may be done by external people looking to send spam anonymously as proxy servers allow the original sender to be hidden from the recipient. We continue to operate the LaBrea "tarpit" program to slow these

scans and hide real TRIUMF addresses, though the amount of traffic has caused problems with ARP cache on the router so we have had to scale back this effort.

In April we wrote a custom interface for the AVP antivirus product running on trmail. This was used to generate more complete virus reports, and also to discard worm-generated e-mail rather than deliver it to the recipient (it generally has no useful content and is sent from a forged address).

The most significant e-mail virus of 2002, in terms of amount of traffic seen at TRIUMF, was Klez. We had few actual virus infections, though an Opaserv infection over the Christmas vacation caused us to block outgoing Windows traffic (incoming was already blocked).

TRIUMF continues to receive an ever-increasing amount of unsolicited commercial e-mail, or "spam", some of it distasteful in nature. Some spammers using a dictionary attack against the site allowed them to discover seldom-used addresses that were not available anywhere on the Internet. There is no easy way to prevent this.

The anti-spam tool "SpamAssassin" was installed in November. This augments the Razor spam signature system by performing rule-based analysis of incoming mail. Internal TRIUMF mail and mail from affiliate institutions is "whitelisted" to avoid misplacing genuine messages. Users can customize their accounts by adjusting the reporting threshold and by adding personal "whitelists" for commercial newsletters (which are often reported as spam).

A number of "spamtrap" e-mail accounts, such as "games" or "ftp" were created. Mail to these spamtrap accounts is fed into the Razor signature database. In August a couple of Solaris machines were hacked and used for IRC activity. They were taken off-line and updated.

Videoconferencing

An ISDN-based computer is still used for a number of conferences as is the VRVS reflector set up for use by the HEP community. The Webcast server "video" was used to record and transmit a number of meetings, including the TRIUMF Users' Group and high school teachers' Pro-D day. Work on setting up an AccessGrid advanced videoconferencing facility (funded by WestGrid) at TRIUMF is in progress.

Network measurements

We continue to participate in the SLAC Pinger and the Oxford Traceping projects for WAN monitoring, as well as monitor the internal TRIUMF network for device availability and location using arpwatch. The search for a comprehensive, affordable, sitewide network monitoring tool continues.

Network data transfer trial

In line with networking requirements of future experiments such as ATLAS at CERN in 2007, CANARIE, Canada's advanced internet development organization, suggested that we participate in iGrid 2002 in Amsterdam by utilizing an international multi-gigabit experimental optical testbed to:

- Demonstrate an end-to-end lightpath between TRIUMF and CERN.
- Experiment with 10 gigabit Ethernet technology and Ethernet channel bonding over such distances.
- Transfer 1 Tbyte of ATLAS Monte Carlo data, single-host to single-host, disk-to-disk, at record speeds.

This required the extension of the end-to-end lightpath from its terminus in downtown Vancouver (BC-NET) to TRIUMF – a distance of 20 km. Figure 166 illustrates the solution that was implemented – namely, the use of a coarse wave division multiplexer (CWDM) to provide 2 bonded GbE in an etherchannel, with 10 GbE technology, whose IEEE 802.3ae specification had just been finalized, at the end-points.

Intel generously supplied alpha versions of their Pro GbE LR server adapters for our end hosts. Extreme Networks enthusiastically loaned two of their Black Diamond 6808 switches with the new 10 GbE Lri blades. This enabled a high speed single stream of data from an end host to the Extreme Switch which could then be switched across to two channel bonded GbE interfaces. The dual GbEs were connected to a Cisco ONS15454 mapped to dual OC-24s and transported end-to-end as shown in Fig. 167.
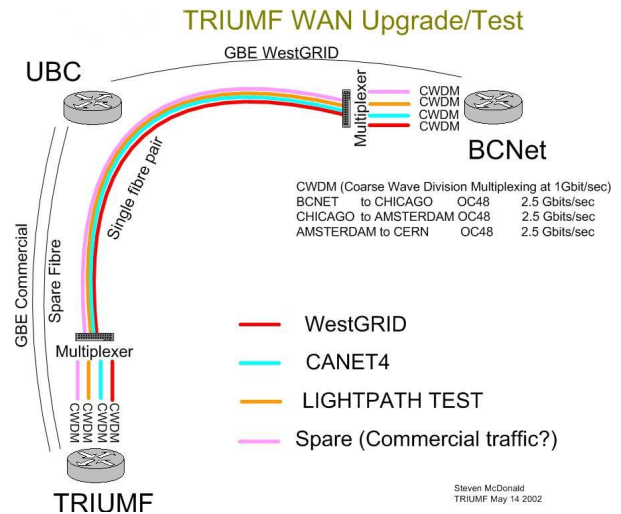
Fig. 166. TRIUMF WAN upgrade/test.

Fig. 167. ATLAS Canada TRIUMF-CERN lightpath test for iGRID2002.

With this configuration we were able to sustain an average rate above 1000 Mbits/sec in the transfer of about 10 Gbytes from disk at TRIUMF to memory in the machine at CERN. Figure 168 shows the transfer rate and total amount transferred as a function of time.

For disk-to-disk transfers, sustained/peak rates using bbFTP were 666/737 Mbps, while using the Tsunami transfer codes they were 700/824 Mbps. Figure 169 illustrates the transfer rates observed on each of the two bonded GbE channels during the successful transfer of over a Tbyte of ATLAS data.

Software developments

Physica

This internationally popular, general purpose data analysis/visualizaton program running on UNIX/Linux platforms has become quite stable. Even
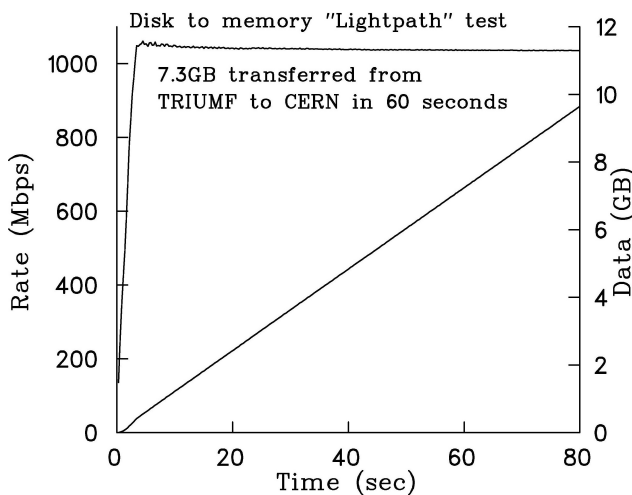
Fig. 168. Record disk to memory transfer rate.
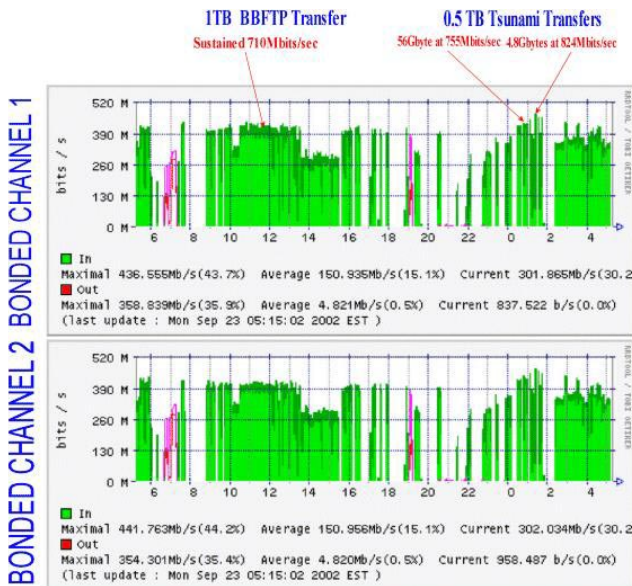
Fig. 169. Record disk to disk transfer rates.

so, it continues to improve as reported bugs (now few and far between) were fixed and requested enhancements were added – such as increasing the maximum number of curves that can be replotted. The port of Physica to the Microsoft Windows platform has progressed from beta testing to the release stage. The list of features in the UNIX/Linux version of Physica that are not in the Windows version has grown short. The Windows version has new improved features not found in the UNIX/Linux versions, such as: more control over the appearance of a graph; true area fill; PostScript Language Level 2 bitmaps; use of TrueType fonts; JPEG output; an integrated graphical user interface; complete session save and restore.

Beam dynamics

GEANT4 – Testing and quality assurance

This year we made further contributions to GEANT4 in the area of Web-tools associated with software testing, debugging, and application development. New facilities installed on TRIUMF's GEANT4 WWW server include ViewCVS, a CVS browser allowing access to the GEANT4 source code repository with displays of revision histories, an excellent graphical diff utility showing changes between versions, and hyperlinked activity logs. Unlike the older CVSWeb package, ViewCVS is tags-aware and therefore a better fit to GEANT4 needs. Also available through ViewCVS is CVSGraph, which creates a hyperlinked graphical representation of the revision tree for any file in the repository, offering a clear view of all main trunk and branch tags. CVSView can be accessed as a stand-alone facility or from LXR, which is a Web-based browser for the GEANT4 source code. These tools can be accessed at http://geant4www.triumf.ca/.

GEANT4 – Visualization

Our Linux-based dual-cpu server for GEANT4 development also functions as a visualization workstation and is configured with a 22 in. flatscreen monitor, 3dLabs high speed graphics card with hardware geometry engine, and Xi Graphics Accelerated X Server software. The latter software, allowing hardware-accelerated graphics to efficiently coexist with the X Window environment on Linux, was definitely "bleeding edge" when we first acquired it, but Xi Graphics has followed through with completely rewritten and much enhanced drivers. This free upgrade was installed and extensively tested, showing improved performance and excellent stability.

ACCSIM

The multiparticle simulation code, ACCSIM, continues to be used in a wide variety of accelerator applications, principally for high-intensity proton synchrotrons and accumulator rings. This year, the work

Accsim 4 Data Management
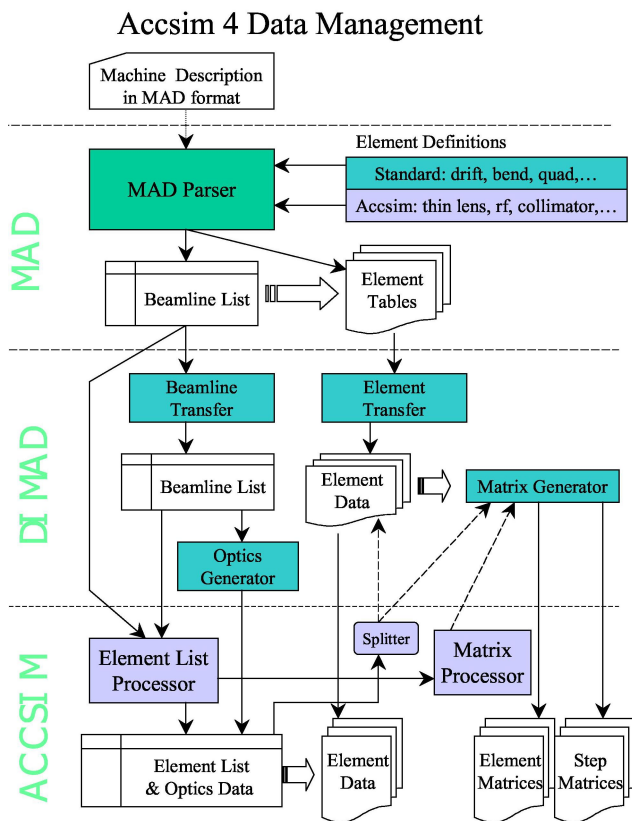
Fig. 170. Part of the architecture of the new ACCSIM. Components from MAD and Dimad are used by permission of the authors.

on "ACCSIM 4" (Fig. 170) was substantially complete and pre-release versions were distributed to users at CERN, KEK, JAERI, and Fermilab. This allowed a few remaining bugs to come out of the woodwork and be fixed, as well as some fine-tuning of features using current applications. The new code is completely stand-alone and allows the input of lattice descriptions in the standard MAD format, with automatic computation of the lattice optics, tunes, chromaticity, and transport coefficients, including step-matrices for space-charge tracking within magnetic elements. This represents a step forward in user convenience for this type of simulation code, which typically relies on a separate program such as MAD or Dimad to process the lattice description and compute the necessary machine data for input to the simulation.

Japanese Hadron Facility

A member of our group visited the Japan Atomic Energy Research Institute (JAERI), the site of JHF (later rechristened as J-PARC), the high intensity proton accelerator facility being built in partnership with KEK. The main objective was to introduce the ACCSIM code to JAERI accelerator physicists and to develop new simulations for the JHF 3 GeV synchrotron,

whose design has been substantially revised since the original JHF proposal.

ACCSIM 4 was installed on several machines at JAERI and KEK and informational seminars were given at both labs. Further development work included a new treatment of bump dipoles, allowing the off-axis orbits and fringe fields to be computed correctly while still maintaining a conventional (local, on-axis) coordinate system for tracking. This will be used to model the 3 GeV machine's sophisticated injection region incorporating 8 orbit-bump dipoles and 2 quadrupoles. Loss management is also a primary concern for this machine. Using ACCSIM 4, a simulation with collimator elements, including proton interactions with the materials, could be rapidly set up and was found to give distributed loss estimates that were in good agreement with MARS code results previously obtained at JAERI.

Parallel computing

Using a small commodity Linux cluster set up originally as a test-bed for cluster management software, this year we inaugurated parallel computing at TRIUMF, at least on a small scale. In conjunction with the collaboration with CERN on LHC beam dynamics, a multiparticle beam-beam simulation code, BeamX, was extended from a 2D beam interaction model to a 3D scenario involving longitudinal subdivision ("slicing") of the counter-rotating proton bunches. The low-cost cluster of 6 CPUs, configured as a private network, provided an excellent development platform on which to parallelize this code using the MPI and LAM toolkits (standard with Red Hat 7.3) and to work out an effective algorithm for the inter-process communication which maintains consistent information between processors as each computes the interaction between particular slice pairs.

In search of additional resources, BeamX has since proliferated to the THOR cluster at the University of Alberta, while production runs also continue at TRIUMF. BeamX is a useful "seed" application for future parallel computing on the larger cluster (WestGrid) soon to come.

Miscellaneous

To underscore the advances in computing power, our standard floating point intensive application ACCSIM, which took 187 minutes on a VAX-780 now takes about 9 seconds on a 2.8 GHz Xeon based machine (using the Intel compiler which reduced it from 15 seconds using g77).

Data Acquisition Systems

(R. Poutissou, TRIUMF)

Overview

In 2002, the DAQ group continued to support a wide array of experimental groups and test stations. Peter Green, who had been with the group for many years, retired at the end of June. He has been replaced by Konstantin Olchansky who had come to TRIUMF two years ago to work with the TWIST group after several years at Brookhaven National Laboratory in data acquisition systems, software analysis and Linux system management.

The TRIUMF data acquisition system MIDAS is currently deployed over 26 stations managed by the DAQ group around the laboratory. These machines also provide some off-line analysis resources and disk storage.

MIDAS software

The MIDAS software continued to evolve and mature. Stefan Ritt, the main author of MIDAS software, spent two weeks at TRIUMF in the early summer to discuss and implement improvements of interest to the TRIUMF systems in collaboration with Pierre Amaudruz. Konstantin Olchansky joined the effort in July. The work on the MIDAS software during this year has been focused on the integration of an event builder, current MIDAS tools optimization and Web interface improvement integrated in a new release of MIDAS version 1.9.1

This new release specifically addressed the following tasks: mevb, logger, lazylogger, mhttpd, elog, history and upgraded error handling in the RPC portion of the code. Most of the software improvements have been suggested and tested by the TWIST experiment where MIDAS has been put to stringent use with data collection up to 8 Mb/s and over a dozen slow control devices.

The number of hardware devices supported by MIDAS keeps increasing. New MIDAS drivers for GPIB and USB devices were added as well as support for a SCSI Camac interface. The success of the USB driver has prompted a study to replace the connection of RS232 devices through old Emulex terminal servers by USB serial adapters.

Evaluation of other DAQ hardware such as PCI/VME interface, VME frontend modules (Flash ADC, AMT deadtimeless multihit TDC) and a new VME processor (a Pentium 3 VMIVME 7750 from VMIC) is in progress.

Study of the new MSCB slow control system developed by Stefan Ritt at PSI has been started in order to evaluate its possible implementation and use within TRIUMF for control and monitoring of experimental devices.

Information about MIDAS can be found at http://midas.triumf.ca/docmidas/index.html.

On-line analysis software

The DAQ group had been supporting two on-line analysis packages. The first one is called NOVA, developed and maintained by Peter Green. The second one is the MIDAS analyzer using the HBOOK/PAW/CERNLIB histogramming software suite.

With the retirement of Peter last June, the development of NOVA has stopped. Limited support for this package is expected to last until the end of 2003. With the development of HBOOK also being static, it was time for the DAQ group to embark on a new avenue. After consultation with the 8π group, Stefan Ritt and TRIUMF computing services, it was decided to begin a development effort using ROOT which is a new C++ analysis framework supported at CERN and widely embraced by the high energy physics community as well as by GSI. The 8π group put in a big

Table XV. Computer systems with MIDAS software managed by the DAQ group.

Name	Location	Type
isdaq01	ISAC-LE, βNMR, TRINAT	2xPII/450
isdaq02	ISAC-LE, GP2, LTNO	PIII/500
isdaq03	ISAC-HE, TUDA	2xPIII/550
isdaq04	ISAC-HE, DRAGON	2xPIII/550
isdaq05	ISAC-LE, ISAC users	PIII/1000-256
isdaq06	ISAC-HE ISAC users	PIII/1000
isdaq08	ISAC-LE, 8π	2xPIII/1000
midtis01	TRINAT DAQ	2xPIII/550
midtis02	Detector Facility	PPro/200
midtis03	LTNO platform DAQ	PII/350
midtis04	GP2 DAQ	2xPIII/550
midtis05	8π cryo	PII/300
midtis06	ISAC floor DAQ	AMD/XP/350
midmes01	Detector Facility	PIII/500
midmes02	DRAGON	2xPIII/550
midmes03	RMC DAQ	2xPIII/550
midmes04	Detector Facility	PII/300
midmes05	Detector Facility	PPro/200
midmes06	8π cryo backup	PII/166
daqtest	M11 users	PII/400
e614slow	TWIST Slow Control	PII/400
midtwist	TWIST DAQ	2xPIII/1000
midm9b	M9B μSR DAQ	2xPIII/1000
midm15	M15 μSR DAQ	2xPIII/1000
midm20	M20 μSR DAQ	2xPIII/1000
dasdevpc	DAQ development and Web server	PIV/1700

effort to develop a GUI and macros for ROOT while Konstantin provided a MIDAS analyzer capable of producing ROOT histograms via shared memory and integrated MIDAS RPCs into ROOT. In 2003, the effort will continue in collaboration with Stefan Ritt to provide a full interface to ROOT as well as a versatile GUI to satisfy the on-line analysis needs of former NOVA and HBOOK users.

DAQ systems

POL and βNMR at ISAC

Further modifications and improvements were made to the βNMR data acquisition system. Support has been added for various scans of devices controlled by Epics (from the ISAC control system) and by CAMP systems (specific βNMR slow control systems). Extensive documentation accessible through any Web browser is now available for this experiment.

A second DAQ called POL was installed on the second leg of the βNMR beam line. It supports a polarimeter for beam studies. The software had to be made versatile enough for use by βNMR users and other experimenters (Osaka) setting their experiment in that area. The experience gained in developing reliable scans of EPICS devices was made available to other MIDAS experiments, specifically to the Osaka group.

μSR systems

The new Linux-based TD-μSR DAQ system was completed (including a graphical user interface written by Donald Arsenault). It has been installed on all three μSR beam lines and was successfully used during the fall beam periods.

A large part of a prototype Linux-based system to replace I-μSR has been written and debugged.

TWIST

Development continued on the TWIST DAQ system. To boost the data rate, the logging media was changed from a DLT8000 to a Super DLT III drive bringing the data rate to the level of 10 Mb/s sustained while lowering the tape costs by a factor of 2.

As mentioned above, this demanding DAQ required a number of MIDAS improvements in all aspects of MIDAS. Much work was done, mainly in the slow control category, in particular, the implementation of M13 B1 and B2 magnet regulators and improvement of the USB camera readout for the TWIST alignment system (including modifications to the Linux ov511 driver). Three of the FASTBUS TDCs had failed and required repairs. One had to be sent to an external company but Andrew Daviel was able to diagnose the problem FPGA in the other cases. Replacement of the chip was done in-house by the Electronics group.

The TWIST experimental group is now exclusively using Elog, the MIDAS electronic logbook facility, instead of a paper logbook. Elog is accessible through any Web interface making it possible for all members of the group, locally or externally based, to follow the progress of the experiment and make timely contributions.

Other experimental stations

The 8π group switched from a VMS based DAQ to VME and MIDAS in the first half of the year with the help of the DAQ group. They also developed a ROOT on-line analysis package as mentioned above.

Half a dozen other requests for DAQ ranging from small test bench set-ups to real experiments have been handled. Support for external MIDAS users has been strong with more than 10 labs around the world requesting help on DAQ hardware selection and/or installation.

Detector Facility
(R. Henderson, TRIUMF)

This year has been an active one for the detector facility.

For the first six months the group was busy completing the spare detector modules for the TWIST project (E614). This project is a sophisticated experiment at TRIUMF which hopes to measure the Michel parameters to ten times the present precision. The various subsystems of this experiment are functioning superbly, including the 56 high-precision drift chambers and the complex gas system fabricated in the facility. A great deal of data has been collected already. A low pressure Time-Expansion-Chamber (TEC) has also been designed for use just upstream of the TWIST spectrometer. This TEC will be built and tested in the facility and will be used to measure the muon beam properties.

The last ATLAS modules have been shipped to CERN and the facility involvement in this project has finished. The completion of the modules frees up two of the facility's clean rooms, adjacent floor space and office space in the facility.

The scintillator shop continues to function as the heavily used machining centre for the facility. This year has seen a wide variety of scintillators fabricated for μSR, the $G\emptyset$ experiment (at JLab) and the 8π experiment. The larger mill in the scintillator shop was previously retrofitted as a 4-axis NC mill for the TWIST project, and this allows us to machine the complex curved scintillator pieces for $G\emptyset$. The $G\emptyset$ scintillator designs were significantly delayed by the $G\emptyset$ group. The first scintillator sector has been finished and we are waiting for the testing before producing the other

seven sectors. More KOPIO prototype detectors continue to be fabricated in this shop.

Design and prototyping have continued for the proposed KOPIO preradiator modules. KOPIO is awaiting approval by the US funding agencies. Robert Henderson spent the majority of this year working in the KOPIO group. If approved, this project will be a very large detector project at TRIUMF – considerably larger and more complex than previous projects such as the ATLAS calorimeter fabrication, the BABAR drift chamber, or the HERMES TRDs.

CFI funding for LADD has been approved. This money will be used to boost the detector development infrastructure at TRIUMF. LADD will take considerable time and effort to set up and is planned to give TRIUMF a world class facility for continuing development of detector technologies, not just for physics experiments but potentially for a wide range of R&D projects including a variety of medical detectors.

Experimental Support
(C. Ballard, TRIUMF)

The Experimental Support group, which includes the Beam Lines group, is responsible for the installation, alignment and maintenance of the experimental facilities at TRIUMF as well as support for the primary beam lines and maintenance, repair and operation of the secondary channels. As in 2001, the group supplied technical assistance to the existing experiments as well as technical support to ISAC and the CERN collaboration. The Beam Lines group continued to provide alignment assistance to ISAC, TWIST, Remote Handling and the RF group.

Meson hall

In January, efforts were focused on the upgrade of beam line 1A. Other projects in the meson hall included the continuation of the overhaul of the M9 separator; repairs to the M15 separator, M13 beam blocker and M9 beam blocker; upgrades to the M11 area and the TNF. The group also performed preventative maintenance on the water packages, vacuum systems and magnet power leads as well as ongoing technical assistance to the proton irradiation facility, proton therapy, PET, ATLAS and μSR.

CERN collaboration

The CERN collaboration involved two technicians and a summer student on the assembly of nine pulse forming network (PFN) tanks. The tanks will be used in the LHC collider at CERN. Each tank weighs over 2 tonnes and consists of a bank of capacitors and resistors bathed in a silicon-based oil. The assembled tanks will be tested at TRIUMF and sent to Geneva.

ISAC

2A beam line

The beam line to the east target station was installed and aligned. The first 15 degree bender was moved to a second position. The 2A Wye magnet was installed in its place with steering magnets and "bunny" quads also installed and aligned. The Wye magnet can switch beam from the west target station to the east target station. The overall project took about 2 months.

β-NMR

A permanent telescope mount was placed after the GPS 2 alignment port to align the cryostat in the β-NMR experiment. This allowed the position of the sample to be checked without compromising the vacuum.

DRAGON

Two lead shielding frames in the DRAGON beam line were installed to protect personnel from X-rays emitted from the diagnostic boxes inside.

A DRAGON target analysis telescope was designed and installed. An Opti-Cal program was used to calculate the lenses required for focusing on the DRAGON gas target. The photograph obtained using an astronomical colour camera illustrated the hydrogen gas target beam glow.

GPS 2

A beam tube in the LEBT line was modified with glass view-ports to see the polarimeter without breaking vacuum.

TWIST

The TWIST Hall probe alignment table for mapping the magnetic field inside the TWIST solenoid in M13 was assembled, installed and aligned. The project involved redesigning a linear guide rail parallel to the axis of the coil to achieve the tolerances required for the map. The automatic system consisted of Hall probes mounted to a rotating aluminum tube that travelled along the axis of the magnet via a ball screw. The location of the Hall probes was to be reproducible to ± 0.010 in. Special modifications were required to maintain the tolerances during rotation as well as translation.

M13 slits

These were installed back into M13 for the TWIST experiment. A cover plate was used off-line to test the mechanism, motor drives and alignment of the slits prior to installation. A temporary motor control was run to a panel where the slits could be operated until the final controls hardware was ready. The M13 beam blocker/gate valve was reassessed because the limit switches were apparently not engaging. It was

decided to remove the valve from the M13 beam line and replace the actuator arm with a welded assembly. This could take place during the January shutdown.

Magnets

The old M8 bender magnet was rebuilt and installed in the off-line ion source test stand. The magnet needed new lifting lugs and the pole gaps were shimmed to meet the specifications for bending the beam into the analysis station after going through the charge state booster. The water manifolds and hoses were replaced as well as the thermo-switched interlocks. The magnet was field mapped and assembled on the stand and aligned in the test stand beam line.

GEANT4
(P. Gumplinger, TRIUMF)

The GEANT4 Collaboration was established in late 1998 with the purpose of transferring the results of earlier R&D activities of the CERN RD44 Project to a supported production service that would provide a software toolkit for simulation of the passage of particles through matter, and in particular would serve as a modern object-oriented (OO) toolkit to build particle detector simulation programs. To this end, a number of institutions from around the world signed a Memorandum of Understanding (MoU) taking specific commitments and pledging resources toward the common goal. The Collaboration, initially formed to provide the high energy physics (HEP) community with a flexible toolkit for simulation, has expanded to include institutions whose primary work is in space science, medicine, industrial research, and commercial applications. TRIUMF is represented in both the GEANT4 Collaboration Board (CB) which administratively manages the collaboration, and the Technical Steering Board (TSB) which manages the execution of the project.

GEANT4 has grown rapidly from the R&D phase to the production stage. The Collaboration is moving toward making GEANT4 a robust and performant simulation package. A fully operational product now exists with impressive capabilities in HEP and other fields. Attention to professional software engineering methods has led to a maintainable and high-quality software product. The investments early in the project to adopt modern software methods are clearly paying off. GEANT4's object-oriented design allows external code, e.g. visualization and Graphical User Interfaces (GUIs), to be more easily incorporated. Leveraging of external resources allows GEANT4 to rapidly expand its repertoire. One of the strengths of the GEANT4 design is its modularity and flexibility in the choice of physics processes. Since the physics processes are the primary focus of a detector simulation program, a comprehensive validation program is key to the success of the product. In fact, a satisfactory implementation of hadronic models is mission-critical for the LHC experiments.

GEANT4 is gaining widespread acceptance as the tool of choice. Over the past few years, the size of the user community has grown significantly faster than the collaboration itself and will undoubtedly continue to grow. Adoption of GEANT4 by an expanding community means there are many more novice users with no previous ties to the developers of GEANT4. The collaboration has addressed many of the issues in support of the novice user. The updated documentation, tutorials and Web publication of the set of standard physics lists for hadronic physics has also been a big step in helping the users inside and outside the collaboration get started with the code. The collaboration added a Web based user requirement entry and tracking system. Three user workshops in the span of one year, at SLAC, CERN, and the European Space Agency, and the addition of Hypernews has helped improve communication, in general, and the dialog with the LHC experiments, in particular.

The GEANT4 optical photon transport modelling of Čerenkov and scintillation detectors was developed by TRIUMF collaborators and has seen substantial improvements during the past year. This specific GEANT4 functionality is now employed worldwide in experimental simulations as diverse as ALICE, ANTARES, AMANDA, Borexino, Icarus, LHCb, HARP, KOPIO, the Pierre Auger Observatory, and the GATE (Imaging in Nuclear Medicine) Collaboration. In the near future, it will also be exploited as part of the investigation to understand the optical properties of extruded plastic scintillator tiles for KOPIO and for the Near Detector of the Long Base-Line Neutrino Experiment at J-PARC/SuperK. Since the GEANT4 Collaboration has been built on a model of distributed support, TRIUMF personnel are constantly responding to inquiries posted on the G4 User Forum regarding the optical photon tracking. Questions and feedback arrive from people working in medical PET research, cosmic shower research, neutrino detectors, HEP experiments and also from corporate research laboratories. We have also attended two of the three user workshops during the past year, as well as the annual GEANT4 collaboration meeting at CERN in October.

Locally, we have encouraged and supported the TIGRESS collaboration at ISAC-II to base their simulation studies on GEANT4. This initiative was mostly carried out by two undergraduate students, Mike Schumaker and Paul Finlay, and their supervisor Carl Svensson, from the University of Guelph, and generated a contribution to the recent G4 user's workshop at CERN.

The GEANT4 group maintains a Web server at http://geant4www.triumf.ca/ for use by GEANT4 collaborators, application developers and others interested in Web tools to help with the development and testing of large software systems. At present, the server is dedicated to the following facilities: LXR, ViewCVS, CVSGraph, and Tinderbox.

LXR provides a powerful source-code viewer and browser for the entire GEANT4 package including examples and tests. Searches are available through the full text, identifiers, and filenames. The C++ code is fully cross-referenced, with hyperlinks for identifiers such as class names and methods, allowing immediate access to their definitions and occurrences.

ViewCVS is a CVS browser which gives full visual query and browsing capabilities for the GEANT4 source code repository. It provides displays of revision histories, hyperlinked activity logs, source file contents, and an excellent graphical diff utility showing changes between versions. A key element for the adoption of ViewCVS, rather than the popular CVSWeb package, is its support for CVS tags. The tag annotations and tag-based queries are essential for GEANT4's scheme of version control.

CVSGraph also accesses the GEANT4 source code repository and provides, for any source file, a hyperlinked graphical representation of its revision tree and, in particular, the attachment of tags to revision numbers. This is a great help in dealing with the sometimes voluminous tag information kept by CVS.

The above three tools have been interconnected so that the user can quickly jump between different information displays for a given source file. Since the CVS repository for GEANT4 is maintained on AFS file space at CERN, to implement the Web tools requires a copy of it to be maintained on geant4www. This is updated frequently and efficiently using rsync, but there is necessarily a short delay before CVS checking becomes visible in the local repository.

Tinderbox is a Web-based testing and archiving facility that is supplementary to the main system testing activities performed continuously at CERN. By giving visual representation of test-job status, and hyperlinked logs of test results, it is useful for both problem diagnosis and debugging, and for testing on unsupported or variant platforms that are not part of the routine test cycle. There are now more elaborate Web-based testing systems to be considered, but we have found Tinderbox to be a lightweight and reliable design and will be pursuing further applications for it such as "Large N" tests and the evaluation of new compilers.

The GEANT4 Collaboration Board has decided to convene periodic external reviews to make an assessment of the collaboration activities and to provide feedback to the CB with the aims of improving the collaboration and guiding the choice of its future objectives. The first such review was held at CERN on June 18–21, 2001, followed by a Delta Review, also at CERN, on October 9–11, 2002. The two reports at http://wwwinfo.cern.ch/asd/geant4/geant4.html contain many recommendations but also compliment the collaboration on their tremendous success.

GEANT4 collaborators at TRIUMF include: P. Gumplinger, F.W. Jones, C.J. Kost and M. Losty.

Scientific Services
(M. Comyn, TRIUMF)

The Scientific Services group encompasses the Publications Office, Library, Information Office, and Conferences. Its activities during 2002 included: producing the 2001 Annual Report, the abstracts book and proceedings for the 14th International Conference on Electromagnetic Isotope Separators and Techniques Related to Their Applications (EMIS-14), and the TRIUMF preprints; updating the functionality of the database system for the Library; coordinating TRIUMF tours and assisting with the production of public relations materials; and supporting twenty past, present and future conferences and workshops. The primary focus of the group throughout the year concerned all aspects of hosting the EMIS-14 conference in Victoria in May.

Publications Office

The TRIUMF Annual Report Scientific Activities has been truly electronic since 1998. Electronic files have been used throughout, from initial contributor submission, through editing, transmission to the printer, and subsequent direct printing on a Xerox Docutech system. The same files are used for the WWW versions of the report which are available at http://www.triumf.ca/annrep in both Portable Document Format and PostScript file formats. Unlike the monochrome paper version, the electronic versions allow those figures which were submitted in colour to be both viewed and printed in colour. The WWW version of the 2001 report was available to readers two weeks before the printed version. During the last two months of 2002, over 300 people accessed the 2001 Annual Report via the WWW. The Annual Report mailing list has been reduced and the trend is expected to continue as people become more accustomed to accessing the information over the WWW. This will result in less copies having to be printed, with subsequent cost savings.

In an attempt to aid and encourage authors to submit Annual Report contributions in the correct format, the instructions available on the WWW were refined. The LaTeX 2_ε skeleton file was unchanged but the in-

structions document which all authors should consult was expanded to include additional information on the correct production of Encapsulated PostScript files for the figures and the submission of original file formats.

Illegal code embedded in Encapsulated PostScript files continues to be a major problem in electronic publishing. Some software packages, such as the TRIUMF graphics routines, fully conform to the Encapsulated PostScript specifications, whereas many do not. In order to alert authors to problems encountered with files they submitted the previous year, and in an attempt to prevent similar problems recurring, a post-mortem of the 204 figures in the 2001 Annual Report was produced and included on the Web site to supplement those for the 1998–2000 Annual Reports. This analysis and explanation of solutions is viewed as an ongoing project which will evolve as new procedures are devised and software packages become available for editing bad PostScript code. Superior TRIUMF scientific publications should result. See http://www.triumf.ca/annrep/figures.html for details.

TRIUMF preprints are now only produced electronically, and immediately posted on the WWW at http://www.triumf.ca/publications/home.html to allow rapid dissemination of the publications. This has replaced the traditional distribution of paper copies by mail, resulting in significant savings of both cost and labour.

In addition to the Annual Report and TRIUMF preprints, the Publications Office also produced the book of abstracts and proceedings for the EMIS-14 conference. Having produced a $\text{\LaTeX}\,2_\varepsilon$ template and instructions for abstract submission and posted them on the EMIS-14 Web site in November, 2001, 155 abstracts were received by the February 1 deadline. These were processed, edited, entered on a database, and made available to the international advisory committee on a secure Web site to facilitate determination of which abstracts should be presented as contributed oral talks or as poster session papers. Once the conference program was finalized, authors were informed of their abstract designation and given manuscript preparation instructions. With assistance from the SFU TRIUMF secretary, a book of abstracts was produced for the conference delegates. The refereed conference proceedings were to be published by Elsevier Science as a dedicated issue of Nuclear Instruments and Methods in Physics Research Section B, Beam Interactions with Materials and Atoms. The functionality of the abstract database was extended to accommodate the many steps that would be necessary to track manuscripts from their initial submission, allocation and sending to the referee, return from the referee, possible return to author for correction and re-submission,

and in some cases multiple loops of the procedure. A set of forms and a filing system were also produced that would be used to track the manuscripts. Most of the manuscripts were received at the conference proceedings office in May and wherever possible they were given to the referees during the conference. Some extremely diligent referees even completed their task before the end of the conference and returned their allocated manuscripts indicating whether they were approved with or without corrections. The task of tracking and chasing the manuscripts took until early December. Some manuscripts were in transit up to eight times between TRIUMF, referee and author. The 129 accepted manuscripts were sent to the publisher in both electronic and hard copy format before Christmas, along with the additional material to appear at the front and back of the proceedings. A May, 2003 publication date is anticipated.

Substantial Web site support was provided for the Summer Nuclear Institute at TRIUMF (SNIT 2002) held June 10–21. Apart from creating and maintaining the Web site, PDF files of all the lectures were created from a variety of original file formats and posted on the site.

Support was provided for the Italian-Canadian Interface for the Development and Exploitation of Stable and Exotic Ion Beams which was held at TRIUMF October 16–20, 2002. A conclusions and abstracts booklet was produced.

Work for the Joint Accelerator Conference Website (JACoW) committee included: presenting two papers at the 3rd JACoW Team Meeting held in Thoiry, France, in February; collaborating on the publication of the electronic proceedings of the European Particle Accelerator Conference (EPAC 2002), held in Paris, France, in June; and co-chairing the Database Workshop and presenting a paper at the 4th JACoW Team Meeting held at Lawrence Berkeley National Laboratory in November.

Library

The Library budget was increased in 2002 to compensate for rising journal subscription costs and unfavourable exchange rates for 2003 renewals, thereby maintaining the list of journals which have been acquired since the last cutbacks in 1998. However, the journal subscription budget and electronic access alternatives are constantly under review.

The Library made a few book purchases in 2002 and continues to rely on donations for most of its acquisitions.

The Oracle database system implemented in 2000 was upgraded to facilitate efficient Library operations. It allows accurate tracking of the journal subscription acquisitions and hence aids subsequent timely requests

to publishers for any missing volumes. It also identifies any volumes which have been illegally removed from the Library prior to the annual spring bookbinding exercise. All books loaned from the TRIUMF Library are entered in the database and automatic e-mails are sent to borrowers who fail to return a book after a month, followed by weekly reminders. This system has proved to be extremely successful at ensuring the prompt return of books, with the added advantage that several borrowers have also returned books which have been out for extended periods. Records for books acquired before 1970 have to be entered manually whenever they are first loaned, and all new acquisitions have to be entered. Outstanding loan reports can be generated easily.

The Library operates on a self-serve basis and manages with minimal support for day-to-day operations.

Information Office

The Information Office coordinated tours for 2,178 people during 2002, the highest number since 1997. The general public tours were conducted by a summer student during the June to August period when tours were offered twice a day. 245 people took a record number of tours (77) during the three month period. Throughout the remainder of the year for the twice weekly general public tours, and for the many prearranged tours given to high school students and others, a small, dedicated group of TRIUMF staff acted as tour guides.

Table XVI shows the number of people taking tours, the number of tours, and the number of tour guides required to conduct them (groups of more than 15 require multiple tour guides) for each of the years 1999–2002 plus the totals. A steady increase can be observed. The numbers are broken down into four categories:

- General public: tours provided for members of the general public twice a week September–May, and twice a day June–August on a drop-in basis.
- Science: pre-arranged tours conducted for university/college physics, chemistry or science students with a specific interest in TRIUMF, scientists at TRIUMF for a conference or workshop, and scientific groups.
- Students: pre-arranged tours conducted for elementary and high school students and university/college non-science students.
- VIP: Specific tours, often conducted by senior management personnel, arranged for VIPs, review/advisory committee members, and the media.

Table XVI. Breakdown of TRIUMF tour numbers for the period 1999–2002.

Category	1999	2000	2001	2002
General Public				
# people	350	368	421	499
# tours	96	107	110	131
# tour guides	96	107	111	134
Science				
# people	384	294	383	592
# tours	18	20	30	23
# tour guides	33	26	43	57
Students				
# people	794	612	839	894
# tours	46	40	30	40
# tour guides	70	53	60	70
VIP				
# people	145	171	258	193
# tours	37	37	59	53
# tour guides	38	40	65	55
Total				
# people	1,673	1,445	1,901	2,178
# tours	197	204	229	247
# tour guides	237	226	279	316

The summer student assisted with the production of a MS PowerPoint version of a slide presentation often given by TRIUMF staff to high school students. A Japanese translation was also produced.

The TRIUMF Welcome Page, which is accessible directly at http://www.triumf.ca/welcome or via the TRIUMF WWW Home Page, continues to receive well over 5,000 visits each year. The series of WWW pages were developed by two co-op students and are intended to provide an overview of TRIUMF in a format understandable to the general public. The Information Office responds to any questions posed by visitors to the site. Some limited maintenance of the pages was performed during the year. A Web site committee met frequently during the year in an effort to use outside resources to totally overhaul those parts of the TRIUMF Web site directed at the general public.

Various TRIUMF images found on the WWW pages continue to be in demand for use in text books and on other Web pages.

Use of the Sony VPL-PX20 LCD data projector purchased in 2000 increased dramatically as more speakers gave seminars and presentations using MS PowerPoint, Star Office, Adobe Acrobat, and other applications. It was also used at the WRNPPC'02 and EMIS-14 conferences.

Support was provided to the TRIUMF Users' Group throughout the year by the TUEC Liaison Officer.

Conferences

2002 was an extremely busy year for conferences and workshops. Apart from the EMIS-14 conference, support was provided for twelve other conferences, workshops and meetings. Seven occurred within the busy April–July period. Registration databases were created and managed for most of the conferences.

In addition, support was provided in the electronic proceedings office of the European Particle Accelerator Conference (EPAC 2002), held in Paris, France, June 3–7.

TRIUMF hosted or supported the following conferences and workshops in 2002:

- Joint Belle-BaBar Worshop on Detector Issues, TRIUMF, February 14–16 (31 delegates).
- Workshop on Low Energy Precision Electroweak Measurements (LEPEM2002), TRIUMF, April 4–6 (68 delegates).
- TITAN Workshop, TRIUMF, April 11–13 (37 delegates).
- Alpha Therapy Workshop, TRIUMF, April 29 (72 delegates).
- 14th International Conference on Electromagnetic Isotope Separators and Techniques Related to Their Applications (EMIS-14), Victoria, May 6–10 (159 delegates).
- Summer Nuclear Institute at TRIUMF (SNIT 2002), TRIUMF, June 10–21 (43 delegates).
- 5th International Conference on Hyperons, Charm and Beauty Hadrons (BEACH 2002), UBC, June 25–29 (116 delegates).
- Workshop on Big DRAGON: a Recoil Separator for ISAC-II at TRIUMF, TRIUMF, July 18–19 (35 delegates).
- Symposium on Symmetries and the Weak Interaction: in Celebration of the 80th Birthday of Sir Denys Wilkinson, TRIUMF, September 5 (52 delegates).
- TRIUMF Five-Year Plan Town Meeting, TRIUMF, September 21–22 (75 delegates).
- Italian-Canadian Interface for the Development and Exploitation of Stable and Exotic Ion Beams, TRIUMF, October 16–20 (36 delegates).
- Physics Teachers Professional Development Day Workshop, TRIUMF, October 25 (85 delegates).
- TRIUMF Users' Group Annual General Meeting, TRIUMF, December 11 (41 delegates).

In addition, preparations were made for the following future conferences and workshops.

- Functional Imaging PET Workshop, UBC, June 26–27, 2003.

- Summer Nuclear Institute at TRIUMF (SNIT 2003), TRIUMF, July 21 – August 1, 2003.
- GEANT4 2003 Workshop, TRIUMF, September 2–6, 2003.
- International Union of Pure and Applied Physics (IUPAP) Meeting, October 10–11, 2003.
- HEPiX-HEPNT Autumn 2003 Meeting, TRIUMF, October 20–24, 2003.
- Eighth International Symposium on Nuclei in the Cosmos (NIC8), Vancouver, July 19–23, 2004.
- Fifth International Symposium on Radiohalogens (5ISR), Whistler, September 11–15, 2004.

The DRAGON Facility
(J.M. D'Auria, SFU)

The primary purpose of the DRAGON (Detector of Recoils And Gammas Of Nuclear reactions) facility, located in the ISAC-I experimental hall, is to measure the astrophysical S-factor or resonance strengths in sub-Coulomb barrier, radiative proton and alpha capture reactions. These reactions are studied using inverse kinematics with gaseous targets of hydrogen or helium bombarded with stable and radioactive heavy ion beams of energies from 0.15 to 1 MeV/u. The rates of such reactions are of interest to increasing our understanding of explosive nucleosynthesis phenomena in nova, supernova, and X-ray bursts. Funding for the DRAGON facility was received April, 1998 and DRAGON began taking data for Expt. 824 in October, 2001. Described herein are upgrade changes made to the facility over the last 12 months along with commissioning studies.

Figure 171 is a schematic representation of the DRAGON facility. It is composed of a windowless, recirculating gas (hydrogen or helium) target (with a cold trap) surrounded with a gamma detection array (30 BGO units), an electromagnetic separator (EMS) and a recoil detection system. The separator will accept heavy recoil products of radiative capture reaction. Their momentum is essentially the same as the beam itself. The design philosophy of the EMS is to select one charge state of the beam and reaction products to pass through slits located after the first magnetic dipole. Beam and reaction products are then separated in the first electrostatic dipole, due to their difference in kinetic energy. Additional separation/beam suppression is achieved in the second stage. In the focal plane detection system the main detector used has been a DSSSD (double sided silicon strip detector), which provided both energy and spatial information, both singly and in coincidence with the gamma system. More complete descriptions can be found elsewhere [Hutcheon *et al.*, Nucl. Instrum. Methods (in press); Liu *et al.*, *ibid.*].

DRAGON
Detector of Recoils And Gammas Of Nuclear reactions
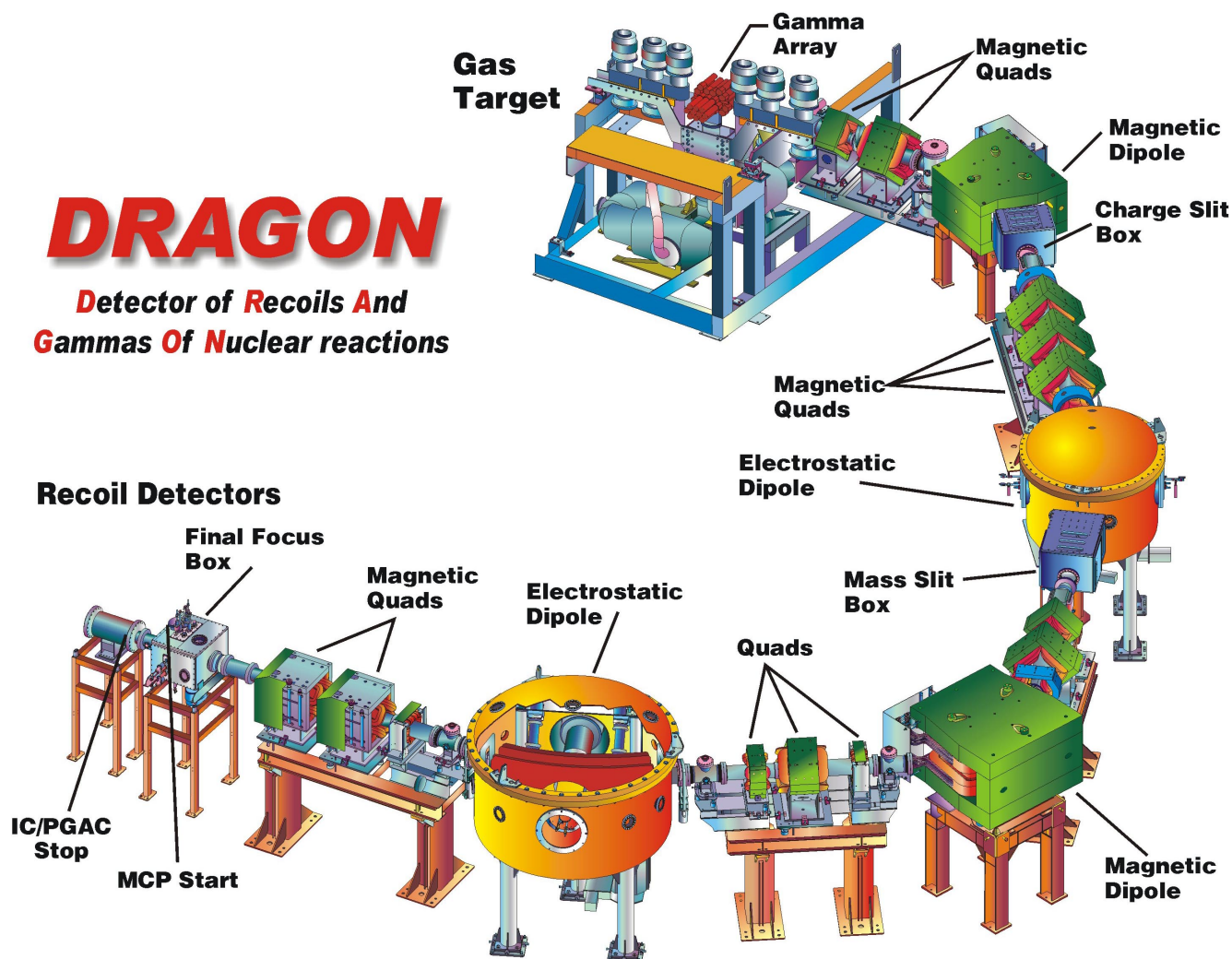
Fig. 171. Schematic view of DRAGON.

Synopsis of facility changes

A number of hardware improvements were made in 2002. These included:

1. Installation and testing of a segmented ionization chamber for detection and identification of the recoil products at the exit of the EMS.
2. Installation and testing of the microchannel plate system to be used at the focal plane for timing and position information.
3. Testing of a novel optical viewing system to allow tuning of the beam while it is intercepting the gas in the target.
4. Improvements in the EPICS-based DRAGON separator tuning program.
5. Replacements of older-model dipole power supplies.
6. Construction and installation of a safety fence around the complete facility.

7. Installation of lead-filled shields around mass and charge slit chambers.

Commissioning

Considerable time was devoted in the past year to using stable beams of ^{14}N, ^{20}Ne, ^{21}Ne, and ^{24}Mg over a wide range of energies to understand and improve the operation of the facility. Approximately 125 shifts in total, with runs in almost every month, were delivered to DRAGON. In particular these studies were devoted to:

1. Calibration of a technique of measuring the incident beam energy.
2. Calibration of the overall absolute efficiency of the DRAGON.
3. Studying the response of DRAGON for a wide resonance.
4. Testing focal plane detection systems.

162

Table XVII. Reaction resonances used for energy calibration studies.

Reaction	E_{lit} (keV)	E_{meas}(keV)	$E_{\mathrm{m}}/E_{\mathrm{l}}$
^{20}Ne$(p,\gamma)^{21}$Na	1112.6 ± 0.6	1110.9 ± 0.8	0.998
^{21}Ne$(p,\gamma)^{22}$Na	731.5 ± 1.6	732.1 ± 0.5	1.001
^{24}Mg$(p,\gamma)^{25}$Al	214.0 ± 0.8	214.5 ± 0.4	1.002

Table XVIII. Efficiency calibration studies.

Reaction	E_{cm} (keV)	$\omega\gamma_{\mathrm{pub}}$	$\omega\gamma_{\mathrm{meas}}$	$\omega\gamma_{\mathrm{meas}}/\omega\gamma_{\mathrm{pub}}$
^{20}Ne$(p,\gamma)^{21}$Na	1112.6	1.13 ± 0.07 eV	0.92 ± 0.17 eV	0.81
^{21}Ne$(p,\gamma)^{22}$Na	258.6	82.5 ± 12.5 meV	209 ± 35 meV	2.27
^{21}Ne$(p,\gamma)^{22}$Na	731.5	3.95 ± 0.79 eV	3.85 ± 0.50 eV	0.97
^{24}Mg$(p,\gamma)^{25}$Al	214.0	12.7 ± 0.09 meV	11.7 ± 0.2 meV	0.92
^{24}Mg$(p,\gamma)^{25}$Al	402.2	41.6 ± 2.6 meV	56.4 ± 8.7 meV	1.36
^{24}Mg$(p,\gamma)^{25}$Al	790.4	532 ± 41 meV	576 ± 39.3 meV	1.08

Beam energy

Beam energy at DRAGON is measured using the first dipole, MD1. Beam is centered through a 2 mm opening in the slits at a focus after MD1. Energies calculated from MD1 NMR magnetic field readings were checked against known resonance energies. The results are shown in Table XVII.

System efficiency

Since the DRAGON is used to measure the absolute resonance strength of unknown reactions involving radioactive reactants, studies were performed to understand the operation (transmission, etc.) under different settings (e.g. slit settings, tuning, etc.). A beam deflection magnet, temporarily replacing the gas target was used to study transmission properties. In addition, a number of known resonance strengths were measured using stable beams (Table XVIII). Such studies will continue.

Wide resonance

DRAGON was designed specifically to study resonances whose widths are much less than the energy loss in the gas target chamber. However, there is interest in broad resonances and non-resonant capture reactions also, and beam time was devoted to explore and measure the response of DRAGON in those cases. This study involved the ^{21}Na radioactive beam for the resonance at $E_{\mathrm{cm}} = 821$ keV and the results are displayed in Figure 172. The resonance strength, $\omega\gamma$, of this broad resonance was measured to be 556 ± 77 meV while the width, Γ, was estimated to be 16.1 ± 2.8 keV.

Focal plane detectors

The specially designed ionization chamber for detecting reaction products at the end of DRAGON was tested (for Expt. 811) using the ^{21}Ne$(p,\gamma)^{22}$Na reaction. Excellent separation was noted between neon and
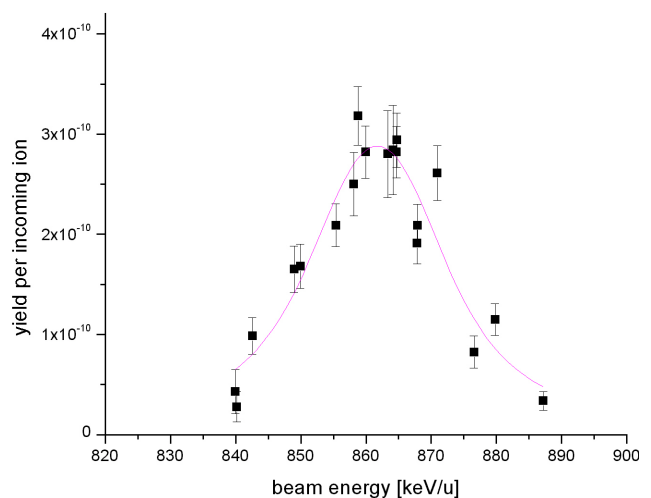
Fig. 172. Preliminary data for Expt. 824.

sodium ions at 0.5 MeV/u both singly and in coincidence with the gamma array.

Science with DRAGON

Radioactive ^{21}Na beam was delivered to DRAGON for Expt. 824 for 2.5 weeks in April/May and about 3 weeks in November/December. Studies of resonances in the ^{21}Na$(p,\gamma)^{22}$Mg reaction at $E_{\mathrm{cm}} = 212, 336, 461, 545,$ and 747 keV are discussed elsewhere in this Annual Report.

Outlook for 2003

Beam time (both stable and radioactive) will be requested for approved experiments 811 (U. Greife, spokesperson, the study of the ^{19}Ne$(p,\gamma)^{20}$Na reaction), and 805 (J. King / J. D'Auria, spokespersons, the ^{13}N$(p,\gamma)^{14}$O reaction). Both of these require the use of the ISAC ECR ion source, which is expected to be operational by April, 2003.

In addition, several new experiments were approved by the EEC and could run in 2003 with, at most, minor

changes to the DRAGON facility. These include studies of the ^{17}F$(p, \gamma)^{18}$Ne, ^{12}C$(\alpha\ , \gamma)^{16}$O, and ^{12}C$(^{12}$C, $\gamma)^{24}$Mg reactions. Some longer-term proposals, requiring more extensive changes to the BGO array or gas target include a revised ^{8}Li$(\alpha, n)^{11}$B study or phase II of ^{12}C$(\alpha, \gamma)^{16}$O. In addition, studies are in progress to explore the feasibility of producing a sufficient amount of ^{15}O (for Expt. 813) with the TR13 cyclotron using a (p, n) reaction, with an on-line gas transfer (of C^{15}O) to OLIS for the production of an accelerated beam.

Summary

The DRAGON facility is now operational with the completion of the first study, Expt. 824; a number of commissioning studies have also been performed. In addition to presentations at conferences and several manuscripts submitted or accepted for publication on DRAGON related studies, one M.Sc. thesis has been completed and four other thesis projects (two Ph.D., two M.Sc.) are essentially completed.

8π Spectrometer
(G.C. Ball, TRIUMF)

Since the 8π γ-ray spectrometer was moved to TRIUMF in 2000, it has undergone significant modifications to optimize its performance for β-decay studies with the non-accelerated radioactive beams available in the low energy area of ISAC (see 2000 and 2001 Annual Reports for details). The first radioactive beam, ^{26}Na, was delivered to the spectrometer in May, 2002. At that time all 20 Compton suppressed HPGe detectors were operational and the original signal-processing and acquisition system was used. This test run demonstrated that the LEBT was able to cleanly deliver a radioactive beam to the spectrometer without dumping radioactive beam on any slits in close proximity to the detector array. The experiment also demonstrated the proof-of-principle of the technique for measuring β-decay lifetimes using γ-rays.

During the next three months a major upgrade of the 8π spectrometer data acquisition system was carried out. This upgrade was needed to meet the requirements of the superallowed β-decay program for precision branching ratio and lifetime measurements (see C. Svensson, Expt. 909). The cost of this upgrade was shared with LLNL. The original system which was based on the LeCroy CAMAC booster (CAB) was replaced with one utilizing FERA readout. The new system uses Ortec ADCs for digitizing pulse heights, LeCroy multihit TDCs for the Ge times and pile-up markers and a LeCroy universal logic module acting as a latching scaler to give an absolute event tag, time stamp and dead time on an event by event basis. The data is streamed into a 64 kword VME triple port memory unit and readout with standard TRIUMF

supported data acqusition hardware/MIDAS software. This upgrade has resulted in a factor ten increase in through-put from under 4000 Hz to a theoretical maximum rate of 50000 Hz. In addition, at instantaneous rates of 30000 triggers/s, less than 1 in 10000 events is lost between the FERA and the on-line analyzer.

A new on-line spectrum viewer was also developed by the 8π collaboration based on ROOT, the object-oriented data analysis framework developed at CERN to replace PAW.

ROOT is a very powerful and versatile tool but also requires a knowledge of C++, therefore it was decided to provide a user-friendly viewer. Following recent developments at GSI, a graphical user interface, GUI, was produced by linking ROOT with QT, a commercial software specialized for designing GUIs. The project was completed over a six month period by F. Sarazin and B. Eshpeter, a summer student, with the support of the TRIUMF DAQ group who converted MIDAS data to ROOT formatted data. The spectrum viewer provides a wide range of display options and specialized features including: one and two dimensional spectra, isometric projections, simultaneous display of multiple spectra, peak fitting etc. Following the early success of the implementation of the new 8π GUI, TRIUMF has decided to develop and support ROOT based graphical software for on-line monitoring of ISAC experiments.

The first 8π development run using the upgraded data acquisition and on-line monitoring system was carried out in August, 2002. With a beam of 10^{4--6}/s ^{26}Na the system was operated at various rates in several different modes to thoroughly understand all possible sources of systematic error for precision lifetime measurements. Approximately 100 GB of data were obtained; the analysis is in progress (see C. Svensson, Expt. 909 for more details). A study of the β-decay of ^{11}Li was also carried out this time (see page 65, β-decay of ^{11}Li). In addition, three experiments were done with the 8π spectrometer using long-lived radioactive sources, namely ^{176}Lu, ^{178}Hf and ^{150}Eu (see page 64, Other studies with the 8π spectrometer).

There are currently seven approved ISAC experiments that will use the 8π spectrometer (Expts. 909, 921, 929, 954, 955, 957 and 961) including four which were approved by the TRIUMF EEC in December, 2002. Several of these experiments are β-γ coincidence studies requiring the scintillating electron positron tagging array (SCEPTAR) that is currently under development. The design goals of SCEPTAR are to provide high β detection efficiency, a low energy threshold, minimum sensitivity to γ-rays, high count rate capability and a detector granularity comparable to the HPGe array. An integral part of SCEPTAR is a fast tape transport system being designed by E. Zganjar (LSU)

to remove long-lived daughter activities from the focus of the array. During the past year the development of prototype detectors was completed. A detailed design of the array, the associated vacuum chamber and moveable support stand was also carried out and machining of the components is in progress. Fabrication and assembly of the complex detector array is scheduled for completion in February, 2003 with installation and initial beam tests in April, 2003.

Finally, during the past year a total of 40 collaborators from 12 institutions actively participated in the development and or/use of the 8π spectrometer, including: 10 undergraduate students, 4 graduate students and 7 post-doctoral fellows.

Towards TIGRESS
(G. Hackman, TRIUMF)

To take full advantage of the physics opportunities presented by ISAC-II beams, a state-of-the-art γ-ray detector array with high efficiency and high resolution is needed. In 2002 the TIGRESS (TRIUMF-ISAC gamma-ray escape suppressed spectrometer) team was pro-active in its goals of building the detector in stages for early implementation in 2005 and full implementation in 2009. The full array will have 16 elements, the active detector elements of each being a high-purity germanium (HPGe) multi-crystal high-resolution spectrometer of the "clover" variety with eight-fold segmented outer contacts, each clover surrounded by reconfigurable bismuth germanate (BGO) and CsI(Tl) suppression shields. Progress involving major contributions from TRIUMF staff in 2002 includes: a) optimization of the suppressor shield design; b) conceptual design of the support structure; c) procurement of a prototype HPGe detector; d) design, construction, and testing of a reliable LN$_2$ control system for maintaining the HPGe detectors at cryogenic operating temperatures; and e) submission of a Major Installation Grant RTI-3 to NSERC for funding of the full array.

Suppressor design evaluation

GEANT-4 simulations were performed to decide between two possible suppressor designs, one with a monolithic suppressor shield and one with multi-component shields as shown in Fig. 173, comprising a "back-catcher" of CsI(Tl) fixed directly to the HPGe cryostat, a "back-side" shield of BGO also fixed to the cryostat, and side BGO shields that could move independently of the HPGe. In the simulations, the latter design exhibited far superior performance while providing the ability to reconfigure the components to maximize either photopeak efficiency ϵ or photopeak-to-total ratio P/T, whichever is apropos for a given experiment. In the close-packed configuration, with the BGO retracted and the HPGe inserted to a radius of
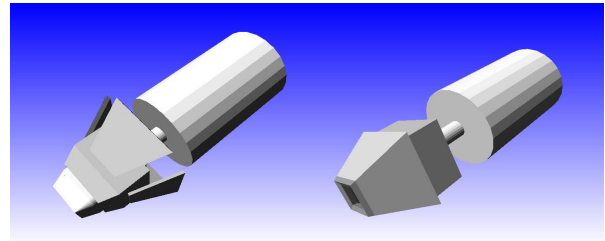
Fig. 173. Schematic of TIGRESS module configured for maximum efficiency (left) or maximum peak-to-total (right).

11 cm, $\epsilon = 27\%$ and P/T = 64% for 1 MeV γ-rays. In the pulled-back configuration the HPGe are withdrawn to 14 cm and the side suppressor shields are inserted between, $\epsilon = 14\%$ and P/T = 73%.

Mechanical design

The mechanical support structure for the array required a detailed conceptual design study. Figure 174 shows the overall support superstructure while Fig. 175 shows the mechanism for insertion and
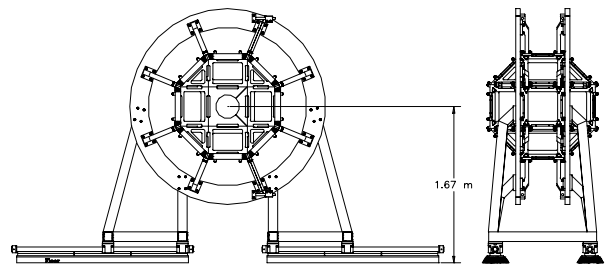
Fig. 174. Mechanical superstructure design.
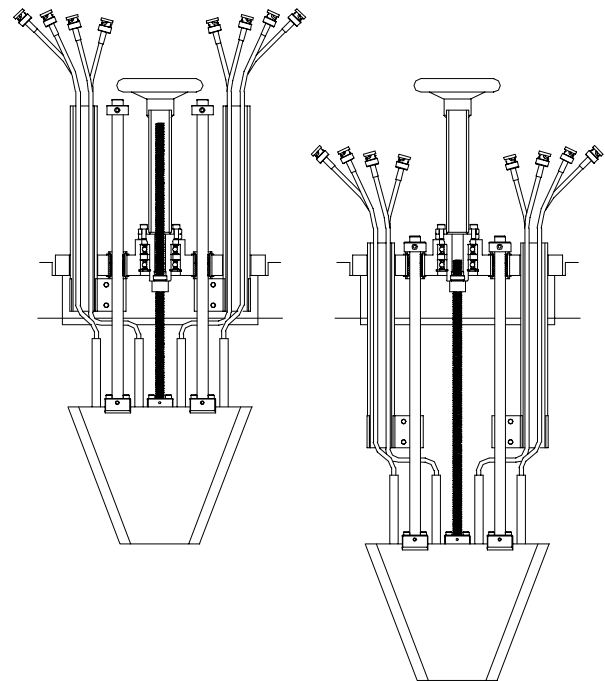
Fig. 175. Side BGO retraction mechanism.

withdrawal of the BGO side shields. This design provides the ability to adapt the array to, for example, a large downstream recoil spectrometer. In addition, this design permits manual reconfiguration from close-packed to maximum-peak-to-total in an afternoon. Cost estimates for final design and component fabrication were also determined.

Prototype HPGe

The TIGRESS team has procured a prototype HPGe detector of the "clover" configuration, with four HPGe crystals in a single cryostat. The outer contacts are electrically split into 8 segments arranged in two layers of four quadrants per crystal, with the lateral segmentation 20 mm from the front of the crystal. With this segmentation it is possible to localize γ-ray interactions within a quadrant and also obtain some indication of the depth within the crystal. Furthermore, such an outer-contact configuration, in conjunction with advanced digital-signal processing techniques, can allow for determination of the first-interaction location to within a few millimeters. This feature will be needed for the full TIGRESS array for Doppler-shift correction of γ-rays emitted from the products of reactions involving high-energy radioactive beams from ISAC-II. A prototype design study carried out by Aptec was funded by TRIUMF and the detector was ordered in April, funded by a CFI-OIT grant obtained by C. Svensson (Guelph). The detector arrived at the end of 2002 (see Fig. 176). Initial tests showed that all 36 contacts functioned; in particular, the 32 outer contacts were operating well within specified resolution for a ^{60}Co source. An extensive testing and characterization program to measure the position sensitivity of the detector will commence in 2003.

LN$_2$ system

A prototype, compact, portable, and reliable LN$_2$ distribution control system was developed to maintain the prototype HPGe at operating temperature (Fig. 177). The system is based on Modicon PLCs, and all process control is self-contained. A graphical interface is provided through the ISAC standard EPICS system.

Submission of NSERC grant request

The R&D developments described herein were included in an NSERC grant request with C.E. Svensson (University of Guelph) as lead spokesman, and J.C. Waddington and Alan Chen (McMaster University), J.P. Martin and C. LeRoy (Université de Montréal), R. Roy and L. Beaulieu (Université Laval), T. Drake (University of Toronto), J.M. D'Auria (Simon Fraser University), and G.C. Ball and G. Hackman (TRIUMF) as grant-elligible collaborators.

Finally, the team held a mini-workshop at the UBC campus following the Big DRAGON workshop in July.

The mini-workshop was attended by A. Boston (Liverpool), C. Gross and D. Bardayan (Oak Ridge), C. Beausang (Yale), J.M Casandjian (GANIL), A. Shotter, J.-M. Poutissou and R. Poutissou (TRIUMF). The mini-workshop provided an opportunity for team members to share their progress and also to obtain expert input and feedback.

The TIGRESS team is large and growing. From TRIUMF, the core group in 2002 was G.C. Ball, J. Braun, K. Cheung, R. Churchman, F. Cifarelli, G. Hackman, F. Sarazin, H. Scraggs and M.B. Smith. We also received valuable technical assistance and support from P. Gumplinger (GEANT4), R. Roper (cost estimates), D. Bishop, D. Dale, R. Keitel and D. Morris (LN$_2$). The performance simulations were performed in collaboration with P. Finlay, M. Schumaker and C.E. Svensson (University of Guelph).
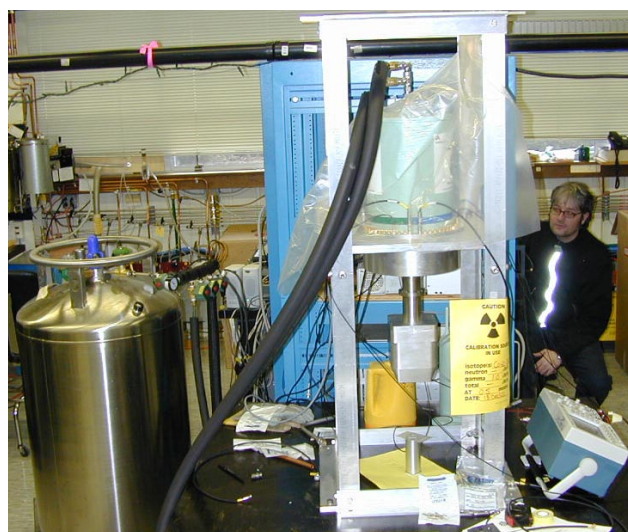
Fig. 176. The prototype clover detector, with its pale green LN$_2$ holding dewar and with the HPGe in the tapered-rectangular vacuum cryostat, is shown mounted on an aluminum testing frame and connected to the LN$_2$ distribution manifold to the left.

Fig. 177. PLC-based LN$_2$ control system in the centre, with interface computer displaying EPICS monitoring page on the left.

RFQ Cooler and Buncher Developments for TITAN
(J. Dilling, TRIUMF)

RFQs filled with buffer gas, operating as coolers and bunchers, are widely used or under construction at almost all radioactive nuclear beam facilities, for example at ISOLDE/CERN, GSI, Argonne and MSU. This is due to their proven ability to provide a 10–50-fold improvement in beam quality and their capability to convert a dc beam into well defined bunches with an overall efficiency of up to 60%.

The basic principle is the following: the incoming ion beam is electrostatically retarded and guided into a segmented four rod structure where alternating potentials generate a quadrupole field. Interactions with the buffer gas cool the ion beam and applied potentials allow for both an accumulation of the ions and an extraction as a bunch with well-defined transverse and longitudinal properties.

The developments at TRIUMF include two significant changes over existing devices:

1. The RFQ can be installed both horizontally and vertically, allowing one to extract the beam both at the entrance side and the top side in the latter orientation.
2. Employ very high rf amplitudes (we intend to go to 10 kV) instead of the typical 100–500 V peak-to-peak voltage.

The modification for a vertical set-up will allow other experiments at the ISAC beam line level to make use of a cooled and bunched beam, for example for co-linear laser spectroscopy in the polarized beam line. This will be possible with the new concept of a square support structure to hold the segmented rods on insulator bars (see Figs. 178 and 179). The system will be mounted to the lid of the vacuum-housing box, allowing one to lift out the structure for easy access. Moreover, the vacuum vessel and alignment system provides for set up in both orientations.

The advantage of going to higher rf amplitudes is to raise the space charge limit. The pseudo-potential, and hence the number of charges that can be stored until the outer trapping force and the repelling Coulomb force are in equilibrium, is proportional to the rf amplitude. At present, our collaboration partner at McGill University has reached amplitudes of 6 kV, employing new coupling techniques. The high fields are required in order to provide large samples of cooled bunched ions, needed for example for β-NMR experiments.

Intensive calculations and simulations have been carried out which show that a 100% acceptance of the ISAC beam (emittance of $\epsilon_{\text{trans}} = 40\,\pi$ mm mrad at 60 keV) can be reached. For the extracted beam
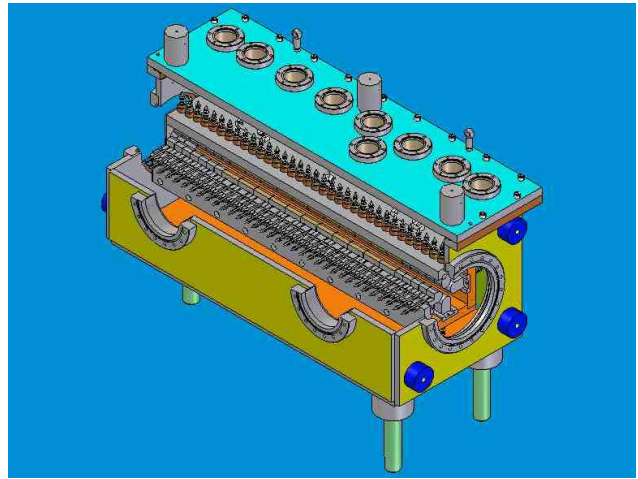
Fig. 178. The RFQ rods are supported by a squared structure, which allows for a vertical and horizontal orientation of the system.
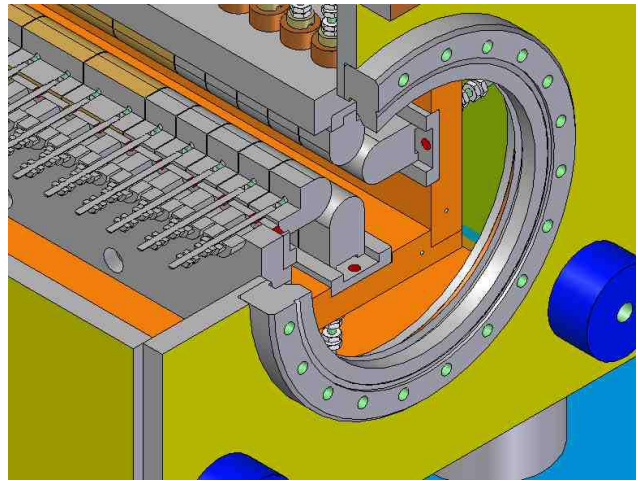
Fig. 179. Design drawing detail of the RFQ structure including the vacuum housing (small inlet).

an emittance of $\epsilon_{\text{trans}} = 1\,\pi$ mm mrad at 2 keV can be expected, corresponding to an improvement by a factor of over 50. The longitudinal energy spread is $\epsilon_{\text{long}} < 5\,\text{eV}\,\mu\text{s}$. The kinetic energy of the extracted beam can be adjusted using a drift tube, where the potential can be rapidly ramped to ground.

These features are ideally suited for further beam manipulation of the ISAC beam in, for example, charge-breeding devices, like the EBIT system in the case of the TITAN facility or the ECR charge breeder. For the latter one the improvement in emittance should make a significant difference in the overall performance, leading to increased breeding efficiencies.

The entire system has been designed and is partially in the fabrication stage awaiting assembly in the TITAN test area being set up in the proton hall extension.

The rf driver for the RFQ has been designed and is being built in conjunction with the TRIUMF Control group and will be finished in September, 2003. Plans are initially to carry out tests to characterize the performance of the RFQ system. Later, a coupling to the ECR charge breeder in horizontal orientation will allow for tests to determine the effect of the beam quality improvement (spring/summer 2004). Finally, this RFQ system will be installed in a vertical configuration at the ISAC beam line as part of the TITAN system and for use as cooler and buncher for the polarized beam line employed for β-NMR or laser spectroscopy experiments.

TRINAT Off-line Laser Lab
Progress in precision optical pumping
(S. Gu, TRIUMF)

When polarizing nuclei using optical pumping, there are quantum field effects of laser-atom interactions that must be considered. Complete polarization of alkali atoms like ^{41}K and ^{37}K requires two frequencies of circularly polarized laser light, one for each hyperfine-split ground state. When the difference between the two frequencies matches the ground state splitting, there can be coherent transfer of population between the states, and the states are mixed by the interaction. The new eigenstates of the full Hamiltonian are linear combinations of the bare atom eigenstates, with phase determined by the laser light phase. The result is one eigenstate that does not absorb laser light, and that eigenstate is not optically pumped so that atoms remain unpolarized. We have found that such states are very fragile and easily destroyed, so they are not a practical impedance to achieving high polarization. The following is a more detailed characterization of similar phenomena explored as part of our group's participation in the Canadian Institute for Photonics Innovations.

Coherent population trapping refers to the process described above. In constrast with coupled atoms ($|C>$) which interact with the laser, atoms that are coherent population trapped don't interact with the laser and are hence denoted as un-coupled atoms ($|UC>$) [Arimomdo, Progress in Optics **XXXV**, 257 (1996)].

We have experimentally studied hyperfine $|UC>$ with cold ^{41}K atoms in a magneto-optical trap. The results are compared and agree with our numerical solutions of the optical Bloch equations for the time evolution of the density matrix. We have also proposed a "pseudo 3-level" theoretical model which explains hyperfine $|UC>$ behaviour well.

In the experiment we used a right-circularly polarized bichromatic D_1 laser beam to optically pump atoms in a magnetic field (**B**) to the fully polarized $F =$

2 $m = 2$ sub-state. When the two laser frequencies ν_1 and ν_2 satisfy the Raman resonance $h(\nu_1 - \nu_2) = W_m$ condition, certain atoms will be trapped in that pair of m sub-states, i.e. in $|UC>$ (where $W_m(m = -1, 0, 1)$ is the ground state hyperfine level splitting of the m sub-state in the given **B** field). Unlike most experiments in which $|UC>$ are mixed with $|C>$, in our experiment we have successfully realized pure $|UC>$. Our study shows that $|UC>$ is physically characterized by the off-diagonal "hyperfine coherence" terms of the density matrix, rather than the on-diagonal populations. This is made manifest by off-Raman resonance oscillations (ORRO), an experimental technique we developed for studying the hyperfine coherence.

In realizing the ORRO experiment, we first feed rf into two acousto-optic modulators to shift the diode laser frequency into two frequencies satisfying the Raman resonance condition. After $|UC>$ has been prepared with this bichromatic laser light, we then change the rf so that the laser frequencies are switched off the Raman resonance, that is, $h(\nu_1 - \nu_2) - W_m = h\Delta\nu$. Under this condition the atomic system won't be in pure $|UC>$ anymore and will oscillate between $|UC>$ and $|C>$ at the frequency $\Delta\nu$, that is ORRO. We experimentally study the ORRO process by observing the fluorescence from those original $|UC>$ atoms. We can see from Fig. 180 that the initial phase of the recorded oscillation curves is different. We have realized that it
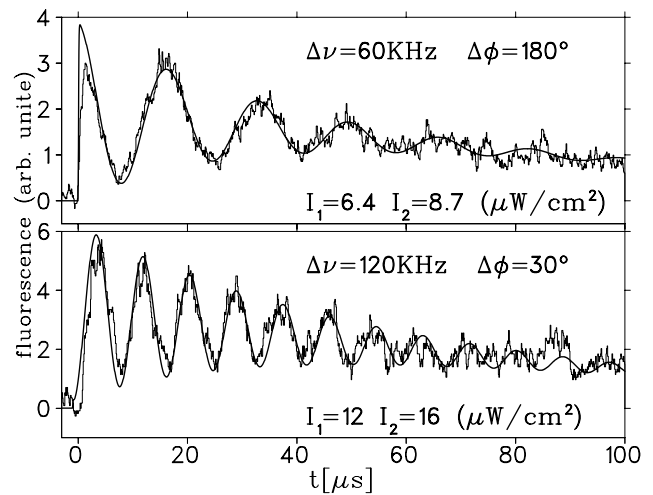
Fig. 180. Experimental measurements of off-Raman resonance oscillations compared to full optical Bloch equation calculations. With lasers on the Raman resonance, $h(\nu_1 - \nu_2) = W_0$, atoms were pumped for $900\,\mu$s to prepare $|UC>$ with $m = 0$ hyperfine states. Then (at $t = 0$) ν_1 and ν_2 were switched off-resonance, $\nu_1 \rightarrow \nu_1 + \Delta\nu/2$, $\nu_2 \rightarrow \nu_2 - \Delta\nu/2$ for the ORRO process. In the calculation $\Delta\phi$ was fit to the corresponding ORRO curve, and laser intensity was calibrated by fitting incoherent fluorescence data during the optical pumping process. $B = 1.74$ G was measured from the Zeeman shift of the rf frequency of the $\Delta m = 1$ Raman resonance.

is from "phase jumping". Note the change in phase between the two lasers before and after the rf is switched to be $\Delta\phi$. Including $\Delta\phi$ into the optical Bloch equations, it can be seen in Fig. 180 that the experimental function can be reproduced.

We have experimentally realized ORRO with uncertainty of $\Delta\nu$ less than $600\,\text{Hz}$, but have not been able to experimentally control the switching time precisely enough to control the phase jumping. We fit the theoretical calculations to the experimental curves by varying $\Delta\phi$. From Fig. 180 it is seen that the first oscillation peak of the $\Delta\nu = 60\,\text{kHz}$ curve is cut by about half a period. By comparing to the calculated curve we concluded that in the switching process corresponding to this curve the phase jumping $\Delta\phi$ is about

$(2n+1)\pi$, while the other data in Fig. 180 correspond to $\approx (2n+1/6)\pi$.

Since the oscillations occur at a rate equal to the detuning of the laser frequency difference from the hyperfine ground state splitting, this technique could be used to determine the hyperfine splitting of radioactive isotopes, as the lasers do not need to be scanned over the resonance.

The ORRO provide a way to study $|UC>$ with which we have proven $|UC>$ is characterized by hyperfine coherences. Because the frequency can be precisely controlled by tuning rf, and the oscillation curve can be manipulated by $\Delta\phi$, with better control of $\Delta\phi$, ORRO could have applications in quantum information.

CYCLOTRON OPERATIONS DIVISION

INTRODUCTION

During 2002 the cyclotron was available for $\sim$90% of the hours scheduled, a satisfactory result considering a few problems that arose at the end of the winter shutdown and during the first part of the beam production schedule. The total number of available hours was 4,845, exceeding that achieved in 2001 and almost equaling the $\sim$5,000 hours achieved in 2000. For high-intensity beams, 2002 was a record year. The total beam charge delivered at 500 MeV was 594 mAh, of which 517 mAh were delivered to BL1A for meson production and 77 mAh were delivered to BL2A for RIB production. Approximately 125 mAh were delivered at 85 MeV to rubidium targets in beam line 2C4 for the production of ^{82}Sr that is used for medical diagnostics. The total beam charge extracted was 20% greater than that produced in previous years. The total beam current extracted and available for experiments increased from 220 μA to 250 μA. During development shifts a total average current of 280 μA was achieved, 20 μA shy of our 300 μA goal for ISAC-I. This 280 μA limit corresponded to the total maximum intensity accepted by the extraction beam lines (170 μA in BL1A, 40 μA in BL2A, and 70 μA in 2C4).

The 90% availability of the cyclotron was lower than the 92.4% achieved in 2001. The main cause was a period of frequent rf sparking that lasted until the September shutdown. The resulting rf downtime in the first weeks of beam operation was three times higher than that in a similar period following the 2001 shutdown. The effect of frequent rf sparking and of corresponding beam interruptions is rather disruptive for the production of the radioactive ion beams that is critically dependent on stable operating temperatures of the RIB targets. Sparking could have been cured by retuning the position of ground-arm-tips through their remote control system. However, that system was malfunctioning and could not be used. A refurbished control system had been planned, but was not yet available because of other site priorities. Priorities were readdressed; the new system was constructed and was installed during the one week shutdown in September. The rf sparking rate following that shutdown was reduced by a factor of 2.5.

The highlights during the winter shutdown were the repair of several water leaks on BL1A and refurbishing modifications around 1AT2. The total loss of cooling water had reached the rate of 74 l/h at the end of the beam production period in December, 2001. Leaks were repaired on the quadrupole triplet in the extremely active area downstream of 1AT2 and on the first quadrupole and first dipole of the M20 me-son beam line. The triplet leak appeared in an easily accessible position on a soldered joint on a cooling-water pipe. This was repaired promptly without high-dose exposure. There were a few other leaks that were more difficult to repair. Other work in the 1AT2 area included the removal of the M8 meson channel, and the refurbishing of the shielding structure south of and above the triplet. Shielding was configured in a manner that would ease replacement of the triplet that is scheduled for the 2003 winter shutdown. A few crumbling concrete shielding blocks were replaced by new units. The 1AT2 area refurbishing effort required close, efficient collaboration between the Remote Handling, Beam Lines, Plant, and Safety groups. This was key to the completion of this delicate operation that was concluded successfully on schedule in mid-April.

In May, during the high-intensity beam production, BL1A was plagued by a substantial water leak in the coils of the M11 septum. Attempts to repair the leak with a special "colloidal solution" in the coolant failed. As soon as it was realized that *ad hoc* repairs were not feasible, it was decided to let the leak grow in a controlled fashion to $\sim$80 l/h. This occurred at the end of July at which time beam delivery to M11 was discontinued. Installation of a new septum is planned for winter, 2005.

The total average intensity extracted from the cyclotron had never exceeded a maximum of $\sim$220 μA, despite several attempts to obtain higher values using the combined maximum-current capabilities of BL1A and BL2C4. The reasons for this limit were analyzed and were traced to thermal problems caused by beam losses in the centre region. The following improvements were introduced during the winter shutdown.

1. A water-cooled copper absorber was installed inside the first quarter-turn orbit to absorb radial beam losses caused by ions not matching the cyclotron rf phase acceptance.

2. The centre region correction plates, showing evidence of beam damage and found to be vertically misaligned, were carefully realigned so that they would no longer protrude into the beam volume intended to be available for acceleration.

3. The back edge of an rf contact, found to be protruding vertically into the beam volume, was also adequately tailored.

Over-temperature problems at $\sim$220 μA disappeared after the shutdown and improved high-intensity conditions were immediately achieved. This was in part due to the above centre region modifications and in part to an improved beam tune that had been established in the ion source/injection line systems. Cyclotron transmission from axial injection to extraction could be

increased above 60%, implying good beam matching through the centre region, for all beam intensities up to 325 μA total. The following results were recorded.

On July 16 a record 250 μA at 100% duty cycle were extracted with good transmission over a 2 hour period. Two weeks later a record 275 μA at 100% duty cycle were extracted over 3 hours with better than 60% transmission. The extracted beams appeared to be reasonably stable (see Fig. 181). On the same day, 300 μA were extracted over 2 hours at 90% duty cycle with good transmission. This was followed by 325 μA (75% duty cycle, 60% transmission) and 350 μA (40% duty cycle, 57% transmission). On subsequent development shifts in August, September, October and November the 300 μA tune was reproduced easily. We failed, however, to reproduce the 350 μA tune. The cause was traced to the rf voltage on the dees being actually lower (by about 10%) than indicated by the rf PA system. After recalibration of the rf we easily reproduced the 350 μA at 10% duty cycle and greater than 60% transmission in the last development shifts before Christmas. In addition, we obtained 380 μA also at 10% duty cycle and better than 60% transmission. We believe that 400 μA cw are now well within reach.

The next goal will be to demonstrate 400 μA with 60–70% duty cycle, good transmission, and reasonable stability over a period of several hours. To demonstrate operation at 100% duty cycle, additional beam dump capacity will be required. For this we are studying the possibilities of increasing the capability of beam line 1A to accept up to 200 μA at 500 MeV and of installing a dedicated beam dump in the vault that would allow simultaneous extraction of another 200 μA at a lower energy (70–85 MeV).

In conclusion, the results achieved indicate that the cyclotron can now be refurbished to operate reliably and stably at total currents up to 400 μA. This is 100 μA in excess of the previous goal set for simultaneous 1A, 2C4, and ISAC operation. It is now conceivable to extract an additional ~100 μA from a fourth high-intensity beam line (for instance, beam line 4V North) to feed a separate target and to provide a second simultaneous beam of radioactive ions for ISAC users. Part of the high-intensity beam for ISAC may have to be extracted at lower energy, i.e. 450 MeV, to avoid electromagnetic stripping between 450 and 500 MeV and thus keep beam losses in the cyclotron within reasonable limits. This scenario is now being considered for the next five-year development plan for the laboratory.
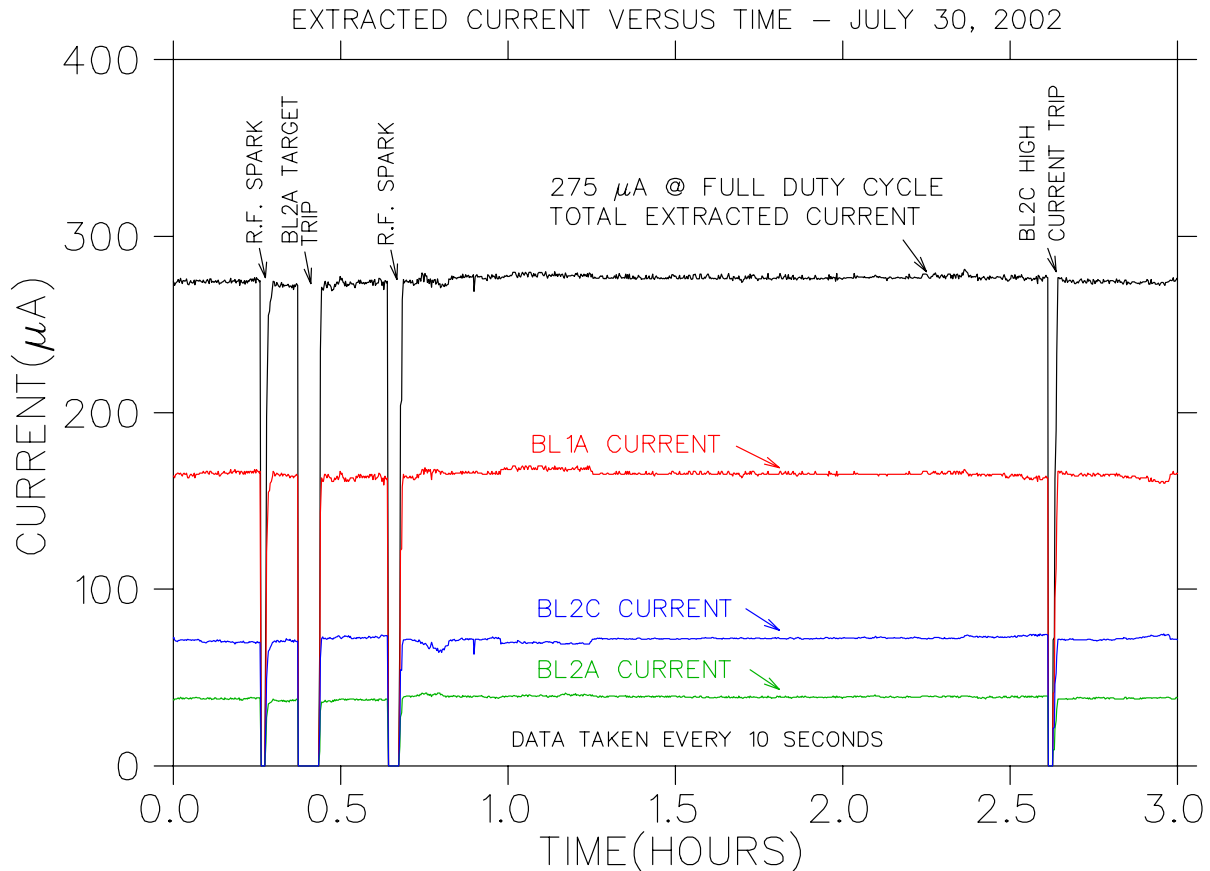
Fig. 181. Beam currents extracted at 100% duty cycle over a three hour period.

Cyclotron refurbishments continued according to the program initiated in year 2000. For the 1AT2 area, the work mentioned above represents only the first phase of the total refurbishing action required. During the 2003 shutdown, we will replace the 1AQ14/15/16 triplet and complete the replacement of adjacent crumbling shielding blocks. The 1AT2 area is given the highest priority because it is the weakest link in the reliable production of high-intensity proton beams.

High priority was also given to the refurbishment of the rf resonator and amplifier systems because historically these have been a major cause of cyclotron downtime. In addition to the centre region improvements described above, metallic pads that were originally applied as vibration dampers to the bellows of the cooling circuit are being replaced with fibreglass units. Occasionally over the years the metallic dampers have caused arcing situations leading to water leaks, the repair of which has required interruption of beam production for two to three weeks each time. The plan is to gradually change these metallic dampers wherever possible. RF diagnostics are being upgraded with improved multiplexing and first-event counters.

Significant progress was achieved on the rf amplifier system. A new waster load was tested at about 500 kW. Two rebuilt combiners were tested at full power and the first one was installed for operation before the year end. Two more combiners are planned for installation in 2003 and 2004. In 2004 we will be able to switch the whole rf amplifier system to the waster load for off-line tests and repair. The goal is to achieve by the 2005 shutdown a rf generator that, in emergencies, can operate with two amplifiers instead of four. Thus, in case of failure, a partial system may be used until repairs can be made during scheduled maintenance.

The refurbishing work on probes and diagnostics was limited by insufficient budget and personnel resources. The group was also heavily involved in the production of diagnostics devices for ISAC. However, a milestone was achieved when it was demonstrated that gas-filled multi-wire chamber monitors can be replaced by lower sensitivity secondary-emission multi-wire harps that can operate in a vacuum. In high radiation areas, gas-filled monitors require frequent maintenance for seal replacement, therefore causing dose exposure problems. A new electronic system was designed that makes the readout of the harp wires more sensitive by two orders of magnitude, thus making the secondary-emission harps preferable for radiation environments. For the cyclotron, a refurbished high-energy probe was designed; this probe is more functional, reliable, and precise than the present ones. Construction and assembly of this probe are planned for 2003.

Refurbishment of the cyclotron central control sys-

tem (CCS) was also limited by budget restrictions. However, progress was achieved by installing a new fibre-channel storage system in the cluster to provide superior performance and reliability. Tape back-up systems were upgraded to high-density drives, and two obsolete production computers were replaced with Alpha units. New LCD monitors have improved console displays in the Control Room, the RF Room, and the Proton Therapy Control Room. Controls integration with beam diagnostics during operation and development shifts was well organized and very helpful.

Finally, a major effort was undertaken to improve the reliability of the safety system that protects against prompt radiation hazards. In response to requests from the CNSC, a study group and an action group were created to study, recommend, and implement improvements. By the end of 2002 almost all of the suggested improvements and actions were completed. These included shielding improvements and the implementation of two separate, parallel systems (a gamma monitoring system and a neutron monitoring system) to interrupt beam in case of radiation in non-exclusion areas. Other improvements included modifications to minimize the risk of tampering with the safety systems, routine periodic testing to verify the functioning of safety-critical devices, and the introduction of additional redundancy. This resulted in the safety systems satisfying the stringent requirement that the probability of serious accidents be less than 10^{-5} per year. It should be stressed that the present safety record of TRIUMF for prompt radiation hazard is very good because no significant problems have been encountered over the (more than) 25 year life of the project. However, it is reassuring to have established that our system is also in line with the prescribed minimum-risk guidelines. Recommended improvements will be completed during the 2004 shutdown with the completion of the restructuring of the safety-critical gamma and neutron monitoring systems such that they become completely independent and without the possibility of a common-mode failure.

In conclusion, the cyclotron is still operating (after 28 years from first beam) at the familiar 90% level of availability. As a result of recent developments and refurbishments, the system can now be expanded to provide an increase of at least 30% in output beam current. This additional output may be used to construct a second, parallel source of exotic ions for the scientific program.

BEAM PRODUCTION

Beam delivery for 2002 was again quite successful with 500 MeV charge production up 20% from the previous year. Cyclotron performance continued to be

enhanced by the use of the rf booster, which was on during most of the high-current running, partly to satisfy the occasional demand for 2 ns pulse-width beam but also to improve the cyclotron transmission (typically between 62% and 66%) and reduce the measured tank beam spill (usually below $2.5\,\mu$A). Sixteen weeks of shutdown left 5,386 scheduled operational hours of which 4,845 were achieved for an average availability of 90%. These totals include 288 hours used for development and tuning and, as shown in Fig. 182, were split roughly 5:1 between scheduled high-current beam production and lower intensity operation. For the latter, the proton irradiation facility (PIF, using BL1B and BL2C1) usually ran in parallel with BL2A. BL2C1 was also used at 74 MeV for ocular melanoma treatments for nine patients during four proton therapy (PT) sessions. Again this year there was no BL4 operation and no polarized source operation except for a viability test of the latter for a few hours.

As Fig. 183 shows, the total beam charge delivered to meson hall experiments along BL1A was 517 mAh or 96% of the 538 scheduled, one of the best results for the past ten years. The average current delivered to BL1A

was 135 μA. In addition to this, there were 126 mAh delivered at 85 MeV to rubidium targets in the solid target facility (STF) in beam line 2C4 for the production of radiopharmaceutical generators. Another 77 mAh, twice the charge of the previous year, was delivered to the west target station in BL2A2 for the production of radioactive ion beams (RIB) for experiments in ISAC. The total current extracted to the three high-current beam lines was normally around 210 μA, but was pushed to 230 μA for some shorter production periods. The higher currents were possible because of the continuing development efforts.

The annual downtime of 484 hours (Fig. 184) was a little above average with the rf responsible for the greatest share of this time (47%), followed by power supply problems (10%), and power failures (9%). RF downtime, chiefly from sparking, was tamed considerably in the latter part of the year, dropping from 8 hours per week in the first beam schedule to 3 hours per week in the second beam schedule. The operational record and beam to experiments for 2002 are given in Tables XIX and XX.
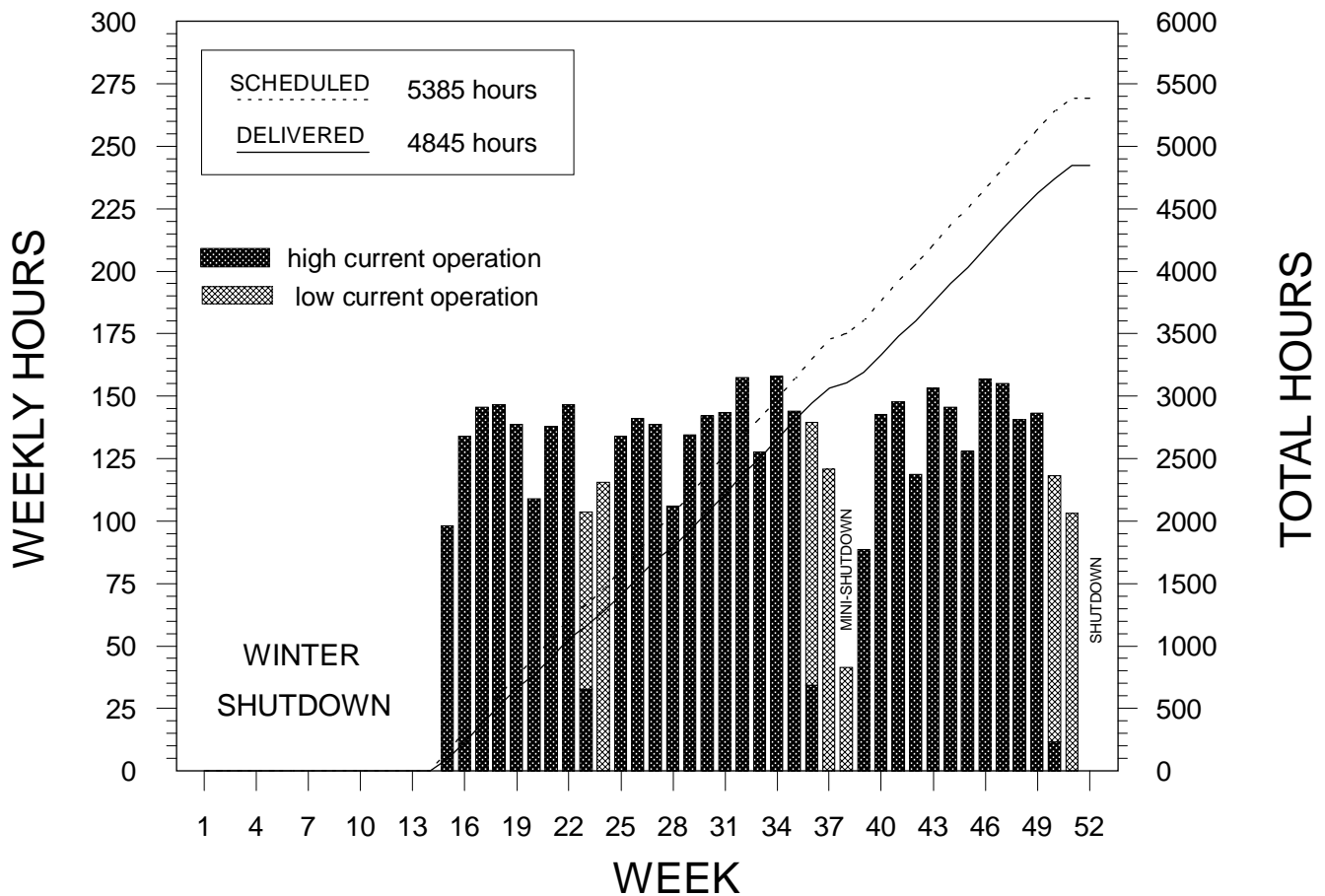
Fig. 182. Operational hours for 2002.

173
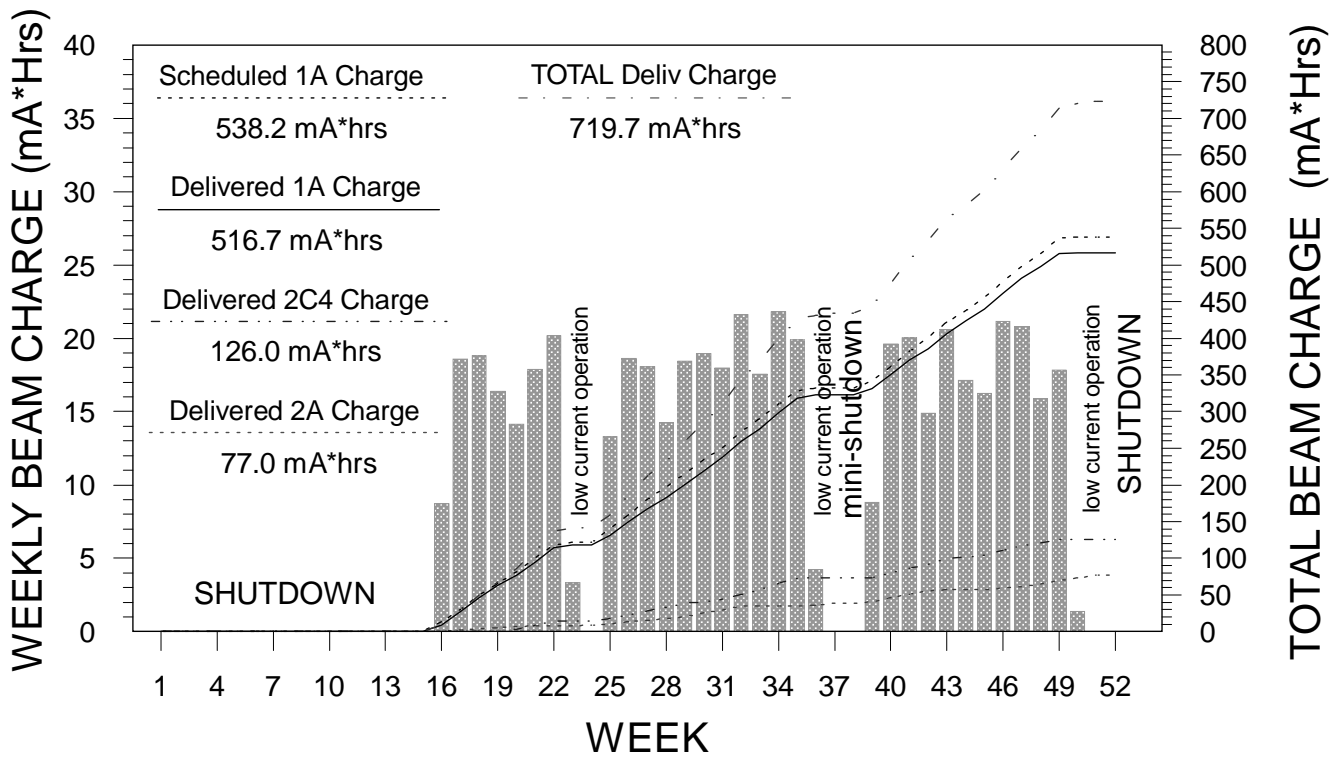
Fig. 183. Beam delivery for 2002.
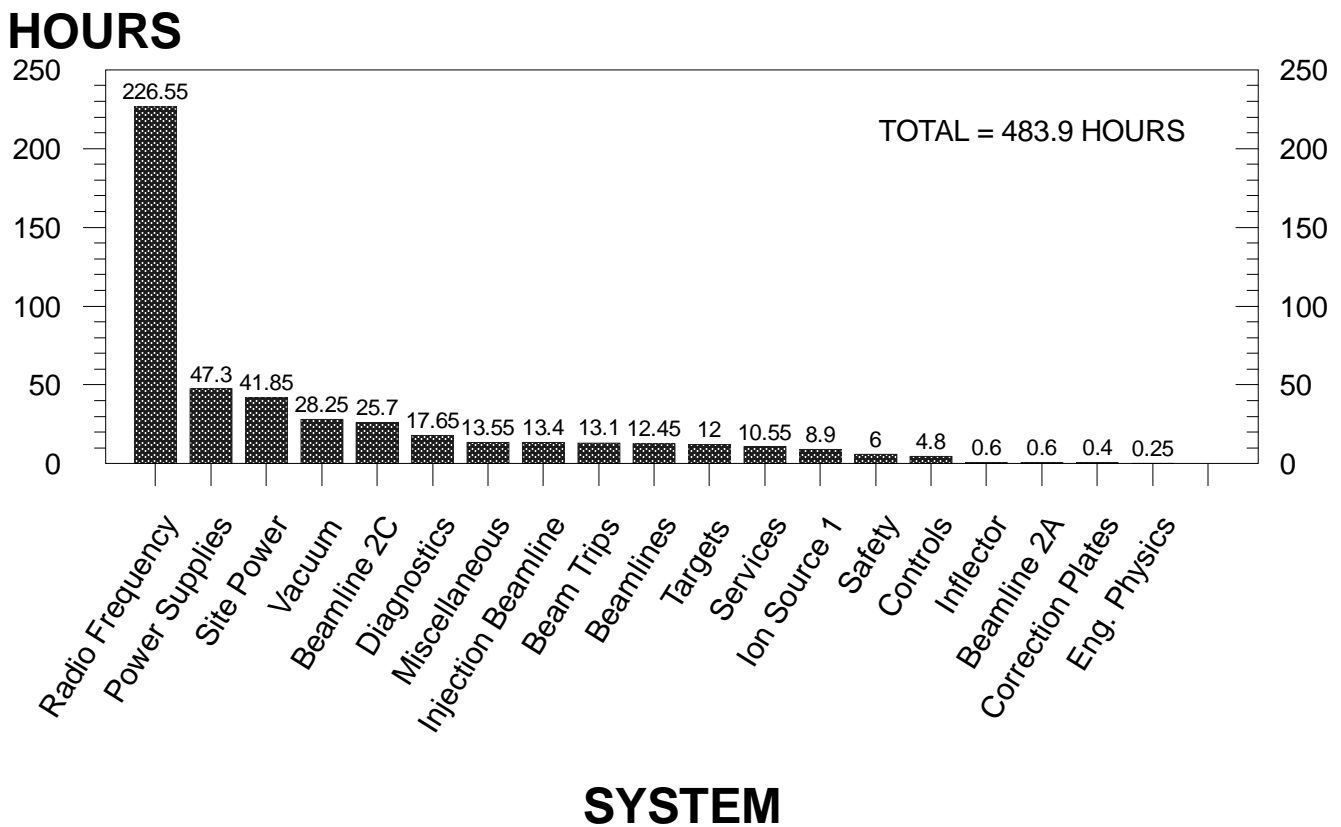
Fig. 184. Cyclotron downtime for 2002.

174

Table XIX. Operational record for 2002.[*]

	Scheduled hours	Actual hours
Cyclotron off:		
Maintenance	454.0	485.20
Startup	243.0	210.05
Shutdown	2,562.0	2,560.00
Other	18.0	25.60
Cyclotron downtime	0.0	483.90
Overhead	73.5	126.05
Totals	3,350.5	3,890.80
Cyclotron on:		
Development	174.0	125.00
Cyclotron tuning	419.0	162.75
Beam to experiments	4,792.0	4,557.45
Totals	5,385.5	4,845.20

Actual/Scheduled = 4845.2/5385.5 = 90.0% availability

	Scheduled hours	Actual hours
Beam to experiments:		
1A Production	4,007.0	3,834.40
1A Development/tuning	0.0	17.35
1A Down/open/no user	266.5	268.50
1B Production	323.0	63.10
1B Development/tuning	0.0	3.75
1B Down/open/no user	196.0	370.35
Total 1A+1B production	4,330.0	3,897.50
2A2 Production	3,820.5	2,868.50
2A2 Development/tuning	0.0	24.00
2A2 Down/open/no user	972.0	1,664.95
2C1 Production/tests	617.5	155.05
2C1 Development/tuning	0.0	5.45
2C1 Down/open/no user	604.0	913.85
2C4 Production/tests	3,346.0	2,811.00
2C4 Development/tuning	0.0	9.05
2C4 Down/open/no user	225.0	663.05
1A Beam charge (μAh)	538,160.0	516,704.00
2A Beam charge (μAh)	96,582.0	76,973.00
2C4 Beam charge (μAh)	147,810.0	125,987.00

[*] There was no BL4 production this year and the polarized source (I4) was not used.

Table XX. Beam to experiments for 2002.

Experiment *	Channel	Scheduled		Delivered	
		h	μA h	h	μA h
614	M13	3332.0	456650	3212.15	434579
768	M15	148.0	19470	133.00	18099
775	M20	127.0	17550	107.95	13766
782	M15	119.0	15470	111.50	15261
791	M15	447.5	60695	415.90	53033
814	M15	127.0	16740	107.95	14703
814	M20	127.0	17780	134.80	18725
822	M11	1182.5	159415	1098.90	151652
822	M15	208.0	28890	189.15	25026
834	M20	265.0	35700	237.60	32403
842	M9	146.5	19505	141.95	19819
843	M20	69.0	9660	69.20	9614
846	M15	127.0	17780	129.25	17566
846	M20	127.0	16740	107.95	14703
847	M15	392.0	52110	416.10	47532
848	M15	127.0	17780	137.75	19578
848	M20	162.0	22680	173.10	24560
865	M15	150.0	21000	150.20	20882
877	M9	127.0	16740	107.95	14703
883	M20	254.0	34290	285.60	31049
888	M9	193.5	25155	160.35	18501
890	M20	127.0	16510	126.25	16226
891	M15	342.5	45675	329.95	44612
891	M20	119.0	15470	111.50	15261
894	M15	115.0	16100	109.00	13595
894	M20	127.0	17780	136.10	18484
895	M15	277.0	38780	284.25	38531
895	M20	81.0	11340	73.75	10213
898	M20	138.0	15410	117.55	14728
912	M15	150.0	21000	138.50	18059
912	M20	219.0	30660	214.00	27144
914	M15	150.0	21000	144.55	21018
915	M15	127.0	17780	136.10	18484
916	M20	343.5	46155	292.40	36499
917	M15	128.0	17920	131.05	18018
917	M20	271.0	37940	265.70	39474
918	M15	121.0	16940	121.15	18456
930	M9	638.0	85360	606.80	82645
931	M15	138.0	17940	113.45	15007
931	M20	115.0	16100	114.85	15900
932	M9	277.0	38780	285.00	39607
933	M20	150.0	19500	145.15	18683
934	M20	148.0	19470	133.00	18099
935	M9	546.0	74960	506.65	71339
936	M15	150.0	21000	132.05	17998
937	M20	146.5	19505	141.95	19819

Table XX (cont'd.)

Experiment *	Channel	Scheduled		Delivered	
		h	μA h	h	μA h
938	M20	11.0	1540	11.75	1387
939	M20	277.0	38780	267.75	35625
940	M20	300.0	42000	304.00	40726
942	M20	128.0	17920	131.05	18018
943	M9	254.0	35560	273.85	38062
943	M15	138.0	15410	117.55	14728
944	M15	150.0	21000	154.55	20920
G∅	M9	115.0	16100	109.00	13595
ISAC RIB†	2A2	3820.5	96582	2868.50	76973
ISOPROD	2C4	3346.0	147810	2811.00	125987
PIF	2C1	557.5	0	138.85	0
PIF	1B	323.0	0	63.10	0
P.THERAPY	2C1	60.0	0	16.20	0

* See Appendix D for experiment title and spokesman.

† Total proton beam on target for all ISAC RIB experiments and tests.

Winter Shutdown

BL1A shutdown activities began in early January with the removal of many shielding blocks from the meson hall to a temporary storage location by the Machine Shop. The original work schedule slipped a little at first because of an unanticipated need to quickly put together two shipments of radioactive waste for disposal and then later from obstacles encountered along the way (welded steel shielding, additional water leaks, new crumbling blocks). The extent and complexity of some of the BL1A tasks, most of them in high radiation fields, resulted in some higher than usual doses for a few workers. Three each received between 5 and 7 mSv of a total summed shutdown dose of 150 mSv that was distributed among 110 workers.

Jobs undertaken in the meson hall by the Remote Handling (RH), Beam Lines (BL), Vacuum, and Diagnostics groups included removal of the front-end elements of the M8 channel; replacement and reconfiguration of shielding (new shielding was designed to fill the M8 void as well as to replace some crumbling blocks); *in situ* repair of three separate water leaks on the 1A triplet; repair of M20Q1 and M20B1 water leaks; a rebuild of the troublesome M13 beam blocker; maintenance of the 1AT1 and 1AT2 targets and their water packages; repair of 1AM8 and 1AM10 monitors; the repair of vacuum leaks at 1AVA8 and M13VA1; and the replacement of the air cylinders of 1AWVA2.

In the vault the cyclotron lid was raised toward the end of January. Radiation fields were about 10% higher than last year (as predicted from the previous beam delivery schedule). As much as possible, remote-handling equipment was used to minimize personnel dose exposure. Apart from the usual heavy schedule of routine diagnostics MRO (including work on the extraction and pop-in probes), a lot of time was spent doing centre region work where, fortunately, the fields were reasonably tolerable. This included the installation of a water-cooled beam absorber in LQ1's detachable quadrant (to help maintain cool centre region temperatures during higher intensity injection); the repair, relocation, and addition of several thermocouples, and the refurbishment of Q1 and Q3 correction plates. At the tank periphery, work included blanking off the unused centring probe feedthroughs and the tricky job of replacing the seals on the gate valve of extraction 1.

There was also a large number of additional jobs and MRO work around the site, not the least of which was the construction and installation of the BL2A3 leg and east target station to eventually provide continuing RIB to ISAC during changeovers of the west target.

Beam Schedule 101

Although the first week of production saw quite a bit of downtime with the site UPS and excessive rf sparking, the performance for these 24 weeks was not too unreasonable with a cyclotron availability of

89%. Other problems included a vacuum failure of the ferrofluidic seals of the 2C extraction probe. These were replaced during a week (originally high current) rescheduled for septum magnet repairs (see below). Downtime totalled 367 hrs with rf being responsible for 190 hours (52%). Power supplies, site power, and vacuum problems (chiefly with the power supply of the main magnet (MMPS), UPS and B-20, respectively) accounted for another 98 hours or 27% of the total downtime.

BL1A usually ran $140\,\mu$A to Be targets at 1AT1 and 1AT2, but saw currents as high as $168\,\mu$A during some development shifts. The charge delivered was $322\,$mAh or 93% of that scheduled. There were minor meson-hall problems, that included continuing intermittent trouble with the M13 beam blocker, but the main setback lay with the septum magnet. In the middle of May, it developed a rapidly growing water leak that prompted an exploratory investigation to see if it could be easily repaired. When it became apparent this was not possible, the water was valved off while an alternative *in situ* repair was pursued. Experts came in mid-June to inject a special sealant into the cooling lines, but on the first two attempts the patch failed as soon as the septum was powered. The third and final attempt saw the septum briefly fully powered immediately after the cooling lines were infused with an injection of the epoxy-clay matrix sealant. This allowed the sealant to penetrate and more thoroughly block the crack that had presumably opened under the strain of the huge electromagnetic forces when the magnet was powered. The septum was back in operation following pressure and power tests a week after this final repair attempt, but started to leak slowly after a few days. Five weeks later at the end of July the water was turned off for good after the leak had steadily grown to about $80\,$l/h, leaving M11 high and dry. The leaking water was well contained, ultimately draining into the active sump. Toward the end of the high-intensity period there was also a failure of the X1 current read-back for which the front-end BL1A toroid signal was substituted.

BL2A took currents from 5 to $45\,\mu$A on two different targets (Ta and TiC), running for 1,727 hours or 70% of its scheduled time and receiving $39\,$mAh or 76% of its scheduled charge. Target trouble and ISAC energy changes were the chief sources of off-time. BL2C4 got off to a slow start because of target float problems but went on to irradiate two rubidium targets for processing by Nordion, running for 1,688 hours or 80% of its scheduled time and receiving $39\,$mAh or 82% of its scheduled charge. Currents averaged about $43\,\mu$A. There were no problems with the corrective steering magnet that continued to be used to compensate for a slightly misaligned STF, but there was some anxiety when it was found that only one of the three new foils was suitable for prolonged high-intensity beam – the other two were found to be somewhat deformed with little or no beam on them. In addition to the above, there were three PT sessions (BL2C1/74 MeV) during which 6 patients were treated and three PIF runs, one at the beginning using 2C1 only (70 and 116 MeV) and the others in June and September using BL1B as well (500, 350 and 200 MeV). The latter provided some cool-down (along with the following PT run) prior to the one-week maintenance period starting mid-September. BL2C1 currents were 5 nA or less and BL1B currents less than 1 nA. There were also three development shifts that utilized 92% of their scheduled 48 hours to improve $300+\,\mu$A equivalent tunes with as much as $275\,\mu$A total extracted down the three high-current proton lines. Some time was also allotted for OPS training during which operators had time to practice machine and beam line tuning and calibrations or to continue with development work.

Fall Mini-Shutdown

This week for extended maintenance work had a reasonably ambitious schedule. BL1 work started when PIF finished in 1B; vault work started a week later once PT had finished. The total shutdown dose was under 5 mSv with no one exceeding 1 mSv. Some of the group's jobs were: Diagnostics MRO (extraction probes 1 and 2A, beam line monitors including 1AM8, fast shutter); Beam lines (repair M13BB and installation of a slit box in M13 F2, removal of 1BBB2 latch mechanism and repair 1BBB3 vacuum leak); Power supplies (MMPS relay and hose MRO, and repair of radiation-damaged feedback wiring of the main magnet); Vacuum (tank cryopump MRO, installation of a turbo pump on cryoline and swap B-20, extensive beam line leak checking, change 2A O-rings near 2AVM1); Services (install new rf room water filter, compressor MRO, ISIS LCW pump MRO, Al ALCW system control valve MRO) and rf (investigate sparking, install and test new combiners, build new GAT control software, check out ISIS rf pickup from tank).

The vault was ready in time for tuning up the cyclotron as scheduled but extraction down BL1A was delayed one day to accommodate last minute work. There were a few lingering details from the shutdown affecting subsequent operation: the M13 beam-blocker worked fine as a blocker, but lost its dual purpose as a beam line gate valve; M20Q1 developed a 1 l/h water leak; and a 1AQ9 over-temperature fault was not found along accessible interlock wiring. Therefore it would be necessary to uncover that quadrupole to determine the exact cause of the fault. In the meantime 1A would have to remain tuned with 1AQ9 off – not

a serious issue because it works in concert with the septum to provide M11 beam. Finally, 1BBB3 needed to be removed to repair a leaking bellows. This made it necessary to run with the 1B area secured until the blocker was fixed. Because the lid was not raised, there was no opportunity to replace the two dud X2C foils. A viewing through the periscope indicated the whiskers were not nicely aligned in the two suspected foils and that the heavily used one remained looking fairly good. After the usual target scans and radiation surveys, the beam intensity was increased over the next two days so that BL1A and BL2A2 were receiving their nominal currents. A few days later 2C4 was slowly brought up to $40 \,\mu A$.

Beam Schedule 102

A Thanksgiving Day failure of the motor driving the main magnet booster pump, an earlier power bump, and later problems with the BL2C vacuum were the chief downtime events in an otherwise productive schedule. The new rf ground-arm-tip (GAT) control system allowed the resonators to be fine-tuned to reduce considerably both leakage and sparking, and was the main contributor to a reduction in downtime from 15 hours per week in the previous beam schedule to 9 hours per week in the latest one. Downtime totalled 117 hrs with rf being responsible for (only) 31% or 37 hours. BL2C vacuum problems accounted for another 25 hours or 21%. For these 13 weeks the cyclotron was available for 1,740 hours or 92% of the scheduled time (1,882 hours), and delivered as much as $230 \,\mu A$ total to the three operating high-current proton lines before ending the schedule with two weeks of low-current production for PIF and 2A only. Again the rf booster was on most of the time helping to maintain a decent cyclotron tune. Three development shifts focused mainly on high-current extraction ($\sim 350 \,\mu A$ equivalent) and made progress in extending those good tunes to the higher-intensity domain. Probe scans done during the last development shift found that the rf dee voltage was 5 to $10 \,kV$ lower than its read-back value (as well as compared to previous scans). This helped to explain some high-current-development limitations and probably also contributed to the lower spark rate.

BL1A ran for 1,453 hours or 97% of its scheduled time, receiving $194 \,mAh$ or 94% of its scheduled charge. The current was normally around 135–$140 \,\mu A$, but was lower toward the end of the run because of a vacuum leak in the 1AT2 area. The M11 channel remained out of commission because of the septum failure and the M9 channel saw little use because of an SCS fridge failure. Water leaks were again a concern as a $1 \,l/h$ drip from M20Q1 grew to a $10 \,l/h$ spray. Other leaks developed in M13Q5 ($\sim 2 \,l/h$) and M13B1 ($\sim 5 \,l/h$). In

mid-November the 1AT2 Be target was determined to be disintegrating after years of use and a new one was selected. BL1A high-current operation wound down in early December, followed by a two-week, low-current schedule that initiated the cool-down period prior to the winter shutdown. This included a very limited amount of BL1B operation for PIF experimenters for whom the 1BBB3 beam blocker had been repaired and reinstalled in October.

BL2A2 ran for 1,166 hours or 85% of its scheduled time, receiving $38 \,mAh$ or 83% of its scheduled charge. There was no proton beam during a two-week ITW target change but $45 \,\mu A$ delivery continued up to the end of the beam schedule as 2A became the sole high intensity user for the last few weeks of beam delivery. There were two instances, a few hours apart, when an output glitch in the 2AVB1 dipole power supply (traced to the local/remote electronics and since repaired) caused not only the 2A tunnel BSMs to alarm but also tripped the ISAC Safety-Critical BSMs and NMs on the ground floor above the electrical room. This was further investigated and quantified during a beam development-shift and found to be non-hazardous should similar events recur.

There were also improvements in the X2A software to eliminate R-Z reproducibility problems that have caused radiation trips in the past. Apart from such spurious trips and some power bumps that were particularly hard on 2A2 because of a faulty UPS unit, beam production was reasonably steady for the scheduled period. However, RIB production from the ITW dropped 2 to 3 orders of magnitude toward the end of the running period before the target somehow rejuvenated itself in the last hour of operation.

BL2C4 ran for 1,126 hours or 90% of its scheduled time, receiving $52 \,mAh$ or 89% of its scheduled charge for an average delivery of $46 \,\mu A$. Most of the 2C4 specific downtime was due to two vacuum leaks, the first in a sliding seal where the corrective steering magnet was installed last year and the second at the indium seal just after the fast valve. The latter occurred a few days before the start of the PIF run for which the 2C1 line was heavily subscribed and therefore required immediate attention. Radiation fields in the area were fairly intense and there were significant space constraints. Some cool-down time was scheduled, and remote handling and beam line experts were involved as well as volunteers in the successful repair that cost about $10 \,mSv$ total dose. It was assumed that the faulty and aging extraction foils were responsible for compromised tunes that gave rise first to somewhat elevated collimator temperatures and eventually to some beam glitches that overheated the vacuum seal. BL2C1 was used for PT (3 patients one session, the other ses-

sion cancelled) as well as for PIF experimenters at 70 and 116 MeV. As with all of the other PT sessions this year, the high-intensity source was on-line so the ISIS pepper pot was required to limit the injected beam current during times of patient treatments.

Most cyclotron systems were turned off by the weekend before Christmas just as holidays and the winter shutdown were beginning. The year then ended as it had begun with the removal of about six dozen large 1A shielding blocks to temporary storage by the machine shop as preparations were made for the next stage of BL1A and meson channel refurbishment and repair.

Apart from the many tasks associated with beam delivery, operators were involved with fire alarm system expansion, card access system installation, Autocad drawings, training and documentation improvements, equipment repair, computer upgrades and maintenance, beam transport modelling, etc., as well as actively helping out with many shutdown jobs, particularly in the areas of remote handling and diagnostics.

CYCLOTRON DEVELOPMENT

Centre Region Upgrade

During the winter 2002 shutdown a great deal of effort was dedicated to improving the cyclotron centre region. Problems were being caused by excessive beam losses on uncooled surfaces in the first few turns. Radial beam losses on the vertical walls of the centre-region rf resonator quadrants were overheating the attached stainless steel reinforcing ribs. At high beam intensities the rib temperature rose above 120°C, triggering protection trips. To solve this problem a water-cooled beam absorber was installed immediately after the injection gap to intercept a large portion of the beam that had previously been hitting the quadrant walls. To install the absorber, the centre region detachable quadrant 1 (Q1) was removed from the cyclotron. Figure 185 shows a centre region view looking towards Q1 before the beam absorber installation. The beam absorber attached to the vertical wall of Q1 is shown in Fig. 186.

Next the quadrant 1 correction plates (CP) (see Fig. 187) were removed from the tank. A detailed inspection of the plates showed a number of deficiencies:

1. The upper tray, which houses the plates, was bent 0.3 in. down toward the median plane of the cyclotron.
2. Evidence of the beam hitting plate 5, one of the plates closest to the median plane, was observed (see Fig. 187).
3. The plates had been made from thin stainless-steel sheet and required realignment.
4. A few ceramic insulators were cracked and/or broken.

5. Some of the insulators near plates exposed to the beam were spattered with metal.

Repairs were made during the shutdown. All damaged insulators were replaced, and the plates were straightened and reassembled. The correction-plate trays were reinstalled and realigned to specifications.

Fig. 185. View into Q1 from slightly above the median plane. The correction plate assembly is on the left.
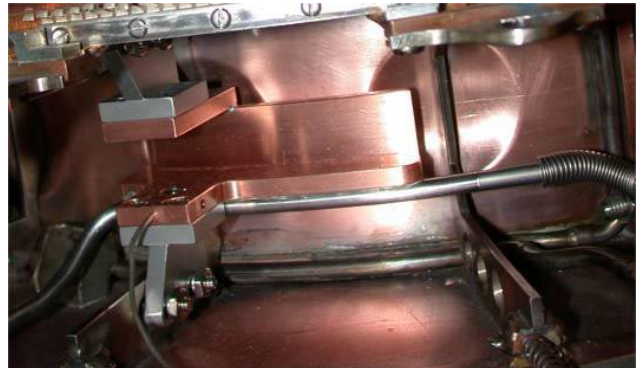
Fig. 186. Cooled beam absorber installed in Q1.
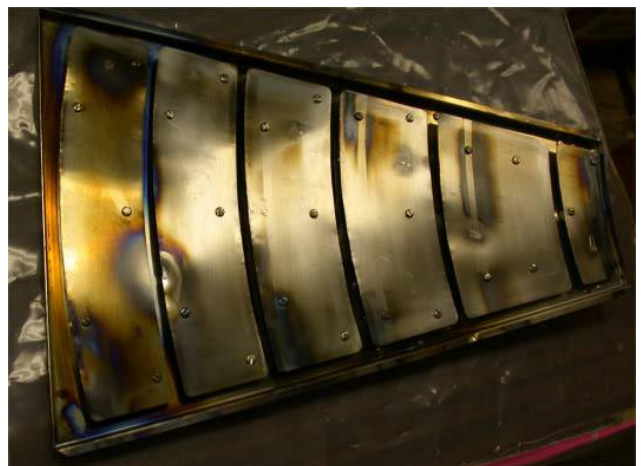
Fig. 187. Q1 correction plates. Notice beam damage spot on the left.

Fig. 188. Protruding M-foil, damaged by beam.

Because similar problems in quadrant 3 were suspected, those plates were also realigned. However, complete servicing had to be postponed until the next shutdown because of time limitations and dose constraints.

Then it was found that the M-foil, designed to provide a good rf connection between adjacent resonators (see right-hand side of Fig. 185), was sticking up into the dee gap. There it was exposed to the beam that caused melting (see Fig. 188). To prevent this from happening again, the excess foil material was trimmed away. Finally, to improve temperature monitoring in the centre region, four new thermocouples were installed and two old thermocouples were relocated.

Observations after the shutdown with the beam back on showed a dramatic decrease in centre region heating. Figures 189 and 190 show the temperature response of the Q1 stainless-steel ribs to rf power and to beam currents of about $200\,\mu$A before and after the installation of the beam absorber. Before shutdown the beam losses heated this rib to about $100°$C. After shutdown the beam did not affect it, and the $8°$C temperature rise was caused by rf losses only.

BEAM DEVELOPMENT

Cyclotron Beam Dynamics Development

The 2002 cyclotron beam dynamics activities focused on increasing the current extracted from the cyclotron. By 2005 it is anticipated that the ISAC target stations will be operating with target currents of $100\,\mu$A. If a second, independent ISAC target facility is eventually constructed, the current requirements of ISAC would increase to $200\,\mu$A. In order to produce these beams without decreasing the beam available to non-ISAC users, the maximum extracted beam from TRIUMF would have to increase from $\sim$$200\,\mu$A to 300 or $400\,\mu$A. During the past year cyclotron beam dynamics studies have focused on extracting $300\,\mu$A
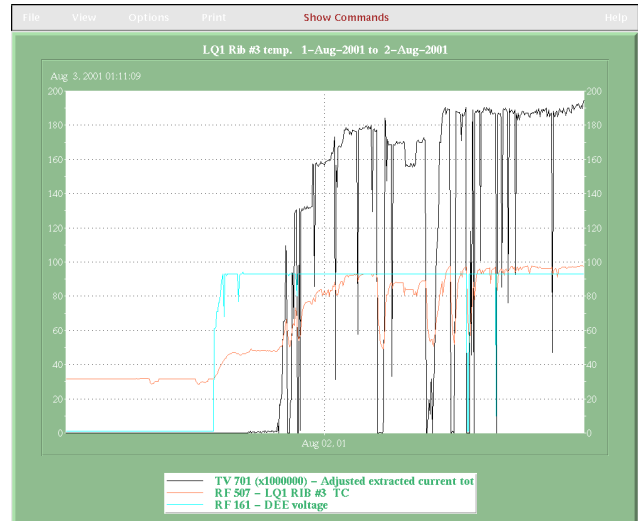
Fig. 189. Temperature response of the Q1 stainless steel ribs to rf power and to beam currents of about $200\,\mu$A before the installation of the beam absorber.
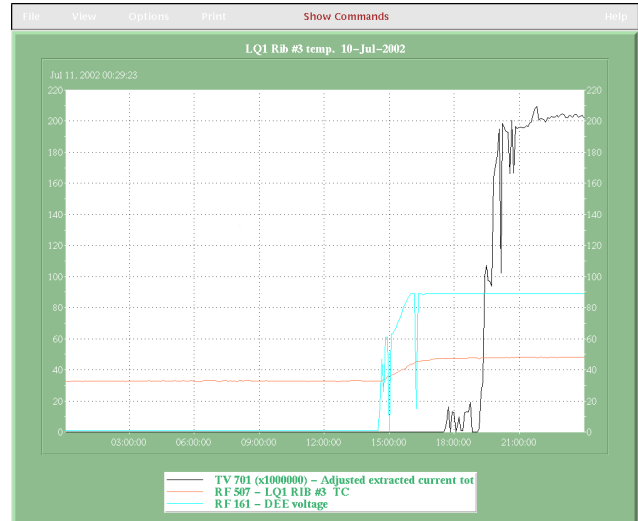
Fig. 190. Temperature response of the Q1 stainless steel ribs to rf power and to beam currents of about $200\,\mu$A after the installation of the beam absorber.

reliably and stably, and on demonstrating the feasibility of $400\,\mu$A extraction.

At the end of 2001, two major roadblocks to $300\,\mu$A extraction had been identified. First, at high current levels radial beam losses on the vertical walls of the centre region rf resonator quadrants were causing overheating. Second, cyclotron transmission at $300\,\mu$A equivalent current appeared to be limited to 50%, substantially lower than the 63% transmission typically obtained with $200\,\mu$A production tunes and the 62% that had been obtained with a $250\,\mu$A development tune. Both of these obstacles were overcome during 2002. In addition, equivalent currents as high as $380\,\mu$A at 10% duty cycle were eventually extracted with greater than 60% cyclotron transmission.

The rf quadrant heating problem was eliminated by the installation of the water-cooled beam stopper to intercept most of the beam that previously was being lost on the quadrant walls. This device was installed during the 2002 winter shutdown and successfully tested with beam after operations resumed. The heating problem was completely eliminated, and the stopper had no discernible effect on the cyclotron transmission to extraction.

After devoting several development shifts to improve the ISIS/cyclotron tunes, on July 30 we extracted $275\,\mu$A at 100% duty cycle with 62% cyclotron transmission for three hours. We were then able to increase the equivalent current extracted to $300\,\mu$A at 90% duty cycle with 61.5% cyclotron transmission for a period of 2 hours, and deliver it to experimenters. The reduction in duty cycle was dictated by the $270\,\mu$A combined current limit on the external beam lines. No thermal problems were encountered, and the beam ran quite stably during this period. We then went on to extract $325\,\mu$A equivalent current at 75% duty cycle and 60% cyclotron transmission, and $350\,\mu$A equivalent current at 40% duty cycle and 57% cyclotron transmission for periods of approximately 1/2 hour each. Operation at $350\,\mu$A appears to be an achievable goal, although some additional centre-region cooling may be required for operation at full duty cycle.

Subsequent beam development shifts were devoted to duplicating and refining the above tunes. Initially it was found that the $300\,\mu$A results could be duplicated on a regular basis; however, it was impossible to duplicate the $350\,\mu$A results. Above $300\,\mu$A, increases in the ion-source current were accompanied by decreases in transmission, preventing an increase in the extracted current. The reason for this is still not completely understood, but part of the problem appeared to be insufficient rf dee voltage. The phase acceptance of the cyclotron increases as the rf voltage is increased, and higher phase acceptances, and hence higher rf voltages, are required at the higher currents where the bunching efficiencies are lower. An analysis of the rf power input to the dees and of the beam's time of flight as measured on high-energy probe HE2 indicated that the actual rf voltage varied throughout 2002, possibly due to the large amount of rf tuning required to reduce sparking. During much of the year, the actual rf voltage was several per cent lower than the voltage being displayed in the control room. Once this was discovered, the rf power was increased to raise the actual rf voltage to $\sim$90 kV, its nominal value prior to 2002. On December 20, after re-optimizing the centre-region correction plates and trim coils, we were able to extract $380\,\mu$A equivalent current at 10% duty cycle with 64% cyclotron transmission. An attempt to raise the duty cycle at this current level was thwarted by lack of rf power – a problem that has now been solved. Although this initial result appears promising, additional work will have to be done on this tune in order to reduce the ISIS/tank spills to levels that would allow operation at full duty cycle.

It is anticipated that cyclotron beam dynamics for 2003 will continue to concentrate on high-current development. Emphasis will be placed on refining and understanding the behaviour of the high current tunes at increased duty cycles. Major goals will be reproducibility and stability.

ISIS Beam Dynamics Development

The high-intensity CUSP ion source and injection line continued to operate well for the past year. The major development activity undertaken was trying to model its optics better. The beam profiles were measured periodically, with 13 wire scanners along the beam line. As an example, Fig. 191 shows the 2σ beam widths measured for dc currents of 345 and 575 μA. It can be seen that the beam widths all stay within 0.4 in. diameter, except near the cyclotron where the beam is bunched, resulting in strong space charge. In the horizontal periodic section, the beam is seen to be well-matched, because it is of quite uniform size.

Comparison of the two currents in the figure shows the effect of space charge on the beam. Because it uses the space-charge-loaded equations of motion of the second moments of the beam, the computer code TRANSOPTR can be used to determine the magnitude of the space charge neutralization, if any. Three wire scanners in the horizontal periodic section were used to measure the horizontal and vertical rms beam sizes for a number of different settings of the periodic section quadrupole strength at a beam current of 686 μA.
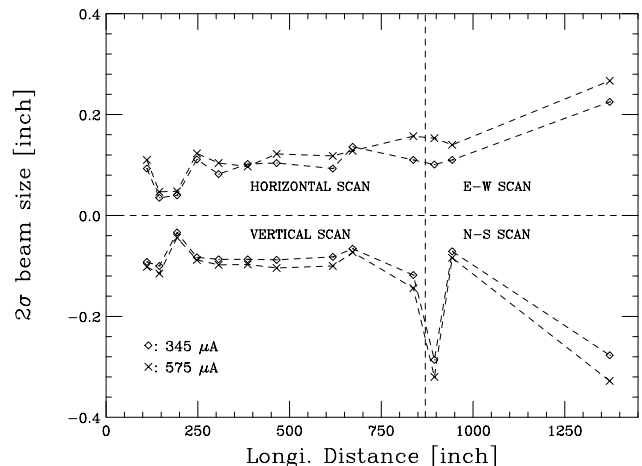
Fig. 191. The 2σ beam sizes in ISIS measured for dc currents 345 and 575 μA. The data points are the measurements. The dashed line is only intended to guide the eye.

These sizes were used in fitting the initial beam parameters and the effective current. In this way, it was found that the (4 rms) beam emittance is $4.3\,\pi$mm-mrad (i.e. $0.11\,\pi$mm-mrad normalized) in both planes, and the effective beam current is $580 \pm 70\,\mu$A. The size of the error is related to the fact that even at $686\,\mu$A, the effect of space charge is to increase the matched 2 rms beam size by only 0.5 mm, from 2.3 mm to 2.8 mm.

Our conclusion is that there is little, if any, neutralization.

RADIO FREQUENCY SYSTEMS

RF Operation

The total rf downtime for the year was 226 hours, 25% higher than last year. Although 80% of this downtime was charged to a combination of sparking and crowbars, it is really the recovery from those events that caused most of the downtime. In the September shutdown a new ground-arm-tip control system was installed and an extensive program of resonator-tip tuning was carried out. Also, in the rf control system, the timing sequence for spark recovery was changed and a software problem was discovered and fixed. As a result the rf downtime was reduced from 8 hrs/wk before the shutdown to 3 hrs/wk after the shutdown. Further work will be done in the January, 2003 shutdown to better diagnose the sparking problem.

Impurities in the LCW cooling system blocked the filter in the line feeding the rf room. The filter was replaced with a finer filter and has been operating reliably since September. Ground-loop interference, which caused unstable performance in the resonator water-pressure regulating system, was investigated and remedied.

RF Refurbishing

A substantial effort was dedicated to rf refurbishing. A 500 kW resistive load was commissioned during the winter shutdown. It is an essential tool for the high-power tests of the rf combiners and for troubleshooting the amplifier system. During the September shutdown, rf combiner #1 was tested to a power level of 460 kW and installed into the rf system. It operated reliably for the rest of the beam run. RF combiner #2 was tested to full power as well and is ready for installation in the next shutdown. All 3 operational combiners were retuned to best matching and isolation values. This reduced the VSWR from 1.3 to 1.15 in transmission-line interconnections within rf room and isolation of the ports from -30 db to -70 db. Two directional couplers were incorporated in the IPA output transmission line to allow tuning for better matching to the rf splitter and easier system troubleshooting. Three water-cooled capacitor stations, which are part of the transmission line matching section, are very difficult to service, especially when a water leak occurs. It was decided to improve their design. An upgraded set of drawings was issued and all the parts were manufactured for installation during the next shutdown. The major improvements were the installation of quick-disconnect water connection, quick-disconnect capacitor electrical connections and the addition of flow interlocks in the cooling system. A multiplexing and diagnostic system was developed that provides first-event detection from as many as 24 voltage pickup probes along the rf power-feed chain. It is a very useful tool for troubleshooting during sparking and rf trips. The system is scheduled for commissioning in spring, 2003.

Cyclotron RF Control

The ground-arm-tip (GAT) motor controller has a long history of unreliable operation. There has been a bug in the system from the beginning that, under some circumstances, will cause all resonator tips to move to maximum travel when only one resonator was selected to move. Several modifications have been made by several people, but this problem was never resolved. As a consequence, movement of the resonator GATs has been kept to a minimum. In an attempt to reduce the sparking rate, which became serious this year, it became evident that we required a more reliable GAT controller.

The GAT motor controller was replaced with a PC-based system. This work was done in collaboration with Jan Miszczak of Warsaw University. With this new system, the GAT motors are energized only during adjustment while under software feedback control. This improves the reliability of the motors and of the power elements in the controller circuits. The relevant data of the GATs and their drive system are stored and retrieved in a relational database. In addition to local control, the system is also connected to the site-wide Ethernet, and the GAT positions can be accessed via an Apache server running in the system.

RF Support

The RF group was also involved in the following major projects in ISAC-I, which are reported in the ISAC section.

1. Maintenance and operation of the ISAC linac.
2. Development of a phase measuring system for the whole ISAC rf system.
3. DTL fine tuner upgrade.
4. DTL power coupler protection and restoration.

CYCLOTRON PROBES

In the fall of this year, we bade a fond farewell to George Mackenzie. "Congratulations on a long and distinguished career! It has been a pleasure working with

you; thank you for all of your help. Now, enjoy your retirement!".

In addition to normal MRO activities and ISAC work, there were a number of major repair jobs completed this year. Good progress was made on the HE probe refurbishment design. The majority of the replacement standard beam line monitor-box gas packages have been prepared for installation; some of these were installed. This year, non-routine repairs were done on the following devices: EX1, 2C1 fast shutter, 2CVM1 MWIC and the ISAC IMS:DB0 Faraday cup.

For more details, the Diagnostics group biweekly meeting notes are available electronically via the Operations CYCINFO information service on the site computer cluster (accessible also through the TRIUMF home page on the WWW). The winter cyclotron shutdown activities, including the report on the ISAC DB0 installation, are summarized in detail in the Diagnostics group meeting notes of May 24, 2002. The fall shutdown report is included in the meeting notes of October 11, 2002.

Probes MRO

Extraction probe EX1 was removed for routine service in February. The L-arm latch-pin design was changed to the same style as used at EX4. It was removed again in September to repair a short circuit on the beam-current pick-up that occurred at the end of beam schedule 101. A very small piece of aluminum swarf was found to have caused the short; new track insulators were installed. The drive tapes and cables were replaced, and the ball-screw disassembled and cleaned.

The air solenoid valve for PIP#4 was replaced and a proper speed control was installed. The valves for the other PIPs will be serviced in future shutdowns.

The ferrofluidic feedthroughs (f/t) were removed from the two decommissioned dee-gap centring probes; blank off flanges were installed. The planned inspection of the slits and flags f/ts was not done this year, but will be done in January, 2003.

Monitor MRO

All vault and standard beam line monitors were serviced during the shutdowns. The monitor refurbishment program was essentially completed. All mechanical assemblies have been built. Monitors 1VM4.6, 1AM6, and 1AM7 were replaced, and replacement of the remaining monitors will begin in January, 2003. New scanning wire monitors were installed in beam line 2C4 and 2C5. The 2CVM1 MWIC was serviced for the first time since its installation: the air solenoids were replaced.

As with all MWIC monitors close to the cyclotron, the gas package seals are susceptible to radiation damage. With the advent of new higher-gain electronics, it is now feasible to operate these devices without gas amplification. Consequently, 2CVM1 was modified to run without gas. It is planned to modify monitors 1VM1, 1VM2, 4VM1, and 4VM2 to use the same advantage and eliminate the need for semi-annual replacement of gas package seals.

The 2C fast shutter seized during operation in late August and was temporarily repaired to permit operation to 2C1 until the scheduled shutdown in September. The assembly was inspected during the shutdown, and found to be in satisfactory condition. A few design improvements have been made to facilitate maintenance, and a spare is being manufactured.

The 1AM8 monitor gas seals leaked due to radiation damage after only six months of operation. A recent service modification has left a shorter park distance from the beam elevation. This monitor becomes another candidate for use without gas. 1AM10 became stuck when a nylon spacer became radiation damaged. The spacer material was changed to brass. 1AM8 and 1AM10 will be refurbished when time permits.

A new MWIC was provided for use of PIF experiments in beam line 2C1/1B.

VACUUM AND ENGINEERING PHYSICS

Vacuum

The vacuum systems of the cyclotron, cyclotron beam lines, ISAC-I targets, and ISAC-I beam lines have been functioning well for beam production during the year. Vacuum problems encountered were dealt with in a timely manner with negligible impact on the beam production.

The ISAC-I east target vacuum system was built and successfully commissioned.

In the cyclotron three instances of problems occurred with the B-20. These were all related to the regenerators on the 20K stage. A new Varian 551 turbo pump was installed on the cryoline connecting B-20 cryogenerator to the cyclotron. This pump replaced the original diffusion pump to shorten the turn-around time during cryogenerator defrosts.

In the beam line vacuum system a large vacuum leak occurred in the 2C4 line because of beam-induced melting of the indium seal caused by an anomalous beam configuration that, in turn, was caused by a deteriorating stripping foil. This seal was replaced. A number of vacuum leaks were diagnosed in beam line 1A. These are scheduled to be fixed during the spring shutdown.

The rest of the group activities concentrated on routine MRO.

Engineering Physics

The Engineering Physics group leader retired this year. In light of this event, some of the group's responsibilities have been assigned to other groups. The correction plates are now serviced by the RF group and responsibility for the inflector/deflector has been moved to the ISIS Group. Manpower for most of these tasks has been allotted from the Engineering Physics Group on an as-required basis. The target development and MRO, as well as the secondary channel front end and TNF MRO responsibilities, now fall under the Primary Beam Lines coordinator.

During the past year the RF group has serviced two sets of correction plates from the cyclotron tank. The other two sets of plates will be serviced during the winter, 2003 shutdown. The inflector/deflector was inspected during the shutdown and was deemed to be serviceable without any intervention. Servicing for the inflector/deflector is now scheduled for the winter, 2003 shutdown.

The TNF system caused a minor inconvenience during the startup last spring because of a known, but inaccessible, vacuum leak. After the vacuum interlock set-point was adjusted and beam was delivered, a gradual improvement in the leak rate was noticed – in accordance with past experience.

During the last high current running period, two beryllium targets, one on each of the 1AT1 and 1AT2 target ladders, showed evidence of deterioration as the secondary-channel count-rates decreased. In both instances, the target ladder held a second beryllium target that was put into service within a few minutes. The failed targets have been in service since 1997 and will be replaced during the winter shutdown.

ISIS

The CUSP ion source and injection line continued to operate well for the past year with only minor down time due to a failed turbo pump. As in the past few years, there were no major projects undertaken because most ISIS personnel were involved in other TRIUMF projects.

Last year we reported the successful effort to extract $700\,\mu$A of H$^-$ current from the ion source. This beam, although with slightly larger emittance, was successfully transported to the cyclotron and used for $300\,\mu$A, 500 MeV, reduced duty cycle (50%) development tests. The transmission through the cyclotron at this current was approximately 48% rather than the usual 63% for typical $230\,\mu$A operation.

Work this year entailed producing a broad ISIS tune at the $300\,\mu$A equivalent extracted current level at better than 60% cyclotron transmission. This tune was developed and frozen to eliminate the use of many of the 120 variable beam-control elements in ISIS. Only a few ion source parameters, the bunchers (variable depending on beam current), and two quadrupoles and steering elements used to match into the cyclotron were available for tuning. In fact, these last elements were also frozen toward the latter part of the year forcing better cyclotron centre-region tunes. This work is described in more detail in the following section.

BEAM DEVELOPMENT

Cyclotron Beam Dynamics Development

The upgrade of the optically-pumped polarized ion source that was started last year has been completed. The new ECR rf power supply, the biased sodium-vapour jet ionizer, and the ionizer solenoid were installed. The ion source delivered $15\,\mu$A unpolarized to the cyclotron using the standard ISIS tune with $8\,\mu$A extracted from the cyclotron. Off-line tests later in the year produced $40\,\mu$A at injection (greater than $21\,\mu$A extracted equivalent). Further tests produced $50\,\mu$A to a beam stop in the horizontal section of ISIS. In all cases the laser system to measure thickness of the alkali target was not available and therefore conservative temperatures were used in both ionizer cells.

These results, coupled with the fact that the extraction optics were not optimized, suggest that the performance of the source can still be improved with further development. The ion source has met the required goal to provide useful polarized beam intensities of $10\,\mu$A that can be used for ISAC lower-intensity beam production in parallel with users requiring polarized beam. (Lower intensity is normally recommended during a three-week period before scheduled shutdowns.) In addition, the source can be used as a lower-intensity $(20\,\mu$A) backup for cyclotron beam production in the event of a major failure of the I1 CUSP-source system.

PRIMARY BEAM LINES

By the end of the last running period of 2001 water leaks had been identified in the triplet as well as in the front-end of the M20 channel downstream of the 1AT2 target region. Because the total water loss from these leaks amounted to $\sim 80\,$l/hour, it was necessary to find and fix them. This was in addition to the decommissioning of the M8 (pion therapy) channel that had already been planned for the 2002 shutdown, the latter being a continuation of the refurbishing program for the primary beam lines.

Work began with the removal of the shielding over the M8 beam line to allow access to the M8 triplet and second dipole M8B2. Electrical, cooling and diagnostic services were disconnected and the vacuum seal separated. M8B2 was removed first and bagged. The triplet was disconnected from the first dipole of the channel,

its exposed beam pipe bagged (because of contamination), and placed in a temporary bunker.

Services to the remaining two elements, M8B1 and M8Q1, of the (M8) channel were removed, and then the elements themselves. The radiation level on the mezzanine above was reduced to $110\,\mu$Sv/hr by installing a new iron shielding block and a new iron suitcase block.

At this point a problem developed in the plans for replacement shielding. Because the M8 channel accepted beam at a forward angle of 30° directly above the primary proton beam, a number of specially shaped shielding blocks had been installed. It was expected that these could be replaced with regular blocks, of which a number had been made. However, it was found that two support blocks had been welded to the 1AT2 target monolith. Consequently, several modifications to the new shielding were required.

The M8-1AT2 flange was sealed with a blanking plate. Four scrapings of the flange face were required before a vacuum seal was successfully obtained. With this operation completed, the M8 channel was successfully decommissioned.

In preparation for work on the 1AQ14/15/16 triplet downstream of the 1AT2 target, shielding over the triplet was removed. A major water leak was found on the return line of 1AQ15. This was cleaned of rust and repaired by welding a solder patch in place. Another leak was found in the supply header to a coil of 1AQ16. Although small (a leak rate of 1–2 drops/s), attempts to tighten the connection were unsuccessful because of a lack of space between the shielding wall and the fitting. The insulator itself was replaced but the small leak remained. After running cooling water overnight it was found that the leak rate had not increased and it was decided to leave the leak rather than expose personnel to further radiation dose.

Electrical shorts in 1AQ15 were found to be caused by an oxidation build-up on the pyrotenax cap insulators and were probably caused by moisture from the large water leak found at that quadrupole. Emery cloth was used to remove the oxidation from those connections that were accessible, resulting in an adequate resistance to allow operation. In addition the trip, warn, and common leads from the magnet's thermocouples were resoldered.

Other problems were encountered with the interlock wiring of the quadrupoles. These were repaired after much troubleshooting had been done. During the troubleshooting it was discovered that a vertical, heavy concrete shielding block near the 1AM10 monitor had disintegrated. Rubble from it had accumulated on the triplet main-header water lines and had displaced them. The debris was removed to reduce any stress on the water lines.

With these repairs completed there remained a water leak of $\sim 3\,$l/hr that could be attributed to the triplet. After relocating some shielding, a camera was used to visually locate the leak. The leak, found on the supply header-cap of 1AQ14, was repaired.

With the completion of the triplet repairs, iron shielding was replaced in the area and shielding was rearranged to allow the work that had been delayed on the M20 channel to proceed. Water was restored to M20Q1 and M20B1 and visual leak checking began. Leaks at both Hansen fittings of M20Q1 and at a solder joint on a coil of M20B1 were observed. The Hansen O-ring sealed fittings of the quadrupole were replaced with spare jumper hoses and the dipole leak was repaired by applying a clamp to the leaking solder joint. Two other similar clamps had been used at other leaks on the dipole. The rubber gaskets of the clamp that was accessible were replaced; however, those of the second were too difficult to reach and were left undisturbed. Water was restored and no indication of further leaks was found.

After restoring the shielding of M20 and from 1AT2 to monitor 1AM10, attention turned to other areas. The window valve upstream of the 1AT2 target had been working improperly and a vacuum leak had been found in the region of the 1AQ10/11 quadrupole doublet downstream of the 1AT1 target. A leak was found in the indium seal between the rotary collimator and 1AQ10. The faulty ring was cleanly removed and a replacement ring was made and installed.

When shielding over the window valve was removed it was found that the air cylinders were leaking badly. The cylinders were removed, new cylinders were installed, and the window valve was tested numerous times with no complications. Shielding over the area was then replaced.

In work around the 1AT1 target, the M13 beam blocker/gate valve assembly was removed, repaired, reinstalled, and the shielding over the area restored. The front end of the M11 channel was opened up to repair the jaws assembly and to locate and repair the last major vacuum leak.

This three-month long shutdown required a lot of planning and arduous work. Many times personnel were required to use their ingenuity when it was found that things were not as they were supposed to be. All of this work was successfully completed despite the high-radiation environment of the work areas. Those involved in the planning and execution of this refurbishment project are to be congratulated for a job well done.

Things ran well until the middle of May when water was found on the floor of the beam line 1A tunnel. By May 22 the leak rate had increased to 15 l/hr. The

M11 septum was identified as the source of the leak; when the area was uncovered it was not possible to find its location. However, with the use of mirrors and a video camera it was possible to see water falling from somewhere above.

It was decided to try a high-technology stop-leak process. One week of high-intensity running was cancelled and a PIF run instituted in order to provide a cool-down period. On June 13 the first infusion of an epoxy-clay matrix sealant was made. Following one day of air curing, a pressure test with water gave some indication of a leak and was confirmed when the septum was powered to 3,000 A. A second infusion followed by a longer curing period gave the same results. It was felt that the high electromagnetic fields of the septum were forcing the crack open.

One more infusion was attempted. This time the septum was briefly, but fully, powered immediately following the injection of the sealant. After a one week curing period the water was slowly turned on. At full water pressure and full power (3,850 A) there was no sign of a leak. On July 1 a leak rate of 2 l/hr was noted and by July 8 this had increased to 35 l/hr. The septum was valved off when not required by the M11 channel experimenters. By the end of July the leak had increased to 80 l/hr. At this time the septum was considered to be unrepairable and its power and water were turned off.

In mid September there was a short, one-week shutdown. The M13 beam blocker was repaired and a slit box installed at the second focus of the channel. To prevent the beam blocker from hanging up, the latch mechanism of the 1BBB2 was removed. The 1B beam blocker 3 was removed and its bellows repaired after which the blocker was reinstalled.

In the January shutdown of 2003 it is planned to replace the 1AQ14/15/16 triplet on beam line 1A. Three 8 in. bore, radiation-hard quadrupoles, nominally identical to those presently installed, were found on the vault roof of the cyclotron. One of these was found to have a shorted coil, so another, shorter quadrupole was substituted for it.

In order that services be accessible from the top of the magnets, their orientation was changed from horizontal to vertical. Water services were changed so that each quadrupole has its own cooling circuit rather than the parallel feed from a single header that had been used previously. The new electrical and water services were installed on these quadrupoles and each was field mapped. They were then installed on a dummy track and aligned. During the January, 2003 shutdown their alignment will be compared with that of the existing triplet and any required corrections made before the new triplet is installed in the beam line.

In addition to the above, the Beam Lines group was involved with other MRO and site activities. The filters of the active cooling system were changed and a new slit assembly for M13 installed. Interlock problems at 1AQ9 were investigated, the M15 separator serviced, and the M20 window changed. A window assembly was installed for Expt. 614 and assistance given for installation and alignment of the solenoid for the TWIST experiment.

In ISAC related work, beam line 2A was reconfigured for the installation of the new east target. Alignment support for both the east and west targets and their modules, as well as in the experimental areas, was given. Ongoing support for the DRAGON experiment continued.

In all, it was a busy year for both the Beam Lines and the Remote Handling groups. That the work load was completed successfully and on time is a tribute to the dedication and cooperation of these personnel.

Beam Line 2C

This year the major use of the 2C beam time continued to be the production of the radioisotope ^{32}Sr in the solid-target facility (STF) on beam line 2C. Operating time increased from 107 days in 2001 to 148 days in 2002. The beam line ran very well on limited support with the only significant downtimes arising from a vacuum leak at the 2C4 steering magnet in November and one between the 2C fast valve and the quadrupole triplet in December. The dose was increased from 81.14 mAh and a yield of 31.12 Ci in 2001 to 123.35 mAh and a yield of 45.08 Ci on 2002. There were eight natural rubidium targets irradiated this year compared with five targets the previous year. The last target irradiated was not processed because it received a small dose of only 609 μAh. This irradiation was terminated because of the vacuum leak between the 2C fast valve and the quadrupole triplet.

The beam extraction foil that is used for isotope production is a 0.250 in. wide curtain of 0.001 in. diameter pyrolytic graphite fibres. Two foils had been loaded in 2001 and one had failed during the run. Thus one foil was pushed to 75.77 mAh, which is 80% of the total 2001 dose and is about 50% higher than the dose on any previous foil. Three foils were loaded in 2002 to share the dose, but two of the foils split, creating a beam halo that could not be tuned out of the beam. Of the total dose this year, 116.26 mAh were put on the good foil and 8.29 mAh and 22 μAh on the split foils. The tuning difficulties and the large beam halo contributed to the vacuum leaks in the beam line, and the (known) misalignment of the STF makes high-current operation very sensitive to the beam halo. Splitting of the foils will be investigated in the 2003 shutdown and

the STF misalignment will be corrected in the 2004 shutdown. An upgrade of the 2C diagnostics in the 2003 shutdown will also assist in tuning.

The target-handling apparatus in the 2C STF hot cell was repaired and another manipulator was added there. The resin can on the STF was modified to facilitate replacing the resin and the STF conductivity meter was repaired. A jig was built for the STF target assemblies and all of the target assemblies were repaired and realigned or disposed of. All of the long overdue maintenance was done with the assistance of the Remote Handling group.

There were 36 days scheduled for proton therapy on 2C1 and 33 days were scheduled in the proton irradiation facility (PIF) on that beam line.

PROMPT RADIATION HAZARD

Introduction

Prompt radiation is produced only while an accelerator is in operation and hence, if required, can be rapidly terminated by interlocks that shut off the beam. In the present context it consists of a mixture of the many different particles that are produced when high-energy protons from the 500 MeV cyclotron interact with any type of material. Of this prompt radiation, high-energy neutrons are the most penetrating. At TRIUMF the safety systems that protect against this hazard have functioned for over 25 years without a failure leading to a significant exposure from prompt radiation.

As a result from the Canadian Nuclear Safety Commission (CNSC) we evaluated "the reliability of the engineered safety systems to provide a timely response under fault conditions must be under fault conditions". The purpose was to establish that the safety systems are sufficiently reliable in turning off the proton beam in response to high beam loss so as to reduce the probability of serious radiation exposures to anyone outside the shielding to well below significant levels ($< 10^{-5}$/year). The "Prompt Radiation Hazards Study Group" was formed to address the question of reliability of the safety systems and to formulate a response to the CNSC. The study group investigated the status of the safety systems and identified 11 action items that could be implemented to guarantee the desired reliability. Later this number was expanded to 15 items by the CNSC.

Immediate Action Group

A "Prompt Radiation Hazard Immediate Action Group" was appointed in March, 2000 to implement the actions that had been identified. The group proceeded to address these issues and also examined the overall rationalization of the safety system. Before the

end of 2002 this work had been largely completed. In several cases progress had been driven beyond the original mandate.

Work Accomplished

To examine all of the work that has been done would be too long for this report, but a short summary is possible.

A policy has been developed that specifies the maximum dose-rate levels outside shielding due to prompt radiation. This policy applies to both normal and abnormal beam-loss conditions of the licensed proton-beam current.

The active machine protection and active personnel protection systems are now treated as separate systems. The existing radiation monitoring has been reconfigured into two independent "safety-critical" radiation safety systems, one using γ-ray detectors and one, neutron detectors. However, both systems trip the same set of beam control devices to shut off the beam. Reliability requirements have been established and testing to verify that these requirements are met is now routinely done. Operator training is being updated to include training on the new safety system configurations and on the calibration and testing requirements.

The above two systems have been examined for ways to reduce their vulnerability to tampering. A number of improvements have been implemented. The monitoring and trip components have been evaluated for single point-of-failure mechanisms and changes have been made to reduce vulnerability to common failure modes. One remaining change is being actively pursued.

A policy has been established that defines the action to be followed when there is a malfunction of some part of the safety systems and that specifies the conditions and measures to be taken to allow continuing operation of the accelerator or beam line for a limited time until repairs have been completed. Improvements to the documentation describing the safety systems have been completed. A system of configuration control for safety-critical beam control devices has been established.

The definition of an "initiating event", that is, an event that could lead to a substantial prompt radiation exposure outside the shielding should the active safety-critical not respond, has been given a precise definition. This was required in order to be able both to clearly identify such events and to count them for the purpose of verifying the safety system reliability in terms of the probability of potential accidents.

The reliability of the pepper pot, a device used to restrict beam current during low-intensity operating configurations, has been re-evaluated and the device

once again found to be safe.

Work Arising

The remaining issue, one that arose from the immediate action items as a very desirable enhancement, was to make the beam-trip configurations for each of the gamma and neutron monitoring systems completely separate and redundant. A concept has been proposed and has been accepted. An engineering design is now being developed. Implementation is planned for the winter, 2004 shutdown.

CONTROLS

The Central Control System (CCS) continued to run well throughout 2002 and was responsible for only 4.8 hours of beam downtime as recorded by the Operations group. This is 2.7 hours less than the previous year. The major part of the downtime was due to hardware failures. Considering the size of the CCS and the age of many of its components, the downtime is minimal. The CCS runs reliably, performs well, and is flexible in meeting new needs. However, because of the many old components, there is serious concern about maintainability of some items. As a result, the importance of refurbishing is considered to be of the highest priority.

The goals set for this year were largely attained. These include continuing to replace the existing secondary beam line controls, phasing out VAX with Alpha machines, replacing the DSSI disk systems with fibre channel disk systems, and starting to replace the aging PC-based ISIS wire scanner system.

CCS Facilities

The major applications such as XTpage (cyclotron display pages), Xstrip (trending package) and Scan (machine protections scans) have received numerous enhancements and new features. Constant modifications and additions to XTpage have been made to keep pace with changes in various systems such as safety, vacuum, and beam lines, and for requirements of the Operations group. Purchase of the source code for the commercial XRT/graph widget, which is used by applications including Xstrip, has made changes and bug fixes much easier. For the Scan application, new keywords have been added to better handle data-acquisition error conditions (hardware failures). Scan also has new features tailored for Operations use. The DOSE program that the Safety group uses to keep track of dosimeter records was successfully ported to the Controls clusters, as anticipated in the previous year.

On the refurbishing front, a new fibre-channel storage has been installed in the Production Cluster to phase out the old DSSI disk storage system. Together with the existing fibre-channel system in the Development Cluster, they provide superior performance and reliability. Continued effort has been made to move file structures from the old disks to the new one. So far, three old disks have been retired in the Development Cluster. In addition, two new fibre-channel disks for the Safety DOSE data storage have been installed, one for each cluster. For the PC Servers Cluster, the fibre-channel hardware has been purchased and will be installed next year.

The tape backup systems in both Production and Development Cluster have been upgraded to high density SuperDLT drives. This provides needed capacity and performance. The backup procedure has been improved to make the incremental backup automatic.

The Production node CCSCS3 has been replaced with a faster Alpha (617 MHz DS10), and the VAX that was used as Diagnostics node DEVDG0 in Development Cluster has been phased out and replaced by a 466 MHz DS10.

New LCD monitors have been installed in locations such as the control room, the rf room, and the proton therapy control room. They were favourably received, in part for their non-susceptibility to stray magnetic fields, slightly larger screens, and light weight. In the next year we plan to replace the old X Window terminal system using VXT terminals and Infoservers with a higher-performance system. The old system has run extremely well for more than 10 years, but is much slower than required. Further, the VXTs do not support secure connections.

To prepare phasing out the last VAX, called DEVBN1, most of its unique functionalities have been ported to DEVBN2 (an Alpha CPU). We plan to remove this last VAX node in the next year.

Secondary Beam Lines

The replacement of the secondary beam line control systems with a new EPICS based system has progressed well. To date, two beam line systems, M13 (TWIST) and M20, have been converted. The M13 control system has been used in production mode. It provides the same functionality as the old system and new features such as finer steering of the beam. The M20 system has been fully converted and is ready for field testing. The M9B and M15 systems and a multiplet tuning program to facilitate μSR tuning are all planned to be done next year. Documentation has been compiled and is available in the Secondary Beam Lines Web site under the CCS home page.

The new EPICS system uses two Sunblade 100s, one for production and the other for development. The latter doubles up as a "hot spare" in case of a failure of the production computer. The usefulness of this con-

figuration was demonstrated when the system disk of the production computer crashed and a switch-over to the development computer was performed.

Additional measures have been taken to improve system reliability. These include setting up a tape drive for routine backup and installing a firewall for the front-end processor (input/output controller). In the area of diagnostics, programs have been developed to facilitate the investigation of faults.

Other Systems

A new system to control and readout data from the VME based electronics for the multi-wire chamber monitors in beam line 2A has been installed. It includes a PC running Windows 2000 for acquiring data from the VME module. This system integrates seamlessly with existing display and control of monitors in other beam lines. Controls have also been provided for the new 2A3 beam line. These include various scans and display pages.

For the proton therapy facility, UPS has been provided as planned and made available to the CAMAC crate, terminal server, and a display terminal. This ensures the equipment is protected from power disturbance. The dose and error-log printers, which were rather older models, were upgraded to more modern units. During the next year the proton therapy computer will be upgraded to a DS10 and the existing computer will be freed up to act as a spare for the beam line 2C CPU.

Miscellaneous

Work has begun on a replacement for the old PC-based ISIS wire scanner system. Display page and device controls are in place and preliminary tests have been completed successfully. Unlike the old system, the new system will allow widely distributed remote control using an X Window interface. It will provide display of statistical parameters together with new features such as saving and restoring scan sets. Further enhancements are planned for next year.

To maintain the CCS software in an up-to-date status, upgrades have been performed on Oracle (to version 9i) and Multinet (version 4.4). An upgrade of VMS to 7.3-1 is planned for next year.

OPERATIONAL SERVICES

Remote Handling

Cyclotron servicing

The winter shutdown presented an uneventful routine of copper blocker and shadow-shield handling, along with video and radiation surveys. The 2C extraction probe was removed remotely for service and replaced at the end of shutdown. Once again, other than routine maintenance, major servicing on the cyclotron elevating system was postponed because of conflicting ISAC work loads.

Beam line servicing

Major beam line refurbishment began in the 1AT2 area this year with removal of the decommissioned M8 pion therapy beam line. All M8 components from the 1AT2 target station downstream were disconnected and removed from the line; the large elements were stored for future-service evaluation. The vacuum flange joint to 1AT2 was cleaned and blanked off.

Miscellaneous parts were packaged for disposal at a radiation waste facility. Low-level activity steel shielding of unique and unusable configuration as well as water-damaged crumbling concrete shielding blocks removed from the beam line also were packaged and transported to the off-site radiation waste disposal facility. Over 32 tons of new concrete and 100 tons of new steel shielding blocks were installed to replace the original components and unique shielding in the area.

Work in the area uncovered a number of water leaks on the beam line 1A triplet magnet assembly. A steady increase in water loss as well as resultant electrical ground faults from this unit had threatened continued operation of the beam line prior to the scheduled shutdown. A water leak at a silver-solder joint on a 1AQ15 cooling header was repaired with a patch soldered *in situ*. A water leak at a ceramic insulator fitting on 1AQ16 required removal of adjacent shielding to allow proper access. Water erosion at the fitting joint due to a long term leak prevented an absolute repair. Even after replacement of the insulator a small leak persisted (1 drop every 2 s). Yet a third leak at a seal plug on a 1AQ14 header was fixed with a replacement plug and metal washer. Pyrotenax coil insulators on 1AQ15 were hand cleaned to remove oxidization products.

Thermal-switch interlock wiring on the triplet assembly was found to be damaged and required rewiring to enable power supply interlocks. Faulty radiation beam-spill monitors in the area also required replacement.

During the shutdown, shielding over the M20 beam line front end was removed to access other known water leaks. Quick disconnect, rubber O-ring sealed fittings on M20Q1 were found to be leaking and were replaced with spare jumper hoses. A new leak on M20B1 was found at a split at a copper coil termination. This is now the third of three identical splits in coil terminations, and is not solder-repairable. A specialized design of rubber clamp was installed to stop this leak. At this time the rubber seal in the one similar, accessible clamp on another coil was also replaced.

A concrete core sample through the meson hall floor adjacent to 1AT2 was drilled and removed at the beginning of the shutdown by outside contractors. The sample is required for information in preparing the TRIUMF Safety decommissioning report.

Miscellaneous beam lines work required replacement of the pneumatic actuator cylinders on the 1AWVA2 window valve between 1AT1 and 1AT2, and an indium vacuum seal on the rotary collimator-to-1AQ10 magnet. The horizontal 12 in. diameter indium metal seal on the 2CVBB1/M1 monitor was replaced.

In May a serious water leak developed on the M11 septum magnet. After removal of shielding in the area, we used closed circuit television in an unsuccessful attempt to locate the actual source of the leak.

In December a vacuum leak in the cyclotron vault at the 2CVF2/2CVQ1 joint required replacement. Initial installation of the beam line had not left sufficient clearance for free removal of the indium carrier ring. The 2CQ1/2/3 quadrupole triplet was permanently relocated approximately 1 cm downstream to improve future access to the joint.

Hot cells and targets

Routine production target maintenance for the year required removal and exchange of the 1AT1 and 1AT2 targets, measurement confirmation of target elevation, resin can exchange at both 1AT1 and 1AT2 cooling packages, replacement of the water flow transducer for collimator "A", and repair of a damaged water return line at 1AT2 package during M8 beam line removal.

Beam lines support saw the replacement of the M20Q1 water quick-disconnect fitting O-rings in the warm cell, and the rebuilding of the spool and pilot valve in one of two beam line 1A air-pressure amplifier units. The storage pit was also prepared toward the end of the year for scheduled 1AM10 monitor removal.

Throughout the year assistance was given to 2C hot cells operation with the retrieval of a misplaced target holder, the repair of the target-flipper mechanism, the replacement of a rubidium target, service maintenance on a pivoting-tong manipulator, and help with the design and drawings for a floating-target jig. A resin can at the 2C cooling package was prepared and exchanged, and a water-outlet fitting replaced. Later in the year a standard 1AT1/1AT2 resin can was adapted and installed at the 2C cooling package, and the package conductivity meter was replaced.

The Safety group was assisted in the design and detailed drawings for a portable neutron source flask, and the addition of 3/4 in. thick aluminum back-up plate for the industrial trash compactor.

Magnet Power Supplies

2002 saw the installation of beam line select switches to enable future beam delivery to the east target station for ISAC.

Many water leaks were encountered in the old M8 power supplies, which were installed for DRAGON. These were repaired as they arose and a decision was taken to replace the power supplies for MD1, MD2, Q9, Q10, SX3, and SX4. Replacement supplies were purchased for installation and commissioning during the spring shutdown, 2003.

Water leaks in the remaining 20–30 year old supplies, which were part of the original TRIUMF installation, continue to be a problem. This is being addressed by the installation of new heat sinks, which should provide better service.

The main cyclotron magnet power supply exhibited signs of instability. This was traced to radiation damage to wiring that had been installed on the cyclotron lid in the early days of power supply commissioning. The wiring provides feedback from trim coil 54 to stabilize the magnetic field. The cable, type 8451, exhibits the characteristic that the insulation turns to powder. A portion of this cable was replaced and further inspection of this type of cable used in the vault is scheduled for the spring, 2003 shutdown.

Further work was done to ensure stability and reproducibility of the M13 power supplies. This was done in conjunction with the Controls group and the Electronics Shop.

Water leaks in the hosing of the main magnet supply indicated that the silicon hoses were reaching the end of their practical lifetime. They were installed in 1982. New hoses will be installed during the spring shutdown, 2003.

Other activities involved provision of experimental support and as normal MRO.

Shutdown coordination was provided for the PCB transformer replacement, the removal of the M8 beam line, and other activities.

Electrical Services

Electrical systems

About 40 engineering and installation work-orders were completed in support of site requirements, including the cyclotron and the experimental program. Among them worth noting are the cooling tower variable-speed drives, UPS power to the proton therapy facility, services for the rf waster load, interlocks for the data acquisition system for Expt. 614, the upgrade of the fire alarm system, extension of the emergency power capacity in the main office building required for the new Card Access system, and site lighting improvements.

However, the ISAC project continued to be an important focus of the engineering efforts. Work on those projects will be covered in the ISAC report. In addition, continuing engineering support was provided to Nordion for the new TR30-2 radioisotope production facility project and to the ATG group for maintaining the operating facility.

TRIUMF uses two types of light fixtures: fluorescent and high discharge (mostly metal halide). Because of advances in lighting technology, we investigated the possibility of significant Hydro savings through replacement of existing lighting by more efficient units. The study indicated that we could save about $60,000 per year in electricity consumption. If approved by BC Hydro, this program would be eligible for some funding under the Power Smart incentive program.

Maintenance-based activities formed the bulk of the work of the Electrical Services group. Approximately 200 calls were answered and completed with an additional 20 carried forward to 2003. Typical maintenance activities included servicing lighting systems, motors, air-conditioning controls, panel boards and transformers, high-voltage switchgear, breakers, and capacitor banks. In addition, the maintenance of the approximately 10,000 fixtures of site lighting continued to keep the crew very busy throughout the year. Ground water has found its way into the conduit housing the 15 kV cable feeding the main office building. The cable still appears to be in fair condition, but it was determined prudent to replace it next spring. Work commenced on the variable-speed control for the cooling tower motors. We plan to put the new system in service by February, 2003.

The electrical crew saw its number decrease when the apprentice quit early in the summer. This placed additional burden on an already understaffed group. The addition of ISAC-II buildings will not make things easier. The service continuity and reliability may suffer if the staffing level does not match the increased workload.

Power delivery

This was a relatively smooth year with only one outage. The current power management program has been administered manually. With the addition of ISAC-I, ISAC-II, and the TR30-2, we began exploring ways to network the power monitoring and ground-fault alarming for better efficiency and response. The monthly averaged peak power demand remained essentially unchanged (6,834 kVA). However, the maximum peak demand increased by 1% to 8,944 kVA and was reached in August (Fig. 192). Electricity consumption inched up by about 2.5% to 53.3 GWh (Fig. 193). The largest consumption also occurred in August (5.89 GWh). The power factor (PF), averaged over the cal-

endar year, remained unchanged at 96.1% (Fig. 194). However, the PF of a typical production month decreased slightly.

YEAR	TOTAL	MONTH AVERAGE	UNITS
1999	47.4	3.950	GWh
2000	53.2	4.434	GWh
2001	52.0	4.332	GWh
2002	53.3	4.440	GWh
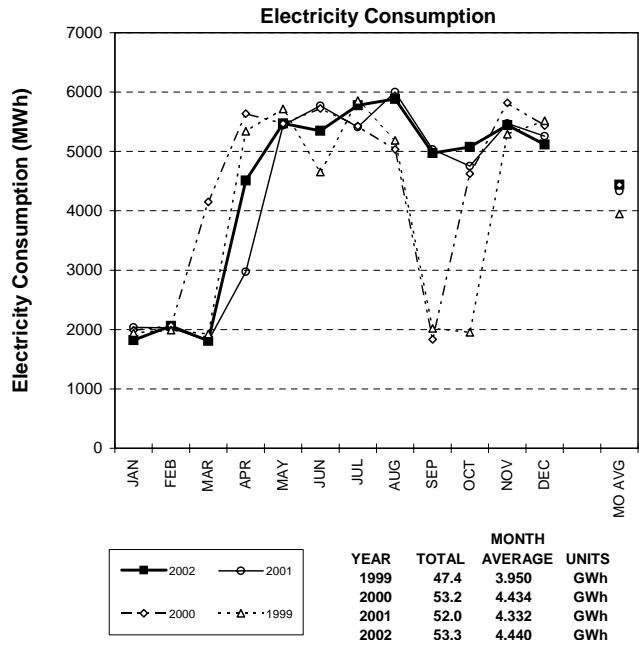
Fig. 192. Electrical system power demand – four year comparison.

YEAR	MONTH AVERAGE	UNITS
1999	5968	kVA
2000	6736	kVA
2001	6857	kVA
2002	6834	kVA
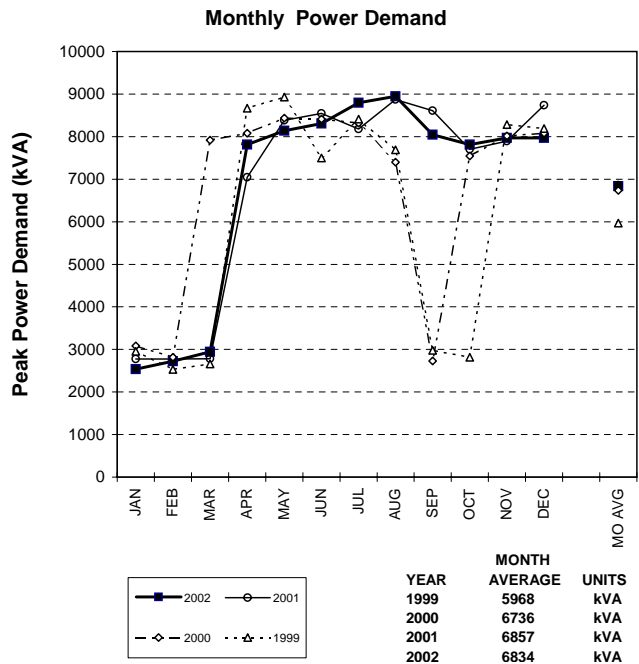
Fig. 193. Electrical system energy consumption – four year comparison.
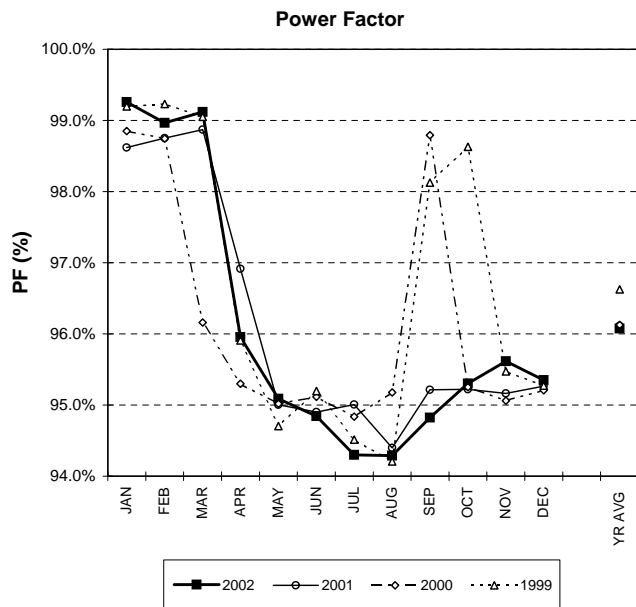
Power Factor

Fig. 194. Electrical system power factor – four year comparison.

Mechanical Services

The majority of effort at TRIUMF can be roughly divided up into two areas of activity: provision of new or maintenance of existing services piping, and heating, ventilation, and air conditioning (HVAC). New piping service jobs included the rf dummy load and CERN kicker magnet, while upgrades included M15 and M20 vacuum pump exhausts, M9 rf separator, M11 and M15 water manifolds, and a new filter for cooling water in the rf room. A large number of MRO jobs were completed. Typical examples would be the repair of leaks in the main magnet power supply and in the Machine Shop hot water system, and the replacement of failed valves. Work was started to replace one of the original perimeter ground-water drainage sump pumps along with connecting piping. Orders were issued for the supply of speed controls for eight of the fourteen cooling tower fans. The completion of this job in the next year will see better rf stability because of better regulated water temperature, and reduced maintenance and power consumption.

New HVAC services were provided to trailer A, PH extension room 204, trailer Gg room 30, and PH extension shower room. An exhaust system was provided for the new TR13 fume hood. A large effort was made in maintenance of existing site HVAC equipment. The list comprised a large fraction of the total inventory: MOB air handling units 1 (a complete overhaul) and 8, board room, trailer Gg, medical annex, ISIS clean room, both service annex machines, telephone exchange room, ATLAS clean room, chemistry annex computer room, and various Buffalo units. A new BL1A exhaust fan was installed.

Annual inspections and deficiency correction were completed for the site fire sprinklers and lifting equipment.

The air compressor formerly known as MRS has been rehabilitated and put to use as a site backup machine. The area around it has been cleared, and a new NOMONOX (breathable air quality) treatment system installed.

Engineering assistance in various areas was provided to Nordion for their new building project.

The Plant group welcomed the addition of technician Rob Walker.

ISAC DIVISION

INTRODUCTION

This full year of ISAC operation has been both rewarding and challenging. Operational experience has highlighted the need for the east target station and increased operating staff. Target and ion source developments are key to a successful ISOL facility. ISOL targets have been developed that accommodate 20 kW of proton beam for extended running periods. Typically the integrated number of protons per target is about 5E+20. Yields of many isotopes continue to increase faster than the proton beam current on target. Target designs capable of handling the full 50 kW are being tested with an electron beam heater off-line. Initial tests were carried out with stable beams from an ECR ion source on the recently completed east target station. It is expected that the ECR source will be commissioned with RIB in 2003. OLIS has become an important part of the accelerated beam science program in ISAC and was modified to accommodate three ion sources to increase the range of stable isotopes. In collaboration with the group from the University of Mainz, a resonant laser ion source has been successfully tested on the modified target conditioning station. The accelerators have been modified to improve reliability during operation. One of the major changes to the TRIUMF site this year has been the civil construction of ISAC-II. The new building, which is now nearing completion, provides a marked change in architecture at TRIUMF. The ECR charge state booster, needed for accelerating heavier masses through ISAC-II, was ordered in January and delivered to TRIUMF in November. The ion source test stand is being extended to commission the charge state booster before it is installed in ISAC. Twenty superconducting, bulk niobium, medium-beta, rf cavities have been ordered for delivery in 2003. A temporary superconducting rf laboratory was set up at the nearby BC Research facilities and a number of initial tests were carried out with a prototype rf cavity in a liquid helium cooled cryostat. A mechanical tuner, coupling loop and rf control system for the cavity are being developed.

ISAC OPERATIONS

This year, operation of the ISAC-I low energy facility continued in parallel with the commissioning and operation of stable beam and RIB to the ISAC-I high-energy area. With the exception of a few weeks of stable beam operation from OLIS to DRAGON in February (beam schedule 100A), the first quarter was devoted to shutdown activities of which the most significant was the installation of the east target station. Beam schedule 101 began in the second quarter and
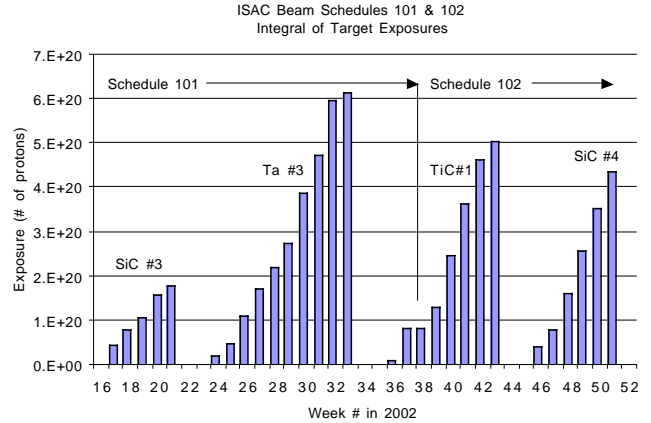
Fig. 195. Integral target exposures by week for RIB delivery in 2002.

carried on through the summer. Beam schedule 102 followed a short shutdown in September. The RIB delivery is shown in Fig. 195. The MEBT and HEBT beam operation continued to command extensive support from the beam dynamic experts, but by the end of the year after informal on-the-job training, all operators had become quite adept at performing routine mass, charge state and energy changes. But as always with complex accelerator systems, there are still occasions that challenge even the experts. The members of the ISAC Operations group take great pride in their contributions to the successes of the experiments and major ISAC milestones that have been highlighted elsewhere in this Annual Report.

Operational performance statistics are provided for the ISAC beam production of RIB from ITW and stable beam from OLIS. These are summarized separately for each beam schedule in Tables XXI to XLII. In some instances OLIS was used by an on-line experiment as part of procedures to change mass or energy. Other times it was used for commissioning or when the RIB was unavailable such as during a maintenance period. The RIB availability as an indicator of operational efficiency is complicated by the incentive to minimize activation when the beam is not required, and by the coincident use of OLIS. Furthermore, uncertainty in the schedule for the completion of the east target station and ECR source affected the beam scheduling of a number of experiments. The availability is quoted in comparison to the actual scheduled hours, but some interpretation is required to extract the relevance of overhead due to operational procedures such as the extensive time required to set up the beam transport and accelerator systems for different beams. This year, a factor has been provided to indicate the expected beam delivery after taking into account system overhead – a factor that can not be scheduled in advance.

The experiment specific factors are given in Table XLI.

The system downtime in terms of total hours of interruption is useful data. In schedule 101, the major interruptions to RIB were: the failure of the SiC #3 target in which the high current ionizer circuit went open after about 4 weeks of operation, requiring an unscheduled target change; a vacuum leak in a feedthrough on the service cap of TM1; various controls problems including IOC trips and the failure of a plc 12 V circuit. The stable beam was interrupted due to vacuum leaks at the L-bend of the microwave guide – caused by sputtering during operation with magnesium beams. In schedule 102, the major problem was the loss of RIB yield in the SiC #4 target after a transient excursion of the ionizer heater. Some of the significant events are indicated in the downtime tables. For example, in schedule 102, 52.6 h of scheduled beam time was devoted to investigating the problem with the loss of yield (Table XXXV) and the RFQ was unavailable for 127 h due to a failed ac breaker (Table XXXIX). For beam schedules 101 and 102, the total unscheduled downtime for RIB and OLIS was 1095.5 hours compared to total scheduled user time of 5322 hours, giving an availability of 79.5% for combined cyclotron, ISAC system performance.

Some of the OLIS downtime is extended due to lower priority when it occurs during parasitic operation simultaneous with RIB to another user. The target histories are given in Table XLII. A concerted effort was undertaken to schedule and perform regular systematic yield measurements in order to track the target performance (RIB yield) as a function of operating hours to better understand how to schedule and operate high power targets. The target yield results are given in the target ion source report. Data are presented for ITE operation although this time was all used for commissioning and development.

One operator was replaced in the first quarter, and the newest recruit was given the latest version of the training program and assigned to shift work at the beginning of the summer. Formal training now takes about 6 months. New operators pair up with an experienced operator for the first three weeks of their on-shift induction. Development of the SAT training program for ISAC Operations was delayed until the fall due to absences and operational priorities. By year-end, the analysis phase (first of five phases) of SAT had been completed and was ready for review. The first release of the ISAC Operations Manual (V1.0) was completed in February. It is available in PDF format on the ISAC Ops Web site.

The staffing complement remains critical, with five on-shift operators required for skeletal operation of a multiple source, complex RIB facility. The operators are assisted by two day-shift coordinators who are responsible for beam quality assurance and the coordination of maintenance activities. The coordinators are also required to stand in for operators who are off shift due to illness or vacation – which is approximately 30% of the time. Including the coordinator absences, beam quality and maintenance tasks are supported at a level less than 60%. There is no contingency for staffing turnover. A recruitment plan has been proposed to increase the resources within ISAC Operations.

In the control room, the EPICS control user interface was transferred to local workstations operating on Linux. This has provided a very stable operating system with the power of a local PC network to perform some of the user applications such as display management and data trending. Four separate workstations with a total of twelve monitor screens are available for operation. Much of this is required for the routine system monitoring and alarm system, so console desk space is scarce during periods of simultaneous operation of RIB with stable beam from OLIS, or other off-line activities. More control space is planned for the new control room in the ISAC-II building. Further console and control system improvements are on-going.

The electronic logbook has been transferred to a secure Web site behind a firewall and has replaced the traditional hard cover logbook, which is no longer maintained. The e-log is available to any on-site user, and the most recent entries are available through a mirrored Web page to off-site readers via the "internal" connection. The Web-based work permit system has been commissioned; improvements are on-going. A number of regular correspondences have been organized into electronic subscription list services. These include weekly maintenance request and maintenance list distributions and the weekly ISAC status meeting notes. An ISAC Operations Web page was created with information useful to ISAC operations and of interest to users.

In the coming year, in addition to providing beam for the scheduled experiments and performing systems maintenance, the major effort will be to establish and complete the SAT training program for ISAC operators.

Table XXI. OLIS beam schedule 100A: December 31 – April 1 (weeks 1–13). OLIS beam to ISAC experiments (hours).

Experiment number	Scheduled	Actual	Tune	Off
DRAGON commissioning	377.50	209.45	22.00	37.25
Development	78.00	48.00	8.00	13.00
Total	455.50	257.45	30.00	50.25

Beam available = 257.45 + 30.00 + 50.25 = 337.70 hours.
OLIS performance = 337.70/455.50 = 74.1 %.

Table XXII. OLIS beam schedule 100A. Breakdown of OLIS beams to ISAC experiments (hours).

Isotope	DRAGON commissioning	Development	Total
Mg-24	31.90	0.00	31.90
Ne-20	153.25	11.00	164.25
Ne-21	24.30	37.00	61.30
Total	209.45	48.00	257.45

Table XXIII. OLIS beam schedule 100A: OLIS systems downtime and overhead.

ISAC systems	Hours
Controls	14.20
Diagnostics	4.00
MEBT rf	2.50
DTL rf	15.20
Charge-exchange stripper	3.00
RFQ	7.10
Ion source	35.00
ISAC maintenance	21.40
ISAC shutdown (Feb. 19 – Apr. 1)	1025.00
ISAC startup	52.00
ISAC idle/no user	592.95
Procedures	41.85
OLIS/LEBT tuning	4.00
RFQ tuning	4.00
MEBT tuning	9.50
DTL tuning	5.50
HEBT tuning	1.00
Other	0.60
Total	1838.80

Table XXIV. ITW beam schedule 101: April 1 – September 23 (weeks 14–38). ITW beam to ISAC experiments (hours).

Experiment number	Scheduled	Expected	Actual	Tune	Off
Etest (ILY)	276	138	110.45	3.80	4.50
E715 (TNT)	336	302	161.35	3.15	4.60
E815 (BMR)	276	221	151.60	28.50	3.00
E824 (DRA)	534	267	195.05	18.10	12.50
E871 (OSA)	120	108	43.90	0.55	7.00
E893 (LTO)	252	126	125.40	2.80	5.00
E903 (OSA)	300	270	155.00	13.00	4.85
E903 (POL)	0	0	33.80	0.00	3.30
E909 (GPS)	80	72	56.75	0.10	4.25
E909 (8PI)	256	230	227.75	2.00	1.75
No scheduled user	(144)				
Total	2430 (2574)	1734	1261.05	72.00	50.75

RIB available = 1261.05 + 72.00 + 50.75 = 1383.80 hours.
Combined cyclotron/ISAC performance = 1,383.80/2430 = 56.9%.
System downtime = 508.40 hours = 508.40/2430 = 20.9%.

Table XXV. ITW beam schedule 101: Breakdown of ITW radioactive beam to ISAC experiments (hours).

Isotope	E715 TNT	E815 BMR	E824 DRA	E871 OSA	E871 POL	E893 LTNO	E903 OSA	E909 GPS	E909 8PI	Total
Yield studies on Li series, K series, Na series, Rb series = 110.45 hours										110.45
^{7}Li (stable)							9.45			9.45
^{8}Li		151.60					6.35			157.95
^{9}Li							29.15			29.15
^{11}Li							110.05		50.85	160.90
^{37}K	83.50									83.50
^{39}K						16.30				16.30
^{21}Na+5			195.05							195.05
^{23}Na				11.00						11.00
^{26}Na				32.90	33.80			56.75	176.90	300.35
^{79}Rb						109.10				109.10
^{80}Rb	77.85									77.85
Total	161.35	151.60	195.05	43.90	33.80	125.40	155.00	56.75	227.75	1261.05

Table XXVI. ITW beam schedule 101: Detail of ITW radioactive beams to HEBT experiments (hours).

Species and energy	Experiment	Current (pA)	Hours	nA-h
^{21}Na+5 215 keV/u	E824 DRA	400 pA	55.80	22
^{21}Na+5 360 keV/u	E824 DRA	150 pA	47.30	7
^{21}Na+5 492 keV/u	E824 DRA	200 pA	11.10	2
^{21}Na+5 504 keV/u	E824 DRA	200 pA	11.90	2
^{21}Na+5 580 keV/u	E824 DRA	200 pA	16.70	3
^{21}Na+5 590 keV/u	E824 DRA	200 pA	3.00	1
^{21}Na+5 850 keV/u	E824 DRA	200 pA	0.10	0
^{21}Na+5 857 keV/u	E824 DRA	200 pA	1.30	0
^{21}Na+5 867 keV/u	E824 DRA	200 pA	2.35	0
^{21}Na+5 878 keV/u	E824 DRA	250 pA	26.00	7
^{21}Na+5 887 keV/u	E824 DRA	200 pA	6.50	1
^{21}Na+5 891 keV/u	E824 DRA	125 pA	0.35	0
^{21}Na+5 901 keV/u	E824 DRA	125 pA	12.65	2
Total			195.05	47

Table XXVII. ITW beam schedule 101: ITW systems downtime and overhead.

ISAC systems	Hours
Downtime – unscheduled	
Beam lines	3.00
Controls (38.6 h plc 12 V fail; 24 h IOC faults)	71.65
DTL rf	6.80
Electrostatic power supplies	1.00
MEBT rf	0.50
Safety	0.10
Site power	7.50
Target/ion source (275.5 h SiC #3 ionizer; 124.5 h vacuum f/t)	416.75
Vacuum	0.10
Other	1.00
Subtotal	508.40
Downtime – scheduled	
Cyclotron maintenance	380.00
Cyclotron development	66.85
Beam line 2A off	242.75
ISAC cooldown	5.50
ISAC shutdown	24.00
ISAC startup	20.50
ISAC maintenance	127.80
ISAC development	7.40
ISAC idle	292.00
Procedures	259.30
Target conditioning	356.90
Target change	432.00
LEBT tuning	24.70
Other	3.75
Total	2751.85

Table XXVIII. OLIS beam schedule 101: OLIS beam to ISAC experiments (hours).

Experiment number	Scheduled	Expected	Actual	Tune	Off
E824 DRAGON	252	126	317.50	22.25	34.40
E870 TUDA	540	432	11.90	12.40	12.80
E871 Osaka	36	32	3.50		
E893 LTNO	60	30	41.75		
E903 TUDA	0	0	11.50	5.00	
Etest GPS	24	22	3.00	8.50	
No scheduled user	(1188)				
Total	912 (2100)	642	389.15	48.15	47.20

Beam available = 389.15 + 48.15 + 47.20 = 484.50 hours.
OLIS performance = 484.50/912.00 = 53.1%.
System downtime = 304.00 hours = 304.00/912.00 = 33.3%.

Table XXIX. OLIS beam schedule 101: Breakdown of OLIS beams to ISAC experiments (hours).

Isotope	E824 DRA	E870 TUD	E871 OSA	E893 LTO	E903 TUD	Etest GPS	Total
^{4}He+1		11.90					11.90
^{15}N+1				25.75			25.75
^{20}Ne+1			3.50				3.50
^{20}Ne+5	60.05				11.50		71.55
^{21}Ne+1				16.00		3.00	19.00
^{21}Ne+5	108.00						108.00
^{24}Mg+6	149.45						149.45
Total	317.50	11.90	3.50	41.75	11.50	3.00	389.15

Table XXX. OLIS beam schedule 101: Detail of OLIS stable beams to HEBT experiments (hours).

Species and energy	Experiment	Current	Hours	nA-h
^{20}Ne+5 360 keV/u	E824 DRA	1 nA	60.05	60
^{21}Ne+5 215 keV/u	E824 DRA	1 nA	3.50	4
^{21}Ne+5 279 keV/u	E824 DRA	1 nA	27.90	28
^{21}Ne+5 287 keV/u	E824 DRA	1 nA	4.70	5
^{21}Ne+5 492 keV/u	E824 DRA	1 nA	3.30	3
^{21}Ne+5 497 keV/u	E824 DRA	1 nA	8.70	9
^{21}Ne+5 500 keV/u	E824 DRA	1 nA	3.30	3
^{21}Ne+5 501 keV/u	E824 DRA	1 nA	0.80	1
^{21}Ne+5 502 keV/u	E824 DRA	1 nA	5.70	6
^{21}Ne+5 503 keV/u	E824 DRA	1 nA	1.00	1
^{21}Ne+5 504 keV/u	E824 DRA	1 nA	1.70	2
^{21}Ne+5 505 keV/u	E824 DRA	1 nA	0.90	1
^{21}Ne+5 506 keV/u	E824 DRA	1 nA	4.85	5
^{21}Ne+5 510 keV/u	E824 DRA	1 nA	1.00	1
^{21}Ne+5 511 keV/u	E824 DRA	1 nA	2.90	3
^{21}Ne+5 515 keV/u	E824 DRA	1 nA	1.00	1
^{21}Ne+5 517 keV/u	E824 DRA	1 nA	14.70	15
^{21}Ne+5 520 keV/u	E824 DRA	1 nA	0.90	1
^{21}Ne+5 523 keV/u	E824 DRA	1 nA	1.00	1
^{21}Ne+5 524 keV/u	E824 DRA	1 nA	1.30	1
^{21}Ne+5 525 keV/u	E824 DRA	1 nA	0.80	1
^{21}Ne+5 526 keV/u	E824 DRA	1 nA	1.40	1
^{21}Ne+5 528 keV/u	E824 DRA	1 nA	0.80	1
^{21}Ne+5 530 keV/u	E824 DRA	1 nA	8.95	9
^{21}Ne+5 590 keV/u	E824 DRA	1 nA	6.90	7
^{24}Mg+6 215 keV/u	E824 DRA	1 nA	0.40	0
^{24}Mg+6 216 keV/u	E824 DRA	1 nA	8.70	9
^{24}Mg+6 219 keV/u	E824 DRA	1 nA	9.00	9
^{24}Mg+6 221 keV/u	E824 DRA	1 nA	7.20	7
^{24}Mg+6 222 keV/u	E824 DRA	1 nA	16.00	16
^{24}Mg+6 224 keV/u	E824 DRA	1 nA	14.60	15
^{24}Mg+6 225 keV/u	E824 DRA	1 nA	2.80	3
^{24}Mg+6 227 keV/u	E824 DRA	1 nA	8.30	8
^{24}Mg+6 228 keV/u	E824 DRA	1 nA	3.50	4
^{24}Mg+6 229 keV/u	E824 DRA	1 nA	4.00	4
^{24}Mg+6 230 keV/u	E824 DRA	1 nA	6.40	6
^{24}Mg+6 236 keV/u	E824 DRA	1 nA	8.00	8
^{24}Mg+6 360 keV/u	E824 DRA	1 nA	1.90	2
^{24}Mg+6 425 keV/u	E824 DRA	1 nA	58.65	59
^{4}He+1 1.50 MeV/u	E870 TUD	1 nA	11.90	12
^{20}Ne+5 1.45 MeV/u	E903 TUD	1 nA	11.50	12
Total			340.90	340

Table XXXI. OLIS beam schedule 101: OLIS systems downtime and overhead.

ISAC systems	Hours
Downtime – unscheduled	
Beam lines	1.00
Controls	12.70
Electrostatic PS (38.3 h IOS:Q3 fail)	39.25
Magnet PS (41.3 h water leak in OLIS:MB1)	42.50
DTL rf (38.3 h tank 2 p/s; 14.5 h tank 5)	37.35
Charge-exchange stripper	3.85
MEBT rf	6.25
RFQ	1.30
Site power	22.00
Ion source (L-bend vacuum failures after Mg beam = 92.3 h in week 18; 40.5 h in week 38)	137.80
Subtotal	304.00
Downtime – scheduled	
ISAC maintenance	210.00
Development	47.50
ISAC idle	1070.30
ISAC shutdown (includes 112 h repair to L-bend in week 38)	289.50
ISAC startup	35.50
Procedures	403.30
LEBT tuning	0.15
Total	2360.25

Table XXXII. ITW beam schedule 102: September 23 – December 30 (weeks 39–52). ITW beam to ISAC experiments (hours).

Experiment	Scheduled	Expected	Actual	Tune	Off	Total
Etest ILY	204	102	52.20	8.20		60.40
Etest 8PI	12	6				0.00
E715 TNT	372	335	319.10	10.05		329.15
E817 BMR	204	163	139.05	1.25	0.80	141.10
E823 GPS	132	119	101.05	5.95	38.05	145.05
E824 DRA	252	126	123.05	2.30	2.00	127.35
E871 OSA	96	86	86.30			86.30
E893 OSA	24	22	21.05	0.25	1.95	23.25
E928 TUD	132	106	105.65	0.70	5.75	112.10
No scheduled user	(156)					
Total	1428 (1584)	1065	947.45	28.70	48.55	1024.70

RIB available = 947.45 + 28.70 + 48.55 = 1024.70 hours.
Combined cyclotron/ISAC performance = 1,024.70/1,428.00 = 71.8%.
System downtime = 111.61 hours = 111.61/1428 = 7.8%.

Table XXXIII. ITW beam schedule 102: Breakdown of ITW radioactive beams to ISAC experiments (hours).

Species	E715 TNT	E815 BMR	E824 DRA	E871 OSA	E893 TUDA	E903 OSA	E909 GPS	Etest 8PI	Total
Multiple				Yield studies = 52.20 hours					52.20
^{7}Li (stable)		1.00							1.00
^{8}Li		138.05							138.05
^{20}Na+5					105.65	18.65			124.30
^{21}Na+5			123.05	77.70		2.40			203.15
^{23}Na (stable)				8.60				0.00	8.60
^{36}K	123.50								123.50
^{37}K	195.60								195.60
^{38}K							101.05		101.05
Total	319.10	139.05	123.05	86.30	105.65	21.05	101.05	0.00	947.45

Table XXXIV. ITW beam schedule 102: Detail of ITW radioactive beams to HEBT experiments (hours).

Energy	Species	Experiment	Hours	nA-h
1.25 MeV/u 2 pA	^{20}Na+5	E928 TUD	73.65	0.1
1.60 MeV/u 2 pA	^{20}Na+5	E928 TUD	32.00	0.1
470 keV/u 100 pA	^{21}Na+5	E824 DRA	6.50	0.7
490 keV/u 100 pA	^{21}Na+5	E824 DRA	15.82	1.6
500 keV/u 100 pA	^{21}Na+5	E824 DRA	7.60	0.8
570 keV/u 100 pA	^{21}Na+5	E824 DRA	41.13	4.1
580 keV/u 100 pA	^{21}Na+5	E824 DRA	1.80	0.2
774 keV/u 5 pA	^{21}Na+5	E824 DRA	40.90	0.2
781 keV/u 100 pA	^{21}Na+5	E824 DRA	9.30	0.9
Total			228.70	8.7

Table XXXV. ITW beam schedule 102: ITW systems downtime and overhead.

ISAC systems	Hours
Downtime – unscheduled	
Controls	8.90
Electrostatic power supplies	3.40
Magnet power supplies	11.50
Q-exchange stripper	0.30
Services	8.80
Site power	13.20
Target/ion source (52.6 h check target after drop in rates)	64.01
Vacuum	1.50
Subtotal	111.61
Downtime – scheduled	
Cyclotron maintenance	206.05
Cyclotron development	13.50
Beam line 2A off	132.54
ISAC shutdown	249.50
ISAC maintenance	7.50
ISAC development	1.40
ISAC idle	73.05
Procedures	97.40
Target conditioning	195.80
Target change	208.00
LEBT tuning	0.70
Subtotal	1185.44
Total	1297.05

Table XXXVI. OLIS beam schedule 102: OLIS beam to ISAC experiments (hours) with microwave source and gases.

Experiment	Scheduled	Expected	Actual	Tune	Off	Total
Etest DEV		60	108.50			108.50
E815 BMR	12	10				
E871 OSA	12	11		0.50		0.50
E824 DRA	264	132	155.60	11.95	9.65	177.20
E870 TUD	204	163	57.05	1.00		58.05
E928 TUD	60	38	50.90	1.50	7.40	59.80
No scheduled user	(852)					
Total	552 (1404)	414	372.05	14.95	17.05	404.05

Beam available = 372.05 + 14.95 + 17.05 = 404.05 hours.
OLIS performance = 404.05/552.00 = 73.2%.
System downtime = 171.50 hours = 171.5/552.00 = 31.1%.

Table XXXVII. OLIS beam schedule 102: Breakdown of OLIS beams to ISAC experiments (hours).

Species	E824 DRA	E870 TUD	E928 TUD	E871 OSA	E817 BMR	Etest DEV	Total
^{12}C+3	54.85						54.85
^{14}N+4	9.10	43.50					52.60
^{20}Ne+5	3.80	13.55	50.90			108.50	176.75
^{21}Ne+5	87.85						87.85
Total	155.60	57.05	50.90	0.00	0.00	108.50	372.05

Table XXXVIII. OLIS beam schedule 102: Detail of OLIS stable beams to HEBT experiments (hours).

Energy	Species	Experiment	Hours	nA-h
1.07 MeV/u 2 nA	^{12}C+3	E824 DRA	23.20	46.4
1.08 MeV/u 2 nA	^{12}C+3	E824 DRA	14.30	28.6
1.11 MeV/u 2 nA	^{12}C+3	E824 DRA	17.35	34.7
410 keV/u 1 nA	^{14}N+4	E824 DRA	9.10	9.1
1.45 MeV/u 200 pA	^{14}N+4	E870 TUD	43.50	8.7
500 keV/u 1 nA	^{20}Ne+5	E824 DRA	3.80	3.8
750 keV/u 2 pA	^{20}Ne+5	E928 TUD	12.00	0.0
1.0 MeV/u 2 nA	^{20}Ne+5	E870 TUD	13.55	27.1
1.25 MeV/u 1 nA	^{20}Ne+5	E928 TUD	34.80	34.8
1.25 MeV/u 2 pA	^{20}Ne+5	E928 TUD	3.10	0.0
1.6 MeV/u 3 pA	^{20}Ne+5	E928 TUD	1.00	0.0
500 keV/u 1 nA	^{21}Ne+5	E824 DRA	6.00	6.0
528 keV/u 1 nA	^{21}Ne+5	E824 DRA	4.20	4.2
543 keV/u 1 nA	^{21}Ne+5	E824 DRA	2.70	2.7
546 keV/u 1 nA	^{21}Ne+5	E824 DRA	8.90	8.9
547 keV/u 1 nA	^{21}Ne+5	E824 DRA	0.30	0.3
548 keV/u 1 nA	^{21}Ne+5	E824 DRA	0.00	0.0
550 keV/u 1 nA	^{21}Ne+5	E824 DRA	1.80	1.8
552 keV/u 1 nA	^{21}Ne+5	E824 DRA	1.80	1.8
553 keV/u 1 nA	^{21}Ne+5	E824 DRA	0.40	0.4
554 keV/u 1 nA	^{21}Ne+5	E824 DRA	2.20	2.2
556 keV/u 1 nA	^{21}Ne+5	E824 DRA	3.60	3.6
557 keV/u 1 nA	^{21}Ne+5	E824 DRA	3.00	3.0
558 keV/u 1 nA	^{21}Ne+5	E824 DRA	2.60	2.6
560 keV/u 1 nA	^{21}Ne+5	E824 DRA	4.70	4.7
774 keV/u 1 nA	^{21}Ne+5	E824 DRA	2.50	2.5
778 keV/u 1 nA	^{21}Ne+5	E824 DRA	0.50	0.5
781 keV/u 1 nA	^{21}Ne+5	E824 DRA	0.00	0.0
799 keV/u 1 nA	^{21}Ne+5	E824 DRA	2.40	2.4
802 keV/u 1 nA	^{21}Ne+5	E824 DRA	2.00	2.0
805 keV/u 1 nA	^{21}Ne+5	E824 DRA	2.00	2.0
808 keV/u 1 nA	^{21}Ne+5	E824 DRA	2.50	2.5
808 keV/u 1 nA	^{21}Ne+5	E824 DRA	3.00	3.0
809 keV/u 1 nA	^{21}Ne+5	E824 DRA	1.50	1.5
810 keV/u 1 nA	^{21}Ne+5	E824 DRA	1.50	1.5
814 keV/u 1 nA	^{21}Ne+5	E824 DRA	9.00	9.0
811 keV/u 1 nA	^{21}Ne+5	E824 DRA	1.50	1.5
817 keV/u 1 nA	^{21}Ne+5	E824 DRA	1.50	1.5
814 keV/u 1 nA	^{21}Ne+5	E824 DRA	1.10	1.1
818 keV/u 1 nA	^{21}Ne+5	E824 DRA	1.75	1.8
820 keV/u 1 nA	^{21}Ne+5	E824 DRA	0.00	0.0
817 keV/u 1 nA	^{21}Ne+5	E824 DRA	1.60	1.6
820 keV/u 1 nA	^{21}Ne+5	E824 DRA	2.80	2.8
824 keV/u 1 nA	^{21}Ne+5	E824 DRA	2.50	2.5
828 keV/u 1 nA	^{21}Ne+5	E824 DRA	3.00	3.0
835 keV/u 1 nA	^{21}Ne+5	E824 DRA	3.00	3.0
Total			263.55	281.1

Table XXXIX. OLIS beam schedule 102: OLIS systems downtime and overhead.

ISAC systems	Hours
Downtime – unscheduled	
Beam lines	6.00
Controls	2.20
Magnet PS	4.80
DTL rf (11.7 h buncher 1 trips November 25,26)	14.50
Charge-exchange stripper	0.30
MEBT rf	5.00
Electrical services (RFQ primary ac breaker failure)	127.00
Site power	7.80
Ion source	3.90
Subtotal	171.50
Downtime – scheduled	
ISAC maintenance	121.95
ISAC idle	354.80
ISAC shutdown	450.50
ISAC startup	44.50
Procedures	193.60
HEBT tuning	6.00
Subtotal	1171.35
Total	1342.85

Table XL. ITE beam schedule 102: ITE systems downtime and overhead with ECR source and gases.

ISAC systems	Hours
Downtime – unscheduled	
Controls	8.50
Diagnostics (IMS:FC0 signal fault)	21.00
Services	6.00
Subtotal	35.50
Downtime – scheduled	
ISAC maintenance	96.00
ISAC development	159.60
ISAC idle	1012.00
Procedures	0.40
Target conditioning	1048.50
Subtotal	2316.50
Total	2352.00

Table XLI. Estimated procedural overhead.

Line	Discount
DEV	5h/wk
ILY	.50
DRA	.50
LTO	.50
TUD	.80
BMR	.80
POL	.80
TNT	.90
GPS	.90
8PI	.90 in schedule 101
	.50 in schedule 102
OSA	.90

Expected hours = scheduled hours × discount factor.

Discount values are estimated from operational experience of experiments on the respective lines. Higher numbers suggest higher uptimes. Generally, HEBT experiments have greater overhead due to multiple energy requirements. Yield runs, scheduled in 12 hour blocks, typically go for the better part of a regular business day. The 8pi run in schedule 102 was for commissioning only.

The target hall and hot cell operation has become quite well organized. The engineering that has been done for the east target station will be applied to upgrade the west target systems, which were installed as prototypes. There were four target changes done this year, each one completed as planned and without incident. The history of operation of ISAC production targets for 2002 is given in Table XLII. Schedule 101 started with SiC #3 – a target of silicon carbide pellets. It failed prematurely due to an open circuit in the tube heater. The remaining targets lasted for the duration of their scheduled beam operation, albeit with decreasing yields as a function of target aging. The next target was Ta foils #3; it received the highest exposure to date: 6.15E20 protons. The next target was TiC #1; although receiving less exposure, this thicker target generated more RIB (exposure × target thickness).

Table XLII. ISAC target history for 2002.

Target ID	In date	Out date	Exposure # of protons	Power μAh*g/cm²	Comments
SiC #3	15-Mar	24-May	1.773E+20	192516	18.9 gSiC/cm² + 5.5 gC/cm²: Failure due to TBHT – open circuit
Ta Foils #3	7-Jun	15-Aug	6.148E+20	596217.98	21.79 g/cm² Ta in the form of 525 × 0.025 mm foils
TiC #1	26-Aug	29-Oct	5.050E+20	993880.32	29.65 gTi/cm² + 14.57 gC/cm² (590 foils 0.11 mmC + 0.25 mm TiC)
SiC#4	1-Nov		4.358E+20	519451.66	14.31 gSi/cm² + 12.47 gC/cm² (425 foils 0.13 mmC + 0.23 mmSiC)

The last target, SiC #4, experienced a precipitous loss of yield after an inadvertent transient spike in the ionizer heater set point. Curiously, the rate mysteriously recovered in the last few hours of operation before the winter shutdown. Hopefully the target inspection will provide some explanations. At these beam powers, considering the operating temperature, the productive life for this generation of targets appears to be about 4–6 weeks.

ISAC TARGETS

ISAC Targets and Beams

During 2002, ISAC target development concentrated on increasing proton beam current limits for refractory carbide target materials (SiC, TiC) and long term operation of a Ta foil target at high proton beam intensity. Three carbide targets (SiC #3, SiC #4 and TiC #1) were operated to provide Na and K beams to both accelerated and low energy experiments. The metal foil target Ta #3 operated from June to August, providing mainly beams of Li isotopes. Ta #3 currently holds the ISAC record for irradiation having received $27,362\,\mu A\,h$ of proton beam, a total of 6.2×10^{20} protons.

Previously at ISAC, compound targets such as SiC, CaO and $CaZrO_3$ had been in the form of pressed powder pellets. The pellets (16 mm diameter, 1 to 2 mm thickness) were stacked inside the 18 mm diameter tantalum target container. The maximum operating proton beam current was limited by the target material's ability to dissipate the proton beam power. Due to the limited contact between target pellets and the inner wall of the target container, beam power deposited in the pellet stack first had to be radiated to the target container and subsequently, from the target container to the surroundings. At the operating temperatures of these target materials (1400–1600°C) radiative heat transfer is not highly efficient. Previously, the maximum operating proton current for pellet targets was $15\,\mu A$ for a SiC pellet target and only $3\,\mu A$ for a $CaZrO_3$ pellet target.

During 2002, higher proton beam current operation for carbide targets was achieved by replacing the target pellets with composite target foils consisting of a thin layer of metal carbide (~ 0.23 mm) on a supporting layer (~ 0.12 mm) of flexible exfoliated graphite foil. The composite foils were loaded into the target container such that good contact with the container wall was maintained allowing beam power to be transferred to the container by conduction rather than radiation. The graphite layer also increased the thermal conductivity of the composite foil allowing metal carbide targets to be treated in a manner analogous to metal foil targets.

Target foils were manufactured by slip casting mixtures of metal carbide powders with appropriate binders, plastisizers, dispersants and solvents. Methods for producing thin, evenly dispersed, compact layers of carbides using both aqueous and non-aqueous systems were developed for SiC, TiC and ZrC. Green densities of up to 65% were achieved for the cast carbides. Prior to on-line operation, the targets were conditioned by heating at operational temperature to decompose and volatilize the organic components and sinter the carbide layers.

The first silicon carbide composite foil target (SiC #3) consisting of 450 composite foils for a total of $18.9\,g\,SiC/cm^2$ operated at a maximum proton current of $30\,\mu A$, twice the beam current of the previous silicon carbide pellet target ($29.9\,g\,SiC/cm^2$). A similar titanium carbide composite target (TiC #1) consisting of 590 foils operated at a maximum current of $40\,\mu A$ for $22,475\,\mu A\,h$ receiving a total of 5.1×10^{20} protons on target. A second silicon carbide composite target (SiC #4) operated with a maximum proton current of $45\,\mu A$ (three times the previous maximum with pellets) operating for $19,397\,\mu A\,h$, a total of 4.4×10^{20} protons.

Yields of alkali beams from both composite foil and pressed pellet targets are presented in Table XLIII. For the sodium beams, the comparison is for silicon carbide target material in different forms. The yields are generally higher by an order of magnitude for the composite foil targets compared to the pressed pellet targets. This reflects the increased production and enhanced diffusion resulting from an increase in maximum beam intensity. Isotopic yields from composite foil and pellet targets operating at the same beam intensity are essentially the same. For the potassium yields, the composite TiC material is compared to a target of pressed pellets of $CaZrO_3$. While the $CaZrO_3$ target maximum beam current is $\leq 3\,\mu A$, the yields of short-lived ^{35}K and ^{36}K are comparable to those from the TiC composite target operating at a $40\,\mu A$ proton current. This reflects the much higher production cross section of light K isotopes from Ca than from Ti. The higher proton flux on the TiC target does not sufficiently compensate for the difference in production. The high yields of neutron rich potassium isotopes from the TiC composite target are consistent with the higher production cross section from Ti.

Table XLIII. Comparison of yields from pressed pellet and composite foil targets.

Beam	Composite target	Yield (/s)	p^{++} (μA)	Pellet target	Yield (/s)	p^{++} (μA)
^{20}Na	SiC	2.6×10^8	46.3	SiC	3.4×10^7	15.4
^{21}Na	SiC	9.9×10^9	46.2	SiC	2.5×10^9	15.3
^{22}Na	SiC	4.8×10^{11}	45.0	SiC	2.0×10^{11}	15.1
^{24g}Na	SiC	6.8×10^{10}	45.0	SiC	7.0×10^9	10.5
^{24m}Na	SiC	1.7×10^8	30.6	SiC	1.3×10^7	10.5
^{25}Na	SiC	3.2×10^9	44.7	SiC	3.7×10^8	10.5
^{26}Na	SiC	3.2×10^7	45.4	SiC	5.2×10^6	10.5
^{26}Na	SiC	1.5×10^6	45.0	SiC	2.2×10^5	10.3
^{35}K	TiC	3.5×10^3	40.6	CaZrO$_3$	2.0×10^3	2.6
^{36}K	TiC	2.1×10^5	40.1	CaZrO$_3$	2.4×10^5	1.0
^{37}K	TiC	6.4×10^7	40.1	CaZrO$_3$	8.5×10^6	1.5
^{38g}K	TiC	1.8×10^{10}	40.1	CaZrO$_3$	7.4×10^8	1.1
^{38m}K	TiC	7.4×10^7	40.1	CaZrO$_3$	1.2×10^7	2.6
^{42}K	TiC	1.5×10^{11}	38.5	−	−	−
^{43}K	TiC	4.6×10^{10}	38.5	−	−	−
^{44}K	TiC	2.6×10^{10}	38.5	−	−	−
^{45}K	TiC	1.6×10^9	38.5	−	−	−

High Power Target Developments at ISAC

Existing target designs using foils of refractory material (Nb, Ta, etc.) can accommodate up to $40 \, \mu$A beam intensities and the available intensities of many radionuclides seem to scale with the proton beam current. Production targets capable of withstanding proton beam intensities up to $100 \, \mu$A without compromising the reliability and the yield of radioactive isotopes will be a future challenge. Several approaches to the dissipation of the power deposited in such targets by the proton beam have been investigated and a realistic solution for the removal of the heat from the target container seems possible. The development of a high power target is the subject of a development program at TRIUMF. In order to go beyond the current limitation one needs to efficiently cool the target. Over the past ten years several concepts were proposed but very few were developed and used satisfactorily on-line. Either the target is too difficult to produce and therefore too expensive, or the cooling is too efficient and the target material never gets to the ideal temperature for fast release of short half-life nuclides. Different schemes have been proposed to overcome these issues and it is clear that radiative cooling offers the simplest approach to cool the target material. If one can increase the effective emissivity of the target container one can increase the beam power deposited into the target. A thick target equipped with radial fins has been developed for this purpose at TRIUMF and the initial tests have been conducted.

Target fabrication

Instead of building a target using the diffusion bonding technique, we considered adding radial fins to a Ta tube. The fins are 55×55 mm cut out from a Ta foil sheet $380 \, \mu$m thick. An undersized hole is punched in the centre and extruded to the tube diameter using a conical shaped tool. Then the fins are installed onto the tube from each side of the central block. Once the fins are installed we use a special tool to expand the Ta tube in order to improve the contact between the tube and the fins. In order to verify if we have a better contact, we measure the electrical resistance between the fins and the tube. We observed a reduction of the resistance by a factor of three across the contact area. The target is equipped with 90 fins in total. Figure 196 shows a photograph of the actual finned target.

Heating tests of the finned target

We ran several tests of the target using the ISAC target conditioning facility. The available power to heat the target comes from a 10 V, 1000 A dc supply. The current passing in the Ta tube directly heats the target. We measured the temperature using a pyrometer and thermocouples. The temperature versus power test has been performed for two types of target: without fins and with fins. The temperature was measured in the interior of the target and on the edge of the fins. Figure 197 shows the heating test results. The filled circles represent the data for the Ta target with no fins and no heat shields. The filled diamonds and the open

Fig. 196. Photograph of the target equipped with fins used for the heating test.
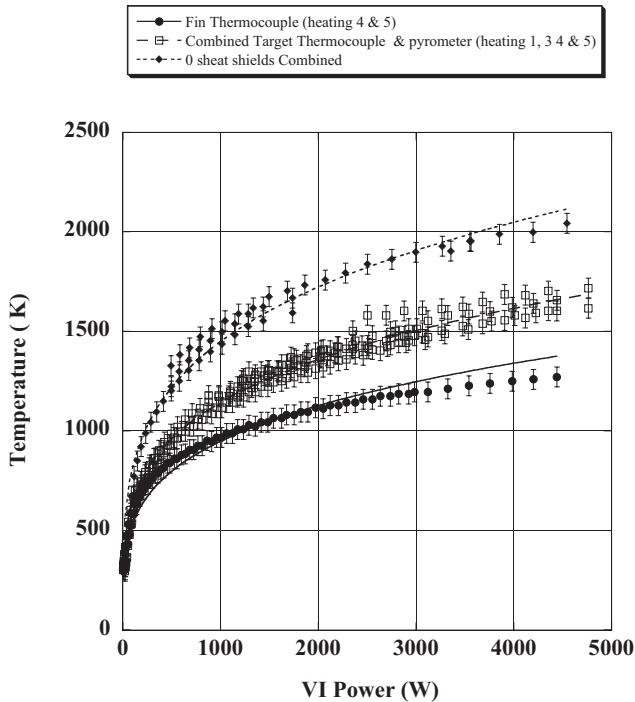
Fig. 197. Heating test of the finned target. The filled circles show the temperature of a Ta tube with no fins and heat shields around it. The filled diamonds show the temperature inside the Ta tube for the finned target. The open squares show the temperature on the target fins. The lines are a fit using the black body radiation law.

squares represent the temperature on the interior wall and on the edge of the fins, respectively.

We can fit the expression for T versus the input power and obtain the value of the emissivity for different targets. The emitting areas are 113.7 and 241.3 cm^2, respectively. We obtain an emissivity of 0.35 for
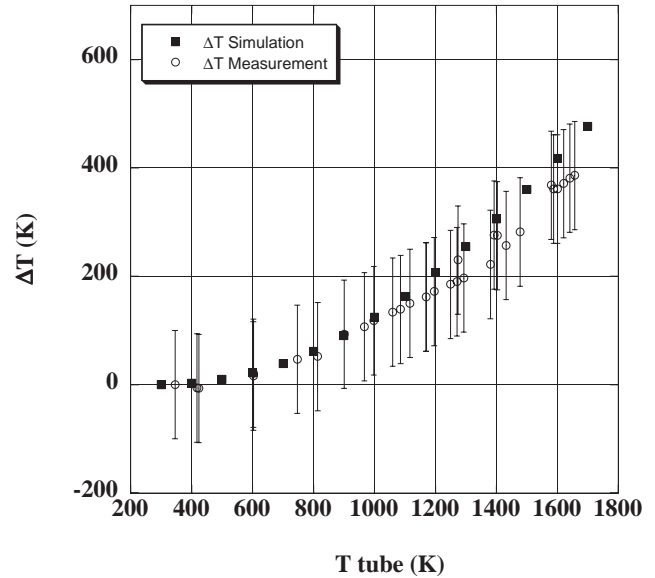
Fig. 198. Plot of the temperature difference ΔT between the target tube interior wall and the edge of the fins. The open circles are the measurements and the filled squares are the results of the simulation.

the target without fins and heat shield, and we obtain an effective emissivity of 0.91 for the target equipped with fins.

The results from the analyses using ANSYS® have been closely comparable to those from pyrometer and thermocouple readings when the target has been heated in a test scenario. Figure 198 shows the temperature difference (ΔT) between the target tube interior wall and the edge of the fins. The filled squares are the results of the simulation and the open circles are the measured temperature differences. As one can see, the ANSYS® simulation is in good agreement with the measurements.

In summary, we have tested a new concept for the fabrication of a target equipped with fins. The fins are fabricated from a square sheet of tantalum installed over a tantalum tube. During the fabrication process we make sure that the thermal contact between the fins and the Ta tube is optimum. We observe an improvement of the resistance across the contact area after the expansion of the Ta tube. The heating tests show that the thermal contact is very good and the simulations also show that we nearly reach a perfect contact between the tube and the fins.

With this target design we are confident that we can go up to the $100\,\mu$A proton beam intensity limit for operation on refractory target foils (Ta, Nb, Mo, etc.) on the condition that the contact between the foil and the Ta tube internal wall is very good. We noticed in our off-line tests that diffusion bonding between the Ta foils and the Ta tube occurred after heating the system at 2000°C for a period of 8 hours.

Before going on-line with such a target we need to test the concept off-line using the same amount of power, say 20 kW. An electron beam heating system is under development to test the target behaviour under such conditions.

Actinide Target Task Force

In March a task force was set up to study the radiation safety problems associated with operating actinide targets at ISAC. The task force prepared a report that both identified the safety issues and defined likely operational changes that would need to be instituted once such targets had been irradiated. The report also outlined a program of proof-of-principle testing that would try to answer issues such as the storage and migration of undesirable alpha-emitting radioactive species and the consequences of their release both on and off site. By year's end a conceptual design had been developed for a testing station that would allow bombardment of ISAC targets at low beam intensities and measurement of the radiological quantities of interest.

ISAC ION SOURCES

Electron Cyclotron Resonance (ECR) Source

The fabrication of a radiation hard ECR source for the ISAC radioactive beam facility has been completed. The ion source was installed in the ion source test stand (ISTS) to evaluate its performance. The source was first high voltage conditioned to the design value of 60 kV. Some weak points have been identified and corrected.

The source delivered a neon beam using helium as a supporting gas. A source ionization efficiency of 10% for Ne^{1+} beam was measured using a calibrated neon leak with leak rate of 1.4×10^{-6} atm cc/s. Figure 199 shows an M/Q scan. In the spectrum the $^{20}Ne^{1+}$ and $^{22}Ne^{1+}$ peaks are clearly seen well separated from the background contribution.

Beam emittance scans were also carried out at the ISTS with the new source. An emittance of $30\,\pi$ mm mrad was measured at 45 keV for a total beam current of $500\,\mu A$. The above results meet the source design and compare quite well with those obtained previously with the non-radiation-hard prototype source.

In December the ion source without the production target was installed in target module #3 for a dry test. The source was operated continuously during the whole month. Again some weak points showed up in the ion source and in part of the beam line downstream of the source. Operation and evaluation of the source will continue throughout January, 2003.

The source will be removed from target module #3 in February, 2003 to carry out some modifications and
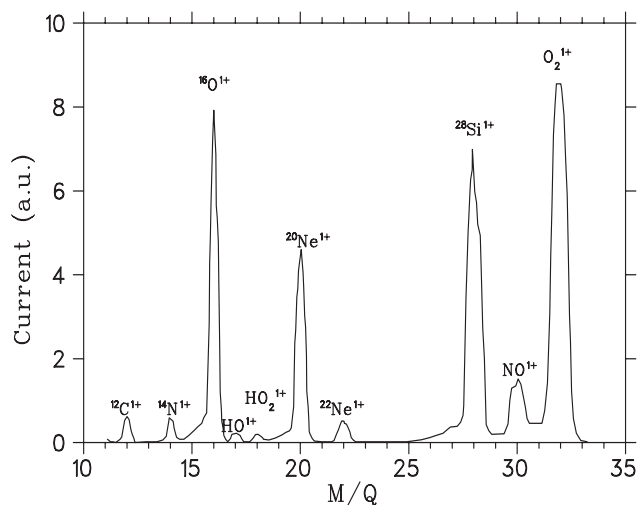
Fig. 199. An M/Q scan of a neon beam. Helium was used as a supporting gas. Two Ne peaks at M/Q = 20 and 22 are clearly seen. The other peaks arise from the residual gases, the silicon most likely coming from the quartz-made plasma chamber.

will be made ready for commissioning with radioactive beams by the middle of April, 2003.

Off-Line Ion Source (OLIS)

OLIS supplied throughout the year beams of ^{21}Ne, ^{15}N, ^{24}Mg, and ^{13}C to the DRAGON and TUDA experiments as well as to other users in the low energy area using the 2.45 GHz microwave source. Some new beams, such as $^{12}C^{2+}$ and $^{14}N^{2+}$ were also delivered.

The source window of the 2.45 GHz microwave source was relocated. As a result of that the lifetime of the source increased; only minor maintenance work was needed within the three months running periods.

A new OLIS terminal has been constructed. It can now support simultaneously three different ion sources (Fig. 200). A surface ion source is being built and will be added to the new terminal in January, 2003. Four high current supplies, to power the three ovens and transfer tube of the surface source, and eight other devices were added to the high voltage rack. The new source will be commissioned in early 2003.

Plans to develop a high breed metal ion source are under way. With this additional source the new OLIS terminal will be producing a large variety of ions to satisfy the multiple experimental requests.
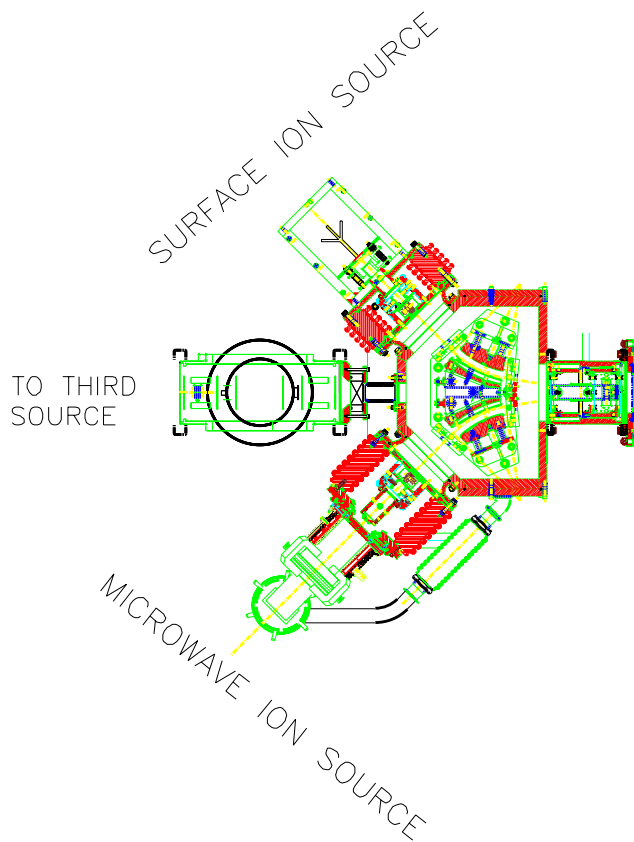
Fig. 200. The new OLIS terminal fitted with the surface and microwave ion sources. A high breed metal ion source will be developed in the near future and will be installed at the centre location of the new OLIS terminal.

Charge State Booster (CSB)

A charge state booster using the electron-cyclotron-resonance (ECR) technique has been developed at the Institute des Sciences Nucléaires (ISN) in Grenoble.

The CSB for TRIUMF, manufactured by PAN-TECHNIK (France) under license by ISN, was ordered in January and delivered to TRIUMF in November.

The 1^+ ion source test bench facility at TRIUMF is being extended to incorporate the CSB for tests and further development prior to its installation in the ISAC hall.

After detailed beam optical calculations the beam transport system has been designed, components have been ordered and their installation is under way. Completion is foreseen by the middle of June, 2003 with beam tests starting in July.

Figure 201 shows the layout of the CSB test facility.
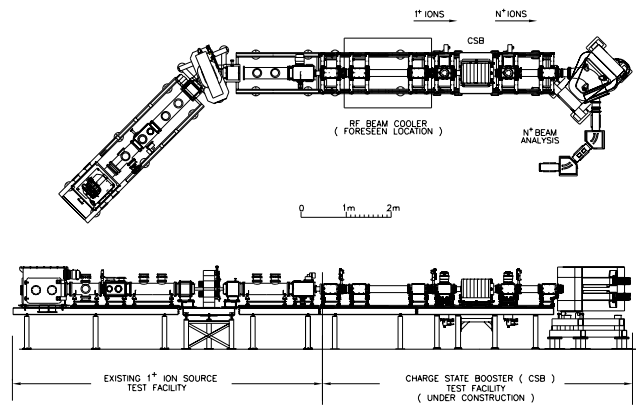
Fig. 201. The existing 1^+ ion source test stand (ISTS) and the charge state booster test facility now under construction. Provision has been made to enable the incorporation of an rf beam cooler in the CSB test bench facility.

Laser Ion Source (LIS)

Within the RIB development at ISAC a resonant laser ion source (TRILIS) is to be set up by 2005 to produce radioactive ion beams to augment the existing ion sources and their capabilities. For this, the position of a "laser ion source spectroscopist" was filled at the end of July. The resonant laser ion source, using multi-step resonant laser ionization, capitalizes on the potential for element selective, efficient photo-ionization, with the major parts of the LIS being located far away from the radioactive target ion source. The current sources are: the surface ion source (good for alkali and alkaline earth elements), and the ECR source (particularly good for noble gases). The resonant laser ion source is to supply beams of metals and transition elements that are otherwise difficult to obtain. The lasers required are tunable, high-power, high repetition rate, narrow bandwidth, and synchronizable pulsed lasers. Typical excitation schemes employ two and, more commonly, three laser excitation steps for ionization, with the laser wavelength for the first excitation step usually being in the blue to ultraviolet region of the spectrum. In a typical laser excitation ladder each further step requires higher spectral energy density.

Current laser ion sources use either excimer- or copper-vapour-lasers, pumping pulsed dye-lasers. The excimer systems have inherently low repetition rates below 1 kHz and, hence, low efficiency due to their poor duty cycle. They are also rather expensive – with the development push going to far UV wavelengths for the semiconductor industries (193 nm), rendering them of increasingly limited use for pumping laser dyes. The efficient laser ion source at CERN ISOLDE uses copper-vapour-laser pumped dye-lasers with post amplification and frequency doubling and tripling. Copper-vapour-lasers emit high power, high repetition rate (about 10 kHz) laser lines in the green

and yellow and are well suited for pumping dye-lasers. However, the copper-vapour laser technology is rather unreliable and out-dated and nowadays is being replaced by other lasers (main application in materials processing) as it is both expensive in installation and maintenance (e.g. the pump lasers at CERN are custom made Russian systems).

Therefore it was decided for the TRIUMF resonant laser ion source (TRILIS) to build on new, diode-pumped solid-state laser based technology. State-of-the-art pump laser technology, mainly frequency doubled YAG lasers, are ideal for pumping solid-state titanium sapphire (Ti:Sa) lasers. This reduces the overall installation and operation cost over the competing copper-vapour-laser dye-laser combination. It does, however, involve the development or adaptation of some technologies, namely the development of:

- new laser ionization schemes, as the wavelength range covered by the Ti:Sa lasers differs from that of the dye-laser systems,
- frequency-tripling for efficient laser excitation of elements such as Be,
- pulse-amplification of Ti:Sa lasers in the final ionization step, similar to that done in dye-lasers,
- improved ion optics and source design for the extraction of the laser generated ions and suppression of background ions (this work also has to be done at CERN-ISOLDE).

To facilitate the development work needed, a clean room grade laser laboratory was constructed adjacent to the ISAC conditioning station (ICB), by expanding and remodelling an existing storage area. These new installations were used for first tests and proof of principle measurements in November. The ICB was upgraded to allow laser access to the target ion source modules, such that development work and off-line tests for TRILIS can be accommodated without affecting the ISAC experimental schedule (Fig. 202). In parallel, floorspace in the TRINAT laser laboratory was cleared, and a laser table together with electrical and other utilities were installed to eventually accommodate the lasers for on-line TRILIS operation. Stable supports for laser-beam transport to the on-line target ion source module in the west target station have been built and installed. Pre-alignment of the laser beams into the on-line target station as well as modifications to the preseparator to accommodate a shuttered, laser grade optical window are under way during the 2002/2003 shutdown.

A state-of-the-art frequency doubled Nd:YAG laser system was purchased and installed in the off-line laser laboratory in the fall (Coherent Corona 75 W, 5 kHz–25 kHz repetition rate), together with a state-of-the-art

Fig. 202. The ISAC conditioning station (ICB) together with the adjacent laser laboratory (not shown) and the lasers under construction are the heart of the off-line TRILIS development. It allows optimum access to all components, lasers as well as the target ion source module and extraction optics.

pulsed and continuous laser wavelength meter (ATOS LM007). This wavelength meter is key to the precise wavelength determination for the resonant laser excitation. As a spin off, the new wavelength meter was also shared in the December polarized beam experiments.

Both instruments were successfully tested in a development/test run in November (just 3 months after project start), when the new off-line laser laboratory and the upgraded ICB were used for the first time (Fig. 203). In this test/development run three automated Ti:Sa laser systems were brought in from our collaborators at the University of Mainz (Dr. Klaus Wendt). These Ti:Sa lasers were operated to resonantly ionize Ca and Ga in ICB and learn about the necessary improvements in ion source and lasers.

The collaboration with the group of Dr. Klaus Wendt from the University of Mainz (Germany), a leader in the field of resonance ionization spectroscopy, was formalized. This group's unique Ti:Sa laser systems that are suitable for efficient resonant laser ionization, as shown by their use in plutonium trace detection, are to be copied for TRILIS. Presently there are no commercial Ti:Sa laser systems available that meet all the requirements for resonant laser ionization. The conditioning station was operated successfully with the help of the Mainz group. The Controls group upgraded the control interface continuously during these initial tests. Different biasing and electrode arrangements were tried in the conditioning station. Resonant laser ionization with a one step resonant, one step non-resonant excitation scheme (1+1′), using two frequency doubled Ti:Sa lasers, was performed on Ca and Ga with encouraging initial results. It was decided
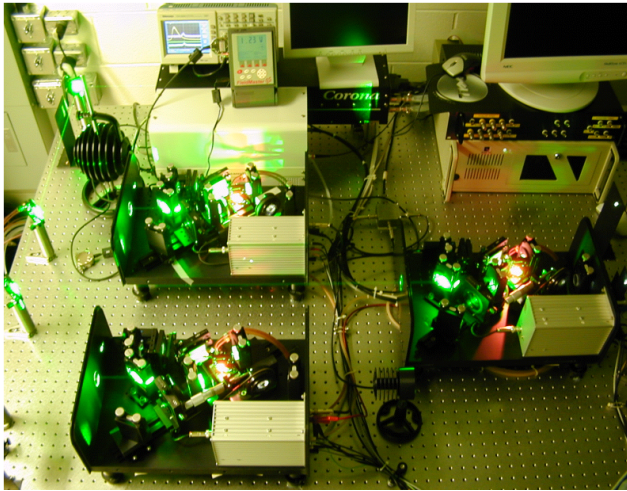
Fig. 203. First TRILIS development/test run in the new TRIUMF off-line laser laboratory adjacent to the ISAC conditioning station. Shown is the compact, state-of-the-art, laser hardware, with the new compact 75 W, 5 kHz–25 kHz repetition rate Corona pump laser (top), the ATOS lambda-meter (adjacent), and the three computer controlled Mainz University narrow bandwidth, tunable Ti:Sa lasers (centre, right and bottom). Not shown are the two Mainz frequency doubling units that were operated in this run as well. The proprietary Mainz Ti:Sa laser systems are now under construction at TRIUMF through our collaboration with the group of Dr. K. Wendt.

that in collaboration with the Mainz group, their proprietary laser systems would be re-built, installed and operated at TRIUMF. Fabrication of components for the lasers and requisition of optics and opto-mechanics for these lasers is under way with first operation of the TRIUMF-Mainz Ti:Sa lasers planned for spring, 2003.

The results from the initial off-line tests of the Mainz laser system and the conditioning station test stand are:

- an efficient TRILIS will have to include a target ion source module with optimized ion optics,
- the simple $(1+1')$ laser excitation for most elements has to be replaced by multi-step resonant laser excitation schemes (e.g. $2+1'$) for higher efficiency.
- the Mainz Ti:Sa lasers proved highly stable and rugged.

For on-line operation the lasers should be located close to the ISAC pre-separator magnet and target ion source, thus the ongoing preparations for an on-line laser laboratory in TRINAT. The overall outlook for 2003 is that the thrust will be towards building three Mainz-type Ti:Sa laser systems with automated controls, set up frequency doubling, as well as to develop, build and test off-line a prototype target-laser ion source module.

ISAC POLARIZER

Polarized beams of ^{8}Li (two β-NMR runs), ^{9}Li and ^{11}Li (one Expt. 903 run), and ^{20}Na, ^{21}Na, ^{26}Na and ^{28}Na (two Expt. 871 runs) were produced for a total of 6 weeks of experimental running time. Polarization was typically 50%, except during the last β-NMR run, when it was greater. The dual frequency Ti:sapphire laser was used for optical pumping during the first β-NMR run. A newly purchased Coherent 899-21 ring dye laser was used for all other runs. The dye laser was performing quite well by the end of the year, although the DCM dye used for pumping Li isotopes has a habit of precipitating out of solution. We are gradually learning how to handle it.

The dye laser frequency lock was upgraded using a new 300 MHz free-spectral-range spectrum analyzer for monitoring the dye laser frequency, in conjunction with a frequency-stabilized He-Ne reference laser. The new spectrum analyzer has higher precision than the original 2 GHz spectrum analyzer. The latter is still required for locking the Ti:sapphire laser and as a reference if the frequency lock (of any laser) is lost. Both spectrum analyzers were enclosed in temperature stabilized, hermetically sealed chambers, which reduced spectrum analyzer drifts by more than an order of magnitude. This eliminated out-of-range problems with the dc voltage offsets to the spectrum analyzer piezoelectric elements. It also eliminated laser frequency drift caused by nonlinearity in the element response.

Slight modifications to the sodium cell design cured a sodium vapour leak and improved the efficiency of the sodium recirculation. The sodium loss rate is now of order 1 mg/hour while operating the sodium reservoir at its maximum temperature of 450° C.

A neutral beam polarimeter was added to the end of the polarizer beam line, downstream of the 3-way bend B21. It measures the beam rate and longitudinal polarization of atoms that are not re-ionized in the helium cell, and which therefore travel straight through the bend. The beam line extension consists of a 5 cm diameter tube with a 5 cm diameter stopper foil inside. The foil has a 5 mm diameter central aperture to allow the laser beam to pass through. Beta particles pass through the tube wall, which is 50 μm thick near the foil, and into upstream and downstream beta detectors in air. Four large Helmholtz coils were added downstream of the helium cell, to preserve the polarization of the neutral beam. A small coil around the stopper foil produces a field of 100 Gs that helps preserve the polarization of the implanted atoms. The neutral beam polarimeter has been used by the β-NMR experimenters as a normalizing monitor for beam intensity and polarization. It is essential whenever the β-NMR

spectrometer is used at low field, when the spectrometer cannot detect backward betas due to the very low solid angle of collection.

REMOTE HANDLING

Modules

This year six new modules for the east target station were built. One each of the exit-1, exit-2, entrance and dump modules, as well as two individual target modules, were constructed. Assembly of the shielding plugs, containment boxes, service ducts and top service caps was completed by Remote Handling technicians seconded to ISAC Engineering. Additional assistance was provided for assembly of the beam optics elements for the two exit modules.

Initially the TM #2 surface source target module was completed and installed for east station beam commissioning, followed directly by the TM #3 target for further development of the new ECR source in this module.

Remote Handling

Remote Handling hot cells activities were primarily in support of scheduled target exchanges for TM #1 in the west target station. Four target replacements were completed this year with differing targets installed as required by the experimental beam schedule.

Residual activity of spent targets varies greatly depending on material and μA h of operation but is documented for future reference. This year the SiC #2 target, removed at the end of February, measured at $1.75\,\mathrm{R/h@}\frac{1}{2}\mathrm{m}$.

At the end of May the SiC #3 target, measuring $4.93\,\mathrm{R/h@}\frac{1}{2}\mathrm{m}$, was removed due to premature failure caused by an electrical short between the ionizer and the outer conductor. Extensive cleaning was required to remove film and other deposits on the extraction column. At this time one containment box cover screw hole was re-tapped in the hot cell, and all box screws replaced as a preventative measure.

Damaged targets are now being systematically disassembled and inspected in the cell to evaluate failure modes. The SiC #2 target proton beam oven was broken in three separate places. SiC #3 target suffered an ionizer transfer tube failure at the weldment to the oven.

The Ta #3 target ($28.3\,\mathrm{R/h@}\frac{1}{2}\mathrm{m}$) was removed in August, disassembled and inspected. It too had experienced a short between the ionizer and the outer conductor and required extensive cleaning. In October the TiC #1 ($16\,\mathrm{R/h@}\frac{1}{2}\mathrm{m}$) was removed and inspected with no major deficiencies noted.

A new SiC #4 was installed during the August target removal. This was the first target to have the inside of the proton beam oven lined with TaC in an attempt to prevent chemical reactions between the target material the and tube wall; a failure mode previously noted during spent target inspection.

Spent targets are now routinely packaged in the hot cell and remotely transported to the spent target storage vault in the target hall. All targets used during the year are now in this storage facility.

Routine hot cell housekeeping required manipulator repairs, work on the tool port feed-throughs to the cell, maintenance of the dry-nitrogen purge system for the Pb-glass shielding windows and work on the module support turntable drive.

Target Hall

Installation continued on the east target station with services laid-in and connected for cooling, power, rf microwave, diagnostics, vacuum and safety interlocks. Pb shielding along the target hall south wall trench was installed for shielding of the active water system between ITE and the cooling package at the west end of the hall.

The RIB beam line between ITE and the preseparator magnet was completed and the ITWIV5 vacuum gate valve was removed from the beam line for adjustment. A new, cooled, proton beam window at the ITE vacuum tank was installed.

EAST TARGET STATION

In January, 2001, the decision was made to complete the east target station, to be operational by spring, 2002. This was not achieved until July, when target module 2 (TM #2) was installed and conditioning commenced. Stable beam was delivered in late August from TM #2 until the end of September, when TM #2 was removed and replaced with TM #3 which housed an ECR source. This was the first time an ECR source had been installed in a target station at TRIUMF. Stable beam commissioning commenced in late October and continued into 2003.

A detailed report, by work package, of the work necessary to bring the east target station into operation was presented in the 2001 Annual Report. The completion of this work in 2002 will be briefly described below.

Modules

East target station entrance and dump modules are mirror images of the west target station units. They do not embody any other design changes and were completed and installed late in 2001.

Exit 1 and exit 2 and the target module all utilized a completely redesigned shield plug and containment box assembly. Redesign was driven by the requirements of the target module, especially the housing of the ECR

source which required five more service connections. Redesign also aimed at improving accessibility for servicing and for improved removal of the service tray and extraction column tray in the hot cell.

The east station exit modules also included redesigned optics in order to be compatible with the ECR source. This, coupled with diagnostics redesign due to the shield plug changes, resulted in basically redesigned exit modules. Installation of the optics and completion of the modules occurred in March and installation of both modules occurred in April. Leak checking and electrical continuity testing followed successfully.

TM #2 was the first module to have the new service connections to the extraction column tray in the containment box. This allows for the complete disconnection of services between the service tray and the extraction column tray such that either can be removed via the hot cell. To achieve this, there are 14 separable water/current junction blocks allowing for the separation of 24 copper service lines which operate at varying voltages – 4 junction blocks are designed to carry currents in excess of 500 A. Routing the 0.25 and 0.375 in. copper tubes with the required spacing to satisfy voltage isolation as well as clearances for tray removal proved to be a formidable challenge and is the main reason the schedule was missed. Due to the close proximity of many joints, soldering was difficult and various techniques had to be perfected. The end result was successful with high voltage checks up to 50 kV achieved to date.

TM #2 was installed in the east station (ITE) in July and delivered stable beam late in August. It was replaced by TM #3 (ECR source) early in October and it delivered stable beam early in November.

East Module Access Area (EMAA)

This is the zone above the modules and vacuum tank and below the 5 removable shield plugs. Experience with the operation of the west target station had indicated that a different approach was required with regard to the running of services in the MAA. The area in the WMAA became congested to the point that general maintenance activities were hindered. To correct this situation, in consultation with the target hall coordinator, a detailed design of the area was produced placing cables in cable trays, rerouting most services to maximize useable floor space, and redesigning the high voltage cage to produce a much neater entry of services to the target module and to allow easier removal. The work was completed during this report period and the results are commendable, as shown in Fig. 204. The west MAA will be reworked in similar
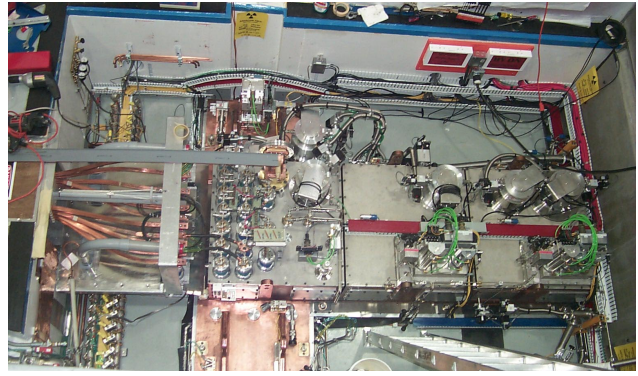
Fig. 204. The east module access area (EMAA).

fashion in the near future. The EMAA also houses the microwave equipment necessary to drive the ECR source. The power supply and controller are located in the electrical room but the magnetron, isolator and auto tuner are located on the south wall of the EMAA, and interface with the wave guide on the top of the ECR target module (TM #3). The EMAA was completed and operational in the summer.

Faraday Cage and High Voltage Chase

Advantage was taken of maintenance days and shutdown periods, during this report period, to complete the installation of power supplies and equipment into the east Faraday cage located in the electrical room adjacent to the target hall. Perhaps the most complex task was routing the ten 0.5×0.5 in. copper high current water-cooled conductors through the bends in the high voltage chase. These are supported by several insulator stands and terminate at a pedestal adjacent to the target module. Flexible cables make the transition from the pedestal to the target module feedthroughs. The chase is then enclosed by shielding blocks and the portion in the MAA is surrounded by the high voltage cage.

ISAC CONTROLS

Highlights of the year include the design and implementation of controls for several new sub-systems:

- Vacuum, optics and diagnostics controls for the east target station including support for an ECR source.
- Completion of controls for the target conditioning station.
- Controls for the ISAC-II cavity test set-up at BC Research.
- Control systems for a target evaporation station and the TIGRESS detector fill system.

During the year, control for 200 new devices was added to the ISAC control system, for a total of 2050 controlled devices.

The distribution of functionality among the EPICS IOCs and PLCs was adjusted in order to decouple different systems as much as possible. The system consists now of 15 IOCs and 8 PLCs.

As in the years before, the Electronics Development Group supplied the hardware support for the ISAC control system, both for design and maintenance.

New Systems

East target station

In order to comply with new specifications for completely independent operation of the east and west target stations, the existing hardware and software had to be reconfigured. One PLC and one VME crate were added to separate west target controls from pre-separator and mass separator controls. Reconfiguring the EPICS software was fairly trivial, but the PLC ladder logic programs needed major surgery. At the same time, all ISAC PLCs were moved and consolidated to one cabinet in the bunker next to the control room.

For the east target station, an additional PLC and VME crate were added to the system. Ladder software and EPICS screens were developed interactively. IOC software and device control panels were generated automatically from the ISAC relational device database. Initially the system was commissioned with a surface ion source. Later in the year, hardware and software support for an ECR ion source was added.

Target conditioning station

Control for 25 optics and diagnostics devices was added to the target conditioning station with the usual complement of EPICS software and displays. Commissioning of the system is complete.

Ion source test stand

The ion source test stand was developed in 1996 as a prototype for the ISAC control system. This year it was upgraded for testing of an ECR ion source. The CAMAC I/O hardware was replaced with ISAC-standard VME hardware, which entailed re-wiring of the diagnostics breakout panel. At the same time, the ladder logic and EPICS software was upgraded to meet the ISAC standards. The test stand is now fully supported by the ISAC device database system.

ISAC-II superconducting cavity

At the BC Research location, the ISAC-II superconducting cavity was supplied with a PLC based vacuum control system and an EPICS system for operator interface and supervision of the rf control system.

In order to streamline the communication between EPICS and the rf system, the EPICS portable channel access server tool was ported to the Windows platform and implemented as a DLL. This makes the rf control

system look and behave like an EPICS IOC and alleviates the need for a special protocol and a bridge-IOC.

For supervision of the BC Research systems from the TRIUMF site, a virtual private network was set up with the help of the TRIUMF networking group.

Other small systems

The PLC system for the mass separator high voltage area lockup was commissioned and integrated into EPICS.

At the target evaporator, a small PLC system (Modicon Momentum series) was taken over from a co-op student. It was reworked and an EPICS operator interface was implemented and commissioned.

For the TIGRESS detectors, an EPICS operator interface for a liquid nitrogen fill system was developed in collaboration with a co-op student, who implemented the underlying Modicon Momentum PLC system.

Functionality Enhancements

All CAN-bus loops and all stepper-motor devices were modified to allow bump-less reboots of IOCs. Each CAN loop was equipped with a monitor module, which takes over the IOC beacon for a programmable time and thus keeps the loop alive while the IOC reboots. The monitor module has a small LCD display, which allows simple diagnostics on the loop. ISAC stepper-motor devices unfortunately have no absolute position read-back and lose their step-count during a reboot. A software work-around was developed, which uses the IOC's non-volatile RAM.

For operator convenience, remote power cycling of VME crates and CAN loops is being implemented. In the first phase of this project, crates and loops in locked-up areas such as mass separator room and electrical services room were connected.

The OLIS IOC, being the earliest installation in the ISAC control system, used commercial VME I/O modules and old TRIUMF NIM current integrators. These were replaced by the standard, TRIUMF-designed VME modules. A diagnostics breakout panel was rewired, the ISAC device database was updated, and the IOC software was regenerated from the database.

For the laser controls of the ILE2 beam line, software was added to support a new dye laser and a new wave-meter. A wave-form replay utility was developed.

For DRAGON, more diagnostics controls were implemented. The NIM NMR modules were provided with signals for remote search range preset.

As a diagnostic help for the RF group, a temperature monitoring system was implemented. Work on a phase measuring system has started. A signal selection system was implemented. The GPIB part of this system is being worked on.

In support of laser tests at the target conditioning station, the fast EPICS binary archiver was installed and tested.

For the diagnostics group, driver and device support was developed for the Highland Technology v680 TDC module. A Motif based GUI for histogram plot was implemented, in order to overcome the plot limitations of the display manager.

For several Faraday cups on the mass separator and the ILT beam line, new current integrator modules were installed, which read lower currents than the VQSX ADC modules.

As a beam tuning help, a program was developed, which dynamically generates a display page with selection buttons for only those Faraday cups involved with the currently selected ion source and beam mode. The selected cup current is routed to meter widgets on the page.

The PLC ladder logic software was reviewed and received minor upgrades for consistency, to accommodate specification changes by the Vacuum group, and to keep track of operational hours for some devices.

System and Development Support

Two more Linux PCs were added to the operations console. This showed the limitations of using the console PCs as X-terminals since they overloaded the SUN display server. To remedy this situation, an EPICS system was built for Linux. Now the display applications run in native mode on Linux, while the SUN is used as an archive and alarm server. In order to resolve problems with the look-and-feel of the EPICS screens across various platforms, an X font server was installed. It is used by all X-servers on the Linux consoles, the development and production Sun workstations, and the Windows based development PCs. The Linux console PCs are managed by Chris Payne from ISAC Operations who, during shutdown periods, was again a valuable addition to the Controls group.

Two more production SUN workstations were added to the system. One serves the target conditioning station, the ion source test stand, the evaporator, and the TIGRESS detector fill system. The other one serves the ISAC-II cavity test at BC Research. Another SUN workstation was converted from a development machine to a production machine to alleviate congestion in serving displays to experiment groups.

Again this year, a considerable amount of time went into system maintenance on the development and production machines, especially into security enhancements, fire-wall improvements and support for the Linux consoles.

A new line of development was started by acquiring x86 based single-board computers on a PC 104 plat-

form. They will be used as low-cost EPICS IOCs for special applications, e.g. small GPIB nodes, supervision of PLCs, etc. The manufacturer's vxWorks board support package was integrated with Tornado II and the BIOS was modified to allow a diskless boot of vxWorks.

More documentation, tutorial material and troubleshooting information was added to the ISAC controls Web site.

As a database exploration project, the ISAC controls asseting database was converted from Microsoft Access to the public domain database system PostgreSQL. This database is accessible by Web browser. The Web interface was implemented using the Perl DBI module.

Commissioning and Operation

After commissioning of the east target station early this year, the support of beam delivery became a priority. This was sometimes difficult as many scheduled maintenance days were used for beam tests with stable beam.

Implementing bump-less IOC reboots reduced the downtime due to controls considerably. The same can be said for the addition and reconfiguration of PLCs and IOCs. A balance, however, had to be achieved between cost and functionality. As a consequence, several of our IOCs operate with a memory load, which is higher than comfortable for extreme operating situations.

VACUUM

The vacuum systems of the cyclotron, cyclotron beam lines, ISAC-I targets, ISAC-I beam lines have been functioning well for beam production during the year.Vacuum problems encountered were dealt with in a timely manner and the impact on the beam production was negligible. The ISAC-I east target vacuum system was built and successfully commissioned.

Cyclotron Vacuum System

Three instances of problems occurred with the B20. These were all related to the regenerators on the 20 K stage.

A new Varian 551 turbo pump was installed on the cryoline connecting the B20 cryogenerator to the cyclotron. The pump replaced the original diffusion pump to shorten the turn around time during cryogenerator defrosts.

Beam Lines

A large vacuum leak occurred in the 2C4 line due to the beam induced melting of the indium seal. This seal was replaced. A number of vacuum leaks were diagnosed in beam line 1A. These are scheduled to be

fixed during the spring shutdown. The rest of the group activities concentrated on routine MRO.

RF SYSTEMS

In 2002 the ISAC rf systems performed well with an overall reliability of about 94%. The major activities include:

- ISAC linac maintenance and operation.
- DTL power couplers protection.
- DTL fine tuner upgrade.
- Phase measuring system development.

RFQ

The RFQ operated quite reliably during the past year. The only trouble experienced was associated with malfunctioning of the ac switchgear system feeding the anode high voltage power supply. Both the conventional breaker and fast switchgear failed. The breaker contacts melted and welded together. The switchgear had difficulties due to transients in the control circuits. Both malfunctioning units were replaced. In order to provide a smooth start up for the system, a dedicated ramping circuit was developed. It is based on SCR elements and allows a slow voltage rise to prevent high inrush currents and very fast power cut off (8 ms compared to 24 ms in the mechanical switch), to reduce ignitron tube overloads.

For the RFQ structure a high power pulsing had been performed twice to reduce the build up of dark currents.

MEBT Rebuncher

Most of the problems with the rebuncher were triggered by unstable operation of the commercial rf amplifier, which could easily go into parasitic oscillations when loaded with an unmatched high-Q resonant load. Poor design of this amplifier made it difficult to reliably adjust or modify. An entirely new 35 MHz, 500 W amplifier was built and commissioned in March and has since operated very reliably.

DTL

DTL systems routinely operated mostly at about 4/9ths of full power (A/q $\approx$ 4) according to scheduled experiments. A lot of effort was dedicated to reliable operation of DTL rf amplifiers, couplers, tuners, troubleshooting and upgrade. During the winter shutdown all the DTL cavities, fine tuners and couplers were opened for inspection and assessed for problem areas (see corresponding sections below). Most of the tank inner surfaces were darkened and sometimes discoloured due to multipactoring. No spark traces were detected on rf structure elements. Similar to last year, soldering flux patches were observed, this time around

Fig. 205. Soldering flux patch in DTL tank #4.

the upstream nose cones of DTL tanks #3 and #4 (see Fig. 205). This is a manufacturing defect, which is very difficult to eliminate. Residuals were cleaned off the surface.

Last spring a safety interlock for the DTL radiation protection cage entrance was commissioned. It allows access to the DTL cavities only when rf is below a predetermined radiation limit. RF cannot be turned on if this safety interlock is not engaged.

In 2001 we faced many interruptions caused by vacuum trips. Replacement of ion gauges, installation of screening grids and distancing the ion gauge from the cavity volume by means of extension pipes did not solve the problem. On the assumption that the problem was caused by a penetration of charged particles ionized and accelerated in the presence of an rf field, extension elbows were installed on all DTL ion gauges and the problem disappeared. Other DTL system interruptions were caused by water flow interlock trips. This was traced down to a grounding loop problem, which led to malfunctioning of the control boards and was subsequently fixed with proper grounding.

DTL amplifiers

All the DTL rf systems are energized by identical 106 MHz amplifiers based on an EIMAC 4CW25000B tube. Last year most of the tubes had reached 10000 hours of operation and a substantial degradation in their performance was observed. One tube showed a

216

grid to cathode short, filament burnt in another one and 4 more aged, providing low cathode emission. Five tubes out of 8 tubes in operation had to be replaced. This triggered a detailed investigation on the tube performance. Two major conclusions were derived as a result.

1. Hairpin filament structure in a different tube type (4CW25000A) is almost insensitive to thermal deformation, while the tube is warming up, compared to the mesh filament structure (4CW25000B). So, application of a type-A tube dramatically cuts the downtime for system conditioning and reduces the probability of a thermal grid-to-filament short circuit.

2. Most of the tubes were running at slightly increased filament voltage, which is good for tube conditioning but not for operation. The supplier claims a 15% reduction in filament voltage should double the tube lifetime.

Based on these findings, we decided to gradually replace all B-type tubes in use with A-type tubes (4CW25000A). Also all filament transformers were replaced with new ones with proper voltage taps and all filament operational voltages were reduced by 15% from the nominal values.

Several amplifier trips due to insufficient water flow in the anode cooling circuit occurred due to a clogged pressure reducing valve with water impurities. In the September shutdown a dedicated filter was installed in the system.

DTL couplers

Due to the number of coupler window failures, infrared temperature sensors were installed on all power couplers to diagnose the problem in the early stages of deterioration. Indeed it helped to detect 4 more coupler deteriorations and save them from being destroyed. In DTL tank #2 a silver alloy evaporated from the coupling loop soldering joint (see Fig. 206) and spattered all the surfaces around including the ceramics (see Fig. 207). Three other couplers failed in DTL tank #5. Couplers were replaced with spare ones and an enhanced study was conducted in order to determine the cause of the trouble. A dedicated vacuum vessel was set up to test the couplers (see Fig. 208). A 106 MHz test amplifier provided rf power up to 8 kW.

Test studies brought us to a conclusion that coupler coating is triggered by a secondary electron emission discharge (multipactoring). In DTL tank #5 it happened during abnormal operation of a starting procedure when switching from pulse to cw mode causing excessive rf voltage. RF controls operational parameters were readjusted and failure never happened again. Buncher #2 coupling loop was copper plated to screen
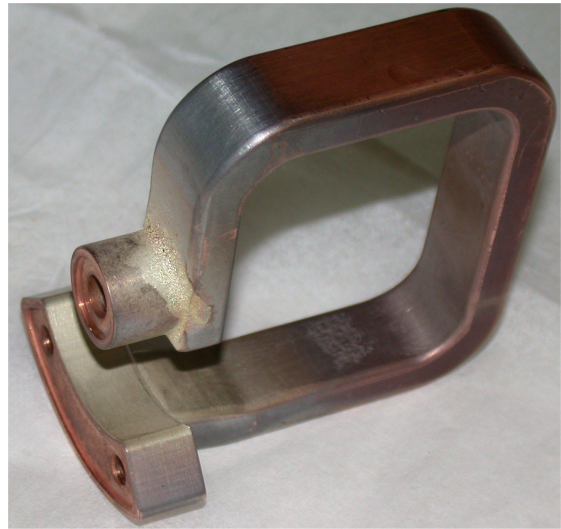
Fig. 206. Buncher #2 coupling loop with a failed soldering.
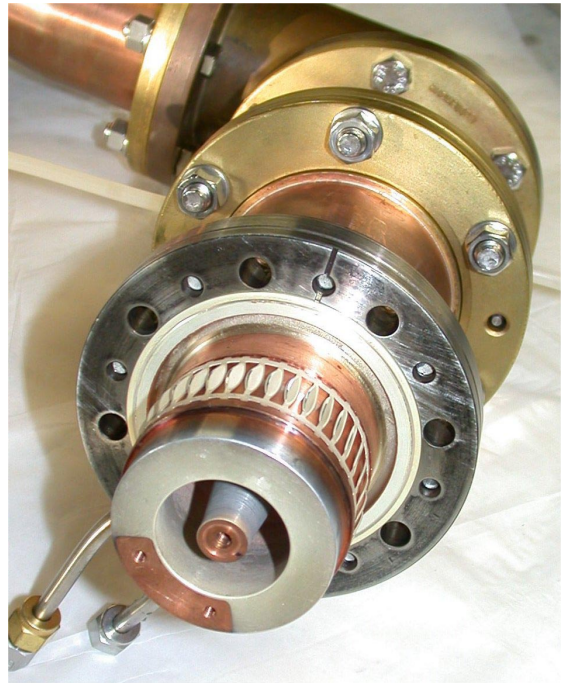
Fig. 207. Buncher #2 coupler – silver spattered.
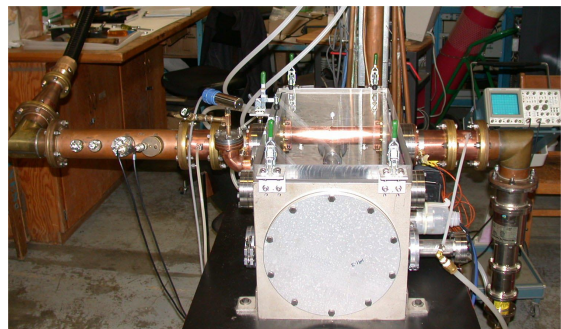
Fig. 208. DTL coupler test stand.

217

the brazing alloy from rf fields. All other coupling loops are scheduled to be copper plated as well during the next shutdown.

An easy and economical restorative solution has been found for the degraded couplers. It involves an abrasive removal of the coating by means of a sand blaster. With this procedure all 4 malfunctioning couplers were rebuilt to their original specifications.

DTL tuners

All DTL systems use capacitive tuners driven by identical drives. The weakest point of this drive appeared to be the rf fingerstock contacts between the moving copper shaft and a ground flange. During shutdown inspection almost all shafts were found scratched. The most damaged MEBT rebuncher tuner shaft is shown in Fig. 209. The reason for this failure is a constantly moving tuner, which operates in a feedback loop for frequency regulation. The fingerstock cannot stand that heavy load. Operating in vacuum without lubrication, they get worn and start scratching the copper shaft. These contacts serve to shield a stainless steel bellows from rf currents, which could result in excessive heat on the bellows. An extensive design review and bench tests were undertaken which led us to the conclusion that the fingerstock could be removed without causing excessive heat on the bellows. Bench tests showed that 25 W dissipated power caused a bellows temperature rise up to 100°C without cooling while application of air cooling allowed 100 W power
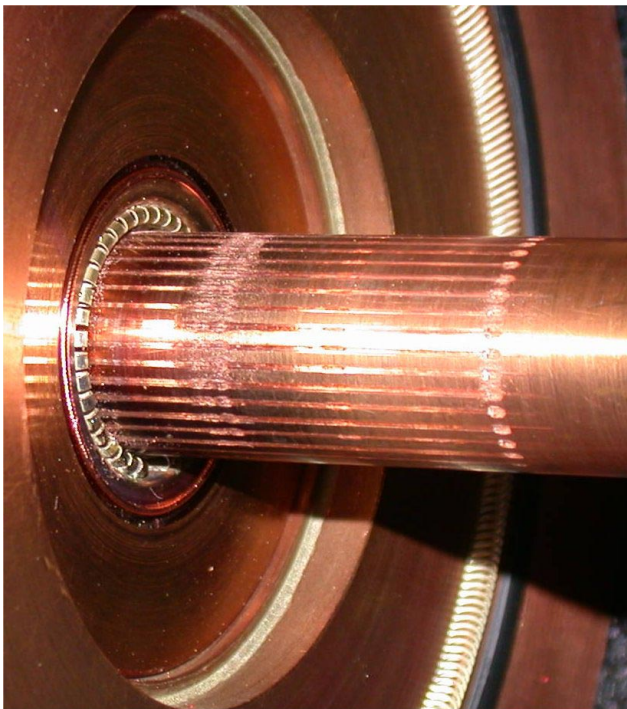
Fig. 209. Damaged MEBT rebuncher tuner shaft.

dissipation with a moderate 40°C temperature rise. A full-scale test on DTL tank #5 confirmed our optimistic assumptions regarding operating the tuner without fingerstock. At a 20 kW power level the bellows temperature rose only by 6°C even without air-cooling. Following this positive outcome we removed the fingerstock from 4 more DTL operational tuners. Subsequently all the modified tuners were equipped with thermocouples to ensure our control over bellows temperature. A few months of operation didn't show any noticeable degradation in system performance. The rest of the tuners are scheduled for modification during the next shutdown.

HEBT High Beta Buncher

The 35 MHz high beta buncher showed reliable operation last year, apart from one failure when a coarse tuner plate disintegrated from the shaft and shorted the rf spiral structure. The cause was traced to the wrong size of lock screw, which connects the plate on the shaft.

Phase Measuring System

An auxiliary phase measuring system has been developed for the ISAC rf system. It provides precise phase difference measurements between the reference rf source and each individual rf device. The need for this system comes from the operation of a multi-cavity variable energy linear accelerator, which dictates very high tolerance (fraction of degree) for rf phase stability and reproducibility. The set-up includes a frequency synthesizer, an rf switcher and a Hewlett Packard vector voltmeter (see Fig. 210). The synthesizer is excited by a 5.89 MHz ISAC rf controls reference signal and provides all ISAC rf system harmonics: 5.89, 11.78, 23.57, 35.36, 106.08 MHz with a very good stability (0.1°) with respect to the reference signal. An rf switcher combined in 6 NIM modules provides proper rf connection of the voltmeter to the desirable rf cavity and corresponding frequency multiple harmonics from the synthesizer. The SW221 chip is a basic element of the switcher. It provides 100% reproducible connection and very high isolation between channels (better than –75 dB). The vector voltmeter measures amplitudes and phase difference between 2 rf signals of the same frequency. Voltmeter phase resolution is about 0.1°. All the rf signals are canalized through semi-rigid phase stable cables in order to reduce temperature dependence and dielectric aging effect. The device is located in the DTL cage vicinity to make all feeding cables shorter and thus further reduce unwanted systematic errors. All hardware was tested and calibrated. An EPICS based control system for this device will be commissioned at the beginning of next year. In
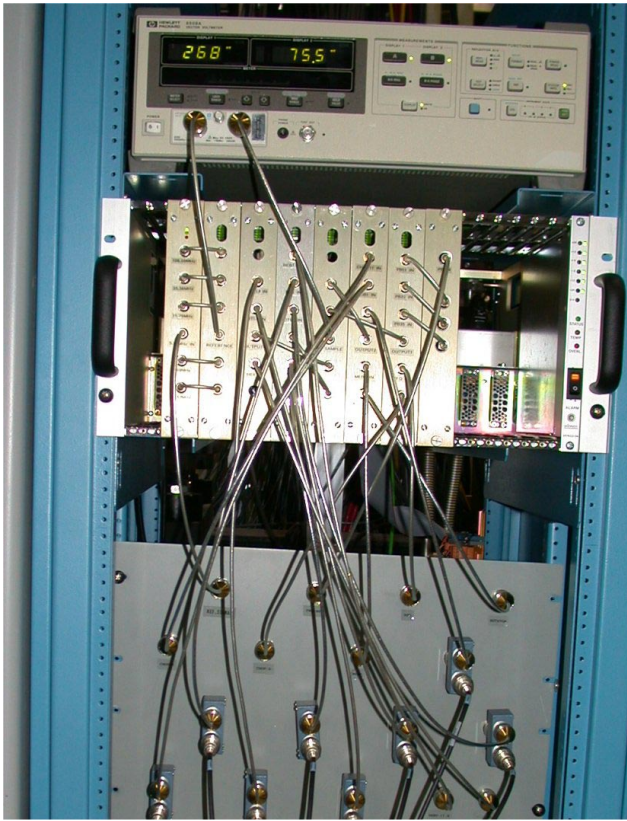
Fig. 210. Phase measuring set-up.

the manual mode this system has already helped us in troubleshooting beam instabilities.

RF Controls

Over the year the RF Controls group regularly provided routine tune up of the rf control system. Upgrade work had been done on the input circuits of the control modules in order to increase stability and reduce rf interference between subsystems.

A sufficient stock of spare modules has been built.

The rf controls system is operated by special software running on personal computers (PC) under Windows-95. Over time these PCs are becoming obsolete. During operation, we have intermittent software crashes due to PC hardware problems, many of them thermal in nature. To improve system reliability, 3 out of 6 operational PCs were replaced with newer units. The rest are scheduled for upgrade during next year.

BEAM DYNAMICS

The ISAC test stand is to be extended to test the charge state booster (CSB) for ISAC-II. Optics were designed to match into the CSB, leaving a 2 m long $-I$ transfer section open to allow for possible later testing of an RFQ cooler. After matching out, beam is directed through a $90°$ magnetic bend and two $45°$ electrostatic

bends. The combination allows a mass resolution of 250 in spite of an energy spread of 2%. All optical elements are standard ISAC LE designs, except for the magnetic dipole, which was inherited from the decommissioned M8 beam line.

The following LE beam line sections were commissioned or re-commissioned: GPS, 8π, Osaka, new bender for the OLIS. All performed as designed, with settings close to theoretical values.

We began development of a graphical user interface (GUI) for beam envelope calculation. The purpose of this is to allow operators to calculate beam envelopes on the fly as they are changing beam line tunes. It is foreseen as a tool to aid in tuning all the ISAC beam lines, as well as ISIS and the cyclotron extracted beam lines.

BEAM COMMISSIONING AND DEVELOPMENT

In 2002 the ISAC accelerator moved from commissioning and training to full beam delivery mode. No new equipment was commissioned during this period. Work instead consisted of operator training as well as standardizing tuning schemes and providing tuning support for new experimental set-ups.

Beam Delivery

Stable beams of ^{4}He^{1+}, ^{12}C^{3+}, ^{14}N^{4+}, ^{20,21}Ne^{5+}, and ^{24}Mg^{6+} were delivered to the two experimental facilities DRAGON and TUDA at various beam energies. Radioactive beams of ^{20,21}Na^{5+} were delivered to DRAGON during two different run periods.

A summary of the stable and radioactive beams delivered to experiments through to the end of 2002 is shown in Fig. 211.
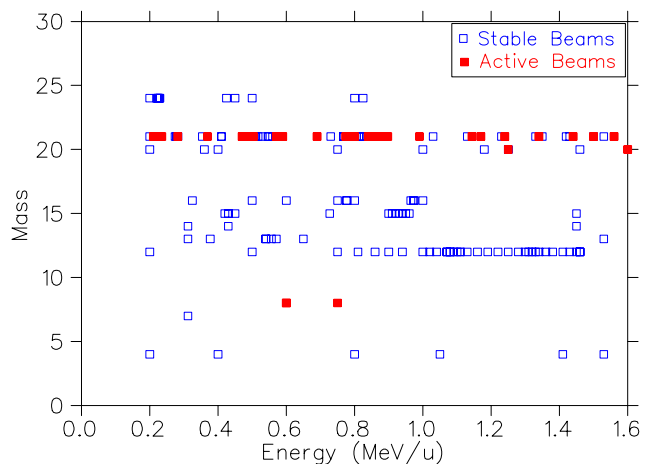
Fig. 211. A summary of stable and radioactive accelerated beams delivered to experiments through to the end of 2002.

Upgrades

The Prague magnet, a 90° analyzing magnet in HEBT, is used for measuring the energy and energy spread of the accelerated beam. The field is set by a Hall probe located on the magnet entrance. Due to the large energy range and A/q range of the delivered beams, the Hall probe has to accurately cover a wide field range. Initially the Hall probe was given two gain ranges. It was found that there was a small offset between the two ranges and so energy measurements at the transition zone were dependent on the gain range selected. A single gain range spanning the full field range has now been implemented.

ISAC DIAGNOSTICS

Fast Faraday Cups

The rf bunching and accelerating fields in ISAC gather the beam into short bunches whose length is measured by fast Faraday cups (FFC). At low beam currents their signal can be buried in noise but the averaging features of the development Tektronix TDS 820 6 GHz oscilloscope enhance the coherent beam related part. There are now several FFC in ISAC and a reconditioned Tektronix TDC8000 6 GHz sampling oscilloscope has been purchased and installed in the HEBT for their use. This oscilloscope can accommodate up to four dual input modules but since these are expensive, only one was purchased and instead a rf signal multiplexer was built. The development oscilloscope is presently on loan serving the MEBT FFC.

Control of the oscilloscopes and the remote display of their screens is performed by a LabVIEW program running on the Sunray control computer. The previous set-up used a National Instruments Ethernet to GPIB adapter with GPIB driver software in LabVIEW to communicate between the control room and the oscilloscope. The adaptors were replaced with units from Agilent that use the VXI-11 protocol of VISA 2.6 and this eliminated the need for the GPIB driver layer of software. The LabVIEW program was revised to take advantage of special features of the TDS 8000 that enhance the display.

The bunch shape at currents below the threshold of the FFC has been measured using a thin gold target to scatter ions into a silicon detector. Analogue nucleonics and a MCA have been used to acquire and display the data. The ISAC Electronics Development group has collaborated in writing an EPICS driver for a Highland VME TDC and this will allow the ISAC control system to display the bunch shape directly to the operators.

The geometry of this first detector used a rather backward scattering angle of 98° in order to observe a well-documented α-C resonance; the choice of angle was also constrained by neighbouring equipment. The data accumulated had almost no background but the count rate was slow and the permanent monitors now being drawn up will use a more forward angle of 30°. The targets have been damaged in the past by vacuum accidents. Flow restrictors have been fitted to both the venting and pump down lines and the new design will retract targets into a sleeve for further protection.

The Electronics group has also built a current integrator and digitizer that, with a small local 12 V power source, could be placed close to the electrical feedthrough of, for example, a Faraday cup in order to reduce the effect of any external pickup and improve the beam measuring sensitivity.

Our standard FFCs extend along the beam axis and are too long to fit into the narrow monitor boxes of the linear accelerator and bunchers. Argonne National Laboratory developed the concept of a FFC based on a stripline placed normal to the beam direction. We have designed and partially assembled such a monitor. It is formed from a copper plated ceramic board and the FOILTEMP program was used to investigate heating of the thin copper mesh that will shield the pickup electrode from the EM field of the approaching beam bunch. It will allow beam bunch shape measurement in the diagnostics boxes of the DTL or ISAC-II provided that a beam current of 10 to 50 enA is available.

Prague Magnet

An air-cooled 90° bending magnet, the Prague magnet, has been used as a spectrometer to commission the ISAC-I accelerators. The current from its power supply is stabilized, at all but the highest values, by a signal from a commercial Hall probe processed by TRIUMF-built electronics. The probe and module had been calibrated against an NMR in a different magnet and the system cross-calibrated against two well known nuclear resonances. The data available led to the belief that the system was linear. Nuclear physicists began to use this spectrometer to measure beam energies and incorporate the results into their analysis. The results accumulated over time implied that the resolution and reproducibility were not sufficiently accurate for their purpose.

The ISAC Electronics group modified the electronics to provide a single scale that spanned the operating range of the magnet and thus eliminated differences in offset between two scales. The probe and electronics were calibrated at finer intervals and a significant non-linearity discovered; it arose chiefly from the electronics. A different probe and a more linear module were obtained and installed in the magnet. The stability of the current from the power supply was measured using a DCCT. Data taken when the supply received

its feedback signal from the Hall probe showed a just acceptable drift.

The magnetic field of the magnet has not been mapped in its entirety because of its shape. This ought to be done since the yoke goes into saturation and becomes sensibly warm at fields required by the more energetic heavier particles and it may be that portions of the iron behave differently from those where the probe is located. An alternative might be to calibrate the system over its momentum range using known nuclear reactions.

Other ISAC Diagnostics

ISAC has delivered beams to several types of experiments over the past two years. Several ion species, both stable and unstable, have been delivered at energies ranging from those emerging from the ion source terminal to ones accelerated by the RFQ and DTL. Diagnostic requirements were re-evaluated in the light of this operating experience and new priorities have been assigned. The top priority is an instrument to measure beam flux at cw currents from a few per second to 5 epA. This is followed closely by a) a device to measure the phase at each tank of the DTL at currents < 5 enA; b) modification of that equipment in HEBT which uses particle detectors or electron multipliers to measure the distribution in time of a low intensity beam bunch to (i) shorten the collection time and (ii) also give the distribution in space; c) installation of such a low intensity profile monitor in front of the MEBT chopper slits and d) elimination of the electrons created by field emission in the DTL that can mask signals from the beam.

A lot of effort early in the year went into equipping the new east production target for ISAC. Profile monitors 2A3M17 and 2A3M18 for the proton beam were installed in the east leg of 2A and also a new secondary emission harp profile 2A2M18 was installed upstream of the west target station. (This was used in the test of the VICA 96 cards described in the Engineering Physics section). A wire scanner and protect monitor were built and installed in the target entry module. Two harp profiles, a shutter monitor, collimators and a Faraday cup were installed in the exit modules leading to the preseparator region mimicking the arrangement on the west side. All were equipped with cables and signal processors, and connected to the control system and tested.

The standard target protection monitors derive their signal from electrons produced as protons pass through their plates. Ground planes are placed between biased plates and signal plates to intercept any leakage currents. A similar construction was used successfully in the manufacture of a quadrant halo plate monitor

for the TUDA collaboration, although in this case ions stop on the plates.

The Faraday cup in the diagnostics box DB0 near the dispersed focal plane of the pre-separator magnet was damaged during a high current test of the stable beam from the ITE ECR source in September, 2001. A temporary repair was made while a new Faraday cup was being designed to permit higher beam power. The repair was done using a special glove box designed specifically for DB0 devices. It was a very useful learning experience in dealing with components contaminated by radioactive dust and ions. Absolute encoders were also installed for improved control of the DB0 slit and Faraday cup motions. The new Faraday cup will be installed in February, 2003. At the same time the DB0 slits will be replaced as an MRO exercise; in part to test the remote handling techniques that have been developed and in part to reduce the accumulated inventory of activation.

A second employee has been taught to lift and mount the 3–5 μg/cm^2 stripping foils used between the RFQ and DTL. A number of foils were prepared and loaded on the MEBT foil changing mechanism. Following the Beam Instrumentation Workshop at Brookhaven, the opportunity was taken to visit the BNL laboratories and shops manufacturing equipment for the electrostatic heavy ion pre-accelerator and the cryogenic synchrotron, RHIC. We were impressed by the stripping foil exchange mechanism designed by BNL; it is more reliable and easier to service with foils than the second hand NEC mechanism presently used in MEBT. Drawings have been obtained from BNL and their design principles will be used for any new foil or target changes required for ISAC-I or II.

ISAC-II

The components in each of the cryomodules being built for ISAC-II will have their alignment checked before installation. A system under development will attach quadrant stripline position monitors to each, solenoid and rf cavity. They will sense the field created when an rf signal travels down a wire stretched parallel to the axis of the module. This system, which will be a major project in the coming year, will be transferred from module to module as they are built.

General

We have purchased a turbo pump and a roughing pump with their necessary controls and gauges. A vacuum station will be set up in the probes lab and used initially for testing equipment before installation and, in the longer term, for various research and development projects.

Once again a significant amount of time has been consumed by routine maintenance work and other gen-

eral activities; this was exacerbated by the illness of the MRO technician. Radiation damaged cables were replaced, modules replaced or repaired and the frequent failures of the 0865 300 V bias supplies has necessitated a program to modify them all. Advice is given regarding interpretation of signals to operators and experimenters and a talk on the Principle of Beam Instrumentation used by Nordion was given to a new group of AT operators.

Meetings

The Diagnostics group biweekly meeting notes are available electronically via the Operations CYCINFO information service on the site computer cluster (accessible also through the TRIUMF home page on the WWW). The winter cyclotron shutdown activities, including the report on the ISAC DB0 installation, are summarized in detail in the Diagnostics group meeting notes of May 24, 2002. The detailed fall shutdown report is included in the meeting notes of October 11, 2002.

EXPERIMENTAL SUPPORT

The Experimental Support group, which includes the Beam Lines group, is part of the Science Division and was responsible for the installation, alignment and maintenance of the experimental facilities at TRIUMF as well as support for the primary beam lines and maintenance, repair and operation of the secondary channels. As in 2001, the group supplied technical assistance to the existing experiments as well as technical support to ISAC. The Beam Lines group continued to provide alignment assistance to ISAC, Remote Handling and the RF group.

2A Beam Line

The beam line to the east target station was installed and aligned. The first 15 degree bender was moved to a second position. The 2A Wye magnet was installed in its place with steering magnets and "bunny" quads also installed and aligned. The Wye magnet can switch beam from the west target station to the east target station. The overall project took about 2 months.

β-NMR

A permanent telescope mount was placed after the GPS 2 alignment port to align the cryostat in the β-NMR experiment. This allowed the position of the sample to be checked without compromising the vacuum.

DRAGON

Two lead shielding frames in the DRAGON beam line were installed to protect personnel from X-rays emitted from the diagnostic boxes inside.

A DRAGON target analysis telescope was designed and installed. An Opti-Cal program was used to calculate the lenses required for focusing on the DRAGON gas target. The photograph obtained using an astronomical colour camera illustrated the hydrogen gas target beam glow.

GPS 2

A beam tube in the LEBT line was modified with glass view-ports to see the polarimeter without breaking vacuum.

Magnets

The old M8 bender magnet was rebuilt and installed in the off-line ion source test stand. The magnet needed new lifting lugs and the pole gaps were shimmed to meet the specifications for bending the beam into the analysis station after going through the charge state booster. The water manifolds and hoses were replaced as well as the thermo-switched interlocks. The magnet was field mapped and assembled on the stand and aligned in the test stand beam line.

CONVENTIONAL FACILITIES AND INFRASTRUCTURES

A number of construction projects were completed and a good number of maintenance activities carried out. Continuing engineering support was lent to ISAC Operations group, the Accelerator group, the Engineering group and the Science Division. General activities included attendance at regular progress and engineering meetings and participation in engineering design review. Dust accumulation continues to be a concern in the experimental hall, where a large number of electronic devices are housed. This problem has to be tackled once the construction of ISAC-II is complete.

Electrical Services

Engineering efforts focused on the experimental facilities, the target conditioning facility and the east target. Completed tasks included services for experiments like DRAGON, TUDA, 8π, the polarimeter, Osaka, the laser spectroscopy experiment, and other facilities like the laser ion source, the target evaporator, the 60 kV bias target conditioning system and upgrade to OLIS. About 40 installation orders were processed for ISAC alone. The majority of wall mounting transformers were retrofit with aircraft cables for seismic anchoring and the grounding around the LEBT was improved. The east target ion source HV terminal and grounding were commissioned in February.

Support to the Safety group continued with the installation of the tamper-proof conduit runs for the radiation monitoring systems and the HV interlock systems.

On the maintenance front, we had a couple of serious problems to address. The RFQ main relay started malfunctioning. As a result, the feeder breaker in MCC-T, the main power distribution centre, failed possibly due to overstress since the over-current protection function of the main RFQ relay had not been working reliably for some time. The breaker was replaced and the breaker-relay time coordination curves revisited. It was determined that the very high start-up (*in-rush*) current requirement of the RFQ input transformer together with a very fast trip function could not be satisfied by a standard industrial breaker or the relay. To limit the in-rush current a soft start device was considered as an addition to the existing RFQ line. The RF group took it upon themselves to install the soft start interface during the upcoming shutdown. One of the power supply cards of the experimental hall UPS failed. The failure revealed a mis-coordination between the UPS unit breaker and the feeder breaker. The latter will be replaced during the next shutdown. A replacement section for MCC-X was purchased and will also be replaced during the upcoming shutdown.

Mechanical Services

A large effort was spent on the completion of ISAC-I. The east target project included installation of cooling water, compressed air, vacuum, and air conditioning service spread over three areas: target hall, electrical room, and BL2A tunnel. New laser installations in room 104 and the experimental hall required ventilation and cooling water service. New water service was provided for the low-β buncher and new filters installed for various rf power supplies. Vacuum roughing lines were provided for GPS and β-NMR. Target lab jobs included water to the evaporator, and vacuum pump exhaust.

Development and MRO work included a new flow switch for the DRAGON hydrogen vent, new circulation pump for the DRAGON cooling package, more fresh air inlets (some to replace those covered up by ISAC-II links) for summers in the experimental hall, new chiller 1 refrigeration compressor, repairs to 8π, TUDA and TRINAT air conditioning, leaks of roof top units, non-active low conductivity water de-ionizer resin catcher, and festooning cable of experimental hall crane.

Various maintenance activities included the replacement of the Chiller #1 unit which failed the previous year, the repair of AHU #3 in the electrical room and regular servicing of the various air conditioning units and the target radiation exhaust system.

Engineering assistance was lent for calculations of gas escape rates in the solenoid helium vessel, and water flow rate through the ECR source.

The ISAC-I distributed digital control (DDC) was converted and integrated with the ISAC-II DDC. The new DDC system allows the operator to interface through EPICS. The conversion proceeded with most of the control systems replaced, installation of new outlets in the main control room and trailer V, and personnel training.

The temporary SCRF lab at BC Research required installation of clean room ventilation, an ultra-pure water supply system for the rinse, and nitrogen lines. Tie-ins for ISAC-II gas, compressed air, and various water systems were made in the existing ISAC-I lines.

ISAC PLANNING

This year the Planning group was involved in planning, scheduling, coordinating and expediting several sub-projects for both ISAC-I and ISAC-II.

Technical details and progress on PERTed activities are described elsewhere in this report under the respective principal group. However, following is a summary of the main projects along with the major milestones achieved.

ISAC-I

Various plans and PERTs were prepared and updated regularly with manpower estimates and analysis to identify critical areas and resolve any problems. ISAC priorities were evaluated and higher priority was assigned to: the east target station that was installed in the winter shutdown; the ECR source (to be installed in TM #3 and tested with beam in November); expedited low energy experimental program that included the β-NMR and Osaka beam line.

East Target Station

This project received high priority and had to be fast-tracked for installation in the January shutdown. The project was broken down into 9 work packages and major highlights included: 2A beam line (2A3 beam line installed in winter shutdown); Faraday cage (most work done in winter shutdown and remainder completed by summer with limited access to electrical room due to ITW beam operation); target hall (included modification and commissioning of south hot cell and alignment components and water package shielding in March); controls (included 2A controls, target protect interlocks and RIB controls for vacuum system, beam optics and beam diagnostic systems completed in the winter shutdown).

The work on the modules required extensive Design Office and Machine Shop effort. Several design modi-

fications were made for better manufacturability and remote handleability. Initially the plan was to make TM #2 and TM #3 interchangeable but later complications associated with installation of the ECR source and the microwave guide and generator excluded that provision. TM #3 was designated as the module for the ECR source at ITE, and TM #2 with surface source at either east or west target stations. Some of the major technical challenges that took longer than anticipated included accurate assembly and installation of 30 tubes and 14 water blocks in the containment box. Consequently the commissioning was delayed significantly as exit modules 1 and 2 were installed in April and TM #2 (with surface source) was installed in July, followed by leak checking, fixing water leaks, and high voltage checks by September. The ECR source was tested on the test stand by September. TM #2 was removed and TM #3 with the ECR source was installed in October, followed by checks and tests with stable beam in November.

Target Conditioning Box

An alternative conditioning system was designed and fabricated by January to expedite the process of changing and conditioning ISAC targets. Assembly continued until April due to lack of manpower.

Experimental Facilities

The Osaka beam line was installed and tested in October/November with new chamber and associated services. The 8π beam line with a simple chamber was commissioned with a test beam in December.

DRAGON and TUDA started commissioning with stable beam followed by RIB. Some of the major hardware items completed for DRAGON included: modular security fence with safety interlocks, service platform, lead shields for charge slits and mass slits diagnostic boxes, and universal alignment fixture.

ISAC-II

PERTs were prepared and monitored for all ISAC-II projects, and activities were coordinated and expedited to meet various milestones. Major milestones achieved for the medium β system included: commissioning tests on Nb cavity with rf controls in June, with mechanical prototype tuner in October, and with μ-metal in November, tuner development and final design released in November, order amplifiers in December, prototype solenoid ordered in October with delivery in March, 2003. Fabricated cavities at Ezanon progressed well with delivery in January, 2003, to be followed by chemical treatment at CERN by April, 2003. Extensive effort was spent in planning cryomodule engineering. The conceptual design was reviewed in November and three designers were allocated to complete the design

of the tank, lid, LN_2 shield, liquid helium reservoir, frame and suspension system, intermodule zone, and jigs and fixture by March, 2003, fabricate and assemble by September, 2003, with an aim to do cold tests and test the cryomodule with rf in October, 2003. The refrigeration system is on critical path because specifications were delayed due to lack of appropriate manpower and information.

Work continued on high β beam dynamics, HEBT transfer line (layout, specifications and concept design of dipoles), and charge state booster (components ordered in February and received in November, design CSB stand in fall, modify analyzing magnet in December), with an aim to test the whole system on the test stand by October, 2003.

CONTRACT ADMINISTRATION

In the past year three contracts were awarded: E. Zanon S.p.A. of Italy manufactured 20 bulk niobium QWR sub-assemblies for the ISAC-II superconducting Linac. DANFYSIK A/S of Denmark manufactured 20 HEBT quadrupole magnets for the ISAC-II transfer line. Pantechnik of France supplied an electron cyclotron resonance ion source, "PHOENIX", to be used as a charge state booster for ISAC-II.

Personnel Resources

ISAC-I

In 2002 the average monthly personnel effort for ISAC-I decreased by approximately 26 people per month to an average of 50.76 FTE people per month (see Fig. 212). In 2001 the FTE effort per month was 76.15 people. The total work effort expended on ISAC-I from the start of the project on January 1, 1996 to December 31, 2002 has been 473.52 years, based on a FTE work-month of 150 hours per person.

Figure 213 shows the FTE persons per month for the various sections of ISAC-I in 2002.

ISAC-II

The recording of work effort for ISAC-II started October 1, 2000 (see Fig. 214). The work effort was recorded as "Project Management and Administration" up until March 31, 2002. Commencing April 1, 2002 the work effort was monitored by section. Figure 215 shows the FTE persons per month for the various sections of ISAC-II in 2002.

Figure 216 shows the FTE years of work effort for each section of ISAC-II since the project began on October 1, 2000 up to December 31, 2002.

The total work effort expended on ISAC-II from the start of the project on October 1, 2000 to December 31, 2002 has been 16.26 years, based on a FTE work-month of 150 hours per person.
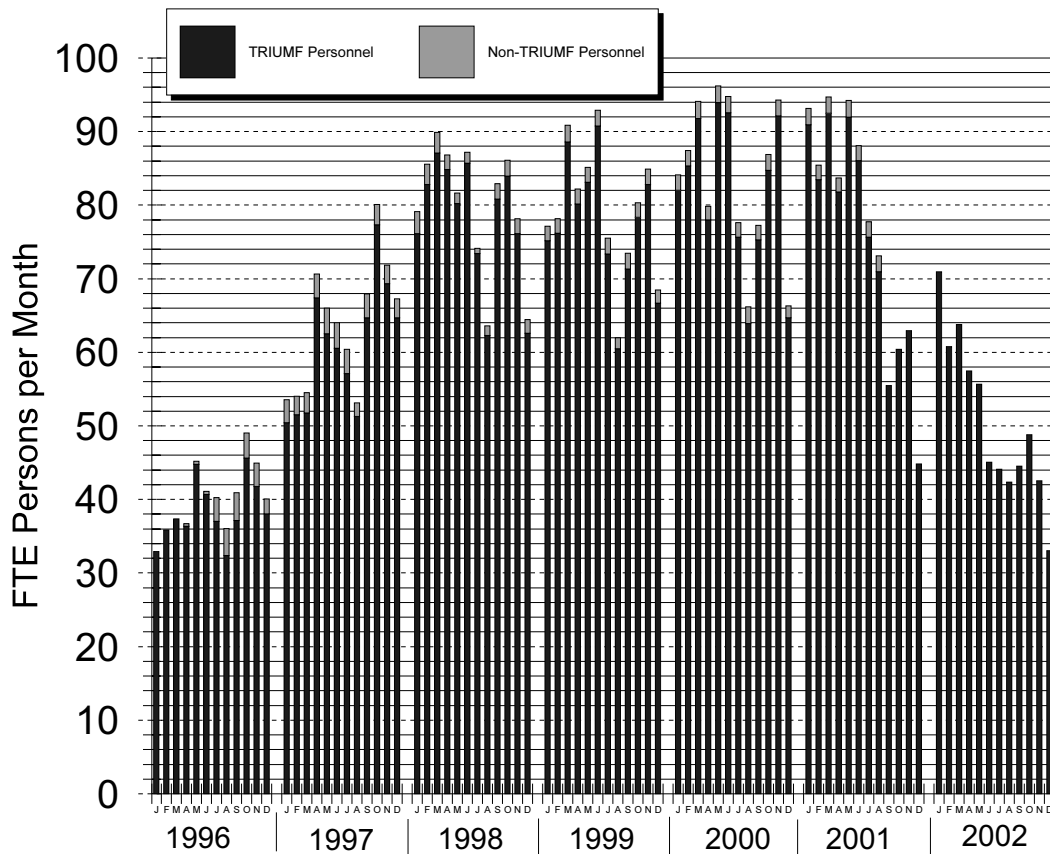
Fig. 212. ISAC-I monthly personnel effort, January 1, 1996 to December 31, 2002.
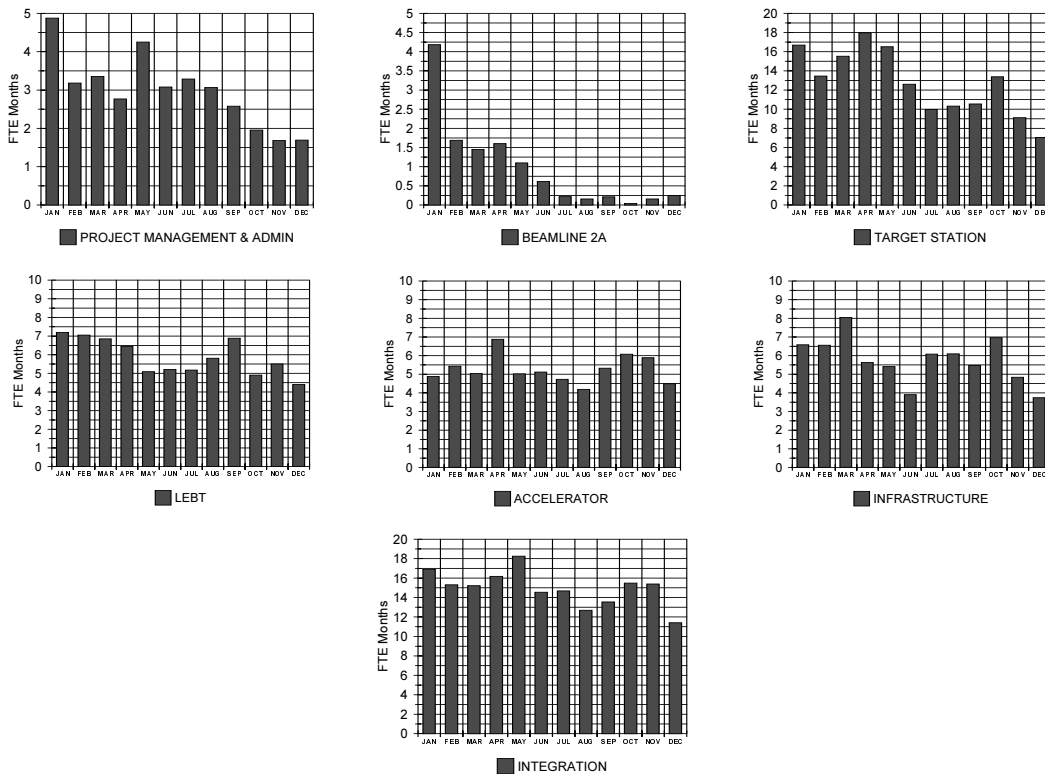
Fig. 213. ISAC-I monthly personnel effort, shown by section for 2002.

225
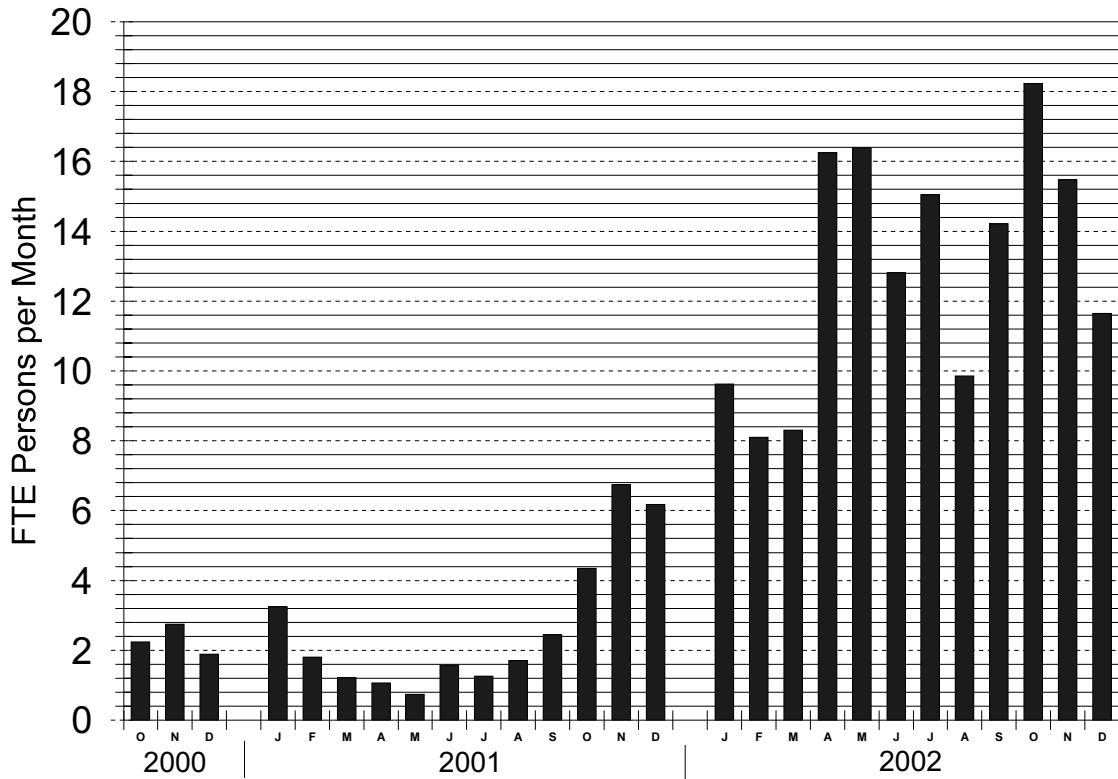
Fig. 214. ISAC-II monthly personnel effort, October 1, 2000 to December 31, 2002.
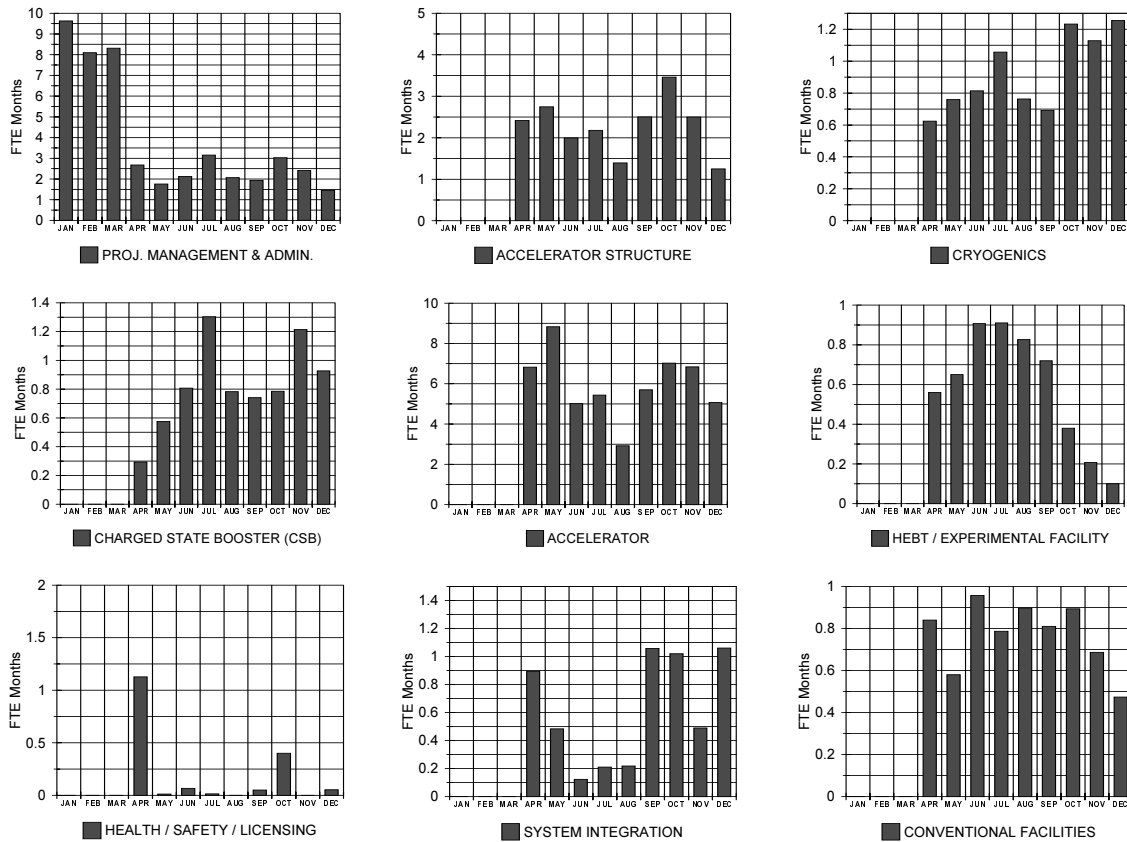
Fig. 215. ISAC-II monthly personnel effort, shown by section for 2002.

226
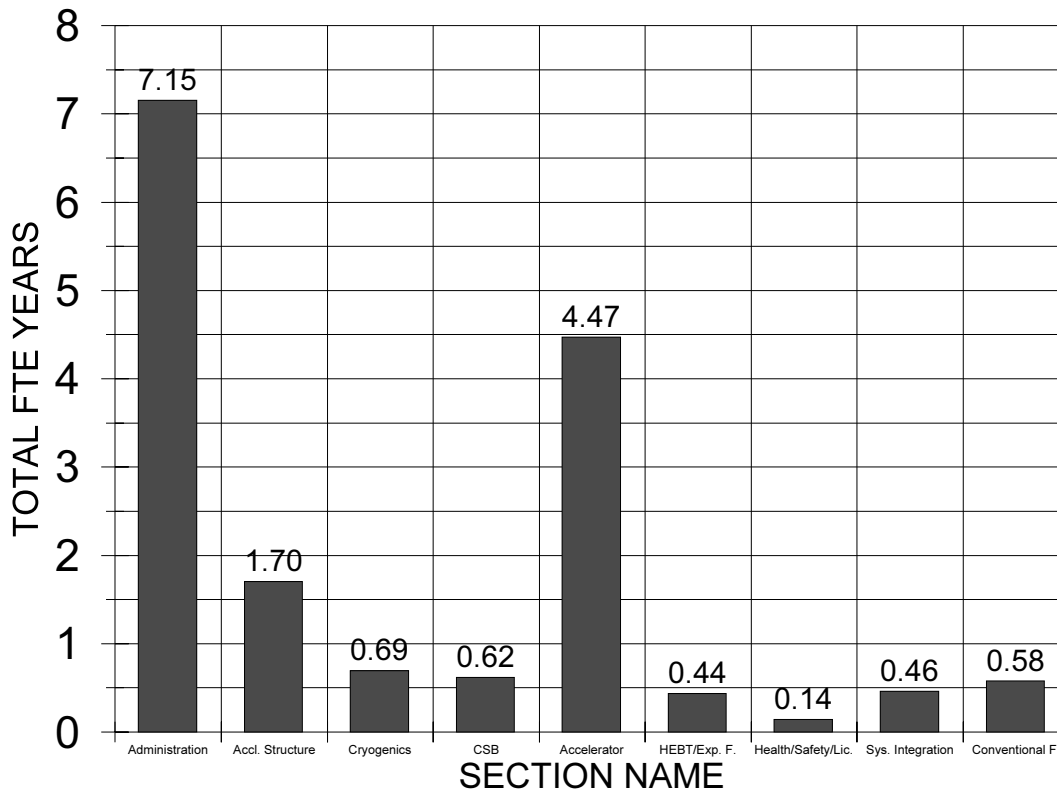
Fig. 216. ISAC-II total personnel effort, October 1, 2000 to December 31, 2002 shown by section.

ISAC-II CONVENTIONAL FACILITIES AND INFRASTRUCTURE

This was the year the ISAC-II laboratory was built. In the design of this laboratory we departed from the approach used in the design of previous buildings and gave the new building a more modern look. The new building has a soft contoured roof over the experimental hall and plenty of glass and architectural features in the office area. The new building is situated north of the ISAC-I experimental hall (see Fig. 217).

Fig. 217. A recent picture of the ISAC-II building. Landscaping is still in progress.

The facility is about 55,000 ft^2 set on two floors, with offices for approximately 90 staff, a clean room for the maintenance of the SCRF cavities, laboratories and technical shops in support of the experimental program and the accelerator.

Under the overall direction and guidance of UMA Management Services Ltd., the conventional facilities (the building portion) of the ISAC-II expansion project were divided into two main sequential construction packages:

- the site preparation package, and
- the main building package.

The site preparation package was tendered and awarded in December, 2001. This package included clearing, grubbing, bulk excavation and site servicing, and was issued ahead of the main building package for scheduling reasons.

Having been tendered and awarded the previous year, this year kicked off with the commencement of the fieldwork of the site preparation construction contract. The atmosphere at TRIUMF changed overnight as the heavy equipment required for the execution of the work, including approximately 600 separate truck trips, became a constant presence north of the existing site. This contract was completed at the end of February.

227

While site preparation was under way, the architect and the consulting engineers completed the specifications and drawings of the main building package. Pre-tender estimates confirmed that the project, as designed, was on budget. Therefore, also in January, the Ministry of Finance officials gave their approval for the tender of the main building package.

The main building package was the second major construction contract. This package was a general construction package and contained the balance of the work to complete the building. It was tendered in late January and throughout February. Tenders were received from pre-qualified general contractors and the successful tender was within budget. Upon receipt of approval to award from the Ministry of Advanced Education, the contract was awarded in March.

Construction work started on site in March in pursuit of an aggressive completion schedule. At the same time, we received the Building Permit issued by UBC, and Permission to Construct from the Canadian Nuclear Safety Commission. Construction continued to advance through the year and at the end of the year stood at 85% complete with Substantial Completion targeted for February 28, 2003.

Milestones achieved during the year include the first concrete pour of the accelerator vault on April 19 and the first structural steel column erected on June 24. The "*lights were turned on*" on January 2, 2003.

A major challenge was the sequencing of the construction due to the simultaneous construction of the nearby Nordion radioisotope laboratory addition. Despite the severely limited lay down space and the sharing of the construction site, both projects proceeded expeditiously, safely and harmoniously to completion. This speaks to the quality and motivation of the people involved at all levels! With careful management, we anticipate that the project will be completed within budget.

TRIUMF engineering staff provided continuing support to both UMA and the engineering consultants during the design stage and throughout the construction phase to ensure that the functional requirements established by TRIUMF were adequately installed. Staff attended weekly construction meetings and commissioning meetings, and participated daily in discussion to expedite construction activities and contractual issues.

With ISAC-II, we installed three capacitor banks for about 1,000 kvar. Capacitors operate to reduce the reactive power demand from the Hydro grid and therefore are a means for controlling the cost increases due to additional power demand. We also added two 40 kW UPS units to serve the ever increasing demand of battery-backed up quality power for better reliability of the data acquisition and computing services, safety systems and beam line controls.

The TRIUMF Data and Voice Communication groups have been preparing to move into the ISAC-II facility to start pulling cabling. Telephone and data services are required to be operational before staff can occupy offices and labs.

In addition, engineering support was lent to the CSB for the preliminary design of the test stand services and to the Refrigeration group in the preparation of the specification package. Preliminary studies started to determine possible configurations of the power supply room and services to the S-bend beam transport system.

ISAC-II ACCELERATOR DEVELOPMENT

In the past year the ISAC-II accelerator design and prototyping was advanced beyond the concept stage to development, design and fabrication. The key achievements were:

- Detailed beam dynamics including the addition of realistic electric and magnetic rf fields were completed. This led to the modification of the first eight medium beta cavities to improve performance. Analysis of the high beta section was completed for two cavity variants.

- An order was placed for twenty medium beta cavities with E. Zanon in Italy. Fabrication of four is now complete and they are ready for chemical polishing in CERN.

- Conceptual and detailed design of the medium beta cryomodule is now in an advanced stage.

- A SCRF lab was established and ten cold tests were performed in 2002. The tests concentrated on establishing cavity preparation and testing procedures, development of the rf controls, mechanical tuner and rf coupling loop as well as a variety of cryogenic tests.

Details of the various achievements are presented below.

Beam Dynamics Studies

Figure 218 shows a schematic for the ISAC-II linac indicating stage 1 and stage 2 installations. Detailed beam dynamics studies have concentrated on the first stage SC linac installation. The linac has been grouped into low, medium and high beta sections corresponding to cavities with design velocities of $\beta_o = 4.2\%$, $\beta_o = 5.7, 7.1\%$ and $\beta_o = 10.4\%$ respectively. The two cavity types in the mid beta section (Fig. 219), composed of eight $\beta_o = 5.7\%$ and twelve $\beta_o = 7.1\%$ cavities, are now being fabricated in industry. A prototype
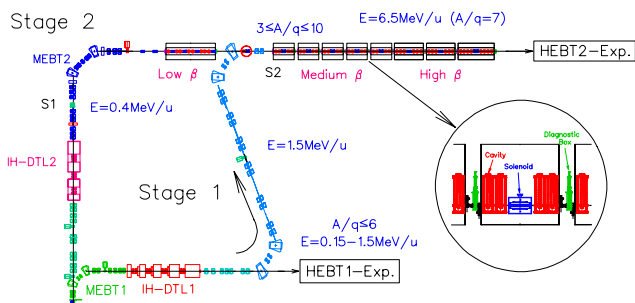
Fig. 218. Stage 1 and stage 2 of the ISAC-II expansion.

(a) Nominal (β=7.1%)   (b) Flat (β=5.7%)
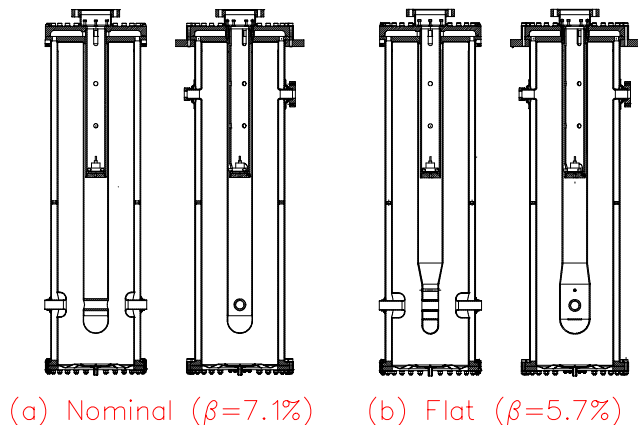
Fig. 219. The two medium beta cavities.

of the $\beta_o = 7.1\%$ cavity has been designed in a collaboration with INFN-LNL, and fabricated in Italy. The *flat* cavity, recently added to the design for improved beam dynamics (see below), borrows from the geometry of the low β cavities on the Piave accelerator at INFN-LNL.

Realistic field studies are now complete for the 10.5 m long medium beta section consisting of five cryomodules with four cavities and one 35 cm long superconducting solenoid in each. Two main asymmetries in the medium beta cavity fields are responsible for differences between a "simple cavity model" and "realistic field" simulations. Inherent in quarter wave cavities are both a vertical electric dipole field and a radial magnetic field that give velocity and phase dependent vertical kicks to the beam. The vertical steering can lead to loss of dynamic aperture and transverse emittance growth especially for multi-charge beams. The steering can be largely cancelled by displacing the cavity vertically so the electric focusing field compensates for the magnetic kick.

The cylindrical stem (Fig. 219a), while simplifying construction, produces an asymmetry in the transverse rf electric fields. The asymmetry leads to a mismatch between horizontal and vertical motion. The degree of mismatch is dependent on the magnitude of the asymmetry and on the relative strength of the defocusing rf

with respect to the focusing optics in the lattice cell. In a quadrupole lattice the two planes are independent and different match conditions can be used to eliminate emittance growth. In a solenoidal lattice the beam is rotated periodically and a mismatch between transverse planes can lead to transverse emittance growth once the beam is delivered to a quadrupole transport system.

To reduce the effects of the focusing asymmetry we alter the original design by adding a new cavity geometry. In the flat cavity (Fig. 219b) the inner conductor is squeezed to 40 mm from 60 mm in the beam direction and the grounded beam ports are extended to maintain the original gap. The transverse deflections from the two cavity types are summarized in Fig. 220 over the operating velocity range required of the cavity for an accelerating gradient of 6 MV/m, an ion of $A/q = 3$, and a phase of $\phi_s = -30°$. The solid lines show the vertical and horizontal defocusing perturbations for a 1 mm displacement from the electrical axis. The dashed lines show the uncorrected, on-axis dipole steering components and the corrected components for cavities shifted down by 0.8 mm in the nominal case and 0.5 mm in the flat case with respect to the beam and solenoid axis.

Studies show that a small but worthwhile improvement in dynamic aperture is gained for light beams by replacing the first eight nominal cavities in the medium beta section with the flat cavities. Adding more than eight flat cavities reduces linac performance because of the reduced β_o.
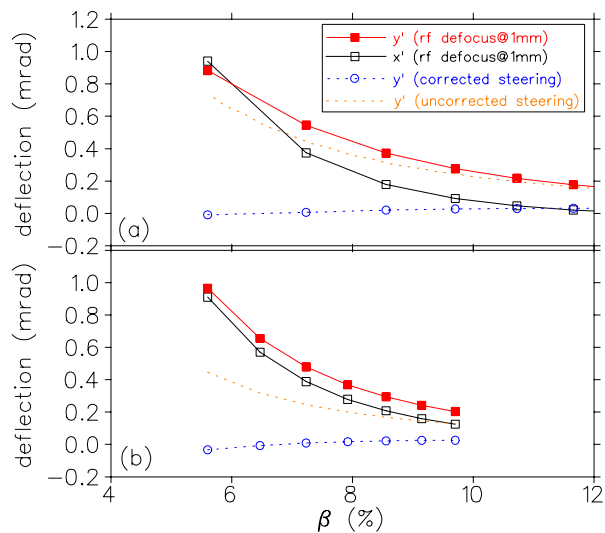
Fig. 220. Focusing and steering perturbations for the two medium beta cavities (a) nominal (b) flat as calculated in HFSS for $E_a = 6$ MV/m, $A/q = 3$, and $\phi_s = -30°$. The dashed lines are the uncorrected (on-axis) and corrected (displaced axis – (a) $\Delta y = 0.8$ mm, (b) $\Delta y = 0.5$ mm) vertical dipole perturbations. The solid lines are the vertical and horizontal defocusing perturbations for a 1 mm displacement from the electrical axis.

In an investigation of misalignment tolerances the realistic fields are used to generate velocity dependent linear matrix elements to speed the calculations. The beam centroid is tracked through the linac for multiple seeds of linac misalignments. For each seed linac, element positions are displaced randomly within a Gaussian distribution. The studies show that the solenoid is at least six times more sensitive to misalignment than the cavities. This assumes that the cavity errors are randomized within the error margin. If the cavity errors are systematic then the negative dynamic aperture is reduced. Since the difficulty of aligning any element is about the same, we can relax the alignment of the cavity by a factor of two with respect to the solenoid and make the engineer's job easier while not impacting the overall performance. The solenoid tolerance is chosen to give less than 20% reduction in the dynamic aperture. In Fig. 221 the single charge state beam centroid shift with steering correction for a randomized solenoid shift of $2\sigma = 200\ \mu$ and cavity shift of $2\sigma = 400\ \mu$ is superimposed on the envelope difference associated with a 20% and 40% reduction in dynamic aperture. The rms beam centre shift is within the 20% envelope.

High Beta Cavity

Beam dynamics studies with realistic fields were done to optimize the high beta cavity design. The cavity choice came down to two cavity variants. One variant has identical transverse dimensions to the medium beta cavity but is designed as a 141 MHz cavity by shortening the overall length. In the other variant the cavity frequency was kept at 106 MHz but the cavity transverse dimensions were scaled to increase the beta from 7.1% to 10.4%. The two cavity variants are shown in Fig. 222.
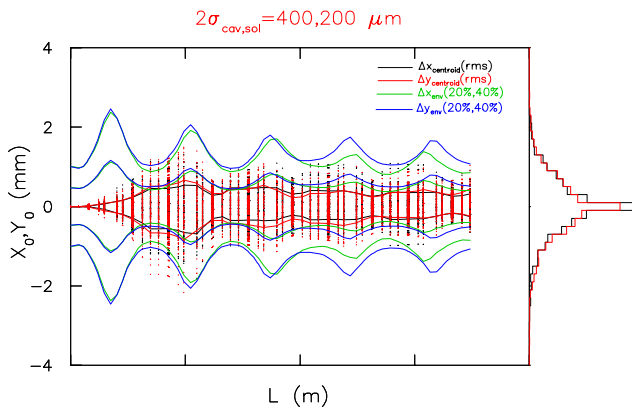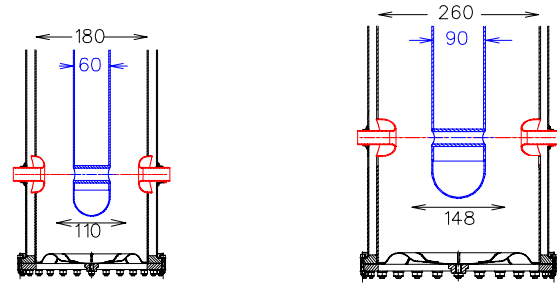
(a) 141MHz Nominal   (d) 106MHz Asymmetric B

Fig. 222. The two cavity variants for high beta beam dynamic studies.

Each cavity has transverse time varying electric and magnetic fields that account for rf defocusing and phase-dependent steering effects. The steering effect can be largely compensated for by shifting the cavity downward by ~ 2 mm with respect to the beam axis. The quadrupole asymmetry noted in the previous section is somewhat larger in the high frequency case by virtue of the smaller inner conductor. The fields associated with the two cavity variants are displayed in Fig. 223.

Beam simulations of the two cavities were completed using the realistic three dimensional electromagnetic cavity fields. The high beta section was composed of three cryomodules with 6,6,8 cavities per module with the high frequency cavity and 4,4,6 cavities per module with the lower frequency cavity as shown in Fig. 224. Both cases use a medium beta section composed of eight flat and twelve round 106 MHz medium beta cavities.

Fig. 221. The single charge state beam centroid shift with steering correction for a randomized solenoid shift of $2\sigma = 200\ \mu$ and cavity shift of $2\sigma = 400\ \mu$ is superimposed on the envelope difference associated with a 20% and 40% reduction in dynamic aperture.
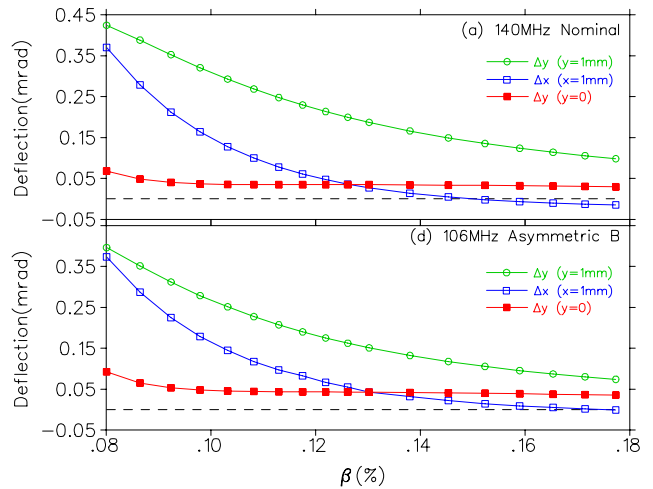
Fig. 223. Focusing and steering perturbations for the two high beta cavity design variants (a) 141 MHz (b) 106 MHz as calculated in HFSS for $E_a = 6$ MV/m, $A/q = 3$, and $\phi_s = -30°$. Shown are the corrected (displaced axis – (a) $\Delta y = xx$ mm, (b) $\Delta y = xx$ mm) vertical dipole perturbations, and the vertical and horizontal defocusing perturbations for a 1 mm displacement from the electrical axis.
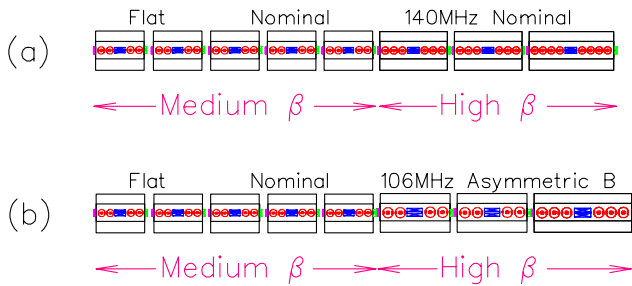
Fig. 224. The two linac variants used in the high beta beam dynamic studies; (a) twenty 141 MHz cavities (b) fourteen 106 MHz cavities.
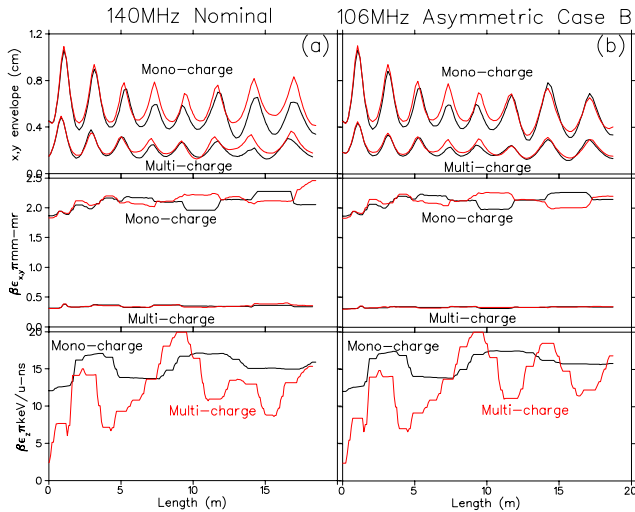
Fig. 225. The transverse beam envelopes and the transverse and longitudinal emittances as a function of longitudinal position along the medium and high beta sections for (a) the 140 MHz high beta variant and (b) the 106 MHz variant. In each case a single charge state beam with intial emittance of 1.8 πmm-mr and 12 πkeV/u-ns (ten times the expected emittances) is simulated. The large beam is used to characterize differences in the effective dynamic aperture of the two variants. Also shown are a multi-charge beam with initial emittances of 0.3 πmm-mr and 2. πkeV/u-ns.

A summary of the beam dynamics calculations is given in Fig. 225. Given are the transverse beam envelopes and the transverse and longitudinal emittances as a function of longitudinal position for the two different variants. In each case a single charge state beam with intial emittance of 1.8 πmm-mr and 12 πkeV/u-ns (ten times the expected emittances) is simulated. The large beam is used to characterize differences in the effective dynamic aperture of the two variants. Also shown are results for a multi-charge beam with initial emittances of 0.3 πmm-mr and 2. πkeV/u-ns. The reduced quadrupole asymmetry in the low frequency cavity results in a reduced envelope. However, the difference in the transverse emittance values is not large. Other considerations such as cost and schedule will be used to choose the cavity type.

Hardware

Work is ongoing on several fronts with the goal of realizing beam delivery in 2005. The first major milestone is the fabrication and cold test of a completed medium beta cryomodule in mid 2003. A summary of the present developments is given below.

Cryomodule design

A prototype of the medium beta cryomodule, shown in Fig. 226, is now in the design phase. The vacuum tank consists of a stainless steel rectangular box and lid. All services and feedthroughs are located on the lid. Unlike elliptical cavity systems, a common vacuum is shared between the thermal isolation space and the cavity/beam space. For this reason the vacuum system is completely oil free with a 340 l/s magnetically levitated turbo pump and scroll backing pump. Each cryomodule has independent gate valves at each end of the beam tubes to allow isolation of a cryomodule unit in case of failure. The initial assembly will be done in a clean room as will all subsequent servicing to the unit. The intermodule space consists of a slim diagnostic box and bellows. An $x - y$ steering magnet fits around the bellows.

A 190 l LHe reservoir and cavity/solenoid support frame is mounted from the lid from supports thermally anchored with LN2. Misalignment studies indicate that the solenoid and cavities must be aligned to a tolerance of ± 200 μm and ± 400 μm respectively. A position monitor using a guide wire carrying an rf signal and pick-ups installed on the devices is being developed for cold alignment. A cold shield is suspended in close proximity to the inner wall of the cryomodule vacuum space and is formed from copper sheet cooled by SS tubing flowing LN2. During nominal operation, a liquid nitrogen load of about 4 liquid l/h is estimated from heat radiation and conductivity load and from experience with our test cryostat. The rf coupling loop is thermally isolated from the cavity and anchored to LN2 through a separate heat exhange loop. Pre-cooling of components is done by delivering
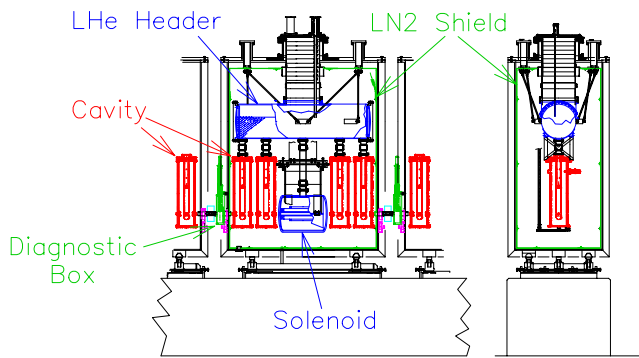
Fig. 226. Medium beta cryomodule for ISAC-II.

231

cold helium vapour to the bottom of each major component. Magnetic shielding in the form of high μ sheet is suspended between the warm wall and the cold shield.

Solenoids

Focusing in the SC LINAC is provided by 9 T 26 mm diameter bore SC solenoids of lengths 16, 34 and 45 cm corresponding to the low, medium and high beta cryomodules respectively. Since the solenoid fringe field could affect the operation of the cavities, the magnets are equiped with active compensation using bucking coils. The operating field at the cavities is specified to be less than 0.1 T. The magnets are mounted in a liquid helium pressure vessel fed from the common helium header. Power leads run from the solenoid through the common helium header to feed-throughs at the top of the cryo-module. A contract has been let for five medium beta solenoids. A prototype medium beta solenoid is being fabricated for delivery in spring, 2003.

Cavities

The cavities are being fabricated at E. Zanon in Italy. Four cavities are now completed and await shipping to CERN for chemical polishing. The remaining sixteen cavities are scheduled for delivery by August, 2003.

SCRF Developments

A temporary superconducting rf test lab of $\sim$100 m^2 is set up in a space rented by TRIUMF in a neighbouring laboratory complex. The laboratory includes a test area with a sunken cryostat pit for high field rf testing, and clean areas for cavity assembly (Class 1000) and high pressure water rinsing (Class 100). In the high pressure rinse area an on-line treatment system delivers 20 l/min of 18 MΩ water at 2000 psi to a manual rinse unit. A prototype rf controls system using a self-excited loop architecture with digital signal processors is in development and has been used to successfully regulate a cold cavity in both self-excited and fixed frequency operation. Cold tests of the prototype cavity are ongoing at the rate of one a month.

Cavity tests

First cold tests were completed in April. Parallel developments of cavity performance, rf controls, cryogenic studies, cleaning procedures and mechanical tuners are ongoing. A summary plot of the measured cavity performance is given in Fig. 227. In initial tests, field emission reduced the Q sharply at field levels above 4 MV/m ($E_p \geq 20$ MV/m). High pressure water rinse (HPWR) treatments gave marked reductions in field emission. Helium conditioning at 4×10^{-5} torr
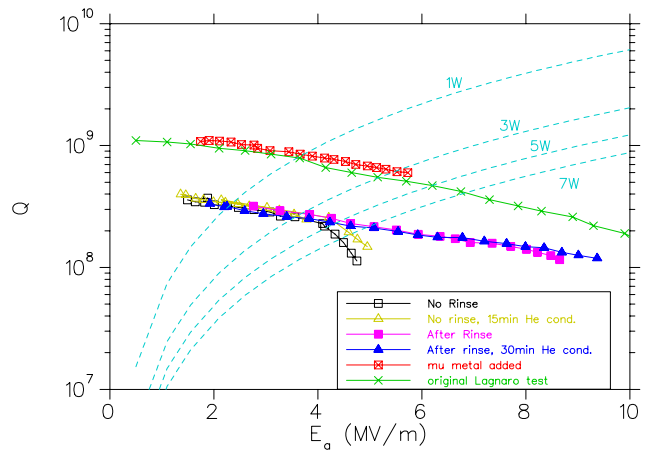
Fig. 227. Measured cavity performance during cold tests at TRIUMF.

for thirty minutes at 9 MV/m gave a further improvement so that we could push the cavity right out to the quench limit ($E_a \geq 9.5$ MV/m,$E_p \geq 48$ MV/m) without significant field emission. These initial tests matched earlier tests at Legnaro except that the measured Q values were lower by a factor of three. The original Legnaro data were finally duplicated after adding a mu-metal shield to reduce the surface resistance caused by trapped flux from the earth's magnetic field.

RF controls

The ISAC-II prototype rf control system is based on the self-excited loop. It consists of two modules: an rf module and a DSP module, housed in a VXI mainframe. A pair of Motorola DSP56002 digital signal processors provide the low level amplitude, phase and tuning regulation. A special circuit is used to pulse through multipactoring. A rack mounted PC provides supervisory controls for these modules. An Apache HTTPD server running on the same PC acquires data from several GPIB-enabled instruments such as power meter, frequency counter, frequency synthesizer and a digital oscilloscope. These data and the computed Q and E_a values can be displayed and plotted in any Web browser. During the series of tests this year the controls system regulated the cavity in both self-excited and frequency locked mode. In one test the cavity frequency was detuned by 10 Hz by increasing the pressure in the helium space ($df/dp \simeq 1$ Hz/torr) while overcoupling to produce a 10 Hz bandwidth. The control system managed to maintain lock both during the slow pressure change and when the pressure was suddenly released. Ongoing developments include optimizing the addition of a mechanical tuner to the control loop.

Tuner development

The mechanical tuner alters the resonant frequency of the cavity by deflection of a niobium tuning plate that encloses the cavity on the bottom high field end.
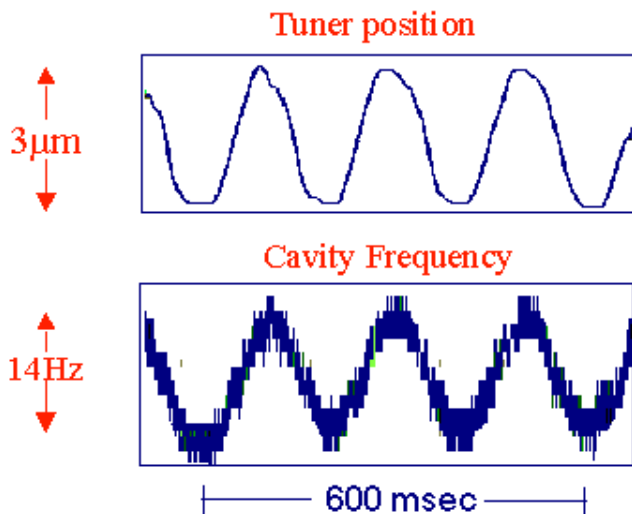
Fig. 228. The tuner position and cavity frequency with tuner driven at 5 Hz and amplitude of ±1.5 μm. The cavity frequency is modulated by ±7 Hz.

Presently a flat plate is being used but we are developing a plate spun with undulations and radial slots to allow a larger tuning range. The plates each give a tuning sensitivity of 7 Hz/μm. The "oil can" spun plate increases the tuning range from about 15 kHz to at least 40 kHz while significantly reducing cavity stresses due to plate distortion. A prototype mechanical tuner is now being tested. It consists of a lever mechanism acting directly on the centre of the cavity tuner plate through a zero backlash hinge and stiff rod connected through a bellows to a precision linear motor located on the top of the cryostat. The tuner is capable of both coarse (20 kHz) and fine (few Hz) frequency adjustments. Initial tests are promising. The tuner plate position has been modulated at mechanical drive frequencies of 0.1 Hz to 10 Hz and amplitudes of 1 μ to 6 μ corresponding to cavity frequency variations of ±5 Hz and ±30 Hz respectively. The self-excited frequency response matches the driving signal with no significant induced microphonics. Figure 228 shows both tuner position and cavity frequency for a 5 Hz, ±1.5 μm tuner variation.

In another study the cavity was phase locked while over coupled, generating a 20 Hz rf bandwidth, and the plate was dithered with a frequency of 8 Hz at ±1 μ without losing phase lock.

ISAC-II CRYOGENIC REFRIGERATION PROJECT

The ISAC-II cryogenic refrigeration workgroup was established early in 2002. The group was charged with preparing specifications and asking for tenders for a helium refrigeration and distribution system for the future ISAC-II superconducting linear accelerator. Since the ISAC-II linac will be installed in two phases, the
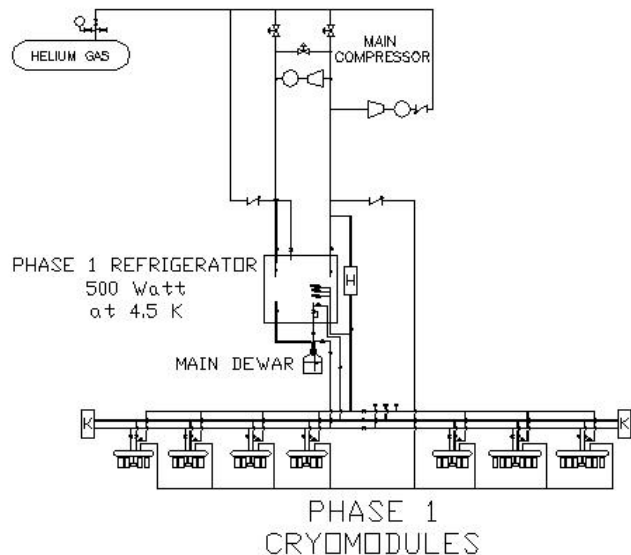
Fig. 229. Reference schematic for phase I refrigeration system.

helium refrigeration system will also be installed in two phases. Phase I will require a 500 W at 4.5 K class helium refrigerator combined with a cryogenic helium distribution system supplying the linac. The current design of the phase II linac will require extending the phase I helium distribution piping and adding another 500 W at 4.5 K class helium refrigerator. The reference schematic for the phase I refrigeration system is shown in Fig. 229. This design has evolved throughout the year after meetings and discussions with potential suppliers and other research laboratories operating similar systems.

In March, meetings were held at Argonne National Laboratory in Illinois. Argonne staff presented the helium refrigeration and distribution system used for the ATLAS linac. The feasibility of using a similar refrigeration system for the ISAC-II was discussed. The ATLAS linac injector cryostats are cooled with a series flow scheme with helium flowing from one cryostat into the next, and on through the remaining cryostats.

Subsequent to the Argonne meetings, the linac cooling methods used at other facilities such as Legnaro in Italy and NSC in India were investigated. Three main methods were considered: series cooling, parallel cooling and supercritical helium cooling for each cryomodule.

A paper titled "Overview of the Cryogenic System for the ISAC-II Superconducting Linac at TRIUMF" was presented to ICEC 19 in Grenoble, France in July. At the ICEC 19 conference several meetings were held with potential suppliers of the ISAC-II helium system. Among the many items discussed were the three cooling distribution methods, the capability of supplying a turn-key system, system sizing and cryogenic piping.

Discussions were also held with representatives from facilities operating cryogenic helium refrigerators such as BNL, NSC in India, CERN, Legnaro, Italy, and SRRC, Taiwan. As a result of the various discussions, it was decided to use the parallel flow distribution scheme in the reference design of the ISAC system. It was concluded that a properly designed parallel flow distribution system would offer better pressure stability and expansion capabilities.

In October an engineering design review of the medium beta cryomodule design and the helium refrigeration specification was held. The review committee included representation from Argonne National Laboratory, JLab and the University of Washington. Among the conclusions reached at the review were that the parallel flow distribution scheme seemed reasonable as long as pressure drops were controlled, and that detailed heat leak calculations should be performed.

Recent data obtained during cooldown tests of the superconducting test cavity have justified the suitability of a 500 W class helium refrigerator. The tendering package for the phase I helium refrigeration and distribution system will be released in March, 2003 with an expected commissioned date of October, 2004.

ISAC-II CRYOMODULES

This report period marked the commencement of the mechanical design of the medium β cryomodules, of which there will be five constructed and installed in the accelerator hall in ISAC-II as part of the superconducting linac.

The medium β cryomodule is a stainless steel vacuum tank housing five cryo elements: four quarter wave resonators and one 9 T solenoid all cooled to $4.2°K$ by liquid helium (see Fig. 230). The cryo elements will be supported by a rigid frame suspended from the vacuum tank lid by thin walled tubular struts with spherical ball ends at both ends to allow for thermal shrinkage during cool down. Positional accuracy of the cryo elements is crucial to the efficient operation of the accelerator, therefore it is imperative that the alignment of these elements relative to the vacuum tank be maintained for repetitive cool down cycles. The liquid helium inventory of 120 l is housed in a 16 in. diameter reservoir, partially filled and connected to the cryo elements by a 3 in. tube and bellows and bolted to the lid via a vertical tower in both the reservoir and lid, the top of which provides a platform for the cryogenic feed throughs, pressure relief valve and burst disk. The latter are provided to allow for perturbations in the operation of the LHe system and, in the event of a vacuum failure in the vacuum tank, to allow the escape of vapour produced by the rapid liquid He boil off. The vacuum tank is lined with 0.040 in. thick μ metal to negate magnetic field effects. Inside the μ metal is
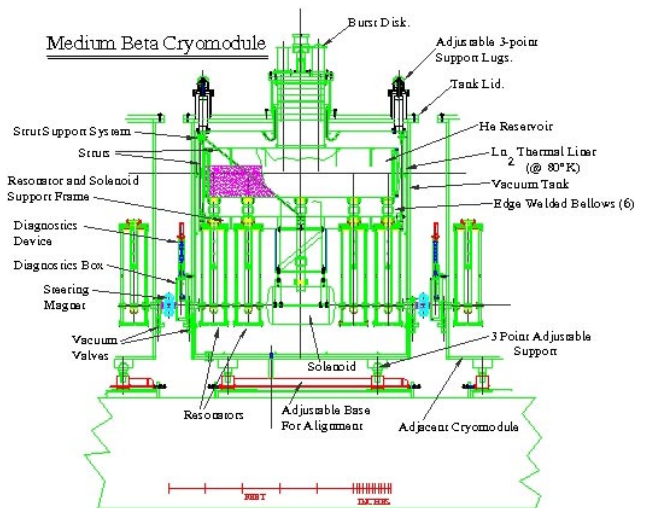
Fig. 230. Medium β cryomodule components.

another liner which is a liquid nitrogen thermal barrier intercepting the heat load from the vacuum tank to the cryo elements. The μ metal liner is screwed to the tank wall and LN_2 liner is placed in the tank sitting on the floor and away from the μ metal by low conductivity stand-offs. The lid will also have a double liner and is 1.25 in. thick stainless steel plate with a central vertical tower matching up with the He reservoir as mentioned.

Access to the cryo elements is achieved by lifting the lid off the vacuum tank, thus removing the contents of the tank except for the μ metal and LN_2 liners. The lid will also provide space for the many other feed throughs related to diagnostics, rf devices, resonator tuning motors, heaters, temperature detectors, alignment equipment feed throughs and suspension lugs.

Each medium β cryomodule will be delivered aligned internally with the tank beam ports (allowing for the internal thermal shrinkage). The lid will be dowelled to the tank and external tank targets will be provided to allow for correct alignment in the accelerator hall. The five cryomodules will sit on a special frame providing three-point mounts which allow for this alignment.

There is a ~30 cm gap between adjacent cryomodules allowing for a diagnostic box, two 2 in. valves, and a short piece of beam tube which is surrounded by a special vertical and horizontal steering magnet. The inter-modular zone is designed in such a way as to allow for removal of a cryomodule from the accelerator without venting the accelerator system. The cryomodule would come away with both beam ports sealed off by the valves, and at one end the diagnostic box, steering magnet and beam tube associated with that cryomodule would be attached to it. The removed cryomodule could be replaced by a section of beam tube to allow the linac to remain operational.

ACCELERATOR TECHNOLOGY DIVISION

INTRODUCTION

The Accelerator Technology Division is responsible for most of the engineering and design at TRIUMF, as well as support of the beam dynamics effort for international collaborations. Other responsibilities include project planning, electronic development and services, Building department and the Design Office and Machine Shop. This year, as for the past number of years, most of the available effort went into supporting the ISAC program. An indication of this is the number of new Requests for Engineering Assistance (REA) that were submitted during the year. There were 34 ISAC related jobs and 21 non-ISAC jobs in mechanical engineering and design. Figure 231 shows the distribution of REAs since they were instituted in 1995. The total may not indicate the overall level of effort required as some requests are for major projects requiring many months of effort and others can be satisfied with a few days of design time.

The Canadian Nuclear Safety Commission requires TRIUMF to develop and adopt a quality assurance program for all activities at the laboratory. A task force, which included two members of the division, was set up to develop this program. For the most part the new plan is adopting many of the policies and procedures that already exist. In some cases the documentation and formalization of the procedures will have to be improved and this will have some impact on the work of the division. Hopefully there will be an overall benefit emerging from this quality management system.

In mechanical engineering, the main job during the first part of the year was the completion of the east target station for ISAC. The system was assembled and then run off-line with a surface source for testing in August. Much of the effort then moved to the design of the cryomodules for the ISAC-II superconducting linac and specification of the refrigeration system. Some remaining work on the DRAGON

spectrometer was completed and a start made on the RFQ cooler for the charge state booster.

The replacement of the BL1A triplet in the high radiation area downstream of the T2 target was a significant effort for the Design Office. This project is being coordinated by the Remote Handling group for installation in the shutdown starting at the end of the year. ISAC projects used about 60% of the design effort. The Machine Shop was fully loaded throughout the year and, in addition to the in-house fabrication work, subcontracted over 200 work packages worth about $500 K to local shops.

There were a number of projects involving TRIUMF's infrastructure role in supporting off-site experiments. An engineer has assisted the KOPIO collaboration in developing the design of the pre-radiator detector. A potential source of inexpensive extruded scintillator was found by working with a local plastics company. The pre-radiator also uses thin aluminum extrusions and possible suppliers for this were investigated. A detector stand assembly for the NPDGamma experiment at Los Alamos was designed, fabricated and delivered to Los Alamos in December.

TRIUMF personnel have been working on components for the ATLAS detector at the LHC for a number of years. Engineering and technical support has been provided by TRIUMF staff at the University of Victoria for the feedthrough project and the assembly of the hadronic endcap calorimeters into their support structure at CERN. An engineer supported by TRIUMF at Carleton University has assisted in the construction of the forward calorimeter modules and assembly and testing at CERN.

The TRIUMF collaboration on accelerator contributions to the LHC is described in another section. A study of the feasibility of a storage ring for the radioactive ions for ISAC was started as a future option for acceleration to higher energies. In addition to this work some initiatives aimed at potential collaborations on other international projects were begun. Studies of micro-bunching at the Brookhaven AGS beam for the KOPIO experiment continued. This experiment also requires upgrades to their kickers to permit higher intensity beams. A CFI grant was awarded to a UBC/TRIUMF collaboration for this AGS upgrade program. However, the grant is dependent on NSF funding of the KOPIO experiment, which has been delayed.

The Kicker group also provided assistance to the Japanese Hadron Facility in the design of a fast extraction/abort kicker for their main ring. A collaboration with this facility is being considered along with
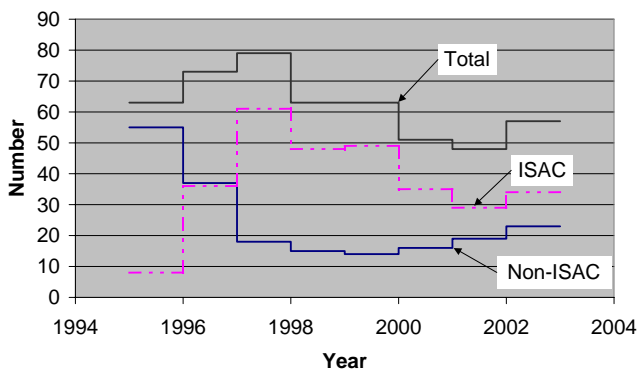
Fig. 231. Distribution of REAs since 1995.

a Canadian involvement in the long baseline neutrino experiment. TRIUMF beam dynamics and kicker personnel attended a SLAC linear collider workshop and the outcome was a proposal to carry out research on the use of high power semiconductor switches to replace thyratrons in kicker systems. Towards the end of the year the Kicker group started a project, financed by an outside experimental group, to build a fast muon kicker for a muon lifetime experiment at PSI.

Field mapping the TWIST magnet was the main effort of the Magnet Measuring group during the first half of 2002. The rad-hard quadrupoles for the replacement BL1A triplet were also measured, along with a number of other magnets. A number of new magnets were designed during the year and the contract to design and build five 9 T superconducting solenoid magnets for the ISAC-II linac was awarded and is being monitored by the magnet engineer.

Hans Mertes, who was responsible for TRIUMF buildings for the past 20 years, retired and was replaced by Dragan Mitrovic. A number of maintenance and minor construction projects were carried out, including the replacement of the roof on the north wing of the main office building.

The Electronics Services group was involved as usual in a large number of support projects from cables and electronic modules for experimenters, to site communications and support of the growing number of PCs at TRIUMF. The Electronics Development group continued to provide all of the hardware installation, maintenance and upgrades for the ISAC control system as well as the development of the prototype data acquisition boards for CERN. Some secondary channel controls for the meson hall are being incorporated into a new EPICS based secondary channel control system.

BEAM DYNAMICS

In line with a recommendation in the Canadian Subatomic Physics Five-Year Plan (2001), studies have begun of the scientific potential and technical feasibility of a storage ring for the radioactive ions from ISAC. Such a ring (the ESR) has been successfully built and used at GSI Darmstadt, and others are being built, proposed or considered at IMP Lanzhou, RIKEN, TU Munich, GSI, and CERN (ISOLDE). Some of the attractive possibilities which a storage ring would open up are:

- measurement of otherwise inaccessible interactions;
- cooling of the beam, significantly improving position, time and energy resolution, and allowing the use of internal gas targets and the achievement of higher luminosities than with solid targets in the ISAC-II beam;

- acceleration to higher energies;
- direct measurement of nuclear and ionic properties (mass, lifetime, ...);
- quasi-simultaneous operation with ISAC-II experiments using the same ions;
- fast extraction of high-intensity pulsed beams for studying interactions with very low cross sections.

Three general scenarios may be considered, in order of increasing complexity and cost:

Mini:

An accumulator ring for ISAC-II beams, with no provision for cooling or further acceleration (similar in purpose to the 5 MeV/u "Recycler" proposed for the Munich Accelerator for Fission Fragments at the high-flux reactor (FRM-II).

Midi:

A storage ring for ISAC-II beams, with cooling and modest acceleration – say to four times greater energies – 26 MeV/u for the heaviest ions and 60 MeV/u for the lightest.

Maxi:

A cooler storage ring capable of handling, say, 100 MeV/u beams delivered by a further ISAC accelerator (linac or cyclotron).

For initial orientation we have considered scaled versions of the TSR at MPI Heidelberg, which has a bending power of 1.5 T-m, a diameter $D \simeq 15$ m, and charge (or momentum) acceptance of $\pm 4\%$. (It is also the basis for the ISOLDE 2.6 T-m test intersecting storage ring (TISR) design.)

The ring diameter required depends on both the maximum energy and the mass/charge ratio (A/q) of the circulating ions. If the ISAC-II beam were to be injected by stripping in a foil, and the associated beam loss could be tolerated, then the A/q for light ions could be reduced from 3 to 2 and that for heavy ions ($Z = 65$) from 7 to 3.2, allowing the bending power $B\rho$ and ring diameter to be correspondingly reduced.

Table XLIV shows approximate values for the major ring parameters for each of the above scenarios and for the TSR and TISR.

One of the main design challenges is to limit ion loss caused by scattering, energy straggling or charge exchange in the injection stripping foil, residual gas or internal target. These effects limit the acceptable thickness for each of these items, and also require the injection energy and transverse and momentum acceptances to be sufficiently high. These issues are currently being explored, with the aim of establishing a basic conceptual design (magnet lattice, injection scheme, and rf, vacuum and cooling requirements) and estimating the

Table XLIV. Storage ring parameters.

Ring	Strip injn.	Z	A/q	Energy (MeV/u)	$B\rho$ (T-m)	D (m)
TSR	No		2	30	1.5	15
Mini	No	6	3	14.6	1.6	
	No	65	7	6.5	2.5	21
	Yes	6	2	14.6	1.1	
	Yes	65	3.2	6.5	1.2	13
Midi	No	6	3	60	3.3	
	No	65	7	26	5.0	36
	Yes	6	2	60	2.2	
	Yes	65	3.2	26	2.4	20
Maxi			2	100	2.9	29
TISR			2	75	2.6	21
			2	300	9.0	66

beam performance achievable (intensity, emittance and charge composition).

Muon Acceleration in an FFAG

Muons present unique challenges for acceleration. First, muons decay; this means that acceleration must be rapid. Second, the 3D emittance of muons emitted from a production target is large; thus, unless there is strong cooling, the accelerator must have extremely large acceptance in all planes. Fixed field alternating gradient (FFAG) magnetic lattices coupled with superconducting rf cavities are a strong candidate to meet these challenges, particularly in the energy range 3–20 GeV, and there is rising interest in these machines at KEK, CERN and in the U.S. Continuing a collaboration with FNAL, we have promoted the non-scaling type FFAG and have further explored options for fixed-frequency acceleration.

Previously the problem of optimizing a single frequency was considered. With the objective of increasing the number of turns and reducing rf voltage, an algorithm that allows cavities to be grouped, and for each group to have its own optimum frequency, has now been devised. Two types of grouping were considered: ABAB and AABB, without restrictions on the number of groups or elements. The program has been applied to muon acceleration in a 300 cell FFAG with 200 MHz rf; cavity parameters were estimated based on existing CERN NC and SC designs. Comparisons were made between several grouping strategies for 5-turn and 6-turn acceleration. The ABAB type grouping typically yields larger transmission than the AABB type. However, for this machine, there are no great improvements in the performance between single-frequency and multi-frequency operation until the number of frequencies becomes large. Thanks to lattice design work at FNAL, and in part to these rf studies, the FFAG accelerator has been costed at BNL,

was the subject of a recent Muon Collaboration (MC) workshop at LBNL, and is considered almost on par with the recirculating linac as part of the U.S. MC baseline proposal.

Micro-Bunching at Brookhaven AGS

It was a significant achievement to document the numerous slow-extraction simulation studies of the previous year. In these studies it was discovered that some 6% of protons, with small betatron amplitude, cross resonance without being extracted. One may choose simply to send them to a beam dump. However, by adiabatic movement of the rf bucket central momentum one may force particles to cross through resonance a second time. To keep the phase spread small, one must also ramp the betatron tune to give a resonance that coincides with the rf bucket. Several schemes of this sort were investigated, but results were disappointing. At best the ramping strategy can extract only an additional 2% of the initial beam; and the micro-bunch phase width is compromised.

RF beam loading of rf cavity

Based on the assumption of minimum reactive power and the smallest rated power tube, resonance frequency tuning and cavity power requirements for the 25 and 100 MHz systems for the proposed KO-PIO experiment were estimated using beam current Fourier components calculated for a micro-bunched slow extraction. The power requirement is dominated by ohmic loss whereas the dynamic tuning range specification is dominated by reactive compensation of the particle beam current. However, due to their ubiquity at BNL, it was subsequently decided to employ a 60 kW tube, a rating 3 times greater than is required, and to reduce the tuning range by having the tube sink 20 kW of reactive beam power.

MAGNETS

In addition to contract supervision on the fabrication of the CERN twin aperture quadrupoles described in the CERN collaboration section, work was carried out on a number of other magnets during the year.

- The conceptual design of a 60 Hz steering magnet to paint the high intensity proton beam on to the ISAC targets was completed, but budget constraints have delayed the detailed design of the magnet [TRI-DN-02-1].
- The second dipole from the decommissioned M8 beam line was modified to act as a charge selector dipole for ISAC's charge state booster [TRI-DN-02-7 and TRI-DN-02-18].
- A small $X-Y$ steering magnet was designed to fit between the ISAC-II cryomodules [TRI-DN-02-17]. At year-end, construction had started on

8 magnets in the TRIUMF shop. The magnetic shielding of the ISAC-II medium beta cryomodules was studied [TRI-DN-02-20].

- Everson Electric Company (Bethlehem, PA) was contracted to design and build five 9 T superconducting solenoids for the ISAC-II medium beta cryomodules. The first magnet is expected to arrive in February, 2003.

Due to the decommissioning of the TRIUMF VAX cluster, considerable effort was spent transferring all old magnet measurement data from magnetic tapes to CDs and to the alph10 computer.

Experiment 614 – TWIST

The first half of 2002 was largely taken up with surveying the TWIST superconducting solenoid in the meson hall. A custom rotating arm survey system was built for this with capacity for 2 Hall probe arms. One probe arm has 7 Hall probes for surveying the main volume of the magnet and the other has the capability of 5 Hall probes for measuring upstream from the magnet, only the probe arm with 7 Hall probes was used for the preliminary surveys.

Another arm, with a NMR probe attached, was also attached to the rotating boom. The whole survey system can rotate through $360°$ and can also move along the Z axis by approximately ± 1.0 m. A second Hall probe channel will be built in early 2003, ready for further measurements. A detailed comparison was made between field maps taken for the TWIST solenoid at a field of approximately 2 T, and predictions obtained using the TOSCA 3D electromagnetic simulation code. There are twelve coils in total, comprising six inner coils and six outer coils. Three main discrepancies were identified in comparison with the TOSCA base model, namely: the measurements had an upstream-downstream asymmetry of 0.7 mT that was not predicted by TOSCA; the reduction in measured field, as one moves away from the centre of the yoke, is greater than TOSCA predictions; and a measured field asymmetry in both X and Y was not predicted. A series of TOSCA simulations, mainly by a co-op student, resulted in the following conclusions:

a) Modifying the model by moving the upstream set of inner and outer coils as well as the downstream set, by a distance of 1.8 mm along the Z-axis towards the centre of the solenoid corrects the predicted field gradient to better match the measured map;

b) A predicted upstream-downstream field asymmetry, similar to the measured asymmetry, can be achieved by appropriately scaling the current (by up to 1.7%) in three of the six inner coils of the solenoid;

c) The measured field asymmetry in both X and Y is predicted when the coils are displaced off-centre by approximately 1.5 mm in X and 1.8 mm in Y.

Detailed field maps obtained from the TOSCA simulations have been supplied for GEANT studies.

Magnet Measurements

Other magnets surveyed this year included the M8CSB dipole (charge state booster dipole), seven ex-Chalk River double steering magnets, HiTime 7 T superconducting solenoid from M15 (surveyed twice), and three radiation hard quadrupoles for 1A triplet (1AQ14, 1AQ15, 1AQ16). These triplets were measured with an 8 in. rotating coil. The 1AQ15 triplet was also measured with the survey table and a Hall probe for comparison.

Kickers

AGS KOPIO collaboration

The Kicker group carried out a conceptual design and budget estimate for upgrades to the AGS kicker systems for a Canadian Foundation for Innovation (CFI) grant submission for the proposed KOPIO experiment at Brookhaven National Laboratory (BNL). Upgrades are required to the booster extraction and AGS injection kickers in order to increase the AGS beam intensity by at least 50%.

NLC collaboration

The Kicker group are collaborating with kicker experts at SLAC carrying out research into the application of high power insulated gate bipolar transistors (IGBTs) for high efficiency, high reliability, and low cost pulsed power modulators for the Next Linear Collider (NLC) (Fig. 232). The IGBTs are stacked in series with a voltage of approximately 140 kV dc per stack. Under normal conditions the IGBTs conduct 3 kA current pulses for 3 μs, and under fault conditions the IGBTs may have to turn off currents of 6 kA or more. The aim of the power IGBT high speed switching project at TRIUMF is to understand and optimize internal designs of the IGBT so that the IGBTs can be reliably used in the pulsed power modulators. A co-op student will commence work on this project during 2003.

JHF collaboration

The TRIUMF Kicker group were approached by the JHF Neutrino Experimental group to consider the feasibility of designing a combined function extraction and abort kicker system for the Japanese Hadron Facility (JHF); at this time a design did not exist for such a kicker system. After making several suggestions for

Fig. 232. Solid state induction modulator developed at SLAC.

PSI MuLan collaboration

An international collaboration plans to measure the lifetime of the muon to a precision of 1 ppm. The "Mu-Lan" experiment will take place at PSI in northern Switzerland. The central idea employed in MuLan invokes an artificial time structure on an otherwise dc beam. The MuLan method requires a fast beam line kicker, which can turn the beam "on" and "off" at a repetition rate of up to 75 kHz: the TRIUMF Kicker group have been asked to design and build the kicker with the goal of shipping the kicker during June, 2003 and commissioning it at PSI in July, 2003. The kicker needs to run with a standard "on-off time cycle" or in a "muon on request" mode. The MuLan kicker will consist of 2 pairs of deflector plates mechanically in series, driven by 4 FET modulators. Each pair of plates is 0.75 m long. One plate of each pair is driven by a ± 12.5 kV FET based modulator and the other plate is driven by a -12.5 kV modulator. The potential difference between a pair of deflector plates is variable up to 25 kV. Each modulator consists of two stacks of FETs operating in push pull mode. The specifications for the kicker demand that the rise and fall times of the deflector plate voltage is not more than 45 ns. There is a requirement for an adjustable output voltage from 0 V to ± 12.5 kV per deflector plate, a minimum pulse duration of 200 ns, and adjustable repetition rate up to a maximum of 75 kHz, continuous. In addition, short turn-on and turn-off delays are required. We have developed a novel concept for the design of the MuLan kicker; a PCB containing a 1 kV MOSFET high-speed driver, power supply, and fibre optic receiver has been prototyped and is currently under test (Fig. 233). The printed circuit board layout for this design is very critical due to the fast switching times (<2 ns on the board) and the presence of kV transients that could otherwise be superimposed on low voltage fibre optic control voltages (5 V). It is planned to finalize the design of this PCB early in 2003.

the combined function kicker system we were invited to be members of an international collaboration designing and constructing the combined function extraction and abort kicker system. We were invited to give a talk at the JHF Neutrino Workshop, Kyoto, Japan in September. To our knowledge, this would be the first time that a combined function kicker has been constructed. The main involvement of the TRIUMF Kicker group will be in the design of the high power semiconductor switches required for the kicker; these switches will probably require high power IGBTs. TRIUMF will also perform PSpice calculations to determine the effect of dispersion on the detailed shape of pulses created with a pulse forming cable feeding a lumped element transmission line kicker magnet. We are also recommending a 32 kV system voltage, rather than 40 kV, to increase reliability. This will involve the design of a 3-cell kicker magnet with good transmission line behaviour, using a design first proposed by TRIUMF in 1994.

An NSERC research grant has been applied for to carry out research into the high power semiconductor switches that will be required for the next generation of kicker systems.

Fig. 233. Prototype PCB developed for MuLan kicker (heat sinks and fibre optic receiver shield not mounted).

239

MECHANICAL ENGINEERING

Mechanical engineering work at TRIUMF is initiated by the submission of a Request for Engineering (REA) form which is assessed and assigned according to the size, complexity and schedule of the task. Large, complex tasks usually require a team approach guided by a project engineer. The ISAC-II superconducting accelerator refrigeration system and cryomodules fall into this category.

During the year there were 34 ISAC REAs and 21 non-ISAC REAs submitted, along with a number carried over from the previous year.

As in the past there was continuous participation of engineering personnel in performing engineering analyses, consideration of safety related issues, design reviews, and other ad hoc engineering related small jobs.

ISAC-I East Target Station

This large project is a carry over from the previous year and was broken down into 6 major work packages as listed and briefly described below.

East module access area (EMAA)

The EMAA is the zone above the modules and below the five removable shield plugs. Although the work commenced in 2001, it could only be done during maintenance days and target changes for the west station, hence the majority of work was accomplished in this report period. A better approach to the layout of the EMAA was required due to problems with accessibility experienced in the WMAA. To correct this shortcoming, and in consultation with the target hall coordinator, a detailed design of the area was produced placing cables in cable trays, re-routing most services to maximize usable floor area, and redesigning the high voltage cage to produce a much neater entry of services to the target module and allow ease of handling during removal. The results of this work have made maintenance work easier in the EMAA, and the WMAA will be upgraded in a similar way in the future. The EMAA also houses some of the microwave equipment necessary to drive the ECR source. The power supply and controller are located in the electrical room but the magnetron, isolator and auto tuner are located on the south wall of the EMAA and connect through a wave guide to the top of the target module. The EMAA was completed and operational in the summer.

Faraday cage and HV chase

The Faraday cage is located in the electrical room adjacent to the target hall and houses the high voltage power supplies and related equipment, and the target gas supply system. Advantage was taken of an extended shutdown early in the year to accomplish a majority of the work.
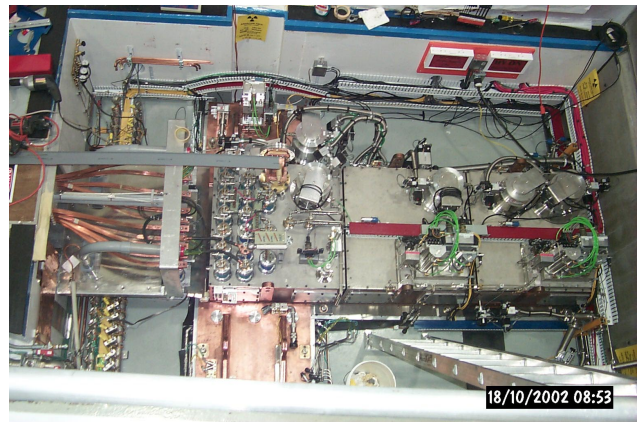
Fig. 234. View of EMAA.

A difficult task was the installation of high voltage conductors in the high voltage chase. The chase is approximately $2 \times 2 \times 20$ ft long with three right angle bends. There are ten 0.5×0.5 in. water-cooled conductors (plus a plastic tube for wires and 4 separate gas lines) that are required to be accurately installed in an H pattern to match several insulation stands in the chase and terminate in a flat array at a pedestal next to the target module. Flexible jumpers are used from the pedestal to the target module. The chase is then enclosed by shield blocks and the portion in the EMAA (Fig. 234) is surrounded by a high voltage cage. All this work was completed in the first half of the year.

Modules

The entrance and dump modules had been completed and installed in 2001. The assembly of TM2 (scheduled to be the surface source module for the east target station) and TM3 (the ECR source module) had commenced in 2001 but the difficult tasks were carried over to this report period. These included the accurate assembly of 30 tubes (0.25 and 0.375 in. diameter) into the service tray and putting them in place, and the accurate fitting of the containment box on to the bottom of the module so that it can be manipulated in the hot cell. The most formidable challenge was bending, fitting and soldering the 14 water blocks in the containment box that connect the service tray tubes to the target extraction column. This is a new, unique design that allows the complete disconnection of services between the service tray and extraction column tray so that either tray can be removed and replaced in the hot cell. This was a painstaking task in a small work space made more difficult by the fact that spacing of the tubes is crucial due to the potential differences during operation (Fig. 235). Due to the complexity of the task, it took an additional two months to accomplish beyond the original scheduled date. However, it
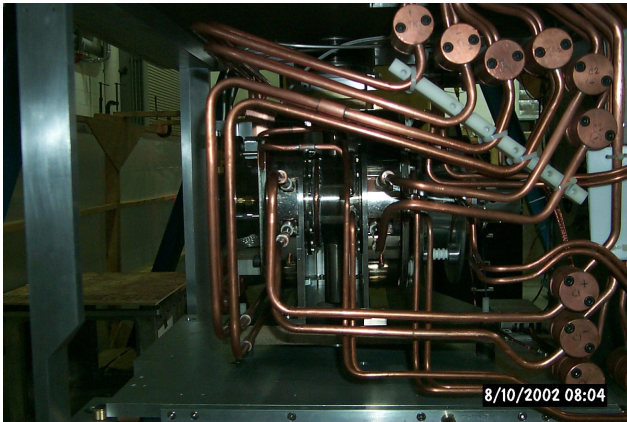
Fig. 235. TM3 water block assembly.

has proved to work well and has accepted voltages up to 50 kV to date.

The exit modules are similar to those in the west target station but incorporate the new shield plug, a slightly different containment box, and redesigned optics for compatibility with the ECR source. The two exit modules were completed in March and installed in April. Leak checking, continuity checks and diagnostic checks were then performed successfully.

TM2 (surface source) was installed in July and was leak, systems, and high voltage checked. It was available for stable beam delivery towards the end of August. This was followed by removal of TM2 and installation of TM3 (ECR source) during the first week of October. After three weeks of checks it was available for stable beam delivery in early November.

DRAGON

The remaining items of the DRAGON beam line were completed as follows:

- Modular security fence, complete with safety interlocks.
- Service platform (walkway) along the west side of the beam line. The platform was built above the cable trays of the power and controls cables using aluminum checker plates. The floor plates can be removed in sections for access to the power cables. The control cables can be accessed by simply lifting the hinged checker plate covers.
- Profile monitors were completed (see Figs. 236 and 237) and awaiting installation.
- Lead shields (about 3000 lbs each) for the charge slits and mass slits diagnostics box, complete with supports, were constructed and installed.
- Multi channel plate (MCP) was assembled and installed in the final slits diagnostic box.
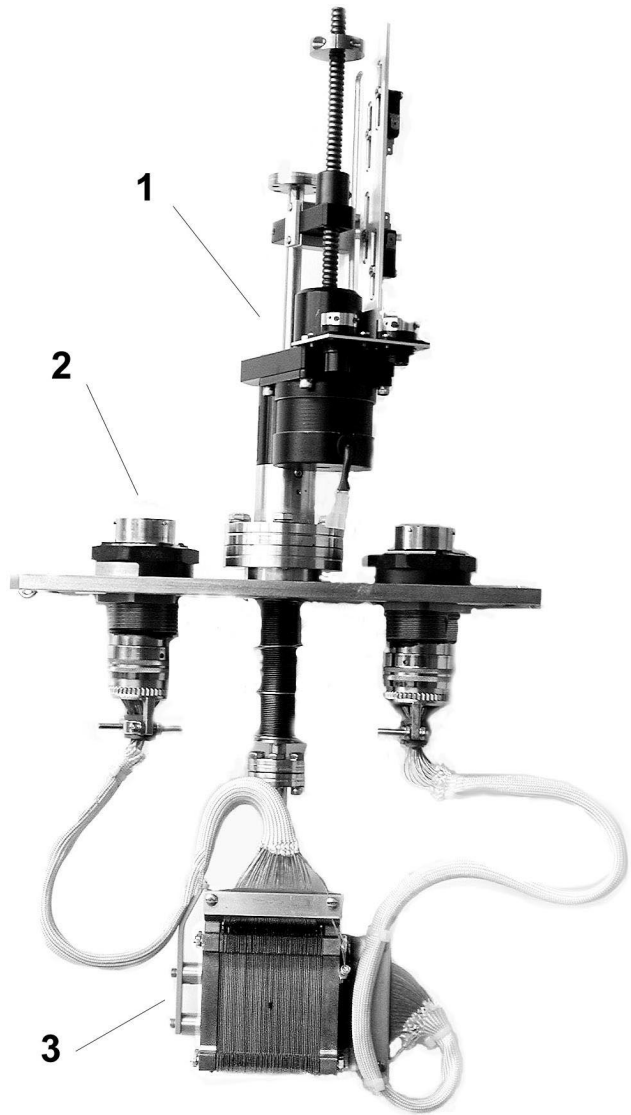
Fig. 236. DRAGON profile monitor showing actuator, vacuum feedthroughs, and monitor head.
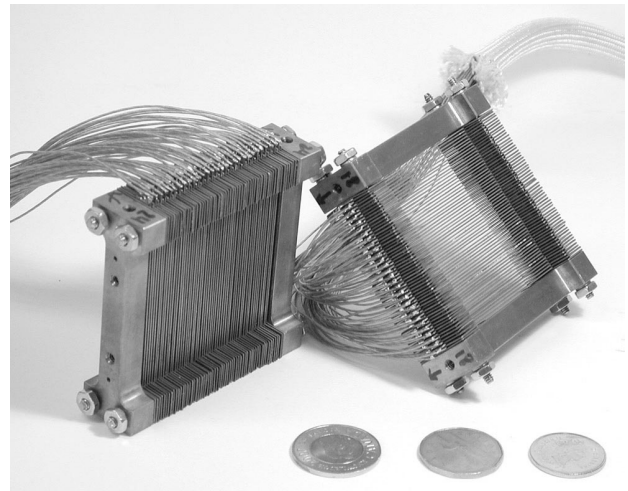
Fig. 237. DRAGON profile monitor showing $X-Y$ monitor heads.

241

- A universal alignment fixture was designed and built. This fixture can be used to pre-align all existing DRAGON diagnostic devices, eliminating alignment of a device in the beam line after repair or when constructing a new device on existing beam line ports.

RFQ cooler

The RFQ cooler captures low energy ion beams, cools the ions, and bunches them before injection into the charge state booster (now being constructed by another group at the ISAC test stand).

Before installing the RFQ cooler in the ISAC test stand, the device will be set up and tested in the former TISOL experimental area in the proton hall extension. The area has been cleared and an exclusion area (semi-clean room) that will house the RFQ cooler is under construction.

The RFQ cooler is a device 2 m long, built on a high voltage platform and protected by a high voltage cage.

The hardware design is about 75% complete. A design review will be done shortly in order to complete the final design and start construction. An overview of the RFQ cooler is shown in Fig. 238.

Engineering – Other

LTNO

The cold beam line of LTNO was redesigned and rebuilt to eliminate binding of the IRIS, and also to eliminate the leak that used to develop when the beam line was cooled to cryogenic temperatures.

KOPIO

Scintillator extrusion

Since a large quantity of scintillator is needed for the KOPIO preradiator, it was desirable to seek an inexpensive scintillator for this experiment as conventional cast scintillator cost would be prohibitive. Fermilab has developed a method of producing inexpensive scintillator using polystyrene and some dopants using extrusion techniques. It is

Fig. 238. RFQ cooler.

also desired that these extruded pieces of scintillator contain holes in their middle plane to accommodate fibres for light collection. Using a local company, Celco Plastics (Surrey, BC), and using the Fermilab method, we have been able to produce scintillator similar to that produced at Fermilab. So far we have produced scintillator with $\frac{1}{2}$ in. $\times 1\frac{1}{4}$ in. cross section and containing 3 holes. Efforts are under way to control the shape of the holes, control the external shape of the cross section to very tight tolerances for an extrusion process, increase the width of the cross section, and hence increase the number of holes in each cross section.

Aluminum extrusions

The KOPIO preradiator requires very thin walled and very tight tolerance aluminum extrusions to provide uniform electric field to the detector wires. One company had been found in Ohio who agreed to try to make such extrusions and indeed produced some samples for the prototypes. However, when this company tried to produce thinner sections, they had trouble doing so and then couldn't even reproduce the original extrusions as the personnel who successfully produced it originally had subsequently retired. Although they are still trying to duplicate what they produced, we have started looking for alternate suppliers. Most companies shy away from this very thin and tight tolerance shape but two companies are willing to try. An order has been placed with one of them to produce what the Ohio company had originally produced.

Other projects

Design and development was carried out for a detector stand assembly with two axis position control and data acquisition system for the NPDGamma experiment at the Los Alamos National Laboratory neutron research facility. The position controlled part of the frame is called the detector array frame and it houses 48 individual cesium iodide detector crystals each weighing about 50 lbs arranged radially around the LHe target cryostat which is also held by a "TRIUMF plate" which holds everything including the "spin flipper". Delivery of the whole system was made to LANL on December 23.

Numerous other thermal, stress and other calculations were done for such things as the ISAC target heat shield, pepperpot beam stop, ISAC-II SCB cryomodule vacuum tank, LHe reservoir, ISAC-II SCB rf cavity, etc.

ISAC-II

January, 2002 marked the beginning of the involvement of engineering on the superconducting linac planned for the accelerator hall in ISAC-II. There were
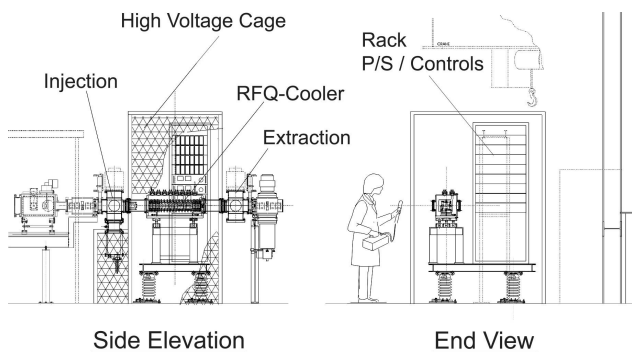
two major work packages assigned to mechanical engineering – (1) the refrigeration system, and (2) cryomodules. The linac is to be installed in two phases. Phase 1 involves the design, manufacture and installation of 5 medium-β cryomodules and 2 high-β cryomodules, the helium refrigeration system, and the helium distribution system to support the operation of this phase of the accelerator. Phase 2 is not at the present time completely defined, but will include an addition to the refrigeration system as well as completion of the high-β cryomodules.

Each resonator in the cryomodule required individual frequency tuning. TRIUMF has developed a design that allows both coarse and fine tuning to be accomplished by the same device and driver. A brief description is included.

Refrigeration system

The refrigeration system is composed of the following major components – an exterior helium storage tank capable of holding the entire phase 1 system inventory as a compressed gas, the main He compressor for this phase of the project housed in a separate compressor room adjacent to the experimental hall, a high pressure delivery system from the compressor to the liquifier housed in the cryogenics room adjacent to the accelerator hall, the liquifier, a turbine expansion machine producing liquid helium, the liquid helium storage dewar, the cryogenic distribution system from the storage dewar to the valve boxes (i.e. one valve box is required per cryomodule), and the transfer line between the valve box and the cryomodule. This system will obviously require a number of sub-systems for operational support that will not be listed here (i.e. He purifier system). Phase 1 (and 2) of the refrigeration system will be a 500 W at 4.5° K system based on the head load of the phase 1 components plus losses, with a suitable margin. It will have a 1000–2000 l liquid He storage dewar allowing for enough liquid He to ensure that cryomodule cooldown is rapid enough to avoid Q disease. A medium-β cryomodule cooldown will require approximately 200 l/hour for a duration of 6 hours.

Both the refrigeration system and distribution control system will be integrated into a two layer single system, consisting of a control layer handling all aspects of device control, and an operation interface (OPI) layer using the EPICS ISAC control system philosophy.

The team looking after the refrigeration system visited other laboratories involved in superconducting accelerators accumulating information, reference data, and related advice, in order to construct a specification to be sent out in a bid package to potential suppliers sometime in early 2003 with a goal of having an operational and accepted system by the end of 2004.

Cryomodules

The mechanical design of the medium-β cryomodules was initiated by the creation of a cryomodule specification based on the beam dynamics design note for relevant dimensions. A medium-β cryomodule is a stainless steel vacuum tank housing 5 cryo elements – 4 quarter-wave resonators and one 9 T solenoid. The cryo elements are supported by a rigid frame suspended from the tank lid by thin walled tubular struts in such a way as to accommodate material shrinkage during cooldown to 4.5° K. Cryo element alignment is paramount for efficient accelerator operation and must be maintained over repetitive cooldown cycles.

120 l of the liquid helium inventory of ∼170 l is held in the 40 cm diameter × 159 cm long helium reservoir and connected to the cryo elements by a 3 in. tube/bellows assembly. The reservoir is supported to the lid by a central tower which also provides a platform for pressure relief valves, a burst disk and cryogenic feedthroughs. The vacuum tank is lined with sheet μ-metal in order to negate the earth's magnetic field effects. Inside this liner is the liquid nitrogen (LN$_2$) liner which intercepts the heat load from the vacuum tank to the cryo elements. The LN$_2$ liner is placed in the tank sitting on the floor and away from the μ-metal by low conductivity standoffs. The lid will also have a double liner overlapping with that of the tank proper. The lid also provides space for other feedthroughs related to diagnostics, rf devices such as resonator tuning and coupling loop tuning, heaters, temperature readout feedthroughs and the frame suspension lugs.

Tests will be performed to investigate material shrinkage and any effects it will have on cryo element alignment (other than vertical). Once material shrinkage has been allowed for, alignment of the cryo elements to the beam ports will be performed in the assembly area and each cryomodule will be delivered aligned with two external alignments for alignment in the beam line on a standard TRIUMF 3-point mounting system.

Between cryomodules there is a diagnostic box, steering magnet, a short retractable beam tube and a 2 in. valve associated with the beam port at one end of each cryomodule; the other end has only a valve and KF40 stub to match the beam tube. This allows for removal of a cryomodule from the beam line without venting the system or the cryomodule. A cryomodule will be able to be replaced by a section of beam tube allowing the accelerator to remain operational.

At the end of this report period the vacuum tank, inter-modular components and some of the support frame have been detailed for release early in 2003. The

goal is to have an operational medium-β cryomodule by late 2003.
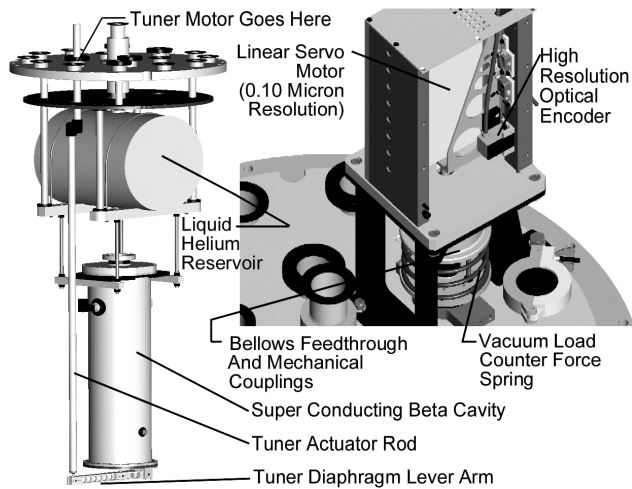
Fig. 239. Resonator tuning diaphragm and actuating mechanism.

Resonator tuning system

A new type of tuner system design was developed and tested successfully for the new ISAC-II superconducting rf cavity. This is the first known application of a direct drive linear motor actuating a tuner diaphragm of this sort to a resolution of ± 0.5 μm through a 5 ft long linkage system from outside the vacuum (Fig. 239). A special contoured tuning diaphragm with radial slots allows a coarse tuning range of $> \pm 2$ mm with an actuation load of ± 10 kg. FEA analysis was used in the design to confirm stress levels at maximum deflection and stiffness to ensure reliability and compatibility with the tuner control system.

Engineering – Victoria

Signal feedthrough project

There is continuing support for the ATLAS feedthrough project where construction of the last of 55 feedthroughs was completed towards the end of the year. All but four of these feedthroughs have arrived at CERN and staff at the University of Victoria will be supporting the integration process into the endcap cryostat of the ATLAS project at CERN. The TRIUMF laboratories at the University of Victoria will still be available to repair any damaged feedthroughs as a result of the installation process.

Hadronic endcap (HEC) module assembly table

Contributions to the ATLAS HEC production structure and manipulation tooling for the assembly of the HEC modules is ongoing. After components of the support structure were manufactured in Canada in 2001, successful delivery to CERN and final inspection were completed in early 2002.

ISAC target development

The targets designed for the ISAC target stations are currently limited to 40 μA at maximum. Additional cooling would be required after this to avoid damage to the target components. A new target has been equipped with fins to increase the surface area to increase the heat dissipation required with the increasing proton beam currents and has been tested off-line. A thermal simulation using finite element software has been conducted and the results from these analyses have closely matched the measurements in the test scenario. These results demonstrate that the new target can withstand proton beam currents up to 100 μA.

With the completion of the manufacturing and testing of ATLAS feedthroughs, the decommissioning of the laboratory space at the University of Victoria has begun, other than leaving a small area for feedthrough repair, if the need arises. At this time a high temperature vacuum test station is being introduced for ISAC target development. Existing equipment is being modified and an effusion cell is being designed to test various materials for potential use in future ISAC targets.

ISAC-II – medium β accelerator design

The University of Victoria has been providing technical support as needed while the design for the medium β cryomodules progresses. This has primarily involved calculations for the heat load on the cryomodules as well as determining the details of the flash vapourization expected of the liquid helium inside the cryogenic components if a loss of vacuum occurs inside the cryomodule tank.

General

The Engineering group at the University of Victoria has continued to provide support for beam line and equipment maintenance at TRIUMF. This has included technical drawings and calculations as required.

Engineering – Carleton

ATLAS forward calorimeters (FCAL)

In July, the FCAL 3C module was packed into a Carleton designed and constructed reusable shipping crate and transported to CERN by truck and air. The total shipping weight of the module and the protective crate was 5154 kg. Once at CERN, the module was moved into a clean room and the installation of signal readout boards was completed (Fig. 240), along with several high voltage tests (Fig. 241) designed to locate shorts in the readout anodes. A cold test, consisting of having the module in a cryostat of liquid argon, was successfully completed in November. This module is now ready for a calibration beam test scheduled for June, 2003. Construction of FCAL module 3A was

completed to the point where only about 5000 tungsten anode rods remain to be inserted. This module is scheduled to be shipped to CERN in April, 2003.

Fig. 240. Installation of FCAL 3C readout boards at CERN.

Fig. 241. Testing of FCAL 3C after arrival at CERN.
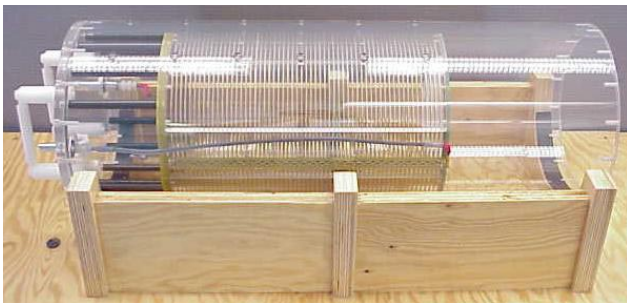
Fig. 242. "See through" TPC readout test chamber.

TPC readout test chamber

In order to test various TPC readout patterns for use in future linear colliders, a small non-magnetic TPC was designed and constructed at Carleton (Fig. 242). The chamber is housed in a 600 mm long,

222 mm diameter acrylic tube. Most of the components are non-metallic with a few that are non-magnetic materials. The chamber was sent to the University of Victoria for testing in a specially built reusable shipping container, the lid of which can also be used as an assembly stand for the inner working of the chamber.

PLANNING

This year the Planning group was involved in planning, scheduling, coordinating and expediting several sub-projects for ISAC-I (east target station, ECR source, 25 MHz cavity, Osaka beam line, and 8π); ISAC-II (BC Research facility, medium-β system, high-β system, transfer line, H-HEBT and charge state booster (CSB)); planning and coordinating activities for two scheduled shutdowns (December 22, 2001–April 17, 2002 and September 19–26); prototype chambers for KOPIO preradiator, M8 decommissioning, 1A triplet repairs and replacement. The Planning group was also involved in preparing preliminary PERTs for the rf cooler and TIGRESS.

ISAC-I

Various plans and PERTs were prepared and updated regularly with manpower estimates and analysis to identify critical areas and resolve any problems. ISAC priorities were evaluated and higher priority was assigned to: the east target station that was installed in the winter, 2002 shutdown; ECR source (to be installed in TM3 and tested with beam in November); install and commission 25 MHz buncher in spring; and expedite low energy experimental program that included the β-NMR and Osaka beam line.

Manpower planning was done, activities were coordinated and expedited, and the above goals were achieved on schedule. However, several technical problems encountered in the installation of the target module at ITE delayed the commissioning until November.

Technical details and progress on PERTed activities are described elsewhere in this report under the respective principal group. However, following is a summary of the main projects along with the major milestones achieved.

East target station

This project received high priority and had to be fast-tracked for installation in the January shutdown. The project was broken down into 9 work packages and major highlights included: 2A beam line (2A3 beam line installed in winter shutdown); Faraday cage (most work done in winter shutdown and remainder completed by summer with limited access to electrical room due to ITW beam operation); target hall (included modification and commissioning of south hot cell and alignment components and water package shielding in

245

March); controls (included 2A controls, target protect interlocks and RIB controls for vacuum system, beam optics and beam diagnostic systems completed in the winter shutdown).

The work on the modules required extensive Design Office and Machine Shop effort. Several design modifications were made for better manufacturability and remote handleability. Initially the plan was to make TM2 and TM3 interchangeable but later complications associated with installation of the ECR source and microwave guide and generator excluded that provision. TM3 was designated as the module for the ECR source at ITE, and TM2 with surface source at either east or west target stations. Some of the major technical challenges that took longer than anticipated included accurate assembly and installation of 30 tubes and 14 water blocks in the containment box. Consequently exit modules 1 and 2 were installed in April and TM2 (with surface source) was installed in July, followed by leak checking, fixing water leaks, and high voltage checks by September. The ECR source was tested on the test stand by September. TM2 was removed and TM3 with ECR source was installed in October, followed by checks and tests with stable beam in November.

Target conditioning box

An alternative conditioning system was designed and fabricated by January to expedite the process of changing and conditioning ISAC targets. Assembly continued till April due to lack of manpower.

Experimental facilities

The Osaka beam line was installed and tested in October/November with a new chamber and associated services. The 8π beam line with a simple chamber was commissioned with a test beam in December.

DRAGON and TUDA started commissioning with stable beam followed by RIB. Some of the major hardware items completed for DRAGON included: modular security fence with safety interlocks, service platform, lead shields for charge slits and mass slits diagnostic boxes, and universal alignment fixture.

ISAC-II

PERTs were prepared and monitored for all ISAC-II projects, and activities were coordinated and expedited to meet various milestones. Major milestones achieved for the medium-β system included: commissioning tests on Nb cavity with rf controls in June, with mechanical prototype tuner in October, and with μ-metal in November, tuner development and final design released in November, order amplifiers in December, prototype solenoid ordered in October with delivery in March, 2003. Fabricated cavities at Ezanon progressed well with delivery anticipated in January, 2003,

to be followed by chemical treatment at CERN by April, 2003. Extensive effort was spent in planning cryomodule engineering. Conceptual design was reviewed in November and three designers were allocated to complete the design of the tank, lid, LN2 shield, liquid helium reservoir, frame and suspension system, intermodule zone, and jigs and fixture by March, 2003, fabricate and assemble by September, 2003, with an aim to do cold tests and test the cryomodule with rf in October, 2003. The refrigeration system is on the critical path because specifications were delayed due to lack of manpower and information.

Work continued on high-β beam dynamics, HEBT transfer line (layout, specifications and concept design of dipoles), and charge state booster (components ordered in February and received in November, design CSB stand in fall, modify analyzing magnet in December), with an aim to test the whole system on the test stand by October, 2003.

Shutdown Activities

There were two shutdowns during the year: the winter shutdown (December 22, 2001–April 17, 2002), and a short maintenance shutdown (September 19–26).

Winter shutdown

BL1A shutdown activities began in early January, with the removal of many shielding blocks from the meson hall to a temporary storage location near the Machine Shop. The original work schedule slipped a little at first because of an unanticipated need to quickly arrange two radioactive waste shipments to the AECL disposal facility to save significant money. Delays were also caused from obstacles encountered along the way – welded steel shielding in M8/T2 area, additional water leaks, new crumbling blocks. Six heavy crumbling shielding blocks were shipped to the Chalk River storage site and removal of additional hidden crumbling blocks, including some underneath the T2 cooling package was delayed to the winter, 2003 shutdown. The extent and complexity of some of the BL1A tasks, most of them in very high radiation fields, resulted in some higher than usual doses for a few workers with three receiving between 5 and 7 mSv. A total shutdown dose of 150 mSv was distributed among 110 workers.

Major jobs completed by the Remote Handling, Beam Lines, Vacuum and Diagnostics groups in the meson hall included: M8 decommissioning that involved removal of the M8 channel front end elements, shielding replacement and reconfiguration (new shielding was designed to fill the void as well as to replace some removed crumbling blocks), the *in situ* repair of three separate water leaks on all three 1A triplet magnets, repair of M20Q1 and B1 water leaks, 1AQ10 ro-

tary collimator vacuum leak, rebuilding of the troublesome M13 beam blocker, T1 and T2 target and water package MRO, repair of 1AM8 and 1AM10 monitors, repair of vacuum leaks at 1AVA8 and M13VA1 (broken bypass line), and replacement of 1AWVA2's air cylinders.

In the vault the cyclotron lid was raised towards the end of January to minimize shutdown dose. Radiation fields were about 10% higher than last year (as predicted from the previous beam delivery schedule), and, as much as possible, remote handling equipment was used to minimize personnel dose exposure. Apart from the usual heavy schedule of routine diagnostics MRO (including work on the extraction and pop-in-probes), there was quite a lot of time spent doing centre region work where, fortunately, the fields were reasonably tolerable. This included installation of a water-cooled beam absorber in LQ1's detachable quadrant (to help maintain cool centre region temperatures during higher intensity injection), repair, relocation and addition of several thermocouples, and the refurbishment of correction plates in Q1 and Q3. At the tank periphery, work included blanking off the unused centring probe feedthroughs and the tricky job of replacing the seals on the extraction 1 gate valve.

There was also a large number of additional jobs and MRO work around the site, including replacement of PCB transformers, construction and installation of the 2A3 leg and east target station.

Fall mini shutdown

This one week of extended maintenance work had a reasonably ambitious schedule. BL1 work started when PIF finished in 1B, while vault work started a week later when proton therapy had finished. The total shutdown dose was under 5 mSv with no one exceeding 1 mSv. Major jobs completed in this mini shutdown included: diagnostics MRO (extraction probes 1 and 2A, beam line monitors including 1AM8, fast shutter), beam lines (repair M13 beam blocker and install slit box in M13 F2, remove 1BBB2 latch mechanism and repair 1BBB3 vacuum leak), power supplies (main magnet power supply relay, water hose, MRO and repair radiation damaged feedback wiring), vacuum (tank cryo pump MRO, install turbo on cryoline and swap B20, extensive BL leak checking, change 2A O-rings near 2AVM1), services (install new rf room water filter, compressor MRO, ISIS LCW pump MRO, aluminum ALCW system control valve MRO), and rf (investigate sparking, install and test new combiners, build new GAT control software, check out ISIS rf pickup from tank).

The vault was ready in time for tuning up the cyclotron as scheduled but extraction down BL1A was delayed one day to accommodate last minute work.

There were a few lingering details from the shutdown affecting subsequent operation. The M13 beam blocker initially worked fine as a blocker but lost its dual purpose as a beam line gate valve, M20Q1 developed a 1 l/h water leak, and a 1AQ9 over temperature fault was not found along accessible interlock wiring. It was recognized that 1AQ9 would therefore require uncovering to determine the exact cause and in the meantime 1A would have to remain tuned with 1AQ9 off. This did not have any major impact on beam operation since it is needed with the septum to provide M11 beam. Finally, 1BBB3 needed to be removed to repair a leaking bellows, making it necessary to run with the 1B area secured until the blocker was fixed. Since the lid was not raised, there was no opportunity to replace the two dead X2C foils. A viewing through the periscope indicated that whiskers were not nicely aligned but also showed that the heavily used one was fairly good. After the usual target scans and radiation surveys, the beam intensity was increased to deliver to BL1A and BL2A2 their nominal currents followed by 40 μA to 2C4.

DESIGN OFFICE

Available hours were up 3.5% over last year to 16,160 with the addition of one full-time junior and a reduction in sub-contracted hours. With ISAC-I under development and ISAC-II being in first stage design, focus has changed.

The ISAC project received 59.5% of design hours available during the calendar year. Specifically and in order of magnitude they were: (a) target module development including TM2, TM3 ECR source and all IT east modules; (b) ISAC-II SCB cryomodule component design, HEBT transfer, cavity refrigeration and experimental prototyping; (c) LE beam transport upgrades; (d) charge state booster development for installation in the ISAC test stand; (e) off-line ion source reconfiguration; and (f) miscellaneous experimental support.

TRIUMF's main program received double the hours of last year at 29.3%. The main projects were (a) BL1A triplet upgrade, (b) cyclotron HE probe upgrades, transmission line upgrade and beam absorber, (c) μSR, (d) M13/TWIST, (e) M11, (f) ISIS, (g) safety and other projects. External projects received 6.7% with most effort concentrated on the pulse forming network, HV switches and power supplies for the CERN collaboration.

Photographic and visual art services continue to grow in support of seminars and conferences. Publications such as the annual financial report are increasingly processed in-house. Instructional aids for the lobby, models, posters and displays are being consistently upgraded. Network 2D CAD is now available

through PC support. 3D is under evaluation. 70% of the legacy archive has now been scanned.

MACHINE SHOP

The TRIUMF Machine Shop, with 19 technicians and 3 apprentices, produced approximately $129,000 worth of fabricated and machined components for various on-site groups each month. The shop charge out rate is $70/hour. The distribution by TRIUMF divisions and other groups is shown in Table XLV. In addition, 228 separate work packages worth more than $464,000 were sub-contracted through the Machine Shop to local industrial companies. The Machine Shop continued to be fully loaded throughout the year with ISAC continuing to be the major user. Two older machines were replaced with a new lathe and milling machine and these were very welcome additions to the ongoing program of updating equipment.

Table XLV. Machine Shop utilization.

ISAC Development	22.29%
Science	20.14%
ISAC Operations	14.13%
Nordion	13.74%
ISAC-II	11.19%
Cyclotron	9.06%
Cyclotron Refurnishing	5.03%
CERN	2.42%
Affiliated Institutions	0.75%
NSERC	0.57%
Site Infrastructure	0.50%

BUILDING PROGRAM

The Building department was involved in the following activities:

Design and management of minor construction projects

The department carried out the following projects: laser rooms in ISAC-I extension hall and service annex, roof access stairs (Fig. 243), additional air intake openings on the ISAC-I building, and proton hall fence, for a total cost of $69,900.

Structural design and engineering review

Structural design was done for the TITAN test area tent steel frame and the 20 ton spreader beam, and engineering review was performed for the new magnet support stand (BL1A triplet).

Construction review

Besides the reviews of minor construction projects managed by the department, the construction review of the new ISAC-II facility was done on a regular basis.

Management of maintenance and repair work

During the course of the year approximately $40,000 was spent on maintenance and repair work

Fig. 243. The new aluminum roof access stairs (before and after).

at various TRIUMF buildings (the annual maintenance and repair contract consumed $31,500). A further $12,800 was spent on interior and exterior painting. The roof of the main office building north wing was replaced at a cost of $65,800.

Drawings library maintenance and services

The department continued with organizing and updating the site and buildings drawings library, and provided services of issuing drawings to many in-house clients.

ELECTRONICS SERVICES

Overview

Electronic Services had a very full year as detailed in the following sections. The personnel in the group worked on virtually all projects and experiments on site and interacted with an estimated half of the site staff. We continue to be one of the most sought out groups with information on every aspect of electronics

from ordering special cables, answering obscure software questions, designing specialized modules and answering just about every PC question. We also have senior personnel that have very valuable historical information on some of the original systems installed at TRIUMF.

Electronics Shop

The Electronics Shop continues to be a major "hub" of TRIUMF. All major and minor ongoing projects are reflected in our daily shop repairs and production. The following were assembled during the year: boards and cables for CERN, flow-switch controllers for ISAC, QSX modules for ISIS, and modules for Jefferson Lab. Cables were made for all groups on site: DRAGON, site communications, PET chemistry, controls, CHAOS, TWIST, β-NMR, beam lines, Osaka, TUDA, University of Guelph, TRINAT, ITE vacuum, Expt. 871, M20, 8π and TRIUMF Stores. The shop also handled a large variety of special, one of cables that experimenters required the day before. The TRIUMF library continues to have ongoing daily support from a member of this group.

Experimental and Target Support

This group spent 80% of its time on CERN contributions including assembly of the PFNs, switch tanks, and help in laying out and testing of bias boards. Cabling of the control system for PFN testing was also done. Assistance was also given to the TWIST experiment in acquisition cabling and the design and installation of a FASTBUS cooling interlock system which has already saved the system from overheating when an air-conditioner failed to restart after a power outage. ISAC was supported with design and installation of the ITE target and dump protection system.

Site Communications

The major effort in site communications was the upgrade to the faster 100 base-T Ethernet standard. These areas included the proton hall extension ground floor and mezzanine floor, TISOL platform, trailer P, service annex ground floor and second floor, ISIS, level 264, service annex extension ground floor and second floor, trailer M, remote handling building, Safety group office, M15 counting room, proton therapy, operations control room, and the Plant group building. All documentation for this work is posted on the TRIUMF Web site. The other major project this year was the planning, specifying, tendering contracts, and ordering of data communications for the new ISAC-II building. Ongoing work included repairs to the site communication system as required, as well as assisting numerous individuals with unique requests for equipment or services.

Technical Support

A large effort of Technical Support went to the Controls group in the design and construction of a new CAMAC based 32-channel 16-bit ADC module incorporating a digital signal processor as well as a CAMAC power and diagnostic module used to monitor the health of individual crates. Another special job for the Controls group was the construction of a replacement sub-assembly for an obsolete DAC on a CAMAC module. This is an ongoing area of concern as many repair parts are not available for some of the 20–30 year old modules on site. For TWIST, some small devices were built and considerable documentation was completed. Proton therapy has a very special PLC system with no backup, so a second fast shutter PLC interface box was constructed. LTNO came in with a request for a precision interval gate generator, stable to one part in four million over one hour. This required acquisition of a specialized oscillator along with the design of a new module.

High Level Software Support

The principal task during 2002 was the development of a control system for the CHAOS polarized proton target on the M11 beam line. All data acquisition and control functions were implemented using the EPICS toolkit and employed a PLC for vacuum control, CAMAC and GPIB for data acquisition, and a Java based acquisition system (JACQ) for data analysis. The system worked well but the beam line had a number of problems. In parallel with CHAOS was the mapping of the TWIST solenoid. The JACQ application was used for this and data was successfully collected using both NMR and hall probes moving within the solenoid cavity. Some supervision of a co-op student took place in association with this work. The proton irradiation facility positioning system was improved by using the JACQ application with a custom front end, co-developed with a co-op student.

Assistance was provided to two co-op students in the development of a PLC based system destined for ISAC. One for the ISAC target implantation system and the other for the 8π TIGRESS liquid nitrogen level controls. Further work was done for TIGRESS to specify an $X - Y$ table for detector calibration. The LTNO experiment required some continuing work for the data acquisition system. This included the implementation of three new instruments into the system and several modifications to existing components.

A complete overhaul of the Bl2A extraction probe control system was completed to improve reliability. The performance was immediately obvious after implementation, and the system has operated fairly reliably since then. The tank thermocouple system was

re-written to improve operation. A new kinetics 3291 dataway display exerciser tool was written for controls hardware. TRIMAC application development is still ongoing using both Fortran and C. The C systems are a good option for small CAMAC based systems requiring some automation. Investigations were made into building a measurement system for the proposed KO-PIO preradiator assembly for Brookhaven. Mechanical positioning systems that could cover over 2 m and allow positional accuracy of 50 μ were researched. Automated image analysis was investigated for fine measurements in two axes using equipment borrowed from PIF. A successful byproduct was the rescue of a PIF experimenter who had lost his computer and was able to collect data as a result of this work. Problems with the M15 separator power supplies resulted in a complete cleaning of all heads and reworking the cooling system. Further work has started to build a test assembly and repair some damaged components.

PC Support/Desktop Services

This year continued to be a busy year for the department. Although the 2001 task numbers are not available for comparison, a comparison to the year 2000 shows a 56% increase to 276 software related tasks, a 40% increase to 167 network related tasks, and a decrease of 32% for the 205 hardware related tasks performed. The decrease in hardware related tasks is presumably due to a greater adherence to the hardware standards defined by this department. These standards are primarily based on reliability and compatibility. With the implementation of a hardware tracking system, it can be seen that a majority of the new Windows based PCs are following these standards.

Several major tasks were completed. A third Net-Ware server called NW02 was purchased and set up to provide imaging services, Web access such as iFolder, iPrint, and a Web server. A new Desktop Services Web site was created to provide an organized and easy to use help desk resource for TRIUMF staff. An Auto-CAD pool of licenses was created from existing stand alone licenses to provide many users access to this application. As of December 31, 30 users are accessing the 9 shared licenses. The PC backup server software was upgraded to allow greater compatibility with Windows 2000 and to make administration easier. The number of users on the NetWare service increased from 74 to 93. Our PC backup service is now serving 42 PCs, up from 26 PCs. The number of virus scan clients has increased to 229 from 167. There has been a noticeable increase in consultations with TRIUMF staff. It is estimated that PC service fielded 3000 consultations this year. These consisted of telephone calls, visits to our offices, and impromptu meetings in hallways with staff seeking advice on every computer topic imaginable.

Electronics Repair Shop – Nucleonics

Considerable time was spent repairing the electronic controls for some of the machines in the Machine Shop, including the electron beam welding machine and numerical readouts for the lathes. Also, repairing detector electronics for E787 at Brookhaven National Laboratory, and repairing and recalibrating high-voltage power supplies borrowed from Fermilab for use in the TWIST experiment at TRIUMF were significant tasks. In total, 282 electronic devices were serviced in some way, including: 40 monitors, 96 power supplies (including 12 NIM units, 10 CAMAC units, 65 high-voltage units, of which 32 were for TWIST, and 9 other units), 64 nucleonics modules (which included 56 NIM devices and 8 CAMAC devices), 24 front end pre-ampliers and amplifiers for E787, 18 pieces of test equipment, 7 printers, and 33 other assorted electronic devices which included 7 from the Machine Shop.

ELECTRONICS DEVELOPMENT

During this year the group's main effort continued in supporting the ISAC control system design and installation along with the data acquisition board (DAB) for CERN. One member of the group was assigned to the quality assurance task force, which has been charged with creating and implementing a QA program acceptable to the CNSC. Travis Howland joined the group as a junior technician.

ISAC Support

The group provided all the hardware installation, maintenance and upgrade support for the ISAC control system. An additional 40 CAN-bus modules for power supply control, and 35 ISAC standard VME modules were installed. CAN-bus code was completed to allow the remote integrator module to communicate with the ISAC control system. Two 4-channel modules were installed on the mass separator platform and the LEBT/yield station section. The ability to read currents of less than 1 pA has improved beam optimization. Optical isolation was added to two more modules and installed on the TUDA chamber.

The ISAC test stand and OLIS controls underwent a complete rebuild to bring the original installations up to the current ISAC control system configuration.

A modification to the CAN-bus controller transition modules in the DTL/HEBT section was made to provide a cleaner installation and easier maintenance.

A temperature measurement sensor was constructed and installed in the 8π shack, and incorporated into the EPICS alarm handler.

Maintenance activities included repair of malfunctioning components as well as development of test pro-

cedures for TRIUMF built devices.

Further development on the VME back plane tester was completed. A second linked module can now test the VME back plane for open and shorts automatically.

A variable current source module was designed and built to automate test procedures for the VQSX module.

CERN

Nine new modules of the latest revision (DABIII) were delivered to CERN in July. Embedded code was written to provide additional functions for orbit batch/bunch acquisition. Two members of the group went to CERN in mid-July to integrate and test the DAB with updated CERN WBTN mezzanine modules. The integration tests with a single DAB module were completed successfully using simulated beam position signals in the laboratory. Scheduled SPS beam tests with real-time data acquisitions using multiple DAB modules were postponed until September to allow time for the completion of SPS equipment installation. Preliminary design based on the new DAB specification was started. The new module will conform to the VME-64x standard.

Engineering Support

An independent PLC system (Modicon Momentum) for the ISAC mass separator high voltage lock-up area was designed and installed according to the Safety group's requirements specification. In addition, an EPICS user interface was implemented and integrated into the ISAC operations console.

For the modular radiation monitoring system the universal detector module design was updated. Ten modules were built, calibrated and shipped to INER in Taiwan.

A gamma radiation detector for PET radiochemistry was designed and built. A photodiode produces a small (fA) current, which is amplified and filtered, producing 10 mV per fA. During testing, the noise level was measured to be 30 fA RMS. Improvements to reduce the noise are being pursued.

Three more VICA harp readout modules were produced for the TRIUMF Diagnostics group.

The Magnet/Kickers group continued to receive support with engineering, design and prototyping of their chopper systems.

The group also provided technical advice to three co-op students with other groups.

Experiment Support

A VME based Gate Logic module was developed for the μSR group. Seven modules were constructed. A third VME frequency synthesizer module was built and delivered. Modifications were completed for enhanced performance of the μSR's ± 1 kV pulser that was built

last year. Some simulation and prototype design was completed for KOPIO high voltage power supplies.

Secondary Channel Support

A failure of the obsolete programming unit for the M9 and M15 vacuum system PLCs precipitated integrating these systems into the ISAC BL2A PLC. The M9 system move was successfully completed. Work was started on the databases and code in preparation for moving the M15 vacuum system. This move, when completed in the spring shutdown, will allow the systems to be fully supported by the new EPICS based secondary channel control system. The addition of a JAW into the M13 beam line required the group to provide a mechanism to control the movement. A temporary controller was constructed so the JAW could be used during the fall beam time. The existing M13 controller will be expanded during the next shutdown, to include this functionality.

New Hardware Designs

Several new modules were designed and built:

- A VME ADC based on the VQSX was designed, built and tested. It incorporates 8 channels of 16-bit ADC and a single channel 16-bit DAC. Any of the input channels can be routed to the DAC output for diagnostic monitoring.
- An 8-channel 12-bit DAC mezzanine card was developed for the VME VQSX module. This card provides analogue monitoring for each of the 8-current inputs.
- An upgraded water flow module was designed, specifically for ISAC requirements. This design allows calibrated flow rates to be read by the ISAC control system via CAN-bus. The board layout has been completed. Installation for the ISAC rf water system is planned for spring, 2003.
- The prototype NMR module auto tuning and pulse detection functions were successfully tested. Full functionality testing continues in parallel with the final module design.
- An accelerometer circuit was constructed in an attempt to correlate readback noise with mechanical vibration. The device is currently being used by the TRIUMF Diagnostics group.

Infrastructure

The growth of the group required replacement of its WindowsNT based file server with a faster larger system. A new system running Linux was assembled utilizing hardware RAID disks. For data security and immediate recovery the files are mirrored on a second server in a different building. In addition, daily incremental backups are performed.

CERN COLLABORATION

INTRODUCTION

TRIUMF's collaboration with CERN on producing accelerator components for the Large Hadron Collider (LHC) is nearing completion. As noted in last year's report three technical projects and two beam dynamics studies are presently being carried out. In October, the directors of TRIUMF and CERN signed an extension to Canada's agreement to contribute to the LHC project, adding a second contribution of $11.5 million to the existing $30 million. Most of these funds are being used to pay for the completion of the contract with ALSTOM.

The series production of the 52 twin-aperture quadrupoles for the beam cleaning insertions in the LHC is going very well at ALSTOM. By the end of 2002, 32 magnets had been produced and the production rate had increased to almost three per month. The magnets are now of high quality and the magnetic field measurements at CERN indicate that the harmonic content is acceptable. The speedy production rate together with a cost increase in the magnet contract meant that there is a cash flow problem this financial year and the next one. This was solved with a repayable loan of $1.5 million from the National Research Council. ALSTOM now expects to complete the contract for the 52 magnets by August, 2003.

The other large contribution consists of components for the LHC injection kicker systems. The five resonant charging power supplies have been tested at high voltage into a dummy load. The nine pulse forming networks are completely assembled and tested at low voltage. The twenty switch tanks are nearing completion. High voltage testing will begin early in 2003 with the first major shipment to CERN about mid year. The shipping container used for the ATLAS calorimeter modules is being modified for shipping the kicker hardware.

A third version of the data acquisition board for the LHC beam pick-up monitors was delivered to CERN in July for testing. A fourth and hopefully final version is now being designed by TRIUMF. This version will be compatible with the newly adopted CERN VME64 standard and uses a new FPGA with more memory and therefore more capability is being requested by CERN.

Two beam dynamics efforts continue to be supported. The study of beam-beam interactions between the LHC beams at the collision points uses a simulation code developed at TRIUMF. This code is being extended to include the longitudinal motion and makes use of parallel computing to obtain acceptable computing time. The beam optics and collimation work is essentially a full time effort for a TRIUMF beam physicist. The collimation system protects the vacuum chamber in the region of the LHC superconducting magnets against beam losses. This year the Dimad technique developed at TRIUMF was compared with a tracking code used at CERN. At CERN it was realized that accidental beam dump failures could cause overheating of the copper collimators if a significant fraction of the beam was dumped locally over a single turn. The solution is to use longer collimators made of lighter material and this requires some changes in the optics to accommodate the longer collimator systems.

BEAM DYNAMICS

Coherent Beam-Beam Effects in the LHC

Our study of beam-beam interactions in the LHC seeks to identify potentially unstable coherent modes excited by the electric forces between counter-rotating bunches of protons as the two beams meet and cross in the collision regions. A multi-particle simulation code, based on 2D models of head-on and long-range interactions, has been used extensively to study these modes under various LHC operational conditions and crossing schemes. This year we entered a new phase of development in which our simulation code, newly dubbed BeamX, is being extended to include the third dimension and also to run in parallel computing environments.

Given the relatively long (0.3 m) bunches in the LHC, we wished to account for effects such as longitudinal motion, crossing angle, and size and density variations in the two beams as they cross each other. Longitudinal motion was included in the macro-particle tracking using the conventional stepwise integration as in many other tracking codes. For beam-beam interactions, a longitudinal subdivision (bunch-slicing) scheme was developed in which the interaction is decomposed into a series of 2D slice-slice interactions. To obtain acceptable computation time, it was crucial here to exploit the obvious parallelism, where, at each stage of beam-beam overlap, each slice-pair interaction (including field solutions and particle transport) can be done on a different processor.

We were fortunate to have unimpeded access to a small "commodity" Linux cluster set up as a test-bed by the Computing Services group at TRIUMF. This allowed some research into various options for parallelizing the simulation code, and led to the development of a suitable parallel algorithm using the MPI toolkit and the LAM environment in a communication topology involving both master-slave and slave-slave messaging. A novel aspect of the method is that it does not use any loops, but rather relies on the flow of inter-

processor messages to optimally conduct the pairwise interactions of bunch slices.

The new code was tested with various numbers of slices and exhibited the expected linear speed-up, allowing us to begin full production runs. However, for a typical run (e.g. 7 slices) the turn-around time is still greater than one day on 1–2 GHz processors, so in 2003 we will likely be seeking further economies, either by improving the communication scheme or by further parallelization, e.g. of the field solver. In addition to ongoing support from TRIUMF resources, this project has been granted access to the University of Alberta THOR cluster, which offers more advanced communication hardware and larger numbers of processors.

Beam Optics and Collimation

Studies performed this year had the goal of verifying that the collimation system protects the vacuum chamber in the arcs against secondary halo protons in conditions close to operational, i.e. for particle beam, optics, and collimator alignment, all with imperfections. The need to treat correctly the off momentum halo implies that arc sextupoles must be included and a fully chromatic model of the ring has been adopted for multi-turn particle tracking by the program Dimad, which now includes the Monte Carlo module from the program Struct which simulates particle-in-media propagation.

As a benchmark, the inefficiency of the ideal system has been computed with Dimad and the results compared with those from a tracking program developed at CERN by Assmann, and the deviation between them attributed to different Monte Carlo models of the scattering; Dimad reports a factor 2.5 larger inefficiency.

By approximating the vacuum chamber around the ring by a pipe of 2 cm radius, and assuming the use of 50 cm long copper secondary collimators, the losses corresponding to steady operation have been evaluated both at injection and collision. For injection energy only, orbit error and collimator misalignment were included and tolerances were set. An important result is that the chamber wall losses are caused mainly by a highly off-momentum halo generated by energy losses as particles traverse the collimators.

The schematic shows a sample error orbit at injection (Fig. 244). The orbit is corrected with four kicks placed at the entrance and exit of each IR3 and IR7. The errors are closed orbit 4 mm peak-to-peak in the arc, and random transverse jaw misalignment with amplitude 0.5 mm. The fractions of halo lost in different vacuum chamber sections are given in Table XLVI.
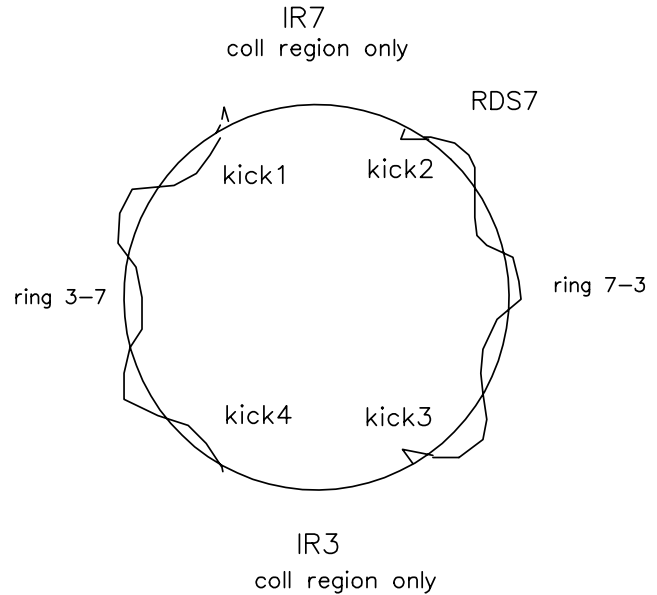
Fig. 244. Dimad model of the LHC ring with a sample error orbit.

Table XLVI. Simulated loss rates on the vacuum chamber wall within the right dispersion suppressor of IR7 (RDS7) and total in all arcs (ring 7-3 plus 3-7, see Fig. 244).

	No errors	With errors
RDS7	1.35×10^{-3}	2×10^{-3}
Arcs	1.6×10^{-4}	7.6×10^{-4}

It was concluded, based on the halo consideration, that the nominal system satisfies the design criteria, and this opinion is held by the CERN team also. However, it was realised recently that accidental dump failures (expected to happen at least once per year) may cause a large fraction of the LHC beam to impact one or several collimators in a single turn. The presently foreseen copper jaws can withstand only 2×10^{-5} of the total beam intensity, which is about 400 times less than the accidental loss. To rectify this, CERN has adopted longer secondary collimators made of lighter material. The next task is to provide around 3 m space for each collimator tank, by changing both optics and collimator locations, and to minimize any loss of performance.

CONTROLS AND INSTRUMENTATION

LHC Orbit System Components

The data acquisition board (DAB) is intended to process signals from the wide-band time normalizer units (WBTN) of the LHC beam pick-up monitors (BPM). The DABII revision, delivered in 2001, differed from DABI by the addition of histogram and post-mortem functions. The DABIII version designed and assembled this year adds a further capability: to replace, optionally, the position card with a fast in-

tegrator card to support a beam current transformer (BCT) application. In addition to some hardware fixes, the DABIII includes the following hardware modifications:

- Monitoring for all WBTN power supplies.
- Extra control pins to WBTN interface to support the BCT integrator mezzanine.
- Extra pins on VME interface for ±15 V to BCT integrator module.
- Improved functionality for selecting test signals for front panel monitoring.
- LVDS buffering for the turn clock and 40 MHz bunch clock signals.

After successful local tests of the design and its application software, nine DABIII cards were delivered to CERN in July: six for the SPS position measurement, one card for the BCT, and two for laboratory tests with a revised WBTN mezzanine module. Trajectory and orbit acquisition modes were fully tested including batch and bunch sum modes. In the last machine development period of the year the transverse positions of 4 batches of bunches were individually monitored at each of 4 BPM locations during the injection and acceleration process in the SPS (which is a test bed for LHC). Figure 245, which confirms a 50 μm resolution, shows example signals from individual batches at a single BPM. In another test, the WBTN was replaced with the BCT mezzanine and the DABIII was successfully used for bunch by bunch intensity measurements, as shown in Fig. 246.

Following the lead of the LHC experiments, the CERN controls group has adopted the VME64x chassis; a new DABIV compliant with this standard will be developed during 2003. In addition to new 12-bit lookup tables for horizontal and vertical trajectory data normalization, the final prototype card will incorporate a VME64x front panel, plug-and-play compatibility and other features including:
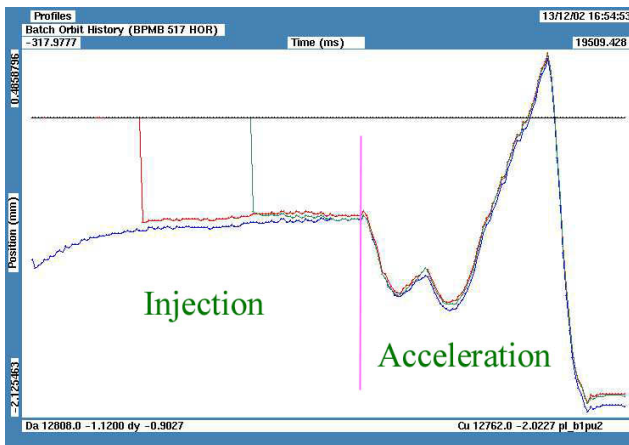
Fig. 245. Signals of three batches (red, green, blue) at a beam position monitor in the SPS.
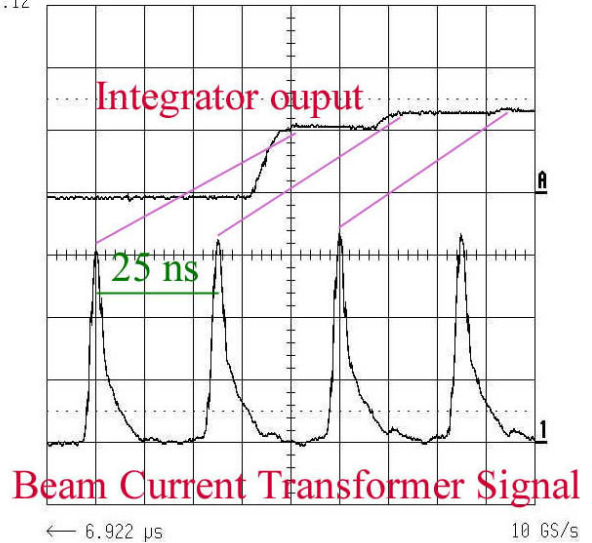
Fig. 246. Time domain signal, and its integral, from 40 MHz bandwidth current monitor in the SPS.

- Two post mortem memories.
- On-line offset subtraction for BCT integrator.
- VME64x configuration/status registers for system auto configure.
- Solder-side covers for hot swap.
- Electrostatic discharge protection.
- Maintenance bus for JTAG board diagnosis.

Filter pairs

2150 pairs of matched filters were purchased from Lorch Microwave for use in the LHC beam position monitor circuits. A network analyzer, driven by a custom-written LabVIEW program, was used to test a sample of 85 of the filter pairs. Early in March, the filters, along with the TRIUMF measurements and the manufacturer's production data, were delivered to CERN.

MAGNET DEVELOPMENT

Series production of the twin-aperture resistive quadrupole magnets for the LHC cleaning insertion began at ALSTOM Canada Inc. (Tracy, Quebec) with an order placed for the first 17 magnets in September 1999. In 2001, the contract was extended from 17 to 52 magnets after the funding was assured from the new five-year plan, and ALSTOM delivered 3 production magnets. In 2002, ALSTOM delivered 29 more magnets bringing the total to 32. Figure 247 shows the production schedule that has been achieved to date. The original estimate called for magnets to be produced at a rate of two per month. Recently ALSTOM is producing a magnet every 10 to 12 days and now expects to finish the contract in August, 2003.

MQW Magnet Production Schedule
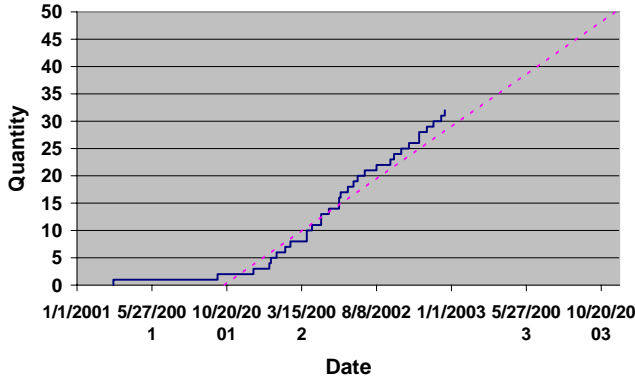
Fig. 247. Production schedule achieved to date.

Prior to shipping the magnets to CERN, a number of acceptance tests are carried out at the factory. These include the alignment measurement with the pole distance measurement device, electrical, water flow and temperature measurements and excitation of the magnet to the nominal peak current of 710 A. The magnetic field is measured using a hall plate mounted on a special holder for reproducible location in the quadrupole field. The acceptance tests are witnessed by an independent local firm LVM Fondatec Inc., with reports sent to TRIUMF to get shipping approval. TRIUMF and CERN engineers have visited the factory several times during the year for more detailed discussions on the progress of the contract.

Detailed magnetic field measurements are carried out at CERN using a rotating coil arrangement to determine the harmonic content of the magnetic field. Figure 248 shows several of the quadrupole magnets and the CERN team collaborating on this project. Table XLVII lists some of the relevant parameters measured during the accurate field mapping of the first few magnets. By the end of 2002, 9 magnets had been measured at CERN.

Fig. 248. Several quadrupole magnets and the CERN team collaborating on this project.

Table XLVII. Relevant parameters measured during accurate field mapping of the first few magnets.

	Current A	Left Aper n=2 Integ.	Right Aper n=2 Integ.	Left Aper n=3*	Right Aper n=3*
MQW001	710	0.4385	0.4377	−39.7	45.7
MQW008	710	0.4368	0.4367	−43.6	47.1
MQW010	710	0.4390	0.4395	−43.4	44.4

KICKER MAGNETS

In collaboration with CERN, TRIUMF has designed and built 4 CERN LHC injection kicker systems plus spares. Each LHC injection kicker system will consist of 1 resonant charging power supply (RCPS), two 5 Ω pulse forming networks (PFNs), 4 thyratron switch tanks, and 2 kicker magnets. The LHC injection kicker magnet systems must produce a kick of 1.3 T m each with a flat-top duration variable up to 7.86 μs, a rise time of 900 ns, and a fall time of less than 3 μs. The combination of ripple and stability in the field from all kicker system components must be less than ±0.5%. A full size prototype kicker magnet has been built and tested at CERN up to 60 kV with the magnet under ultra high vacuum. Nine PFNs have been designed and completely assembled at TRIUMF, with all damping resistors installed and tested at low voltage. The design of the thyratron switch tank and the terminating resistors was completed. Twenty switch tanks are close to completion and the components for 10 terminating resistors have all been received. High voltage testing will commence early in 2003 with the first major shipment to CERN in mid 2003.

RCPS, PFN and Thyratron Switch Test Area

The kicker lab has been reconfigured to accommodate 4 racks of CERN controls which have been interfaced to a RCPS (Fig. 249) which is set up to pulse either 2 off of 66 kV dummy loads or one dummy load and one PFN. The control system computers are connected to CERN via the internet to allow CERN to update control software. The control system commissioning has been completed.

Cable trays have been installed, as well as a copper ground plane under the RCPS racks, the CERN control racks, the PFN test area, and the dummy loads. The front of the cabinets shown in Fig. 249 are in the low voltage area. The high voltage area is fenced off behind and beside the cabinets and contains the PFN, switch tanks under test, and the dummy loads. The gates to the HV area are interlocked. High voltage testing is anticipated to begin in the spring of 2003.

255
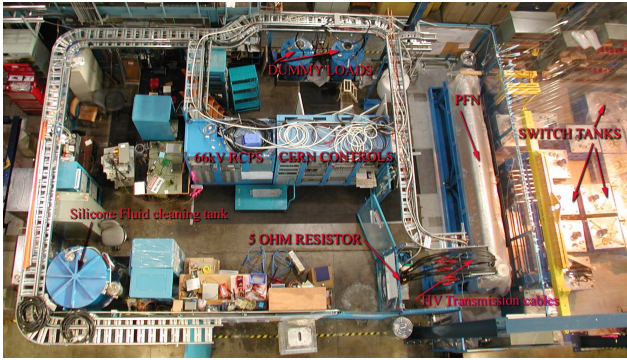
Fig. 249. CERN control system interfaced to PFN, dummy loads, and RCPS, ready for HV tests at TRIUMF.

RCPS

An RCPS has two parallel outputs to charge two 5 Ω PFNs to up to 66 kV. The RCPS has a 2.6 mF storage capacitor bank charged to up to 3 kV. A thyristor is used to switch the energy on the capacitor bank onto the primary of a 1:23 step-up transformer of low leakage inductance. The output of the secondary is transferred to two 5 Ω (PFNs) through two coaxial cables, two diode stacks and two 70 Ω resistors. The RCPS is designed so that the PFNs can be charged up to 66 kV in less than 1 ms at a repetition rate of 0.2 Hz.

Six RCPS, including the prototype, have been assembled at TRIUMF. The prototype RCPS has been extensively tested at CERN. All of the 5 production models have been successfully tested at TRIUMF at 66 kV operation into two dummy loads. An extensive maintenance manual is almost completed and will be stored on CDs.

PFN

Each 5 Ω PFN is composed of two parallel 10 Ω lumped element delay lines consisting of 4.3 m long precision wound coils, high voltage and high current capacitors and damping resistors. There is a thyratron switch tank at each end of the 5 Ω PFN. Nine PFNs were built in 2001 without damping resistors installed and tested at low voltage at TRIUMF. The damping resistors were installed in 2002 and the tanks then filled with silicone fluid to cover the resistors. Seven hundred litres of silicone fluid are required to cover the resistors, and an additional 325 l for high voltage operation. It is necessary to store the resistors in silicone fluid; otherwise the resistance values can change considerably. All of the PFNs, with numbering from 2 through 10, were measured with damping resistors installed: the ripple with damping resistors is less than ±0.2% on all 9 PFNs and the spread in the average magnitude is ±0.3% (Fig. 250). The pulse duration of all PFNs, from 50% of the rise time to 50% of the fall time, is 10.82 μs ±15 ns. The results of low voltage
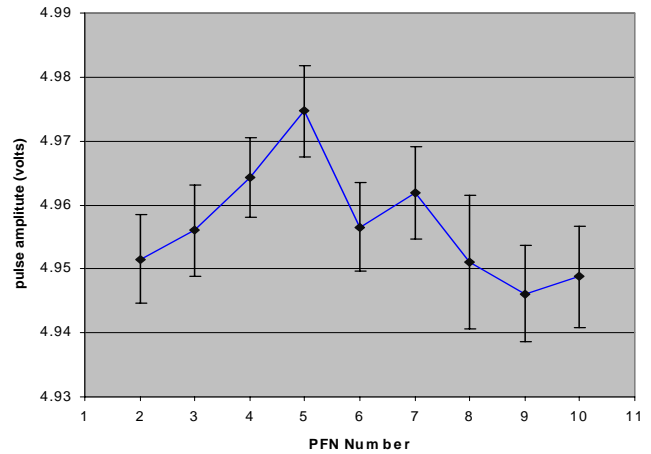
Fig. 250. Average PFN pulse amplitude (2 μs to 9 μs) for 10 V PFN charge error bars show peak ripple. All PFNs complete with damping resistors and filled with silicone fluid.

measurements are in excellent agreement with PSpice predictions.

Thyratron switch tanks

The thyratron switch tanks will mount on the ends of the PFN tanks. The main switch (MS) thyratron will be connected to a 5 Ω transmission line kicker magnet, via 10 parallel 50 Ω coaxial cables. The dump switch (DS) thyratron will also be connected to a 5 Ω resistive terminator mounted on top of its switch tank (Fig. 251).

The TRIUMF Kicker group in collaboration with CERN has designed a HV grid bias circuit for the thyratrons. TRIUMF has built and tested 37 bias boards; 20 of these will be used in the LHC injection kickers, 14 have been sent to CERN for use in the MKE (SPS extraction) CERN kicker system, and there are 3 spares. The bias circuits will be installed in the thyratron switch tanks in early 2003 (Fig. 252).

We have received 3 thyratrons from CERN that need to be assembled into switch tanks for HV tests.

Fig. 251. View of some of the 20 assembled thyratron switch tanks at TRIUMF.

Fig. 252. One of the bias boards, without Faraday cage, cover mounted in a dump switch tank.

Terminating resistors

We completed the design for the dump switch terminating resistor assemblies, placed orders for their fabrication, and received all components by the end of 2002. We plan to start assembly of these high power terminating resistors in February, 2003.

Shipping container

We obtained a 20 ft shipping container that was used to ship components of the ATLAS detector from TRIUMF to CERN. We have made preliminary designs to permit RCPSs and PFNs to be mounted in the container for shipping; shock absorbers are built into the shipping container. The roof and back of the container must be modified for the CERN RCPSs and PFNs. Over the next two years the container will make 6 round trips to CERN for shipment of the LHC kicker system components.

TECHNOLOGY TRANSFER DIVISION

INTRODUCTION

The Technology Transfer Division at TRIUMF is responsible for the commercial interactions for the laboratory. It is composed of a small group dedicated to optimizing the commercialization technologies emanating from TRIUMF research, plus the Applied Technology group that is responsible for the operations of the on-site commercial cyclotrons on behalf of MDS Nordion.

TECHNOLOGY TRANSFER

The mandate of the Division is the pursuit of all financially and technically viable opportunities for commercializing technologies emanating from the research at TRIUMF. This mandate must recognize the pre-eminence of the scientific research at the laboratory, and proceed in a manner that optimizes the impact on TRIUMF and the Canadian economy while minimizing the impact on scientific activities at the facility.

The current Contribution Agreement between the National Research Council (NRC) and TRIUMF includes the requirement for TRIUMF to enhance its impact on the Canadian economy. This impact is measured through the benefits provided to Canadian industry, both through the transfer of TRIUMF's technical knowledge and through its purchasing practices.

APPLIED TECHNOLOGY GROUP

500 MeV Isotope Production Facility

During this year, the 500 MeV irradiation facility received 199 mAh. Eight targets were irradiated, six targets delivered to produce ^{82}Sr/^{82}Rb for MDS Nordion.

CP42 Facility

The total beam delivery for 2002 was 982 mAh. The weekly beam delivery graph is shown in Fig. 253 and the quarterly time evolution of the beam delivery is shown in Fig. 254. The downtime and maintenance statistics are analyzed in Fig. 255 and compared with the TR30.

Work is still proceeding on the CP42 control system upgrade.

TR30 Facility

The total beam delivery for 2002 was 3267.5 mAh. The weekly beam delivery graph is shown in Fig. 256 and the quarterly time evolution of the beam delivery is displayed in Fig. 254. The downtime and maintenance statistics are analyzed in Fig. 255 and compared with the CP42.

A new type of a radiation hard target station has been installed on the south beam line (2B) and tested successfully at proton beam currents in excess of 0.5 mA (30 MeV). ATG is planning on replacing the north high current target station for palladium production (1B) within the next year.

ATG Development Projects

ATG continues to be actively involved in the commissioning of the new TR30 cyclotron facility. Two improved high current target stations have been built and installed.

ATG started the production of carbon foils to be used in the extractors of the CP42 and TR30 cyclotrons. Films of up to 150 μg/cm^2 have been manufactured and tested successfully.

RADIOISOTOPE PROCESSING (MDS NORDION)

During the year 2002, MDS Nordion shipped large quantities of short-lived medical radioisotopes produced using the TR30 and CP42 cyclotrons. The main radioisotopes produced and shipped were iodine-123 used for thyroid imaging and research, palladium-103 used in prostate brachytherapy, and indium-111 used for monoclonal antibody imaging.

The facility expansion commenced during the year. By year end, the building was completed and commissioned. The cyclotron and beam lines were installed and are being commissioned. The plan is to have the facility and cyclotron operational in early 2003.
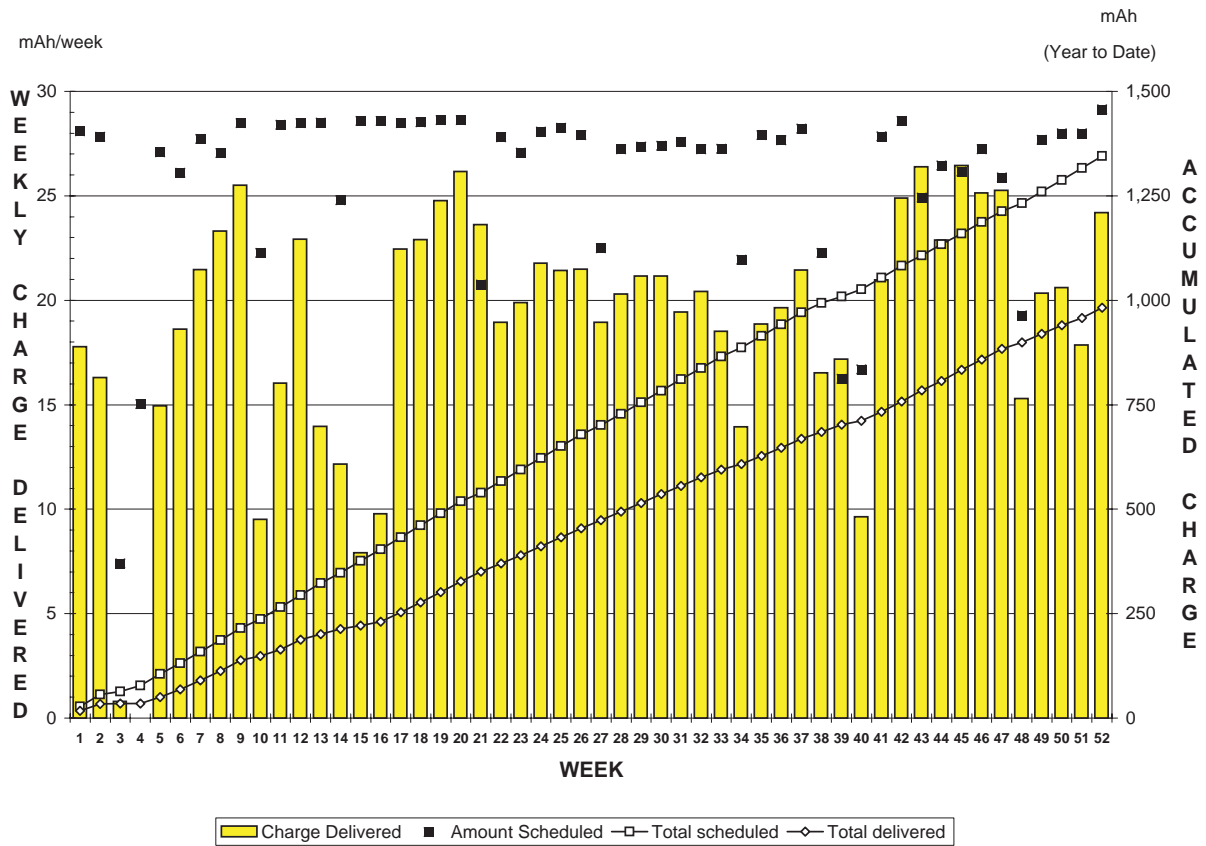
Fig. 253. Weekly beam delivery for the CP42.
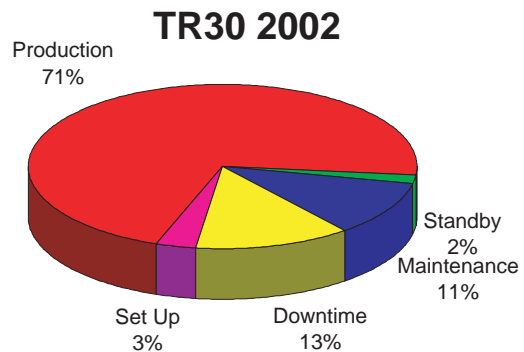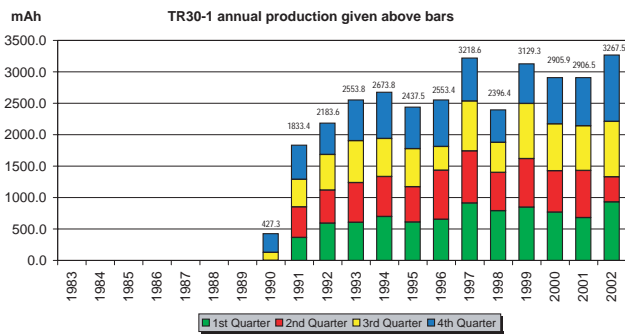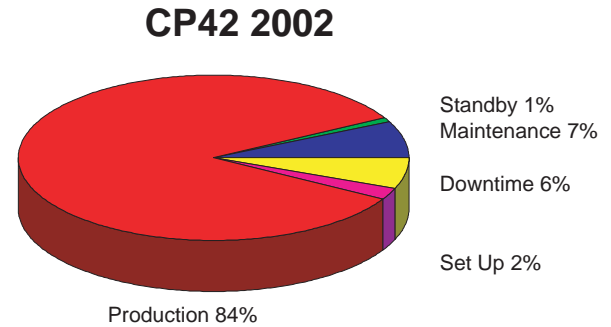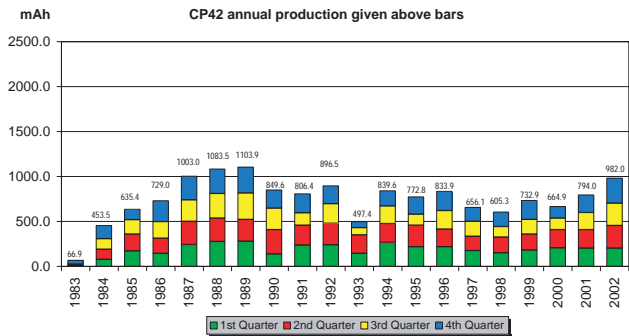
Fig. 254. Annual time evolution of the beam delivery for the CP42 (top) and the TR30 (bottom).

Fig. 255. Breakdown of downtime and maintenance for the CP42 (top) and the TR30 (bottom) during operational hours.

259
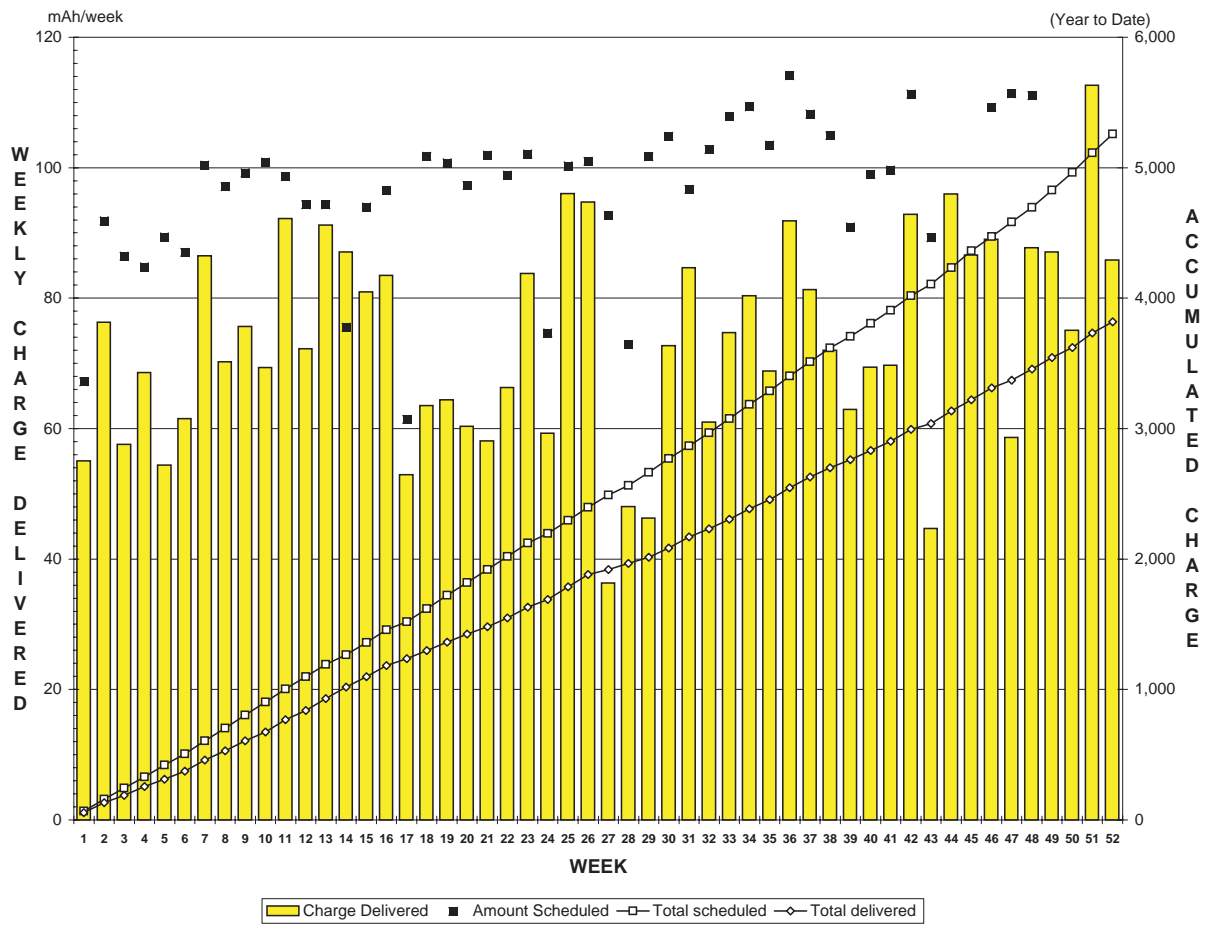
Fig. 256. Weekly beam delivery for the TR30.

ADMINISTRATION DIVISION

INTRODUCTION

The Administration Division is made up of Human Resources and Administration, Accounting and Materials Control, Administrative Computing, and Safety. The manager of each group reports to the Director. A summary of Division activities is included in this report.

HUMAN RESOURCES AND ADMINISTRATION

All employees are reviewed for performance on an annual basis. The period covered for Performance Planning and Review coincides with the calendar year. The Hiring and Promotion Guidelines for Professional and Supervisory staff were revised and approved by the TRIUMF Board of Management for implementation.

In 2002 TRIUMF cancelled its agreement with the University of British Columbia for the supply of clerical and support staff. While this meant that ten new positions were created at TRIUMF, this had no effect on the salary budget since TRIUMF reimbursed the university for all salary and benefits costs.

TRIUMF has a very strong student program and hires on average some 35 summer students per year in addition to the university co-op student programs that it supports throughout the year.

The insurance program was renewed with an approximate 25% increase in premium from the previous year as a result of market conditions. Third party liability coverage remains at $50 M. All buildings operated by TRIUMF are owned by the University of British Columbia and insurance coverage for these buildings and contents is provided by the Canadian Universities Reciprocal Insurance Exchange (CURIE).

TRIUMF awarded a contract for the installation of a security card access system in December. This photo security card will be required to access the main office building and the area behind the security fence. It is expected the system will be operational early in 2003 and all employees and long term visitors will be required to wear a photo ID card. All short-term visitors will be required to wear a Visitor badge. TRIUMF Management has decided not to install a system that would have included the installation of motion detectors with cameras behind the security fence. Security guard coverage continues between 6:00 pm and 6:00 am on working days with twenty-four hour coverage on weekends and statutory holidays. All vehicles accessing the site behind the security fence are required to have a permit.

Construction of the ISAC-II building is nearing completion with beneficial occupancy expected in March, 2003.

There are currently five full member and six associate member universities in the Joint Venture. Each full member university has two voting members on the Board of Management. Two additional voting members are appointed by the Board from the private sector. The associate members each retain one non-voting member on the Board. In 2002 the TRIUMF Board of Management instituted a Technology Transfer Sub-Committee of the Board to review technology transfer activities and TRIUMF's IP policies.

TRIUMF has an Operating Committee (OPCOM) that is made up of representatives from the full member universities along with representatives from the TRIUMF users community and staff. In 2002 the "Terms of Reference" were revised so that communication between the universities and TRIUMF can be enhanced.

TRIUMF must now comply with Federal Treasury Board requirements under a Results-based Management and Accountability Framework. The purpose of this framework is to establish a mechanism to help the National Research Council and TRIUMF: i) collect performance information related to this initiative; ii) track delivery of commitments and reporting; iii) describe how the success of TRIUMF will be evaluated over time; and iv) provide direction for on-going and future planning. This report was submitted in late summer and accepted by the Treasury Board.

ENVIRONMENTAL HEALTH AND SAFETY

Licensing

A second hearing into the application by TRIUMF for a new operating licence was held on February 28, 2002 at the Canadian Nuclear Safety Commission (CNSC) headquarters in Ottawa. A delegation spearheaded by Dr. J.W. McDonald and Dr. A. Shotter made a presentation successfully defending TRIUMF's application and a new licence was issued at the beginning of May. A new licence was required because of the change in the regulatory environment when the former Atomic Energy Control Board (AECB) was replaced by the CNSC.

The new licence carried two conditions: that TRIUMF develop a Quality Assurance Program acceptable to the CNSC and that TRIUMF prepare a "Preliminary Decommissioning Plan".

The first condition was addressed by the members of the QA Task Force who produced a "Quality Manual" and eight "Standard Operating Procedures" that, for the most part, defined how quality was already being achieved at TRIUMF. However, there were a num-

ber of aspects of the present, rather informal system, that require improvement, especially documentation and ongoing assessment. The CNSC staff comments on the proposed QA Program were received by the end of the year and we are making a number of minor revisions to be re-submitted by mid February, 2003.

The preparation of a "Preliminary Decommissioning Plan" (PDP) was contracted out to a consulting firm that specializes in such work. Together with TRIUMF staff, a program of measurement was carried out during the spring in order to define the magnitude of any eventual decommissioning. The TRIUMF site was divided into a number of "work packages" for the purpose of determining costs and manpower. The PDP was close enough to completion by the end of the year that TRIUMF staff could start its review of the document prior to submission to the CNSC.

Training

The Radiation Safety Course was offered a total of four times in 2002 (January, May, July and September) with 49 trainees attending. There was a 100% pass rate with an average of 90% on the final exam. The two most senior Radiation Surveyors (Lynne LeMessurier and Peter Biglowe) took over the instructional duties of the Contamination/Decontamination module. These two people have brought more practical on-the-job radiation protection experience to the course.

The development of the formal accelerator operator training program continued during this year. The four operations groups, 500 MeV OPS, ATG, ISAC and TR13, under the guidance of the training coordinator, Phil Jones, applied the systematic approach to training (SAT) in developing their programs. Each developed a task list that was analyzed in order to determine which tasks required formal training. In phase two of the SAT design, documents were created from the task lists. These documents were then used in developing the lessons and job performance measures required for each of the training programs.

Occupational Health and Safety

The fire alarm system, sprinkler systems and fire extinguishers were all inspected and verified during 2002. Representing both management and workers, the members of the TRIUMF Accident Prevention Committee (TAPC) through their regular program of inspections continue to assist OH&S by doing an excellent job raising safety awareness on the site.

The project management for both the new MDS Nordion TR30-2 and the ISAC-II building gave TRIUMF full co-operation in terms of personnel safety during construction. The TRIUMF Housekeeping Committee formed last year has made a noticeable improvement in the overall appearance of the TRIUMF site.

A clean and orderly work environment has reduced injuries and accidents while promoting worker's pride in the workplace.

Personnel Dosimetry

The collective dose for TRIUMF personnel for the year 2002 was 420.6 mSv as measured by the direct reading dosimeter service. Table XLVIII shows the breakdown of the collective dose by various work groups.

Table XLVIII. Collective dose for TRIUMF personnel by group.

Group	Dose (mSv)	Fraction of Total (%)	Median (mSv)
Applied Technology	123.1	29.3	4.5
500 MeV Operations	41.4	9.8	1.9
Safety Group	34.4	8.2	1.0
Life Sciences	33.8	8.0	1.8
Remote Handling	27.1	6.4	2.0
Vacuum Group	23.2	5.5	3.7
Tech Support	18.1	4.3	0.5
RF Group	14.9	3.5	1.8
Plant Group	14.5	3.4	0.5
Beam Lines/Probes	12.1	2.9	2.4
ISAC Operations	7.9	1.9	0.1
ISIS	3.0	0.7	0.3
Outside Contractors	2.9	0.7	0.4
Others	72.1	17.1	—
Total	420.6	100.0	0.6

Interlocks and Monitoring

Further improvements were made to the 500 MeV facility radiation safety system. A number of radiation monitors that had been identified as "critical" were upgraded so as to make them less prone to tampering by enclosing them in locked cabinets and rerouting the cabling in conduit. An analysis of the two radiation safety systems for common failure modes indicated that additional reliability could be achieved by completely separating the trip circuitry used by the two systems to shut down the 500 MeV cyclotron. A conceptual design to achieve this was developed. A number of tests were performed in order to determine the magnitude of the proton beam loss and the resulting radiation fields outside shielding when the settings on the two dipoles in beam line 2A were varied. It was established that no setting of these dipoles could result in a radiation dose above the regulatory limit.

The ISAC Radiation Monitoring System was extended to cover the growing network of ion beam lines delivering beam to a number of new experimental stations. A number of improvements were also made to the system's display functions.

The interlocks for the ISAC east target station were installed. A new exclusion area was created on top of the ISAC target shielding to control access during conditioning of one target station while the other is being bombarded. Because the two target stations share the same cooling water circuit, access to this area cannot be allowed for such a configuration due to expected high radiation fields from the cooling water.

ADMINISTRATION COMPUTING AND COMMUNICATIONS

Management Information Systems

Many of the developments in MIS in 2002 were made possible by the increased use of Web and email technologies:

- Electronic information distribution: The volume of paper produced by the Business Office was reduced dramatically by the implementation of a system that allowed management reports to be "printed" as PDF files instead of paper. Users were given the option of having monthly reports emailed, resulting in a reduction of over 30% in the amount of paper distributed. Additionally, almost all large reports produced in the accounting department were stored on CD-ROM instead of being printed, reducing the in-house printing requirements by over 90%.
- Electronic notification: An automated system was implemented so that requisitioners could receive immediate email notification whenever purchase-orders were placed, or when requisitioned goods were received at TRIUMF.
- More information available via the Web: New Web applications were developed so that division heads, account holders, and their alternates could view up-to-the-minute account status in the "Personalized Portal" on the Administration Web site.
- Interactive use of the Web: For the first time, account holders were able to use forms on the Web to place requests for summer/coop students. Entries in these forms were stored in a database, to allow the Student Coordinator and Human Resources to manage the requests efficiently using a Web interface.
- Improvements to existing Web applications: Many of the existing Web applications were improved; for example, the Stores Catalogue application was updated to include both thumbnail and full-size photographs of many items.

Word Processing Systems

The project to migrate all word processing clients to a standardized Windows 2000 based platform was completed near the start of 2002. Aside from an increase in the number of client systems, no major changes were made to the word processing environment.

Telephones

The site telephone system saw only incremental changes in 2002. No modifications were made to the central systems themselves, though some preparation was done to accommodate the upcoming ISAC-II expansion. Most of this preparatory work involved planning and laying cables to, and within, the new building.

Major reductions in dial-in usage were observed, allowing the number of dial-in lines to be cut to 10 from 18.

A new system was put in place to simplify running long-distance teleconferences. This system allows callers to join a TRIUMF teleconference by dialling a toll-free number. Usage of this system increased throughout the year.

OUTREACH ACTIVITIES

In 2002 TRIUMF began developing a new Science Education Outreach Program which aims to bring the excitement of subatomic physics research in Canada to as broad a public audience as possible. At the outset, the Outreach Program will focus its attention on introducing high school science teachers to the TRIUMF research experience. The teachers will in turn share their knowledge with their students and encourage talented young students to consider careers in science. TRIUMF has been actively pursuing external sources of funding for these initiatives, which presently are not accounted for in its present five-year plan. At time of writing, a substantial contribution of matching funds has been secured from the private Vancouver Foundation, and further funding is being sought.

High School Teacher Internships

A key component of the new Outreach initiative is a program to bring high school science teachers to TRIUMF for brief "internships". Teachers will join and participate fully on a running experiment at TRIUMF for 3–5 days. In the end, the teachers will work with the Outreach office in producing resource materials for their classrooms and the general public, based on their internship experience. This model was tested in August with two teachers from Penticton, who were very enthusiastic about the program and highly recommended it to their science teacher colleagues in an article written for their monthly journal. The near-term goal will be to accommodate roughly 6 such internships each year with teachers across the province, aiming for the longer term perhaps double that number with teachers from across Canada.

Professional Development Day

On October 25, TRIUMF, together with the BC Association of Physics Teachers, hosted a professional development day for high school science teachers. Eighty-five high school teachers attended, most of them from the Vancouver area, but a few from as far away as Prince George and Vancouver Island. The attendees were offered a variety of lectures and hands-on demonstrations on topics such as the standard model of particle physics, medical imaging techniques, synthesis of radioactive ^{13}N with the TR-13 cyclotron, measurement of penetration of different types of radiations, γ-ray spectroscopy, and charged particle beam optics. The organizers judged the day to be an unqualified success, and a follow-up event is planned for 2003.
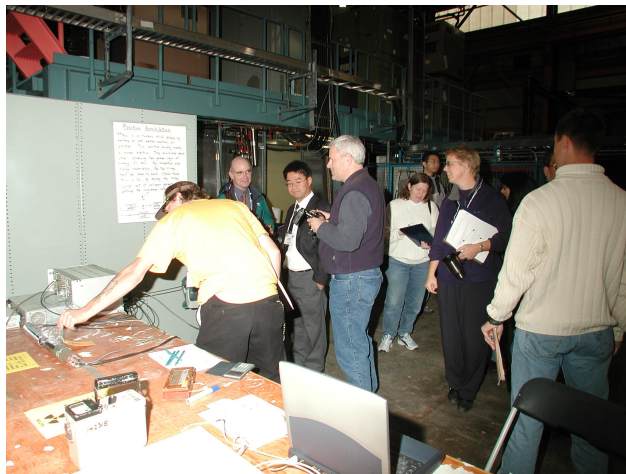
Fig. 257. Attendees at TRIUMF-hosted professional development day.

CONFERENCES, WORKSHOPS AND MEETINGS

JOINT BELLE-BABAR WORKSHOP ON DETECTOR ISSUES

The Joint Belle-BaBar Workshop on Detector Issues was held at TRIUMF February 14–16. Belle, located at KEK in Japan, and BaBar, located at the Stanford Linear Accelerator Center in California, are similar experiments with the common physics goal of studying CP violation and heavy-flavour physics.

This meeting – the first joint meeting of the two collaborations – allowed the groups to compare experiences with detector operations and plans for future upgrades. There were 10 participants from Belle and 19 from BaBar.

The program included plenary presentations from each collaboration on the major detector subsystems: tracking, calorimetry, particle identification, vertexing, trigger, data acquisition, and computing. Detailed discussions were held in parallel sessions on several of these topics. Informal discussion – one of the most rewarding aspects of the meeting – continued at a reception and banquet.

Detailed information about the meeting, including copies of all presentations, is available at http://www.triumf.ca/people/desilva/index.html.

2002 LAKE LOUISE WINTER INSTITUTE: FUNDAMENTAL INTERACTIONS

The 17th Lake Louise Winter Institute (February 17–23) was devoted to a variety of topics of current interest. The invited speakers did a wonderful job of presenting pedagogical lectures that brought the present status of development of each area of interest. The audience consisted of 70 participants with 35 of them being students. The rest were faculty members and post-doctoral fellows from many countries of Europe and Asia in addition to North America. The Winter Institute had the following main lecturers:

- E.G. Adelberger, *Ultraweak Forces*
- S. Bhadra, *QCD in Lepton Hadron Collisions*
- A. Manohar, *Heavy Quark Physics*
- R.D. Pisarski, *QCD and Heavy Ion Physics*
- M.H. Shaevitz, *Neutrino Physics*

The pedagogical lectures were complemented by 48 contributed talks that brought the latest information on experimental and theoretical developments. All the major experiments had sent representatives to present the latest data and new results. The presence of participants from different experiments and countries brings to reality that physics is really universal and the Lake Louise Winter Institute, with the outstanding facilities of the Chateau Lake Louise, is glad to provide a forum for these presentations and in-depth discussions. The invited lectures and the contributed talks will appear as proceedings to be published by World Scientific. The format for the Winter Institute was to have lectures in the morning and evening and the afternoons were left free for the participants to enjoy the scenery and the excellent skiing offered by the location. The participants fully utilized the facilities and in the process made new friends and perhaps future collaborations.

The Winter Institute was made possible by financial assistance from TRIUMF, the Institute of Particle Physics, the University of Alberta conference fund and the Dean, Faculty of Science, University of Alberta. The infrastructure support of the Physics Department, University of Alberta is invaluable in making this event possible, for which the organizers are grateful. Finally, thanks go to Lee Grimard, Secretary, who did a great deal of the organizational work to make the Winter Institute a success.

Organizing Committee: Faqir Khanna, Bruce Campbell, Manuella Vincter and Alan Astbury.

WORKSHOP ON LOW ENERGY PRECISION ELECTROWEAK MEASUREMENTS

Considerable interest has developed in low-energy precision electroweak observables, stimulated by a number of recent measurements which have searched for a deviation from standard model predictions, e.g., deep inelastic neutrino-nucleus scattering, g-2 of the muon, and cesium atomic parity violation. Together with the apparent deviation of the CKM matrix from unitarity, such results may provide new clues about physics which lies beyond the standard model, complementing what can be learnt from high energy collider studies and neutrino physics.

Against this backdrop, an array of new precision measurements – either under way or being planned – will provide additional insights about the shape of the "new" standard model. These measurements include: the neutron lifetime and beta-decay correlation coefficients; the pion beta-decay branching ratio; the weak charges of the electron and proton; "isotope ratios" in atomic parity violation; the Michel parameters in muon decay; and μ to e conversion in the nuclear domain.

The objectives of the workshop (held April 4–6) were to bring together a group of particle, nuclear, and atomic theorists and experimentalists to address two primary questions: 1) In what ways do precision low-energy measurements and high-energy collider studies (at the Tevatron, LHC, Tesla, etc.) provide complementary information about new physics? 2) What theoretical and experimental work should be undertaken

to ensure that low-energy measurements can be cleanly interpreted in terms of new physics?

To address these questions, the workshop included speakers representing both the low- and high-energy perspectives. Attendance (68 delegates) and participation in the workshop exceeded all expectations. Details of the program of the workshop and copies of the transparencies shown during the various discussions can be found on the Web site. The workshop concluded with a panel discussion with open participation, which resulted in the following specific recommendations:

(I) Establish a working group dealing with low-energy precision electroweak measurements. Michael J. Ramsey-Musolf and Jens Erler were charged with organizing this working group of experimentalists and theorists. The purpose of the working group is:

- to create a coherent and noticeable "voice" for this emerging subfield; many experimental efforts are ongoing worldwide at various different facilities. The working group is to provide cohesion to these efforts.
- to ensure proper representation of these efforts at major meetings by proposing invited talks, topical sessions, and so on.
- to organize its own workshops on a regular basis (with a frequency of once every two years).
- to establish a Web site with: 1) a listing of important measurements at an easily accessible site; 2) a file with the more important graphical depictions; 3) a listing of links to experiments; 4) a listing of links to relevant experimental and theoretical publications.
- to produce an annual progress report.
- to fulfill the role of advocacy for this emerging subfield where required.

(II) Strongly encourage an increase in the funding supporting the subdiscipline. It was noted that there are at present very few permanent theory positions for the subdiscipline. It is apparent that a preponderance of electroweak radiative corrections have to be calculated to realize the full impact of the precision electroweak measurements program.

In summary, the workshop placed great emphasis on performing precision electroweak measurements testing various aspects of the standard model, e.g., neutron beta-decay and the question of unitarity of the CKM matrix; nuclear beta-decay and extraneous interactions with right-handed gauge bosons; atomic parity violation, parity violating Moeller scattering, parity violating electron-proton scattering (and their intercomparison), as well as high energy collider efforts (the latter at Q^2 values beyond the Z^0 pole) and the search for a superweak force; g-2 of the muon and the question of supersymmetry; the muon decay Michel parameters and right-handed gauge bosons; deep inelastic neutrino-nucleus scattering (is the anomaly a mere isospin effect?); improved precision measurements for various kaon decays. Clearly this is a multifaceted program of experiments and one can add to this several other experiments, like the searches for electric dipole moments, double beta-decay searches, and CP non-conservation, which were not discussed at the workshop. The complementarity of the lower energy experiments with very high energy experiments needs to be stressed. The experiments are extremely challenging and require great attention to detail. Theoretical predictions require sophistication in particular where it concerns radiative corrections. Almost all experiments have lurking hadronic effects at some level. There is a paucity of in-depth evaluations of hadronic structure effects.

Certainly the standard model is a restricted concept of an ultimate description of the physical world. There are indications of the physics beyond the standard model. The recent data on solar and atmospheric neutrinos give evidence of new physics. The quest for such physics is to be pursued vigorously. This requires that substantial resources and funding be made available. The emerging subdiscipline of low-energy precision electroweak measurements invokes great excitement and presents a great challenge! It is to be noted that in the latest Nuclear Science Advisory Committee Report the search for physics beyond the standard model is categorized by the nuclear physics community as one of four forefront research thrusts to be pursued in the immediate future.

The workshop was organized by: Roger Carlini, Jlab (carlini@jlab.org); John Ng, TRIUMF (misery@triumf.ca); Michael J. Ramsey-Musolf, Caltech (mjrm@krl.caltech.edu), Willem T.H. van Oers, Manitoba (vanoers@physics.umanitoba.ca).

TITAN WORKSHOP

The ion trap workshop was held April 11–13 at TRIUMF. The organizing committee consisted of Pierre Bricault, Elly Driessen, and Jens Dilling. Funding for the workshop was provided by TRIUMF.

The Canadian Subatomic Physics Five Year Planning Committee had given, in its 2001 report, the recommendation "to establish a state-of-the-art Penning trap facility at TRIUMF ... to exploit the available high intensity beams of exotic nuclei at ISAC".

Together with H.-Jürgen Kluge (GSI), who was at TRIUMF for a 6 month sabbatical, a concept for such a Penning trap system was developed. A Letter of Intent to the TRIUMF Experiments Evaluation Committee (EEC) for an ion trap facility at ISAC/TRIUMF was

received very positively at the meeting in December, 2001. The Committee "strongly encourages the development" of such a system.

The aim of the workshop was to present the new concept of the TITAN project (TRIUMF's ion trap for atomic and nuclear science) and to further explore the research potential of the system for experiments in a broad range of science, e.g., nuclear, atomic, astro, and solid-state physics, and to discuss technical issues of this unique facility. The workshop also provided the opportunity to motivate a collaboration which will coordinate efforts towards funding requests, preparation of experiments and theoretical support.

Approximately 40 scientists and students from various universities and national laboratories in Canada, the United States, Europe and Asia participated in the meeting, which consisted of 27 talks including a TRIUMF special seminar. Lively question rounds followed the talks, and discussions in the breaks contributed to the successful and fruitful atmosphere at the workshop. The workshop was structured in two days of presentations, and on the third day an excursion to Whistler provided additional opportunities for plenty of "informal" discussion. Overall, the clear message was that a system such as TITAN would have tremendous potential and deserves strong support.

The program for the first two days was as follows, with time for discussions in between and a conclusion and discussion session at the end:

April 11:

- J.-M. Poutissou, TRIUMF, *Welcome*
- P. Schmor, TRIUMF, *ISAC overview*
- J. Dilling, TRIUMF, *TITAN overview*
- B. Moore, McGill U., *Cooling concepts in RFQs*
- D. Douglas, UBC, *Collisions, cooling, linear quadrupole ion guides and traps*
- V. Shapiro, *Idea of rotating RFQ traps and coolers*
- S. Schwarz, MSU, *Ion beam manipulation and transport in the LEBIT project*
- F. Buchinger, McGill U., *Collinear laser spectroscopy on pulsed exotic beams. What do we gain?*
- H.-J. Kluge, GSI, *Radioactive and highly-charged ions (HCIs) in traps: the European networks*
- G. Bollen, MSU, *Ion traps – precision measurements and more* (TRIUMF Seminar)
- J. Crawford, McGill U., *Laser spectroscopy in Paul traps*
- R. Thompson, U. Calgary, *Laser-induced fluorescence: more than just a spectroscopic tool*
- M. Wada, RIKEN, *On-line collection of energetic ^8Li ions by RF ion-guide*

- H. Schüssler, Texas A&M, *Mass measurements with parametric exc. and a linear trap*

April 12:

- R. Marrs, LLNL, *EBIT concept and design*
- J. Crespo López-Urrutia, MPI Heidelberg, *EBIT experiments at MPI HD*
- D. Fischer, MPI Heidelberg, *Experiments with extracted HCIs*
- E. Pinnington, U. Alberta, *M1 transition rates in HCIs*
- F. Ames, LMU Munich, *Accumulation, cooling and charge breeding for REXISOLDE*
- T. Beier, GSI, *QED investigations with HCIs*
- M. Pearson, TRIUMF, *HCIs for experiments with polarized atoms in gas*
- K. Blaum, CERN, *Accuracy limits on mass measurements with Penning traps / mass measurements of highly-charged ions in a Penning trap*
- G. Bollen, MSU, *The Penning trap system at MSU*
- S. Rainville, MIT, *Single ion mass spectrometry at 100 parts per trillion and beyond*
- K. Sharma, U. Manitoba, *Recent on-line results from CPT*
- J.M. Pearson, U. Montreal, *Hartree-Fock mass formulas and exotic nuclei*
- M. Wiescher, U. Notre Dame, *Masses for nuclear astrophysics*

ALPHA THERAPY WORKSHOP

In an attempt to identify research areas for the next 5 year plan for TRIUMF, a series of workshops were organized for the various user communities. One of these focused on the use of the ISAC facilities for the Life Sciences program. This workshop, held on April 29, explored the possibility of producing high specific activity alpha emitting radionuclides for radioisotope therapy (RIT).

There were 72 attendees with 22 from outside the Lower Mainland. The workshop was Webcast and viewed by interested parties from Europe and Australia as well as from eastern Canada and the US. Web viewers were provided the opportunity to email questions for live interaction with the speakers.

Six invited speakers plus two contributed talks covered topics from the very basic radiobiology of the interaction of radiation with living matter to the chemistry for the isolation and incorporation of radioactive species in biologically active molecules. A couple of presentations described ongoing clinical trials using ^{211}At and ^{213}Bi as therapeutic agents. The topics extended beyond alpha emitters to discuss the utility of beta emitters as well.

One presentation of particular relevance described the use of the ISOLDE facility at CERN for the production and isolation of alpha emitting radionuclides. This was followed by a presentation on the unique capabilities of ISAC.

Following the formal presentations there was a round table discussion on the future of radioisotope therapy and the role for facilities such as ISAC.

There are at least three separate camps:

- Fundamental studies on the interaction of radiation with matter (low dose and low dose rates radiation).
- Studies in animal models of human disease (dosing regimens).
- Human clinical trials using α-emitting radioisotopes coupled with the potential for full scale use in treating cancer (with commercial spin-offs).

One of the primary issues to be dealt with is matching biological clearance (half-life) with the useful physical half-life of the tracer. The known useful α-emitters have $t_{1/2}$ ranging from 46 minutes to 10 days.

The Director of TRIUMF pointed out that TRIUMF cannot meet the needs of the clinical trial demands. However, the participants felt that there is definitely potential for world class research in fundamental radiation biology and the use of α-therapy in animal models for which ISAC could play a major role.

14th INTERNATIONAL CONFERENCE ON ELECTROMAGNETIC ISOTOPE SEPARATORS AND TECHNIQUES RELATED TO THEIR APPLICATIONS

The 14th meeting of the International Conference on Electromagnetic Separators and Techniques Related to their Applications (EMIS-14) was held in Victoria, BC, from May 6–10. The conference also included a special visit (on May 11) for conference participants to the new TRIUMF-ISAC facility. There were 159 delegates (see Fig. 258).

This conference is part of a series of such international meetings on the use of electromagnetic isotope separators for scientific purposes. The previous conferences were held at Harwell (1955), Amsterdam (1957), Vienna (1960), Orsay (1962), Aarhus (1965), Asilomar (1967), Marburg (1970), Skövde (1973), Kiryat Anavim (1976), Zinal (1980), Los Alamos (1986), Sendai (1991), and Bad Dürkheim (1996).

The goal of this series of conferences is to bring together the scientific, technical and professional experts involved with the design, building and use of electromagnetic isotope separators from around the world. In the past this has concentrated mainly on ISOL (isotope separation on-line) systems. The exciting new aspect of the Victoria conference was the growing focus on radioactive beam facilities, both ISOL and projectile fragmentation based systems, in operation and the challenges that exist in the building of the next generation facilities.
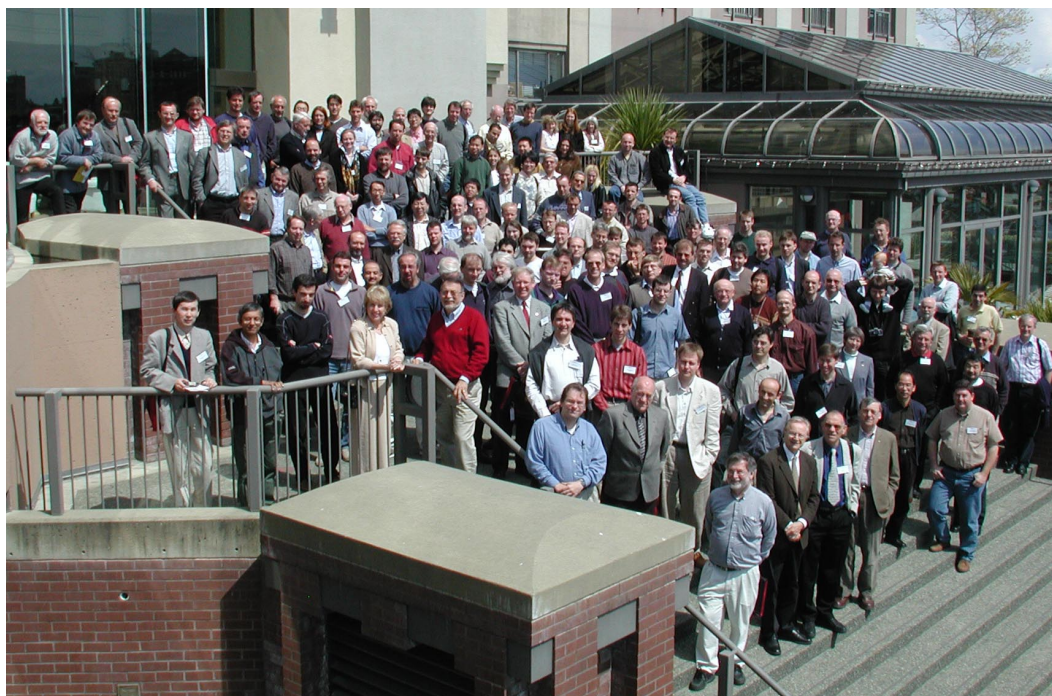
Fig. 258. The EMIS-14 participants outside the Delta Victoria Ocean Pointe Resort where the conference was held.

Today, radioactive beam facilities (which are based upon EMIS type devices) are used to perform a wide range of disciplines including nuclear astrophysics, nuclear spectroscopy, nuclear reactions, studies of exotic nuclides far from stability, condensed matter physics, nuclear medicine and fundamental symmetries among others. The need for developing ever improving facilities, based upon the mature technique of electromagnetic separation, to service this wide and diverse group of interdisciplinary research areas requires that experts in these fields gather to discuss the challenges. In this conference many of these new approaches and ideas were described, disseminated and discussed. One of the bright highlights of the conference was the large number of young scientists and professionals of both genders who participated and presented their studies.

The proceedings of this conference will appear in Nuclear Instruments and Methods B.

During the conference, the International Advisory Committee met and selected France as the location of the next conference. The GANIL Laboratory has agreed to assume the responsibility of organizing EMIS-15.

One essential aspect for a successful conference is the financial arrangements. Organizing such events is becoming expensive and participants cannot always meet the rising costs of registration fees. EMIS-14 was a success in part due to the contributions of the sponsors, namely, NSERC (Natural Sciences and Engineering Research Council of Canada), the Provincial Government of British Columbia, Simon Fraser University, Canberra, Dehnel Consulting, Gamble Technologies, MDS Nordion, Scionix, the UMA group, and VARIAN. A special thanks goes to the TRIUMF laboratory which not only contributed financially, but also with a number of its scientists and professionals who played key roles in all aspects of the conference.

Apart from the chair of EMIS-14, John M. D'Auria, a number of individuals who volunteered their time and efforts for this conference must also be acknowledged. Special thanks go to Martin Comyn for his patience and extra efforts keeping all of the devices needed in the presentations running properly. He also played a key role in preparing the abstracts properly. Jana Thomson worked very diligently on both the abstracts and the conference proceedings. Elly Driessen was very important in putting together a successful social program. Thanks also go to Anna Gelbart for the preparation of the poster and all art work, Mindy Hapke for the excellent photos, Don Hunter and Anthony Lee for putting together the Web page, Irene Tsui for help with financial aspects, Lorraine King for help with the manuscripts and operation of the conference, and Glenn Jones for ensuring that Internet oper-

ations worked well for all registrations. Both the Local Organizing Committee and the International Committee (see Fig. 259) were also essential in assisting with the organization of this conference.
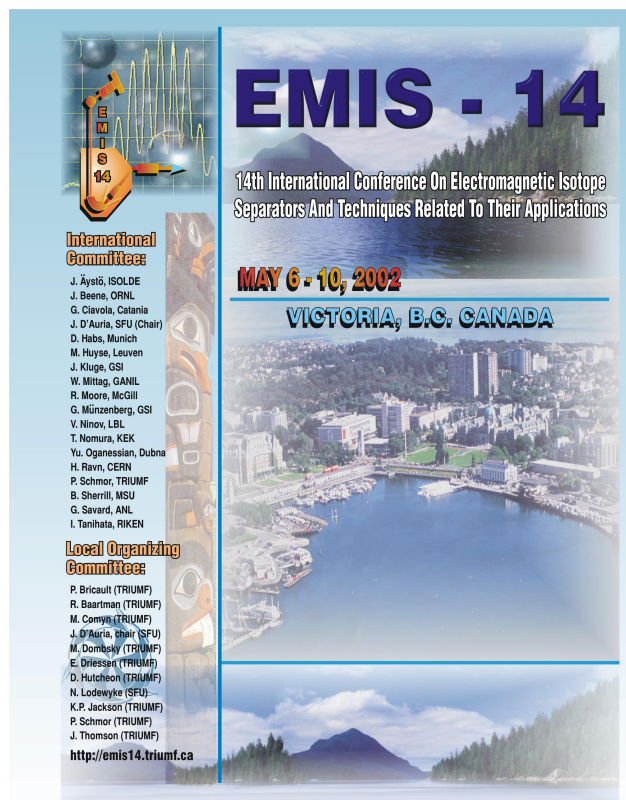
Fig. 259. The EMIS-14 conference poster showing the organizing committees.

SUMMER NUCLEAR INSTITUTE AT TRIUMF (SNIT) – NUCLEAR ASTROPHYSICS: OBSERVATION, EXPERIMENT, THEORY

Nuclear astrophysics is concerned with the impact and influence of nuclear structure and nuclear reactions on astrophysical processes from the beginning of the universe in the big bang through the evolution of stars. It was the goal of this year's Summer Nuclear Institute at TRIUMF (SNIT 2002, June 10–21) to give an introduction to this exciting field.

The summer institute attracted a record number of participants (43), mostly graduate students, but also one undergraduate student and 2 postdocs. The participants came from Canada (19), the United States (15), Europe (7), and Asia (2); 37 work in experimental physics, 6 in theory. About one quarter of the students received graduate credit for SNIT 2002. The eleven invited lecturers came from TRIUMF, the United States, Denmark and Germany and covered a variety of important aspects of the field:

- L. Buchmann, TRIUMF, *Selected problems in low energy nuclear scattering*
- C.W. Johnson, San Diego State U., *The nuclear shell model, with applications to astrophysics*
- D.L. Lambert, U. Texas at Austin, *Nuclear astrophysics – observations*
- K. Langanke, Aarhus U. (Denmark), *Supernovae and nuclear physics*
- G.C. McLaughlin, North Carolina State U., *Neutrino oscillations: theory and application to astrophysics*
- B.S. Meyer, Clemson U., *Explosive nucleosynthesis*
- C. Rolfs, Ruhr-U. Bochum (Germany), *Experimental nuclear astrophysics, an introduction*
- H. Schatz, Michigan State U., *Experimental nuclear astrophysics with radioactive beams*
- A. Shotter, TRIUMF, *Nuclear astrophysics – a general view and the TRIUMF connection*
- K.A. Snover, U. Washington in Seattle, *The $^7Be(p, \gamma)^8B$ reaction and solar neutrinos*
- E.W. Vogt, TRIUMF, *Nuclear halo states*

Despite the great weather, attendance at the lectures was high, the homework assignments were taken very seriously, and the discussion sessions revealed intelligent, probing questions. A large group of about 30 participated in the two-hour tour of TRIUMF, given by Marcello Pavan.

The social program consisted of a pizza reception and a banquet at Brock House. In addition, Peter Jackson organized spontaneously (upon popular demand) a beer-and-pizza party at TRIUMF and Lothar Buchmann made his private cabin available for a weekend get-together. These informal meetings served as a great forum for discussions between the lecturers and the students.

For those who are interested, lecture notes and photos from SNIT 2002 are available at http://www.triumf.ca/snit/2002/.

The 2002 Summer Institute was organized by Jutta Escher, Lothar Buchmann, Greg Hackman, and Byron Jennings.

5th INTERNATIONAL CONFERENCE ON HYPERONS, CHARM AND BEAUTY HADRONS

The 5th International Conference on Hyperons, Charm and Beauty Hadrons was held June 25–29 at the University of British Columbia. It was the fifth in a series of particle physics meetings started in 1995 centred on the physics of heavy quarks and hyperons. Heavy quark physics has figured prominently in the Canadian particle physics community, and we were

pleased to have Canada host this conference for the second time.

Conference history	
BEACH 1995	Strasbourg, France
BEACH 1996	Montreal, Canada
BEACH 1998	Genoa, Italy
BEACH 2000	Valencia, Spain
BEACH 2002	Vancouver, Canada
BEACH 2004	Chicago, USA

The conference was formatted as four and a half days of plenary sessions only. It was well attended, with 116 participants from 21 countries, including 14 graduate students. The participants were approximately half theorists, half experimentalists, with most of the major heavy quark and hyperon particle physics experiments represented.

Full details on the conference, program, bulletins, electronic versions of talks, link to published proceedings (when available), participants and their email addresses, are available from the conference Web pages: http://beach2002.physics.ubc.ca.

TRIUMF Director Dr. Alan Shotter gave a brief set of opening remarks, welcoming participants to Vancouver, reminding visitors from around the world that we have TRIUMF, Canada's national subatomic laboratory, here in Vancouver. He described highlights of the locally based research program, and stressed that TRIUMF also plays a key role in providing infrastructure to many Canadian particle/subatomic experiments, including international experiments based at CERN, SLAC, SNO, BNL, DESY, as well as at TRIUMF.

Professor Aneesh Manohar of the University of California, San Diego, gave an excellent opening overview talk on the physics of beauty, charm and hyperons, presenting his perspectives on some of the new and controversial issues/results that would be presented later in the conference.

UBC Vice-President of Research, Professor Indira Samarasekera, sponsored the opening reception and gave a heart-warming address on the importance of physics research in Canada in general and in particular, particle physics here at UBC.

The very difficult task of closing the conference with the Summary Talk was superbly done by Professor Jonathan Rosner of the University of Chicago and the Enrico Fermi Institute; there has been much theoretical activity and many new experimental results in the fields of heavy quarks and hyperons in the past year, and Rosner's summary was very well done.

The conference talks were all plenary, grouped into seven sessions:

- Heavy Baryons
- Heavy Quark Physics at the Z Pole and Beyond
- Results from the B Factories and CP Violation
- Beauty and Charm Decays and CKM Elements
- Hadronic Heavy Quark Decays and Effective Field Theories
- Charmonium, Charm Production and Decay
- Hyperon and Kaon Decays

The conference banquet was held at the UBC Museum of Anthropology. A half day excursion to Grouse Mountain and the North Shore took place in the middle of the conference.

The organizing committee was:

- Janis McKenna, UBC (Chair)
- Tom Mattison, UBC
- John Ng, TRIUMF/UBC
- Marco Bozzo, U. Genoa/INFN Genoa
- Calvin Kalman, Concordia U. (Chair International Advisory Committee)
- Zoltan Ligeti, Lawrence Berkeley National Lab
- Miguel Angel Sanchis-Lozano, Universitat de Valencia/IFIC Valencia
- Paul Singer, Technion-Israel Inst. of Technology

Proceedings were submitted for publication in November, 2002, and will appear in Nuclear Physics B (Proc. Suppl.) 115 in February, 2003.

BEACH 2004 will be held in Chicago, USA, organized by the Illinois Institute of Technology and the University of Chicago, and will include a session dedicated to Leon Lederman's 80th birthday.

The organizing committee thanks sponsors:

- The Institute of Particle Physics of Canada – for generous subsidization of every graduate student's registration fee.
- The Office of the Vice-President of Research, Professor Indira Samarasekera, for sponsorship of the conference opening reception.
- The Faculty of Graduate Studies, Professor Frieda Granot, for the 4 student conference assistants: Travis Beals, Patrick Bruskiewich, Mark Laidlaw and Douglas Thiessen.
- The Department of Physics and Astronomy – for unfailing secretarial assistance from Mabel Ng and Janet Johnson.
- TRIUMF – Anna Gelbart who designed the popular conference logo and provided excellent advice and guidance for the poster.
- CAP Particle Physics Division.

WORKSHOP ON BIG DRAGON: A RECOIL SEPARATOR FOR ISAC-II AT TRIUMF

A workshop on the science with, and technology of, a recoil separator for use with the radioactive ion beams to be delivered by the ISAC-II facility was held on July 18–19 at TRIUMF. Such a separator will be one of the main components of the ISAC-II experimental program. The first part of the workshop focused on the science program of ISAC-II, the present status of the facility, and planned experimental stations at ISAC-II. This was followed by presentations on several existing recoil separators at facilities worldwide, with an emphasis on present achievements and challenges. Other topics discussed included potential targets and focal plane detectors for the separator.

The workshop, sponsored by TRIUMF, was well attended and drew over 35 attendees from various laboratories. The invited speakers included:

- P. Schmor, *ISAC-II Overview*
- A. Chen, TRIUMF/McMaster U., *Nuclear Astrophysics at ISAC-II*
- D. Dean, ORNL/U. Tennessee, *Nuclear Structure at ISAC-II*
- M. Stoyer, Lawrence Livermore National Lab, *Heavy Element Physics at ISAC-II*
- Y. Oganessian, JINR, *Heavy Element Research at Dubna*
- G. Hackman, TRIUMF, *The TIGRESS Spectrometer*
- J. Dilling, TRIUMF, *Ion Traps*
- B. Fulton, York U. (UK), *ISAC-II Physics with a Charged Particle Array and Recoil Separator Combination*
- F. Sarazin, TRIUMF, *Particle Detector Arrays and Target Set-ups*
- D. Hutcheon, TRIUMF, *The DRAGON Recoil Separator*
- C. Davids, ANL, *The Fragment Mass Analyzer at Argonne*
- C. Gross, ORNL, *The HRIBF Recoil Mass Spectrometer: Its Capabilities and Science*
- F. Strieder, Bochum, *The ERNA Recoil Separator*
- D. Bardayan, ORNL, *Nuclear Astrophysics Studies using the Daresbury Recoil Separator at the ORNL Holifield Radioactive Ion Beam Facility*
- C. Beausang, Yale, *SASSYER and the Future*
- B. Tribble, Texas A&M, *Radioactive Beams with MARS and their Applications in Nuclear Astrophysics and Weak Interactions*
- A. Yeremin, JINR, *Status of the VASSILISSA and other Recoil Separators at the FLNR-JINR*
- J.M. Casandjian, Ganil, *EXOGAM/VAMOS*

- K. Gregorich, LBL, *The Berkeley Gas-filled Separator*

Overall, the calibre of the talks was very high, resulting in interesting and fruitful discussions during the workshop. The meeting concluded with a round table discussion on possible design concepts for the new recoil separator, and on taking steps toward establishing an international collaboration. The workshop was organized by U. Greife (chair), A. Chen, J. D'Auria, and D. Hutcheon.

SYMPOSIUM ON SYMMETRIES AND THE WEAK INTERACTION: IN CELEBRATION OF SIR DENYS WILKINSON'S 80th BIRTHDAY

On September 5, a symposium and dinner were held at TRIUMF in celebration of the 80th birthday of Sir Denys Wilkinson and also for the past fifteen years of his retirement during which he has spent substantial time at TRIUMF each year and has been remarkably productive in science ideas.

The Symposium on Symmetries and the Weak Interaction had a program of four talks:

- Viktor Flambaum, Sydney, Australia and Seattle, *Time Reversal and Parity Violation in Heavy Atoms*
- W. Clark Griffith, Seattle, *The Search for a Permanent Electric Dipole Moment of Hg Atoms*
- Peter Jackson, TRIUMF, *The TRIUMF Neutral Atom Trap (TRINAT)*
- Sir Denys Wilkinson, TRIUMF, *Remarks*

The remarks in the last talk pertained to Sir Denys' many recent papers on the analysis of nuclear beta decays to obtain information about the elements of the Cabbibo-Kobayashi-Maskawa quark-mixing matrix and about the unitarity of the matrix. Denys guided his audience through the multitudinous and delectable corrections to the matrix elements of beta decay as analyzed for this purpose.

The dinner following the symposium was held at the Seasons in the Park restaurant. The symposium and dinner were attended by about forty TRIUMF participants and about a dozen out-of-town participants who came to Vancouver for this purpose. In his remarkable career Sir Denys has had a wonderful influence on the development of TRIUMF.

THE ITALIAN-CANADIAN INTERFACE FOR THE DEVELOPMENT AND EXPLOITATION OF STABLE AND EXOTIC ION BEAMS

A group of 36 Italian and Canadian scientists held a meeting at TRIUMF October 16–20, to present work done at their respective laboratories and to discuss projects of mutual interest. The Italian delegation comprised five delegates: G. deAngelis and G. Fortuna (Laboratorio Nationale di Legnaro), A. Bracco (University of Milano), M. Lattuada and E. Migneco (Laboratorio Nationale di Sud). TRIUMF was represented by the Director and several research scientists as well as university faculty members.

The program started with an introduction to TRIUMF including a tour which largely concentrated on ISAC. Next day the guests gave an overview of their home institutions, i.e. the Laboratorio Nationale di Legnaro (LNL), close to Padova, and the Laboratorio Nationale di Sud in Catania, and the physics programs performed there. This included descriptions of the accelerator systems and experimental facilities. Thereafter, the experimental physics done as part of the nuclear and nuclear astrophysics program in Italy and Canada was presented and extensively discussed.

The next day started with a discussion of applications of the nuclear program on both sides, many of them concerning condensed matter problems. The subject then shifted to future facilities of short term and long term range both at TRIUMF and the Italian nuclear laboratories. These projects either concern future radioactive beam facilities or experimental stations at such facilities. The day included a tour of the superconducting cavity development facility at BC Research, an area where TRIUMF and LNL work closely together. The meeting concluded with a round table discussion of future possibilities for collaboration.

TRIUMF USERS' GROUP ANNUAL GENERAL MEETING

The TRIUMF Users' Group Annual General Meeting was held on Wednesday, December 11, sandwiched between the Subatomic and Materials Science two-day EEC meetings. The meeting had 41 paid registrants attending the majority of the talks, double that number for certain talks, and over 25 people who were unable to travel to TRIUMF watched the live video stream on the Web via http://video.triumf.ca/ where the sessions are archived.

Graeme Luke, the chair of the TRIUMF Users' Executive Committee (TUEC), opened the meeting by welcoming both the Users in the Auditorium and those around the world watching the video stream. He then went on to pay tribute to Nate Rodning, the past chair of TUEC, who had died so unexpectedly in late April.

The very full agenda began with the traditional status reports by the Director and division heads. Alan Shotter outlined the accomplishments of the past year and the challenges ahead, including preparations for the Five Year Plan review. Jean-Michel Poutissou re-

ported on the scientific achievements of the past year and the results and publications anticipated before the review committee visit in 2003. Gerardo Dutto described the cyclotron refurbishments performed since the present five year plan funding began in April 2000, the work to be performed in future shutdowns, and the overall performance of the cyclotron with regard to reliability and increased accelerated and extracted beam currents. Paul Schmor reviewed the performance and future developments of ISAC-I, the status of ISAC-II civil construction, and progress on the ISAC-II accelerator systems.

After lunch two of the DRAGON graduate students, Sabine Engel and Shawn Bishop, gave talks on the commissioning and early results from DRAGON. These were followed by a discussion of the Five Year Plan. Alan Shotter outlined the anticipated timetable, which was unfortunately still dynamic and shrinking. He described the discussions, meetings and planning which had occurred to date, the formation of the committee of protagonists that would draft the plan, and the role of the Users. Graeme Luke described the discussions and input from TUEC over the year, summarized the presentations and discussions at the Town Meeting held at TRIUMF on the weekend of September 21–22, and emphasized the need for ongoing input from the Users. The meeting was then opened for discussion from the floor.

A number of shorter topics were presented after the coffee break. Peter Jackson and Rob Kiefl described the positive outcomes of the NSERC reallocations exercise with respect to the two grant selection committees that fund the majority of TRIUMF experiments. Byron Jennings presented his ideas concerning a TRIUMF Virtual University. Marcello Pavan described the creation of the TRIUMF Outreach program, applications for funding, initiatives for high school science teachers, and the successful professional development day event hosted at TRIUMF on October 25 in conjunction with the BC Association of Physics Teachers which eighty-five high school teachers attended. Jim Hanlon gave an update on the status of the negotiations with UBC concerning the location, design and cost of the new TRIUMF House.

Graeme Luke reported on the activities of TUEC during the year. He announced that, by acclamation, J.E. Sonier (SFU) had been elected as chair-elect for 2003; and, after a vote, T.A. Porcelli (UNBC) and A. Chen (McMaster U.) had been elected as members for 2003/2004. TUEC nominates two members to represent the Users on the TRIUMF Operating Committee. In 2002 S. Yen (TRIUMF) moved from being alternate

to member, replacing G.M. Marshall (TRIUMF), and L. Lee became his alternate. G.M. Luke (McMaster U.) and J.E. Sonier (SFU) remained as the other member and alternate, respectively.

The afternoon session ended with Willem van Oers presenting a proposal for the formal organization of the nuclear physics community in Canada, along the same broad lines as the Institute of Particle Physics (IPP). The Users discussed his ideas informally during the buffet dinner and then returned to the Auditorium for the final session where an open discussion ensued under his chairmanship. The AGM ended almost twelve hours after it had begun.

Welcome	Graeme Luke
State of the Laboratory	Alan Shotter
Science Division Report	Jean-Michel Poutissou
Cyclotron Refurbishing	Gerardo Dutto
ISAC-I, ISAC-II Developments	Paul Schmor
The Awakening of the DRAGON: Commissioning and Operation	Sabine Engel
Nuclear Astrophysics at DRAGON: the ^{21}Na$(p,\gamma)^{22}$Mg Reaction and Oxygen-Neon Novae	Shawn Bishop
Five Year Plan	Alan Shotter / Graeme Luke
NSERC GSC Reallocations	Peter Jackson / Rob Kiefl
TRIUMF Virtual University	Byron Jennings
TRIUMF Outreach	Marcello Pavan
TRIUMF House	Jim Hanlon
TUEC Business Meeting	Graeme Luke
Proposal for the Formal Organization of the Nuclear Physics Community	Willem van Oers
Dinner at TRIUMF	
Open Discussion	Willem van Oers

TUEC Membership for 2002

G.M. Luke	McMaster U.	*Chair*
N. Rodning	U. Alberta	*Past Chair*
W.D. Ramsay	U. Manitoba	*Chair Elect*
G.D. Morris	LANL	2001/2002
J.E. Sonier	SFU	2002
G.S. Hackman	TRIUMF	2002/2003
M.M. Pavan	U. Regina/TRIUMF	2002/2003
M. Comyn	TRIUMF	*Liaison Officer*

ORGANIZATION

Board of Management (BOM)

The Board of Management of TRIUMF manages the business of the facility and has equal representation from each of the five member universities. The Board met 4 times during the year. At the end of 2002 the Board comprised:

University of Alberta	Dr. W.J. McDonald	Chairman
	Dr. A. Noujaim	
University of British Columbia	Dr. D. Brooks	
	Dr. B. Turrell	
Carleton University	Dr. R. Carnegie	
	Dr. F. Hamdullahpur	
Simon Fraser University	Dr. W.S. Davidson	
	Dr. C.H.W. Jones	
University of Victoria	Dr. R. Keeler	
	Dr. M. Taylor	
Private Sector	Ms. G. Gabel	Environmental Sensors Inc.
	Dr. H. Ing	Bubble Technologies Inc.

Towards the end of 1987, Board membership was expanded in anticipation of a broadening of the TRIUMF joint venture to include a more national representation of Canadian universities long associated with the TRIUMF experimental program. The University of Manitoba and Université de Montréal became associate members, and the University of Toronto joined as an observer. At the end of 1988, University of Toronto's status changed from that of observer to associate member. In March, 1989 the University of Regina became an associate member. In December, 1998 Carleton University and Queen's University became associate members. In March, 2000 Carleton University's status changed from that of associate member to full member. In 2001 two private sector positions were added. In October, 2001 McMaster University became an associate member. Associate membership at year-end:

Non-voting Associate members:	Dr. W.T.H. van Oers	University of Manitoba
	Dr. A.J. Berlinsky	McMaster University
	Dr. C. Leroy	Université de Montréal
	Dr. A. Hallin	Queen's University
	Dr. K. Bergman	University of Regina
	Dr. R. Orr	University of Toronto
ex officio members:	Dr. W. Davidson	National Research Council
	Dr. P. Sinervo	ACOT
	Dr. A. Shotter	Director, TRIUMF
	Dr. J.-M. Poutissou	Associate Director, TRIUMF
	Mr. J. Hanlon	TRIUMF, Recording Secretary

Administration

Under the directorship of Dr. A. Shotter, TRIUMF personnel were grouped into Divisions, with Division Heads as follows:

Division Head, Science Division	J.-M. Poutissou
Division Head, Accelerator Technology Division	E.W. Blackmore
Division Head, Cyclotron Operations Division	G. Dutto
Division Head, Technology Transfer Division	P.L. Gardner
Division Head, ISAC Division	P.W. Schmor
Division Head, Administration Division	A. Shotter

Operating Committee

The TRIUMF Operating Committee is responsible for the operation of the facility. It reports to the Board of Management through its Chairman, the Director, Dr. A. Shotter. The Operating Committee consists of one voting member from each of the five universities, two voting members representing the interests of the Users, and one representing TRIUMF staff. The Associate Director is a non-voting member. The Operating Committee met 6 times in 2002. Members of the committee (alternate members in parentheses) at the end of 2002 were:

Dr. A. Shotter	Chairman	Director	
Dr. J.-M. Poutissou	*(ex officio)*	Associate Director	
Dr. J. Pinfold		University of Alberta	(TBA)
Dr. G. Oakham		Carleton University	(TBA)
Dr. K.P. Jackson		Simon Fraser University	(Dr. J.M. D'Auria)
Dr. R. Kowalewski		University of Victoria	(Dr. M. Lefebvre)
Dr. D. Bryman		University of British Columbia	(Dr. T. Mattison)
Dr. G.M. Luke		Users	(Dr. J. Sonier)
Dr. S. Yen		Users	(Dr. L. Lee)
Mr. R. Ruegg		TRIUMF Employee Group	(Mr. R. Baartman)
Mr. J. Hanlon	Recording Secretary	TRIUMF	
Dr. W. Davidson	*(ex officio)*	National Research Council	

NRC Advisory Committee on TRIUMF (ACOT)

The Advisory Committee on TRIUMF advises the National Research Council on all aspects of the TRIUMF program insofar as they relate to the determination and administration of the federal contribution to TRIUMF. The Committee provides scientific program advice to the Director of TRIUMF. The Committee reports to the National Research Council each year on its findings and recommendations, with particular reference to the arrangement entered into by the National Research Council and TRIUMF under which contribution payments are made, thereby ensuring that TRIUMF utilizes its program in support of its defined role as a national facility and works with all constituencies of the Canadian subatomic physics community to sustain a national program in the field of research, within the context of the funds available.

Dr. P. Sinervo	Chairman	University of Toronto
Dr. W. Davidson	Secretary	National Research Council
Dr. J. Äystö		University of Jyväskylä
Dr. W.J.L. Buyers		National Research Council
Dr. A. Fenster		J.P. Robarts Research Institute
Dr. J. Guigné		Guigné International Ltd.
Dr. G. Kalmus		Rutherford Appleton Laboratory
Dr. W. Nazarewicz		University of Tennessee
Dr. C. Rolfs		Ruhr-Universität Bochum
Dr. J. Siegrist		University of California, Berkeley
Dr. P. Vincett		FairCopy Services Inc.
Dr. R. Keeler	*(ex officio)*	University of Victoria
Dr. N. Lockyer	*(ex officio)*	University of Pennsylvania
Dr. W.J. McDonald	*(ex officio)*	University of Alberta
Ms. K. Wilson	*(ex officio)*	Natural Sciences and Engineering Research Council

Agency Committee on TRIUMF (ACT)

The role of the Agency Committee on TRIUMF is to oversee the Government of Canada's investment in TRIUMF and the economic benefits derived from that investment, with a particular focus on financial and commercialization matters. The Committee provides advice to the Minister of Industry, in conjunction with the reports of the NRC Advisory Committee on TRIUMF on scientific matters. The Agency Committee on TRIUMF usually meets twice a year.

Dr. A.J. Carty	Chairman	President, National Research Council
Dr. T. Brzustowski		President, Natural Sciences and Engineering Research Council
Mr. V.P. Harder		Deputy Minister, Industry Canada
Dr. W. Davidson	Secretary	National Research Council

TRIUMF Safety Management Committee

Dr. A. Shotter	Director, TRIUMF
Dr. J.-M. Poutissou	Associate Director/Head, Science Division
Dr. E.W. Blackmore	Head, Accelerator Technology Division
Dr. G. Dutto	Head, Cyclotron Operations Division
Mr. P.L. Gardner	Head, Technology Transfer Division
Dr. P.W. Schmor	Head, ISAC Division
Mr. M. Stenning	Head, Operations Group
Mr. D. Preddy	TAPC Chairman
Mr. G. Wood	Industrial Safety Officer/TAPC
Mr. L. Moritz	Head, Environmental Health & Safety
Mr. J. Hanlon	Manager, Human Resources & Administration
Dr. S. Zeisler	Head, Applied Technology Group
Dr. B. Abeysekera	MDS-Nordion
Mrs. K. Gildert	Recording Secretary

Experiments Evaluation Committees (EEC)

In July, 1994 the Experiments Evaluation Committee was formally split into two committees representing subatomic physics and μSR physics. In 2000 the μSR Committee changed its name to the Materials Science Committee. In 2002 these committees comprised:

Subatomic Committee:

Dr. I.S. Towner	Chairman	Queen's University
Dr. J.-M. Poutissou	Associate Director/*(ex officio)*	TRIUMF
Dr. B. Jennings	Secretary	TRIUMF
Dr. J.H. Brewer	*(ex officio)*	TUEC Past Chairman/UBC
Dr. S.J. Freedman		Lawrence Berkeley Laboratory
Dr. H.-O. Meyer		Indiana University
Dr. B.M. Sherrill		NSCL/Michigan State University
Dr. F.K. Thielemann		Universität Basel

Materials Science Committee:

Dr. I.K. Affleck	Chairman	Boston University
Dr. J.-M. Poutissou	Associate Director/*(ex officio)*	TRIUMF
Dr. P.W. Percival	Secretary/*(ex officio)*	SFU/TRIUMF
Dr. G.M. Luke	*(ex officio)*	TUEC Chairman/McMaster University
Dr. S.F.J. Cox		Rutherford Appleton Laboratory
Dr. B. Gaulin		McMaster University
Dr. S. Roorda		Université de Montréal
Dr. G.A. Sawatzky		University of British Columbia
Dr. T.W. Swaddle		University of Calgary

Life Sciences Project Evaluation Committee (LSPEC)

Dr. A. Fenster	Chairman	J.P. Robarts Research Institute
Dr. J.-M. Poutissou	Associate Director/*(ex officio)*	TRIUMF
Dr. L.P. Robertson	Secretary	University of Victoria
Dr. R.F. Dannals		Johns Hopkins PET Center
Dr. S. Houle		PET Center – CAMH/University of Toronto
Dr. J. Link		University of Washington
Dr. A.J.B. McEwan		Cross Cancer Clinic
Dr. C.J. Thompson		Montreal Neurological Institute, McGill University

PUBLICATIONS

This appendix lists publications describing work performed at TRIUMF and also work conducted elsewhere by TRIUMF personnel and TRIUMF users.

Journal Publications

Particle, Nuclear and Atomic Physics

A.M. Laird, S. Cherubini, A.N. Ostrowski, M. Aliotta, T. Davinson, A. Di Pietro, P. Figuera, W. Galster, J.S. Graulich, D. Groombridge, J. Hinnefeld, M. Lattuada, P. Leleux, L. Michel, A. Musumarra, A. Ninane, M.G. Pellegriti, A.C. Shotter, C. Spitaleri, A. Tumino, J. Vervier and P. Woods, *Indirect study of the astrophysically important $^{13}O(\alpha,\gamma)\,^{19}Ne$ reaction through $^2H(\,^{18}Ne,\,^{19}Ne)\,^1H$*, Phys. Rev. **C66**, 0488011 (2002).

D. Groombridge, A.C. Shotter, W. Bradfield-Smith, S. Cherubini, T. Davinson, A. Di Pietro, J. Gorres, J.S. Graulich, A.M. Laird, P. Leleux, A. Musumarra, A. Ninane, A.N. Ostrowski, J. Rahighi, H. Schatz, M. Wiescher and P.J. Woods, *Breakout from the hot CNO cycle via the $^{138}Ne(\alpha,p)\,^{21}Na$ reaction. II: Extended energy range $E_{c.m.} \sim 1.7 - 2.9$ MeV*, Phys. Rev. **C66**, 0558021 (2002).

A.N. Ostrowski, S. Cherubini, T. Davinson, D. Groombridge, A.M. Laird, A. Musumarra, A. Ninane, A. Di Pietro, A.C. Shotter and P.J. Woods, *A double sided silicon strip detector for radioactive nuclear beam experiments*, Nucl. Instrum. Methods **A480**, 448 (2002).

P. Tischhauser, R.E. Azuma, L. Buchmann, R. Detwiler, U. Giesen, J. Görres, M. Heil, J. Hinnefeld, F. Käppeler, J.J. Kolata, H. Schatz, A. Shotter, E. Stech, S. Vouzoukas and M. Wiescher, *Elastic $\alpha - \,^{12}C$ scattering and the $^{12}C(\alpha,\gamma)\,^{16}O$ E2 S-factor*, Phys. Rev. Lett. **88**, 072501 (2002).

L.M. Boone, J.A. Hinton, D. Bramel, E. Chae, C.E. Covault, P. Fortin, D.M. Gingrich, D.S. Hanna, R. Mukherjee, C. Mueller, R.A. Ong, K. Ragan, R.A. Scalzo, D.R. Schuette, C.G. Théoret and D.A. Williams, *STACEE observations of Markarian 421 during an extended gamma-ray outburst*, Astrophys. J. **579**, L5 (2002) [astro-ph/0209194].

A. Starostin, H.M. Staudenmaier, V. Bekrenev, W.J. Briscoe, A. Koulbardis, N. Kozlenko, S. Kruglov, I. Lopatin, A. Marusic, S. McDonald, B.M.K. Nefkens, N. Phaisangittisakul, S. Prakhov, J.W. Price, A. Shafi, I. Slaus and I. Supek, *In-medium production of $2\pi^0$, η, and π^0 by π^- at 750 MeV/c*, Phys. Rev. **C66**, 055205 (2002).

D. Anthony, L. Buchmann, P. Bergbusch, J.M. D'Auria, M. Dombsky, U. Giesen, K.P. Jackson, J.D. King, J. Powell and F.C. Barker, *β-delayed deuteron emission from ^6He*, Phys. Rev. **C65**, 034310 (2002).

D.R. Rich *et al.*, *A measurement of the absolute neutron beam polarization produced by an optically pumped ^3He neutron spin filter*, Nucl. Instrum. Methods **A481**, 431 (2002).

A.D. Davies *et al.*, *Beta asymmetry measured following ^{75}Ga decay*, Bull. Am. Phys. Soc. **47**, 38 (2002).

A.C. Morton, J.C. Chow, J.D. King, R.N. Boyd, N.P.T. Bateman, L. Buchmann, J.M. D'Auria, T. Davinson, M. Dombsky, W. Galster, E. Gete, U. Giesen, C. Iliadis, K.P. Jackson, J. Powell, G. Roy and A. Shotter, *β-delayed particle decay of ^{17}Ne*, Nucl. Phys. **A706**, 15 (2002).

J.C. Chow, J.D. King, N.P.T. Bateman, R.N. Boyd, L. Buchmann, J.M. D'Auria, T. Davinson, M. Dombsky, E. Gete, U. Giesen, C. Iliadis, K.P. Jackson, A.C. Morton, J. Powell and A. Shotter, *β-delayed particle decay of ^{17}Ne into $p + \alpha + \,^{12}C$ through the isobaric analog state in ^{17}F*, Phys. Rev. **C66**, 064316 (2002).

A.R. Lipski and M.R. Pearson, *Development of thick gold targets for the production of radioactive beams of francium*, Nucl. Instrum. Methods **A480**, 156 (2002).

G.D. Sprouse, R.P. Fliller III, J.S. Grossman, L.A. Orozco and M.R. Pearson, *Traps for neutral radioactive atoms*, Nucl. Phys. **A701**, 597 (2002).

G.D. Sprouse, S. Aubin, E. Gomez, J.S. Grossman, L.A. Orozco, M.R. Pearson and M. True, *Atomic probes of electromagnetic and weak interactions with trapped radioactive atoms*, Eur. Phys. J. **A13**, 239 (2002).

K.J. Kim, J.M. Sisterson, P.A.J. Englert, M.W. Caffee, R.C. Reedy, J. Vincent and C. Castaneda, *Experimental cross-sections for the production of ^{10}Be from natural carbon targets with 40.6 to 500 MeV protons*, Nucl. Instrum. Methods **B196**, 239 (2002).

J.L. Clark, M.E. Sevior, H. Clement, J. Grater, R. Meier, G.J. Wagner, P.-A. Amaudruz, L. Felawka, G.J. Hofman, D. Ottewell, G.R. Smith, A. Ambardar, M. Kermani, G. Tagliente, P. Camerini, E. Fragiacomo, N. Grion, R. Rui, E.L. Mathie, R. Tacik, D.M. Yeomans, E.F. Gibson, J.T. Brack and M. Schepkin, *Semiexclusive pionic double charge exchange on ^4He*, Phys. Rev. **C66**, 054606 (2002).

J.D. Patterson, G.J. Hofman, J.T. Brack, P. Camerini, J. Clark, P.P.J. Delheij, L. Felawka, E. Fragiacomo, E.F. Gibson, N. Grion, B. Jamieson, E.L. Mathie, R. Meier, D. Ottewell, R.J. Peterson, K. Raywood, R.A. Ristinen, R. Rui, M.E. Sevior, G.R. Smith, R. Tacik, G. Tagliente, G.J. Wagner and D.M. Yeomans, *Analyzing powers for πp elastic scattering between 57 and 139 MeV*, Phys. Rev. **C66**, 025207 (2002).

M.A. Caprio, R.F. Casten, N.V. Zamfir, G.C. Ball, K.P. Jackson, P.-A. Amaudruz and J.-C. Thomas, *Properties of the low lying $K^\pi = 0^+$ excitations in ^{162}Er*, Phys. Rev. **C66**, 014307 (2002).

S. Tripathi, D.S. Armstrong, M.E. Christy, J.H.D. Clark, T.P. Gorringe, M.D. Hasinoff, M.A. Kovash, D.H. Wright and P.A. Zolnierczuk, *Observation of double radiative capture on pionic hydrogen*, Phys. Rev. Lett. **89**, 252501 (2002) [nucl-ex/0204013].

P.A. Zolnierczuk, T.P. Gorringe, M.D. Hasinoff, M.A. Kovash, S. Tripathi and D.H. Wright, *Search for D^* dibaryon by double radiative capture on pionic deuterium*, Phys. Lett. **B549**, 301 (2002) [nucl-ex/0208001].

G.M. Huber, G.J. Lolos, Z. Papandreou, J. Hovdebo, S.I.H. Naqvi, D.F. Ottewell, P.L. Walden and G. Jones, *The (π^+, pd) and (π^+, dd) reactions on light nuclei at 100 MeV and 165 MeV incident pion energies*, Nucl. Phys. **A705**, 367 (2002) [nucl-ex/0009010].

N.J. Tagg, A. Hamer, B. Sur, E.D. Earle, R.L. Helmer, G. Jonkmans, B.A. Moffat and J.J. Simpson, *The ^8Li calibration source for the Sudbury Neutrino Observatory*, Nucl. Instrum. Methods **A489**, 178 (2002) [nucl-ex/0202024].

C. Ruiz, F. Sarazin, L. Buchmann, T. Davinson, R.E. Azuma, A.A. Chen, B.R. Fulton, D. Groombridge, L. Ling, A. Murphy, J. Pearson, I. Roberts, A. Robinson, A.C. Shotter, P. Walden and P.J. Woods, *Strong resonances in elastic scattering of radioactive ^{21}Na on protons*, Phys. Rev. **C65**, 042801(R) (2002).

M. Samri, F. Grenier, G.C. Ball, L. Beaulieu, L. Gingras, D. Horn, Y. Larochelle, R. Moustabchir, R. Roy, C. St-Pierre and D. Theriault, *Fusion and reaction mechanism evolution in $^{24}Mg + {}^{12}C$ at intermediate energies*, Phys. Rev. **C65**, 061603(R) (2002).

L. Gingras, A. Chernomoretz, Y. Larochelle, Z.Y. He, L. Beaulieu, G.C. Ball, F. Greiner, D. Horn, R. Roy, M. Samri, C. St. Pierre, D. Theriault and S. Turbide, *Origins of intermediate velocity particle production in heavy ion reactions*, Phys. Rev. **C65**, 061604(R) (2002).

N.S. Kelsall, D.P. Balamuth, G.C. Ball, M. Carpenter, R.M. Clark, P. Fallon, S.M. Fischer, R.V.F. Janssens, D.G. Jenkins, C.J. Lister, A.O. Macchiavelli, D.G. Sarantites, D. Seweryniak, C.E. Svensson, S. Vincent, R. Wadsworth, A.N. Wilson, A.V. Afanasjev, S. Frauendorf, I. Ragnarsson and R. Wyss, *Testing mean-field models near the $N = Z$ line: gamma ray spectroscopy of the $T_Z = \frac{1}{2}$ nucleus ^{73}Kr*, Phys. Rev. **C65**, 044331 (2002).

D.G. Jenkins, N.S. Kelsall, C.J. Lister, D.P. Balamuth, M.P. Carpenter, T.A. Sienko, S.M. Fisher, R.M. Clark, P. Fallon, A. Gorgen, A.O. Macchiavelli, C.E. Svensson, R. Wadsworth, W. Reviol, D.G. Sarantites, G.C. Ball, O. Jillet and P. Van Isacker, *T=0 and T=1 states in the odd-odd nucleus ^{70}Br*, Phys. Rev. **C65**, 064307 (2002).

T. Haseyama, K. Asahi, J.D. Bowman, P.P.J. Delheij, H. Funahashi, S. Ishimoto, G. Jones, A. Masaike, Y. Masuda, Y. Matsuda, K. Morimoto, S. Muto, S.I. Penttila, V.R. Pomeroy, K. Sakai, E.I. Sharapov, D.A. Smith and V.W. Yuan, *Measurement of parity nonconserving rotation of neutron spin in the 0.734 eV p-wave resonance of ^{139}La*, Phys. Lett. **B534**, 39 (2002) [nucl-ex/0111018].

A.R. Junghans, E.C. Mohrmann, K.A. Snover, T.D. Steiger, E.G. Adelberger, J.M. Casandjian, H.E. Swanson, L. Buchmann, S.H. Park and A. Zyuzin, *$^7Be(p,\gamma)\,^8B$ astrophysical S-factor from precision cross section measurements*, Phys. Rev. Lett. **88**, 041101 (2002) [nucl-ex/0111014].

D. Karlen, *The number of light neutrino types from collider experiment*, Rev. Part. Phys. **D66**, 387 (2002).

B. Dowler *et al.* (ATLAS Liquid Argon HEC collaboration), *Performance of the ATLAS hadronic end-cap calorimeter in beam tests*, Nucl. Instrum. Methods **A482**, 94 (2002).

B. Aubert *et al.* (BABAR collaboration), *Measurement of $B^0 \bar{B}^0$ flavor oscillations in hadronic B^0 decays*, Phys. Rev. Lett. **88**, 221802 (2002) [SLAC-PUB-9061, BABAR-PUB-01-02, hep-ex/0112044].

B. Aubert *et al.* (BABAR collaboration), *A study of time dependent CP violating asymmetries and flavor oscillations in neutral B decays at the $\Upsilon(4S)$*, Phys. Rev. **D66**, 032003 (2002) [SLAC-PUB-9060, BABAR-PUB-01-03, hep-ex/0201020].

B. Aubert *et al.* (BABAR collaboration), *Measurement of $B \to K^*\gamma$ branching fractions and charge asymmetries*, Phys. Rev. Lett. **88**, 101805 (2002) [SLAC-PUB-8952, BABAR-PUB-01-04, hep-ex/0110065].

B. Aubert *et al.* (BABAR collaboration), *Measurement of branching fractions for exclusive B decays to charmonium final states*, Phys. Rev. **D65**, 032001 (2002) [SLAC-PUB-8909, BABAR-PUB-01-07, hep-ex/0107025].

B. Aubert *et al.*, *The BABAR detector*, Nucl. Instrum. Methods **A479**, 1 (2002) [SLAC-PUB-8569, BABAR-PUB-01-08, hep-ex/0105044].

B. Aubert *et al.* (BABAR collaboration), *Measurement of the branching fractions for $\psi(2S) \to e^+e^-$ and $\psi(2S) \to \mu^+\mu^-$*, Phys. Rev. **D65**, 031101 (2002) [SLAC-PUB-8953, BABAR-PUB-01-13, hep-ex/0109004].

B. Aubert *et al.* (BABAR collaboration), *Measurement of D_s^+ and D_s^{*+} production in B meson decays and from continuum e^+e^- annihilation at $\sqrt{s} = 10.6$ GeV*, Phys. Rev. **D65**, 091104 (2002) [SLAC-PUB-9131, BABAR-PUB-01-17, hep-ex/0201041].

B. Aubert *et al.* (BABAR collaboration), *Search for the rare decays $B \to K\ell^+\ell^-$ and $B \to K^*\ell^+\ell^-$*, Phys. Rev. Lett. **88**, 241801 (2002) [SLAC-PUB-9102, BABAR-PUB-01-19, hep-ex/0201008].

B. Aubert *et al.* (BABAR collaboration), *Search for T and CP violation in $B^0 - \bar{B}^0$ mixing with inclusive dilepton*

events, Phys. Rev. Lett. **88**, 231801 (2002) [SLAC-PUB-9149, BABAR-PUB-01-20, hep-ex/0202041].

B. Aubert *et al.* (BABAR collaboration), *Study of the CP violating asymmetries in* $B^0 \to \pi^+\pi^-$, $K^+\pi^-$ *decays*, Phys. Rev. **D65**, 051502 (2002) [SLAC-PUB-9012, BABAR-PUB-01-21, hep-ex/0110062].

B. Aubert *et al.* (BABAR collaboration), *Measurement of the* $B^0\bar{B}^0$ *oscillation frequency with inclusive dilepton events*, Phys. Rev. Lett. **88**, 221803 (2002) [SLAC-PUB-9096, BABAR-PUB-01-22, hep-ex/0112045].

B. Aubert *et al.* (BABAR collaboration), *Direct CP violation searches in charmless hadronic B meson decays*, Phys. Rev. **D65**, 051101 (2002) [SLAC-PUB-9065, BABAR-PUB-01-23, hep-ex/0111087].

B. Aubert *et al.* (BABAR collaboration), *Measurement of the* B^0 *lifetime with partially reconstructed* $B^0 \to D^{*-}\ell^+\nu_\ell$ *decays*, Phys. Rev. Lett. **89**, 011802 (2002); erratum *ibid.* 169903 (2002) [SLAC-PUB-9128, BABAR-PUB-02-02, hep-ex/0202005].

B. Aubert *et al.* (BABAR collaboration), *Study of* $\mathcal{B}(B^\pm \to J/\psi\pi^\pm)/ \mathcal{B}(B^\pm \to J/\psi K^\pm)$ *decays: measurement of the ratio of branching fractions and search for direct CP violating charge asymmetries*, Phys. Rev. **D65**, 091101 (2002) [SLAC-PUB-8942, EXP SLAC-PEP2-BABAR].

B. Aubert *et al.* (BABAR collaboration), *Measurement of the CP violating asymmetry amplitude sin2β*, Phys. Rev. Lett. **89**, 201802 (2002) [SLAC-PUB-9293, BABAR-PUB-02-008, hep-ex/0207042].

B. Aubert *et al.* (BABAR collaboration), *Measurements of branching fractions and CP violating asymmetries in* $B^0 \to \pi^+\pi^-$, $K^+\pi^-$, K^+K^- *decays*, Phys. Rev. Lett. **89**, 281802 (2002) [SLAC-PUB-9317, BABAR-PUB-02-009, hep-ex/0207055].

S.C. Adler *et al.* (E787 collaboration), *Further evidence for the decay* $K^+ \to \pi^+\nu\bar{\nu}$, Phys. Rev. Lett. **88**, 041803 (2002) [BNL-68713, KEK-2001-138, PRINCETON-HEP-2001-2, TRI-PP-01-35, hep-ex/0111091].

S.C. Adler *et al.* (E787 collaboration), *Search for the rare decay* $K^+ \to \pi^+\gamma$, Phys. Rev. **D65**, 052009 (2002) [BNL-68328, PRINCETON-HEP-2001-1, TRI-PP-01-09, KEK-PREPRINT-2001-26, hep-ex/0108006].

S.C. Adler *et al.* (E787 collaboration), *Search for the decay* $K^+ \to \pi^+\nu\bar{\nu}$ *in the momentum region* $P_\pi < 195\,MeV/c$, Phys. Lett. **B537**, 211 (2002) [hep-ex/0201037].

A. Airapetian *et al.* (HERMES collaboration), *Single spin azimuthal asymmetry in exclusive electroproduction of* π^+ *mesons*, Phys. Lett. **B535**, 85 (2002) [DESY-01-223, hep-ex/0112022].

G. Abbiendi *et al.* (OPAL collaboration), *Investigation of the decay of orbitally-excited B mesons and first measurement of the branching ratio* $BR(B_J^* \to B^*\pi(X))$, Eur. Phys. J. **C23**, 437 (2002) [CERN-EP-2000-125, hep-ex/0010031].

G. Abbiendi *et al.* (OPAL collaboration), *Search for single leptoquark and squark production in electron photon scattering at* $\sqrt{s_{ee}} = 189\ GeV$ *at LEP*, Eur. Phys. J. **C23**, 1 (2002) [CERN-EP-2001-040, hep-ex/0106031].

G. Abbiendi *et al.* (OPAL collaboration), *Measurement of* Z/γ^* *production in Compton scattering of quasi-real photons*, Eur. Phys. J. **C24**, 1 (2002) [CERN-EP-2001-053, hep-ex/0107047].

G. Abbiendi *et al.* (OPAL collaboration), *Measurement of the hadronic cross section for the scattering of two virtual photons at LEP*, Eur. Phys. J. **C24**, 17 (2002) [CERN-EP-2001-064, hep-ex/0110006].

G. Abbiendi *et al.* (OPAL collaboration), *Particle multiplicity of unbiased gluon jets from* e^+e^- *three jet events*, Eur. Phys. J. **C23**, 597 (2002) [CERN-EP-2001-076, hep-ex/0111013].

G. Abbiendi *et al.* (OPAL collaboration), *Search for Yukawa production of a light neutral Higgs boson at LEP*, Eur. Phys. J. **C23**, 397 (2002) [CERN-EP-2001-077, hep-ex/0111010].

G. Abbiendi *et al.* (OPAL collaboration), *Search for doubly charged Higgs bosons with the OPAL detector at LEP*, Phys. Lett. **B526**, 221 (2002) [CERN-EP-2001-082, hep-ex/0111059].

G. Abbiendi *et al.* (OPAL collaboration), *Search for leptoquarks in electron photon scattering at* $\sqrt{s_{ee}}$ *up to 209 GeV at LEP*, Phys. Lett. **B526**, 233 (2002) [CERN-EP-2001-093, hep-ex/0112024].

G. Abbiendi *et al.* (OPAL collaboration), *Measurement of the hadronic photon structure function* F_2^γ *at LEP-2*, Phys. Lett. **B533**, 207 (2002) [CERN-EP-2002-014, hep-ex/0202035].

G. Abbiendi *et al.* (OPAL collaboration), *Measurement of the charm structure function* $F_{2,c}^\gamma$ *of the photon at LEP*, Phys. Lett. **B539**, 13 (2002) [CERN-EP-2002-031, hep-ex/0206021].

G. Abbiendi *et al.* (OPAL collaboration), *Search for charged excited leptons in* e^+e^- *collisions at* $\sqrt{1/2} = 183\,GeV$ *to* $209\,GeV$, Phys. Lett. **B544**, 57 (2002) [CERN-EP-2002-043, hep-ex/0206061].

G. Abbiendi *et al.* (OPAL collaboration), *Search for associated production of massive states decaying into two photons in* e^+e^- *annihilations at* $\sqrt{1/2} = 88\,GeV$ *to* $209\,GeV$, Phys. Lett. **B544**, 44 (2002) [CERN-EP-2002-045, hep-ex/0207027].

G. Abbiendi *et al.* (OPAL collaboration), *Search for scalar top and scalar bottom quarks at LEP*, Phys. Lett. **B545**, 272 (2002), erratum, *ibid.* **B548**, 258 (2002) [CERN-EP-2002-050, hep-ex/0209026].

G. Abbiendi *et al.* (OPAL collaboration), *Measurement of neutral current four fermion production at LEP-2*,

Phys. Lett. **B544**, 259 (2002) [CERN-EP-2002-052, hep-ex/0210026].

G. Abbiendi *et al.* (OPAL collaboration), *Measurement of the B quark forward backward asymmetry around the Z^0 peak using an inclusive tag*, Phys. Lett. **B546**, 29 (2002) [CERN-EP-2002-053, hep-ex/0209076].

G. Abbiendi *et al.* (OPAL collaboration), *Charged particle multiplicities in heavy and light quark initiated events above the Z^0 peak*, Phys. Lett. **B550**, 33 (2002) [CERN-EP-2002-079, hep-ex/0211007].

Q.R. Ahmad *et al.* (SNO collaboration), *Direct evidence for neutrino flavor transformation from neutral current interactions in the Sudbury Neutrino Observatory*, Phys. Rev. Lett. **89**, 011301 (2002) [nucl-ex/0204008].

Q.R. Ahmad *et al.* (SNO collaboration), *Measurement of day and night neutrino energy spectra at SNO and constraints on neutrino mixing parameters*, Phys. Rev. Lett. **89**, 011302 (2002) [nucl-ex/0204009].

Instrumentation/Accelerator Physics/Computing Sciences

A. Zyuzin, L. Buchmann, K.R. Buckley, A.R. Junghans, E.C. Mohrmann, S.H. Park, K.A. Snover, T.D. Steiger and J. Vincent, *The fabrication of metallic ^7Be targets with a small diameter for $^7Be(p,\gamma)^8B$ measurements*, Nucl. Instrum. Methods **B187**, 264 (2002).

E. Fosshag, M. Hecht, K.R. Buckley, D.W. Becker, K. Jayamanna, J.M. D'Auria, J.S. Vincent and T.J. Ruth, *A target system for the production of ^{15}O beams for ISAC*, Nucl. Instrum. Methods **A480**, 124 (2002).

E. Grein, C. Duzenli, T. Pickles, R. Ma, K. Paton, W. Kwa, R. Harrison and E. Blackmore, *Proton radiation therapy in Canada*, Phys. in Canada, March/April, 87 (2002).

Chemistry and Solid-State Physics

A.U.B. Wolter, A. Bosse, D. Baabe, I. Maksimov, D. Mienert, H.H. Klauss, F.J. Litterst, D. Niemeier, R. Michalak, C. Geibel, R. Feyerherm, R. Hendrikx, J.A. Mydosh and S. Süllow, *Structure and magnetic order of the Heusler compound Co_2NbSn*, Phys. Rev. **B66**, 174428 (2002).

M.D. Lumsden, S.R. Dunsiger, J.E. Sonier, R.I. Miller, R.F. Kiefl, R. Jin, J. He, D. Mandrus, S.T. Bramwell and J.S. Gardner, *Temperature dependence of the magnetic penetration depth in the vortex state of the pyrochlore superconductor, $Cd_2Re_2O_7$*, Phys. Rev. Lett. **89**, 147002 (2002).

R. Kadono, *Quantum diffusion of positive muons and muonium atoms*, Current Opinion in Solid State and Mat. Sci. **6**, 141 (2002).

Y. Fudamoto, I.M. Gat, M.I. Larkin, J. Merrin, B. Nachumi, A.T. Savici, Y.J. Uemura, G.M. Luke, K.M. Kojima, M. Hase, T. Masuda and K. Uchinokura, *Muon spin relaxation in spin-ring system Cu_3WO_6: quasi-static spin freezing at $7.0K$*, Phys. Rev. **B65**, 174428 (2002).

J.A. Chakhalian, R.F. Kiefl, S.R. Dunsiger, W.A. MacFarlane, R. Miller, J.E. Sonier and J.E. Fischer, *Evidence for local moment formation around a positive muon in graphite*, Phys. Rev. **B66**, 155107 (2002).

J.D. Dow and D.R. Harshman, *Explanation of high-temperature superconductivity without cuprate planes*, Philosophical Magazine **B82**, 1055 (2002).

D.G. Eshchenko, V.G. Storchak, J.H. Brewer and R.L. Lichti, *Influence of impurities on short range electron transport in GaAs*, Phys. Rev. Lett. **89**, 226601 (2002).

V.G. Storchak, D.G. Eshchenko, J.H. Brewer, S.P. Cottrell and S.F.J. Cox, *Coherent quantum diffusion of muonium in a highly disordered medium*, Phys. Lett. **A306**, 243 (2002).

R. Kadono, W. Higemoto, A. Koda, Y. Kawasaki, M. Hanawa and Z. Hiroi, *Quasiparticle excitation in the superconducting pyrochlore $Cd_2Re_2O_7$ probed by muon spin rotation*, J. Phys. Soc. Jpn. **71**, 709 (2002).

W. Higemoto, A. Koda, R. Kadono, Y. Kawasaki, Y. Haga, D. Aoki, R. Settai and Y. Onuki, *μSR studies on heavy fermion superconductors $CeIrIn_5$ and $CeCoIn_5$*, J. Phys. Soc. Jpn. **71**, 1023 (2002).

T. Asano, H. Nojiri, W. Higemoto, A. Koda, R. Kadono and Y. Ajiro, *μSR study of Cu benzoate at very low temperature – existence or nonexistence of long range order in coupled chains*, J. Phys. Soc. Jpn. **71**, 594 (2002).

C.R. Wiebe, J.E. Greedan, G.M. Luke and J.S. Gardner, *Spin-glass behavior in the $S = 1/2$ fcc ordered perovskite Sr_2CaReO_6*, Phys. Rev. **B65**, 144413 (2002).

J. Sugiyama, H. Itahara, T. Tani, J.H. Brewer and E.J. Ansaldo, *Magnetism of layered cobalt oxides investigated by muon spin rotation and relaxation*, Phys. Rev. **B66**, 134413 (2002).

A.T. Savici, Y. Fudamoto, I.M. Gat, T. Ito, M.I. Larkin, Y.J. Uemura, G.M. Luke, Y.S. Lee, M.A. Kastner, R.J. Birgeneau and K. Yamada, *Muon spin relaxation studies of incommensurate magnetism and superconductivity in stage-4 $La_2CuO_{4.11}$ and $La_{1.88}Sr_{0.12}CuO_4$*, Phys. Rev. **B66**, 014524 (2002) [cond-mat/0202037].

A.N. Price, R.I. Miller, R.F. Kiefl, J.A. Chakhalian, S.R. Dunsiger, G.D. Morris, J.E. Sonier and P.C. Canfield, *Anomalous vortex state of superconducting $LuNi_2B_2C$*, Phys. Rev. **B65**, 214520 (2002).

D.G. Eshchenko, V.G. Storchak, J.H. Brewer, G.D. Morris, S.P. Cottrell and S.F.J. Cox, *Excess electron transport and delayed muonium formation in condensed rare gases*, Phys. Rev. **B66**, 035105 (2002).

S.F.J. Cox, R.L. Lichti and E.A. Davis, *Hydrogen in group III-V nitrides, studied by muon spin resonance*, J. Phys. D: App. Phys. **D35**, 586 (2002).

I. McKenzie, B. Addison-Jones, J.-C. Brodovitch, K. Ghandi, S. Kecman and P.W. Percival, *Detection of the*

muoniated methyl radical, J. Phys. Chem. **A106**, 7083 (2002).

K. Ghandi, B. Addison-Jones, J.-C. Brodovitch, I. McKenzie, P.W. Percival and J. Schüth, *Near-diffusion-controlled reactions of muonium in sub- and supercritical water*, Phys. Chem. Chem. Phys. **4**, 586 (2002).

D.G. Fleming, M.Y. Shelley, D.J. Arseneau, M. Senba, J.J. Pan and E. Roduner, *Hyperfine and host-guest interactions of the Mu-cyclohexadienyl radical in NaY zeolite*, J. Phys. Chem. **B25**, 6395 (2002).

J.E. Sonier, J.H. Brewer, R.F. Kiefl, R.H. Heffner, K. Poon, S.L. Stubbs, G.D. Morris, R.I. Miller, W.N. Hardy, R. Liang, D.A. Bonn, J.S. Gardner, C.E. Stronach and N.J. Curro, *Correlations between charge ordering and local magnetic fields in overdoped $YBa_2Cu_3O_{6+x}$*, Phys. Rev. **B66**, 134501 (2002) [cond-mat/0108479].

A. Koda, W.Higemoto, R. Kadono, Y. Kawasaki, K. Ishida, Y. Kitaoka, C. Geibel and F. Steglich, *Evidence for the coexistence of superconductivity and the magnetic A-phase in $CeCu_2Si_2$ proved by muon Knight shift*, J. Phys. Soc. Jpn. **71**, 1427 (2002).

K. Ohishi, K. Kakuta, J. Akimitsu, W. Higemoto, R. Kadono, J.E. Sonier, A.N. Price, R.I. Miller, R.F. Kiefl, M. Nohara, H. Suzuki and H. Takagi, *Nonlocal effects and shrinkage of the vortex core radius in YNi_2B_2C probed by μSR*, Phys. Rev. **B65** Rapid Comm., 140505 (2002).

D.R. Noakes, G.M. Kalvius and O. Hartmann, *Random anisotropy causes wide distributions of relaxation rates in Tb-Mg-Zn quasicrystals and amorphous DyAg*, Phys. Rev. Lett. **B65**, 132413 (2002).

D.E. MacLaughlin, O.O. Bernal, J.E. Sonier, R.H. Heffner, T. Taniguchi and Y. Miako, *Susceptibility inhomogeneity and non-fermi-liquid behavior in $Ce(Ru_{0.5}Rh_{0.5})_2Si_2$*, Phys. Rev. **B65**, 184401 (2002).

D.E. MacLaughlin, J.E. Sonier, R.H. Heffner, O.O. Bernal, B.-L. Young, M.S. Rose, G.D. Morris, E.D. Bauer, T.D. Do and M.B. Maple, *Muon spin relaxation and isotropic pairing in superconducting $PrOs_4Sb_{12}$*, Phys. Rev. Lett. **89**, 157001 (2002).

R.I. Miller, R.F. Kiefl, J.H. Brewer, J.E. Sonier, J. Chakhalian, S. Dunsiger, G.D. Morris, A.N. Price, D.A. Bonn, W.H. Hardy and R. Liang, *Evidence for static magnetism in the vortex cores of ortho-II $YBa_2Cu_3O_{6.50}$*, Phys. Rev. Lett. **88**, 137002 (2002).

D.H. Ryan, J.M. Cadogan and J. van Lierop, *Reply to Comment on "The field dependence of the transverse spin freezing transition"*, Phys. Rev. **B65**, 176402 (2002).

J. van Lierop and D.H. Ryan, *Dynamics in fine particle magnets*, Phys. Rev. **B65**, 104402 (2002).

J. van Lierop, D.H. Ryan and J.M Cadogan, *A study of spin dynamics in the a-$Fe_{90}Sc_{10}$ spin-glass*, J. Appl. Phys. **91**, 8263 (2002).

R.L. Lichti, S.F.J. Cox, E.A. Davis, B. Hitti and S.K.L. Sjue, *Positively charged muonium centers in aluminum and gallium nitrides*, Physica B **308-310**, 73 (2002).

R.L. Lichti, K.H. Chow, B. Hitti, E.A. Davis, S.K.L. Sjue and S.F.J. Cox, *Motional properties of positive muonium in gallium III-V compounds*, Physica B **308-310**, 862 (2002).

Life Sciences

R. de la Fuente-Fernandez and A.J. Stoessl, *Parkinson's disease: imaging update*, Curr. Opin. Neurol. **15**, 477 (2002).

A.D.M. Glass, D.J. Britto, B.N. Kaiser, H.J. Kronzucker, A. Kumar, M. Okamoto, M.Y. Siddiqi and J.J. Vidmar, *The regulation of nitrate and ammonium transport systems in plants*, J. Exp. Bot. **53**, 855 (2002).

H.G. Dunn, A.J. Stoessl, H. Ho, P.M. MacLeod, K.J. Poskitt, D.J. Doudet, M. Schulzer, D. Blackstock, T. Dobko, B. Koop and G.V. de Amorim, *Rett syndrome: investigation of 9 patients, including PET scanning*, Can. J. Neurol. Sci. **29**, 345 (2002).

E.M. Strome, G.H. Wheeler, D. Higley, D.L. Loriaux, S.J. Suomi and D.J. Doudet, *Intracerebroventricular corticotrophin-releasing factor increases limbic glucose metabolism and has social context-dependent behavioral effects in non-human primates*, PNAS **99**, 15749 (2002).

R. de la Fuente-Fernandez and A.J. Stoessl, *The biochemical bases for reward: implications for the placebo effect*, Eval. and the Health Prof. **25**, 387 (2002).

S. Furtado, M. Farrer, Y. Tsuboi, M.L. Klimek, R. de la Fuente-Fernandez, J. Hussey, P. Lockhart, D.B. Calne, O. Suchowersky, A.J. Stoessl and Z.K. Wszolek, *SCA-2 presenting as Parkinsonism in an Alberta family: clinical, genetic and PET findings*, Neurology **59**, 1625 (2002).

A.J. Stoessl, *"Stiff in the closet" – Who provides care for Parkinsonian patients?*, Can. J. Neurol. Sci. **29**, 203 (2002).

S.E. McCormick and A.J. Stoessl, *Blockade of pallidal and nigral opioid receptors suppresses vacuous chewing movements in a rodent model of tardive dyskinesia*, Neuroscience **112**, 851 (2002).

R. de la Fuente-Fernandez and A.J. Stoessl, *The placebo effect in Parkinson's disease*, Trends in Neurosciences **25**, 302 (2002).

J.Q. Lu and A.J. Stoessl, *Somatostatin modulates the behavioral effects of dopamine receptor activation in Parkinsonian rats*, Neuroscience **112**, 261 (2002).

R. de la Fuente-Fernandez, M. Schulzer and A.J. Stoessl, *The placebo effect in neurological disorders*, Lancet Neurology **1**, 85 (2002).

S. Armstrong, D. Worsley and G.K. Blair, *Pediatric surgical images: PET evaluation of papillary thyroid carcinoma recurrence*, J. Pediatr. Surg. **37**, 1648 (2002).

M.J. Adam, *Radiohalogenated carbohydrates for use in PET and SPECT*, J. Lab. Compd. Radiopharm. **45**, 1 (2002).

E.T.C. Ngan, C.J. Lane, T.J. Ruth and P.F. Liddle, *Immediate and delayed effects of risperidone on cerebral metabolism in neuroleptic naïve schizophrenic patients: correlations with symptom change*, J. Neurol. Neurosurg. Psychiatry **72**, 106 (2002).

J.E. Holden, S. Jivan, T.J. Ruth and D.J. Doudet, *In-vivo receptor assay with multiple ligand concentrations: an equilibrium approach*, J. Cereb. Blood Flow Metab. **22**, 1132 (2002).

D.J. Doudet, S. Jivan, T.J. Ruth and J.E. Holden, *Density and affinity of the dopamine D2 receptors in aged symptomatic and asymptomatic MPTP-treated monkeys: PET studies with [^{11}C]raclopride*, Synapse **44**, 198 (2002).

D.J. Doudet, J.E. Holden, T.J. Ruth, T.A. Aigner and R.J. Wyatt, *In-vivo PET studies of the dopamine D1 receptors in rhesus monkeys with long-term MPTP-induced Parkinsonism*, Synapse **44**, 111 (2002).

R.A. Hauser, S. Furtado, C.R. Cimino, H. Delgado, S. Eichler, S. Schwartz, D. Scott, G.M. Nauert, E. Soety, V. Sossi, D.A. Holt, P.R. Sanberg, A.J. Stoessl and T.B. Freeman, *Bilateral human fetal striatal transplantation in Huntington's disease*, Neurology **58**, 687 (2002).

M.E. Daube-Witherspoon, J.S. Karp, M.E. Casey, J. Fernando, H. Hines, G. Muehllehner, V. Simcic, C. Stearns, P. Vernon, L-E. Adam, S. Kohlmyer and V. Sossi, *PET performance measurements using the NU-2-2001 standard*, J. Nucl. Med. **43**, 1398 (2002).

V. Sossi, R. de la Fuente-Fernandez, J.E. Holden, D.J. Doudet, J. McKenzie, A.J. Stoessl and T.J. Ruth, *Increase in dopamine turnover occurs early in Parkinson's disease: evidence from a new modeling approach to PET ^{18}F-fluorodopa data*, J. Cereb. Blood Flow and Metab. **22**, 232 (2002).

R. de la Fuente-Fernandez, A.G. Phillips, M. Zamburlini, V. Sossi, D.B. Calne, T.J. Ruth and A.J. Stoessl, *Dopamine release in human ventral striatum and expectation of reward*, Behavioural Brain Research **136**, 359 (2002).

L.N. Yatham, P.F. Liddle, I.-S. Shiah, R.W. Lam, E. Ngan, G. Scarrow, M. Imperial, J. Stoessl, V. Sossi and T.J. Ruth, *PET study of the effects of valproate on dopamine D(2) receptors in neuroleptic- and mood-stabilizer-naïve patients with nonpsychotic mania*, Am. J. Psych. **159**, 1718 (2002).

L.N. Yatham, P.F. Liddle, I.-S. Shiah, R.W. Lam, E. Ngan, G. Scarrow, M. Imperial, J. Stoessl, V. Sossi and T.J. Ruth, *A positron emission tomography study of [^{18}F]6-fluoro-L-dopa uptake in neuroleptic and mood stabilizer naïve first episode non-psychotic mania: effects of treatment with Divalproex sodium*, Am. J. Psych. **159**, 768 (2002).

Theoretical Program

T.S. Park, H. Jung and D.P. Min, *In-medium effective pion mass from heavy-baryon chiral perturbation theory*, J. Korean Phys. Soc. **41**, 195 (2002) [SNUTP-99-053, USC-NY-01-03, nucl-th/0101064].

O. Teoderescu, A.K. Dutt-Mazumder and C. Gale, *Aspects of meson properties in dense nuclear matter*, Phys. Rev. **C66**, 015209 (2002) [nucl-th/0112035].

A.D. Lahiff and I.R. Afnan, *Unitarity and the Bethe-Salpeter equation*, Phys. Rev. **C66**, 044001 (2002) [nucl-th/0205076].

N. Mathur, R. Lewis and R.M. Woloshyn, *Charmed and bottom baryons from lattice NRQCD*, Phys. Rev. **D66**, 014502 (2002) [hep-ph/0203253].

S. Ando, H.W. Fearing and D.P. Min, *Polarized photons in radiative muon capture*, Phys. Rev. **C65**, 015502 (2002) [USC-NT-REPORT-01-1, TRI-PP-01-02, SNUTP-00-037, nucl-th/0104077].

T. Ebertshauser, H.W. Fearing and S. Scherer, *The anomalous chiral perturbation theory meson Lagrangian to order p^6 revisited*, Phys. Rev. **D65**, 054033 (2002) [MKPH-T-01-22, TRI-PP-01-34, hep-ph/0110261].

E.C.Y. Ho and H.W. Fearing, *Radiative muon capture by ^{3}He*, Phys. Rev. **C65**, 065501 (2002) [TRI-PP-01-37, nucl-th/0112019].

G. Rupak and N. Shoresh, *Chiral perturbation theory for the Wilson lattice action*, Phys. Rev. **D66**, 054503 (2002) [TRI-PP-01-38, BUHEP-02-04, hep-lat/0201019].

A.Z. Mekjian, *Particle multiplicity distributions: connections with a Feynman-Wilson gas and a Ginzburg-Landau theory*, Phys. Rev. **C65**, 014907 (2002).

H.-J. He, D.A. Dicus and J.N. Ng, *Minimal schemes for large neutrino mixings with inverted hierarchy*, Phys. Lett. **B536**, 83 (2002) [hep-ph/0203237].

D. Chang, W.-F. Chang and W.-Y. Keung, *New constraint from electric dipole moments on chargino baryogenesis in MSSM*, Phys. Rev. **D66**, 116008 (2002) [hep-ph/0205084].

W.-F. Chang and J.N. Ng, *CP violation in 5-D split fermions scenario*, J. High Energy Phys. **0212**, 077 (2002) [hep-ph/0210414].

W.-F. Chang, I.-L. Ho and J.N. Ng, *Lepton universality, rare decays and split fermions*, Phys. Rev. **D66**, 076004 (2002) [hep-ph/0203212].

C.Q. Geng and C.-W. Hwang, *Lepton pair decays of the K_L meson in the light front model*, Phys. Rev. **D66**, 034005 (2002) [hep-ph/0112164].

C.-H. Chen and C.Q. Geng, *Probing new physics in $B \to K^{(*)}\ell^+\ell^-$ decays*, Phys. Rev. **D66**, 094018 (2002) [hep-ph/0209352].

C.-H. Chen and C.Q. Geng, *T violation in B →
K*ℓ⁺ℓ⁻ from SUSY*, Phys. Rev. **D66**, 014007 (2002) [hep-
ph/0205306].

C.-H. Chen, and C.Q. Geng, *Analysis of B → K*ℓ⁺ℓ⁻ de-
cays at large recoil region*, Nucl. Phys. **B636**, 338 (2002)
[hep-ph/0203003].

C.-H. Chen and C.Q. Geng, *Long distance contributions in
B → K*ℓ⁺ℓ⁻ decays with polarized K***, Phys. Rev. **D66**,
034006 (2002) [hep-ph/0207038].

C.Q. Geng, J.N. Ng and T.H. Wu, *CP violation in the
decay η → π⁺π⁻γ*, Mod. Phys. Lett. **A17**, 1489 (2002)
[hep-ph/0201191].

C.Q. Geng, C.-W. Hwang and C.C. Liu, *Study of rare
$B_c^+ → D_{d,s}^{*+}\ell\bar\ell$ decays*, Phys. Rev. **D65**, 094037 (2002) [hep-
ph/0110376].

C.-H. Chen, C.Q. Geng and J.N. Ng, *T violation in
$Λ_b → Λℓ⁺ℓ⁻$ decays with polarized Λ*, Phys. Rev. **D65**,
091502 (2002) [hep-ph/0202103].

D. Chang, W.-F. Chang, W.-Y. Keung and N. Sinha,
Squark mixing contributions to CP violating phase gamma,
Phys. Rev. **C65**, 055010 (2002) [IMSC-2001-09-50, hep-
ph/0109151].

S. Kondratyuk, *Pion nucleon amplitude near threshold: the
sigma-term and scattering lengths beyond few loops*, Nucl.
Phys. **A710**, 329 (2002) [nucl-th/0204050].

S. Kondratyuk and O. Scholten, *Low-energy Compton scat-
tering on the nucleon and sum rules*, Phys. Rev. **C65**,
038201 (2002) [nucl-th/0109038].

K. Maltman and J. Kambor, *Decay constants, light quark
masses and quark mass bounds from light quark pseu-
doscalar sum rules*, Phys. Rev. **D65**, 074013 (2002)[ZU-
TH-26-01, YU-PP-I-E-KM-5-01, hep-ph/0108227].

J.C. Da Silva, F.C. Khanna, A. Matos Neto and A.E. San-
tana, *Generalised Bogoliubov transformation for confined
fields: application for the Casimir effect*, Phys. Rev. **A66**,
052101 (2002).

W. Zhao and F.C. Khanna, *Screening length, dispersion re-
lations and quark potential in thermo field dynamics*, Int.
J. Mod. Phys. **A17**, 1 (2002).

E. Truhlik and F.C. Khanna *On radiative muon cap-
ture in hydrogen*, Phys. Rev. **C65**, 045504 (2002) [nucl-
th/0102006].

D.U. Matrasulov, F.C. Khanna, Kh.Yu. Rakhimov and
Kh.T. Butanov, *Spectra of baryons containing two heavy
quarks*, Eur. Phys. J. **A14**, 81 (2002).

F. Khanna, A. Mann, M. Revzen and S. Roy, *Bell's in-
equality and symmetry*, Phys. Lett. **A294**, 1 (2002).

A.E. Santana, F.C. Khanna and M. Revzen, *Entropy of
entangled states and SU(1,1) and SU(2) symmetries*, Phys.
Rev. **A65**, 032119 (2002).

J. Escher and B.K. Jennings, *One-body overlap func-
tions, equations of motion, and phenomenological poten-
tials*, Phys. Rev. **C66**, 034313 (2002) [TRI-PP-02-11].

J. Escher and A. Leviaton, *Partial dynamical symmetry in
the symplectic shell model*, Phys. Rev. **C65**, 054309 (2002)
[TRI-PP-00-57, nucl-th/0110030].

H.W. Griesshammer and G. Rupak, *Nucleon polarizabili-
ties from Compton scattering on the deuteron*, Phys. Lett.
B529, 57 (2002) [NT-UW-00-022, TRI-PP-00-62, TUM-
T39-00-18, nucl-th/0012096].

W.C. Haxton, C.P. Liu and M.J. Ramsey-Musolf, *Nuclear
anapole moments*, Phys. Rev. **C65**, 045502 (2002) [nucl-
th/0109014].

D.H. Wilkinson, *Super-allowed fermi beta-decay revisited*,
Nucl. Instrum. Methods **A488**, 654 (2002).

D.H. Wilkinson, *Evaluation of G_V^* and G_A^*: CKM unitarity*,
Nucl. Instrum. Methods **A495**, 65 (2002) [TRI-PP-02-04].

S.J.Q. Robinson and L. Zamick, *Effects of T=0 two body
matrix elements on M1 and Gamow-Teller transitions:
isospin decomposition*, Phys. Rev. **C66**, 034303 (2002)
[nucl-th/0201058].

Journal Publications In Press or Submitted

Particle, Nuclear and Atomic Physics

P. Camerini, E. Fragiacomo, N. Grion, S. Piano, R. Rui, J.
Clark, L. Felawka, E.F. Gibson, G. Hofman, E.L. Mathie,
R. Meier, G. Moloney, D. Ottewell, K. Raywood, M.E. Se-
vior, G.R. Smith and R. Tacik, *General properties of the
pion production reaction in nuclear matter* (submitted to
Nucl. Phys. A).

A. Toyoda *et al.*, *New insights in muon-catalyzed dd fusion
by using ortho-para controlled solid deuterium* (Phys. Rev.
Lett., in press).

W. Liu *et al.*, *Charge state studies of low energy heavy ions
passing through hydrogen and helium gas* (Nucl. Instrum.
Methods A, in press).

S. Bishop, R.E. Azuma, L. Buchmann, A.A. Chen, M.L.
Chatterjee, J.M. D'Auria, S. Engel, D. Gigliotti, U. Greife,
M. Hernanz, D. Hunter, A. Hussein, D. Hutcheon, C.
Jewett, J. Jose, J. King, S. Kubono, A.M. Laird, M.
Lamey, R. Lewis, W. Liu, S. Michimasa, A. Olin, D. Ot-
tewell, P.D. Parker, J.G. Rogers, F. Strieder and C. Wrede,
²¹Na(p,γ)²²Mg reaction and oxygen-neon novae (Phys.
Rev. Lett., in press).

G.F. Grinyer, J.C. Waddington, C.E. Svensson, R.A.E.
Austin, G.C. Ball, G.S. Hackman, J.M. O'Meara, C. Os-
borne, F. Sarazin, H.C. Scraggs and H.D.H. Stover, *The
half-life of ¹⁷⁶Lu* (Phys. Rev. C, in press).

C.D. O'Leary, C.E. Svensson, S.G. Frauendorf, D.E. Ap-
pelbe, R.A.E. Austin, G.C. Ball, J.A. Cameron, R.M.

Clark, M. Cromaz, P. Fallon, D.F. Hodgson, N.S. Kelsall, A.O. Macchiavelli, D. Sarantites, J.C. Waddington, R. Wadsworth, D. Ward, A. Afanasjev and I. Ragnarsson, *Evidence for isovector neutron-proton pairing from high-spin states in* ^{74}Rb (Phys. Rev. C, in press).

A. Piechaczek, E.F. Zganjar, G.C. Ball, B. Bricault, J. D'Auria, J.C. Hardy, D.F. Hodgson, V. Iacob, P. Klages, W.D. Kulp, J.R. Leslie, M. Lipoglavsek, J.A. Macdonald, H.-B. Mak, D.M. Moltz, G. Savard, J. von Schwarzenberg, C.E. Svensson, I.S. Towner and J.L. Wood, *High precision branching ratio measurements for the superallowed β-decay of ^{74}Rb: a prerequisite for exacting tests of the standard model* (submitted to Phys. Rev. C).

S. Gu, J.A. Behr, M.N. Groves and D. Dhat, *Coherent population trapping states with cold atoms in a magnetic field* (Optics Communications, in press).

S. Gu and J.A. Behr, *Study of coherent population trapping using off-Raman resonance oscillations* (submitted to Phys. Rev. A).

S. Gu and J.A. Behr, *Off-Raman resonance effects of hyperfine coherences* (submitted to Phys. Rev. A).

M. Trinczek, A. Gorelov, D. Melconian, W.P. Alford, D. Asgeirsson, D. Ashery, J.A. Behr, P.G. Bricault, J.M. D'Auria, J. Deutsch, J. Dilling, M. Dombsky, P. Dubé, S. Eaton, J. Fingler, U. Giesen, S. Gu, O. Häusser, K.P. Jackson, B. Lee, J.H. Schmid, T.J. Stocki, T.B. Swanson and W. Wong, *Novel search for heavy ν mixing from the β^+ decay of ^{38m}K confined in an atom trap* (Phys. Rev. Lett., in press).

A.R. Berdoz, J. Birchall, J.B. Bland, J.D. Bowman, J.R. Campbell, G.H. Coombes, C.A. Davis, A.A. Green, P.W. Green, A.A. Hamian, R. Helmer, S. Kadantsev, Y. Kuznetsov, L. Lee, C.D.P. Levy, R.E. Mischke, N.T. Okumusoglu, S.A. Page, W.D. Ramsay, S.D. Reitzner, T. Ries, G. Roy, A.M. Sekulovich, J. Soukup, G.M. Stinson, T. Stocki, V. Sum, N.A. Titov, W.T.H. van Oers, R.J. Woo, S. Zadorozny and A.N. Zelenski (E497 collaboration), *Parity violation in proton-proton scattering at $221\,MeV$* (submitted to Phys. Rev. C) [TRI-PP-02-18, nucl-ex/0211020].

B. Aubert *et al.* (BABAR collaboration), *Study of inclusive production of charmonium mesons in B decay* (Phys. Rev. D, in press) [SLAC-PUB-9327, BABAR-PUB-02-04, hep-ex/0207097].

B. Aubert *et al.* (BABAR collaboration), *A measurement of the $B^0 \rightarrow J/\psi \pi^+ \pi^-$ branching fraction* (Phys. Rev. Lett., in press) [SLAC-PUB-9261, BABAR-PUB-02-06, hep-ex/0209013].

B. Aubert *et al.* (BABAR collaboration), *Measurement of the branching fraction for inclusive semileptonic B meson decays* (Phys. Rev. D, in press) [SLAC-PUB-9306, BABAR-PUB-02-011, hep-ex/0208018].

M.C. Vetterli *et al.* [HERMES collaboration], *Deep inelastic scattering on nuclei* (submitted to Phys. Lett. B)

[DESY-02-091, hep-ex/0210068].

A. Airapetian *et al.* (HERMES collaboration), *Evidence for quark-hadron duality in the proton spin asymmetry A_1* (Phys. Rev. Lett., in press) [hep-ex/0209018, DESY-02-137].

A. Airapetian *et al.* (HERMES collaboration), *The Q^2-dependence of nuclear transparency for exclusive ρ^0 production* (Phys. Rev. Lett., in press) [DESY-02-152, hep-ex/0209072].

A. Airapetian *et al.* (HERMES collaboration), *The Q^2-dependence of the generalized Gerasimov-Drell-Hearn integral for the deuteron, proton and neutron* (Eur. Phys. J., in press) [DESY-02-172, hep-ex/0210047].

A. Airapetian *et al.* (HERMES collaboration), *Measurement of single-spin azimuthal asymmetries in semi-inclusive electroproduction of pions and kaons on a longitudinally polarised deuterium target* (Phys. Lett. B, in press) [hep-ex/0212039, DESY 02-226].

A. Airapetian *et al.* (HERMES collaboration), *Double-spin asymmetries in the cross section of diffractive ρ^0 and ϕ production at intermediate energies* (Eur. Phys. J. C, in press) [hep-ex/0302012, DESY-02-230].

M.A. Aliev *et al.* (KEK-E470 collaboration), *Measurement of direct photon emission in $K^+ \rightarrow \pi^+ \pi^0 \gamma$ decay using stopped positive kaons* (Phys. Lett. B, in press) [hep-ex/0212048].

W.J. Murray *et al.* (MuScat collaboration), *Status of the MuScat experiment* (J. Phys. G, in press).

G. Abbiendi *et al.* (OPAL collaboration), *Measurement of the mass of the W boson in $e^+ e^-$ collisions using the fully leptonic channel* (Eur. Phys. J. C, in press) [CERN-EP-2002-022, hep-ex/0203026].

G. Abbiendi *et al.* (OPAL collaboration), *Decay mode independent searches for new scalar bosons with the OPAL detector at LEP* (Eur. Phys. J., in press) [CERN-EP-2002-032, hep-ex/0206022].

G. Abbiendi *et al.* (OPAL collaboration), *Inclusive analysis of the B quark fragmentation function in Z decays at LEP* (submitted to Eur. Phys. J. C) [CERN-EP-2002-051, hep-ex/0210031].

G. Abbiendi *et al.* (OPAL collaboration), *Measurement of the cross-section for the process $\gamma\gamma \rightarrow p\bar{p}$ at $\sqrt{s_{ee}} = 183$–$189\,GeV$ at LEP* (submitted to Eur. Phys. J. C) [CERN-EP-2002-056, hep-ex/0209052].

G. Abbiendi *et al.* (OPAL collaboration), *Charged particle momentum spectra in $e^+ e^-$ annihilation at $\sqrt{1/2} = 192$–$209\,GeV$* (Eur. Phys. J., in press) [CERN-EP-2002-057, hep-ex/0209048].

G. Abbiendi *et al.* (OPAL collaboration), *Search for a low mass CP odd Higgs boson in $e^+ e^-$ collisions with the OPAL*

detector at LEP-2 (Eur. Phys. J. C, in press) [CERN-EP-2002-058, hep-ex/0209068].

G. Abbiendi *et al.* (OPAL collaboration), *Search for the standard model Higgs boson with the OPAL detector at LEP* (Eur. Phys. J. C, in press) [CERN-EP-2002-059, hep-ex/0209078].

G. Abbiendi *et al.* (OPAL collaboration), *Multi-photon production in e^+e^- collisions at $\sqrt{s} = 181$–$209\,GeV$* (submitted to Eur. Phys. J.) [CERN-EP-2002-060, hep-ex/0210016].

G. Abbiendi *et al.* (OPAL collaboration), *Search for nearly mass degenerate charginos and neutralinos at LEP* (submitted to Eur. Phys. J.) [CERN-EP-2002-063, hep-ex/0210043].

G. Abbiendi *et al.* (OPAL collaboration), *A measurement of the $\tau^- \rightarrow \mu^- \bar{\nu}_\mu \nu_\tau$* (Phys. Lett. B, in press) [CERN-EP-2002-085, hep-ex/0211066].

G. Abbiendi *et al.* (OPAL collaboration), *Di-jet production in photon-photon collisions at $\sqrt{s_{ee}}$ from 189 to 209 GeV* (submitted to Eur. J. Phys. C) [CERN-EP-2002-093, hep-ex/0301013].

G. Abbiendi *et al.* (OPAL collaboration), *A measurement of semileptonic B decays to narrow orbitally excited charm mesons* (submitted to Eur. J. Phys. C) [CERN-EP-2002-094, hep-ex/0301018].

J. Wozniak *et al.* (TRIUMF Muonic Hydrogen collaboration), *Scattering of $p\mu$ muonic atoms in solid hydrogen* (submitted to Phys. Rev. A) [nucl-ex/0212005].

Instrumentation/Accelerator Physics/Computing Sciences

P.G. Bricault, *First laser ions at an off-line mass separator of the ISAC facility at TRIUMF* (submitted to Nucl. Instrum. Methods B).

S. Zeisler, R.A. Pavan, J. Orzechowski, R. Langlois, S. Rodrigue and J.E. van Lier, *Production of ^{64}Cu on the Sherbrooke TR-PET cyclotron* (J. Radioanal. Nucl. Chem., in press).

R.A. Pavan, W.Z. Gelbart and S.K. Zeisler, *Thermal modelling of high current solid targets* (J. Radioanal. Nucl. Chem., in press).

K. Jayamanna, D. Yuan, M. McDonald, M. Olivo, P. Schmor and G. Stanford, *Commissioning the TRIUMF/ISAC ECR source for radioactive ion beams* (Rev. Sci. Instrum., in press).

N.J. Buchanan and D.M. Gingrich, *Proton radiation effects in XC4036XLA field programmable gate arrays* (IEEE Trans. Nucl. Sci., in press).

D. Hutcheon *et al.*, *The DRAGON facility for nuclear astrophysics at TRIUMF-ISAC: design, construction and operation* (Nucl. Instrum. Methods A, in press).

P. Gumplinger, F. Jones, S. Agostinelli *et al.* (GEANT4 collaboration), *GEANT4 – a simulation toolkit* (Nucl. Instrum. Methods A, in press).

M. Abe *et al.*, *Apparatus for a search for T-violating muon polarization in stopped-kaon decays* (Nucl. Instrum. Methods A, in press).

Chemistry and Solid-State Physics

Y.J. Uemura, *Superfluid density of high-T_c cuprate systems: implication on condensation mechanisms, heterogeneity and phase diagram* (Solid State Comm., in press).

J.J. Pan, D.J. Arseneau, M. Senba and D.G. Fleming, *Gas phase Mu+CO termolecular kinetics* (submitted to J. Chem. Phys.).

R.I. Miller and R.F. Kiefl, *Magnetism in the cuprates induced by an external magnetic field* (Solid State Comm., in press).

I. McKenzie, J.-C. Brodovitch, P.W. Percival, T. Ramnial and J.A.C. Clyburne, *The reactions of imidazol-2-ylidenes with the hydrogen atom: a theoretical study and experimental confirmation with muonium* (submitted to J. Am. Chem. Soc.).

K. Ghandi, B. Addison-Jones, J.-C. Brodovitch, B. McCollum, I. McKenzie and P.W. Percival, *Enolization of acetone in superheated water detected via radical formation* (submitted to J. Am. Chem. Soc.)

R. Kadono, W. Higemoto, A. Koda, M.I. Larkin, G.M. Luke, A.T. Savici, Y.J. Uemura, K.M. Kojima, T. Okamoto, T. Kakeshita, S. Uchida, T. Ito, K. Oka, M. Takigawa, M. Ichioka and K. Machida, *Expansion of vortex cores at low magnetic induction in $La_{2-x}Sr_xCuO_4$* (submitted to Phys. Rev. Lett.).

W. Higemoto, K. Satoh, A. Koda, K. Nishiyama, K. Shimomura, R. Kadono, A. Hanaoka, S. Koiwai, Y. Uwatoko and N. Mori, *μSR study of magnetism of $CeRh_2Si_2$ under a high pressure* (Physica B, in press).

I.M. Gat-Malureanu, A. Fukaya, M.I. Larkin, A.J. Millis, P.L. Russo, A.T. Savici, Y.J. Uemura, P.P. Kyriakou, G.M. Luke, C.R. Wiebe, Y.V. Sushko, R.H. Heffner, D.E. MacLaughlin, D. Andreica and G.M. Kalvius, *Field dependence of muon spin relaxation rate in MnSi* (submitted to Phys. Rev. Lett.).

A. Fukaya, Y. Fudamoto, I.M. Gat, T. Ito, M.I. Larkin, A.T. Savici, Y.J. Uemura, P.P. Kyriakou, G.M. Luke, M.T. Rovers, K.M. Kojima, A. Keren, M. Hanawa and Z. Hiroi, *Muon spin relaxation and susceptibility studies of pure and doped spin 1/2 Kagome-like system $(Ca_x Zn_{1-x})_3 V_2 O_7 (OH)_2$-$2(H_2 O)$* (submitted to Phys. Rev. Lett.).

Y. Fudamoto, I.M. Gat, M.I. Larkin, J. Merrin, B. Nachumi, A.T. Savici, Y.J. Uemura, G.M. Luke, K.M. Kojima, M. Isobe, Y. Ueda, S. Taniguchi and M. Sato, *μSR*

studies of two-dimensional antiferromagnets CaV_3O_7 and SrV_3O_7 (Physica B, in press).

J.A. Chakhalian, R.F. Kiefl, R.I. Miller, J.H. Brewer, S.R. Dunsiger, G.D. Morris, W.A. MacFarlane, J.E. Sonier, S. Eggert, I. Affleck, A. Keren and M. Verdaguer, *Local magnetic susceptibility of the positive muon in the quasi 1D $S = 1/2$ antiferromagnet dichlorobis (pyridine) copper (II)* (Phys. Rev. Lett., in press).

D.R. Harshman, W.J. Kossler, X. Wan, A.T. Fiory, A.J. Greer, D.R. Noakes, C.E. Stronach, E. Koster, A. Erb, and J.D. Dow, *Nodeless pairing state in single-crystal $YBa_2Cu_3O_7$* (submitted to Phys. Rev. B).

D.R. Harshman, W.J. Kossler, A.J. Greer, D.R. Noakes, C.E. Stronach, E. Koster, M.K. Wu, F.Z. Chien, J.P. Franck, I. Isaac and J.D. Dow, *Spin-glass behavior, spin-fluctuations and superconductivity in $Sr_2Y(Ru_{1-u}Cu_u)O_6$* (Phys. Rev. B, in press).

A.J. Greer, D.R. Harshman, W.J. Kossler, A. Goonewardene, D.Ll. Williams, E. Koster, W. Kang, R.N. Kleiman and R.C. Haddon, *A µSR study of the $(TMTSF)_2ClO_4$ system* (submitted to Physica C).

D.R. Harshman, J.D. Dow, W.J. Kossler, D.R. Noakes, C.E. Stronach, A.J. Greer, E. Koster, Z.F. Ren and D.Z. Wang, *Muon spin rotation study of $GdSr_2Cu_2RuO_8$: implications* (submitted to Philosophical Magazine).

J. Sugiyama, J.H. Brewer, E.J. Ansaldo, H. Itahara, C. Xia and T. Tani, *Hidden magnetic transitions in thermoelectric layered cobaltites* (submitted to Phys. Rev. Lett.).

J. Sugiyama, C. Xia and T. Tani, *Anisotropic magnetic properties of $Ca_3Co_4O_9$; the evidence of a spin density wave transition at $27K$* (Phys. Rev. B, in press).

J. Sugiyama, J.H. Brewer, E.J. Ansaldo, H. Itahara, S. Hirano and T. Tani, *μ^+SR studies on thermoelectric oxides* (Physica B, in press).

V.G. Storchak, D.G. Eshchenko, R.L. Lichti and J.H. Brewer, *Weakly bound muonium state in GaP: validity of the effective mass approximation* (Phys. Rev. B, in press).

K. Ghandi and P.W. Percival, *Prediction of rate constants for reactions of the hydroxyl radical in water at high temperatures and pressures* (submitted to J. Phys. Chem. A).

J.-C. Brodovitch, B. Addison-Jones, K. Ghandi, I. McKenzie, P.W. Percival and J. Schüth, *Free radicals formed by H(Mu) addition to fluoranthene* (Can. J. Chem., in press).

D.C. Walker, S. Karolczak, G.B. Porter and H. A. Gillis, *No "delayed" muonium-formation in organic liquids* (J. Chem. Phys., in press).

D.C. Walker, S. Karolczak, H.A. Gillis and G.B. Porter, *Hot model of muonium formation in liquids* (Can. J. Chem., in press).

S. Karolczak, H.A. Gillis, G.B. Porter and D.C. Walker,

Solvent-dependent rate constants of muonium atom reactions (Can. J. Chem., in press).

K. Ohishi, T. Muranaka, J. Akimitsu, A. Koda, W. Higemoto and R. Kadono, *Quasiparticle excitations outside the vortex cores in MgB_2 probed by muon spin rotation* (J. Phys. Soc. Jpn., in press).

D.H. Ryan, A.D. Beath, E. McCalla, J. van Lierop and J.M. Cadogan, *Transverse spin freezing in $a\text{-}(Fe_{1-x}Mn_x)_{78}Si_8B_{14}$: a site-frustrated metallic glass* (Phys. Rev. B, in press).

A.D. Beath and D.H. Ryan, *Ordering in the site frustrated Heisenberg ferromagnet revisited* (J. Appl. Phys., in press).

R.L. Lichti, S.F.J. Cox, B. Hitti and R.J. Molnar, *Evolution of muonium states in n-type GaN* (submitted to Phys. Rev. B).

J.E. Sonier, K.F. Poon, G.M. Luke, P. Kyriakou, R.I. Miller, P. Fournier and R.L. Greene, *Paramagnetic vortex state in $Pr_{2-x}Ce_xCuO_4$ single crystals* (Physica B, in press).

J.E. Sonier, K.F. Poon, G.M. Luke, P. Kyriakou, R.I. Miller, R. Liang, C.R. Wiebe, P. Fournier and R.L. Greene, *Superconductivity and field-induced magnetism in $Pr_{2-x}Ce_xCuO_4$ single crystals* (submitted to Phys. Rev. Lett.).

Life Sciences

T.E. Barnhart, A.K. Converse, K.A. Dabbs, R.J. Nickles, K. Buckley, S. Jivan, T.J. Ruth and A.D. Roberts, *Water-cooled grid support system for high power irradiation with thin target windows* (Appl. Radiat. Isotopes, in press).

A. Studenov, S. Jivan, K.R. Buckley and M.J. Adam, *Efficient in-loop synthesis of high specific radioactivity $[^{11}C]$Carfentanil* (JLRC, in press).

A.J. Stoessl and R. de la Fuente-Fernandez, *Dopamine receptors in Parkinson's disease: imaging studies* (Advances in Neurol., in press).

J.E. Holden, V. Sossi, G. Chan, D.J. Doudet, A.J. Stoessl and T.J. Ruth, *Effect of population k2 values in graphical estimation of DV ratios of reversible ligands* (submitted to J. Cereb. Blood Flow).

A. Kishore, G.L.-Y. Chan, T. Dobko, M. Schulzer, V. Sossi, R. de la Fuente-Fernandez, E. Mak, T.J. Ruth, D.B. Calne and A.J. Stoessl, *Dopamine D1 and D2 receptors and motor complications in idiopathic Parkinsonism: a PET study* (submitted to Brain).

Z. Huang, R. de la Fuente-Fernandez and A.J. Stoessl, *Etiology of Parkinson's disease* (Can. J. Neurol. Sci., in press).

D.T. Britto and H.J. Kronzucker, *Can unidirectional influx be measured in higher plants? A mathematical approach using parameters from efflux analysis* (New Phytol., in press).

M.Y. Siddiqi, H.J. Kronzucker, D.T. Britto and A.D.M. Glass, *Effect of increasing NH_4^+ on growth of a tomato crop* (J. Plant Nutr. Soil Sci., in press).

S.E. Unkles, D. Zhou, M.Y. Siddiqi, J.R. Kinghorn and A.D.M. Glass, *Apparent genetic redundancy facilitates ecological plasticity for nitrate transport* (EMBO J., in press).

V. Sossi, *Positron emission tomography (PET) advances in neurological applications* (submitted to Nucl. Instrum. Methods A).

R. de la Fuente-Fernandez, S. Furtado, M. Guttman, Y. Furukawa, C.S. Lee, D.B. Calne, T.J. Ruth, S.J. Kish and A.J. Stoessl, *Expression of vesicular monoamine transporter type 2 is not linked to dopamine synthesis: in-vivo evidence from human PET studies* (submitted to Ann. Neurol.).

R. de la Fuente-Fernandez, A.S. Lim, V. Sossi, M.J. Adam, T.J. Ruth, D.B. Calne, A.J. Stoessl and C.S. Lee, *Age and severity of nigrostriatal damage at onset of Parkinson's disease* (Synapse, in press).

V. Sossi, J.E. Holden, R. de la Fuente-Fernandez, T.J. Ruth and A.J. Stoessl, *The effect of dopamine loss and the metabolite 3-O-methyl-[^{18}F]fluorodopa on the relationship between the ^{18}F-fluorodopa tissue input uptake rate constant K_{occ} and the ^{18}F-fluorodopa plasma input uptake rate constant K_i* (J. Cereb. Blood Flow and Metab., in press).

C.S. Lee, M. Schulzer, R. de la Fuente-Fernandez, E. Mak, V. Sossi, T.J. Ruth, D.B. Calne and A.J. Stoessl, *Degeneration of dopamine neurons is self-limiting in Parkinson's disease: causation by an event?* (submitted to Science).

H. Dougan, J.I. Weitz, A.R. Stafford, K.D. Gillespie, P. Klement, J.B. Hobbs and D.M. Lyster, *Evaluation of DNA aptamers directed to thrombin as potential imaging agents* (submitted to Nucl. Med. and Biol.).

Theoretical Program

W.F. Chang and J.N. Ng, *Radiative neutrino masses in 5D SU(5) unification* (submitted to Phys. Rev. D).

E. Vogt, *Single neutron halos in the valley of stability* (submitted to Phys. Lett.) [TRI-PP-02-03].

J. Escher and B.K. Jennings, *Magic numbers and a special class of intruder states* (submitted to Phys. Rev. Lett.) [TRI-PP-02-13].

D.H. Wilkinson, *Super-allowed fermi beta-decay: CKM unitarity* (J. Phys. G: Nucl. Part. Phys., in press) [TRI-PP-02-14].

J. Escher and B.K. Jennings, *Contemplating a new measure for nuclear shell closures* (Revista Mexican de Fisica, in press).

C.P. Liu, G. Prézeau and M.J. Ramsey-Musolf, *Hadronic parity violation and inelastic electron deuteron scattering* (Phys. Rev. C, in press) [nucl-th/0212041].

K. Tsushima and F.C. Khanna, *Properties of charm and bottom hadrons in nuclear matter: a plausible study* (Phys. Lett. B, in press).

K. Tsushima and F.C. Khanna, *Λ_c and Λ_b hypernuclei* (Phys. Rev. C, in press).

C. Barbieri and W.H. Dickhoff, *Extension of the random phase approximation including the selfconsistent coupling to two phonon contributions* (submitted to Phys. Rev. C) [nucl-th/0212025].

A.K. Dutt-Mazumder, *Omega meson propagation in dense nuclear matter and collective excitations* (Nucl. Phys. A, in press) [nucl-th/0207070].

S. Ando, Y.H. Song, T.S. Park, H.W. Fearing and K. Kubodera, *Solar neutrino reactions on deuteron in effective field theory* (Phys. Lett. B, in press) [USC-NT-02-2, SNUTP-02-014, TRI-PP-02-07, nucl-th/0206001].

T. Gorringe and H.W. Fearing, *Induced pseudoscalar coupling of the proton weak interaction* (submitted to Rev. Mod. Phys.) [TRI-PP-02-08, nucl-th/0206039].

R. Lewis, W. Wilcox and R.M. Woloshyn, *The nucleon's strange electromagnetic and scalar matrix elements* (Phys. Rev. D, in press) [BU-HEPP-02-10, TRI-PP-02-15, hep-ph/0210064].

G. Rupak and X. Kong, *Quartet S-wave $p - d$ scattering in EFT* (Nucl. Phys. A, in press) [TRI-PP-01-13, nucl-th/0108059].

E. Vogt, *Pervasive and extreme neutron halos* (resubmitted to Phys. Rev. C) [TRI-PP-01-23].

Conference Publications

Particle, Nuclear and Atomic Physics

C.A. Miller *et al.* (HERMES collaboration), *Single-spin/azimuthal asymmetries in semi-inclusive and exclusive DIS*, Proc. **7th Conf. on Intersections Between Particle and Nuclear Physics (CIPANP 2000), Quebec City, PQ, May 22–28, 2000** (AIP Conf. Proc. **549**, 2002), p.712.

A.S. Levchenko *et al.* (KEK-PS E246 collaboration), *Test of exotic scalar and tensor interactions in K_{e3} decay using stopped positive kaons*, Proc. **3rd Int. Conf. on Nonaccelerator New Physics (NANPino 01), Dubna, Russia, June 19–23, 2001** (Physics of Atomic Nuclei (Yad. Fiz.) **65**, 2002) p.2232 [hep-ex/0111048].

E.F. Zganjar, A. Piechaczek, G.C. Ball, B. Bricault, J.M. D'Auria, J.C. Hardy, D.F. Hodgson, V. Iacob, P. Klages, W.D. Kulp, J.R. Leslie, M. Lipoglavek, J.A. Macdonald, H.-B. Mak, D.M. Moltz, G. Savard, J. von Schwarzenberg, C.E. Svensson, I.S. Towner and J. Wood, *Tests of the standard model from superallowed Fermi β-decay studies: the ^{74}Rb β-decay*, Proc. **3rd Int. Conf on Exotic Nuclei and Atomic Masses (ENAM 2001), Hameenlinna, Finland, July 2–7, 2001** (Eur. Phys. J. **A15**, 2002) p.229.

L. De Nardo, *Measurement of the spin structure function g_1 at HERMES*, Proc. **Advanced Study Inst. on Symmetries and Spin (PRAHA SPIN 2001), Prague, Czech Republic, July 15–28, 2001** (Czech. J. Phys., 2002).

B. Aubert *et al.* (BABAR collaboration), *Investigation of $B \to D^{(*)}\bar{D}^{(*)}K$ decays with the BABAR detector*, Proc. **20th Int. Symp. on Lepton and Photon Interactions at High Energies (LP 01), Rome, Italy, July 23–28, 2001** (Int. J. Mod. Phys., **A17**, 2002) [SLAC-PUB-8924, BABAR-CONF-01-01, hep-ex/0107056].

B. Aubert *et al.* (BABAR collaboration), *Measurement of the branching fraction for the decay $B^0 \to D^{*+}D^{*-}$, ibid.* [SLAC-PUB-8925, BABAR-CONF-01-03, hep-ex/0107057].

B. Aubert *et al.* (BABAR collaboration), *Study of CP violating asymmetries in $B \to \pi^{\pm}\pi^{\mp}, K^{\pm}\pi^{\mp}$ decays, ibid.* [SLAC-PUB-8929, BABAR-CONF-01-05, hep-ex/0107074].

B. Aubert *et al.* (BABAR collaboration), *Search for $B^0 \to a_0^+(980)\pi^-$, ibid.* [SLAC-PUB-8930, BABAR-CONF-01-07, hep-ex/0107075].

B. Aubert *et al.* (BABAR collaboration), *Measurements of B^0 decays to $\pi^+\pi^-\pi^0$, ibid.* [SLAC-PUB-8926, BABAR-CONF-01-10, hep-ex/0107058].

B. Aubert *et al.* (BABAR collaboration), *Study of T and CP violation in $B^0\bar{B}^0$ mixing with inclusive dilepton events, ibid.* [SLAC-PUB-8927, BABAR-CONF-01-17, hep-ex/0107059].

B. Aubert *et al.* (BABAR collaboration), *Measurement of D_s^+ and D_s^{*+} production in B meson decays and from continuum e^+e^- annihilations at $\sqrt{s}$ = 10.6 GeV, ibid.* [SLAC-PUB-8928, BABAR-CONF-01-27, hep-ex/0107060].

R. Meier, *Low-energy pion-proton scattering at TRIUMF and PSI*, Proc. **9th Int. Symp. on Meson-Nucleon Physics and the Structure of the Nucleon (MENU 2001), Washington, DC, July 26–31, 2001** (πN Newsletter **16**, 2002) p.19.

M.M. Pavan, I.I. Strakovsky, R.L. Workman and R.A. Arndt, *The pion nucleon Σ term is definitely large: results from a GWU analysis of πN scattering data, ibid.* 110 [hep-ph/0111066].

H. Denz, *Pion-proton cross sections in the Coulomb-nuclear interference region, ibid.* 302.

M. Croni, B. van den Brandt, R. Bilger, J. Breitschopf, H. Clement, J. Comfort, H. Denz, K. Fohl, E. Friedman, J. Grater, P. Hautle, G.J. Hofman, P. Jesinger, J.A. Konter, S. Mango, R. Meier, M. Pavan, J. Patzold, G.J. Wagner and F. von Wrochem, *Measurement of analyzing powers in πp scattering, ibid.* 305.

B. Seitz, *Single spin asymmetry in hard exclusive electroproduction of π^+ and real photons at HERMES, ibid.* 412.

S.T. Clark *et al.*, *Empirical investigation of extreme single-particle behavior of nuclear quadrupole moments in highly collective $A \sim 150$ superdeformed bands*, Proc. **Int. Nuclear Physics Conference: Nuclear Physics in the 21st Century (INPC), Berkeley, CA, July 30 – August 3, 2001** (AIP, New York, **610**, 2002) p.825.

B. Aubert *et al.* (BABAR collaboration), *Search for B decays into $K^0\bar{K}^0$*, Proc. **9th Int. Symp. on Heavy Flavor Physics, Pasadena, CA, September 10–13, 2001**, eds. A. Ryd and F.C. Porter (AIP, New York, **618**, 2002) [SLAC-PUB-8978, BABAR-CONF-01-04, hep-ex/0109005].

B. Aubert *et al.* (BABAR collaboration), *Study of semi-inclusive production of η' mesons in B decays, ibid.* [SLAC-PUB-8979, BABAR-CONF-01-08, hep-ex/0109034].

B. Aubert *et al.* (BABAR collaboration), *Search for direct CP violation in quasi two body charmless B decays, ibid.* [SLAC-PUB-8980, BABAR-CONF-01-09, hep-ex/0109006].

B. Aubert *et al.* (BABAR collaboration), *Measurement of the branching fraction for $B^+ \to K^{*0}\pi^+$, ibid.* [SLAC-PUB-8981, BABAR-CONF-01-12, hep-ex/0109007].

B. Aubert *et al.* (BABAR collaboration), *Study of $B \to D^{(*)}\bar{D}^{(*)}$ decays with the BABAR detector, ibid.* [SLAC-PUB-8982, BABAR-CONF-01-28, hep-ex/0109009].

B. Aubert *et al.* (BABAR collaboration), *Search for a lifetime difference in D^0 decays, ibid.* [SLAC-PUB-8983, BABAR-CONF-01-29, hep-ex/0109008].

R.L. Helmer *et al.* (SNO collaboration), *First results from the Sudbury Neutrino Observatory*, Proc. **5th KEK Topical Conf.: Frontiers in Flavor Physics (KEKTC5), Tsukuba, Japan, November 20–22, 2001** (Nucl. Phys. B. Proc. Suppl. **111**, 2002), p.122.

W.T.H. van Oers (for the $G\emptyset$ collaboration), *Parity violating electron-proton scattering experiments*, Proc. **Int. Symp. on Electromagnetic Interactions in Nuclear and Hadron Physics (EMI 2001), Osaka, Japan, December 4–7, 2001**, eds. M. Fujiwara and T. Shima (World Scientific, Singapore, 2002) [TRI-PP-02-02].

Y. Itow, T. Kajita, K. Kaneyuki, M. Shiozawa, Y. Totsuka, Y. Hayato, T. Ishida, T. Ishii, T. Kobayashi, T. Maruyama, K. Nakamura, Y. Obayashi, Y. Oyama, M. Sakuda, M. Yoshida, S. Aoki, T. Hara, A. Suzuki, A. Ichikawa, T. Nakaya, K. Nishikawa, T. Hasegawa, K. Ishihara, A. Suzuki and A. Konaka, *The JHF-Kamioka neutrino project*, Proc. **3rd Workshop on Neutrino Oscillations and Their Origin (NOON 2001), Kashiwa, Japan, December 5–8, 2001**, eds. Y. Suzuki *et al.* (World Scientific, Singapore, 2003) p.239 [KEK-REPORT-2001-4, ICRR-REPORT-477-2001-7, TRI-PP-01-05, hep-ex/0106019].

B. Aubert *et al.* (BABAR collaboration), *Improved measurement of the CP violating asymmetry amplitude sin2β*, Proc. **16th Les Rencontres de Physique de la Vallee d'Aoste: Results and Perspectives in Particle Physics,**

La Thuile, Aosta Valley, Italy, March 3–9, 2002, ed. M. Greco (INFN, Frascati, 2002) [SLAC-PUB-9153, BABAR-CONF-02-01, hep-ex/0203007].

D. Bryman, *Rare kaon decays: progress and prospects*, Proc. **Flavor Physics and CP Violation (FPCP), Philadelphia, PA, May 16–18, 2002**, ed. R.G.C. Oldeman (www.slac.stanford.edu/econf/C020516/, 2002) [hep-ex/0206072].

B. Aubert *et al.* (BABAR collaboration), *Evidence for the $b \rightarrow u$ transition $B^0 \rightarrow D_s^+ \pi^-$ and a search for $B^0 \rightarrow D_s^{*+} \pi^-$, ibid.* [SLAC-PUB-9231, BABAR-CONF-02-08, hep-ex/0205102].

B. Aubert *et al.* (BABAR collaboration), *Measurements of the branching fractions of charmless three body charged B decays, ibid.* [SLAC-PUB-9232, BABAR-CONF-02-09, hep-ex/0206004].

B. Aubert *et al.* (BABAR collaboration), *Measurements of charmless two body charged B decays with neutral pions and kaons, ibid.* [SLAC-PUB-9270, BABAR-CONF-02-11, hep-ex/0206053].

A. Olin, S. Bishop, L. Buchmann, M.L. Chatterjee, A. Chen, J.M. D'Auria, S. Engel, D. Gigliotti, W. Greife, D. Hunter, A. Hussein, D. Hutcheon, C. Jewett, J. King, S. Kubono, M. Lamey, A.M. Laird, R. Lewis, W. Liu, S. Michimasa, D. Ottewell, P. Parker, J. Rogers, F. Strieder, M. Wiescher and C. Wrede, *Nuclear astrophysics at ISAC with DRAGON: initial studies*, Proc. **Int. Conf. on Classical Nova Explosions, Sitges, Spain, May 20–24, 2002**, eds. M. Hernanz and J. José (AIP **637**, 2002) p.119.

P. Savard, *et al.* (CDF and D0 collaborations), *Top and Higgs physics at the Tevatron*, Proc. **22nd Physics in Collision Conf. (PIC 2002), Stanford, CA, June 20–22, 2002** (eConf C020620:SABT05, 2002; also in Stanford 2002, Physics in Collision, 304) [FERMILAB-CONF-02-292-E, PIC-2002-SABT05, hep-ex/0209061].

A.W. Poon *et al.* (SNO collaboration), *Solar neutrino observations at the Sudbury Neutrino Observatory*, Proc. **30th SLAC Summer Institute on Particle Physics: Secrets of the B Meson (SSI 2002), SLAC, Menlo Park, CA, August 5–16, 2002** (SLAC Electronic Proceedings Archive, eConf C020805:TTH01, 2002) [hep-ex/0211013].

Instrumentation/Accelerator Physics/Computing Sciences

P. Bricault, R. Baartman, M. Dombsky, A. Hurst, C. Mark, G. Stanford and P. Schmor, *TRIUMF-ISAC target station and mass separator commissioning*, Proc. **5th Int. Conf. on Radioactive Nuclear Beams (RNB5), Divonne, France, April 3–8, 2000**, eds. H.L. Ravn, T. Lettry and T. Nilsson (Nucl. Phys. **A701**, 2002) p.49 [TRI-PP-00-12].

S. Engel, S. Bishop, A. Chen, C. Dale, J.M. D'Auria, U. Giesen, U. Greife, R. Henderson, D. Hunter, D. Hutcheon, R. Openshaw, J. Rogers, C. Rolfs and A. Shotter, *Development of detection systems for low-energy heavy ions at DRAGON, ibid.* 228 [TRI-PP-00-17].

C.D.P. Levy, R. Baartman, K. Jayamanna, R. Kiefl, T. Kuo, M. Olivo, G.W. Wight, D. Yuan and A.N. Zelenski, *A polarized beams project at ISAC, ibid.* 253 [TRI-PP-00-13].

P.W. Schmor, *Target handling at high-intensity RNB facilities, ibid.* 480 [TRI-PP-00-14].

M. Dombsky, P. Bricault, T. Hodges, A. Hurst and P. Schmor, *Online isotope separation at ISAC with a $10\,\mu A$ proton driver beam, ibid.* 486 [TRI-PP-00-15].

J. D'Auria, *Astrophysics with a DRAGON at ISAC, ibid.*, 625 [TRI-PP-00-10].

R.E. Laxdal, R.A. Baartman, P. Bricault, G. Dutto, R. Poirier, P. Schmor and G. Stanford, *RNB post-accelerator for ISAC at TRIUMF – present and future, ibid.*, 647 [TRI-PP-00-16].

R.E. Laxdal, *ISAC at TRIUMF: status of the post-accelerator*, Proc. **Int. Workshop on Production of Radioactive Ion Beams (PRORIB 2001), Puri, India, February 12–17, 2001** (Indian J. Phys. **76S**, 2002) [TRI-PP-01-03].

R. Baartman, *Low energy beam transport design optimization for RIBs, ibid.* 149.

N.J. Buchanan and D.M. Gingrich, *Radiation concerns in high-energy physics and the switched capacitor array controller in ATLAS*, Proc. **Lake Louise Winter Institute on Fundamental Interactions, Lake Louise, AB, February 18–24, 2001** (World Scientific, Singapore, 2002) p.134.

P.-A. Amaudruz, R. Poutissou *et al.*, *Real time control/monitoring and data acquisition system for nuclear polarization experiments with implanted radioactive ions*, Proc. **12th IEEE Real Time Conf. on Nuclear and Plasma Sciences, Valencia, Spain, June 4–8, 2001** (IEEE Trans. Nucl. Sci. **49**, 2002).

A. Radu, R.K. Mommsen, J.T.M. Baines, A. Baratella, P. Morettini, F. Parodi, B.L. Caron, R.A. Davis, J. Pinfold, A. Di Mattia, S. Falciano, A. Nisati, S. Robins, M. Elsing, D. Wicke, B. Epp, V.M. Ghete, A. Nairz, B. Gonzalez-Pineiro, R. Hauser, S. George, D. Hutchcroft, W. Li, S. Gonzalez, S. Qian, W. Wiedenmann, T. Hansl-Kozanecka, N. Nikitin, F. Rizatdinova, S. Sivoklokov, A. Negri, G. Polesello, D. Scannicchio, V. Vercesi, J. Shank, C. Slowe, P. Sherwood, M. Smizanska, T. Shears, M. Sessler, S. Tapprogge and M. Wielers, *High-level triggers in ATLAS, ibid.* 377, erratum *ibid.* 2037.

M. Barnes and G. Wait, *A FET based kicker for a charge booster for the TRIUMF-ISAC project*, Proc. **13th IEEE Int. Pulsed Power Conf., Las Vegas, NV, June 17–22, 2001** (IEEE, 2002) p.1245 [TRI-PP-01-12].

P.W. Schmor, *Ion sources for radioactive ion beams in ISOL facilities*, Proc. **9th Int. Conf. on Ion Sources, Oakland, CA, September 3–7, 2001** (Rev. Sci. Instrum. **73**, 2002) p.707.

T. Lamy, J.L. Bouly, J.C. Curdy, R. Geller, A. Lacoste, P. Sole, P. Sortais, T. Thuillier, J.L. Vieux-Rochaz, K. Jayamanna, M. Olivo, P. Schmor and D. Yuan, *Charge state breeding applications with the ECR PHOENIX source: from low to high current production, ibid.* 717.

K. Jayamanna, D. Yuan, M. Dombsky, P. Bricault, M. McDonald, M. Olivo, P. Schmor, G. Stanford, J. Vincent and A. Zyuzin, *A design of an ECR ion source for radioactive ion beams for ISAC on-line facility at TRIUMF, ibid.* 792.

A. Zelensky, J. Alessi, B. Briscoe, H. Huang, A. Kponou, A. Lehrach, V. Lodestro, D. Raparia, J. Ritter, G. Dutto, P. Levy, G. Wight, S. Kokhanovsky, V. Klenov, V. Zoubets, Y. Mori, M. Okamura and T. Takeuchi, *Optically pumped polarized H^- ion source for RHIC spin physics, ibid.* 888.

T. Kuo, R. Baartman, G. Dutto, S. Hahto, J. Ärje and E. Liukkonen, *A high intensity DC H^- source for low energy injection, ibid.* 986.

G. Dutto, P. Bricault, R. Baartman, K. Fong, R.E. Laxdal, G. Mackenzie, M. Pasini, R. Poirier, P.W. Schmor, G. Stinson and A. Facco, *Completion of the ISAC-I accelerator for radioactive ions and extension to ISAC-II*, Proc. **2nd Asian Particle Accelerator Conf. (APAC01), Beijing, China, September 17–21, 2001** (Inst. of High Energy Physics, Chinese Acad. of Sciences, Beijing, 2002) p.143 [TRI-PP-01-24].

R. Assmann, J.B. Jeanneret and D. Kaltchev, *Status of robustness studies for the LHC collimator, ibid.* 204.

K. Fong, M. Laverty and S. Fang, *RF control systems for the TRIUMF ISAC rf, ibid.* 642.

G. Clark, *Construction and measurements of the pre-series twin aperture resistive quadrupole magnet for the LHC beam cleaning insertions*, Proc. **17th Int. Conf. on Magnet Technology (MT17), Geneva, Switzerland, September 24–28, 2001** (IEEE Trans. Appl. Superconductivity, 2002).

G. Clark, *Analysis of lamination measurements for CERN's twin aperture quadrupoles, ibid.*

M. Aleksa, S. Amet, L. Bottura, M. Buzio, P. Ferracin, O. Pagano, V. Remondino, S. Russenschuck, S. Sanfilippo, W. Scandale, E. Todesco and Z. Ang, *Measurement and analysis of the field quality of LHC prototype and pre-series superconducting dipoles, ibid.* [CERN-LHC-PROJECT-REPORT-558].

W. Venturini Delsolaro, Z. Ang, L. Bottura, S. Sanfilippo, A. Siemko, D. Tommasini and L. Walckiers, *Field quality of the short superconducting dipole models for the LHC, ibid.* [CERN-LHC-PROJECT-REPORT-563].

A. Zelenski, J. Alessi, B. Briscoe, G. Dutto, H. Huang, A. Kponou, S. Kokhanovski, V. Klenov, A. Lehrach, P. Levy, V. Lodestro, Y. Mori, M. Okamura, D. Raparia, J. Ritter, T. Takeuchi, G. Wight and V. Zoubets *An optically-pumped polarized H^- ion source for RHIC SPIN physics*, Proc. **9th Int. Workshop on Polarized Sources and Targets (PST2001), Nashville, IN, September 30–October**

4, 2001, eds. V.P. Derenchuk and B. von Przewoski (World Scientific, Singapore, 2002), p.194.

W.D. Ramsay *et al.*, *A high precision scanning polarimeter for the TRIUMF proton-proton parity violation experiment, ibid.* 289.

C.D.P. Levy, R. Baartman, J.A. Behr, A. Hatakeyama, Y. Hirayama, R.F. Kiefl, G.D. Morris, R. Nussbaumer, R. Poutissou and G.W. Wight, *A highly polarized $^8Li^+$ ion beam at ISAC, ibid.* 334.

A. Hatakeyama, Y. Hirayama, J.A. Behr, H. Izumi, C.D.P. Levy, D. Melconian and T. Shimoda, *Optical pumping at the ISAC polarizer, ibid.* 339.

D. Karlen, *Credibility of confidence intervals*, Proc. **Advanced Statistical Techniques in Particle Physics, Durham, UK, March 18–22, 2002**, eds. M.R. Whalley and L. Lyons (IPPP, Durham, 2002) p.53.

I.L. Azhgirei, R. Assmann, I.S. Baishev, J.B. Jeanneret, D. Kaltchev, T. Kurtyka and A. Wroblewski, *Beam loss and collimation at LHC*, Proc. **20th ICFA Advanced Beam Dynamics Workshop on High Intensity and High Brightness Hadron Beams (ICFA - HB2002), Batavia, IL, April 8–12, 2002**, eds. W. Chou, Y. Mori, D. Neuffer, J.-F. Ostiguy Melville (AIP Conf. Proc. **642**, 2002) [CERN-LHC-PROJECT-REPORT-603, LHC-PROJECT-REPORT-603].

C.J. Johnstone and S. Koscielniak, *Rapid acceleration in an FFAG using high-frequency rf, ibid.* 207 [FERMILAB-CONF-02-223-T].

R. Baartman, *Isochronous and scaling FFAGs, ibid.*

D. Kaltchev and F. Zimmermann, *On the transparency of the electron cloud to synchrotron radiation*, Proc. **Mini Workshop on Electron Cloud Simulations for Proton and Positron Beams (ECLOUD'02), Geneva, April 15–18, 2002**, eds. G. Rumolo and F. Zimmermann (CERN, Geneva, 2002) p.243 [CERN-2002-001].

R.W. Assmann, I. Baishev, M. Brugger, L. Bruno, H. Burkhardt, G. Burtin, B. Dehning, C. Fischer, B. Goddard, E. Gschwendtner, M. Hayes, J.B. Jeanneret, R. Jung, V. Kain, D. Kaltchev, M. Lamont, R. Schmidt, E. Vossenberg, E. Weisse and J. Wenninger, *Requirements for the LHC collimation system*, Proc. **8th European Particle Accelerator Conf.: a Europhysics Conf. (EPAC 2002), Paris, France, June 3–7, 2002**, eds. T. Garvey *et al.* (European Physical Society Interdivisional Group on Accelerators and CERN, 2002) p.197 [CERN-LHC-PROJECT-REPORT-599, LHC-PROJECT-REPORT-599].

R.W. Assmann, J.B. Jeanneret and D. Kaltchev, *Efficiency for the imperfect LHC collimation system, ibid.* 293 [CERN-LHC-PROJECT-REPORT-598, LHC-PROJECT-REPORT-598].

S. Koscielniak, *New potential function for RFQ accelerator cells, ibid.* 918.

290

M. Pasini, R.E. Laxdal and P.N. Ostroumov, *Beam dynamics studies on the ISAC-II post-accelerator at TRIUMF, ibid.* 933.

M. Pasini and R.E. Laxdal, *An isopath achromatic bending section for multi-charge ion beam transport at ISAC-II, ibid.* 1175.

C. Johnstone and S. Koscielniak, *Recent progress on FFAGs for rapid acceleration, ibid.* 1261.

T. Lamy, J.C. Curdy, R. Geller, C. Peaucelle, P. Sole, P. Sortais, T. Thuillier, D. Voulot, K. Jayamanna, M. Olivo, P. Schmor and D. Yuan, *Charge breeding method results with the PHOENIX ECR ion source, ibid.* 1724.

M. Mouat, E. Klassen, K.S. Lee, J.J. Pon and P.J. Yogendran, *Disk storage upgrade in TRIUMF's central control system, ibid.* 2037.

A.K. Mitra, Z.T. Ang, I.V. Bylinskii, K. Fong, P. Harmer, R.E. Laxdal, J. Lu, R.L. Poirier and B. Waraich, *RF test and commissioning of the low and high beta bunchers for the TRIUMF ISAC facility, ibid.* 2178.

K. Fong, S. Fang and M. Laverty, *RF control system for ISAC-II superconducting cavities, ibid.* 2226.

M.J. Barnes, G.D. Wait and L. Ducimetière, *Low voltage measurements on nine PFNs for the LHC injection kicker systems, ibid.* 2520 [TRI-PP-02-09].

W. Zhang, J. Sandberg, J. Tuozzolo, R. Cassel, L. Ducimetière, C. Jensen, M. Barnes, G. Wait and J. Wang, *An overview of high voltage dielectric material for traveling wave kicker magnet application*, Proc. **25th Int. Power Modulator Conf. and High Voltage Workshop, Hollywood, CA, June 30 – July 3, 2002** (IEEE, 2002) p.674 [TRI-PP-02-10, SLAC-REPRINT-2002-194, FERMILAB-CONF-02-166-E].

D.M. Gingrich, N.J. Buchanan, L. Chen and S. Liu, *Ionizing radiation effects in EPF10K50E and XC2S150 programmable logic devices*, Proc. **2002 IEEE Nuclear and Space Radiation Effects Conf. (NSREC 2002), Phoenix, AZ, July 15–19, 2002**, ed. S.C. Witczak (IEEE Trans. Nucl. Sci. **49**, 2002) p.41.

P. Paillet, J.R. Schwank, M.R. Shaneyfelt, V. Ferlet-Cavrois, R.L. Jones. O. Flament and E.W. Blackmore, *Comparison of charge yield in MOS devices for different radiation sources, ibid.* 2656.

Chemistry and Solid-State Physics

H.-H. Klauss, W. Wagener, W. Kopmann, D. Baabe, D. Mienert, F.J. Litterst, M. Hücker and B. Büchner, *Magnetic stripe order in $La_{1.8-x}Eu_{0.2}Sr_xCuO_4$*, Proc. **2001 Strongly Correlated Electron Systems Conf. (SCES 2001), Ann Arbor, MI, August 6–10, 2001** (Physica **B312-313**, 2002) p.71.

J.E. Sonier and J.H. Brewer, *μSR detection of weak magnetism in superconducting $YBa_2Cu_3O_{6+x}$, ibid.* 77.

D.R. Noakes, G.M. Kalvius, H. Nakotte, E. Schreier and R. Wäppling, *Magnetic ordering in UPdSn and CeCuSn, ibid.* 292.

H.-H. Klauss, M.A.C. de Melo, S. Süllow, H. Walf, D. Mienert, D. Baabe, F.J. Litterst and C. Geibel, *The magnetic phases of $Ce(Cu_{1-x}Ni_x)_2Ge_2$, ibid.* 425.

D.E. MacLaughlin, O.O. Bernal, R.H. Heffner, G.J. Nieuwenhuys, M.S. Rose, J.E. Sonier, B. Andraka, R. Chau and M.B. Maple, *Slow spin dynamics in non-Fermi-liquid $UCu_{5-x}Pd_x$, x = 1.0 and 1.5, ibid.* 453.

A. Kratzer, D.R. Noakes, G.M. Kalvius, E. Schreier, R. Wäppling, K. Umeo, T. Takabatake and H.v. Löhneysen, *μSR studies of the heavy fermion compound Ce_7Ni_3, ibid.* 469.

N. Büttgen, A. Krimmel, A. Loidl, M. Klemm, S. Horn, D.R. Noakes, E. Schreier and G.M. Kalvius, *Magnetic correlations in frustrated LiV_2O_4 and ZnV_2O_4, ibid.* 703.

H. Takagiwa, K. Ohishi, J. Akimitsu, W. Higemoto, R. Kadono, F. Iga and M. Sera, *Magnetic properties in phase IV of $Ce_{0.8}Nd_{0.2}B_6$ studied by muon spin relaxation*, Proc. **Int. Conf. on Strongly Correlated Electrons with Orbital Degrees of Freedom (ORBITAL2001), Sendai, Japan, September 11–14, 2001** (J. Phys. Soc. Jpn. Suppl. **71**, 2002) p.118.

K. Ohishi, T. Muranaka, J. Akimitsu, W. Higemoto and R. Kadono, *Physical properties in flux line lattice state in MgB_2 probed by μSR, ibid.*, 335.

R.L. Lichti, *Sites and dynamics for muonium in III-V semiconductors*, Proc. **Hydrogen Workshop 2002** (Hydrogen in Materials and Vacuum Systems, AIP, 2002).

J.D. Dow and D.R. Harshman, *Proofs that high-temperature superconductivity is in BaO, SrO or interstitial-oxygen layers, and is s-wave paired and p-type*, Proc. **10th Int. Ceramics Congress and 3rd Forum on New Materials (CIMTEC 2002), Florence, Italy, July 14–18, 2002**, ed. P. Vincenzini (Techna Pub., S.Rr. L., Faenza, Italy, 2002).

Theoretical Program

A.D. Lahiff and I.R. Afnan, *Pion-nucleon scattering in a Bethe-Salpeter approach*, Proc. **9th Int. Symp. on Meson-Nucleon Physics and the Structure of the Nucleon (MENU 2001), Washington, DC, July 26–31, 2001** (πN Newsletter **16**, 2002) p.92 [nucl-th/0109054].

A.D. Lahiff, *Covariant meson exchange model of the $\bar{K}N$ interaction, ibid.* 385 [nucl-th/0110028].

R. Lewis, N. Mathur and R.M. Woloshyn, *Spin splittings among charmed hadrons*, Proc. **19th Int. Symp. on Lattice Field Theory (Lattice 2001), Berlin, Germany, August 19–24, 2001**, eds. M. Müller-Preussker *et al.* (Nucl. Phys. B, proc. suppl. **106**, 2002) p.370 [hep-lat/0109014].

N. Mathur, R. Lewis and R.M. Woloshyn, *Heavy baryons from lattice NRQCD, ibid.* 400 [TRI-PP-01-22, hep-lat/0110031].

O. Scholten, S. Kondratyuk, L. Van Daele, D. van Neck, M. Waroquier and A.Yu. Korchin, *Compton scattering on the proton and light nuclei in the delta-resonance region*, Proc. **6th TAPS Workshop, Krzyze, Poland, September 9–13, 2001** (Acta Phys. Polon. **B33**, 2002) p.847.

C.Q. Geng and J.N. Ng, *Testing discrete symmetries with the decay* $\eta \to \pi^+ \pi^- \gamma$, Proc. **Workshop on Eta Physics: Prospects of Precision Measurements with the CELSIUS/WASA Facility, Uppsala, Sweden, October 25–27, 2001** (Phys. Scripta **T99**, 2002), p.109.

R. Lewis, W. Wilcox and R.M. Woloshyn, *Strange quark current in the nucleon from lattice QCD*, Proc. **Int. Symp. on Electromagnetic Interactions in Nuclear and Hadron Physics (EMI 2001), Osaka, Japan, December 4–7, 2001**, eds. M. Fujiwara and T. Shima (World Scientific, Singapore, 2002) p.537 [BU-HEPP-06-01, TRI-PP-02-01, hep-ph/0201190].

O. Scholten and S. Kondratyuk, *Compton scattering on the proton, ibid.* 515 [nucl-th/0203077].

R. Allahverdi and M. Drees, *Heavy particle production during reheating*, Proc. **10th Int. Conf. on Supersymmetry and Unification of Fundamental Interactions (SUSY02), Hamburg, Germany, June 17–23, 2002**, eds. P. Nath, P.M. Zerwas and C. Grosche (DESY, Hamburg, **2**, 2002) p.1183 [hep-ph/0210432].

Conference Presentations

Particle, Nuclear and Atomic Physics

D.M. Gingrich, *Search for Higgs bosons and new particles with OPAL*, Proc. **Canadian Association of Physicists, Congress, York, ON, 2002**.

A. Shotter, *Radioactive beams at TRIUMF – current situation – future prospectives*, Proc. **Teatro Congressi, EURISOL, Abano Terme, Italy, January 24–26, 2002**.

L. Buchmann, *Strong resonances in elastic scattering of radioactive ^{21}Na on protons*, Proc. **Western Regional Nuclear and Particle Physics Conf. (WRNPPC'02), Lake Louise, AB, February 15–17, 2002**.

J.-M. Poutissou, *The TWIST experiment at TRIUMF, ibid.*

S.-M. Chen, *Measurement of rare kaon decay* $K^+ \to \pi^+ \nu \bar{\nu}$, Proc. **37th Rencontres de Moriond on Electroweak Interactions and Unified Theories, Les Arcs, France, March 9–16, 2002** [hep-ex/0205031].

B. Aubert *et al.* (BABAR collaboration), *Measurements of branching fractions and CP violating asymmetries in* $B^0 \to \pi^+ \pi^-$, $K^+ \pi^-$, $K^+ K^-$ *decays, ibid.* [SLAC-PUB-9229, BABAR-CONF-02-07, hep-ex/0205082].

B. Aubert *et al.* (BABAR collaboration), *Rare B decays to states containing a J/ψ meson*, Proc. **37th Rencontres de Moriond on QCD and Hadronic Interactions, Les Arcs, France, March 16–23, 2002** [SLAC-PUB-9166, BABAR-CONF-02-06, hep-ex/0203035].

B. Aubert *et al.* (BABAR collaboration), *Measurement of the B^0 lifetime with partial reconstruction of* $\bar{B}^0 \to D^{*+} \rho^-$, *ibid.* [SLAC-PUB-9169, BABAR-CONF-02-003, hep-ex/0203036].

B. Aubert *et al.* (BABAR collaboration), *Measurement of the neutral B^0 lifetime using partially reconstructed* $B^0 \to D^{*-} \pi^+$ *decays, ibid.* [SLAC-PUB-9185, BABAR-CONF-02-02, hep-ex/0203038].

B. Aubert *et al.* (BABAR collaboration), *Branching fraction measurements of the decays* $B \to \eta_c K$, *where* $\eta_c \to K \bar{K} \pi$ *and* $\eta_c \to 4K$, *ibid.* [SLAC-PUB-9170, BABAR-CONF-02-05, hep-ex/0203040].

B. Aubert *et al.* (BABAR collaboration), *A measurement of the $B^0 \to J/\psi \pi^+ \pi^-$ branching fraction, ibid.* [SLAC-PUB-9171, BABAR-CONF-02-04, hep-ex/0203034].

J.A. Behr, *Atom trap studies of beta decay*, Proc. **Low Energy Precision Measurements Workshop (LEPEM), TRIUMF, Vancouver, BC, April 4–6, 2002**.

N. Rodning (TWIST collaboration), *TWIST, a precision measurement of muon decay, ibid.*

J.N. Ng, *Some low energy precision tests of brane models, ibid.*

A. Shotter, *Nuclear astrophysics at TRIUMF*, Proc. **Inst. of Physics, Physics Congress 2002, Brighton, UK, April 8–11, 2002**.

S.A. Page, *Parity violation in the nucleon-nucleon system: recent results and future prospects*, Proc. **APS 2002, Albuquerque, NM, April 20–23, 2002**.

J.M. D'Auria, J. Thomson and M. Comyn (editors), Proc. **14th Int. Conf. on Electromagnetic Isotope Separators and Techniques Related to Their Applications (EMIS-14), Victoria, BC, May 6–10, 2002** (Nucl. Instrum. Methods B, in press).

D. Gigliotti, J.G. Rogers and A.H. Hussein, *Calibration and simulation of a gamma array for DRAGON at ISAC, ibid.* [TRI-PP-02-19].

A.A. Chen *et al.* (DRAGON collaboration), *Results from the development of ionization detection systems for the DRAGON facility, ibid.* [TRI-PP-02-20].

S. Engel *et al.* (DRAGON collaboration), *Commissioning and operation of DRAGON, ibid.* [TRI-PP-02-21].

J.A. Behr, *Neutral atom traps of radioactives, ibid.* [TRI-PP-02-22].

A. Shotter, *Advances at ISOL facilities, ibid.* [TRI-PP-02-23].

R. Baartman, *Low energy beam transport design optimization for RIBs, ibid.* [TRI-PP-02-24].

R.E. Laxdal, *Acceleration of radioactive ions, ibid.* [TRI-PP-02-25].

G.-J. Beyer and T.J. Ruth, *The role of electromagnetic separators in the production of radiotracers for bio-medical research and nuclear medical application, ibid.* [TRI-PP-02-26].

P. Bricault, M. Dombsky, A. Dowling and M. Lane, *High power target developments at ISAC, ibid.* [TRI-PP-02-27].

D. Melconian, D. Ashery, G. Ball, J.A. Behr, P. Bricault, B.A. Brown, M. Dombsky, K.P. Jackson, S. Fostner, A. Gorelov, M.N. Groves, S. Gu, M.R. Pearson, I.S. Towner, M. Trinczek and I. Vollrath, *Measuring isospin mixing in ^{36}Ar using a polarized, neutral atom trap, ibid.* [TRI-PP-02-28].

R.F. Kiefl, W.A. MacFarlane, P. Amaudruz, D. Arseneau, R. Baartman, T.R. Beal, A. Hatakeyama, B. Hitti, S.R. Kreitzman, C.D.P. Levy, R. Miller, M. Olivo, R. Poutissou, G.D. Morris, S.R. Dunsiger, R. Heffner, K.H. Chow, Y. Hirayama, H. Izumi, C. Bommas, E. Dumont and L.H. Greene, *Low energy spin polarized radioactive beams as a probe of thin films and interfaces, ibid.* [TRI-PP-02-29].

J. Dilling, P. Bricault, M. Smith, H.-J. Kluge *et al.* (TITAN collaboration), *The proposed TITAN facility at ISAC for very precise mass measurements on highly charged short-lived isotopes, ibid.* [TRI-PP-02-30].

M. Dombsky, P. Bricault, P. Schmor and M. Lane, *ISAC target operation with high proton currents, ibid.* [TRI-PP-02-31].

S. Lapi, T.J. Ruth, A. Zyuzin and J.M. D'Auria, *Development of an intense ^{15}O radioactive ion beam using low energy protons, ibid.* [TRI-PP-02-32].

C.D.P. Levy, A. Hatakeyama, Y. Hirayama, R.F. Kiefl, R. Baartman, J.A. Behr, H. Izumi, D. Melconian, G.D. Morris, R. Nussbaumer, M. Olivo, M. Pearson, R. Poutissou and G.W. Wight, *Polarized radioactive beam at ISAC, ibid.* [TRI-PP-02-33].

S. Engel, L. Buchmann, A. Chen, J.M. D'Auria, D.A. Hutcheon, C.S. Galovich, D. Gigliotti, U. Greife, D. Hunter, A. Hussein, C.C. Jewett, W. Liu, A. Olin, D. Ottewell and J. Rogers, *Testing the ISAC radioactive ion accelerator beam specifications using the $H(^{15}N, \alpha\gamma)^{12}C$ reaction, ibid.*

C. Wrede, A. Hussein, J.G. Rogers and J. D'Auria, *A double sided silicon strip detector as a DRAGON end detector, ibid.*

C.E. Svensson, R.A.E. Austin, G.C. Ball, P. Finlay, P.E. Garrett, G.F. Grinyer, G.S. Hackman, C.J. Osborne, F. Sarazin, H.C. Scraggs, M.B. Smith and J.C. Waddington, *Radioactive beam experiments with large gamma-ray detector arrays, ibid.*

W.T.H. van Oers *Proton-proton parity violation experiments*, Proc. **APS North West Section Meeting, Banff, AB, May 17–18, 2002**.

A. Shotter, *ISAC nuclear physics programme, ibid.*

D. Sinclair, *The international facility for underground science*, Proc. **National Academy for the Advancement of Science, Washington, DC, June, 2002**.

W.T.H. van Oers *Proton-proton parity violation experiments*, Proc. **CAP Annual Congress, Quebec City, PQ, June 2–5, 2002**.

J. Dilling *et al.* (TITAN collaboration), *The proposed TITAN facility for high precision mass measurements and more, ibid.*

A. Konaka, *Neutrino oscillation, ibid.*

A. Shotter, *The TRIUMF nuclear astrophysics mission, ibid.*

D. Bryman, *The rare kaon decays $K^+ \rightarrow \pi^+\nu\bar{\nu}$ and $K_L^0 \rightarrow \pi^0\nu\bar{\nu}$: progress and prospects*, Proc. **14th Rencontres De Blois: Matter – Anti-Matter Asymmetry, Chateau de Blois, France, June 17–22, 2002** [TRI-PP-02-17].

J.-M. Poutissou and K. Yoshimura, *Non-neutrino physics working group summary*, Proc. **4th NuFact'02 Workshop (Neutrino Factories based on Muon Storage Rings), London, UK, July 1–6, 2002** (J. Phys. G, in press).

S.H. Park, A.R. Junghans, E.C. Mohrmann, K.A. Snover, T.D. Steiger, E.G. Adelberger, J.M. Cajandian, H.E. Swanson, L. Buchmann, A. Zyuzin and A. Laird, *A new measurement of $^7Be(p,\gamma)^8B$ cross section and its astrophysical meaning*, Proc. **7th Int. Symp. on Nuclei in the Cosmos (NIC7), Fuji-Yoshida, Japan, July 8–12, 2002** (Nucl. Phys. A, in press).

R.E. Azuma, S. Bishop, L. Buchmann, M.L. Chatterjee, A.A. Chen, J.M. D'Auria, T. Davinson, S. Engel, B.R. Fulton, D. Gigliotti, U. Greife, D. Groombridge, D. Hunter, A. Hussein, D. Hutcheon, C. Jewett, J.D. King, N. Khan, S. Kubono, A.M. Laird, M. Lamey, R. Lewis, L. Ling, W. Liu, S. Michimasa, A.S. Murphy, A. Olin, D. Ottewell, P. Parker, J. Pearson, I. Roberts, A. Robinson, J.G. Rogers, G. Roy, C. Ruiz, F. Sarazin, A.C. Shotter, H. Sprenger, F. Strieder, P. Walden, P.J. Woods and C. Wrede, *Results of $^{21}Na + p$ experiments at ISAC, ibid.*

J.C. Blackmon, D.W. Bardayan, W. Bradfield-Smith, R. Brummit, A.E. Champagne, A.A. Chen, T. Davinson, L. Dessieux, M.W. Guidry, K.I. Hahn, G.M. Hale, W.R. Hix, R.L. Kozub, Z. Ma, P.D. Parker, G. Rajbaidya, R.C. Runkle, C.M. Rowland, A.C. Shotter, M.S. Smith, L.A. Van Wormer, D.W. Visser and P.J. Woods, *The $^{14}O(\alpha,p)^{17}F$ reaction rate, ibid.*

S. Bishop, R. Azuma, L. Buchmann, A.A. Chen, M.L. Chatterjee, J.M. D'Auria, S. Engel, D. Gigliotti, U. Greife, D. Hunter, A. Hussein, D. Hutcheon, C. Jewett, J. King,

S. Kubono, M. Lamey, R. Lewis, W. Liu, S. Michimasa, A. Olin, D. Ottewell, P.D. Parker, J. Rogers and C. Wrede, *Nuclear astrophysics studies at DRAGON: the $^{21}Na(p,\gamma)^{22}Mg$ reaction and oxygen-neon novae, ibid.*

D.A. Hutcheon, S. Bishop, L. Buchmann, M.L. Chatterjee, A.A. Chen, J.M. D'Auria, S. Engel, D. Gigliotti, U. Greife, D. Hunter, A. Hussein, C. Jewett, N. Khan, A. Lamey, W. Liu, A. Olin, D. Ottewell, J.G. Rogers, G. Roy, H. Sprenger and C. Wrede, *The DRAGON facility for nuclear astrophysics at TRIUMF-ISAC, ibid.*

F. Sarazin, L. Buchmann *et al.* (TUDA collaboration), *($^{3}He,p$) as an alternative to resonant elastic scattering, ibid.*

S. Michimasa, S. Kubono, S.H. Park, T. Teranishi, Y. Yanagisawa, N. Imai, Zs. Fülöp, X. Liu, T. Minemura, C.C. Yun, J.M. D'Auria and K.P. Jackson, *Study on the $^{21}Na(p,\gamma)^{22}Mg$ stellar reaction by the (p,t) reaction, ibid.*

B. Aubert *et al.* (BABAR collaboration), *A study of the rare decays $B^0 \to D_s^{(*)+}\pi^-$ and $B^0 \to D_s^{(*)-}K^+$*, Proc. **31st Int. Conf. on High Energy Physics (ICHEP 2002), Amsterdam, July 24–31, 2002** (Elsevier Science BV, in press) [SLAC-PUB-9302, BABAR-CONF-02-034, hep-ex/0207053].

B. Aubert *et al.* (BABAR collaboration), *A study of time dependent CP asymmetry in $B^0 \to J/\psi\pi^0$ decays, ibid.* [SLAC-PUB-9298, BABAR-CONF-02-015, hep-ex/0207058].

B. Aubert *et al.* (BABAR collaboration), *A search for the decay $B^0 \to \pi^0\pi^0$, ibid.* [SLAC-PUB-9310, BABAR-CONF-02-32, hep-ex/0207063].

B. Aubert *et al.* (BABAR collaboration), *Measurements of branching fractions and direct CP asymmetries in $\pi^+\pi^0$, $K^+\pi^0$ and $K^0\pi^0 B$ decays, ibid.* [SLAC-PUB-9304, BABAR-CONF-02-13, hep-ex/0207065].

B. Aubert *et al.* (BABAR collaboration), *Measurement of the branching fraction for $B^\pm \to \chi_{e0}K^\pm$, ibid.* [SLAC-PUB-9316, BABAR-CONF-02-22, hep-ex/0207066].

B. Aubert *et al.* (BABAR collaboration), *Search for CP violation in $B^0\bar{B}^0$ decays to $\pi^+\pi^-\pi^0$ and $K^\pm\pi^\mp\pi^0$ in regions dominated by the $\rho^\pm$ resonance, ibid.* [SLAC-PUB-9303, BABAR-CONF-02-033, hep-ex/0207068].

B. Aubert *et al.* (BABAR collaboration), *A search for $B^+ \to K^+\nu\bar{\nu}$, ibid.* [SLAC-PUB-9309, BABAR-CONF-02-027, hep-ex/0207069].

B. Aubert *et al.* (BABAR collaboration), *Measurement of $sin2\beta$ in $B^0 \to \phi K_s^0$, ibid.* [SLAC-PUB-9297, BABAR-CONF-02-016, hep-ex/0207070].

B. Aubert *et al.* (BABAR collaboration), *Simultaneous measurement of the B^0 meson lifetime and mixing frequency with $B^0 \to D^{*-}\ell^+\nu_\ell$ decays, ibid.* [SLAC-PUB-9307, BABAR-CONF-02-21, hep-ex/0207071].

B. Aubert *et al.* (BABAR collaboration), *Measurement of time dependent CP asymmetries and the CP odd fraction in the decay $B^0 \to D^{*+}D^{*-}$, ibid.* [SLAC-PUB-9299, BABAR-CONF-02-14, hep-ex/0207072].

B. Aubert *et al.* (BABAR collaboration), *Search for the exclusive radiative decays $B \to \rho\gamma$ and $B^0 \to \omega\gamma$, ibid.* [SLAC-PUB-9319, BABAR-CONF-02-024, hep-ex/0207073].

B. Aubert *et al.* (BABAR collaboration), *$b \to s\gamma$ using a sum of exclusive modes, ibid.* [SLAC-PUB-9308, BABAR-CONF-02-25, hep-ex/0207074].

B. Aubert *et al.* (BABAR collaboration), *Determination of the branching fraction for inclusive decays $B \to X_s\gamma$, ibid.* [SLAC-PUB-9301, BABAR-CONF-02-026, hep-ex/0207076].

B. Aubert *et al.* (BABAR collaboration), *Measurement of $B^0 \to D_s^{(*)+}D^{*-}$ branching fractions and polarization in the decay $B^0 \to D_s^{*+}D^{*-}$ with a partial reconstruction technique, ibid.* [SLAC-PUB-9321, BABAR-CONF-02-20, hep-ex/0207079].

B. Aubert *et al.* (BABAR collaboration), *Measurement of the CKM matrix element $|V_{ub}|$ with charmless exclusive semileptonic B meson decays at BABAR, ibid.* [SLAC-PUB-9305, BABAR-CONF-02-030, hep-ex/0207080].

B. Aubert *et al.* (BABAR collaboration), *Measurement of the inclusive electron spectrum in charmless semileptonic B decays near the kinematic endpoint, ibid.* [SLAC-PUB-9282, BABAR-CONF-02-012, hep-ex/0207081].

B. Aubert *et al.* (BABAR collaboration), *Evidence for the flavor changing neutral current decays $B \to K\ell^+\ell^-$ and $B \to K^*\ell^+\ell^-$, ibid.* [SLAC-PUB-9323, BABAR-CONF-02-023, hep-ex/0207082].

B. Aubert *et al.* (BABAR collaboration), *Search for decays of B^0 mesons into pairs of leptons, ibid.* [SLAC-PUB-9313, BABAR-CONF-02-028, hep-ex/0207083].

B. Aubert *et al.* (BABAR collaboration), *Measurement of the first hadronic spectral moment from semileptonic B decays, ibid.* [SLAC-PUB-9314, BABAR-CONF-02-029, hep-ex/0207084].

B. Aubert *et al.* (BABAR collaboration), *Measurement of the $B^0 \to D^{*-}a_1^+$ branching fraction with partially reconstructed D^*, ibid.* [SLAC-PUB-9315, BABAR-CONF-02-010, hep-ex/0207085].

B. Aubert *et al.* (BABAR collaboration), *Measurement of the branching fractions for the exclusive decays of B^0 and B^+ to $\bar{D}^{(*)}D^{(*)}K$, ibid.* [SLAC-PUB-9322, BABAR-CONF-02-19, hep-ex/0207086].

B. Aubert *et al.* (BABAR collaboration), *Measurement of the branching ratios and CP asymmetries in $B^- \to D^0_{(CP)}K^-$ decays, ibid.* [SLAC-PUB-9311, BABAR-CONF-02-18, hep-ex/0207087].

B. Aubert *et al.* (BABAR collaboration), *Dalitz plot analysis of D^0 hadronic decays $D^0 \to K^0 K^- \pi^+$, $D^0 \to \bar{K}^0 K^+ \pi^-$ and $D^0 \to \bar{K}^0 K^+ K^-$, ibid.* [SLAC-PUB-9320, BABAR-CONF-02-031, hep-ex/0207089].

B. Aubert *et al.* (BABAR collaboration), *Measurement of branching fractions of color suppressed decays of the $\bar{B}^0$ meson to $D^0 \pi^0$, $D^0 \eta$, and $D^0 \omega$, ibid.* [SLAC-PUB-9324, BABAR-CONF-02-17, hep-ex/0207092].

J. Dilling *et al.* (TITAN collaboration), *The proposed TITAN facility at TRIUMF: a next generation Penning trap mass spectrometer for high charged ions*, Proc. **Int. Conf. on Trapped Charged Particles and Fundamental Interactions (TCPFI 2002), Wildbad Kreuth, Germany, August 25–30, 2002**.

M.C. Vetterli, *Nucleon spin physics at HERMES: ECT**, Proc. **Workshop, Structure of the Nucleon, European Centre for Theoretical Studies in Nuclear Physics and Related Areas, Trento, September, 2002**.

S. Engel *et al.*, *Measurements with DRAGON on resonances in the $^{21}Na(p,\gamma)\,^{22}Mg$ reaction with a radioactive beam*, Proc. **17th Int. Nuclear Physics Divisional Conf. of the EPS, September, 2002** (Nuclear Physics A, in press).

D. Sinclair, *The international facility for underground science*, Proc. **Int. Conf. on Dark Matter, York, UK, September, 2002**.

J. Dilling *et al.* (TITAN collaboration), *High precision mass measurements and other applications for highly charged ions with the proposed TITAN facility at TRIUMF*, Proc. **Int. Conf. on Highly Charged Ions (HCI), Caen, France, September 1–5, 2002**.

W.D. Ramsay, *Parity violation in pp and np experiments*, Proc. **15th Int. Spin Physics Symp. (SPIN 2002), Brookhaven, NY, September 9–14, 2002** (AIP, in press) [TRI-PP-02-16].

C.A. Miller, *New results on semi-inclusive DIS measurements, ibid.*

A. Shotter, *Nuclear astrophysics with radioactive beams: a TRIUMF perspective*, Proc. **17th Int. Nuclear Physics Divisional Conf. of the European Physical Society (NPDC-17), Budapest, Hungary, September 30–October 4, 2002** (Nucl. Phys. A, in press).

M. Abe *et al.* (KEK-E246 collaboration), *Further search for T violation in the decay $K^+ \to \pi^0 \mu^+ \nu$*, Proc. **16th Int. Conf. on Particles and Nuclei (PANIC 02), Osaka, Japan, September 30 – October 4, 2002** (Nucl. Phys. A, in press) [hep-ex/0211049].

T. Numao, T. Awes, S. Berridge, W. Bugg, V. Cianciolo, Y. Davydov, Y. Efremenko, R. Gearhart, Y. Kamyshkov, S. Ovchinnikov, J.-M. Poutissou and G. Young, *π^- capture in water and light materials, ibid.*

J.-M. Poutissou *et al.*, *The TWIST experiment (TRIUMF weak interaction symmetry test), ibid.*

J.-M. Poutissou *et al.*, *A precision measurement of muon decay, ibid.*

A. Olin *et al.*, *Nuclear astrophysics at ISAC with DRAGON: initial studies, ibid.*

A. Konaka, *Rare K decay results and future prospects, ibid.*

A.A. Chen, *Present and future studies with DRAGON*, Proc. **APS Division of Nuclear Physics Meeting, East Lansing, MI, October, 2002**.

G. Hackman, *Gamma spectroscopy at TRIUMF-ISAC: the current and future 8π program, ibid.*

A.A. Chen, *The ISAC-II radioactive beam facility*, Proc. **Joint Inst. for Nuclear Astrophysics Workshop on the r-process: New Experimental, Theoretical, and Observational Opportunities, Gull Lake, MI, October, 2002**.

D. Sinclair, *The Sudbury Neutrino Observatory*, Proc. **Symp. on the 10th Anniversary of the LVD, Gran Sasso, Italy, November, 2002**

A. Shotter, *ISAC at TRIUMF: status and future*, Proc. **3rd Int. Conf. on Fission and Properties of Neutron-Rich Nuclei, Sanibel Island, FL, November 3–9, 2002** (World Scientific, in press).

A.A. Chen *et al.*, *Measurement of the $^{21}Na(p,\gamma)\,^{22}Mg$ reaction with the DRAGON facility at TRIUMF-ISAC*, Proc. **17th Int. Conf. on the Application of Accelerators in Research and Industry (CAARI), Denton, TX, November 13–17, 2002**.

J. Dilling *et al.* (TITAN collaboration), *The proposed TITAN facility at TRIUMF: a next generation Penning trap mass spectrometer for highly charged ions, ibid.*

Instrumentation/Accelerator Physics/Computing Sciences

D.M. Gingrich *et al.*, *A radiation tolerant controller for a switched capacitor array*, Proc. **Single Event Effects Symposium, Los Angeles, CA, 2002**.

M. Comyn, *Status of mirror sites*, Proc. **3rd Joint Accelerator Conf. Website (JACoW) Team Meeting, Thoiry, France, February 18–19, 2002**.

M. Comyn, *Font and graphics rendering problems encountered with Adobe Acrobat PDF, ibid.*

P. Gumplinger, *Optical processes in GEANT4*, Proc. **GEANT4 Users' Workshop, SLAC, Stanford, CA, February 18–22, 2002**.

J.-M. Poutissou, *Muon facilities/experimental program at TRIUMF*, Proc. **Int. Workshop on Future of Muon Science, KEK, Riken, Japan, March 7–9, 2002**.

D. Gray and B. Minato, *Simple "package design" ion chamber monitors for TRIUMF's proton beamlines*, Proc. **Beam Instrumentation Workshop (BIW 2002), Upton, NY, May 6–9, 2002** (AIP, in press) [TRI-PP-02-06].

P. Bricault, *Laser ion source for the ISAC facility*, Proc. **Int. Conf. on Laser Probing, LAP2002, Leuven, Belgium, July 7–12, 2002**.

W. Andersson, R.E. Laxdal, I. Sekachev and G. Stanford *Overview of the cryogenic system for the ISAC-II superconducting linac at TRIUMF*, Proc. **19th Int. Cryogenic Engineering Conf. (ICEC 19), Grenoble, France, July 22–26, 2002** (Narosa, New Delhi, in press) [TRI-PP-02-34].

A.K. Mitra, P.J. Bricault, I.V. Bylinsky, K. Fong, G. Dutto, R.E. Laxdal and R.L. Poirier, *RF test and commissioning of the radio frequency structures of the TRIUMF ISAC-I facility*, Proc. **XXI Int. LINAC Conf., Gyeongju, Korea, August 19–23, 2002**.

A.K. Mitra, Z.T. Ang, R. Hohbach, R.E. Laxdal, J. Lu and R.L. Poirier, *Design test and commissioning of a dual frequency chopper for the TRIUMF ISAC facility, ibid.*

R.E. Laxdal, G. Clark, K. Fong, A. Mitra, M. Pasini, R. Poirier, I. Sekachev and G. Stanford, *Superconducting accelerator activities at TRIUMF/ISAC, ibid.*

K. Sachs *et al.*, *GEM TPC R&D in Canada, ibid.*

R.E. Laxdal, *ISAC-I and ISAC-II at TRIUMF: achieved performance and new construction, ibid.*

R.E. Laxdal, M. Pasini and L. Root, *Beam dynamics design study and beam commissioning of the ISAC two frequency chopper, ibid.*

P.N. Ostroumov *et al.*, *A new generation of superconducting solenoids for heavy ion linac application, ibid.*

D. Karlen, *Review of detector concepts*, Proc. **Int. Linear Collider Workshop, Jeju Island, Korea, August 26–30, 2002**.

D. Karlen, *Pad geometry study for a linear collider TPC, ibid.*

G. Dutto, *Recent achievements at TRIUMF*, Proc. **XXXIII European Cyclotron Progress Meeting, Warsaw, Poland, September 17–21, 2002** (Nukleonika, Poland, in press).

C. Kost, S. McDonald, B. Caron and W. Hong, *ATLAS Canada lightpath data transfer trial*, Proc. **iGrid2002, Amsterdam, Netherlands, September 23–26, 2002** (Elsevier Science, in press).

M.J. Barnes and G.D. Wait, *JHF 50 GeV ring combined fast extraction and abort kicker*, **Int. Workshop on Nuclear and Particle Physics at 50 GeV PS (NP02), Kyoto, Japan, September 27–29, 2002**.

J. Doornbos, *Options for beam optics and beam scraping for the proton transfer line at 30 to 50 GeV, ibid.*

J. Doornbos, *Possibilities for low energy stopped kaon beams at the JHF, ibid.*

S. Koscielniak, *High frequency, short bunch width, slow extraction for KOPIO*, Proc. **10th ICFA Mini-Workshop on Slow Extraction, Upton, NY, October 15–17, 2002**.

L. Moritz, *Radiation safety at ISAC*, Proc. **SAFERIB Workshop at CERN, Geneva, Switzerland, October 30–November 1, 2002** (CERN report, in press).

M. Comyn and I. Andrian, *Report of the JACoW workshop on databases for conference programmes and proceedings*, Proc. **Database Workshop and 4th Joint Accelerator Conf. Website (JACoW) Team Meeting, Berkeley, CA, November 4–7, 2002**.

M. Comyn, *Use of jpeg2ps with JPEG figures in LaTeX 2ε ibid.*

D. Karlen, *GEM-TPC resolution studies*, Proc. **ECFA-DESY, Linear Collider Workshop, Prague, Czech Republic, November 15–18, 2002**.

Chemistry and Solid-State Physics

T.L. Estle, R. Lichti, B. Hitti and S. Kreitzman, *Muonium in Si: low temperatures and high fields and metastability*, Proc. **European Workshop for High Field MuSR, Paul Scherrer Inst., Switzerland, January 15–16, 2002**.

S. Kreitzman, *High magnetic field μSR: technical issues and solutions, ibid.*

P.W. Percival, K. Ghandi, B. Addison-Jones and I.D. McKenzie, *Reactions of the light hydrogen isotope Mu in sub- and supercritical water*, Proc. **Gordon Research Conf. on Isotopes in the Biological and Chemical Sciences, Ventura, CA, February 17–22, 2002**.

J.D. Dow and D.R. Harshman, *Ruthenate and cuprate high-temperature superconductivity*, Proc. **Int. Conf. on Superconductivity, CRM and Related Materials: Novel Trends (SCRM 2002), Giens, France, June 1–8, 2002**.

P.W. Percival, *Muonium chemistry*, Pre-conference tutorial on μSR, Proc. **9th Int. Conf. on Muon Spin Rotation/Relaxation/Resonance (MuSR 2002), Williamsburg, VA, June 3–7, 2002** (Physica B, in press).

D.R. Noakes, R.H. Heffner and P.W. Percival (editors), Proc. **9th Int. Conf. on Muon Spin Rotation/Relaxation/Resonance (MuSR 2002), Williamsburg, VA, June 3–7, 2002** (Physica B, in press).

S. Kreitzman, *An overview of high field/timing resolution and RF/μwave μSR methods, ibid.*

J.C. Brodovitch, B. Addison-Jones, K. Ghandi, I.D. McKenzie and P.W. Percival, *^{13}C hyperfine coupling constants of MuC_{70} in solution, ibid.*

K. Ghandi, B. Addison-Jones, J.-C. Brodovitch, S. Kecman, I. McKenzie and P.W. Percival, *Muonium kinetics in sub- and supercritical water, ibid.*

296

V.G. Storchak, D.G. Eshchenko, J.H. Brewer, G.D. Morris, S.P. Cottrell and S.F.J. Cox, *Coherent tunnelling dynamics of muonium in a disordered medium, ibid.*

D.J. Arseneau, D.G. Fleming, C.A. Fyfe and M. Senba, *Observation of muonium in zeolites, ibid.*

P.W. Percival, J.C. Brodovitch, D.J. Arseneau, M. Senba and D.G. Fleming, *Formation of the muoniated ethyl radical in the gas phase, ibid.*

I. McKenzie, J.C. Brodovitch, K. Ghandi, S. Kecman and P.W. Percival, *Formation and spectroscopy of α-muoniated radicals, ibid.*

D.G. Eshchenko, V.G. Storchak, J.H. Brewer, S.P. Cottrell, S.F.J. Cox, E. Karlsson and R. Wäppling, *Ionization of a shallow muonium state in a semiconductor, ibid.*

R.L. Lichti, *Properties of muonium defect centers in III-V nitrides, ibid.*

K.H. Chow, *Isolated positively charged muonium and the analog of hydrogen passivation, ibid.*

K.H. Chow, B. Hitti, D.G. Eshchenko, V.G. Storchak, S.R. Kreitzman and J.H. Brewer, *Avoided level crossing measurements of electric field enhanced diamagnetic states in gallium arsenide, ibid.*

D.G. Eshchenko, V.G. Storchak, R.L. Lichti and J.H. Brewer, *Short range electron transport in GaAs, ibid.*

V.G. Storchak, D.G. Eshchenko, R.L. Lichti and J.H. Brewer, *Weakly bound muonium state in a semiconductor, ibid.*

R.L. Lichti, K.H. Chow, E.A. Davis, B. Hitti, Y.G. Celebi and S.F.J. Cox, *Muonium–acceptor interactions in gallium phosphide, ibid.*

P.J.C. King, R.L. Lichti and I. Yonenaga, *Muonium behaviour in Czochralski $Si_{1-x}Ge_x$ alloys, ibid.*

K.L. Hoffman, K.H. Chow, R.F. Kiefl, B. Hitti, T.L. Estle and R.L. Lichti, *Frequency shifts and local spin susceptibility of muonium in heavily-doped Si and GaAs, ibid.*

B. Hitti and S.R. Kreitzman, *Muonium dynamics in silicon at high temperature, ibid.*

R.F. Kiefl, W.A. MacFarlane, G.D. Morris, P. Amaudruz, D. Arseneau, H. Azumi, R. Baartman, T.R. Beals, J. Behr, C. Bommas, J.H. Brewer, K.H. Chow, E. Dumont, S.R. Dunsiger, S. Daviel, L. Greene, A. Hatakeyama, R.H. Heffner, Y. Hirayama, B. Hitti, S.R. Kreitzman, C.D.P. Levy, R.I. Miller, M. Olivo and R. Poutissou, *Low-energy spin-polarized radioactive beams as a nano-scale probe of matter, ibid.*

T.R. Beals, R.F. Kiefl, W.A. MacFarlane, K.M. Nichol, G.D. Morris, C.D.P. Levy, S.R. Kreitzman, R. Poutissou, S. Daviel, R.A. Baartman and K.H. Chow, *Range straggling of low energy $^8Li^+$ in thin metallic films using β-NMR, ibid.*

W.A. MacFarlane, G.D. Morris, K.H. Chow, R.A. Baartman, S. Daviel, S.R. Dunsiger, A. Hatakeyama, S.R. Kreitzman, C.D.P. Levy, R.I. Miller, K.M. Nichol, R. Poutissou, E. Dumont, L.H. Greene and R.F. Kiefl, *Quadrupolar split ^8Li β-NMR in $SrTiO_3$, ibid.*

W.A. MacFarlane, G.D. Morris, T.R. Beals, K.H. Chow, R.A. Baartman, S. Daviel, S.R. Dunsiger, A. Hatakeyama, S.R. Kreitzman, C.D.P. Levy, R.I. Miller, K.M. Nichol, R. Poutissou and R.F. Kiefl, *^8Li β-NMR in thin metal films, ibid.*

D.G. Eshchenko, V.G. Storchak, B. Hitti, S.R. Kreitzman, J.H. Brewer and K.H. Chow, *Radio-frequency μSR experiments in an applied electric field, ibid.*

G.D. Morris and R.H. Heffner, *A method of achieving accurate zero field conditions using muonium, ibid.*

K.H. Chow, R.F. Kiefl, S. Chan, R.I. Miller, P. Amaudruz, R. Poutissou, B. Hitti and D. Arseneau, *MULTI – new detector, new logic, new science, ibid.*

R.I. Miller, R.F. Kiefl, J.H. Brewer, J.C. Chakhalian, S. Dunsiger, A.N. Price, D.A. Bonn, W.H. Hardy, R. Liang and J.E. Sonier, *Penetration depth and core radius μSR measurements in the vortex state near the lower critical field, ibid.*

J.E. Sonier, J.H. Brewer, R.F. Kiefl, R.I. Miller, R.H. Heffner, K.F. Poon, G.D. Morris, W.N. Hardy, R. Liang, D.A. Bonn, J.S. Gardner and C.E. Stronach, *Zero field μSR study of $YBa_2Cu_3O_{6+x}$, $x \geq 0.67$: evidence for charge ordering, ibid.*

K.M. Kojima, S. Uchida, Y. Fudamoto, I.M. Gat, M.I. Larkin, Y.J. Uemura and G.M. Luke, *Superfluid density and volume fraction of static magnetism in stripe-stabilized $La_{1.85-y}Eu_ySr_{0.15}CuO_4$, ibid.*

D. Baabe, H.-H. Klauss, D. Mienert, M. Birke, P. Adelmann, B. Hitti, U. Zimmermann, A. Amato and F.J. Litterst, *Inhomogeneous spin order in the magnetic phase of electron-doped high-T_c superconductors, ibid.*

K. Ohishi, K. Kakuta, J. Akimitsu, A. Koda, W. Higemoto, R. Kadono, J.E. Sonier, A.N. Price, R.I. Miller, R.F. Kiefl, M. Nohara, H. Suzuki and H. Takagi, *Anomalous quasiparticle excitations in $Y(Ni_{1-x}Pt_x)_2B_2C$, ibid.*

G.M. Luke, M.T. Rovers, A. Fukaya, I.M. Gat, M.I. Larkin, A.T. Savici, Y.J. Uemura, K.M. Kojima, P.M. Chaikin, I.J. Lee and M.J. Naughton, *Unconventional superconductivity in $(TMTSF)_2ClO_4$, ibid.*

D.E. MacLaughlin, M.S. Rose, B.-L. Young, O.O. Bernal, R.H. Heffner, G.D. Morris, K. Ishida, G.J. Nieuwenhuys and J.E. Sonier, *μSR and NMR in f-electron non-Fermi liquid materials, ibid.*

D.E. MacLaughlin, M.S. Rose, B.-L. Young, O.O. Bernal, R.H. Heffner, G.J. Nieuwenhuys, R. Pietri and B. Andraka, *μSR in $Ce_{1-x}La_xAl_3$: anisotropic Kondo effect?, ibid.*

G.D. Morris, R.H. Heffner, J.E. Sonier, D.E. MacLaughlin, O.O. Bernal, G.J. Nieuwenhuys, A.T. Savici, P.G. Pagliuso and J.L. Sarrao, *Magnetism and superconductivity in $CeRh_{1-x}Ir_xIn_5$ heavy fermion materials, ibid.*

D.R. Noakes, G.M. Kalvius, H. Nakotte, E. Schreier and R. Wäppling, *μSR magnetic response in UPdSn, ibid.*

D.R. Noakes, G.M. Kalvius, H. Nakotte, E.J. Ansaldo and A.V. Andreev, *$U_{0.94}Y_{0.06}CoAl$: a dilute-moment ferromagnet, ibid.*

J.E. Sonier, R.H. Heffner, G.D. Morris, D.E. MacLaughlin, O.O. Bernal, J. Cooley, J.L. Smith and J.D. Thompson, *μ^+-Knight shift in the superconducting state of $U_{1-x}Th_xBe_{13}$, $x = 0$ and 0.035 single crystals, ibid.*

J.A. Chakhalian, R.F. Kiefl, R. Miller, S.R. Dunsiger, G. Morris, S. Kreitzman, W.A. MacFarlane, J. Sonier, S. Eggert, I. Affleck and I. Yamada, *Local magnetic susceptibility of the positive muon in the quasi-1D $S = 1/2$ antiferromagnet $KCuF_3$, ibid.*

D. Mienert, H.-H. Klauss, A. Bosse, D. Baabe, H. Luetkens, M. Birke, F.J. Litterst, B. Büchner, U. Ammerahl, A. Revcolevschi, A. Amato, U. Zimmermann, B. Hitti and S. Kreitzman, *The interplay of charge order and magnetism in the one-dimensional quantum spin system $Sr_{14}Cu_{24}O_{41}$, ibid.*

A. Fukaya, Y. Fudamoto, I.M. Gat, T. Ito, M.I. Larkin, A.T. Savici, Y.J. Uemura, P.P. Kyriakou, G.M. Luke, M. Rovers, H. Kageyama and Y. Ueda, *Spin dynamics in the two-dimensional spin system $SrCu_2(BO_3)_2$, ibid.*

D.H. Ryan, J. van Lierop and J.M. Cadogan, *μSR and Mössbauer studies of transverse spin freezing, ibid.*

G.M. Kalvius, D.R. Noakes, R. Wäppling, G. Grosse, W. Schäfer, W. Kockelmann, J.K. Yakinthos and P.A. Kotsanides, *Spin dynamics and spin disorder in frustrated $TbCo_xNi_{1-x}C_2$, ibid.*

G.M. Kalvius, D.R. Noakes, R. Wäppling, E. Schreier, N. Büttgen, A. Krimmel, M. Klemm, S. Horn and A. Loidl, *Magnetic properties of geometrically frustrated $Zn_xLi_{1-x}V_2O_4$, ibid.*

S.R. Dunsiger, R.F. Kiefl, J.A. Chakhalian, K.H. Chow, J.S. Gardner, J.E. Greedan, W.A. MacFarlane, R.I. Miller, G.D. Morris, A.N. Price, N.P. Raju and J.E. Sonier, *A comparison of the local magnetic susceptibility in rare earth pyrochlores, ibid.*

R.H. Heffner, J.E. Sonier, D.E. MacLaughlin, G.J. Nieuwenhuys, F. Mezei, G. Ehlers, J.F. Mitchell and S.-W. Cheong, *Inhomogeneity in the spin channel of ferromagnetic CMR manganites, ibid.*

J. Sugiyama, J.H. Brewer, E.J. Ansaldo, H. Itahara, M. Bayer and T. Tani, *μSR studies on layered cobalt oxides, ibid.*

P.W. Percival, *Closing remarks, ibid.*

J.D. Dow and D.R. Harshman, *High-temperature superconductivity: the hole-pairing is s-wave and the holes are on the SrO, BaO or interstitial oxygen*, Proc. **2002 Int. Conf. on the Physics and Chemistry of Molecular and Oxide Superconductors (MOS 2002), Hsinchu, Taiwan, August 13–18, 2002**.

K. Ohishi, K. Kakuta, J. Akimitsu, W. Higemoto, R. Kadono, J.E. Sonier, A.N. Price, R.I. Miller, R.F. Kiefl, M. Nohara, H. Suzuki and H. Takagi, *Anomalous quasiparticle excitations in $Y(Ni_{1-x}Pt_x)_2B_2C$*, Proc. **23$^{\text{rd}}$ Int. Conf. on Low Temperature Physics (LT23), Hiroshima, Japan, August 20–27, 2002**.

J.D. Dow and D.R. Harshman, *SrO and BaO high-temperature superconductivity, ibid.*

Life Sciences

C.S. Lee, S. Mann, M. Zamburlini, S. Lee, V. Sossi, M. Adam, A.J. Stoessl and T.J. Ruth, *PET studies on the extent of cholinergic and dopaminergic neuronal loss in Parkinson's disease, Parkinson's disease with dementia, and dementia with Lewy bodies*, Proc. **Movement Disorders Society, 2002**.

D.J. Doudet and J.E. Holden, *Multiple ligand concentration receptor assays (MLCRA): sequential vs. non-sequential measurements of density and affinity of dopamine receptors with [11C] raclopride. Application to amphetamine effects*, Proc. **NeuroReceptor 2002. NeuroImage 2002**.

R.L. Watts, C.D. Raiser, N.P. Stover, M.L. Cornfeldt, A.W. Schweikert, R.C. Allen, T. Subramanian, D.J. Doudet, C. Honey and R.A.E. Bakay, *Human retinal pigment epithelial cells attached to gelatin microcarriers: a promising new cell therapy for Parkinson's disease*, Proc. **10$^{\text{th}}$ Int. Winter Conf. on Neurodegeneration, Berlin, Germany, February, 2002**.

M.J. Adam, K.R. Buckley, S. Jivan, J. Huser, M. Kovacs, J. Lu, D. Lyster, R. MacDonald, J. Mercer, J. Wilson, J. Wu and T.J. Ruth, *^{18}F-FDG production: a comparison of 3 commercial systems and 2 sources of ^{18}F-fluoride*, Proc. **Annual Canadian Society of Nuclear Medicine Meeting, Edmonton, AB, April 5–7, 2002**.

C.S. Lee, S. Jivan, M.J. Adam, A. Kurish, V. Sossi, J.E. Holden, C. Williams, S. Mann, B. Buck, A. de Feijter, M. Schulzer, I. MacKenzie, A.J. Stoessl, B.L. Beattie and T.J. Ruth, *Extent and topography of cholinergic and dopaminergic denervation in dementia with Lewy bodies, Parkinson's disease and Alzheimer's disease: in vivo positron emission tomographic studies using ^{11}C-DTBZ and ^{11}C-PMP*, Proc. **54$^{\text{th}}$ Annual Meeting of the American Academy of Neurology, Denver, CO, April 13–20, 2002**.

D.J. Doudet, S. Jivan and J.E. Holden, *Amphetamine: evaluation of effects on DA D2 receptors and endogenous synaptic DA*, Proc. **IX Symp. on the Medical Applications of Cyclotrons, Turku, Finland, May, 2002**.

G.-J. Beyer and T.J. Ruth, *The role of electromagnetic separators in the production of radiotracers for bio-medical research and nuclear medical application*, Proc. **14th Int. Conf. on Electromagnetic Isotope Separators and Techniques Related to Their Applications (EMIS-14), Victoria, BC, May 6–10, 2002** (Nucl. Instrum. Methods, in press) [TRI-PP-02-26].

K.R. Buckley, J. Wilson, S. Jivan, M.J. Adam, P. Picconi, E.T. Hurtado and T.J. Ruth, *Operational experience with a niobium target body for the irradiation of $^{18}O - H_2O$*, Proc. **9th Int. Workshop on Targetry and Target Chemistry, Turku, Finland, May 23–25, 2002**.

T.E. Barnhart, K.R. Buckley, S. Jivan, A.D. Roberts and T.J. Ruth, *Performance of a flow-through target for the production of $^{11}C - CH_4$, ibid.*

D.W. Becker, K.R. Buckley, J. Lenz, B. Hagen, P. Piccioni and T.J. Ruth, *Qualitative evaluation of helium-cooling windows, ibid.*

K.R. Buckley, D.W. Becker, R. Dahl, S. Jivan and T.J. Ruth, *Further progress on targetry for the production of ultra-high quantities of ^{18}F-fluoride, ibid.*

K.R. Buckley and T.J. Ruth, *Website for proceedings of the workshops on targetry and target chemistry, ibid.*

K.R. Buckley, *Technology of cyclotrons for radioisotope production, ibid.*

K.R. Buckley, *OPC based control software, ibid.*

E.W. Blackmore, *Results of proton and plaque therapy of chroidal melanoma treated in Vancouver*, Proc. **PTCOG, Catania, Italy, May 29–31 2002**.

D.J. Doudet, C. Honey, A. Schweikert and M. Cornfeldt, *PET imaging of implanted human retinal pigment epithelial (RPE) cells on gelatin microcarriers (Spheramine: SP) in the MPTP-induced primate model of Parkinson's disease (PD)*, Proc. **ASNTR, June, 2002**.

D.J. Doudet, S. Jivan and J.E. Holden, *Evaluation of density and affinity of D2 receptors after methylphenidate (MPh)-induced increase in endogenous dopamine (DA): PET studies with raclopride*, Proc. **Dopamine 2002, Portland, OR, July, 2002**.

E.M. Strome, R.A. Kornelsen, A.P. Zis and D.J. Doudet, *Electroconvulsive shock (ECS) alters D1 binding in rat striatum: differential effects of anesthesia, ibid.*

V. Sossi, M. Zamburlini, J.E. Holden, R. de la Fuente-Fernandez, A.J. Stoessl and T.J. Ruth, *The presence of 3-O-methyl-[^{18}F]fluoro-DOPA (3OMFD) influences the evaluation of the ^{18}F-fluorodopa tissue input uptake rate constant in a disease dependent way: a study in Parkinson's disease*, Proc. **Neuroreceptor Mapping, Oxford, UK, July 19–21, 2002**.

J.E. Holden, S. Jivan, T.J. Ruth and D.J. Doudet, *PET receptor assay with multiple ligand concentrations and true equilibrium: mathematical and neurochemical aspects, ibid.*

T.J. Ruth, *From nuclear spectroscopy to in vivo biochemistry*, Proc. **American Chemical Society, Boston, MA, August, 2002**.

E.M. Strome, A.P. Zis and D.J. Doudet, *Electroconvulsive shock (ECS) alters 5HT2 binding in rat striatum: differential effects of anesthesia*, Proc. **Society for Neuroscience, October, 2002**.

T.J. Ruth, *Production of radioisotopes for imaging and therapy at low energy*, Proc. **7th Int. Conf. on Advanced Technology and Particle Physics, Como, Italy, October, 2002**.

T.J. Ruth, *Design consideration for high power gas targets*, Proc. **17th Int. Conf. on the Application of Accelerators in Research and Industry (CAARI), Denton, TX, November, 2002**.

V. Astakhov, P. Gumplinger, C. Moisan, T.J. Ruth and V. Sossi, *Effect of depth of interaction decoding on resolution in PET: a simulation study*, Proc. **2002 IEEE/Medical Imaging Conf., Norfolk, VA, November 13–16, 2002** (IEEE Trans. Med. Imaging, in press).

V. Sossi, O. Morin, A. Celler, A. Belzberg, T.D. Rempel and C. Carhart, *PET and SPECT performance evaluation of the Siemens HD3 e.camduet: a 1 in. Na(I) hybrid camera, ibid.*

M. Zamburlini, R. de la Fuente-Fernandez, A.J. Stoessl, T.J. Ruth and V. Sossi, *Impact of different realignment algorithms on the SPM analysis of ^{11}C-raclopride PET studies, ibid.*

Theoretical Program

A. Astbury, B. Campbell, F.C. Khanna and M. Vincter (editors), Proc. **Lake Louise Winter Inst. on Fundamental Interactions (LLWI02), Lake Louise, AB, February 17–23, 2002** (World Scientific, Singapore, in press).

D.U. Matrasulov, F.C. Khanna, Kh.Yu. Rakhimov and Kh.T. Butanov, *Spectroscopy of baryons containing two heavy quarks, ibid.*

F.C. Khanna and D.U. Matrasulov, *Properties of hadrons in nuclear matter*, Proc. **Joint CCSM/JHF/NITP Workshop on Physics at the Japan Hadron Facility, Adelaide, Australia, March 14–21, 2002**, eds. V. Guzey *et al.* (World Scientific, Singapore, in press).

I.R. Afnan and A.D. Lahiff, *The Bethe-Salpeter equation and the low-energy theorems for πN scattering*, Proc. **Conf. on Quarks and Nuclear Physics (QNP 2002), Julich, Germany, June 9–14, 2002**, eds. J. Speth, Ch. Elster and Th. Walcher (Eur. Phys. J. A, in press) [nucl-th/0210027].

R. Lewis, W. Wilcox and R.M. Woloshyn, *Strange matrix elements of the nucleon*, Proc. **20th Int. Symp. on Lattice Field Theory (LATTICE 2002), Cambridge, MA,**

June 24–29, 2002 (Nucl. Phys. B Proc. Supp., in press) [hep-lat/0208063].

C.S. Kalman, J. McKenna, M. Bozzo, Z. Ligeti, T. Mattison, J. Ng, M.A. Sanchis-Lozano and P. Singer (editors), Proc. **5th Int. Conf. on Hyperons, Charm and Beauty Hadrons (BEACH 2002), Vancouver, BC, June 25–29, 2002** (Nucl. Phys. **115**, in press).

D.U. Matrasulov, F.C. Khanna, Kh.Yu. Rakhimov and H. Yusupov, *Spectra of heavy flavored hadrons in the relativistic approach, ibid.*

T. Numao (for the E787/949 and KOPIO collaborations at BNL), *Status of $K \to \pi\nu\bar{\nu}$, ibid.*

C.-H. Chen, C.Q. Geng and J.N. Ng, *T violation in $\Lambda_b \to \Lambda\ell^+\ell^-$ decays, ibid.* [hep-ph/-0210067].

J. Escher and B.K. Jennings, *A new signature for nuclear shell closures*, Proc. **7th Int. Symp. on Nuclei in the Cosmos (NIC7), Fuji-Yoshida, Japan, July 8–12, 2002** (Nucl. Phys. A, in press) [TRI-PP-02-12].

M. de Montigny, F.C. Khanna and A.E. Santana, *Metric formulation of Galilean invariance in five dimensions*, Proc. **24th Int. Coll. on Group Theoretical Methods in Physics: GROUP – 24 (ICGTMP 2002), Paris, France, July 15–20, 2002** (Inst. of Phys., in press).

H. Uys, H.G. Miller and F.C. Khanna, *Generalised statistics and high T_c superconductivity*, Proc. **26th Int. Workshop on Condensed Matter Theories (CMT 26), Luso, Portugal, September 2–7, 2002** (Condensed Matter Theories, **18**, in press).

C.-P. Liu, *Nuclear anapole moments and the parity nonconserving nuclear interaction*, Proc. **15th Int. Spin Physics Symp. (SPIN 2002), Brookhaven, NY, September 9–14, 2002** (AIP, in press) [nucl-th/0211095].

M. de Montigny, F.C. Khanna and A.E. Santana, *Physical applications of a five-dimensional metric formulation of Galilean invariance*, Proc. **Workshop on Symmetry in Physics in Memory of Robert T. Sharp, Montreal, PQ, September 12–14, 2002** (CRM Proc. and Lecture Notes, in press).

K. Tsushima and F.C. Khanna, *Properties of nuclear medium and a possibility of charmed nuclei*, Proc. **16th Int. Conf. on Particles and Nuclei (PANIC 02), Osaka, Japan, September 30 – October 4, 2002** (Nucl. Phys. A, in press).

M. de Montigny, F.C. Khanna and A.E. Santana, *Model dependent Lagrangians for fluids in the Galilean covariant formalism*, Proc. **XXIII Brazilian Meeting on Particles and Fields, Sao Paulo, Brazil, October, 2002**.

K. Tsushima and F.C. Khanna, *Properties of charmed and bottom hadrons in nuclear medium: results for Λ_c^+ and Λ_b hypernuclei*, Proc. **YITP-RCNP Workshop on Chiral Restoration in Nuclear Medium, Kyoto, Japan, Octo-**

ber 7–9, 2002 (Prog. Theor. Phys. Suppl., in press) [nucl-th/0212100].

P.L. Gardner, *Unusual challenges in technology transfer*, Proc. **Society of Research Administrators, Tucson, AZ, May, 2002**.

P.L. Gardner, *The globalization of R&D and international technology transfer in the 21st century*, Proc. **Int. Conf. on Management of Innovation and Technology (ISMOT), Hangzhou City, China, October 18–20, 2002** [TRI-PP-02-05].

Books

M.K. Craddock, *Cyclotrons*, in McGraw-Hill Encyclopedia of Science and Technology, 9th Edition (McGraw-Hill, New York, 2002) **v.13**, p.44.

K. Nagamine, *Introductory muon science* (Cambridge Univ. Press, Cambridge, in press).

A.J. Stoessl and S. Furtado, *Positron emission tomography in movement disorders*, in Positron Emission Tomography: Basic Science and Clinical Practice, eds. P.E. Valk *et al.* (Springer-Verlag, London, in press).

Theses

G.A.N. Belanger, *The search for extra dimensions and the ATLAS forward calorimeter* (M.Sc., Physics, Carleton University).

D.F. Hodgson, *Tests of the standard model from superallowed Fermi β-decay studies: β-decay of ^{74}Rb* (M.Sc., Physics, University of Surrey, UK).

P. Kyriakou, *Studies of Zn-doped Bi2212* (M.Sc., Physics and Astronomy, McMaster University).

X. Li, *Improvements to the range stack straw chambers for the measurement of $K^+ \to \pi^+\nu\bar{\nu}$* (M.Sc., Physics, University of British Columbia).

K.F. Poon, *μSR studies of the electron-doped high-T_c superconductor $Pr_{2-x}Ce_xCuO_4$* (M.Sc., Physics, Simon Fraser University).

M. Rovers, *Muon spin relaxation investigation of the spin dynamics of geometrically frustrated chromites* (M.Sc., Physics and Astronomy, McMaster University).

H. Xu, *The pion deuteron breakup reaction* (M. Sc., Physics, University of Regina).

C. Bridges, *Structural and electronic properties of $BaV_{10}O_{15}$, $BaV_{10-x}Ti_xO_{15}$, and $BaVO_{3-x}$* (Ph.D., Chemistry, McMaster University).

M.A. Caprio, *Structure of collective modes in transitional and deformed nuclei* (Ph.D., Physics, Yale University).

J.A. Chakhalian, *Local magnetic susceptibility of the positive muon in graphite and the quasi 1D spin 1/2 chain CPC* (Ph.D., Physics and Astronomy, University of British Columbia).

L. De Nardo, *Measurement of the structure function g_1^d at HERMES and extraction of polarized parton distributions* (Ph.D., Physics, University of Alberta).

I.M. Gat, *Muon spin relaxation measurements of the magnetic system with itinerant electrons in MnSi* (Ph.D., Physics, Columbia University).

K. Ghandi, *Muonium chemistry in sub- and supercritical water* (Ph.D., Chemistry, Simon Fraser University).

R.I. Miller, *Relationship between magnetism and superconductivity in $YBa_2Cu_3O_{6+x}$* (Ph.D., Physics and Astron-

omy, University of British Columbia).

K. Ohishi, *Flux line lattice state in the type-II superconductors probed by muon spin rotation* (Ph.D., Physics, Aoyama-Gakuin University).

J.D. Patterson, *Precision measurement of elastic πp analyzing powers from 57 to 140 MeV* (Ph.D., University of Colorado).

X. Wan, *Effects of longitudinal disorder on the magnetic field distribution in $Bi_2Sr_2CaCu_2O_{8+\delta}$* (Ph.D., Physics, College of William and Mary).

C.R. Wiebe, *Studies of magnetism in rhenium and manganese based perovskite oxides* (Ph.D., Chemistry, McMaster University).

Appendix B

SEMINARS[*]

The following seminars were presented at TRIUMF this year.

14/01   *Heavy Ions at GSI: Status and Future*, H.-Juergen Kluge, GSI, Darmstadt/U. Heidelberg.
16/01   *Chiral Aspects of Hadron Properties Calculated in Lattice QCD*, Anthony W. Thomas, U. Adelaide.
17/01   *Would Freud Have Dreamt of It?: How Physics Helps Imaging the Troubled Mind*, Sylvain Houle, PET Centre, CAMH/U. Toronto.
31/01   *The TRIUMF-Seattle $^7Be(p,\gamma)^8B$ Experiment*, Lothar Buchmann, TRIUMF.
06/02   *Spontaneous Broken Space-Time Symmetry and the Goldstone Theorem*, Ian Low, Harvard U.
07/02   *Noncommutative Field Theories – a Survey*, Moshe Rozali, UBC.
13/02   *Testing the Relativistic Time Dilation With Laser Spectroscopy of Fast Stored Ions*, Gerald Gwinner, MPI, Heidelberg.
18/02   *Polarized H^- Ion Source For RHIC Spin Physics*, Anatoli Zelenski, BNL.
21/02   *Ideas of The World Beyond*, Erich Poppitz, U. Toronto.
22/02   *Long-Range Correlations and the One-Hole Spectral Function of ^{16}O*, Carlo Barbieri, Washington U., St. Louis.
26/02   *Taking a Closer Look at the Dilepton Spectrum of a Quark Gluon Plasma*, Abhijit Majumder, McGill U.
28/02   *Nitrogen Absorption by Plant Roots: From Ecology to Molecular Biology With a Lot of Help From ^{13}N*, Anthony Glass, UBC.
01/03   *Fermion Masses and Mixing and CP Violation in a SUSY $SO(10) \times SU(2)_F$ Model*, Mu-Chun Chen, U. Colorado.
07/03   *Recent Results From the HIGS Facility*, Henry Weller, Duke U./TUNL.
08/03   *Quasideuteron Model and Proton-Neutron Structure in Medium Nuclei*, Alexander Lisetskiy, U. Koln.
19/03   *Muon Capture in Liquid H_2 and Solar-Neutrino Scattering on D_2 in Chiral Perturbation Theory*, Shung-ichi Ando, U. South Carolina.
21/03   *Recent Results From Super-Kamiokande and K2K*, Kate Scholberg, MIT.
25/03   *Accelerators in China and the Proposed RIB at CIAE*, Tianjue Zhang, Chinese Institute of Atomic Energy.
28/03   *TUDA at ISAC*, Pat Walden, TRIUMF.
04/04   *Measurement of the Weak Mixing Angle $sin^2(\theta_W)$ in Neutrino and Anti-Neutrino Scattering*, Heidi Schellman, Northwestern U.
11/04   *Ion Traps – Precision Measurements and More*, Georg Bollen, Michigan State U.
18/04   *Quantum Mass Effects in Muonium Reactivity*, Don Fleming, UBC.
22/04   *A Model-Independent Determination of the $K \to \pi\pi$ Matrix Elements of the Electroweak Penguin Operators Q_7 and Q_8 in the Chiral Limit*, Kim Maltman, York U.
25/04   *Self-Shunted Streamer Chamber Spectrometer For Studying Pion Interactions With Light Nuclei at Energies Below the Delta-Resonance*, Gil Pontecorvo, JINR/Torino.
26/04   *Quantifying Errors of Stellar Abundance Observables Due to Uncertainties in Nuclear Reactions: Oxygen in Red Giants*, Falk Herwig, U. Victoria.
26/04   *Recent Results From SNO*, Neil McCauley, U. Pennsylvania.
02/05   *A New Signature For Shell Closures in Nuclei?*, Jutta Escher, TRIUMF.
09/05   *The PSI $\mu \to e\gamma$ Experiment*, Stefan Ritt, PSI.
14/05   *The Role of Recoil Separators in Nuclear Structure*, Jo Ressler, Yale U.
15/05   *Current Progress of Nuclear Physics Study and BRNBF at CIAE*, Wei-Ping Lui, China Institute of Atomic Energy.
16/05   *Precision Measurements of Isotope Shifts, Fine and Hyperfine Structure in Li I & II*, William van Wijngaarden, York U.
23/05   *TESLA – a New Tool For Science: High Energy Electron-Positron Collider and X-Ray Free Electron Laser (Scientific Potential and Technical Challenges)*, Albrecht Wagner, DESY/U. Hamburg.
30/05   *Supernova Nucleosynthesis, Cosmochronometry and Cosmology*, Taka Nagino and Kaori Otsuki, NAO/Japan, U. Tokyo and Notre Dame.
20/06   *Baryon Resonance Spectroscopy From a Novel Improved Fermion Action*, James Zanotti, U. Adelaide.
04/07   *New Perspectives on Heavy Quarkonium From Nonrelativistic Effective Field Theories*, Nora Brambilla, U. Milan.
18/07   *Heavy Element Research at DUBNA*, Yuri Oganessian, JINR.
22/07   *Muon Cooling*, Raphael Galea, Columbia U.
01/08   *Nuclear Structure From Scratch*, Erich Ormand, LLNL.
07/08   *Precision Low-Energy Measurements and Supersymmetry*, Michael Ramsey-Musolf, Caltech.
08/08   *Exploring the Nuclear Halo*, Jim Al-Khalili, U. Surrey.
15/08   *Anomalons Redux: Anomalous Projectile Fragments, Their Growth and Decay*, Paul Karol, Carnegie Mellon U.
21/08   *A Time Projection Chamber For Physics at the Next e^+e^- Collider*, Madhu Dixit, CRPP/TRIUMF.

04/09   *Do the Fundamental Constants of Nature Vary With Time and Distance?*, Victor Flambaum, INT, Seattle/U. New South Wales.

19/09   *Alpha-Decay Branching Ratio of Near-Threshold States in ^{19}Ne and the Astrophysical Rate of $^{15}O(\alpha,\gamma)^{19}Ne$*, Barry Davids, KVI.

26/09   *Status of the ATLAS Calorimeter*, Monica Wielers, TRIUMF.

03/10   *Comparison of Source Images For Protons, Pions and Λ Hyperons in $6\,A\,GeV\,Au+Au$ Collisions*, Paul Chung, SUNY at Stony Brook.

17/10   *Measuring the Shape of the Proton – More Than Just a Sphere!*, Adam Sarty, St. Mary's U.

21/10   *A Measurement of Particle Branching Ratios in ^{19}Ne Using a Large Area Silicon Array*, Dale Visser, Yale U.

29/10   *Accelerator Production of Radioisotopes at Wisconsin: Methodology For PET and RIB Applications*, Andrew D. Roberts, U. Wisconsin.

31/10   *Developments in Plastic Scintillator*, Anna Pla-Dalmau, Fermilab.

04/11   *Toward an Italian X-Ray FEL Project: the SPARX Proposal and the SPARC R&D Program at INFN-LNF*, Luca Serafini, INFN-Milan/U. Milan.

06/11   *The Canadian Penning Trap Mass Spectrometer – Machine, Method and Measurements!*, Joe Vas, U. Manitoba.

07/11   *GANIL Accelerator Facility: Present Status and Future Upgrade*, Marco Di Giacomo, GANIL.

13/11   *Operation of Titanium Sapphire Lasers at TRIUMF*, Christopher Geppert, U. Mainz.

14/11   *Stochastic Resonance and Human Psychophysics*, Lawrence Ward, UBC.

18/11   *Ion Beam Applications at the Ionenstrahllabor Berlin*, Andrea Denker, Hahn-Meitner-Institut, Berlin.

21/11   *The New Dimensions of Unification*, Graham Kribs, U. Wisconsin.

28/11   *PANDA – Proton ANtiproton at DArmstadt (GSI)*, Klaus Peters, Ruhr-Universität Bochum.

29/11   *Single-Ion Penning Trap Mass Measurements With $\Delta M/M \leq 2 \times 10^{-10}$*, Michael Bradley, MIT.

10/12   *New Results From KAMLAND*, Stuart Freedman, LBNL.

13/12   *GLAST – Mapping the Gamma Ray Sky From Low Earth Orbit*, Richard Dubois, SLAC.

17/12   *Ultracold Neutron Production For Experiments With Confined Neutrons*, Yasuhiro Masuda, KEK.

The following lunchtime seminars were presented at TRIUMF this year.

10/09   *From Sleeplessness to Nightmares: A Post-Mortem of an EPICS System For a Physics Experiment*, David Morris, TRIUMF.

15/10   *TRIUMF Uses a "Lightpath" For High Speed File Transfers to CERN*, Steve McDonald and Corrie Kost, TRIUMF.

---

* All matters concerning TRIUMF seminars should be referred via e-mail to seminar@triumf.ca

The latest listing of TRIUMF seminars can be seen at http://www.triumf.ca/seminars/

USERS GROUPS

TRIUMF USERS' GROUP

From the TRIUMF Users' Group Charter:

The TRIUMF Users' Group is an organization of scientists and engineers with special interest in the use of the TRIUMF facility. Its purpose is:

(a) to provide a formal means for exchange of information relating to the development and use of the facility;

(b) to advise members of the entire TRIUMF organization of projects and facilities available;

(c) to provide an entity responsive to the representations of its members for offering advice and counsel to the TRIUMF management on operating policy and facilities.

Membership of the TRIUMF Users' Group (TUG) is open to all scientists and engineers interested in the TRIUMF program. At the end of 2002 the TUG had 281 members from 12 countries.

TRIUMF Users' Executive Committee (TUEC)

The TRIUMF Users' Executive Committee (TUEC) is a committee of elected members whose role is to represent the interests of the TUG to the TRIUMF administration.

Among other things, TUEC maintains the TUG Web site at http://www.triumf.ca/tug/ where detailed information is available about its membership, that of related committees, and various TUG activities.

TUEC Membership for 2002

G.M. Luke	McMaster U.	*Chair*
N. Rodning	U. Alberta	*Past Chair*
W.D. Ramsay	U. Manitoba	*Chair Elect*
G.D. Morris	LANL	2001/2002
J.E. Sonier	SFU	2002
G.S. Hackman	TRIUMF	2002/2003
M.M. Pavan	U. Regina/TRIUMF	2002/2003
M. Comyn	TRIUMF	*Liaison Officer*

By acclamation, J.E. Sonier (SFU) was elected as chair elect for 2003.

T.A. Porcelli (UNBC) and A. Chen (McMaster U.) were elected as members for 2003/2004.

In addition, TUEC nominated two members to represent the Users on the TRIUMF Operating Committee. In 2002 S. Yen (TRIUMF) moved from being alternate to member, replacing G.M. Marshall (TRIUMF), and L. Lee became his alternate. G.M. Luke (McMaster U.) and J.E. Sonier (SFU) remained as the other member and alternate, respectively.

μSR USERS GROUP

Full details regarding the μSR Users Group and μSR facilities can be obtained via the WWW at http://musr.triumf.ca/.

EXPERIMENT PROPOSALS

The following lists experiment proposals received up to the end of 2002 (missing numbers cover proposals that have been withdrawn or replaced by later versions, rejected, or combined with another proposal). Experiments 1–699 are omitted from this listing (except for those reporting results in this Annual Report). Please refer to the 1999 Annual Report or see http://www.triumf.ca/annrep/experiments.html for a full listing of these earlier experiments. Page numbers are given for those experiments which are included in this Annual Report. Page

560. Low energy $\pi^+ p$ analyzing powers with CHAOS [completed], J. Clark, M.E. Sevior *(U. Melbourne)*, B. Jamieson, P. Tagliente *(UBC)*, P. Delheij, L. Felawka, D.F. Ottewell, K. Raywood, G.R. Smith *(TRIUMF)*, P. Camerini, E. Fragiacomo, R. Rui *(INFN Trieste–U. Trieste)*, N. Grion *(INFN Trieste)*, E.L. Mathie, R. Tacik, M. Yeomans *(U. Regina)*, J. Brack, G. Hofman, J. Patterson, R.J. Peterson, R.A. Ristinen *(U. Colorado)*, E. Gibson *(California State U., Sacramento)*, R. Meier, G. Wagner *(U. Tübingen)* 31

614. Precise measurement of the ρ, σ and $(P_\mu \xi)$ parameters in muon decay [active], W. Andersson, C. Ballard, M. Barnes, Y. Davydov, J. Doornbos, B. Evans, W. Faszer, D.R. Gill, P. Gumplinger, R. Helmer, R. Henderson, D. Maas, J.A. Macdonald, G. Marshall, K. Olchanski, A. Olin, R. Openshaw, J.-M. Poutissou, R. Poutissou, G. Sheffer, S.-C. Wang *(TRIUMF)*, P. Depommier *(U. Montréal)*, A. Gaponenko, P.W. Green, P. Kitching, R. MacDonald, M. Quraan, N. Rodning*, J. Schaapman, J. Soukup, G.M. Stinson, L. Wampler *(U. Alberta)*, M. Hasinoff, B. Jamieson *(UBC)*, E.L. Mathie, R. Tacik *(U. Regina)*, W. Shin *(U. Saskatchewan)*, E. Korkmaz, T. Porcelli *(UNBC)* C.A. Gagliardi, J. Hardy, J.R. Musser, R.E. Tribble, M.A. Vasiliev *(Texas A&M U.)*, D.D. Koetke, P. Nord, T.D.S. Stanislaus *(Valparaiso U.)*, Y. Davydov, A. Khruchinsky, V. Selivanov, V. Torokhov *(KIAE, Moscow)*, R. Mischke *(Los Alamos Nat. Lab)* 5

700. Measuring cross sections of long-lived radionuclides produced by 200-500 MeV protons in elements found in meteorites and lunar rocks [completed], J. Vincent *(TRIUMF)*, J.M. Sisterson *(Harvard U.)*, K. Kim *(San Jose State U.)*, A.J.T. Jull *(U. Arizona)*, M.W. Caffee *(Lawrence Livermore Nat. Lab)*, R.C. Reedy *(Los Alamos Nat. Lab)*

702. Measurement of kaon-nucleon elastic scattering at 16 MeV [active], G.A. Beer, P. Knowles, G.R. Mason, A. Olin, L.P. Robertson *(U. Victoria)*, P. Amaudruz, D.R. Gill, G. Smith, S. Yen *(TRIUMF)*, L. Lee *(U. Manitoba)*, G. Tagliente *(UBC)*

703. Study of the decay $\pi^+ \to e^+ \nu$ phase I – lifetime measurement of the pion [completed], D.A. Bryman, T. Numao, A. Olin *(TRIUMF)*

704. Charge symmetry breaking in $np \to d\pi^0$ close to threshold [completed data-taking], R. Abegg*, P.W. Green, D.A. Hutcheon *(TRIUMF–U. Alberta)*, L.G. Greeniaus *(U. Alberta–TRIUMF)*, R.W. Finlay, A.K. Opper, S.D. Reitzner *(Ohio U.)*, E. Korkmaz, T.A. Porcelli *(UNBC)*, J.A. Niskanen *(U. Helsinki)*, P. Walden *(TRIUMF–UBC)*, S. Yen *(TRIUMF)*, C.A. Davis *(TRIUMF–U. Manitoba)*, D.V. Jordan *(Ohio U.–U. Alberta)*, E. Auld *(UBC)* 32

705. Development of modular gas microstrip chambers as in-target tracking devices for an experiment to detect $\Lambda\Lambda$ hypernuclei at the BNL AGS (BNL885) [completed data-taking], C.A. Davis *(TRIUMF–U. Manitoba)*, B. Bassalleck, R. Stotzer *(U. New Mexico)*, A.R. Berdoz, A. Biglan, D.S. Carman, G.B. Franklin, P. Khaustov, P. Koran, R. Magahiz, R. McCrady, C.A. Meyer, K. Paschke, B. Quinn, R.A. Schumacher, *(Carnegie-Mellon U.)*, J. Birchall, L. Gan, M.R. Landry, L. Lee, S.A. Page, W.D. Ramsay, W.T.H. van Oers *(U. Manitoba)*, T. Bürger, H. Fischer, J. Franz, H. Schmitt *(U. Freiburg)*, D.E. Alburger, R.E. Chrien, M. May, P.H. Pile, A. Rusek, R. Sawafta, R. Sutter *(Brookhaven Nat. Lab)*, A. Ichikawa, K. Imai, Y. Kondo, K. Yamamoto, M. Yosoi *(Kyoto U.)*, F. Takeutchi *(Kyoto Sangyo U.)*, V.J. Zeps *(U. Kentucky)*, P.D. Barnes, F. Merrill *(Los Alamos Nat. Lab)*, V.J. Zeps *(U. Kentucky)*, T. Iijima *(KEK)*, J. Lowe *(U. Birmingham)*

706. μSR studies of spin fluctuations in $CePt_2Sn_2$ and other Kondo spin systems [completed], A. Keren, K. Kojima, G.M. Luke, Y.J. Uemura, W.D. Wu *(Columbia U.)*, K. Andres, G.M. Kalvius *(Tech. U. Munich)*, H. Fujii, G. Nakamoto, T. Takabatake, H. Tanaka *(Hiroshima U.)*, M. Ishikawa *(ISSP, U. Tokyo)*, B. Andraka *(U. Florida)*, D.L. Cox *(Ohio State U.)*

707. μSR measurements on two-dimensional site-diluted antiferromagnets [active], K. Kojima *(Columbia U.–U. Tokyo)*, A. Keren, G.M. Luke, Y.J. Uemura, W.D. Wu *(Columbia U.)*, H. Ikeda *(KEK–KENS)*, R.J. Birgeneau *(MIT)*, K. Nagamine *(U. Tokyo)*

708. The spin relaxation and chemical reactivity of muonium-substituted organic radicals in the gas phase [completed], D.G. Fleming, J.J. Pan, M. Shelley *(UBC)*, D.J. Arseneau *(TRIUMF–UBC)*, M. Senba *(TRIUMF)*, J.C. Brodovitch, P.W. Percival *(SFU)*, H. Dilger, E. Roduner *(U. Zürich)*, S.F.J. Cox *(Rutherford Appleton Lab)*

709. $^{90,92,94,96}\mathrm{Zr}(n,p)^{90,92,94,96}\mathrm{Y}$ reaction at 200 MeV [completed data-taking], A.G. Ling, P.L. Walden *(TRIUMF)*, J. Rapaport *(Ohio U.)*, D.A. Cooper, D.L. Prout, E.R. Sugarbaker *(Ohio State U.)*, M. Halbert *(Oak Ridge Nat. Lab)*, D. Mercer *(U. Colorado)*, J. Campbell *(U. Manitoba–TRIUMF)*, M. Hartig *(U. Muenster)*

710. Dynamics of muonium in Ge and GaAs [completed], R.L. Lichti *(Texas Tech. U.)*, S.F.J. Cox *(Rutherford Appleton Lab)*, R.F. Kiefl *(UBC)*, K.H. Chow *(Lehigh U.)*, T.L. Estle *(Rice U.)*, B. Hitti *(TRIUMF)*, E.A. Davis *(Leicester U.)*, C.R. Schwab *(CNRS, Strasbourg)*

712. μSR study of superconducting spin glasses [completed], V. McMullen, D.R. Noakes , C.E. Stronach *(Virginia State U.)*, E.J. Ansaldo *(U. Saskatchewan)*, J.H. Brewer *(UBC)*, G. Cao, J.E. Crow *(NHMFL)*, S. McCall *(Florida State U.–NHMFL)*

713. Muonium chemistry in supercritical water [completed], B. Addison-Jones, J.-C. Brodovitch, K. Ghandi, I. McKenzie, P. Percival *(SFU)*, J. Schüth *(U. Bonn)*

714. Atomic PNC in francium: preparations [inactive], J.A. Behr, L. Buchmann, M. Dombsky, P. Jackson, C.D.P. Levy *(TRIUMF)*, J.M. D'Auria, P. Dubé, A. Gorelov, D. Melconian, T. Swanson, M. Trinczek *(SFU)*, O. Häusser *(SFU–TRIUMF)*, U. Giesen *(U. Alberta)*, I. Kelson, A.I. Yavin *(Tel Aviv U.)*, J. Deutsch *(U. Catholique de Louvain)*, J. Dilling *(SFU–Heidelberg)*

715. Weak interaction symmetries in β^+ decay of optically trapped $^{37,38m}\mathrm{K}$ [active], J.M. D'Auria, A. Gorelov, D. Melconian, M. Trinczek *(SFU)*, J.A. Behr, P. Bricault, M. Dombsky, K.P. Jackson, B.K. Jennings *(TRIUMF)*, S. Gu, M. Pearson *(UBC)*, U. Giesen *(U. Notre Dame)*, W.P. Alford *(U. Western Ontario)*, J. Deutsch *(U. Catholique de Louvain)*, D.A. Ashery, O. Aviv *(Tel Aviv U.)*, F. Glück *(U. Mainz)*

716. Complete beta-delayed particle emission study of $^{31}\mathrm{Ar}$ [deferred], J. Cerny, D.M. Moltz, T. Ognibene, M.W. Rowe, R.J. Tighe *(Lawrence Berkeley Lab)*, L. Buchmann *(TRIUMF)*, J. D'Auria *(SFU)*, M. Dombsky *(SFU–U. Alberta)*, G. Roy *(U. Alberta)*

717. Muon hyperfine transition rates in light nuclei [completed], J.H. Brewer, E. Gete, M.C. Fujiwara, J. Lange, D.F. Measday, B.A. Moftah, M.A. Saliba, T. Stocki *(UBC)*, T.P. Gorringe *(U. Kentucky)*

718. Superconductivity and magnetism in quaternary boron carbides [completed], A. Keren, G.M. Luke, Y.J. Uemura, W.D. Wu *(Columbia U.)*, K. Kojima *(Columbia U.–U. Tokyo)*, S. Uchida *(U. Tokyo)*

719. $^4\mathrm{He}(\pi^+,\pi^- pp)$ invariant mass measurement with CHAOS [completed data-taking], P. Amaudruz, L. Felawka, D. Ottewell, G. Smith *(TRIUMF)*, E.T. Mathie, R. Tacik, D.M. Yeomans *(U. Regina)*, H. Clement, J. Gräter, R. Meier, G.J. Wagner *(U. Tübingen)*, J. Clark, M. Sevior *(U. Melbourne)*, A. Ambardar, G.J. Hofman, M. Kermani, G. Tagliente *(UBC)*, F. Bonutti, P. Camerini, N. Grion, R. Rui *(U. di Trieste)*, J. Brack, R. Ristinen *(U. Colorado)*, E. Gibson *(California State U., Sacramento)*, M. Schepkin *(ITEP Moscow)*

720. Muonium's nucleophilicity [active], G.B. Porter, D.C. Walker *(UBC)*, J.M. Stadlbauer* *(Hood Coll.)*, K. Venkateswaran *(Hindustan Lever Ltd.)*, M.V. Barnabas *(Proctor & Gamble Ltd.)*

721. The delta nucleon reaction in CHAOS [completed data-taking], F. Farzanpay, P. Hong, E.L. Mathie, N. Mobed *(U. Regina)*, R. Tacik *(TRIUMF–U. Regina)*, P.A. Amaudruz, L. Felawka, R. Meier, D. Ottewell, G.R. Smith *(TRIUMF)*, N. Grion *(INFN, Trieste)*, P. Camerini, R. Rui *(U. di Trieste)*, E. Gibson *(California State U., Sacramento)*, G. Hofman, G. Jones, M. Kermani *(UBC)*, M.E. Sevior *(U. Melbourne)*, J.T. Brack, R.A. Ristinen *(U. Colorado)*

722. Pion initial state interactions in the $^{12}\mathrm{C}(\pi^+,ppp)$ reaction [completed data-taking], T. Mathie, R. Tacik *(U. Regina)*, P.A. Amaudruz, L. Felawka, D. Ottewell, K. Raywood, G.R. Smith *(TRIUMF)* M. Kermani, S. McFarland *(UBC)*, F. Bonutti, P. Camerini, R. Rui *(U. di Trieste)*, N. Grion *(INFN, Trieste)*, E.F. Gibson *(California State U., Sacramento)*, M. Sevior *(U. Melbourne)*, J. Brack, G. Hofman *(U. Colorado)*, R. Meier *(U. Tübingen)*

723. Study of pion-nucleus double-scattering reactions [completed data-taking], R. Tacik *(TRIUMF–U. Regina)*, T. Mathie *(U. Regina)*, P. Amaudruz, L. Felawka, D. Ottewell, K. Raywood, G. Smith *(TRIUMF)*, M. Kermani, S. McFarland *(UBC)*, F. Bonutti, P. Camerini, R. Rui *(U. di Trieste)*, N. Grion *(INFN, Trieste)*, J. Brack, G. Hofman *(U. Colorado)*, R. Meier *(U. Tübingen)*, M. Sevior *(U. Melbourne)*, E. Gibson *(California State U. Sacramento)*

724. μSR measurements on spin ladder systems [completed], A. Keren, G.M. Luke, Y.J. Uemura, W.D. Wu *(Columbia U.)*, K. Kojima *(Columbia U.–U. Tokyo)*, M. Takano *(Kyoto U.)*, K. Nagamine *(U. Tokyo)*

725. Pion double charge exchange reactions on $^{3,4}\mathrm{He}$ in the energy range 50–100 MeV [completed], P. Amaudruz, L. Felawka, R. Meier, D. Ottewell, G. Smith *(TRIUMF)*, T. Mathie, R. Tacik, M. Yeomans *(U. Regina)*, J. Graeter, G. Wagner *(U. Tübingen)*, J. Clark, M. Sevior *(U. Melbourne)*, G. Hofman, M. Kermani, P. Tagliente *(UBC)*, F. Bonutti, P. Camerini, N. Grion, R. Rui *(U. di Trieste)*, J. Brack, R. Ristinen *(U. Colorado)*, E. Gibson *(California State U., Sacramento)*, O. Patarakin *(Kurchatov Inst.)*, E. Friedman *(Hebrew U. Jerusalem)*

726. Beta-delayed proton and γ-decay of ^{65}Se, ^{69}Kr and ^{73}Sr [active], D. Anthony, J. D'Auria, M. Trinczek *(SFU)*, R.E. Azuma, J.D. King *(U. Toronto)*, L. Buchmann, K.P. Jackson, J. Vincent *(TRIUMF)*, M. Dombsky *(SFU–U. Alberta)*, U. Giesen *(TRIUMF–U. Alberta)*, J. Görres, H. Schatz, M. Wiescher *(U. Notre Dame)*, C. Iliadis *(TRIUMF–U. Toronto)*, G. Roy *(U. Alberta)*

728. Search for population and de-excitation of low-spin superdeformed states in Po-Hg region via β^+ and α decays [completed data-taking], Y.A. Akovali, M. Brinkman *(Oak Ridge Nat. Lab)*, J.M. D'Auria *(TRIUMF–SFU)*, J.A. Becker, E.A. Henry *(Lawrence Livermore Nat. Lab)*, M. Dombsky *(SFU)*, P.F. Mantica *(UNISOR)*, W. Nazarewicz *(Joint Inst. for Heavy Ion)*, J. Rikovska, N.J. Stone *(Oxford U.)*, M.A. Stoyer *(Lawrence Berkeley Nat. Lab)*, R.A. Wyss *(MSI, Sweden)*

729. Gamow-Teller and spin-dipole strengths from ^{17,18}O(n,p) [completed data-taking], D.P. Beatty, H.T. Fortune, P.P. Hui, R.B. Ivie, Z.Q. Mao, M.G. McKinzie, D.A. Smith *(U. Pennsylvania)*, W.P. Alford *(U. Western Ontario)*, K.P. Jackson, A.G. Ling, C.A. Miller, P. Walden, S. Yen *(TRIUMF)*

730. The solar neutrino problem and a new measurement of ^{7}Be$(p,\gamma)^8$B [deferred], R.E. Azuma, J.D. King *(U. Toronto)*, P. Bricault, L. Buchmann, T. Ruth, H. Schneider, J. Vincent, S. Zeisler *(TRIUMF)*, J. D'Auria, R. Korteling *(SFU)*, M. Dombsky *(SFU–U. Alberta)*, U. Giesen *(TRIUMF–U. Alberta)*, C. Iliadis *(TRIUMF–U. Toronto)*, G. Roy *(U. Alberta)*, M. Wiescher *(U. Notre Dame)*

731. Investigation of spin-polarized muonium in metallic semiconductors [completed], K.H. Chow, S. Dunsiger, R.F. Kiefl, W.A. MacFarlane, J. Sonier *(UBC)*, S.F.J. Cox *(Rutherford Appleton Lab)*, E.A. Davis, A. Singh *(Leicester U.)*, T.L. Estle, B. Hitti *(Rice U.)*, R.L. Lichti *(Texas Tech. U.)*, P. Mendels *(Orsay U.)*, C. Schwab *(CRN, Strasbourg)*

732. Quantum impurities in one dimensional spin 1/2 chains [completed], I. Affleck, J.H. Brewer, K. Chow, S. Dunsiger, S. Eggert, R.F. Kiefl, A. MacFarlane, J. Sonier *(UBC)*, A. Keren, Y.J. Uemura *(Columbia U.)*

733. Probing high T_c superconductor with "paramagnetic" (μ^-O) system [active], H. Kojima, I. Tanaka, E. Torikai *(Yamanashi U.)*, K. Nishiyama *(U. Tokyo)*, K. Nagamine *(U. Tokyo–RIKEN)*, I. Watanabe *(RIKEN)*, T.P. Das *(State U. New York)*, S. Maekawa *(Nagoya U.)*

734. Radiative muon capture on nickel isotopes [completed], D.S. Armstrong, P. McKenzie *(Coll. of William & Mary)*, G. Azuelos, P. Depommier *(U. de Montréal)*, P. Bergbusch, P. Gumplinger, M. Hasinoff, E. Saettler *(UBC)*, B. Doyle, T.P. Gorringe, R. Sedlar *(U. Kentucky)*, M. Blecher, C. Sigler *(Virginia Polytechnic Inst.)*, J.A. MacDonald, J.-M. Poutissou, R. Poutissou, D. Wright *(TRIUMF)*

735. Studies of single layer cuprate superconductors [completed], G.M. Luke, B. Nachumi, Y.J. Uemura *(Columbia U.)*, K. Kojima *(Columbia U.–U. Tokyo)*, S. Uchida *(U. Tokyo)*, R.H. Heffner, L.P. Le *(Los Alamos Nat. Lab)*, R. MacLaughlin *(U. California, Riverside)*, M.B. Maple *(U. California, San Diego)*

736. Tests of electro-weak theory using ^{14}O beam [deferred], M. Bahtacharya, A. Garcia, R. Rutchi, M. Wayne *(U. Notre Dame)*, L. Buchmann *(TRIUMF)*, C. Iliadis *(TRIUMF–U. Toronto)*, B. Fujikawa *(Lawrence Berkeley Lab)*, S.J. Freedman, J. Mortara *(U. California, Berkeley)*

737. Magnetic and superconducting behaviour in selected oxide materials [completed], R.H. Heffner, L.P. Le *(Los Alamos Nat. Lab)*, D.E. Maclaughlin *(U. California, Riverside)*, G. Luke, B. Nachuma, Y.J. Uemura *(Columbia U.)*, K. Kojima *(Columbia U.–U. Tokyo)*

740. Irradiation of silicon tracker components [completed], R. Lipton, L. Spiegel *(Fermilab)*, K.F. O'Shaughnessy *(U. California, Santa Cruz)*, B. Barnett, J. Cameratta, J. Skarha *(Johns Hopkins U.)*, N. Brunner, M. Frautschi, M. Gold, Y. Ling, J. Matthews, S. Seidel *(U. New Mexico)*, D. Bortoletto, A. Garfinkel, A. Hardman, K. Hoffman, T. Keaffaber, N.M. Shaw *(Purdue U.)*

741. Beta-delayed proton decay of ^{17}Ne to α-emitting states in ^{16}O [completed], R.E. Azuma, J. Chow, J.D. King, A.C. Morton *(U. Toronto)*, L. Buchmann, M. Dombsky *(TRIUMF)*, U. Giesen *(U. Notre Dame)*, T. Davinson, A.C. Shotter *(U. Edinburgh)*, R.N. Boyd *(Ohio State U.)*, C. Iliadis *(U. North Carolina)*, J. Powell *(U. California, Berkeley)*,

742. Scattering of muonic hydrogen isotopes [completed], V.M. Bystritsky, V.A. Stolupin *(JINR)*, R. Jacot-Guillarmod, P.E. Knowles, F. Mulhauser *(U. Fribourg)*, G.M. Marshall *(TRIUMF)*, M. Filipowicz, J. Wozniak *(Fac. Phys., Nucl. Tech., Krakow)*, A. Adamczak *(Inst. Nucl. Physics, Krakow)*, A.R. Kunselman *(U. Wyoming)*, V.E. Markushin, C. Petitjean *(PSI)*, T.M. Huber *(Gustavus Adolphus Coll.)*, G.A. Beer, M. Maier, A. Olin, T.A. Porcelli *(U. Victoria)*, P. Kammel *(U. California, Berkeley)*, M.C. Fujiwara *(UBC)*, J. Zmeskal *(IMEP Vienna)*, S.K. Kim *(Jeonbuk Nat. U.)*

743. Gamow-Teller strength in ^{64,66,68}Zn and ^{63,65}Cu(n,p) [completed data-taking], W.P. Alford *(U. Western Ontario)*, D. Beatty, H.T. Fortune, P.P. Hui, R.B. Ivie, Z. Mao, M.G. McKinzie, D.A. Smith *(U. Pennsylvania)*, S. Yen *(TRIUMF)*

744. Hadronic weak and electromagnetic form factors via $\pi^- p \to e^+ e^- n$ [active], P. Gumplinger, M.D. Hasinoff *(UBC)*, E. Christy, B.C. Doyle, T.P. Gorringe, M.A. Kovash, S. Tripathi, P. Zolnierchuk *(U. Kentucky)*, D.H. Wright *(SLAC)*

745. μ^-SR measurements on one-dimensional spin systems [active], K. Kojima *(Columbia U.–U. Tokyo)*, K. Nagamine, K. Nishiyama, S. Uchida *(U. Tokyo)*, G.M. Luke, B. Nachumi, Y.J. Uemura *(Columbia U.)*, I. Affleck, S. Dunsiger, S. Eggert, R.F. Kiefl *(UBC)*

746. Muonium dynamics in Si, Ge and GaAs studied by RF-μSR and μW-μSR [active], S.R. Kreitzman *(TRIUMF)*, T.L. Estle, B. Hitti *(Rice U.)*, R. Lichti *(Texas Tech. U.)*, K. Chow *(UBC)*, S.F.J. Cox *(Rutherford Appleton Lab)*, E.A. Davis *(Leicester U.)*, C. Schwab *(CRN Strasbourg)*

747. μSR study of re-entrant spin glasses a-FeMn, AuFe, and $Fe_{70}Al_{30}$ [completed], I.A. Campbell *(U. Paris Sud Orsay)*, S. Dunsiger, R.F. Kiefl *(UBC)*, M.J.P. Gingras *(TRIUMF)*, M. Hennion, I. Mirebeau *(Saclay, LLB)*, K. Kojima, G.M. Luke, B. Nachumi, Y.J. Uemura, W.D. Wu *(Columbia U.)*

749. Muonium-substituted free radicals [completed], B. Addison-Jones, J.C. Brodovitch, K. Ghandi, I. McKenzie, P.W. Percival *(SFU)*, J. Schüth *(U. Bonn)*

750. Liquid chemistry μSR [completed], G.B. Porter, D.C. Walker *(UBC)*, J.M. Stadlbauer* *(Hood Coll.)*, K. Venkateswaran *(Lever Hindustan Ltd.)*, M.V. Barnabas *Procter & Gamble Ltd.)*

751. Tests in preparation for μSR measurements of off-axis internal magnetic fields in anisotropic superconductors [active], E. Csomortani, W.J. Kossler, X. Wan *(Coll. of William & Mary)*, D.R. Harshman *(Physikon Research Inc.)*, A. Greer *(Gonzaga U.)*, E. Koster, D.L. Williams *(UBC)*, C.E. Stronach *(Virginia State U.)*

752. Muonium centres in Si and GaAs [completed], K.H. Chow *(Oxford U.)*, S.F.J. Cox *(Rutherford Appleton Lab)*, E.A. Davis *(Leicester U.)*, S. Dunsiger, R.F. Kiefl, W.A. MacFarlane *(UBC)*, T.L. Estle *(Rice U.)*, B. Hitti *(TRIUMF)*, R.L. Lichti *(Texas Tech. U.)*, C. Schwab *(CRN Strasbourg)*

753. Studies of magnetic correlations in planar oxides [completed], K. Kojima *(Columbia U.–U. Tokyo)*, M. Larkin, G.M. Luke, J. Merrin, B. Nachumi, Y.J. Uemura *(Columbia U.)*, B.J. Sternlieb *(Brookhaven Nat. Lab)*, S. Uchida *(U. Tokyo)*

754. A search for the muonium substituted hydroxyl radical [deferred], T.A. Claxton, G. Marston *(Leicester U.)*, S.F.J. Cox *(Rutherford Appleton Lab)*, D. Arseneau, D. Fleming, M. Senba, P. Wassell *(UBC)*, J.-C. Brodovitch, P.W. Percival *(SFU)*

755. Muonium formation in Zn-spinels [deferred], G.M. Kalvius, A. Kratzer, W. Potzel *(Tech. U. Munich)*, R. Wäppling *(U. Uppsala)*, D.R. Noakes *(Virginia State U.)*, S.R. Kreitzman *(TRIUMF)*, A. Martin *(U. Jena)*, M.K. Krause *(U. Leipzig)*

756. Mu+NO spin relaxation: electron exchange or paramagnetism? [deferred], D.G. Fleming, J.J. Pan, M. Senba, M. Shelley *(UBC)*, D.J. Arseneau *(TRIUMF)*, E. Roduner *(U. Zürich)*

757. Study of muon dynamics in ferroelectric materials and proton ionic conductors – comparison with proton dynamics [completed], W.K. Dawson, K. Nishiyama, S. Ohira, K. Shimomura *(U. Tokyo)*, K. Nagamine *(U. Tokyo–RIKEN)*, S. Ikeda *(KEK)*, S. Shin *(U. Tokyo –ISSP)*, N. Sata *(Tohoku U.)*

758. Electronic structure of muonium and muonium-lithium complexes in graphite and related compounds [completed], J. Brewer, J. Chakhalian, S. Dunsiger, R.F. Kiefl, W.A. MacFarlane, R. Miller, J. Sonier *(UBC)*, J. Dahn *(Dalhousie U.)*, J. Fischer *(U. Pennsylvania)*, B. Hitti, S.R. Kreitzman *(TRIUMF)*

759. Study of the isotropic hyperfine coupling constant of muonium at high temperature and under uniaxial pressure [completed], W.K. Dawson, K. Nishiyama, S. Ohira, K. Shimomura *(U. Tokyo)*, K. Nagamine *(U. Tokyo–RIKEN)*, T.P. Das *(U. New York, Albany)*

761. Parity violation in $p-p$ scattering at 450 MeV [deferred], J. Birchall, C.A. Davis, L. Lee, S.A. Page, W.D. Ramsay, A.W. Rauf, G. Rutledge, W.T.H. van Oers *(U. Manitoba)*, R. Helmer, R. Laxdal, C.D.P. Levy *(TRIUMF)*, P.W. Green, G. Roy, G.M. Stinson *(U. Alberta)*, N.A. Titov, S. Zadorozhny, A.N. Zelenski *(INR, Moscow)*, J.D. Bowman, R.E. Mischke, S. Penttila, W.S. Wilburn *(Los Alamos Nat. Lab)*, E. Korkmaz, *(UNBC)*, M. Simonius *(ETH Zürich)*, J. Bisplinghoff, P.D. Eversheim, F. Hinterberger *(U. Bonn)*, W. Kretschmer, G. Morgenroth *(U. Erlangen)*, H. Schieck *(U. Cologne)*, P. von Rossen *(KFA Jülich)*

762. Gamow-Teller and spin-flip dipole strengths near $A=90$ [completed data-taking], W.P. Alford *(U. Western Ontario)*, D.P. Beat- ty, H.T. Fortune, P.P. Hui, R.B. Ivie, D. Koltenuk, J. Yu *(U. Pennsylvania)*, A. Ling, S. Yen *(TRIUMF)*, S. El-Kateb *(King Fahd U.)*

763. Muon cooling and acceleration in an undulating crystal channel [deferred], S.A. Bogacz, D.B. Cline, D.A. Sanders *(UCLA)*, L.M. Cremaldi, B. Denardo, Q. Jie, D.J. Summers *(U. Mississippi–Oxford)*, G.M. Marshall *(TRIUMF)*

764. Calibration of a segmented neutron detector [completed], E. Korkmaz, G. O'Rielly *(UNBC)*, D.A. Hutcheon *(TRIUMF)*, A.K. Opper *(U. Alberta)*, G. Feldman, N.R. Kolb *(U. Saskatchewan)*

766. The ortho-para transition rate in muonic molecular hydrogen [completed data-taking], D.S. Armstrong, J.H.D. Clark, P. King *(Coll. of William & Mary)*, T.P. Gorringe, S. Tripathi, P.A. Żołnierczuk *(U. Kentucky)*, M.D. Hasinoff, T. Stocki *(UBC)*, D.H. Wright *(TRIUMF)*

767. Direct measurement of sticking in muon catalyzed $d - t$ fusion [inactive], J.M. Bailey *(Chester Technology, UK)*, G.A. Beer, M. Maier, G.R. Mason, T.A. Porcelli *(U. Victoria)*, K.M. Crowe, P. Kammel *(U. California, Berkeley–LBL)*, M.C. Fujiwara, E. Gete, T.J. Stocki *(UBC)*, T.M. Huber *(Gustavus Adolphus Coll.)*, S.K. Kim *(Jeonbuk Nat. U.)*, A.R. Kunselman *(U. Wyoming)*, G.M. Marshall, A. Olin *(TRIUMF)*, C.J. Martoff *(Temple U.)*, V.S. Melezhik *(JINR, Dubna)*, F. Mulhauser *(U. Fribourg)*, C. Petitjean *(PSI)*, J. Zmeskal *(IMEP Vienna)*

768. Generalized Fulde-Ferrell-Larkin-Ovchinnikov state in heavy fermion and intermediate valence systems [active], J. Akimitsu, K. Oishi, T. Muranaka *(Aoyama Gakuin U.)*, W. Higemoto, R. Kadono, A. Koda *(KEK-IMSS)*, M. Nohara, H. Suzuki, H. Takagi *(U. Tokyo)*, R.F. Kiefl, R.I. Miller, A.N. Price *(UBC-TRIUMF)*, J.E. Sonier *(SFU)* 72

769. Effects of uniaxial stress on muonium in semiconductors [completed], K.H. Chow *(Oxford)*, B. Hitti *(TRIUMF)*, R.F. Kiefl *(UBC)*, T.L. Estle *(Rice U.)*, R. Lichti *(Texas Tech. U.)*

770. μSR studies of organic conductors: (BEDT-TTF)$_2$– X and (TMTTF)$_2$Br [completed], K. Kojima, M. Larkin, G.M. Luke, J. Merrin, B. Nachumi, Y.J. Uemura *(Columbia U.)*, P.M. Chaikin *(Princeton U.)*, G. Saito *(Kyoto U.)*

771. μSR studies of geometrically frustrated S = 1/2 spin systems [completed], K. Kojima, M. Larkin, G.M. Luke, J. Merrin, B. Nachumi, Y.J. Uemura *(Columbia U.)*, M.J.P. Gingras *(TRIUMF)*, S. Dunsiger, R.F. Kiefl *(UBC)*, D.C. Johnston, S. Kondo *(Iowa State U.)*, S. Uchida *(U. Tokyo)*, R.J. Cava *(AT&T Bell Labs)*

772. Search for the $\Delta - \Delta$ dibaryon [inactive], R. Abegg*, C.A. Miller, P. Walden, S. Yen *(TRIUMF)*, R. Bent *(Indiana U.)*, T.Y. Chen, F. Wang, C.H. Ye *(Nanjing U.)*, W. Falk *(U. Manitoba)*, D. Frekers, M. Hartig *(U. Muenster)*, T. Goldman *(Los Alamos Nat. Lab)*, M. Heyrat, C.W. Wong *(UCLA)*, G. Jones *(UBC)*, E. Korkmaz, G. O'Rielly *(UNBC)*, C. Rangacharyulu *(U. Saskatchewan)*, I. Strakovsky *(Virginia Tech. Inst.)*, Z.X. Sun, J.C. Xu *(Inst. Atomic Energy, China)*, T. Walton *(Cariboo U. Coll.)*

773. Muon-electron interaction in n-type silicon [completed], D. Arseneau, B. Hitti, S.R. Kreitzman *(TRIUMF)*, J.H. Brewer, R.F. Kiefl, G. Morris *(UBC)*, K. Chow *(Oxford U.)*, S.F.J. Cox *(Rutherford Appleton Lab)*, D.G. Eshchenko *(INR, Moscow)*, T.L. Estle *(Rice U.)*, R. Lichti *(Texas Tech. U.)*, V.G. Storchak, *(Kurchatov Inst.)*

774. Muonium dynamics in GaAs studied by rf and μ-wave μSR [active], B. Hitti, S.R. Kreitzman *(TRIUMF)*, T.L. Estle *(Rice U.)*, R. Lichti *(Texas Tech. U.)*

775. Electron transport in insulators, semiconductors and magnetic materials [active], J.H. Brewer, A. Izadi, D.M.C. Liu, K.M. Nichol, S. Sivanandam, A.T. Warkentin *(UBC)*, G.D. Morris *(TRIUMF)*, V.G. Storchak *(Kurchatov Inst.)*, D.G. Eshchenko *(INR, Moscow)*, J.D. Brewer *(SFU)*

776. Rare earth materials with disordered spin structures [completed], J.H. Brewer *(UBC)*, K. Fukamichi *(Tohoku U.)*, G.M. Kalvius *(Tech. U. Munich)*, D.R. Noakes, C.E. Stronach *(Virginia State U.)*, R. Wäppling *(Uppsala U.)*

777. Vortex state of s-wave superconductors investigated by muon spin rotation [active], J.C. Chakhalian, K. Chow, R. Miller, A.N. Price *(UBC)*, J.H. Brewer, R.F. Kiefl *(UBC–TRIUMF)*, G.M. Luke *(McMaster U.)*, J.E. Sonier *(SFU)*

778. $\pi^{\pm}p$ differential cross sections in the Coulomb-nuclear interference region [completed data-taking], P. Amaudruz, D. Ottewell, *(TRIUMF)*, P. Camerini, E. Fragiacomo, N. Grion, S. Piano, R. Rui *(INFI Trieste–U. Trieste)*, K. Babcock, E. Mathie, H. Xu, D.M. Yeomans *(U. Regina)*, G. Hofman, M.M. Pavan, K.J. Raywood, R. Tacik *(Regina–TRIUMF)*, J. Breitschopf, H. Denz, R. Meier, F. von Wrochem, G. Wagner *(U. Tübingen)*, G. Moloney, M. Sevior *(U. Melbourne)*, J. Brack, J. Patterson, R. Ristinen *(U. Colorado)*, E. Gibson *(California State U., Sacramento)*, O. Patarakin *(Kurchatov Inst.)*, G. Smith *(Jefferson Lab)* 39

779. Accelerator mass spectrometry experiments at ISAC [inactive], S. Calvert, A. Glass, R.R. Johnson, T. Petersen *(UBC)*, Z. Gelbart, D. Ottewell *(TRIUMF)*, R. Schubank *(unaffiliated)*, C.S. Wong *(Inst. of Ocean Sciences)*, J. Clague *(Geological Survey Canada)*, M. Paul *(Hebrew U. Jerusalem)*

780. Deeply bound pionic states through $^{208}\text{Pb}(p,^3\text{He})^{206}\text{Pb}\bigotimes\pi^-$ [completed], D. Frekers, W. Garske, K. Grewer, M. Hartig, H. Wörtche *(U. Muenster)*, H. Machner *(KFA, Jülich)*, D. Hutcheon, P. Walden, S. Yen *(TRIUMF)*, A. Opper *(U. Ohio)*

781. Investigations of the $\pi\pi$ invariant mass distributions of nuclear $(\pi^+, \pi^-\pi^+)$ reactions with the CHAOS detector [completed data-taking], J. Clark, G. Moloney, M.E. Sevior *(U. Melbourne)*, L. Felawka, G. Hofman, D.F. Ottewell, K. Raywood, G.R. Smith *(TRIUMF)*, R. Meier *(U. Tübingen)*, P. Camerini, E. Fragiacomo, R. Rui *(INFN Trieste–U. Trieste)*, N. Grion, S. Piano *(INFN, Trieste)*, E.L. Mathie, R. Tacik, *(U. Regina)*, E.F. Gibson *(Cal. State U., Sacramento)* 39

782. Non-fermi-liquid behaviour and other novel phenomena in heavy-fermion alloys [active], D.E. MacLaughlin *(U. California, Riverside)*, R.H. Heffner, G.D. Morris *(Los Alamos Nat. Lab)*, Y.J. Uemura *(Columbia U.)*, M.B. Maple *(U. California, San Diego)*, O.O. Bernal *(Cal. State U., Los Angeles)*, G.M. Luke *(McMaster U.)*, J.E. Sonier *(SFU)*, B. Andraka, G.R. Stewart *(U. Florida)* 73

783. Paramagnetic frequency shifts in unconventional superconductors [active], R.H. Heffner, G.D. Morris *(Los Alamos Nat. Lab)*, D.E. MacLaughlin *(U. California, Riverside)*, G.J. Nieuwenhuys *(U. Leiden)*, O.O. Bernal *(Cal. State U., Los Angeles)*, J.E. Sonier *(SFU)*

784. μSR studies of spin singlet states in oxides [active], A. Fukaya, I. Gat, M. Larkin, A. Savici, Y.J. Uemura *(Columbia U.)*, T. Ito *(Columbia U.–ETL)*, H. Kageyama, K. Ueda, Y. Ueda *(U. Tokyo)*, P.P. Kyriakou, G.M. Luke, M.T. Rovers *(McMaster U.)*

785. Pion double charge exchange on ^{3}He with CHAOS [completed data-taking], R. Tacik *(TRIUMF–U. Regina)*, E.L. Mathie, M. Yeomans *(U. Regina)*, H. Clement, J. Graeter, R. Meier, J. Petzold, G.J. Wagner *(U. Tübingen)*, E. Friedman *(Hebrew U. Jerusalem)*, N. Grion *(INFN Trieste)*, P. Camerini, E. Fragiacomo, R. Rui *(U. Trieste)*, L. Felawka, D. Ottewell, K. Raywood, G.R. Smith *(TRIUMF)*, G. Hofman, B. Jamieson, G. Tagliente *(UBC)*, J. Clark, G. Molony, M.E. Sevior *(U. Melbourne)*, E. Gibson *(California State U. Sacramento)*, H. Staudenmeyer *(U. Karlsruhe)*, S. Filippov, Y. Gavrilov, T. Karavicheva *(Moscow Meson Factory)*

786. Low energy structures in the β-delayed particle decays of ^{9}C, ^{12}N and ^{17}Ne [completed data-taking], N. Bateman *(TRIUMF–SFU–U. Toronto)*, L. Buchmann, K.P. Jackson, T. Shoppa *(TRIUMF)*, J. Chow, J.D. King, C. Mortin *(U. Toronto)*, T. Davison, A. Ostrowski, A. Shotter *(U. Edinburgh)*, J. D'Auria *(SFU)*, E. Gete, D. Measday *(UBC)*, U. Giesen *(U. Alberta)*

788. Nuclear and atomic physics with the CPT spectrometer [inactive], B. Barber, K.S. Sharma *(U. Manitoba)*, X. Feng *(U. Manitoba–McGill U.)*, F. Buchinger, J. Crawford, S. Gulick, J. Lee, B. Moore *(McGill U.)*, E. Hagberg, J. Hardy, V. Koslowsky, G. Savard *(Chalk River Nuclear Lab)*

789. μSR studies of magnetic fluctuations in hydronium jarosites, model Kagomé antiferromagnets [completed], A. Harrison, A.S. Wills *(U. Edinburgh)*, Y. Fudamoto, K. Kojima, M. Larkin, G.M. Luke, J. Merrin, B. Nachumi, Y.J. Uemura *(Columbia U.)*, T. Mason *(U. Toronto)*

790. μSR studies of stripe order in La$_{1.6-x}$Sr$_x$Nd$_{0.4}$CuO$_4$ modified cuprate superconductors [completed], Y. Fudamoto, K. Kojima, M. Larkin, G.M. Luke, J. Merrin, B. Nachumi, Y.J. Uemura *(Columbia U.)*, M. Crawford *(Du Pont)*, A. Moodenbaugh *(Brookhaven Nat. Lab)*, S. Uchida *(U. Tokyo)*

791. Electronic structure and dynamics of charged muonium and muonium-dopant centers in semiconductors [active], K.H. Chow *(Oxford U.)*, R.F. Kiefl *(UBC)*, B. Hitti *(TRIUMF)*, T.L. Estle *(Rice U.)*, R. Lichti *(Texas Tech. U.)*, S.F.J. Cox *(Rutherford Appleton Lab)*, C. Schwab *(CRN, Strasbourg)*

792. Muonium in III-V semiconductors: identification of states and transitions [completed], K.H. Chow *Oxford U.)*, S.F.J. Cox *(Rutherford Appleton Lab)*, B. Hitti *(TRIUMF)*, T.L. Estle *(Rice U.)*, R.L. Lichti *(Texas Tech. U.)*, C. Schwab *(CRN, Strasboug)*

793. Production of an intense ^{15}O beam for ISAC [completed], J. D'Auria, R. Lange *(SFU)*, M. Dombsky, T. Ruth, J. Vincent *(TRIUMF)*, K. Carter *(Oak Ridge Nat. Lab)*, B. Zhuikov *(INR, Moscow)*

794. μ^+SR study on the magnetic properties of LaCoO$_3$ and La$_{1-x}$Sr$_x$CoO$_3$ [completed], V.V. Krishnamurthy, I. Watan- abe *(RIKEN)*, K. Asai, N. Yamada *(U. Electro-communications)*, K. Nagamine *(U. Tokyo–RIKEN)*

795. μSR study on non fermi liquid behaviour [completed], Y. Miyako, Y. Yamamoto *(Osaka U.)*, S. Murayama *(Muroran Inst. Tech.)*, K. Nagamine *(U. Tokyo)*, K. Nishiyama *(U. Tokyo-RIKEN)*

796. μSR studies in ionic crystals doped with either colour centres or impurity [deferred], Y. Miyake, K. Nagamine, K. Nishiyama, K. Shimomura *(U. Tokyo)*, A. Matsusita *(RIKEN)*

797. Magnetic correlations in the ternary equiatomic Ce compounds CeTSn [completed], G. Grosse, G.M. Kalvius A. Kratzer *(Tech. U. Munich)*, R. Wäppling *(U. Uppsala)*, T. Takabatake *(Hiroshima U.)*, D.R. Noakes, C.R. Stronach *(Virginia State U.)*, Y. Echizen *(Hiroshima U.)*, H. Nakotte *(New Mexico State U.)*, H.v. Löhneysen *(U. Karlsruhe)*

798. μSR studies on the competition of RKKY exchange and Kondo effect in CeT$_2$X$_2$ compounds (T=transition metal, X=Si,Ge) [completed], H.-H. Klauss, W. Kopmann, F.J. Litterst, W. Wagener, H. Walf *(Tech. U. Braunschweig)*, E. Baggio Saitovitch, M.B. Fontes *(CBPF Rio de Janeiro)*, A. Krimmel, A. Loidl *(U. Augsburg)*

799. Hyperfine structure and site determination of (μ^-O) system in LaSuCuO high T_c superconductors [completed], H. Kojima, I. Tanaka, E. Torikai *(Yamanashi U.)*, K. Nishiyama *(U. Tokyo–RIKEN)*, K. Nagamine, K. Shimomura *(U. Tokyo)*, I. Watanabe *(RIKEN)*, T.P. Das *(State U. New York)*

801. Studies of multi-phonon states via β-decay [completed data-taking], C.J. Barton, M.A. Caprio, R.F. Casten, N.V. Zamfir *(Yale U.)*, D.S. Brenner *(Clark U.)*, G.C. Ball, K.P. Jackson *(TRIUMF)*

802. Superdeformation and smooth band termination on and near the $N = Z$ line: Part 1 ^{60}Zn [active], J.A. Cameron, S. Flibotte, D.S. Haslip, J. Nieminen, C. Svensson, J.C. Waddington, J.N. Wilson *(McMaster U.)*, G. Ball *(TRIUMF)*, A. Galindo-Uribarri, D.C. Radford *(Oak Ridge Nat. Lab)*, D. Ward *(Lawrence Berkeley Nat. Lab)*

803. Experimental studies of interaction and properties of neutron-rich nuclei at ISAC [inactive], A.S. Iljinov, A.V. Klyachko, E.S. Konobeevsky, M.V. Morodovskoy, M.A. Prohvatilov, A.I. Reshetin, Yu.V. Ryabov, K.A. Shileev, V.A. Simonov, V.M. Skorkin, S.V. Zuyev *(INR, Moscow)*

804. Muonium in gallium nitride [active], B.A. Bailey, R.L. Lichti *(Texas Tech. U.)*, K.H. Chow *(U. Alberta)*, B. Hitti *(TRIUMF)*, S.F.J. Cox *(Rutherford Appleton Lab)*, E.A. Davis *(Leicester U.)*

805. A study of the ^{13}N$(p,\gamma)^{14}$O reaction with a ^{13}N beam [active], R.E. Azuma, J. Chow, J.D. King, A.C. Morton *(U. Toronto)*, N. Bateman *(TRIUMF–Toronto)*, L. Buchmann, K.P. Jackson, T. Shoppa *(TRIUMF)*, J.M. D'Auria *(SFU)*, U. Giesen *(SFU–TRIUMF)*, G. Roy *(U. Alberta)*, W. Galster *(U. Catholique de Louvain)*, A.C. Shotter *(U. Edinburgh)*, R.N. Boyd *(Ohio State U.)*, U. Greife, C. Rolfs, F. Strieder, H.-P. Trautvetter *(Ruhr U. Bochum)*

806. Excitation of high-spin isomeric states and compound nucleus formation by intermediate energy protons and stopped pions [completed data-taking], A.S. Iljinov, V.M. Kokhanyuk, B.L. Zhuikov *(INR, Moscow)*, I. Liu, J. Vincent, A.Z. Zyuzin *(TRIUMF)*

808. Spin glass order in magnets frustrated by competing ferro- and antiferromagnetic exchange [completed], G.M. Kalvius, A. Kratzer, E. Schreier *(Techn. U. Munich)*, R. Wäppling *(U. Uppsala)*, D.R. Noakes *(Virginia State U.)*, J. Gal *(Beer Sheva U.)*, W. Schäfer *(Bonn U.)*

809. Quantum diffusion of muonium in crystals with orientational degrees of freedom [completed], D. Arseneau, B. Hitti, S.R. Kreitzman *(TRIUMF)*, J.H. Brewer, A. Izadi, G.D. Morris *(UBC)*, D.G. Eshchenko *(INR, Moscow)*, V.G. Storchak *(Kurchatov Inst.)*, J.D. Brewer *(SFU)*

810. First direct study of the ^{23}Mg$(p,\gamma)^{24}$Al reaction with a recoil mass separator (DRAGON) [active], N.P.T. Bateman, J.M. D'Auria, D. Hunter, R. Korteling *(SFU)*, R.N. Boyd *(Ohio State U.)*, L. Buchmann, R. Helmer, D. Hutcheon, K.P. Jackson, A. Olin, J. Rogers *(TRIUMF)*, U. Giesen, G. Roy *(U. Alberta)*, L. Gialanella, U. Greife, C. Rolfs, F. Strieder, H.-P. Trautvetter *(Ruhr U. Bochum)*, A. Hussein *(UNBC)*, M. Junker *(INFN Gran Sasso)*, J.D. King *(U. Toronto)*, P.D. Parker *(Yale U.)*, A. Shotter *(U. Edinburgh)*, M. Wiescher *(U. Notre Dame)*

811. A direct study of the ^{19}Ne$(p,\gamma)^{20}$Na reaction with a recoil mass separator (DRAGON) [active], N.P.T. Bateman, J.M. D'Auria, D. Hunter, R. Korteling *(SFU)*, R.N. Boyd *(Ohio State U.)*, L. Buchmann, R. Helmer, D. Hutcheon, K.P. Jackson, A. Olin, J. Rogers *(TRIUMF)*, U. Giesen, G. Roy *(U. Alberta)*, L. Gialanella, U. Greife, C. Rolfs, F. Strieder, H.-P. Trautvetter *(Ruhr U. Bochum)*, A. Hussein *(UNBC)*, M. Junker *(INFN Gran Sasso)*, J.D. King *(U. Toronto)*, P.D. Parker *(Yale U.)*, A. Shotter *(U. Edinburgh)*, M. Wiescher *(U. Notre Dame)*

812. Proposed study of the ^{8}Li$(\alpha,n)^{11}$B reaction [active], R.N. Boyd, A. Murphy, L. Sahin, E. Smith, M. Zahar *(Ohio State U.)*, L. Buchmann, P. Walden *(TRIUMF)*, J.M. D'Auria *(SFU)*, J.D. King *(U. Toronto)*, M. Nishimura, S. Nishimura, I. Tanihata *(RIKEN)*

813. A study of the ^{15}O$(\alpha,\gamma)^{19}$Ne reaction at the astrophysically important energy [active], N.P.T. Bateman, J.M. D'Auria, D. Hunter, R. Korteling *(SFU)*, R.N. Boyd *(Ohio State U.)*, L. Buchmann, R. Helmer, D. Hutcheon, K.P. Jackson, A. Olin, J. Rogers *(TRIUMF)*, U. Giesen, G. Roy *(U. Alberta)*, U. Greife, C. Rolfs, F. Strieder, H.-P. Trautvetter *(Ruhr U. Bochum)*, A. Hussein *(UNBC)*, J.D. King *(U. Toronto)*, P.D. Parker *(Yale U.)*, A. Shotter *(U. Edinburgh)*, M. Wiescher *(U. Notre Dame)*

814. μSR studies of unconventional superconductivity in Sr$_2$RuO$_4$ [active], Y. Fudamoto, K.M. Kojima, M. Larkin, G.M. Luke, J. Merrin, B. Nachumi, Y.J. Uemura *(Columbia U.)*, Y. Maeno *(Kyoto U.)*, R.J. Cava *(Princeton U.)*

815. β-NMR investigation of magnetic multilayers and giant magnetoresistance [active], J. Chakhalian, W.A. MacFarlane, R. Miller, *(UBC)*, J.H. Brewer, R.F. Kiefl *(UBC–TRIUMF)*, P. Amaudruz, R. Baartman, T.R. Beals, J. Behr, S. Daviel, S.R. Kreitzmann, T. Kuo, C.D.P. Levy, M. Olivo, R. Poutissou, Z. Salman, G.D. Wight *(TRIUMF)* S.R. Dunsiger, R. Heffner, G.D. Morris *(Los Alamos Nat. Lab)*, C. Bommas *(U. Bonn)*, A. Hatakeyama, Y. Hirayama, T. Shimoda *(Osaka U.)*, K.H. Chow *(U. Alberta)*, J.E. Elenewski, L.H. Greene *(U. Illinois-Urbana-Champaigne)*

75

816. Semiconductor quantum wells investigated by β-NMR [active], J.H. Brewer, J.C. Chakhalian, S. Dunsiger, R. Miller, T. Tiedje *(UBC)*, M. Gingras *(U. Waterloo)*, B. Ittermann *(U. Marburg)*, B. Hitti, P. Levy, S.R. Kreitzman, A. Zelenski *(TRIUMF)*, R.F. Kiefl *(TRIUMF–UBC)*   75

817. β-NMR investigation of type II superconductors [active], D. Bonn, J.H. Brewer, J.C. Chakhalian, S. Dunsiger, W. Hardy, R. Liang, R.F. Kiefl, W.A. MacFarlane, R. Miller, J. Sonier *(UBC)*, M. Gingras *(U. Waterloo)*, R. Heffner *(Los Alamos Nat. Lab)*, B. Itterman *(U. Marburg)*, B. Hitti, P. Levy, S.R. Kreitzman, A. Zelenski *(TRIUMF)*, G.M. Luke *(Columbia U.)*, J.W. Brill *(U. Kentucky)*   75

818. μ^+SR study of magnetic ordering in the one-dimensional spin-1/2 antiferromagnet copper benzoate [completed], J.C. Chakhalian, S. Dunsiger, R.F. Kiefl, W.A. MacFarlane, R. Miller, J. Sonier *(UBC)*, C. Broholm, D.C. Dender, P. Hammar, D. Reich *(Johns-Hopkins U.)*, G. Luke, T. Uemura *(Columbia U.)*

819. μ^+SR studies of the antiferromagnetic instability and metastable state in colossal magnetoresistance system $(\mathrm{Nd}_{1-y}\mathrm{Sm}_y)_{1/2}\mathrm{Sr}_{1/2}\mathrm{MnO}_3$ ($y = 0.875$) [completed], W. Higemoto, I. Watanabe *(RIKEN)*, K. Nishiyama *(KEK)*, K. Nagamine *(RIKEN–KEK)*, A. Asamitsu, H. Kuwahara, Y. Tokura *(JRCAT, U. Tokyo)*

821. Shape coexistence and shape mixing in neutron-deficient platinum isotopes: on-line nuclear orientation studies of the decays of ^{182}Au and ^{186}Au [active], K.S. Krane *(Oregon State U.)*, J.L. Wood *(Georgia Inst. Tech.)*, J. D'Auria *(SFU)*

822. Effect of disorder on quantum spin liquid state [active], W. Higemoto, R. Kadono, A. Koda, K. Ohishi, *(KEK-IMSS)*, M. Nohara, H. Takagi, H. Ueda, C. Urano *(U. Tokyo)*   77

823. Pure fermi decay in medium mass nuclei [active], G.C. Ball, R. Beaton, P. Bricault, G. Hackman, P. Klages, J.A. Macdonald, E. Vandervoort *(TRIUMF)*, D.F. Hodgson *(U. Surrey–TRIUMF)*, J. Cerny, D.M. Moltz, J. Powell *(Lawrence Berkeley Lab)*, G. Savard *(Argonne Nat. Lab)*, J.C. Hardy, V. Iacob *(Texas A&M U.)*, S. Bishop, J. D'Auria *(SFU)*, J.R. Leslie, H.-B. Mak, I.S. Towner *(Queen's U.)*, D. Kulp, J.L. Wood *(Georgia Inst. Tech.)*, E.F. Zganjar, A. Piechaczek *(Louisiana State U.)*   41

824. Measurement of the astrophysical rate of the ^{21}Na$(p, \gamma)^{22}$Mg reaction [active], S. Bishop, J.M. D'Auria, D. Hunter, M. Lamey, W. Liu, C. Wrede, *(SFU)*, L. Buchmann, D. Hutcheon, A.M. Laird, A. Olin, D. Ottewell, J.G. Rogers *(TRIUMF)*, S. Engel, F. Strieder *(Ruhr U.)*, D. Gigliotti, A. Hussein *(UNBC)*, R. Azuma, J.D. King *(U. Toronto)*, R. Lewis, P.D. Parker *(Yale U.)*, S. Kubono, S. Michimasa *(U. Tokyo)*, M. Chatterjee *(Saha Inst., Calcutta)*, U. Greife, C. Jewett *(Colorado School of Mines)*, A.A. Chen *(McMaster U.)*, M. Hernanz, J. José *(Inst. d'Estudis Espacials de Catalunya, Barcelona)*   43

826. Studies of ultrathin magnetic films with implanted isotopes [active], R. Kiefl, J. Pond, B.G. Turrell *(UBC)*, C.A. Davis, P.P.J. Delheij *(TRIUMF)*, K.S. Krane. J. Loats, P. Schmelzenbach, C. Stapels *(Oregon State U.)*, D. Groh, W. Kumarasiri, P. Mantica *(Michigan State U.)*, D. Kulp, J.L. Wood, *(Georgia Inst. Tech.)*

827. Parity violation in ^{182}W [active], J. D'Auria *(TRIUMF–SFU)*, C.A. Davis P.P.J. Delheij *(TRIUMF)*, R. Kiefl, A. Kotlicki, J. Pond, B. Turrell *(UBC)*, K.S. Krane *(Oregon State U.)*

828. Nuclear moments in the mass-100 region [active], K.S. Krane, J. Loats, P. Schmelzenbach, C. Stapels *(Oregon State U.)*, D. Kulp, J.L. Wood *(Georgia Inst. Tech.)*, C.A. Davis, P.P.J. Delheij *(TRIUMF)*, D. Groh, W. Kumarasiri, P. Mantica *(Michigan State U.)*, R. Kiefl, J. Pond, B.G. Turrell *(UBC)*

829. Muonium as a hydrogen isotope: reactions in solution [completed], D.P. Chong, G.B. Porter, D.C. Walker *(UBC)*, K. Venkateswaran *(Hindustan Lever Ltd.)*, H.A. Gillis *(St. Francis Xavier U.)*

830. The hot entropy bubble and the decay of ^{9}Li [active], N. Bateman *(TRIUMF–SFU–Toronto)*, L. Buchmann, K.P. Jackson, S. Karataglidis, T. Shoppa, E. Vogt *(TRIUMF)*, J. Chow, J.D. King, C. Mortin *(U. Toronto)*, T. Davison, A. Ostrowski, A. Shotter *(U. Edinburgh)*, J. D'Auria, U. Giesen *(SFU)*, E. Gete, D. Measday *(UBC)*

831. Magnetic properties of $\mathrm{REBa_2Cu_3O}_x$ [completed data-taking], D. Andreica, F.N. Gygax, M. Pinkpank, A. Schenck *(ETH Zürich)*, B. Hitti *(TRIUMF)*, A. Amato *(PSI)*, J.H. Brewer *(UBC–TRIUMF)*

832. Study of the non-magnetic-magnetic transition in the $\mathrm{Yb(Cu_{1-x}Ni_x)_2Si_2}$ system [completed data-taking], D. Andreica, F. Gygax, M. Pinkpank, A. Schenck *(ETH Zürich–PSI)*, A. Amato *(PSI)*, B. Hitti *(TRIUMF)*

833. μSR studies of doped MnSi and $\mathrm{V_{2-y}O_3}$: non-fermi-liquid behaviour, spin fluctuations and itinerant magnetism [active], A. Fukaya, I.M. Gat, M. Larkin, A.J. Millis, P.L. Russo, A.T. Savici, Y.J. Uemura *(Columbia U.)*, P.P. Kyriakou, G.M. Luke, C.R. Wiebe *(McMaster U.)*, Y.V. Sushko *(U. Kentucky)*, R.H. Heffner *(Los Alamos Nat. Lab)*, D.E. MacLaughlin *(U. California, Riverside)*, D. Andreica *(PSI)*, M. Kalvius *(Tech. U. Munich)*   79

834. μSR study of transverse spin freezing in bond-frustrated magnets [active], A.D. Beath, D.H. Ryan, *(McGill U.)*, J.M. Cadogan *(U. New South Wales)*, J. van Lierop *(U. Michigan)*   80

835. μSR studies of intercalated HfN and Bi2212 superconductors [active], R. Breslow, Y. Fudamoto, A. Fukaya, I.M. Gat, K. Groves, M.I. Larkin, A. Savici, Y.J. Uemura *(Columbia U.)*, P. Kyriakou, G.M. Luke, M. Rovers *(McMaster U.)*, K.M. Kojima *(U. Tokyo)*, S. Yamanaka *(Hiroshima U.)*, T. Ito *(Columbia U.–CERC)*

312

836. Elasticks [active], R.E. Azuma, J.D. King *(U. Toronto)*, G. Ball, L. Buchmann, K.P. Jackson, B. Jennings, S. Karataglidis, E. Vogt *(TRIUMF)*, N. Bateman *(TRIUMF–SFU–U. Toronto)*, T. Davison, A. Ostrowski, A. Shotter *(U. Edinburgh)*, J. D'Auria *(SFU)*, W. Galster *(U. Catholique de Louvain)*, G. Roy *(U. Alberta)*

837. Pion-induced errors in memory chips [completed], J.T. Brack, G. Hofman, J. Patterson R.J. Peterson, R.A. Ristinen *(U. Colorado)*, J.F. Ziegler *(IBM)*, M.E. Nelson *(US Naval Academy)*, G. Smith *(TRIUMF)*

838. Measurement of the $\pi^- p \to \gamma\gamma n$ capture mode of pionic hydrogen [completed data-taking], T. Gorringe, M. Kovash, S. Tripathi, P. Żołnierczuk *(U. Kentucky)*, D. Armstrong, J. Clark *(Coll. of William & Mary)*, M. Hasinoff *(UBC)*, D. Healey, D. Wright *(TRIUMF)*

839. Thermal test of prototype high power ISAC target [completed], D. Drake, D. Liska, W.L. Talbert, M. Wilson *(Amparo Corp.)*, P. Bricault, M. Dombsky, P. Schmor *(TRIUMF)*, E. Dalder, C. Landram, K. Sale, D. Slaughter *(Lawrence Livermore Nat. Lab)*, J. Nolen, G. Savard *(Argonne Nat. Lab)*, G. Alton *(Oak Ridge Nat. Lab)*

840. Muon transfer from excited states of muonic hydrogen with x-ray measurement [active], S. Sakamoto, K. Shimomura *(KEK)*, K. Nagamine *(KEK–RIKEN)*, K. Ishida, N. Kawamura, Y. Matsuda, T. Matsuzaki, S.N. Nakamura, P. Strasser *(RIKEN)*

841. ISAC beam and target development [active], P. Bricault, M. Dombsky *(TRIUMF)*

842. Muonium-substituted free radicals in sub- and supercritical water [active], J.-C. Brodovitch, S. Kecman, B. McCollum, I. McKenzie, P.W. Percival *(SFU)*, B. Addison-Jones *(Douglas College)*   82

843. Quadrupole ordering in dense Kondo system studied by μLCR [active], J. Akimitsu, K. Kakuta, K. Ohishi *(Aoyama Gakuin U.)*, W. Higemoto, R. Kadono *(KEK–IMSS)*, T. Yokoo *(CREST)*   83

844. Quantum impurities in one dimensional spin 1/2 chains [completed], I. Affleck, J. Brewer, J. Chakhalian, S. Dunsiger, R.F. Kiefl, R. Miller, A. Price *(UBC)*, S. Eggert *(Chalmers U.)*, B. Hitti *(TRIUMF)*, A.A. Keren *(Israel Inst. Tech.)*, W.A. MacFarlane *(U. Paris-Sud)*, G. Morris *(UBC–TRIUMF)*, Y.J. Uemura *(Columbia U.)*, M. Verdaguer *(CNRS)*, I. Yamada *(Chiba U.)*

845. μSR studies of vortex phases in $(Ba,K)BiO_3$ [completed], G.M. Luke, M.A. Lumsden *(McMaster U.)*, Y. Fudamoto, M.I. Larkin, Y.J. Uemura *(Columbia U.)*, K.M. Kojima *(U. Tokyo)*, M. Gingras *(U. Waterloo)*, I. Joumard, T. Klein, J. Marcus *(U. Grenoble)*

846. Complex order parameter symmetry in $YB_2Cu_3O_{7-\delta}$ at low T and high magnetic field [completed data-taking], D.A. Bonn, J.H. Brewer, W.N. Hardy, R.F. Kiefl, R.X. Liang, J.-M. Ménard, R.I. Miller *(UBC)*, D. Babineau, K.F. Poon, J.E. Sonier *(SFU)*, C.E. Stronach *(Virginia State U.)*   84

847. Electron-doped high-T_c superconductors [active], P. Kyriakou, G.M. Luke, C.R. Wiebe *(McMaster U.)*, P. Fournier *(U. Sherbrooke)*, K.F. Poon, J.E. Sonier *(SFU)*, R.X. Liang, R.I. Miller *(UBC)*, C.E. Stronach *(Virginia State U.)*   85

848. μSR investigation of the vortex state of $YBa_2Cu_3O_{6+x}$ [completed], D.A. Bonn, J.C. Chakhalian, K. Chow, W.N. Hardy, R.X. Liang, R. Miller, A.N. Price *(UBC)*, J.H. Brewer, R.F. Kiefl *(UBC–TRIUMF)*, J. Sonier *(SFU)*

849. Spin structure and magnetic volume fraction of La214 systems: revisiting "1/8", "stripes", "spin glass", and "swiss cheese" [completed], K.M. Kojima *(U. Tokyo)*, Y. Fudamoto, I.M. Gat, M.I. Larkin, A.T. Savici, Y.J. Uemura *(Columbia U.)*, G.M. Luke *(McMaster U.)*, M.A. Kastner, Y.S. Lee *(MIT)*, R.J. Birgeneau *(MIT–U. Toronto)*, K. Yamada *(Kyoto U.)*

850. Effects of dilute (Cu,Zn) substitution in spin gap systems $SrCu_2O_3$ and $CuGeO_3$ [completed], Y. Fudamoto, I. Gat, M.I. Larkin, Y.J. Uemura *(Columbia U.)*, K.M. Kojima, K. Manabe, K. Uchinokura *(U. Tokyo)*, G.M. Luke *(McMaster U.)*, M. Azuma, M. Takano *(Kyoto U.)*

851. μSR in ruthenate and cuprate high-T compounds [active], D.R. Harshman *(Physikon Research Corp.)*, M.K. Wu *(Nat. Tsing Hua U.)*, F.Z. Chien *(Tamkang U.)*, J.D. Dow *(Arizona State U.)*, A.J. Greer *(Gonzaga U.)*, A. Goonewardene, W.J. Kossler, X. Wan *(Coll. of William & Mary)*, E. Koster, D.Ll. Williams *(UBC)*, D.R. Noakes, C.E. Stronach *(Virginia State U.)*, A.T. Fiory *(New Jersey Inst. Tech.)*, A. Erb *(Walther-Meissner-Inst. Tieftemperaturforschung, Garching)*, J.P. Franck, I. Issac *(U. Alberta)*, Z.F. Ren, D.Z. Wang *(Boston College)*, R.N. Kleiman *(Bell Labs)*, R.C. Haddon *(U. California, Riverside)*, W. Kang *(U. Chicago)*   87

852. Magnetic phases in geometrically frustrated rare earth pyrochlores [active], R. Kiefl *(UBC–TRIUMF)*, B.D. Gaulin, G. Luke *(McMaster U.)*, M.J.P. Gingras *(U. Waterloo)*, S. Dunsiger, G.D. Morris *(Los Alamos Nat. Lab)*, R. Miller, A.N. Price *(UBC)*, J.S. Gardner *(NRC)*, S.T. Bramwell *(U. College London)*, K. Chow *(U. Alberta)*, R. Jin, M.D. Lumsden, D. Mandrus *(Oak Ridge Nat. Lab)*, J.E. Sonier *(SFU)*

856. μSR study on CuO [active], W. Higemoto, K. Nishiyama, K. Shimomura *(KEK)*, M. Suzuki, S. Tanaka, N. Tsutsumi, X.G. Zheng *(Saga U.)*

857. Investigation of the magnetic properties of the cerium compound probed by negative muon [active], W. Higemoto, K. Nagamine, K. Nishiyama, K. Shimomura *(KEK)*, V.V. Krishnamurthy *(RIKEN)*

858. Repolarization of muonic atom in semiconductors by laser optical pumping in solids [active], W. Higemoto, R. Kadono, K. Nagamine, K. Nishiyama K. Shimomura *(KEK)*

859. A search for non-Markovian μ^+ diffusion in solids: μ^+ spectral spin hopping in high transverse field [inactive], G. Alexandrowicz, A. Grayevsky, N. Kaplan, T. Tashma *(Racah Inst. Physics)*, A. Schenck *(ETH Zürich)*

860. Mass and charge transport in disordered media: orientational glasses [active], J.H. Brewer, A. Izadi, D.M.C. Liu, K.M. Nichol, S. Sivanandam, A.T. Warkentin *(UBC)*, G.D. Morris *(TRIUMF)*, V.G. Storchak *(Kurchatov Inst.)*, D.G. Eshchenko *(INR, Moscow)*, J.D. Brewer *(SFU)*

862. Polarization observables in the $\vec{p}(\pi^\pm, \pi^+, \pi^\pm)$ reactions: a test of chiral perturbation theory [active], P. Amaudruz, D. Ottewell *(TRIUMF)*, K. Craig, G. Hofman, M.M. Pavan, K.J. Raywood, R. Tacik *(Regina–TRIUMF)*, K. Babcock, E. Mathie, H. Xu, M. Yeomans *(U. Regina)*, P. Camerini, E. Fragiacomo, N. Grion, R. Rui *(U. di Trieste)*, J. Breitschopf, H. Denz, R. Meier, G. Wagner *(U. Tübingen)*, G. Smith *(Jefferson Lab)*, E. Gibson *(California State U. Sacramento)*, C. Riedel *(Montana State U. Bozeman)*   46

863. Magnetic dipole moments measurements of ^{75,77,79}Ga using low temperature nuclear orientation and β-NMR [active], A. Davies, D. Groh, P.F. Mantica, A.C. Morton *(Michigan State U.)*, C.A. Davis, P.P.J. Delheij *(TRIUMF)*, B. Turrell *(UBC)*   47

864. Measurement of the two-photon capture mode of the pionic deuterium atom [completed data-taking], S. Arole, T. Gorringe, C. Nenkov, S. Tripathi, P. Żołnierczuk *(U. Kentucky)*, D. Armstrong, J. Clark *(Coll. of William & Mary)*, M. Hasinoff *(UBC)*, D. Wright *(TRIUMF)*

865. Electronic structure and diffusion kinetics of muonium in group III nitrides [active], W. Higemoto, R. Kadono, K. Nishiyama, K. Shimomura *(KEK–IMSS)*, M. Mizuta *(NEC Corp.)*, M. Saito *(NEC Inf. Syst. Ltd.)*

866. $S = 0$ doping to the 1d spin chain: comparison between the $S = 1/2$ and $S = 1$ chains [active], I. Eisaki, K.M. Kojima, T. Masuda, S. Uchida, K. Uchinokura *(U. Tokyo)*, Y. Fudamoto, I. Gat, M.I. Larkin, Y.J. Uemura *(Columbia U.)*, G.M. Luke *(McMaster U.)*

867. μSR studies of magnetic properties of strontium/calcium ruthenates [active], Y. Fudamoto, I. Gat, M. Larkin, A. Savici, Y.J. Uemura *(Columbia U.)*, G.M. Luke *(McMaster U.)*, K. Kojima *(U. Tokyo)*, S. Ikeda, Y. Maeno *(Kyoto U.)*

868. Magnetic correlations in impurity doped one dimensional spin systems [active], D. Baabe, H.-H. Klauss, W. Kopmann, F.J. Litterst, D. Mienert *(Tech. U. Braunschweig)*, U. Ammerahl, B. Büchner *(U. Köln)*, C. Geibel *(MPI Dresden)*

869. Measurement of the ^{1}H$(\pi^-, \pi^0)n$ differential cross section at 100–140 MeV/c and forward angles [completed data-taking], S. Arole, T. Gorringe, M. Kovash, S. Tripathi, P. Żołnierczuk *(U. Kentucky)*, M. Hasinoff *(UBC)*, D. Armstrong *(Coll. of William & Mary)*, M. Pavan *(TRIUMF)*

870. Breakout from the hot CNO cycle via the ^{18}Ne$(\alpha, p)^{21}$Na reaction [active], T. Davinson, A. Ostrowski, F. Sarazin, A. Shotter, P. Woods *(U. Edinburgh)*, L. Buchmann, J. D'Auria *(TRIUMF)*, J. Daly, J. Görres, M. Wiescher *(U. Notre Dame)*, P. Leleux *(U. Catholique de Louvain)*   48

871. Meson and quark effects in nuclear β-decay of ^{20}Na [active], M. Fukuda, K. Matsuta, M. Mihara, T. Minamisono, T. Nagatomo, M. Ogura, T. Sumikama *(Osaka U.)*, R. Baartman, J. Behr, P. Bricault, M. Dombsky, K.P. Jackson, P. Levy *(TRIUMF)*, R. Kiefl *(UBC)*, K. Koshigiri *(Osaka Kyoiku U.)*, M. Morita *(Josai Int. U.)*, K. Minamisono *(JSPS–TRIUMF)*   48

872. Weak interaction studies with trapped radioactive ions [active], J. Dilling, D. Melconian *(SFU)*, G. Savard *(Argonne Nat. Lab–U. Chicago)*, G.C. Ball, J.A. Behr, P. Bricault, K.P. Jackson *(TRIUMF)*, F. Buchinger, J.E. Crawford, J.K.P. Lee, R.B. Moore *(McGill U.)*, K.S. Sharma *(U. Manitoba)*

874. Study of ^{19}Ne α-decay properties related to the hot-CNO breakout reaction ^{15}O$(\alpha, \gamma)^{19}$Ne [active], T. Davinson, D. Groombridge, A.M. Laird, A.N. Ostrowski, F. Sarazin, K. Schmidt, A.C. Shotter, P.J. Woods *(U. Edinburgh)*, L. Buchmann *(TRIUMF)*, S. Cherubini, P. Leleux *(U. Catholique de Louvain)*, J. Hinnefeld *(U. South Bend)*

875. Muon scattering in low Z materials for muon cooling studies [active], M. Curtis-Rouse, T.R. Edgecock, M. Ellis, J. Lidbury, W. Murray, P.R. Norton, K.J. Peach *(Rutherford Appleton Lab)*, K. Ishida, Y. Matsuda *(RIKEN)*, T. McMahon, J.A. Wilson *(U. Birmingham)*, G. Barber, A. Jamdagni, K. Long, E. McKigney *(Imp. Coll., London)*, W. Allison *(U. Oxford)*, S. Benveniste, D. Cline, Y. Fukui, K. Lee, Y. Pischalnikov *(UCLA)*, R. Fernow *(Brookhaven Nat. Lab)*, P. Gruber, A. Lombardi *(CERN)*, S.N. Nakamura *(U. Tohoku)*, G. Marshall *(TRIUMF)*   51

876. Disordered magnetism near magnetic instabilities in f-electron materials [completed], D.R. Noakes, C.E. Stronach *(Virginia State U.)*, G.M. Kalvius *(Tech. U. Munich)*, A. Loidl *(Augsburg U.)*, H. Nakotte *(New Mexico State U.)*, R. Wäppling *(Uppsala U.)*, A.V. Andreev *Charles U.)*

877. μSR studies of strongly correlated electron systems under a high pressure [active], W. Higemoto, R. Kadono, A. Koda, K. Nishiyama *(KEK–MSL)*, K. Satoh *(Saitama U.)*, Y. Kitaoka, K. Ishida *(Osaka U.)*, K. Nagamine *(RIKEN–KEK–MSL)*   88

878. μ^+SR studies on magnetism of layered compounds $Cu_2(OH)_3X(X=Cl,Br,I)$ [active], G. Maruta, K. Nishiyama *(KEK-MSL)*, S. Takeda *(Gunma U.)*

879. Proton-^{21}Na elastic scattering at astrophysical energies [active], L. Buchmann *(TRIUMF)*, T. Davinson, A. Ostrowski, F. Sarazin, A. Shotter, P. Woods *(U. Edinburgh)*, R.E. Azuma, J.D. King *(U. Toronto)*, A. Chen *(TRIUMF–SFU)*, J. Daly, J. Görres, M. Wiescher *(U. Notre Dame)*, J. D'Auria *(SFU)*, E.S. Konobeevsky, M.V. Mordovskoy, V.A. Simonov, A.V. Stepanov, V.P. Zavarzina *(INR, Moscow)*

880. Ortho-para effect of muon catalyzed fusion in solid deuterium [completed], K. Ishida *(RIKEN–KEK)*, K. Nagamine *(KEK–RIKEN)*, A. Toyoda *(U. Tokyo–RIKEN–KEK)*, K. Shimomura *(KEK)*, S.N. Nakamura *(RIKEN–Tohoku U.)*, Y. Matsuda *(RIKEN)*

881. Magnetism of Ce-based heavy fermion superconductor [active], W. Higemoto, R. Kadono, A. Koda, K. Ohishi *(KEK-IMSS)*, K. Ishida, Y. Kawasaki, Y. Kitaoka *(Osaka U.)*, C. Geibel, F. Steglich *(Max-Planck Inst.)*   89

882. μSR studies of unconventional superconductivity in an organic superconductor $(TMTSF)_2ClO_4$ [active], I.M. Gat, M.I. Larkin, A. Savici, Y.J. Uemura *(Columbia U.)*, T. Ito *(Columbia U.–ETL)*, P. Kyriakou, G.M. Luke, M. Rovers *(McMaster U.)*, K.M. Kojima *(U. Tokyo)*, P.M. Chaikin, I.J. Lee *(Princeton U.)*, M.J. Naughton *(Boston Coll.)*

883. Muonium-substituted methyl and associated free radicals [active], J.-C. Brodovitch, J. Clyburne, S. Kecman, I. McKenzie, P.W. Percival *(SFU)*, B. Addison-Jones *(Douglas College)*   89

884. μSR studies on magnetic ground state of $S = 1/2$ kagomé spin system $Cu_3V_2O_7(OH)-2\cdot2H_2O$ [active], A. Fukaya, I.M. Gat, M.I. Larkin, A. Savici, Y.J. Uemura *(Columbia U.)*, T. Ito *(CERC–AIST)*, A. Keren *(Technion-Israel Inst. of Tech.)*, P.P. Kyriakou, G.M. Luke, M.T. Rovers *(McMaster U.)*, Z. Hiroi *(U. Tokyo)*

885. High-TF line-shape measurement of impurity-doped high-T_c cuprates [active], K.M. Kojima, Y. Kojima, Y. Maeda, T. Okamura, S. Uchida *(U. Tokyo)*, I. Gat, T. Itoh, A. Kinkhabwala, M.I. Larkin, Y.J. Uemura *(Columbia U.)*, G.M. Luke *(McMaster U.)*, S.R. Dunsiger, R.F. Kiefl, R. Miller *(UBC)*, J.E. Sonier *(Los Alamos Nat. Lab)*

886. Study of field dependent T_1 relaxation and coexistence of order parameters in the (anti)ferromagnetic ruthenate-cuprate superconductors $RuSr_2(Gd,Eu,Y)Cu_2O_8$ [active], C. Bernhard *(Max Planck Inst.)*. C. Niedermayer, V. Oehmichen *(U. Konstanz)*, E.J. Ansaldo *(U. Saskatoon)*, J.L. Tallon *(NZIIRD)*

887. Search for broken time reversal symmetry in high temperature superconductors [active], P. Kyriakou, G.M. Luke, M. Rovers *(McMaster U.)*, R.H. Heffner *(Los Alamos Nat. Lab)*, M.I. Larkin, Y.J. Uemura *(Columbia U.)*, J. Sonier *(SFU)*, K.M. Kojima *(U. Tokyo)*

888. Test of delayed-muonium model for hydrocarbon liquids [active], D.C. Walker *(UBC–TRIUMF)*, H.A. Gillis *(St. Francis Xavier U.)*, G.B. Porter *(UBC)*, S. Karolczak *(Politechnika, Poland)*   91

889. Study of field induced gap in Cu benzoate [active], Y. Ajiro, T. Asano, Y. Inagaki *(Kyushu U.)*, H. Nojiri *(Tohoku U.)*, W. Higemoto, R. Kadono, A. Koda *(KEK-IMSS)*

890. Anisotropic Kondo effect in $Ce_{0.8}La_{0.2}Al_3$? [completed], D.E. MacLaughlin *(U. California, Riverside)*, O.O. Bernal *(Cal. State U., Los Angeles)*, R.H. Heffner *(Los Alamos Nat. Lab)*, G.M. Luke *(McMaster U.)*, G.J. Nieuwenhuys *(U. Leiden)*, J.E. Sonier *(SFU)*, B. Andraka *(U. Florida)*

891. Superconductivity and magnetism in $Ce_nT_mIn_{3n+2m}$ [active], R.H. Heffner, G.D. Morris, J. Sarrao *(Los Alamos Nat. Lab)*, J.E. Sonier *(SFU)*, D.E. MacLaughlin *(U. California, Riverside)*, G.J. Nieuwenhuys *(U. Leiden)*, O.O. Bernal *(Cal. State U., Los Angeles)*   93

892. Resonance ionization spectroscopy of stable and radioactive nuclides at TISOL [deferred] F. Buchinger, J.E. Crawford, S. Gulick, J.K.P. Lee *(McGill U.)*, K. Sharma *(U. Manitoba)*, J. Pinard *(Lab Aimé Cotton, Orsay)*

893. Hyperfine field of Rb in the ferromagnets Fe, Ni, Co [active], C.A. Davis, P.P.J. Delheij *(TRIUMF)*, S. Cottenier *(K.U. Leuven)*, H. Haas *(Hahn Meitner Inst.)*, K.S. Krane, J. Loats, P. Schmelzenbach, C. Stapels *(Oregon State U.)*, R. Kiefl, J. Pond, B. Turrell *(UBC)*, D. Kulp, J. Wood *(Georgia Inst. Tech.)*, A.D. Davies, D. Groh, P. Mantica, A.C. Morton *(Michigan State U.)*   53

894. Muonium kinetics and free radical formation in solutions of fullerenes [active], B. Addison-Jones *(Douglas College)*, J.-C. Brodovitch, S. Kecman, I. McKenzie, P.W. Percival *(SFU)*   94

895. The vortex structure and magnetism of electron-doped cuprate superconductors [active], <u>K.M. Kojima</u>, S. Uchida *(U. Tokyo)*, W. Higemoto, <u>R. Kadono</u>, A. Koda *(KEK)*, M. Azuma, M. Fujita, M. Takano, K. Yamada *(Kyoto U.)*, K. Ishida, Y. Kawasaki, Y. Kitaoka *(Osaka U)*, M.I. Larkin, Y.J. Uemura *(Columbia U.)*   95

896. Investigation of spin liquid behaviour in chromium and manganese spinels [active], H. Dabkowska, J. Greedan, P.P. Kyriakou, <u>G.M. Luke</u>, <u>M.T. Rovers</u> *(McMaster U.)*, I.M. Gat, M.I. Larkin, A.T. Savici, Y.J. Uemura *(Columbia U.)*, <u>K.M. Kojima</u> *(U. Tokyo)*

897. Absolute magnetic penetration depth in the Meissner state of superconductors measured with low frequency beta-NMR [active], D. Bonn, J.H. Brewer, K.H. Chow, W. Hardy, R. Liang, R. Miller, <u>G. Morris</u> *(UBC)*, S. Dunsiger, B. Heffner *(Los Alamos Nat. Lab)*, <u>R.F. Kiefl</u> *(UBC–TRIUMF)*, S. Kreitzman, P. Levy *(TRIUMF)*, G. Luke *(McMaster U.)*, <u>J. Sonier</u> *(SFU)*, C. Stronach *(Virginia State U.)*

898. MULTI development with applications in superconductors and semiconductors [active], P. Amadruz, D. Arseneau, S. Chan, <u>K.H. Chow</u>, B. Hitti, G. Morris, R. Poutissou *(TRIUMF)*, J. Chakhalian, S. Dunsiger, <u>R.F. Kiefl</u>, R. Miller *(UBC)*

900. A determination of the $\alpha+{}^{15}$O radiative capture rate by a measurement of the ^{15}O$({}^6$Li,$d){}^{19}$Ne reaction [active], <u>B.R. Fulton</u>, B. Greenhalgh, J. Pearson, D.L. Watson *(U. York)*, N.M. Clarke *(U. Birmingham)*, T. Davinson, N. Farrington, P. Monroe, C. Ruiz, F. Sarazin, K. Schmidt, A.C. Shotter, P.J. Woods *(U. Edinburgh)*, L. Buchmann, P. Walden *(TRIUMF)*, J. D'Auria *(SFU)*

902. Muon capture on ^{45}Sc, ^{51}V, ^{55}Mn and ^{59}Co [active], <u>D.F. Measday</u> *(UBC)*, T.P. Gorringe *(U. Kentucky)*

903. Spectroscopic study of ^{11}Be with polarized ^{11}Li beam [active], A. Hatakeyama, Y. Hirayama, H. Izumi, <u>T. Shimoda</u>, M. Yagi, H. Yano *(Osaka U.)*, H. Miyatake *(IPNS, KEK)*, K.P. Jackson, C.D.P. Levy *(TRIUMF)*   55

907. Improving S$_{E1}$(300): the $\beta - \alpha$ branching ratio of ^{16}N [deferred] <u>R.E. Azuma</u>, J.D. King *(U. Toronto)*, <u>L. Buchmann</u> *(TRIUMF)*

909. Isospin symmetry breaking in superallowed Fermi beta decays [active], P. Finlay, G.F. Grinyer, M. Schumaker, <u>C.E. Svensson</u> *(Guelph U.)*, R.A.E. Austin, J.A. Cameron, J.C. Waddington *(McMaster U.)*, G.C. Ball, P. Bricault, G. Hackman, J.A. Macdonald, F. Sarazin, H.C. Scraggs, M.B. Smith *(TRIUMF)*, J.C. Hardy, V. Iacob *(Texas A&M U.)*, J.R. Leslie *(Queen's U.)*, D.M. Moltz *(Lawrence Berkeley Nat. Lab)*, G. Savard *(Argonne Nat. Lab)*, J.L. Woods, W.D. Kulp, J. von Schwarzenberg *(U. Georgia)*, P.E. Garrett *(Lawrence Livermore Nat. Lab)*, A. Piechaczek, E.F. Zganjar *(Louisiana State U.)*, C.J. Osborne, P.M. Walker *(U. Surrey)*   59

910. Study of the ground state proton emitter ^{73}Rb and implications for the astrophysical rp-process [active], <u>A. Piechaczek</u>, E.F. Zganjar *(Louisiana State U.)*, G.C. Ball *(TRIUMF)*, J.C. Batchelder *(Oak Ridge Assoc. U.)*, D. Kulp, B.D. MacDonald, J.L. Wood *(Georgia Inst. Tech.)*

911. Test of aerogel proto-type detector for $G\emptyset$ phase II [active], J. Birchall, W. Falk, L. Lee, S. Page, W.D. Ramsay, A. Rauf, G. Rutledge, W.T.H. van Oers *(U. Manitoba)*, C. Davis *(TRIUMF)*, L. Hannelius, J. Martin *(Caltech)*, E. Korkmaz, T. Porcelli *(UNBC)*, S. Kox, G. Quemener, R. Tieulent *(ISN Grenoble)*, <u>D. Beck</u> *(U. Illinois, Urbana)*

912. Formation, structure, and dynamics of muonium in GaAs studied by EF-ALC-RF μ^+SR [active], B. Hitti, <u>S.R. Kreitzman</u> *(TRIUMF)*, <u>K.H. Chow</u> *(U. Alberta)*, J.H. Brewer *(UBC)*, D.G. Eshchenko *(U. Zurich–PSI)*, <u>V.G. Storchak</u> *(Kurchatov Inst.)*   96

913. Photo-induced dynamics and reactivity of spin polarized ^{8}Li in semiconductors [active], <u>K.H. Chow</u> *(U. Alberta)*, T. Beals, <u>R.F. Kiefl</u>, R.I. Miller *(UBC)*, P. Amadruz, D. Arseneau, S. Daviel, B. Hitti, S.R. Kreitzman, P. Levy, R. Poutissou *(TRIUMF)*, R.L. Lichti *(Texas Tech. U.)*, G.D. Morris *(Los Alamos Nat. Lab)*, C. Bommas *(U. Bonn)*

914. Zero-field μSR in Bi2212 and Bi2201 searching for effects related to the pseudo-gap [active], Y. Ching, M. Greven, N. Kaneko, P.K. Mang *(Stanford U.)*, A. Fukaya, I.M. Gat, M.I. Larkin, P.L. Russo, A. Savici, <u>Y.J. Uemura</u>, J. Zhang *(Columbia U.)*, H. Dabkovska, P. Kilyakiu, <u>G.M. Luke</u>, M. Rovers *(McMaster U.)*

915. Muonium in semiconductor alloys [active], <u>R.L. Lichti</u> *(Texas Tech. U.)*, K.H. Chow *(U. Alberta)*, <u>P.J.C. King</u> *(Rutherford Appleton Lab)*, J.M. Gil *(U. Coimbra)*, B. Hitti *(TRIUMF)*   97

916. QLCR of diamagnetic states in GaP [active], <u>R.L. Lichti</u>, W. Nusbaum *(Texas Tech. U.)*, K.H. Chow *(U. Alberta)*, S.F.J. Cox *(Rutherford Appleton Lab)*, <u>B. Hitti</u> *(TRIUMF)*   98

917. Correlation between magnetism and transport properties of thermoelectric oxides [active], K. Dohmae, H. Itahara, Y. Seno, J. Sugiyama, T. Tani, C. Xia *(Toyota Central R&D Labs Inc.)*, <u>J.H. Brewer</u> *(UBC–TRIUMF)* E.J. Ansaldo *(U. Saskatchewan)*, B. Hitti *(TRIUMF)*   99

316

918. High field study of La_2CuO_4 based superconductors [active], I.M. Gat, M.I. Larkin, P.L. Russo, A. Savici, Y.J. Uemura *(Columbia U.)*, P.P. Kyriakou, G.M. Luke, M.T. Rovers *(McMaster U.)*, K.M. Kojima, S. Uchida *(U. Tokyo)*, T. Ito *(AIST, Tsukuba)*, Y.S. Lee *(Nat. Inst. Standards Technology)*, K. Yamada *(Kyoto U.)*, M. Greven, M. Kaneko *(Stanford U.)*   101

919. Proton irradiation effects in SOI devices [active], P. Dodd, G. Hash, R. Loemker, J. Schwank, M. Shaneyfelt *(Sandia Nat. Lab)*, V. Ferlet-Cavrois, P. Paillet *(CEA)*

920. Nuclear charge radii and moments of short lived neutron deficient Lanthanum isotopes [active], H.A. Schuessler *(Texas A&M U.)*, P. Levy *(TRIUMF)*, H. Iimura *(Japan Atomic Energy Res. Inst.)*, F. Buchinger, J. Crawford, J. Lee *(McGill U.)*, R.I. Thompson *(U. Calgary)*

921. High-K isomers in neutron-rich $A = 170$–190 nuclei [active], A.A. Hill, Z. Podolyák, P.H. Regan, P.M. Walker, C. Wheldon, R. Wood *(U. Surrey)*, G.C. Ball, P. Bricault, G. Hackman *(TRIUMF)*, C.E. Svensson *(U. Guelph)*, R. Austin, J.C. Waddington *(McMaster U.)*, A. Piechaczek, E.F. Zganjar *(Louisiana State U.)*

922. On the production of ^{26}Al in novae: measurement of the ^{25}Al$(p, \gamma)^{26}$Si reaction rate [pending], S. Bishop, A.A. Chen, J.M. D'Auria, D. Hunter, M. Lamey, C. Wrede *(SFU)*, L. Buchmann, D.A. Hutcheon, K.P. Jackson, A. Olin, J. Rogers *(TRIUMF)*, S. Engel *(Ruhr-U. Bochum)*, C.S. Galovich *(U. Northern Colorado)*, D. Gigliotti, A. Hussein *(UNBC)*, U. Greife, C.C. Jewett *(Colorado School of Mines)*, J. José *(UPC/IEEC Barcelona)*, P.D. Parker *(Yale U.)*

923. Measurement of ^{25}Al $+ p$ resonances through elastic scattering [active], A.A. Chen, J.M. D'Auria *(SFU)*, L. Buchmann, F. Sarazin, A. Shotter, P. Walden *(TRIUMF)*, T. Davinson, A. Murphy, I. Roberts, A. Robinson, C. Ruiz, P. Woods *(U. Edinburgh)*, B. Fulton, D. Groombridge, J. Pearson *(U. York)*, P.D. Parker *(Yale U.)*

924. The hot CNO cycle and the ^{14}O$(\alpha, p)^{17}$F reaction [active], M. Aliotta, T. Davinson, A. Murphy, I. Roberts, A. Robinson, P.J. Woods *(U. Edinburgh)*, L. Buchmann, A. Chen, P. Walden *(TRIUMF)*, B. Fulton, D. Groombridge, J. Pearson *(U. York)*, P. Leleux *(U. Catholique de Louvain)*, R. Azuma *(U. Toronto)*

925. Isospin mixing in ^{36}Ar via spin-polarized observables in ^{36}K β^+ decay [active], J.M. D'Auria, D. Melconian *(SFU)*, G.C. Ball, J.A. Behr, P. Bricault, M. Dombsky, K.P. Jackson *(TRIUMF)*, S. Gu, M. Pearson *(UBC)*, W.P. Alford *(U. Western Ontario)*, D.A. Ashery, O. Aviv *(Tel Aviv U.)*, I.A. Towner *(Queen's U.)*, S. Karataglidis *(Los Alamos Nat. Lab)*, B.A. Brown *(Michigan State U.)*   61

926. Measurement of charge radius and β^+-decay Q-value of laser-trapped ^{74}Rb [active], S. Gu, M. Pearson *(UBC)*, J.A. Behr, P. Bricault, M. Dombsky, K.P. Jackson *(TRIUMF)*, D. Melconian *(SFU)*, D.A. Ashery, O. Aviv *(Tel Aviv U.)*

927. Using $(^3$He,$p)$: spectroscopy of proton unbound ^{19}Na [active], G.C. Ball, L. Buchmann, G. Hackman, A. Laird, F. Sarazin, A. Shotter, P. Walden *(TRIUMF)*, A.A. Chen *(SFU)*, T. Davinson, I. Roberts, A. Robinson, C. Ruiz, P. Woods *(U. Edinburgh)*, B. Fulton, D. Groombridge, J. Pearson *(U. York)*, C.E. Svensson *(U. Guelph)*, J. Waddington *(McMaster U.)*

928. Level structure of ^{21}Mg: nuclear and astrophysical implications [active], M. Aliotta, T. Davinson, A.St.J. Murphy, A. Robinson, P.J. Woods *(U. Edinburgh)*, J.M. D'Auria *(SFU)*, R. Azuma *(U. Toronto)*, R. Boyd *(Ohio State U.)*, L. Buchmann, A. Chen, D. Hutcheon, A. Laird, P. Walden *(TRIUMF)*, B. Fulton *(U. York)*   62

929. Octupole deformation and spin-exchange polarization of odd-A radon isotopes: toward radon electric dipole moment measurements at ISAC [active], C.E. Svensson *(U. Guelph)*, S.B. Bayram, T.E. Chupp, K. Coulter, W. Lorenzen *(U. Michigan)*, D.E. Appelbe *(Daresbury)*, R.A.E. Austin, J.C. Waddington *(McMaster U.)*, G.C. Ball, J.A. Behr, P. Bricault, G.S. Hackman, K.P. Jackson, J.A. Macdonald *(TRIUMF)*, P. Garrett *(Lawrence Livermore Nat. Lab)*, M.E. Hayden *(SFU)*, D. Kulp, J.L. Wood *(Georgia Tech. U.)*, M.R. Pearson *(UBC)*, A. Piechaczek, E.F. Zganjar *(Louisiana State U.)*

930. Measurement of π^- absorption in water [completed data-taking], T. Awes, V. Cianciolo, G. Young *(Oak Ridge Nat. Lab)*, S. Berridge, W. Bugg, Yu. Efremenko, R. Gearhart, Yu. Kamyshkov, S. Ovchinnikov *(U. Tennessee)*, Yu. Davydov, T. Numao, J.-M. Poutissou *(TRIUMF)*   63

931. Magnetic properties of multinuclear, open-shell coordination complexes and polymers probed by μSR [active], N. Draper, D.B. Leznoff, G. Mund, K.F. Poon, C. Shorrock, J.E. Sonier *(SFU)*   102

932. Improving μ^-SR performance [active], J.H. Brewer, D.F. Measday *(UBC)*, G.M. Marshall, M.M. Pavan *(TRIUMF)*, K. Ghandi *(UBC–TRIUMF)*   103

933. Effects of nonlocality in superconductors [completed], R. Miller, R. Kiefl *(UBC–TRIUMF)*, S.L. Bud'ko, P. Canfield, V. Kogan *(Iowa State U.)*, P. Poon, J.E. Sonier *(SFU)*

934. MuSR study of polymerized C_{60} [active], A. Fukaya, I.M. Gat, P.L. Russo, A.T. Savici, Y.J. Uemura *(Columbia U.)*, P. Kyriakou, G.M. Luke *(McMaster U.)*, T. Makarova, B. Sundqvist *(Umea U. Sweden)*, V.A. Davydov *(Moscow Inst. High Pressure)*, T. Ito *(AIST, Tsukuba)*   107

935. High pressure study of URu$_2$Si$_2$ [active], J. Garrett, P. Kyriakou, G.M. Luke, C. Wiebe *(McMaster U.)*, I.M. Gat, A. Savici, Y.J. Uemura *(Columbia U.)*, Y. Sushko *(U. Kentucky)*, K.M. Kojima *(U. Tokyo)*

936. Magnetic dynamics in spin ice systems [active], S.T. Bramwell, J. Lago *(U. College London)*, S.R. Dunsiger *(Los Alamos Nat. Lab)*, J.S. Gardner *(NRC)*, M.J.P. Gingras *(U. Waterloo)*, R. Kiefl *(UBC–TRIUMF)*, G.M. Luke *(McMaster U.)*

937. Muonium in hexagonal semiconductors [active], R.L. Lichti *(Texas Tech. U.)*, K.H. Chow *(U. Alberta)*, S.F.J. Cox *(Rutherford Appleton Lab)*, B. Hitti *(TRIUMF)*   108

938. Muonium formation and ionization in semiconductors and insulators [active], J.H. Brewer, *(UBC)*, B. Hitti *(TRIUMF)*, R. Lichti *(Texas Tech. U.)*, D.G. Eshchenko *(U. Zurich–PSI)*, V.G. Storchak *(Kurchatov Inst.)*   109

939. Guest-host interactions and Hfcs of mu-radicals in zeolites [active], M. Bridges, D.G. Fleming, C. Fyfe, G. Patey, A. Wang *(UBC)*, D. Arseneau *(TRIUMF)*, K. Ghandi *(TRIUMF–UBC)*, E. Roduner *(U. Stuttgart)*, M. Senba *(Dalhousie U.)*   110

940. Thermoelectrics II: μSR in layered manganese oxides [active], K. Dohmae, H. Itahara, Y. Seno, J. Sugiyama, T. Tani, C. Xia *(Toyota Central R&D Labs Inc.)*, J.H. Brewer *(UBC)*, E.J. Ansaldo *(U. Saskatchewan)*, B. Hitti *(TRIUMF)*   111

941. Investigation of spin dynamics in geometrically frustrated transition metal oxides [active], J.E. Greedan, G.M. Luke, G. MacDougal, C.R. Wiebe *(McMaster U.)*, P. Russo, A. Savici, Y.J. Uemura *(Columbia U.)*

942. Magnetic fluctuations near metal insulator transitions in ruthenate pyrochlores [active], N. Curro, S.R. Dunsiger, K.H. Kim *(Los Alamos Nat. Lab)*, R.F. Kiefl *(UBC–TRIUMF)*, K.H. Chow *(U. Alberta)*, M.J.P. Gingras *(U. Waterloo)*, W.A. MacFarlane, R.I. Miller *(UBC)*, J.E. Sonier *(SFU)*, S.W. Cheong, *(Rutgers U.–Lucent Tech.)*, N. Hur *(Rutgers U.)*, P.C. Hammel *(Ohio State U.)*   112

943. Muonium and muoniated free radical formation and reactivity in sub- and supercritical carbon dioxide [active], D.J. Arseneau *(TRIUMF)*, M. Bridges *(UBC–TRIUMF)*, D.G. Fleming, K. Ghandi, G. Patey, A. Wang *(UBC)*, M. Pinto *(SFU)*, M. Senba *(Dalhousie U.)*   115

944. Muonium sites and dynamics in silicon carbide [active], R.L. Lichti, W. Nusbaum *(Texas Tech. U.)*, K.H. Chow, *(U. Alberta)*, E.A. Davis *(U. Leicester)*, B. Hitti *(TRIUMF)*, S.F.J. Cox *(Rutherford Appleton Lab)*   117

945. Muoniated radicals formed from carbenes and carbene analogues [active], J.-C. Brodovitch, J.A.C. Clyburne, S. Kecman, B. McCollum, I. McKenzie, P.W. Percival *(SFU)*

946. Energy generation and nucleosynthesis in the HotCNO cycles: measurement of the ^{17}F$(p, \gamma)^{18}$Ne reaction rate [active], A.A. Chen *(U. McMaster–TRIUMF)*, S. Bishop, J.M. D'Auria, M. Lamey, C. Wrede *(SFU)*, L. Buchmann, D.A. Hutcheon, A. Olin, D. Ottewell, J. Rogers *(TRIUMF)*, S. Engel *(Ruhr-Universität Bochum)*, D. Gigliotti, A. Hussein *(UNBC)*, U. Greife, C.C. Jewett *(Colorado School of Mines)*, J. José *(UPC/IEEC Barcelona)*, P.D. Parker *(Yale U.)*

947. Evaluation of the competition between single-step and multi-step γ decay in the ^{12}C$(^{12}$C, $\gamma)$ reaction [active], T. Brown, S.P. Fox, B.R. Fulton, D. Groombridge, D.G. Jenkins, J. Pearson, R. Wadsworth, D.L. Watson *(U. York)*, L. Buchmann, C. Davis, D. Hutcheon, S. Park, J. Rogers *(TRIUMF)*, J.M. D'Auria *(SFU)*, U. Greife *(Colorado School of Mines)*, M.P. Carpenter, R.V.F. Janssens, T.L. Khoo, C.J. Lister, A.H. Wuosmaa *(Argonne Nat. Lab)*, M. Freer *(U. Birmingham)*, F. Azaiez, C. Beck, F. Haas, P. Papka, A. Sanchez *(IReS Strasbourg)*, C. Andreoiu, M. Chartier, R.-D. Herzberg *(U. Liverpool)*

948. Proton radiation effects in silicon-on-insulator and bulk-silicon devices [active], P. Dodd, G. Hash, R. Jones, J. Schwank, M. Shaneyfelt *(Sandia Nat. Labs)*, V. Ferlet-Cavroi, C. D'Hose, P. Paillet, J.-E. Sauvestre *(CEA, France)*, E. Blackmore *(TRIUMF)*

949. μSR study of magnetic order in high-T_c superconductor under high pressure [active], J. Arai, T. Goko, K. Sato, S. Takeshita *(Tokho U. of Science)*, W. Higemoto, K. Nagamine, K. Nishiyama *(KEK-MSL)*

950. High field study of Zn doped/Eu doped/overdoped systems [active], P.L. Russo, A.T. Savici, Y.J. Uemura *(Columbia U.)*, G.M. Luke, C.R. Wiebe *(McMaster U.)*, K.M. Kojima, S. Uchida *(U. Tokyo)*, Y.S. Lee *(Nat. Inst. Standards Technology)*, M.A. Kastner *(MIT)*, R.J. Birgeneau *(U. Toronto)*, K. Yamada *(Kyoto U.)*, R. Kadono *(KEK)*

951. Magnetism and flux line lattice structure of oxychloride superconductors [active], W. Higemoto, R. Kadono, A. Koda, K. Ohishi *(KEK-IMSS)*, M. Azuma, M. Takano, I. Yamada *(Kyoto U.)*, K.M. Kojima *(U. Tokyo)*

952. ^{12}C$(\alpha, \gamma)^{16}$O at DRAGON [active], C. Barbieri, L. Buchmann, D. Hutcheon, A.M. Laird, S. Park, J. Rogers, F. Sarazin, J.M. Sparenberg *(TRIUMF)*, C.R. Brune *(U. Ohio)*, A. Chen *(McMaster U.)*, J.M. D'Auria *(SFU)*, J. Görres, M. Wiescher *(U. Notre Dame)*, U. Greife *(Colorado School of Mines)*, A. Hussein *(UNBC)*, Z. Li, *(Chinese Inst. of Atomic Energy)*, A. Murphy *(U. Edinburgh)*, S. Woosley *(U. California, Santa Cruz)*

953. Spin dynamics and quantum coherence in molecular magnets [active], Z. Salman *(TRIUMF)*, A. MacFarlane, R. Kiefl *(UBC–TRIUMF)*, K. Chow *(U. Alberta)*, S. Dunsiger *(Los Alamos Nat. Lab)*, B. Barbara *(Lab de Magnetisme Louis Néel)*

954. Half-lives of long-lived isotopes/chronology and environment [active] R.A.E. Austin, A. Chen, K.A. Koopmans, M. Lee, N. Novo, B. Singh, J.C. Waddington *(McMaster U.)*, G.C. Ball, G. Hackman, F. Sarazin, H. Scraggs, M.B. Smith *(TRIUMF)*, P.E. Garrett *(Lawrence Livermore Nat. Lab)*, G. Grinyer, C.E. Svensson *(U. Guelph)*

955. Probing shell structure with β- and β-n-delayed γ spectroscopy [active], G.C. Ball, P. Bricault, M. Dombsky, G. Hackman, J. MacDonald, F. Sarazin, H. Scraggs, M.B. Smith *(TRIUMF)*, G. Grinyer, C.E. Svensson *(U. Guelph)*, J.C. Waddington *(McMaster U.)*, E. Zganjar *(Louisiana State U.)*, W.D. Kulp, J. Wood *(Georgia Tech. U.)*, P.E. Garrett *(Lawrence Livermore Nat. Lab)*, P. Walker *(U. Surrey–TRIUMF)*

956. Search for tensor interactions in recoil nucleus singles in decay of polarized ^{80}Rb [active], J.A. Behr, P. Bricault, M. Dombsky, S. Gu, K.P. Jackson, M.R. Pearson *(TRIUMF)*, D. Melconian *(SFU)*, D. Ashery, O. Aviv *(Tel Aviv U.)*

957. Search for high-spin isomeric states in the vicinity of double-magic $N = Z$ ^{100}Sn [active], G.C. Ball, G.S. Hackman, F. Sarazin, H.C. Scraggs, M.B. Smith *(TRIUMF)*, P.M. Walker *(U. Surrey)*, C.E. Svensson *(U. Guelph)*, J.C. Waddington *(McMaster U.)*, E. Zganjar *(Louisiana State U.)*, P.E. Garrett *(Lawrence Livermore Nat. Lab)*, J.L. Wood *(Georgia Tech. U.)*

958. HTF-μ^+SR lineshapes in overdoped high-T_c superconductors [active], D.A. Bonn, J.H. Brewer, M. Franz, W.N. Hardy, R.F. Kiefl, R.X. Liang, W.A. MacFarlane *(UBC)*, F. Callaghan, K.F. Poon, J.E. Sonier *(SFU)*, J. Chakhalian, Z. Salman *(TRIUMF)*, S. Kim, G.M. Luke *(McMaster U.)*, N.N. Kolesnikov *(Russian Acad. of Science)*, C.E. Stronach *(Virginia State U.)*

959. New low field integral method for studies of diamagnetic muonium centers in group IV and II-VI semiconductors [active], K.H. Chow, K. Hoffman *(U. Alberta)*, B. Hitti *(TRIUMF)*, J.M. Gil *(U. Coimbra)*, R.F. Kiefl *(UBC)*

960. Hydrogen (Mu) defect level in II-VI chalcogenides [active], H.V. Alberto, J.M. Gil, R.C. Vilao *(U. Coimbra)*, K.H. Chow *(U. Alberta)*, S.F.J. Cox *(Rutherford Appleton Lab)*, E.A. Davis *(U. Leicester)*, B. Hitti, S.R. Kreitzman *(TRIUMF)*, R.L. Lichti, W. Nusbaum *(Texas Tech. U.)*

961. $A \geq 62$ super-allowed Fermi β decays: constraining unknown corrections with ^{66}As and ^{70}Br decay [active], P.E. Garrett, W.E. Ormand, A. Schiller *(Lawrence Livermore Nat. Lab)*, G.F. Grinyer, C.E. Svensson *(U. Guelph)*, R.A.E. Austin, J.C. Waddington *(McMaster U.)*, G.C. Ball, G. Hackman, F. Sarazin, H.C. Scraggs, M.B. Smith *(TRIUMF)*, J. Allmond, W.D. Kulp, J.L. Wood *(Georgia Tech. U.)*, A. Piechaczek, E. Zganjar *(Louisiana State U.)*

962. μSR study on Na$_{0.33}$V$_2$O$_5$ [active], P.L. Russo, A.T. Savici, Y.J. Uemura *(Columbia U.)*, G.M. Luke, C.R. Wiebe *(McMaster U.)*, Y. Ueda, T. Yamauchi *(ISSP)*

963. Underdoped/undoped cuprate single crystals [active], D.A. Bonn, J.H. Brewer, W.N. Hardy, R.F. Kiefl, R.X. Liang *(UBC)*, F. Callaghan, K.F. Poon, J.E. Sonier *(SFU)*, G.M. Luke *(McMaster U.)*, R.L. Greene *(Maryland U.)*, P. Fournier *(U. Sherbrooke)*, C.E. Stronach *(Virginia State U.)*, R.I. Miller *(Pennsylvania State U.)*

965. Investigation of spin statics and dynamics in the new dipolar spin ice Ho$_2$Ru$_2$O$_7$ [active], J.E. Greedan, S.J. Kim, G.M. Luke, G. MacDougall, C.R. Wiebe *(McMaster U.)*, M.J.P. Gingras *(U. Waterloo)*, P. Russo, A. Savici, Y.J. Uemura *(Columbia U.)*

966. High precision mass determination for CVC tests [active], P. Bricault, J. Dilling, J. Vaz *(TRIUMF)*, K. Sharma *(U. Manitoba)*, M. Trinczek *(MPI-K–TRIUMF)*, M. Smith *(UBC–TRIUMF)*, F. Buchinger, J. Crawford, J. Lee, R.B. Moore *(McGill U.)*

967. Beta decay branching ratio of ^{21}Na [active], S.J. Freedman *(UC Berkeley–LBNL)*, P.A. Vetter *(Lawrence Berkeley Nat. Lab)*, A.P. Craig, M.P. Decowski, N.D. Scielzo *(U. California, Berkeley)*

968. Ortho-para effect of muon catalyzed fusion in liquid deuterium [active], N. Kawamura, K. Nagamine, A. Toyoda *(KEK)*, H. Imao *(U. Tokyo–KEK)*, K. Ishida, T. Matsuzaki *(RIKEN)*

969. Metamagnetic transitions and quantum critical behavior [active], S.R. Dunsiger, R.H. Heffner, G.D. Morris *(Los Alamos Nat. Lab)*, D.E. MacLaughlin *(U. California, Riverside)*, O.O. Bernal *(California State U.)*, G.J. Nieuwenhuys *(U. Leiden)*

*deceased

LIFE SCIENCES PROJECT PROPOSALS

The following lists life sciences project proposals received up to the end of 2002 (missing numbers cover proposals that have been withdrawn or replaced by later versions, rejected, or combined with another proposal). Page numbers are given for those experiments which are included in this Annual Report.   Page

LS0. PET facilities [active], <u>K.R. Buckley</u>, E.T. Hurtado, P. Piccioni *(TRIUMF)*, C. English, S. Jivan, C. Williams *(UBC–TRIUMF)*   119

LS1. Attenuation maps for quantitative SPECT [completed], <u>A. Celler</u> *(UBC–VH&HSC)*, S. McFarland *(UBC)*, S. Barney, M. Limber *(SFU)*

LS2. Synthesis of ^{18}F-glycosides as potential imaging agents for the study of glycosidase activity in the brain [completed], <u>M.J. Adam</u> *(TRIUMF)*, D. Lyster *(VH&HSC)*, G. Matte *(Halifax H.)*

LS3. Synthesis of radiopharmaceuticals for positron emission tomography [active], <u>M.J. Adam</u>, K.R. Buckley, E.T. Hurtado, J. Huser, S. Jivan, J.-M. Lu, T.J. Ruth *(TRIUMF)*   120

LS4. TR13 targets for PET radioisotope production [active], K. Buckley, T. Hurtado, <u>T.J. Ruth</u>, S.K. Zeisler *(TRIUMF)*   121

LS5. Production and on-line separation of ^{124}I from enriched tellurium [inactive], W.Z. Gelbart, E.T. Hurtado, <u>T.J. Ruth</u>, N.R. Stevenson, S.K. Zeisler *(TRIUMF)*, R.R. Johnson *(UBC)*

LS6. Bone calcium resorption studies in pre- and peri-menopausal women using accelerator mass spectrometry [completed], <u>R.R. Johnson</u>, A. Priestman, J.C. Prior *(UBC)*, A. Altman, W.Z. Gelbart, V. Sossi *(TRIUMF)*, D. Berkovits, S. Ghelberg, M. Paul *(Racah Inst., Hebrew U. Jerusalem)*, L.M. Shulman *(Chaim Sheba Med. Centre)*, R. Chechik *(Weizmann Inst.)*, E. Venzel *(SFU)*

LS7. PET 3D data quantification and integration into a research clinical environment [completed], K.S. Morrison, T.J. Ruth, <u>V. Sossi</u>, M.W. Stazyk *(UBC–TRIUMF)*, K.R. Buckley *(TRIUMF)*, J.S. Barney *(VH&HSC)*, D. Sirota, B.J. Snow *(UBC)*

LS8. Radiotracers for the physical and biosciences [active], L. Buchmann, <u>T.J. Ruth</u>, S.K. Zeisler *(TRIUMF)*, A.D.M. Glass, R.R. Johnson, M. Lowe, C.E.R. Orvig *(UBC)*, T.F. Budinger *(Lawrence Berkeley National Lab)*   123

LS10. Biological evaluation of radiohalogenated DNA aptamers [completed], <u>H. Dougan</u> *(TRIUMF)*, J.B. Hobbs, D.M. Lyster *(UBC)*, J.I. Weitz *(McMaster U.)*

LS11. Development of single photon imaging agents [inactive], <u>D. Lyster</u> *(UBC–VH&HSC)*, L. Alcorn, M. Hampong, T. Lutz, C. Vo *(UBC)*

LS12. A simulation platform for the design of position encoding multicrystal detectors [completed], A. Altman, <u>C. Moisan</u>, <u>J.G. Rogers</u> *(TRIUMF)*, E. Hoskinson, G. Tsang *(UBC)*

LS13. Utility of 2-[F-18]-fluoro-2-deoxy-d-glucose SPECT imaging in the evaluation of patients with solitary pulmonary nodules [completed], A. Celler, D. Lyster, <u>D. Worsley</u> *(UBC)*, M. Adam *(TRIUMF)*

LS14. Production of ^{127}Xe from cesium with 90–110 MeV protons [inactive], D. Pearce, <u>J. Vincent</u> *(TRIUMF)*

LS15. Investigation of frame realignment on the reproducibility of ^{18}F-6-fluorodopa positron emission tomography [inactive], <u>K.S. Morrison</u>, T.J. Ruth *(UBC–TRIUMF)*, B.J. Snow *(UBC)*

LS17. Table-top radiocarbon facility [inactive], W. Gelbart, <u>R.B. Schubank</u> *(TRIUMF)*, E. Venczel *(UBC–SFU)*, S. Calvert, R.R. Johnson, J. Nagel, T. Peterson, V. Sossi *(UBC)*, D.E. Nelson *(SFU)*, J. Prior, K. Schoenholzer, R. Sutton, V. Walker *(UBC–VH&HSC)*, R. Middleton *(U. Pennsylvania)*, M. Paul *(Hebrew U. Jerusalem)*, J. Clague, L. Jackson, J. Lutenauer, D. Templeman-Kluit *(Geological Survey of Canada)*, R.N. McNeely, J.-S. Vincent *(GSC Ottawa)*, V. Barrie *(Pacific Geoscience Center)*, D. Prior, K.R. Robertson, G. Vilks *(Bedford Inst. Oceanography)*, R. Brown, S. Wang *(Elemental Research Inc.)*, J. Vogel *(Lawrence Livermore National Lab)*, A.E. Litherland *(U. Toronto)*, S. Dias, S. Sood *(Ontario Hydro)*, H.R. Andrews, R.M. Brown, R.J. Cornett *(AECL)*, D.B. Carlisle *(Environment Canada)*, J. Carron, A. Kabir, R.C.J. Wilkinson *(Canadian Centre for Inland Waters)*, R. Gephart, P. Molton, D. Robertson *(Batelle Pacific Northwest Labs)*

LS18. Cooperative development of ^{82}Sr-Rb generators for human use in Canada [completed], <u>J. Vincent</u> *(TRIUMF)*, R. Beanlands *(U. Ottawa Heart Inst.)*, B. Bowen *(McMaster U.)*, W. Dickie *(Nordion Int.)*

LS19. An ^{15}O-water generator: a feasibility study [inactive], K.R. Buckley, <u>T.J. Ruth</u> *(TRIUMF)*

LS20. Prototype heat-pipe water target for ^{18}F-production [inactive], K.R. Buckley, E.T. Hurtado, <u>T.J. Ruth</u> *(TRIUMF)*, J.W. Lenz *(private consultant)*

LS21. Aluminum kinetics in plants [inactive], A. Glass, R.R. Johnson, L. Oliveira *(UBC)*, K. Buckley, Z. Gelbart *(TRIUMF)*, D. Berkovitz, M. Paul *(Hebrew U. Jerusalem)*, E. Venczel *(SFU)*

LS22. Virtual national biomedical tracer facility [inactive], T.J. Ruth, J.S. Vincent *(TRIUMF)*, E.J. Peterson, D. Phillips *(Los Alamos National Lab)*

LS24. Scanning for early detection and staging of breast cancer: a comparative study using FDG PET and MIBI SPECT [deferred], P.F. Cohen, P. Klimo *(Lions Gate H.–UBC)*, M. Cackette *(EBCO Industries Ltd.)*, J. Whiffen *(JALORN)*, V. Sossi *(TRIUMF–UBC)*, J. Porter *(Nordion Int.)*, R.R. Johnson *(UBC)*

LS25. 3D PET in human neuroreceptor studies: quantification and reconstruction [completed], K.S. Morrison, T. Oakes, T.J. Ruth, V. Sossi *(UBC–TRIUMF)*, K.R. Buckley *(TRIUMF)*, M. Krzywinski, M. Schulzer, J. Stoessl *(UBC)*

LS26. A gaseous planar positron source for routine 3D PET normalization [completed], T. Oakes, T.J. Ruth, V. Sossi *(UBC–TRIUMF)*, K. Buckley, S. Jivan, R. MacDonald *(TRIUMF)*

LS27. The feasibility and efficacy of using 2-(F-18)-fluoro-2-deoxy-D-glucose (18-FDG) to evaluate children with musculoskeletal neoplasm [deferred], R. Anderson, J. Davis, D. Lyster, H.R. Nadel, T.J. Ruth, M. Stilwell, D. Worsley *(UBC)*

LS28. Evaluation of potentially viable myocardium with dobutamine myocardial SPECT imaging [completed], H. Abbey, A.-Y. Fung, L. Hook, D.M. Lyster, D.F. Worsley *(VH&HSC)*, M. Adam, S. Jivan *(TRIUMF)*

LS29. Production and distribution of FDG for clinical studies [completed], D. Lyster, D. Worsley *(VH&HSC)*, P. Cohen *(Lions Gate H.)*, H. Nadel *(Children's H.)*, M.J. Adam, S. Jivan, T.J. Ruth, V. Sossi *(TRIUMF)*   127

LS31. Auger electron emitters for therapy-physics and chemistry [inactive], D. Pearce, T.J. Ruth, J. Vincent, A. Zyuzin *(TRIUMF)*, V. Kokhanyuk, V. Kravchuk, B.L. Zhuikov *(INR Moscow)*

LS32. ^{18}F-H$_2$^{18}O supply to the University of Alberta [completed], S.A. McQuarrie, J.R. Mercer *(U. Alberta)*, A.J.B. McEwan *(CCI)*, R.R. Johnson *(UBC–EBCO)*, T.J. Ruth *(UBC–TRIUMF)*   127

LS33. Evaluation and improvement of a dual head coincidence camera [active], K.S. Morrison, T.J. Ruth, V. Sossi *(UBC–TRIUMF)*, M. Krzywinski *(UBC)*, P. Cohen *(Lions Gate H.)*, P. Klimo *(Lions Gate H.–UBC)*, T.K. Lewellen, D.A. Mankoff *(U. Washington)*   128

LS34. Production of ^{103}Pd [inactive], R.R. Johnson, R. Pavan *(UBC)*, M. Cackette, K.L. Erdman *(EBCO Industries Ltd.)*, Z. Gelbart *(TRIUMF)*

LS35. Development of F-18 labelled nitroimidazole PET imaging agents for tissue hypoxia [active], M.J. Adam *(TRIUMF)*, K. Skov *(BCCRC–UBC)*, S. Evans, C. Koch, A. Kachera *(U. Pennsylvania)*, I. Baird, B. James *(UBC)*   129

LS37. Feasibility of ^{125}Xe implantation as a ^{125}I brachytherapy source [completed], D. Ottewell, T. Ruth, J. Vincent, A. Zyuzin *(TRIUMF)*

LS38. Dopaminergic tracers kinetic modeling with minimally invasive scanning procedures [completed], G. Chan, M. Krzywinski, T.J. Ruth, V. Sossi *(UBC–TRIUMF)*, J. Holden *(U. Wisconsin)*, D. Doudet, J. Stoessl *(UBC)*

LS39. Positron emission profiling (PEP) for pulp and paper fluid dynamic studies [active], M. Martinez, J. Olson *(UBC)*, M.J. Adam, K. Buckley, S. Jivan, T.J. Ruth, V. Sossi *(TRIUMF)*   129

LS40. F-18 FDG cardiac PET scans using a coincidence PET/SPECT camera to assess myocardial viability in patients with fixed abnormalities and low ejection fractions on gated sestamibi stress tests [deferred], P.F. Cohen, J. Imrie, K. Woo *(Lions Gate H.)*, D. Worsley *(Vancouver General H.)*, V. Sossi *(TRIUMF–UBC)*, T. Ruth *(UBC–TRIUMF)*, R.R. Johnson *(UBC)*

LS41. Impact of the ADAC coincidence PET camera in the management of selected cancer patients [deferred], P.F. Cohen, J. Imrie, K. Woo *(Lions Gate H.)*, J. Powe *(Vancouver General H.)*, V. Sossi *(TRIUMF–UBC)*, T. Ruth *(UBC–TRIUMF)*, R.R. Johnson *(UBC)*

LS42. Configuration modeling and image reconstruction studies on a depth encoding research tomograph [active], T. Ruth, V. Sossi *(UBC–TRIUMF)*, V. Astakhov *(UBC)*, K. Buckley *(TRIUMF)*, S. Houle *(Centre Addiction & Mental Health, Toronto)*, C. Moisan *(U. Laval)*   130

LS43. Positron emission mammography system (PEM) [deferred], K. Buckley, S. Jivan, T.J. Ruth, V. Sossi *(TRIUMF)*, M. Stilwell *(B.C. Women's H.)*, P. Gordon *(UBC)*, H. Nadel *(Children's H.)*

LS44. Development of a high-speed formation (areal density) measurement system for paper [active], M. Avikainen, S. Heath, M. Martinez, J. Olson *(UBC)*, K. Buckley, T.J. Ruth, M. Salomon *(TRIUMF)*

LS45. Modelling genetic risk for ionizing radiation exposure in space [deferred], J.G. de Boer, J. Holcroft, S. Zhang *(U. Victoria)*

321

LS46. Modelling of the dopaminergic system in more severely affected PD patients [active], T.J. Ruth, V. Sossi *(UBC– TRIUMF)*, J. Holden *(U. Wisconsin)*, R. de la Fuente-Fernandez, D. Doudet, C.S. Lee, M. Schulzer, J. Stoessl *(UBC)*

LS47. PET imaging of recurrent prostate cancer with 2-F-18-fluoromethy-dimethy-2-hydroxyethylammonia (FCH), [active], M. Gleave, D. Lyster, J. Powe, D. Worsley *(Vancouver General H.–UBC)*, M. Adam *(TRIUMF)*, H. Abbey *(Vancouver General H.)*

LS48. Anorexia nervosa: autonomic dysfunction, the brain and the heart [completed], A.S. Belzberg, C.L. Birmingham, C. Kerr, G.P. Sexsmith, M. Stilwell *(St. Paul's H.)*, M.J. Stock *(St. George's H.)*, P. Beumont *(U. Sydney, Aust.)*, V. Sossi *(UBC–TRIUMF)*

LS49. ^{18}F FDG cardiac PET scans using a third generation coincidence camera to assess myocardial viability in patients who are candidates for cardiac transplantation [deferred], A.S. Belzberg, S. Chan, A. Ignaszewski, M. Kiess, G. Sexsmith, M. Stilwell *(St. Paul's H.)*, V. Sossi *(TRIUMF–UBC)*

LS50. Antisense imaging nucleic acids for Parkinson's disease [active], M. Adam, H. Dougan, T.J. Ruth *(TRIUMF)*, J.B. Hobbs, D.M. Lyster, J. Stoessl *(UBC)*, A.I. Kassis *(Harvard U.)* 132

LS51. Auger therapy for prostate cancer [active], H. Dougan, T.J. Ruth, J.S. Vincent *(TRIUMF)*, C.C. Nelson, P.S. Rennie *(Prostate Centre)*, C.M. Ludgate *(UBC–U. Victoria)*, D.M. Lyster *(UBC)* 132

LS52. Comparison of commercial FDG synthesis systems [completed], T.J. Ruth *(UBC/TRIUMF)*, M. Adam, K. Buckley, S. Jivan *(TRIUMF)*, D. Lyster *(UBC)*, R. McDonald *(IPET)* 133

LS53. Synthesis of ^{99m}Tc and ^{186,188}Re sugar derivatives [active], M.J. Adam *(TRIUMF)*, C. Orvig *(UBC)*, S. Bayly, C. Fisher *(TRIUMF/UBC)*, M. Abrams *(AnorMED)* 133

LS54. Wavelet reconstruction for high resolution three-dimensional positron emission tomography [active], C.-H. Chen, A. Rahmim, K. Raywood *(UBC)*, T.J. Ruth, V. Sossi *(UBC/TRIUMF)*

LS55. Detection of metastases in intermediate thickness melanoma with ^{18}FDG and a coincidence hybrid scanner [active], A. Belzberg, G. Sexsmith, M. Stilwell *(St. Paul's H./UBC)*, A. Lee *(Surrey Memorial H.)*, T.J. Ruth *(UBC/TRIUMF)*

LS56. Synthesis of radiolabelled nucleotides and oligonucleotides [active], M.J. Adam, H. Dougan, A. Studenov *(TRIUMF)*, J. Wilson *(Cross Cancer, Edmonton)*, J. Hobbs *(UBC)*

LS57. Quantitative imaging with the Concorde MicroPET [active], A. Rahmin, V. Sossi *(UBC)*, K. Raywood, T.J. Ruth *(UBC–TRIUMF)*, K. Buckley, P. Piccioni *(TRIUMF)*, C. Thompson *(Montreal Neurological Inst.)*, S. Lapi *(SFU)* 134